Characterisation of late Palaeozoic glacigene sedimentary rocks of the Troubridge and Arckaringa basins and implications for palaeogeographic reconstructions of late Palaeozoic South Australia

by

VERITY JAYNE NORMINGTON

B. Sc (Hons), University of Adelaide, 2009

A thesis submitted in fulfilment of the requirements for the degree of

DOCTOR OF PHILOSOPHY

Department of Earth Sciences, School of Physical Sciences

University of Adelaide

Adelaide, South Australia, Australia

2017

Page intentionally left blank

Statement of Authorship

I certify that this work contains no material which has been accepted for the award of any other degree or diploma in my name, in any university or other tertiary institution and, to the best of my knowledge and belief, contains no material previously published or written by another person, except where due reference has been made in the text. In addition, I certify that no part of this work will, in the future, be used in a submission in my name, for any other degree or diploma in any university or other tertiary institution without the prior approval of the University of Adelaide and where applicable, any partner institution responsible for the joint-award of this degree.

I give permission for the digital version of my thesis to be made available on the web, via the University's digital research repository, the Library Search and also through web search engines, unless permission has been granted by the University to restrict access for a period of time.

I acknowledge the support I have received for my research through the provision of an Australian Government Research Training Program Scholarship.

27/02/2018

Verity Jayne Normington — Date

Dedicated to my Parents,

Dad, you were not here to see me get where I am now but somehow you always knew I would.

Mum, you raised me so that I could withstand the tough times and showed me I could to survive anything.

and

To my Husband,

Adam, you let me follow my dreams no matter where they took us.

Abstract

The majority of southern Australia was covered in ice during the Gondwanan Permo-Carboniferous glaciation. Glacigene sequences associated with this event are preserved within basins including the Late Palaeozoic sediments of the Arckaringa and Troubridge basins in South Australia. In this study, detailed sedimentology, geochronology and geochemistry of these sediments is used to inform an improved palaeogeographic reconstruction of South Australia during the late Palaeozoic and to understand background geochemistry relevant to their use as geochemical exploration media.

Diamictite units with rounded to angular, locally-derived clasts are observed throughout the Troubridge Basin and the south Arckaringa Basin. These are consistent with deposition by ice tongues and icesheets. Diamictite units with subrounded to rounded clasts with both locally- and distally-derived clasts are observed in the eastern margin Arckaringa Basin. These are consistent with sedimentary rocks deposited by valley glaciers. Alternating clay and sandstone beds with lesser diamictite beds are observed in discrete exposures in the Troubridge Basin. These are consistent with a glacial environment where meltwater streams have alternating energy and sediment load. This is due to the periodic melting of the ice mass which fed into glacial lakes. The increasing frequency of diamictite beds up-sequence is indicative of the rapid retreat and melting of the ice mass. Massive to bedded, green glaciomarine clays observed in the Troubridge Basin are consistent with sedimentary rocks deposited in a transitional glacial to marine to deepening glaciomarine setting. Sedimentary rocks deposited during the marine regression are interbedded with increasingly fluvial sedimentary rocks suggesting that freshwater streams were active during the waning stages of the regression. The resulting terrestrial environment consisted of alternating fluvial and lacustrine environment with intermittent formation of coal swamps. Alternating clay and sandstone beds with minor carbonaceous beds are observed in the upper succession of the Arckaringa Basin. These are consistent with sedimentary rocks deposited in an environment where post-glacial isostatic rebound causes alternating fluvial and lacustrine conditions.

Zircon provenance spectra of the glacigene sedimentary rocks of the Troubridge Basin are dominated by ages between ca 500 to 600 Ma. These ages correlate with proximal rock packages of the Kanmantoo Group (Adelaide Rift Complex) and the Transantarctic Mountains of Antarctica. These sources are likely from sources adjacent to and from the south which is consistent with deposition via an icesheet and ice tongue. The zircon provenance spectra for the glacigene sedimentary rocks of the Arckaringa Basin are dominated by ages of ca 900 to 1200 Ma and ca 1700 to 1900 Ma. These ages are typical of rocks from the nearby Adelaide Rift Complex and the Gawler Craton as well as the distal Kanmantoo Group, Transantarctic Mountains, Musgrave Province and Arunta Region. These sources are likely from adjacent highlands and consistent with being deposited via valley glaciers formed in nearby alpine glacial systems.

Major and trace element geochemistry of the minimally weathered clay and silt packages interbedded with diamictite in the Troubridge and Arckaringa basins are similar to PAAS and likely sourced from of the Kanmantoo Group. The depositional setting of the glacigene sediment is shown in SiO_2:Al_2O_3 ratios. High silica end members represent sand-rich lithologies and high Al end members represent clay-rich lithologies. The Al-rich end members include clay matrix diamictites that are most likely the result of glacial deposition (rock flour + clasts). The Si-rich end members represent lithologies where fluvial processes removed the fine-grained clay-rich component. The complexity of the observed geochemical trends and the influence of weathering on the concentration of potential mineral exploration pathfinder (trace) elements highlights the necessity of understanding depositional and post-depositional influences on geochemistry. Weathering processes largely control the major and trace element geochemistry of weathered and indurated glacigene sedimentary rocks. These weathering processes include terraneous weathering (carbonate, sulphate and dolomite), ferruginous weathering and kaolinitic weathering.

The sedimentology, geochronology and geochemistry of the late Palaeozoic glacigene sedimentary rocks of the Troubridge and Arckaringa basins are used to interpret a three-stage model of evolution of the late Palaeozoic

glaciation. Stage 1: Glacial advance (late Palaeozoic). During the Permo-Carboniferous glaciation, the South Australian landscape was dominated by both continental and alpine glaciation. The continental ice sheet spread rapidly north from Antarctica into central South Australia, extending to southern margin of the Arckaringa Basin at the glacial maximum at the Asselian. Ice tongues at the front of the ice sheet scoured, eroded and polished the exposed landscape, forming U-shaped valleys and polished, glaciated pavements. At paleolatitudes north of the continental icesheet alpine glaciers occupied the highlands and valley glaciers transported debris into low-lying depocentres adjacent to the highlands. Stage 2: Glacial retreat and marine transgression (Sakmarian). The ice sheet rapidly melted and retreated from northern South Australia shedding debris into the Troubridge Basin. Melting slowed as it retreated further south. The retreat of the ice mass from northern South Australia opened a seaway into which marine waters entered from the west initiating a marine transgression in northern South Australia. When the marine transgression was at its maximum most of South Australia was inundated with only the eastern Gawler Craton Highlands remaining above seawater. Stage 3: Post-glacial isostatic rebound (late Sakmarian to early Artinskian). During this time the seaway contracted toward the south (Troubridge Basin) and there was a transition to fluviolacustrine conditions in the north (Arckaringa Basin).

Acknowledgements

Firstly, I would like to thank my PhD supervisors, Dr. Steven Hill, Prof. David Giles and Dr. Caroline Tiddy for supporting, mentoring, and encouraging me during this journey. Thank you doesn't seem enough for all the time, effort and patience you have shown and I especially thank you all for sticking by me during my many absences due to illness, lesser people would have given up. Steve was instrumental in inspiring me to continue in the world of geology. His ever present enthusiasm towards my research and never ending support allowed me to steer my research to a place where I could explore and expand my passions. I cannot thank him enough for the hours of discussions and for all the laughs we had along the way.

Dave has been knowledgeable, supportive and patient, his willingness to provide insightful and well-informed advice has allowed me to produce something that I am proud of. His readiness to provide feedback on countless drafts and that he continued to do so after I moved halfway across the country has meant that I have been able to finally finish. Caroline has been a source of never ending support and enthusiasm and her eagerness to read rewrite after rewrite of chapters has been instrumental in creating something that I hope can contribute to the geoscientific understanding of the cover in Australia. But mostly I thank all of you for the friendship, support towards both my research and in my life outside of my PhD and for the belief that I would finish when I sometimes struggled to believe it myself.

I am forever indebted to my follow geologists with whom I shared my journey with. Ashlyn Johnson, Ben van der Hoek and Charlotte Mitchell, thank you for the all advice, support and scientific discussions and I especially thank you for your friendship it will always be cherished. To the University of Adelaide research students not mentioned by name who provided advice and support, thank you also. I also thank my colleagues and friends at the Northern Territory Geological Survey, especially Eloise Beyer, Alison Wiercinski, Jo Whelan and Chris Edgoose without your support, advice both geological and other and encouragement I would still be writing my thesis and not be at this final stage.

I now thank the most important people in my life, my friends and family. To the best friends a girl could ask for, particularly Matt and Chelsea, Belinda, Alison, Eloise, Bianca, Tanya and Mellisa, thank you for being both a distraction and a motivation throughout the years and thank you for listening to my never ending ravings about my research and trying to understand what the hell it is was talking about.

My biggest thank you goes to my family. A special thank you goes to my best friend, Errol; you've been there since the beginning. Thank you for always being there with an open ear, a supportive word, a strong coffee and an even stronger hug. I couldn't have done this without my Sando Family. To my husband and best friend Adam, you have stood with me and supported me throughout this journey from high school to now. Your constant love and encouragement has meant I could follow this dream through to completion. Now we can finally go on a holiday! Thank you to my mum, Erica. You have always supported me without judgement no matter what it was I wanted to do. The strength you have shown over the years is an inspiration to me in all that I do. And thanks to the rest of my family, my baby brother, Dan and his wife Abbey, my grandparents, aunts, uncles and cousins. Thanks for being always being proud of me no matter what.

Table of Contents

Chapter 1: Introduction

Glaciers constitute much of the Earth's cryosphere, the portion of the Earth that is frozen. Currently glaciers cover approximately 10% of the planet and are isolated to Polar, high latitude, and high altitude regions. Icesheets and glaciers have repeatedly advanced and retreated throughout Earth's history. Hoffman and Schrag (2002) hypothesized the 'Snowball Earth Theory', and suggest that during the Neoproterozoic, up to 99% of the Earth's surface, was covered in icesheets and glaciers. During the Last Glacial Maximum (ca 20 000 years ago), it is estimated that up to 30% of the Earth's surface was covered by glaciers (Ehlers and Gibbard 2007), the majority of which covered large areas of the northern hemisphere. The sedimentological and geochemical characteristics of glacigene sedimentary rocks are the result of a combination of processes from source regions through transport, deposition, post-depositional alteration, and weathering. These often reflect global climate, eustasy, geography and landscape evolution during the period of glaciation. Additionally, glacial sedimentary rocks may overlie extensive, economically prospective regions (e.g. Canada; McClenaghan and DiLabio 1993, Finland; Sarala et al. 2009), where they represent a potential geochemical exploration media.

Depositional processes, palaeogeography, climate, and depositional environment of ancient glacial successions can be reconstructed based on an understanding of modern glacial processes. For instance, the glaciated terrane of eastern Greenland (Figure 1:1) is an example of a continental icesheet that has ice tongues extending from the front of the icesheet. These ice tongues along with smaller montaine and valley glaciers feed into the Norwegian Sea (Figure 1:1b). Small glacial lakes can form where icebergs break off and trap glacial waters between the ice tongue and iceberg or between the landmass and iceberg (Figure 1:1b). Valley glaciers originating in the highlands flow into glacial lakes or meet and join ice tongues (Figure 1:1b). Hudson Bay in northeastern Canada (Figure 1:1a) is an area where past glaciation has affected the landscape due to the ice mass in Greenland retreating from where it once covered much of Canada. This post-glacial landscape is currently undergoing post-glacial isostatic rebound (Shilts 1986). Lakes and fluvial streams are forming in low-lying areas surrounding the bay due to the isostatic rebound.

Modern glacial settings have been used to inform reconstructions of the Permo-Carboniferous glaciation (or late Palaeozoic Ice Age; e.g. Le Blanc Smith and Eriksson 1979, Alley and Bourman 1984, Veevers 2006). The Permo-Carboniferous glaciation was a significant glacial period in Earth's history, as the glaciation and subsequent transition to a terrestrial, greenhouse climate had a major impact on Earth's chemical, physical and biological systems (Isbell et al. 2012). Records of the stratigraphic, geochemical and tectonic history preserved in the late Palaeozoic sedimentary rocks have contributed to development and understanding of the palaeogeographic continental arrangement and location of the supercontinent Gondwana (Figure 1:2; Fielding et al. 2008, Isbell et al. 2012). Previous researchers (e.g. Ludbrook 1969b, Alley et al. 1995) suggested that during the Permo-Carboniferous glaciation, most of Gondwana was covered by a continental icesheet, or series of icesheets, that waxed and waned during much of the late Palaeozoic (Figure 1:2). Other models (e.g. Crowell and Frakes 1971a, 1971b, Veevers 2006) suggest the high altitude alpine glaciers also formed during the glaciation. Remnants of the Permo-Carboniferous glaciation have been recorded in sedimentary basins in India, Africa, South America, Antarctica, and Australia (Figure 1:2; Fielding et al. 2008, Isbell et al. 2012).

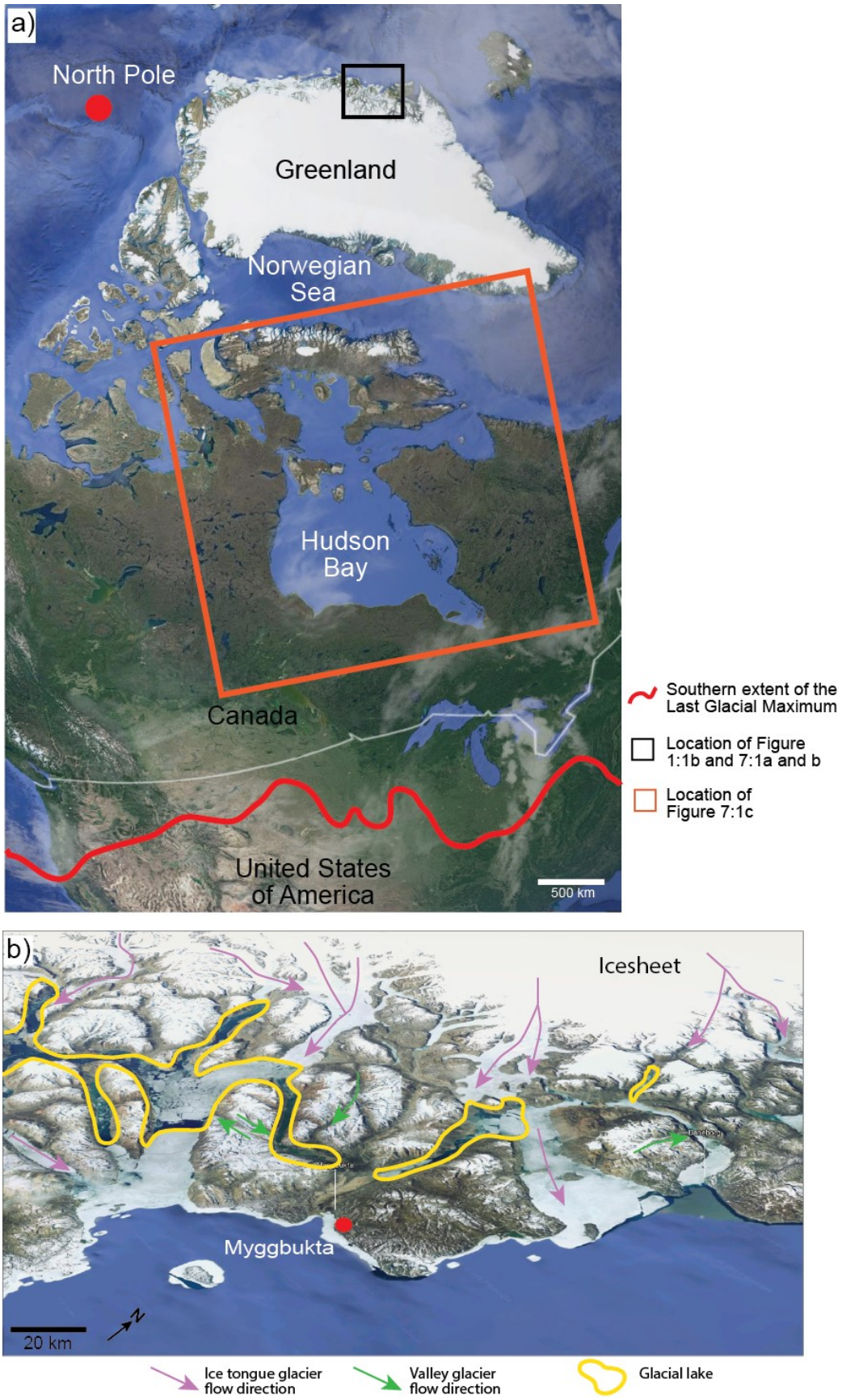

Figure 1:1 Modern glaciated terrane and adjacent landscape of greater Northern America showing the extent of the Last Glacial Maximum (adapted from Margold et al. 2015) and locations areas shown in Figures 1:1b and 7:1. Image from Google Earth.

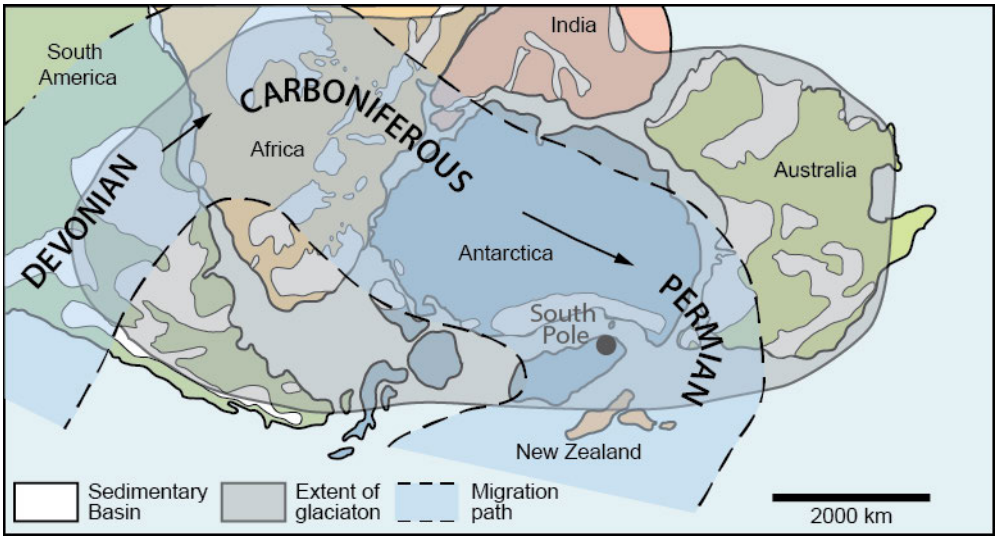

Figure 1:2 The migration of the South Pole through Gondwana from the Devonian to the Triassic, South Pole position shown is during the Permo-Carboniferous glaciation. Grey shading is the area affected by the late Palaeozoic glaciation as interpreted by Crowell (1978), Caputo and Crowell (1985), Scheffler et al. (2003), Veevers (2006), and López-Gamundi and Buatois (2010). Sedimentary basins with remnants of late Palaeozoic glacigene sedimentary rocks are shaded in white as proposed by Alley et al. (1995), and Isbell et al. (2012). Figure adapted from Alley and Bourman (1995), Fielding et al. (2008 and references therein) and Isbell et al. (2012).

There is abundant evidence that large parts of Australia were covered by ice during the Carboniferous and Early Permian (Crowell and Frakes 1971a, 1971b, Caputo and Crowell 1982, Veevers 2006, Playford 2011, Yang et al. 2014). Glacigene sedimentary rocks deposited at this time have been recorded across Australia; including large parts of South Australia, Western Australia and New South Wales (Figure 1:2). During the Permo-Carboniferous glaciation, Australia was located proximal to the South Pole (Figure 1:2). Icesheets and associated ice tongues together with alpine glaciers almost completely covered southern Australia (e.g. Crowell and Frakes 1971b, Pillans 2007). The onset of widespread glaciation was due to the proximity to and rapid migration of Australia towards the South Pole (Isbell et al. 2012, Embleton and Schmidt 1977, Embleton and Valencio 1977). Additionally, orogenesis associated with the Alice Springs Orogeny (ca 300-450 Ma; Flöttmann et al. 2004), which culminated in the amalgamation of Pangea, resulted in development of topographic highs that could accommodate alpine glaciation.

1.1 Late Palaeozoic geology of South Australia

Sedimentary rocks deposited during the Gondwanan Permo-Carboniferous glaciation are preserved across Australia (Figure 1:3). Palynological age constraints indicate that upper units of the glacigene succession are well constrained to Late Asselian to Sakmarian age (290 to 285 Ma; Hibburt 1995). The lowermost units are not well constrained due to poorly preserved foraminifera (Ludbrook 1967, Ludbrook 1969b). Therefore, due to the poorly constrained age of the sedimentary rocks, in this thesis, the sedimentary rocks are referred to as late Palaeozoic rather than Permo-Carboniferous.

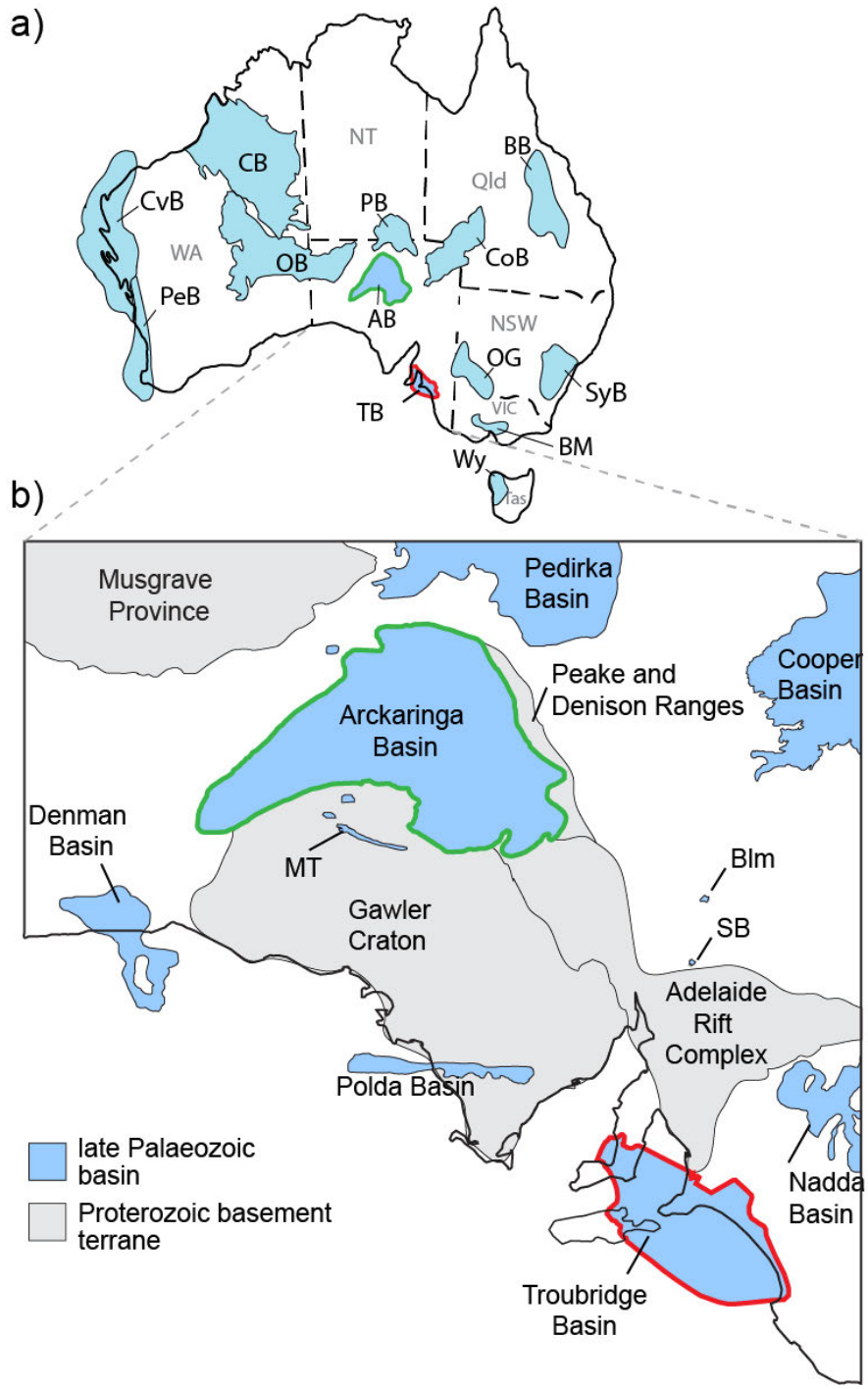

Figure 1:3 a) Distribution of late Palaeozoic sedimentary rocks in Australia, adapted from Veevers (2006). Glacial features have been recorded in the Troubridge Basin (TB: red outline; David and Howchin 1897, Milnes and Bourman 1972, Bourman et al. 1976, Alley and Bourman 1984, Bourman and Alley 1988, 1990, 1995, 1999) Arckaringa Basin (AB: green outline; Ludbrook 1961, 1967, Freytag 1964, DeMaison 1969, Townsend 1973, Heath 1974, Finlayson 1981, Hibburt 1995) of South Australia, the Bacchus Marsh (BM) area in central southern Victoria, the Ovens Graben (OG) in northeastern Victoria (Craig and Brown 1984, Roberts 1984, O'Brien 1986, Holdgate 1995, O'Brien et al. 2003), Wynyard (Wy) in Tasmania (Banks 1962, Fielding et al. 2010) and the Canning and Canarvon basins in Western Australia (CB, CvB; Crowell and Frakes 1971b, Towner 1981). Late Palaeozoic sedimentary rocks have also been recorded in the Bowen Basin (BB; Campbell et al. 1960, Derrington and Morgan 1960, Dickins 1989) and Sydney Basin (SyB; Dickins 1989, Mii et al. 2011) of eastern Australia, the Perth Basin (PeB; Playford et al. 1976, Cadman et al. 1994, Mory et al. 2005) of Western Australia as well as the Officer (OB), Cooper (CoB) and Pedirka (PB) basins in central Australia (Shearer 1994, Alley et al. 1995, Tucker 1997). b) Late Palaeozoic basins and key basement terranes of South Australia, adapted from Alley et al. (1995). Blm: Blinman area; MT: Mulgathing Trough; SB: Springfield Basin.

The sparsity and isolation of the late Palaeozoic sedimentary rocks across Australia has resulted in a series of depositional models as well as palaeogeographic and palaeoclimatic reconstructions derived from extrapolation of observations from small, independent exposures across a region or continent. The majority of these reconstructions utilise observations from exposures preserved in eastern and western Australia with little to no observations of the South Australia glacigene sedimentary rocks (such as Crowell and Frakes 1971a, Embleton and Valencio 1977, Eyles et al. 2002, Veevers 2006; see Figure 1:4). For example, the research by Veevers (2006) is based on previously published research as well as observations made in the Yilgarn Craton and the Canning and Canarvon basins in Western Australia, and from glacial exposures in Queensland, New South Wales and eastern Australia. While the model of Crowell and Frakes (1971a and 1971b; Figure 1:4) was based on till and glaciated basement distribution as well as detailed till facies observations in Tasmania, Victoria and New South Wales. The lack of direct observations and data from the late Palaeozoic rocks of South Australia within these models has resulted in a series of reconstructions and models that do not specifically address the glacial environment of South Australia, and therefore cannot be directly and holistically related to depositional processes, palaeoclimate and palaeogeography within this region during the time of glaciation.

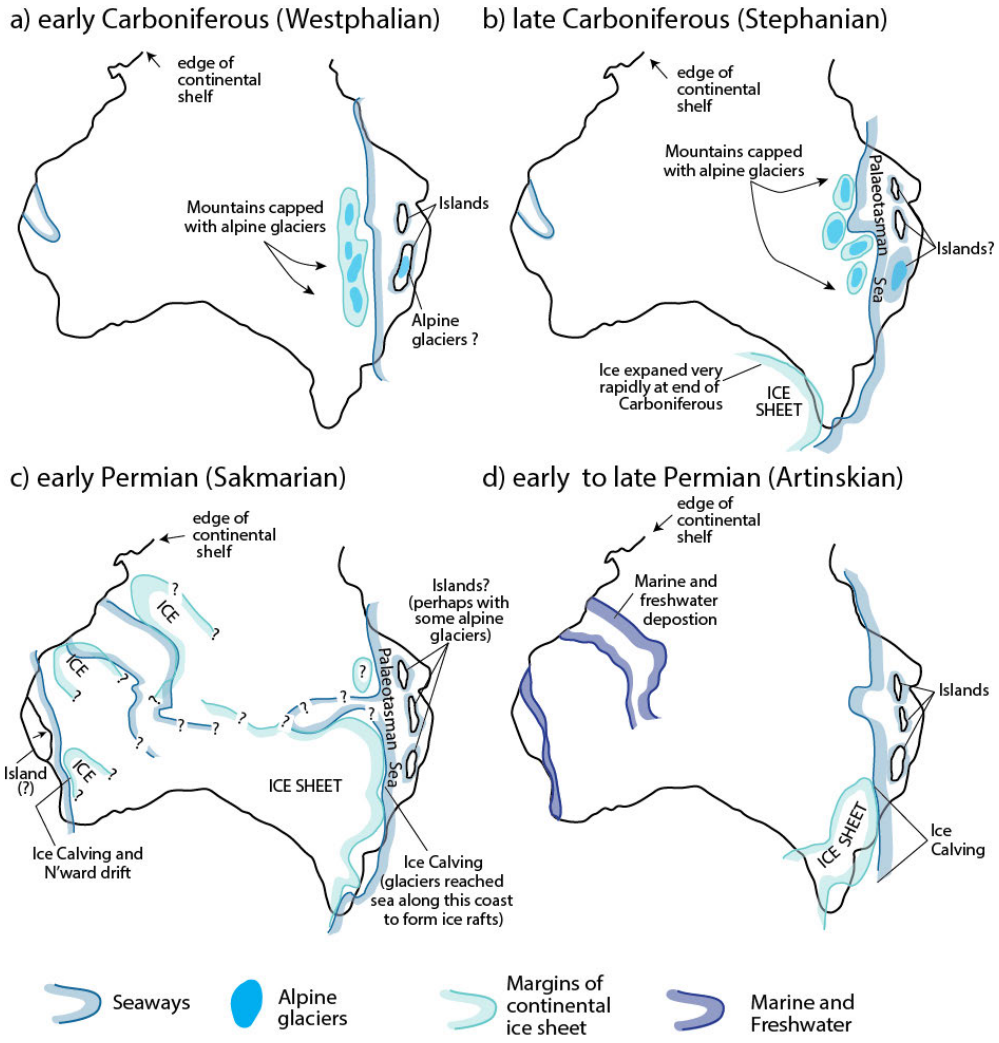

Figure 1:4 Palaeogeographic sketch maps of Crowell and Frakes (1971a) showing alpine glaciers in high altitude zones of Australia during the Permo-Carboniferous glaciation (a to d), the advancing and retreating icesheets (b to d) followed by the opening of seaways during the late Permian (d).

It is generally postulated that a wet-based (temperate), continental icesheet advanced in a northerly to northeasterly direction from Antarctica across South Australia into central Australia (Figure 1:4; e.g. Ludbrook 1969b, Crowell and Frakes 1971a, McGowran 1973, Alley and Bourman 1984, Crowell 1978, Bourman and Alley 1988, 1990, 1995, 1999, 2013, Alley et al. 1995, Hibburt 1995). The ice movement direction has been reconstructed using a variety of indicators including the distribution of striae, chatter marks and erratics (David and Howchin 1897, Milnes and Bourman 1972, Bourman et al. 1976, Bourman and Alley 1988, 1990, 1995, 1999). Glacial features and sedimentary rocks are exposed throughout Australia (Figure 1:3a), and are most intensely studied in South Australia in the well exposed regions of the Troubridge Basin (Figure 1:3b).

Depositional and palaeogeographic models have been proposed using observations of the late Palaeozoic sedimentary rocks of South Australia. These depositional models are largely based on extrapolation of data from investigations of small, but mostly complete measured sections (e.g. Figure 1:5). Sedimentary rocks deposited during this time are preserved in the late Palaeozoic basins of South Australia (Figure 1:3; Alley et al. 1995).

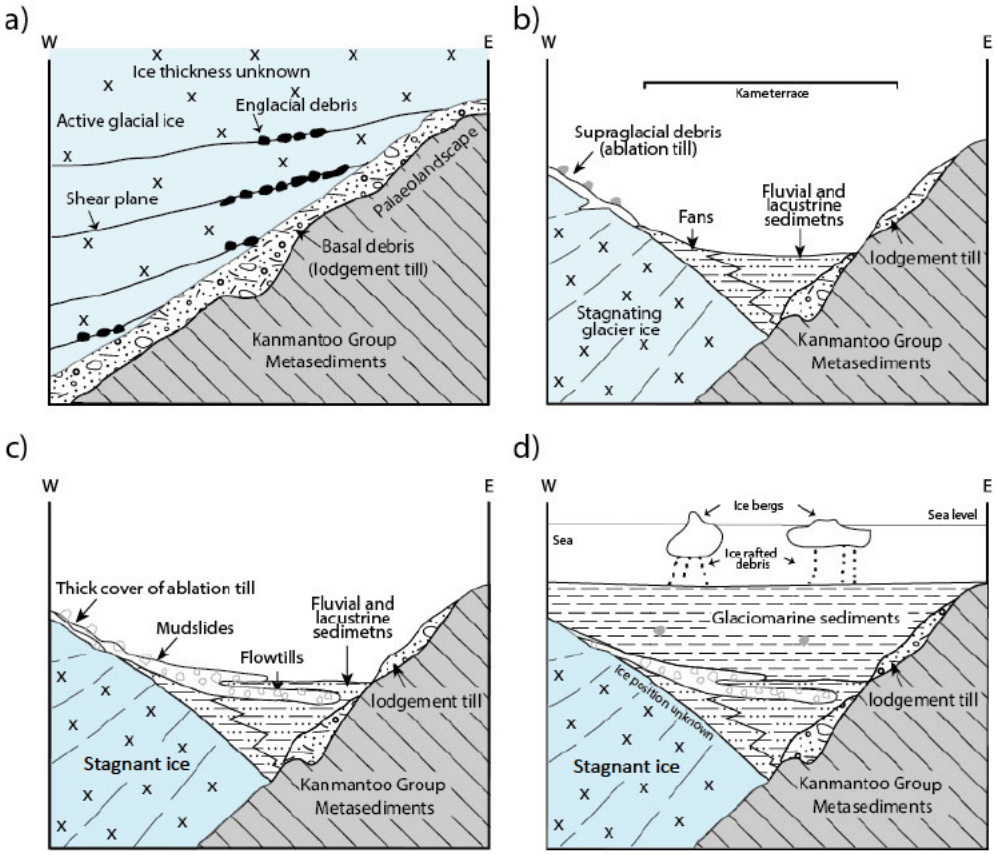

Figure 1:5 Depositional model of Cape Jervis Formation by Bourman and Alley (1984) showing the relationship between the icesheet and the deposition of the glacigene sedimentary rocks; a) Lodgement till was laid down over remnants of proglacial sediments (not shown); b) Deglaciation led to ice stagnation, exposing the underlying basement and the preservation of the lodgement till in the low-lying areas of the palaeosurface; c) Further downwasting of the ice lead to the thick cover of supraglacial debris, unstable debris flows formed flow till beds; d) Eustatic rise lead to a rapid marine transgression depositing glaciomarine sediments with isolated pebbles and boulders dropped from ice bergs.

The widely accepted model, based on sedimentary rocks of the Troubridge Basin, postulated by Howchin (1912), and expanded upon by Alley and Bourman (1984) and Alley et al. (1995) proposes that a wet-based, continental-size icesheet advanced from Antarctica in a generally northward direction into central Australia. As the icesheet advanced, glacigene and fluvioglacial sediment and

later glaciolacustrine and glacigene sedimentary rocks were deposited in the Troubridge Basin suggesting the stagnation, rapid melting, and southerly retreat of the icesheet (Figure 1:5). This retreat initiated a eustatic rise which resulted in the deposition of glaciomarine sedimentary rocks during the northern marine transgression. No sedimentary rocks preserving the retreat and subsequent marine transgression have been reported in the Troubridge Basin. Instead McGowran (1973) suggested that as the ice mass in the Arckaringa Basin began to retreat towards the south, a rise in sea level triggered a marine incursion from the south, which eventually covered most of southern Australia. After the marine transgression, a period of freshwater fluvial and lacustrine deposition is interpreted to have occurred in the north of the Arckaringa Basin (Townsend 1973) and Rogers et al. 1996b). This model is supported by observations made by Alley et al. (1995) who reported deposition of non-marine sedimentary rocks in the northern Arckaringa, Denman, Pedirka and Cooper basins (Figure 1:3b).

Crowell and Frakes (1971a, 1971b) and Veevers (2006) proposed an alternative model (Figure 1:4) whereby a northward moving continental icesheet accompanied by piedmont (valley) glaciers occupied the highlands where the modern Gawler Craton is now recognised. Along with material derived from the continental icesheet, the highlands supplied water and additional sediment (through erosion) into the basins. Crowell (1978) and Veevers (2006) suggest that the icesheet then retreated rapidly in the early Permian as the climate warmed and Australia migrated northwards away from the South Pole while the alpine glaciation was stagnant before retreating as Australia moved away from the South Pole.

1.2 Contributions of this study

The local depositional setting of glacigene sedimentary rocks within South Australia, particularly in the Troubridge Basin, have been inferred from detailed lithological descriptions of key sections (Alley and Bourman 1984, Bourman and Alley 1990, 1995, 1999, Alley et al. 2013). Accompanying these descriptions are palynological studies (such as Ludbrook 1967, Ludbrook 1969a, 1969b, Foster 1974, Townsend and Ludbrook 1975) that constrain the age of the rocks. These studies do not include petrology and mineralogy of the glacigene sedimentary rocks, nor have there been any investigations into the whole rock geochemistry or radiogenic isotope geochronology signatures of the sedimentary rocks that can be used to constrain provenance, depositional and post-depositional processes. These elements are required to construct a comprehensive understanding of the late Palaeozoic glacial and post-glacial conditions in South Australia.

The aim of this study is to characterise the late Palaeozoic sedimentary rocks of South Australia with the intention to produce a holistic palaeogeographic reconstruction that details depositional setting and palaeoclimate. To achieve this a detailed investigation into the glacigene sedimentary rocks of the Troubridge and Arckaringa basins of South Australia (Figure 1:3b) was carried out. The investigations included;

- Sedimentology of late Palaeozoic glacigene sedimentary rocks from which the glacigene depositional processes will be constructed;
- Radiogenic isotopic geochronology which will provide a constraint of the provenance of the glacigene sedimentary rocks; and
- Whole rock geochemistry to establish provenance, depositional and post-depositional processes the sedimentary rocks have undergone as well as establishing the background

geochemistry of the sedimentary rocks and assessing their potential use in mineral exploration.

Data for these investigations were collected from key measured sections in conjunction with systematic surface samples of the glacigene sedimentary rocks in the Troubridge and Arckaringa basins (Figure 1:3).

This thesis is structured as five chapters written so they can be submitted as independent publications. These chapters are bookended by this introduction and a short conclusions chapter. The sedimentology of the Troubridge and Arckaringa basins is addressed individually in Chapters 2 and 3 respectively. The provenance of the glacial sedimentary rocks from both basins is addressed using geochronology (Chapter 4). The influence of depositional processes and weathering on the geochemistry of the sedimentary rocks is addressed in Chapter 5. Chapter 6 presents a series of reconstructions of the palaeogeography of South Australia during the glacial and post-glacial interval of the late Palaeozoic.

Chapter 2: Sedimentology of the late Palaeozoic Cape Jervis Formation

Foreword

This chapter presents the results of the sedimentology of the sedimentary rocks carried out on five measured sections of the Cape Jervis Formation in the Troubridge Basin. Measured sections were systematically logged and sampled by the author and Dr Steve Hill during field trips between July 2010 and February 2012. Analytical methods include observations of the physical characteristics of the sedimentary rocks including detailed petrology and mineralogy. Petrological analysis was conducted by the author at Adelaide Microscopy at the University of Adelaide using thin sections prepared by Pontifex and Associated Pty. Ltd. in Adelaide. Mineralogical (spectroscopic) analysis and data processing was conducted by Georgina Gordon using the Hylogger^{TM} 3-3 at the Department of State Development, Geological Survey of South Australia Core Store Facility in Glenside, Adelaide.

This chapter builds on research initially conducted by Ludbrook (1967) and expanded upon by Alley and Bourman (1984) and Bourman and Alley (1990, 1995, 1999) which focused on the millimetre- to centimetre-scale sedimentology as well as the depositional setting of the sedimentary rocks of the Cape Jervis Formation. These are duly referenced throughout this chapter. The depositional settings of the glacigene sedimentary rocks of the Troubridge Basin; based on the sedimentology are presented herein. This chapter has been written as an independent publication and is structured accordingly.

Abstract

The late Palaeozoic Cape Jervis Formation of the Troubridge Basin in southern South Australia provides a sedimentological record of the glacial environment during the Permo-Carboniferous glaciation. The sedimentary sequence is divided into five informal units that make up the Cape Jervis Formation, and preserve sedimentological features that have been used to constrain the glacial setting and associated depositional mechanisms during this time. Landscape features such as glaciated pavements and the presence of lodgement till diamictite suggest that the glacial setting was a wet-based, continental icesheet with ice tongue glaciers at the front margin of the icesheet. The icesheet advanced in a north to northeast direction forming glaciated bedrock surfaces and depositing lodgement till. The fluviolacustrine beds suggest that the icesheet was stagnant, which facilitated the formation of glacial lakes and meltwater streams. The icesheet then began to decay and retreat southward. Ablation of the ice resulted in deposition of a flow till complex, and caused a eustatic rise that resulted in a marine transgression and subsequent deposition of glaciomarine sedimentary rocks.

2.1 Introduction

Palaeogeographic reconstructions of Australia during the late Carboniferous to earliest Permian, supported by palaeomagnetic data (Creer 1968, Embleton and Valencio 1977, Embleton and Schmidt 1977, Isbell et al. 2012) and numerous lines of geological evidence (e.g. Crowell and Frakes 1971b, Martin 1981, Archbold 1982, Caputo and Crowell 1982, Ireland et al. 1998, Scheffler et al. 2003, Foden et al. 2006, Veevers 2006); consistently place Australia and Antarctica in an amalgamated high-latitude southerly configuration; as part of the supercontinent Gondwana. There is consensus amongst researchers that a large continental ice mass grew over Antarctica and spread across southern Australia as Gondwana drifted across the South Pole (Crowell and Frakes 1971a, Alley et al. 1995). The Australian portion of the ice mass is suggested to have developed by the end of the Carboniferous and reached its greatest extent by the earliest Permian, after which it rapidly decayed (Alley et al. 1995).

The most definitive evidence for the late Palaeozoic glaciation in South Australia is preserved within the sedimentary rocks of the Cape Jervis Formation. The Cape Jervis Formation is exposed across most of the Fleurieu Peninsula, the southeastern coastal cliffs of the Yorke Peninsula and eastern Kangaroo Island in a geographic area referred to by Wopfner (1972) as the Troubridge Basin (Figure 2:1a). Glaciated pavements are extensive throughout the Fleurieu Peninsula (Figure 2:1b), and glacially-derived sedimentary rocks have been observed across most of the basin. It is likely that the Troubridge Basin and the other now disconnected basins are remnants of a much larger glacial system.

Small-scale depositional models localised around key sections of the Cape Jervis Formation have been derived from sedimentological studies (e.g. Alley and Bourman 1984, Bourman and Alley 1990, 1995, 1999). Basin- to continental-scale models that interpret the evolution of glaciation have also been developed (e.g. Crowell and Frakes 1971b, Embleton and Valencio 1977, Veevers 2006). Further definition of the depositional setting of the sedimentary rocks of the Cape Jervis Formation requires correlation of the sedimentology across the basin, identification of differences between units at the key sections, as well as differences within the same unit across the basin. The widespread and extensive exposure of the Cape Jervis Formation provides an opportunity for such an investigation.

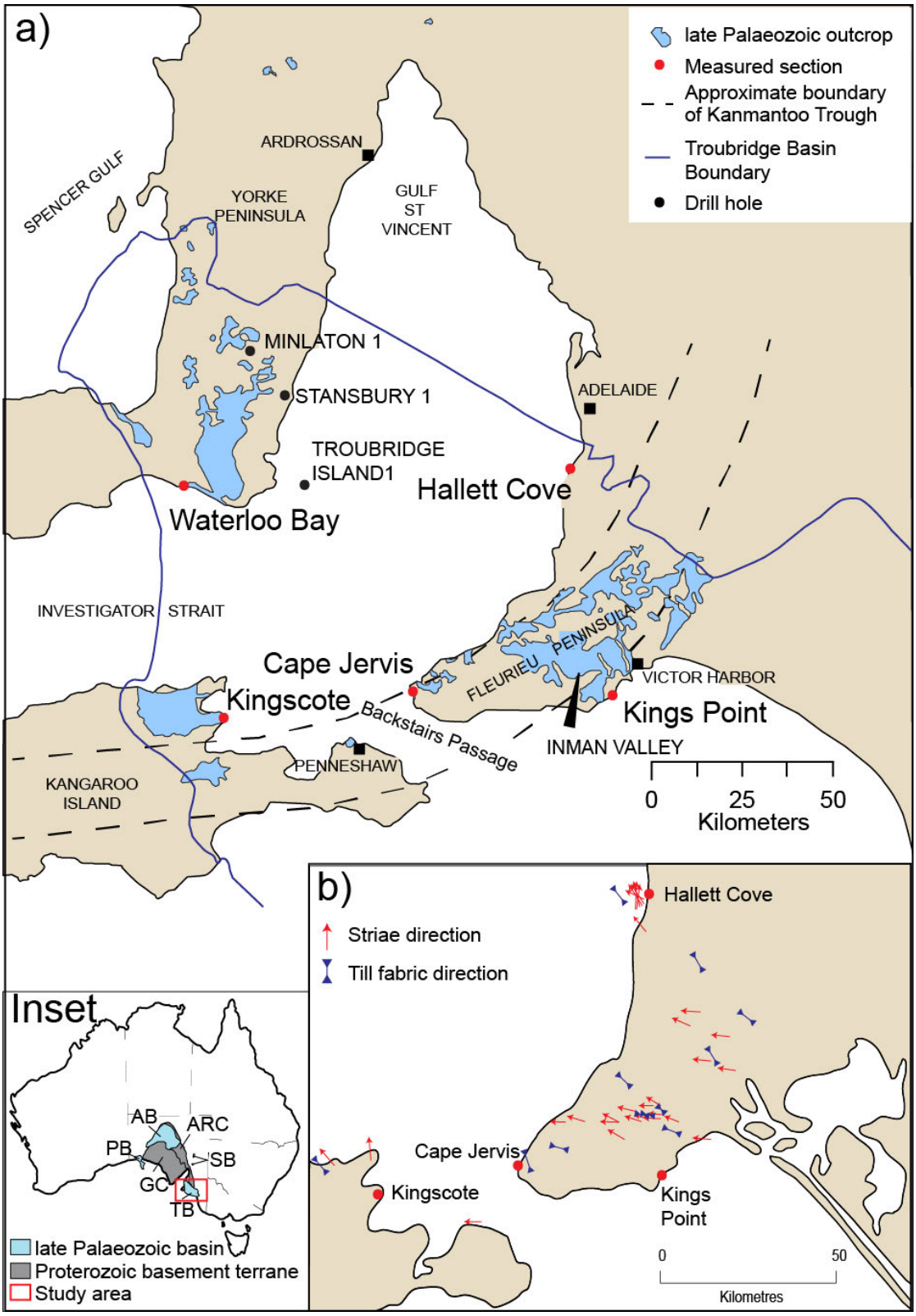

Figure 2:1 a) Approximate limits of the Troubridge Basin adapted from Alley and Bourman (1995), showing exposures of the late Palaeozoic Cape Jervis Formation adapted from Thompson and Horwitz (1962), Crawford (1960) and Fairclough (2007). Key locations and drill holes are also shown; b) Ice movement direction in the Troubridge Basin based in till fabrics and striae orientations adapted from Bourman and Alley (1990); Inset: location of study area (red box) in relation to Australia and significant basement terranes (grey) and late Palaeozoic basins (blue). AB: Arckaringa Basin; ARC: Adelaide Rift Complex; GC: Gawler Craton; PB: Polda Basin; SB: Springfield Basin; TB: Troubridge Basin.

The composition and mineralogy of the sedimentary rocks would provide a greater insight to the glacial environment as well as the degree of transport and post-depositional alteration the sedimentary rocks have undergone. This would provide information relevant to which sedimentary rocks could be targeted for geochemical analysis to provide the most accurate representation of the sedimentary rocks prior to surficial alteration such as oxidation.

This chapter builds on previous studies of the glacigene sedimentary rocks within the Troubridge Basin and adds to them by re-examining the sedimentology (including at microscopic scale) with emphasis on the mineralogy and composition of the Cape Jervis Formation at key sections across the Troubridge Basin. The recognition of subtle sedimentary features and changes to the clast morphology allows a more detailed and specific depositional setting to be constructed. This chapter also discusses lateral variations in the sedimentological record and depositional environment of individual units. Sedimentological differences across the basin that may have resulted from subtle changes in the glacial environment as it progressed across the basin are discussed.

2.1.1 Geological setting

The Troubridge Basin was first defined by Wopfner (1972). The sediments were assigned to the Cape Jervis Formation by Alley and Bourman (1984 after Ludbrook 1967) who nominated the coastal cliffs of Cape Jervis as the type section. The Cape Jervis Formation varies in thickness from <5 to 50 m where it is exposed on shore but is locally in excess of 1000 m where it has been intersected in offshore drill holes (Flöttmann and Cockshell 1996). The Cape Jervis Formation is the only unit within the Troubridge Basin and unconformably overlies a variety of Cambrian to Neoproterozoic rocks and is partially overlain Jurassic to Quaternary-aged sedimentary rocks (Crawford 1965, Johnson 1982a, 1982b, Alley and Bourman 1984, Bourman and Alley 1990, 1999, Zang and Hore 2001, 2003).

The Cape Jervis Formation has an upper age constraint of Sakmarian (295 – 290 Ma; Table 2:1) age based on foraminifera observed at Cape Jervis and Waterloo Bay and in drill holes Minlaton 1, Stansbury 1 and Troubridge Shoal 1 (Figure 2:1; Ludbrook 1967, 1969b, Harris and McGowran 1971, Foster 1974). Age constraints of individual units are summarised in Table 2:1. As yet no dates have been ascertained for unit one of the Cape Jervis Formation and hence the age of initial deposition remains unconstrained. However, it has been postulated that the glaciation initiated in the late Carboniferous and reached its maximum extent by the early Permian (Sakmarian; Alley and Bourman 1984, Alley et al. 2013).

In addition to Alley and Bourman's (1984) formation defining study, there have been a series of studies focussed on key stratigraphic sections of the Cape Jervis Formation. Studies at Kangaroo Island (Bourman and Alley 1999, Alley et al. 2013), Kings Point (Bourman and Alley 1995) and Hallett Cove (Bourman and Alley 1990) included the identification and stratigraphic logging of the Cape Jervis Formation glacigene sedimentary rocks and refinement of their interpreted depositional setting. Other investigations have concentrated on exposures of the Cape Jervis Formation away from coastal cliffs on the Fleurieu Peninsula (including Mawson 1962, Milnes and Bourman 1972, Bourman et al. 1976, Bourman and Milnes 1976, Milnes et al. 1981) and identified glacial landscape features such as roche moutonnée, erratic fields and glaciated pavements. Crawford (1965) identified and described the sedimentary rocks of the Cape Jervis Formation across the Yorke Peninsula while Foster (1974) investigated the palynology of the sedimentary rocks in the coastal cliffs of Waterloo Bay, southern Yorke Peninsula.

Alley and Bourman (1984) divided the Cape Jervis Formation into five informal units with each reflecting a different depositional setting: 1) basal fluvioglacial and glaciolacustrine sedimentary rocks; 2) lodgement till; 3) fluviolacustrine beds; 4) flow till complex; and; 5) glaciomarine sediments (Alley and Bourman 1984). The characteristics of each unit are summarised in Table 2:1.

Table 2:1 Summary table of characteristics for each of the units within the Cape Jervis Formation and description of lithologies used to correlate sections within the Troubridge Basin. Unit characteristics are based on observations by the author, Alley and Bourman (1984) and Bourman and Alley (1990, 1995). Age of the units is constrained by palynological studies by [1,2]Ludbrook (1967, 1969b), [3]Harris and McGowran (1971), [4]Foster (1974), [5]Bourman and Alley (1990) and [6]Alley and Bourman (1995). Palaeoenvironmental interpretation is based on observations made by [a]Eyles et al. (1998), [b]Miall (2000) and [c]Bennett and Glasser (2009).

Unit, unique lithology, age	Characteristic of unique lithologies	Overall unit characteristic	Palaeoenvironmental interpretation
Glaciomarine sediments (unit 5) – clay, Late Asselian-Sakmarian (295 – 290 Ma)[1,2, 3, 4]	- Green - Massive - Prismatic fracturing	Dominated by clay, with occasional sandstone beds	Ice influenced cold water, relatively deep water slope [a, c]
Flow till complex (unit 4) - diamictite	- Unconsolidated or clast-supported - Typically coarsen upwards	Diamictite beds interbedded with sandstone, silt clay and pebble beds	Subglacial or subaqueous deposition with intermittent fluviolacustrine and debris flow depositional processes [a, b, c]

Fluvioglacial beds (unit 3) – clay	- Grey-green clay
	- Fine to coarse sandstone beds
	- Finely laminated, thin beds
	- Variable matrix-supported diamictite - clay to coarse-grained sand
	- Clasts
	  o up to 40 cm
	  o large proportion subrounded to rounded
	  o lithology variable
		Clay beds interbedded with sandstone and diamictite beds with rounded and striated dropstones	Subaqueous or subglacial deposition with sediment heavy flows, channel fill, ice rafted debris flows and minor channel flows [a,b]

Lodgement till (unit 2) – diamictite, Asselian (298 – 295 Ma) age[5,6]	- Matrix-supported
	- Sandstone matrix
	- Clasts
	  o up to 10 cm
	  o angular to rounded
	  o dominantly locally sourced
	  o faceted and striated
	- Massive, structureless and well consolidated
		Only diamictite seen in the unit	Subglacial deposition with debris flow [a,b,c]

Basal fluviolacustrine and glaciolacustrine sedimentary rocks (unit 1)	Not observed	Fine-grained, cross-bedded sandstone with thin lenses of diamictite and occasional dropstones,	Fluvioglacial deposition with scour fill and subglacial fluvial flows [a,b]

The basal fluviolacustrine and glaciolacustrine sedimentary rocks of unit one (Table 2:1) are interpreted to have been deposited during the initial stages of glaciation in a basin where glacial lakes formed at the front of an icesheet (Alley and Bourman 1984). Alley and Bourman (1984) note that the sedimentary rocks of unit one were observed in an excavation at the base of the Cape Jervis type section, however, this excavation is now covered in scree. Unit two has been interpreted by Alley and Bourman (1984) as a lodgement till. Numerous frost-shattered, polished, striated and glaciated pavements on the Fleurieu Peninsula and Kangaroo Island (Figure 2:1b) are immediately overlain by sedimentary rocks assigned to unit two (Table 2:1). Alley and Bourman (1984) inferred that unit two was deposited at the base of a wet-based glacier. Local differences in ice movement direction recorded by striations (Figure 2:1b) reflect deviation of the icesheet around topographic features (Bourman 1986).

Bourman and Alley (1990, 1995) suggest that the alternating clay, sand and diamictite beds of the fluviolacustrine beds (unit three; Table 2:1) are the result of variable ice decay rates. They also postulated that the icesheet was stagnant in the Gulf St Vincent, and that materials were deposited around the icesheet via the meltwater streams. Small lakes formed, some of which contained icebergs that released dropstones as they melted. Unit four is interpreted as flow till complex by Alley and Bourman (1984) which is in sharp contact with the underlying fluvioglacial sedimentary rocks. Unit four is interpreted to have been deposited as the icesheet retreated, resulting in meltwater streams with increased energy and sediment load. The uppermost unit of the Cape Jervis section (unit five) marks an abrupt change to glaciomarine sediments (Alley and Bourman 1984). These sedimentary rocks were deposited in shallow marine conditions that are influenced by the fluvial input of glaciers and icebergs melting nearby (Alley and Bourman 1984).

The initial migration of the icesheet caused gelifract (fracturing of the bedrock via freezing of the substrate prior to ice presence; Alley and Bourman 1984), scouring of U-shaped valleys and glacial pavements and deposition of diamictite (Bourman and Alley 1988). The evolution from unit one to unit five has been interpreted by successive workers (e.g. Bourman 1973, Alley and Bourman 1984, Bourman 1986, Bourman and Alley 1990, 1995, 1999) to represent a cycle of broadly northward glacial advance beginning in the late Carboniferous (unit one and two), followed by stagnation in the Gulf St Vincent resulting in the deposition of sandstone and clay units, suggesting meltwater streams and glacial lakes formed during this stage (unit three; Bourman and Alley 1990). Southward decay of the icesheet and further retreat deposited diamictite units with sandstone beds (unit four) was then followed by the final stage of deglaciation. The final wasting of the glacier lead to an eustatic rise and deposition of glaciomarine clay and sand units (unit five; Alley and Bourman 1984).

2.2 Methods

2.2.1 Sample collection

Suitable sites for logging and sampling were selected based on the exposure being extensive enough to allow sampling through the stratigraphic profile. Profiles sampled for this study were from Cape Jervis, Kings Point, Hallett Cove, Kingscote, and Waterloo Bay (Figure 2:1). These sections are in the same or similar locations to the sections investigations by previous researchers as these sites are the most complete, best exposed and accessible sections across the basin. The previous studies provided a guide to the basic lithology of the sedimentary rocks.

Samples were collected at each change in lithology or every metre if no change occurred. Five to ten centimetres of overlying material was removed prior to sample collection to reduce risk of surface contamination. Approximately 0.5 kg of sample was then removed using a geo pick and put into a clean, plastic snap lock bag. Each bag was labelled with a predetermined sample number and location name. For each sample, a GPS location was recorded along with a description of the sediment lithology and any overprinting and weathering that was apparent. Surrounding field relationships were also recorded as well as information such as vegetation growth or proximity to possible contaminants such as roads or the possibility of sea spray. Samples were collected for investigations into the petrography and mineralogy of the sedimentary rocks as well as detailed sedimentological descriptions. Splits of selected samples were used for geochronological and geochemical analysis. The samples were of varied lithologies including sand, clay, silt and diamictite with varying degrees of weathering.

2.2.2 Mineralogical analysis

The mineralogy of samples was investigated using petrographic and spectroscopic analysis. Petrographic analysis of thin sections determined relationships between grains and matrix as well as alteration. Petrologic analysis was performed on representative samples from each unit within the Cape Jervis section. These samples were selected based on being representative of each of the preserved units, having minimal post-depositional alteration and their consolidated nature.

Petrological thin sections (dimensions: 7.5 by 2.5 cm) of consolidated sediment were prepared by Pontifex and Associates Pty. Ltd., Adelaide. Slides are polished and are without a cover-slip. Petrographical analysis was done at Adelaide Microscopy, University of Adelaide using a Nikon Petrographic Microscope.

Spectroscopic analysis was used to determine the bulk mineralogy of samples and was performed on all samples collected. A representative split of each sample was placed into black chip trays and analysed in black chip trays using the HyLogger™3-3 at the Department of State Development Core Storage Facility in Glenside, Adelaide. HyLogger™ Core Scanning and HyChips™ modes were used to detect the visible to shortwave infrared (Vis-SWIR: 380-2500nm), and the thermal infrared (TIR: 6000-14500nm, core logging mode only) wavelengths. The minerals identified using infrared wavelengths include white micas, kaolinite, carbonate minerals in the SWIR, and tectosilicates such as pyroxene, silica, feldspars and garnets in the TIR. High resolution images were taken on every sample every 2mm. HyLogger™ core logging mode analysis was done by scanning across each sample four times, allowing for overlap to maximise the viable spectra. HyChip™ mode analysis was done by scanning three times using only Vis-SWIR wavelengths. Three readings were taken per sample.

Results were processed using The Spectral Geologist (TSG) HotCore software to allow viewing in the free TSG Viewer software provided by AusSpec International Inc. Data processing included removal of data from any non-sample material (e.g. black plastic of the chip trays). Processing did not account for geological context of the samples or removal of any specific mineral species prior to processing. Routine machine calibrations were performed prior and post-analyses.

2.3 Sedimentology and mineralogy

In this section, the field observations, spectroscopic mineralogy and petrography of the sedimentary rocks within the Cape Jervis Section have been described in detail as the section is the type section for the Cape Jervis Formation. Other measured sections investigated are discussed in relation to how the

sedimentary rock differ from the type section. Stratigraphic logs and field images are provided for each section. Detailed descriptions of measured sections away from Cape Jervis are in Appendix 1.

2.3.1 Cape Jervis section

The most complete section of the Cape Jervis Formation is within two coastal cliffs of Cape Jervis, north of the lighthouse (Figure 2:2a). The type section occurs within two, steep erosional gullies. The southern gully (here informally termed section A; Figure 2:2a) was originally described by Ludbrook (1967). Alley and Bourman (1984) used Section A and a second gully to the north (here informally termed Section B; Figure 2:2a) to define the Cape Jervis Formation and develop a composite type section. The composite section begins approximately ten metres above the shore platform and extends for approximately 50 m to where the Cape Jervis Formation is overlain by limestone and calcareous sandstone of the Quaternary Point Ellen Formation with calcrete at the top of the cliff. The Cape Jervis Formation overlies the very steeply dipping, Cambrian Kanmantoo Group metasedimentary rocks, and the section is in part deposited against the steeply sloping bedrock valley surfaces of the cliffs and U-shaped valleys (Alley and Bourman 1984). All five units of the Cape Jervis Formation as defined by Alley and Bourman (1984) are preserved within the section, however, unit one is now not exposed and covered by scree.

The base of the section (0 to 1.5 m) comprises frost-shattered (or gelifract) Cambrian Kanmantoo Group metasedimentary rocks (here called bedrock), or gelifract bedrock and approximately 1m of bedrock rubble (Figure 2:3a). The Cambrian metasedimentary rocks are bedded at decimetre to metre-scale and vary from metagreywacke to metasiltstone (Figure 2:3a). They are dark-grey and contain abundant quartz, minor feldspar and lithics and a variable pelitic component characteristic of relatively immature turbiditic sedimentary rocks. Muscovite, goethite, hematite and nontronite have been identified by hyperspectral analysis (Figure 2:2b). Amongst the scree deposits, on the shore platform, and near the gelifract at the base of the section are large, rounded, polished and occasionally striated Encounter Bay Granite erratics, some of which are up to five metres in diameter (Figure 2:3b).

Unit two (1.5 to 7 m) has an unusual depositional geometry, being deposited against the sloping bedrock surface of the valley where it is overlain by other units of the sequence. The unit is dominated by matrix-supported diamictite with angular to rounded, polished and faceted clasts, mostly less than one centimetre diameter but occasionally up to ten centimetres, comprising approximately 30% of the rock. Pebbles and cobbles, up to 20 cm diameter, become more common toward the top of the unit. The clasts are dominantly metasedimentary rocks comparable to the underlying Kanmantoo Group with lesser granitic rocks that are texturally and mineralogically comparable to the Encounter Bay Granite which is exposed in the Victor Harbour region about 55 km to the south southeast. The matrix of the diamictite is buff-coloured, poorly-sorted, medium- to coarse-grained and relatively unconsolidated sand. The sand is dominated by quartz grains that range from 300 to 1200 µm and average about 500 µm (Figure 2:3c). Subrounded to rounded grains of feldspar (largely altered to kaolinite; Figure 2:3c) and muscovite are also present. These grains are surrounded and supported by a cement of clay, Fe-oxide minerals (identified as kaolinite and goethite in the hyperspectral data) and lesser siderite (Figure 2:2b, 2:3c).

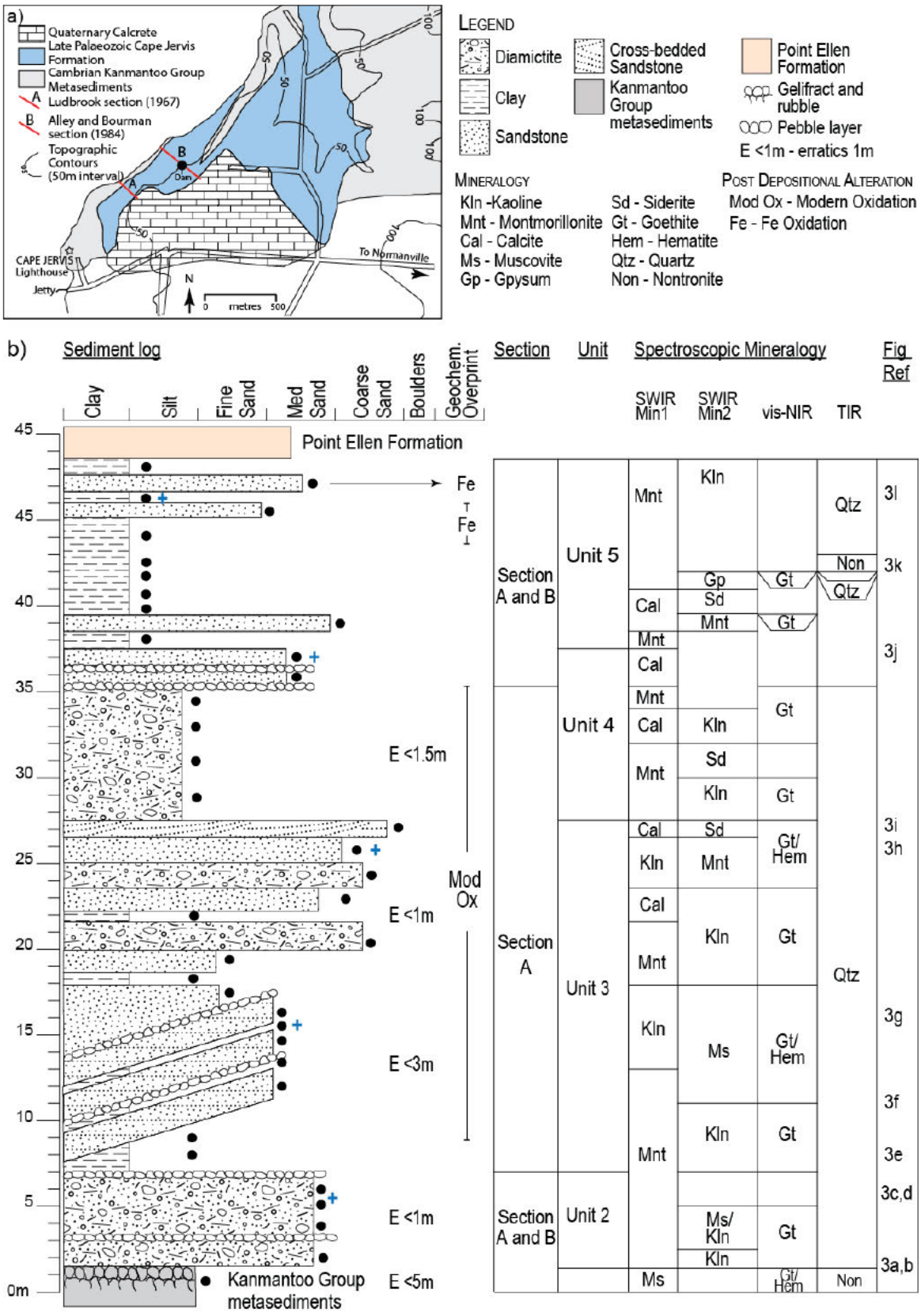

Figure 2:2 a) Simplified regional geology of the Cape Jervis area adapted from Alley and Bourman (1984) showing section locations; b) Stratigraphic log of the sedimentary rocks including an indication of which section units are within, the unit and the spectroscopic mineralogy. The location of Cape Jervis is shown in Figure 2:1. Blue cross: thin section location; black dot: sample location of HyLogger™ analysis. Units as described by Alley and Bourman (1984).

Two lenses of poorly sorted, clast-supported pebble and cobble lenses up to 20 cm thick are preserved within the diamictite at approximately 4 and 7 m. These lenses comprise rounded, faceted clasts, mostly less than ten centimetres in diameter with some (<10%) up to 50 cm (Figure 2:3d, e). The clast lithologies are consistent with those in the diamictite being dominated by metasedimentary rocks and granite. Large (up to one metre) clasts of granite occur throughout unit two. Rounded, polished and occasionally striated granite erratics, some of which are up to five metres in diameter (presumably sourced from unit two) are scattered along the foreshore (Figure 2:3b).

Unit three comprises 20 m of heterolithically bedded clay and sand beds with occasional beds of diamictite, pebble and cobble lenses and isolated boulders (Figure 2:2f). The lower 7.5 m of unit three (7 to 14.5 m) is dominated by very thinly bedded (centimetre-scale), fine-to medium-grained, yellow to orange sand and minor clay. At the type section, bedding is tilted toward the east at 15-20° (Figure 2:3f), in comparison to the flat-laying underlying unit two and overlying upper unit three. The sedimentary rocks are poorly-sorted, with grain sizes ranging from 20 to 500 µm, and dominated by subangular to subrounded grains of quartz and feldspar (Figure 2:3g). Occasional subrounded rock fragments greater than 500 µm are also present (Figure 2:3g). The grains are surrounded by a cement of secondary minerals of mixed clay and Fe-oxide minerals (identified as kaolinite, montmorillonite, goethite and hematite in the hyperspectral data; Figure 2:2b). Two pebble and cobble lenses are preserved within the tilted beds at 10 and 14.5 m (Figure 2:2b). These lenses are approximately 20 cm wide and are dominated by rounded, polished, striated and faceted metasedimentary rocks and minor granites that are 5 to 10 cm in diameter (Figure 2.3f).

The upper 12.5 m of unit three (14.5 to 27.5 m) comprises flat-lying beds of sandstone, diamictite and minor clay interbedded at metre-scale (Figure 2:2b). The sand and sandstone dominated horizons are typically yellow to brown, poorly-sorted with angular to subrounded grains of quartz, feldspar, lithic fragments and a mixed clay and Fe-oxide mineral cement. Individual horizons differ on the basis of their finest fraction, which increases up-sequence from fine- to coarse-grained sand. Clasts up to five centimetres in diameter comprise <20% of the rock and are dominated by metasedimentary material comparable to the underlying Kanmantoo Group. The uppermost sandstone bed (27 m) in unit three is distinctive in that it exhibits poorly-preserved, 1 to 10 cm cross-beds (Figure 2:2b, 2:3i). The sandstone beds from 26 to 27.5m in unit three (Figure 2:3i) do not contain clasts larger than one centimetre diameter. The diamictite beds within the upper parts of unit three (between 20 and 25 m) are up to 20 cm thick in 1.5 m bed sets (Figure 2:2b). Clasts within the matrix-supported diamictite are poorly-sorted, subrounded to rounded, up to four centimetres in diameter within a matrix of coarse-grained sand.

Scattered throughout unit three are isolated pebbles and boulders of metasedimentary rock and granite that are typically polished, faceted and striated. The sedimentary rocks immediately underneath some of the metasedimentary boulders are compressed, while the overlying beds are draped over the stone, consistent with the boulders being deposited as dropstones. In contrast, the granite boulders do not appear to contort the underlying sedimentary rocks; rather the sedimentary rocks are often deposited against the granite boulders suggesting they had been in place prior to the deposition of unit three.

Within the upper five metres of unit three (22.5 to 27.5 m), calcite commonly forms a crystalline cement that efficiently fills the intergranular spaces of one centimetre diameter (Figure 2:3h). This is a significant change compared to the Fe-oxide and clay minerals that occupy the pore spaces in unit two (Figure 2:3c) and the lower parts of unit three (Figure 2:3g).


a
b
c
Fe
PS
RF
Fe/Kln
Fe
Kln
Qtz
Sd
Qtz
Qtz
PS
Qtz
Fe
Fe/Kln
Kln
500 µm
d
e
GLAD
SNAP LOCK
f
Kanmantoo
Metasediment
erratic
Encounter Bay
Granite erratic
g
Fe/Kln
Kln
Kln
RF
Qtz
Fe
Qtz
RF
Fe/Kln
Qtz
Kln
Qtz
Fe
PS
Qtz
Fe
Kln
Qtz
500 µm
Fe
h
Kln
Kln
RF
Qtz
Qtz
RF
Cal
Fe
Qtz
Qtz
Fe
Qtz
Cal
Qtz
Cal
RF
Kln
Kln
Kln
Cal
500 µm

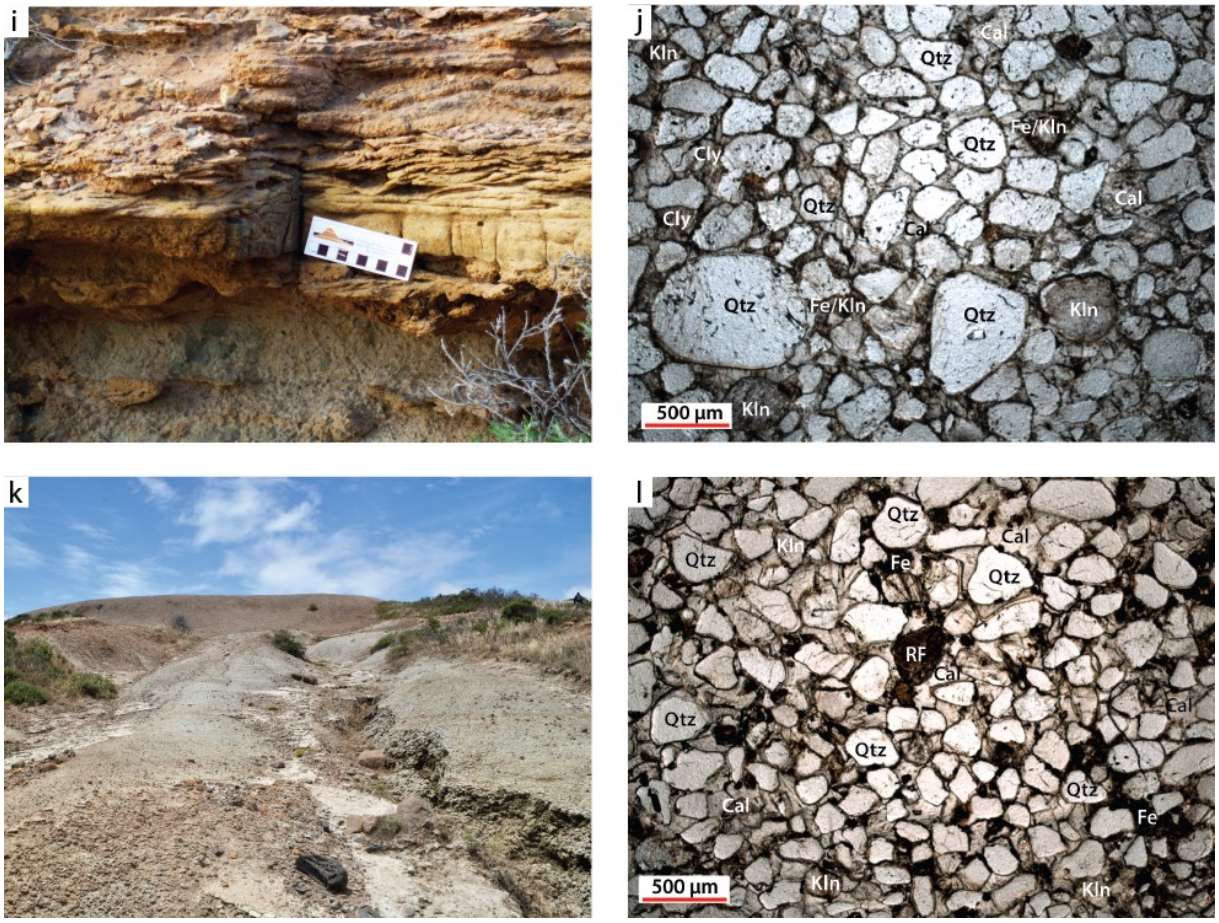

Figure 2:3 Cape Jervis Section a) Fractured (gelifract) Kanmantoo Group metasedimentary rocks at the base of the Cape Jervis Section (at 0 to 1.5 m), orange lichen commonly grows on the exposed surfaces; b) Large Encounter Bay Granite erratic at the base of the Cape Jervis Formation type section; c) Photomicrograph of the matrix-supported diamictite of unit two. The sample a was collected from a height of five metres; d) Striated and faceted Kanmantoo Group metasediment dropstone within the diamictite of unit two (at 6 m); e) Pebble and cobble layer within unit two at a height of seven metres, showing the rounded nature and size (up to 10 cm) of the clasts. Matrix-supported diamictite containing smaller (>5 cm) clasts can be seen below the pebble and cobble layer; f) Tilted beds from 7 to 14.5 m (as outlined by dotted lines) of the base of the fluviolacustrine beds (unit three). Erratics of Kanmantoo metasedimentary rocks (approximately one m) and Encounter Bay Granite (approximately three m) can be seen in the foreground; g) Photomicrograph of clay bed at 15.25 m within the tilted beds of unit three showing very fine-grained to clay sized subrounded to angular quartz grains within a ferruginous cement; h) Photomicrograph of flat-lying beds within the fluviolacustrine beds (unit three) at 25.25 m comprising of subrounded quartz grains and rock fragments; i) Laminated sandstone beds of unit three at 26.5 m the top of the unit three, flaggy beds above the scale bar have poorly preserved cross-beds; j) Photomicrograph of laminated sandstone at 37.2 m near the top of unit four showing angular to rounded quartz grains within a calcareous cement; k) Massive, green grey clay of unit five at 39.5 to 45 m. Photo taken looking up section B to the southeast; l) Photomicrograph of the first sandstone lens at 46.3 m within the of unit five, the quartz grains are <100 µm with clay cement. Qtz: quartz; Kln: kaolinite; Cal: calcite cement; Sd: siderite; Fe: Fe-oxide mineral cement; Fe/Kln: Fe-oxide mineral and kaolinite cement; cly: clay mineral; RF: rock fragment; PS: pore space; approximate location of photos are shown in Figure 2:2b.

The base of *unit four* (27.5 m) is a buff-coloured, clast-supported diamictite that is 8.5 m thick (Figure 2:2b). Smaller clasts (<5 cm) within the diamictite are rounded to angular metasedimentary rocks with comparable composition to the underlying Kanmantoo Group. Larger clasts (up to 20 cm) are subrounded to rounded, mostly polished, faceted and striated and are metasedimentary or granitic in composition. The loosely consolidated matrix of the diamictite is medium- to coarse-grained sand with approximately 40% silt.

Overlying the diamictite, at 35 to 37.5 m, is 2.5 metres of laminated, calcareous, fine-grained sandstone interbedded with lesser medium- to coarse-grained sand lenses and two narrow pebble and cobble lenses (Figure 2:2b). The sandstone is buff to yellow and dominantly comprises poorly sorted, angular to subrounded quartz grains up to 500 µm. Minor detrital feldspar, now altered to kaolinite, with the same size and shape as the quartz grains is also present (Figure2:3j). Sand lenses have the same characteristics as the sandstone but are friable and typically unconsolidated. The pebble and cobble lenses are unconsolidated, and comprise rounded pebbles up to ten centimetres in diameter within a matrix of fine-grained sand with a minor clay component. The clasts up to ten centimetres in diameter are either metasedimentary or granitic. Calcite is an abundant phase throughout unit four, forming an intergranular cement within pore spaces along with minor kaolinite, montmorillonite and Fe-oxide minerals (Figure 2:3j).

Unit five is approximately 11 m (37.5 to 48.5 m) of massive to bedded, green clay beds interlayered with occasional thin sandstone beds (Figure 2:2b). The massive clay (37.5 to 45 m) is up to 7.5 m thick (Figure 2:2b, 2.3k). Prismatic fracturing occurs within the clay immediately overlying the sandstone at the top of unit four. Bedding within the clay becomes more defined upwards. The clay comprises montmorillonite and kaolinite with minor siderite (Figure 2:2b). The clay is mostly green in colour (Figure 2:3k). Several red to orange beds are preserved in the middle of the clay unit and are silty and gritty. The clay is interbedded with medium-grained, buff to yellow sandstone beds, up to 20 cm thick, these occur at 39, 45 and 47 m. The sandstone beds comprise poorly sorted, angular to subrounded quartz and occasional kaolinite grains that range from <50 to 500 µm (Figure 2:3l). Calcite and minor goethite cement completely fills the pore spaces. (Figure 2:2b, 2:3l). Unit five has a sharp contact with the overlying calcareous, coarse-grained sands, limestone and calcrete of the Quaternary Point Ellen Formation.

2.3.2 Hallett Cove section

The northernmost known occurrence of the Cape Jervis Formation on the Fleurieu Peninsula is in the coastal cliffs of Hallett Cove (Figures 2:1, 2.4a). The area is host to a well-preserved exposure of Cape Jervis Formation and the underlying glaciated pavements. The section investigated begins at the edge of the shore platform and is exposed in a 30m interval in the incised gullies of Sugarloaf Creek (Figure 2:4a). Units two and three are observed at the Hallett Cove section.

The basement rocks within the Hallett Cove area dominantly comprise Neoproterozoic Wilpena Group as opposed to the type section that is underlain by the Kanmantoo Group. The Wilpena Group at Hallett Cove comprises green-grey and purple micaeous siltstone. These sedimentary rocks are well preserved as a glaciated pavement, which is best exposed at the top of Black Cliff, north of Sugarloaf Creek (Figure 2:5a). The glaciated pavement has been polished and striated and preserves chatter marks and grooves (Figure 2:5a). Bourman and Alley (1990) calculated a northwesterly ice movement direction using measurements of the striae and till fabric studies. There is no exposed glacial bedrock pavement at the base of the measured section, at Sugarloaf Creek, however, diamictites overlie polished pavement at Black Cliff (Figure 2:5b). There are no polished pavements at the type section.

Unit two at Hallett Cove is up to 6 m thick, although only 2 m is exposed. The matrix-supported diamictite (0 to 2 m) differs from the type section in that clasts comprise up to 70% of the whole rock and range from 1 to 45 cm in size. At the type section there is a lesser percentage of smaller clasts. The clast composition is dominated by the underlying stratigraphy as it is at the type section. The diamictite

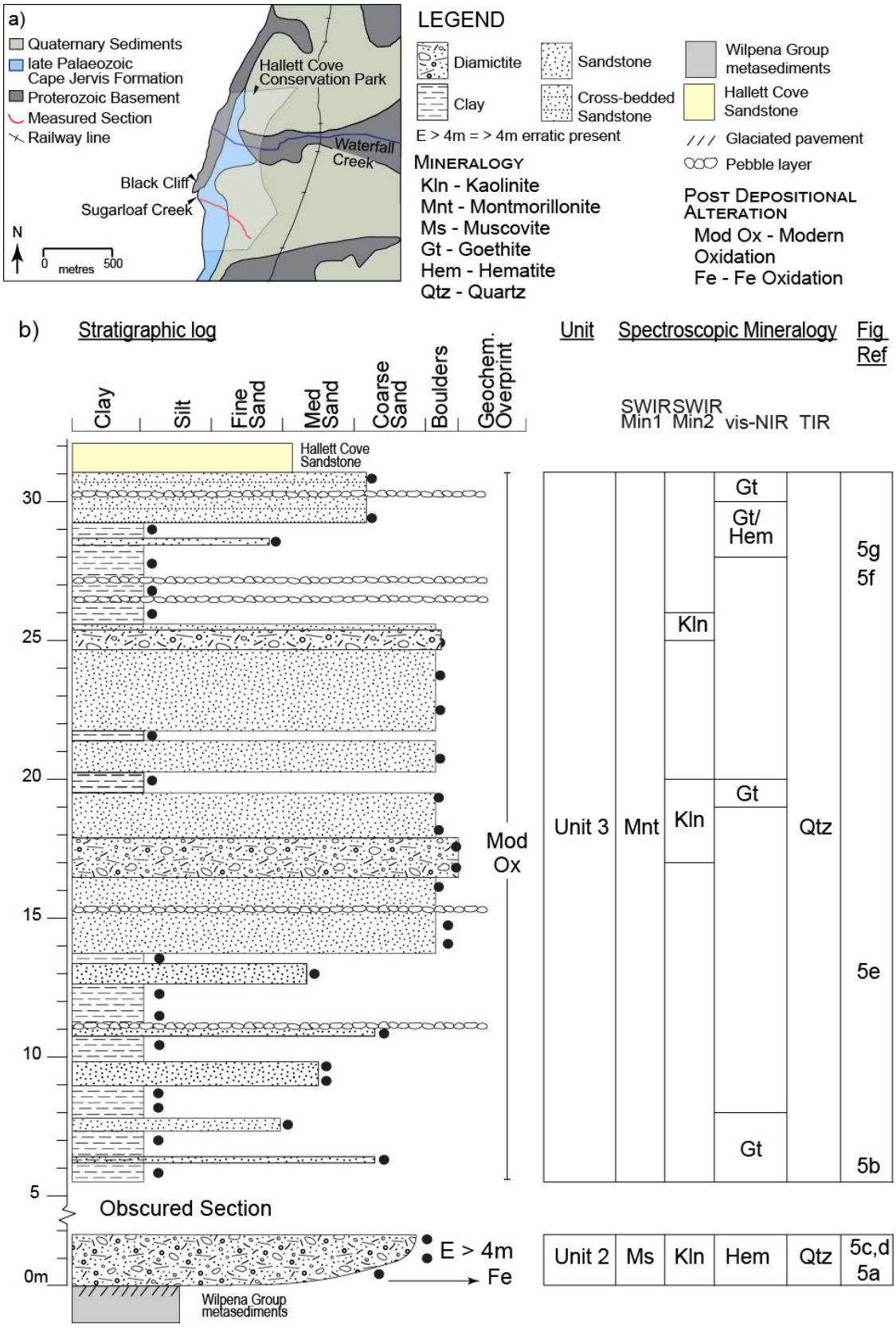

Figure 2:4 a) Simplified regional geology of the Hallett Cove area adapted from Bourman and Alley (1990) showing section locations; b) Stratigraphic log, spectroscopic mineralogy and unit for Sugarloaf Creek in Hallett Cove area. The location of Hallett Cove is shown in Figure 2:1. Black dots: sample location for HyLogger™ analysis. Units as described by Bourman and Alley (1990).

matrix coarsens upward from grey-green sandy clay to buff coloured coarse-grained sand (Figure 2:4b). The top of unit two and bottom of unit three in this area is obscured by approximately four metres of grasses and aeolian sands (Figure 2:4b).

Unit three (5.5 to 31 m) in the Hallett Cove area comprises ~26 m of clay, silt and medium- to coarse-grained sand beds with minor diamictite and cobble and pebble beds (Figures 2:4b, 2:5e to g). The lowermost eight metres of unit three (5.5 to 13.8 m) comprises silty clay (clay with 50 to 70% silt) beds interbedded with lesser medium to coarse-grained sand beds. The silty clay beds are pale grey with orange and red mottles and up to two metres thick. Silty clay beds were not observed at the type section (Figure 2:2b), instead 8.5 m of tilted, fine- to medium-grained sandstone beds dominate the base of the unit.

The sand, sandstone, clay beds with occasional diamictite beds from 13.8 to 31 m (Figure 2:4b) are similar to those at the top of unit three at the type section (Figure 2:2b). From 13.8 to 22 m, red and purple, medium- to coarse-grained sandstone beds interbedded with occasional diamictite and clay beds (Figure 2:5e) dominate. The sand and sandstone beds vary from consolidated to friable. The sandstone comprises coarse-grained, angular quartz sand with clay mineral cement. The diamictite beds are 0.5 to 2 m thick. The characteristics of these sand and sandstone beds are similar to those at the type section however the colour of the Hallett Cove sand is different.

In the pebble and cobble layer at 15.2 m, 50% of the layer is pebbles and cobbles, which are up to 35 cm size and comprise dominantly of Wilpena Group rocks. The matrix-dominated diamictite at 16.5 m, has clasts that comprise 40% of the whole rock, are angular, up to 5cm and consists mostly of Wilpena Group sedimentary rocks. The matrix of the diamictite is coarse- to very coarse-grained sand. A pebble lens is preserved within one of the lower sandstone beds (Figure 2:4b).

Similar to the top of unit three at Cape Jervis, a coarse-grained, buff to yellow sandstone and a thick (~50 cm) matrix-supported diamictite lens occurs from 22 to 25.7 m (Figure 2.4b). In both sections, the sandstone and diamictite are coarse- to very coarse-grained. In the Hallett Cove section, several <1m size dropstones occur within the sandstone. The majority of the dropstones are between the diamictite lenses and are rounded, polished and occasionally striated. Some of the dropstones have disturbed the sedimentary rocks directly below them (Figure 2:5f, g).

At the top of the exposed unit three (25.7 to 31 m), which includes much of the Sugar loaf, is up to three metres silty clay beds and up to two metres of partially consolidated, medium- to coarse-grained, yellow, bedded sandstone. Several metres of loosely consolidated Pliocene Hallett Cove Sandstone overlie the top of the exposed Cape Jervis Formation in this area.

Next page: Figure 2:5 Hallett Cove Section a) Striated glacial pavement of Wilpena Group basement at the top of Black Cliff, Hallett Cove; b) Looking southeast upstream of Sugarloaf Creek (from 5 m of the section) towards the Sugar loaf. Silty clay beds of unit three make up the banks of Sugarloaf Creek; c) Shore platform of Hallett Cove (at 0.5 m) exposed at low tide showing sandy clay diamictite and scattered clasts and erratics. Encounter Bay Granite erratic in foreground is approximately one metre diameter and the Wilpena Group erratic is approximately five metres in diameter; d) Wilpena Group metasediment clast within coarse-grained matrix diamictite at the outlet of Sugarloaf Creek, at 1.8 m. Polished, rounded and striated clasts greater than 50 cm are accumulated at the mouth of Sugarloaf Creek; e) Purple medium-grained sandstone beds (5.5 to 12.5 m) overlying buff, coarse-grained sandstone beds (12.5 to 16 m); f) Red, fine-grained laminated sandstone preserving a dropstone at 27.2 m. The beds have draped over the drop stone, (blue solid line). The dotted blue line shows the probable continuation of the laminations under the weathered surface; g) Bedded clay and fine sands at the top of unit three of the Hallett Cove section at 28.3 m. Dropstones have disturbed the bedding below and above them (blue lines). Approximate locations of photos are shown in Figure 2:4b.


a
Ice movement direction
b
Sugar Loaf
c
Wilpena Group erratics
Lodgement till diamictite
Encounter Bay Granite erratic
d
Nikon
e
f
g
Dropstone
Dropstone
Dropstone

2.3.3 Kings Point section

The coastal cliffs of Kings Point preserve 14 m of Cape Jervis Formation exposed in two erosional gullies (Figure 2:6a). Both sections unconformably overlie the Cambrian Petrel Cove Formation of the Kanmantoo Group (Bourman and Alley 1995). It is not clear whether the late Palaeozoic sedimentary rocks of the southwestern gully directly overlie the late Palaeozoic sedimentary rocks of the eastern gully or if some late Palaeozoic sedimentary rocks have been eroded creating a disconformity between the sections. Units three and four are observed at the Kings Point section.

The base of the section (0 to 5.2 m) is exposed in the eastern erosional gully and includes rocks of the lower part of *unit three* (Figure 2:6b). The sediments in unit three are not tilted, however, the sedimentological characteristics of the silty clay, clay and fine-grained sandstone beds are similar to the type section. The clay beds include rounded and polished 40 cm clasts derived from the local metasedimentary rocks (Figure 2:7a) and smaller (up to 20 cm) granitic clasts also occur throughout the clay beds.

Unit four of the Cape Jervis Formation is exposed in the southwestern gully (5.6 to 14.2 m; Figure 2:6a). Unit four of the Kings Point section differs from that of the type section as there is a greater occurrence of sandstone beds throughout the unit as well as the differing diamictite characteristics. The matrix- to clast-supported diamictite beds from 5.6 to 9.8 m (Figure 2:6b) have clasts which comprise of 25 to 75% of the whole rock, are mostly 20 cm, can be up 40 cm, and are rounded to angular in shape. The diamictite matrix coarsens upward from clay to coarse-grained sand, diamictite and becomes increasingly clast-supported up section (Figures 2:6b, 2:7b).

The upper four metres (9.8 to 25.2 m) consists of diamictite and coarse-grained sandstone beds. These sandstone beds are different to those at the top of unit three in the type section as they are poorly sorted with rock fragments. Diamictite beds are not observed in this part of the type section. The gully at Kings Point is littered with Encounter Bay Granite erratics that are up to 2.5 m, rounded and polished (Figure 2:7c), and were not observed at the type section. The Cape Jervis Formation is overlain by up to ten metres of Cenozoic undifferentiated sands.

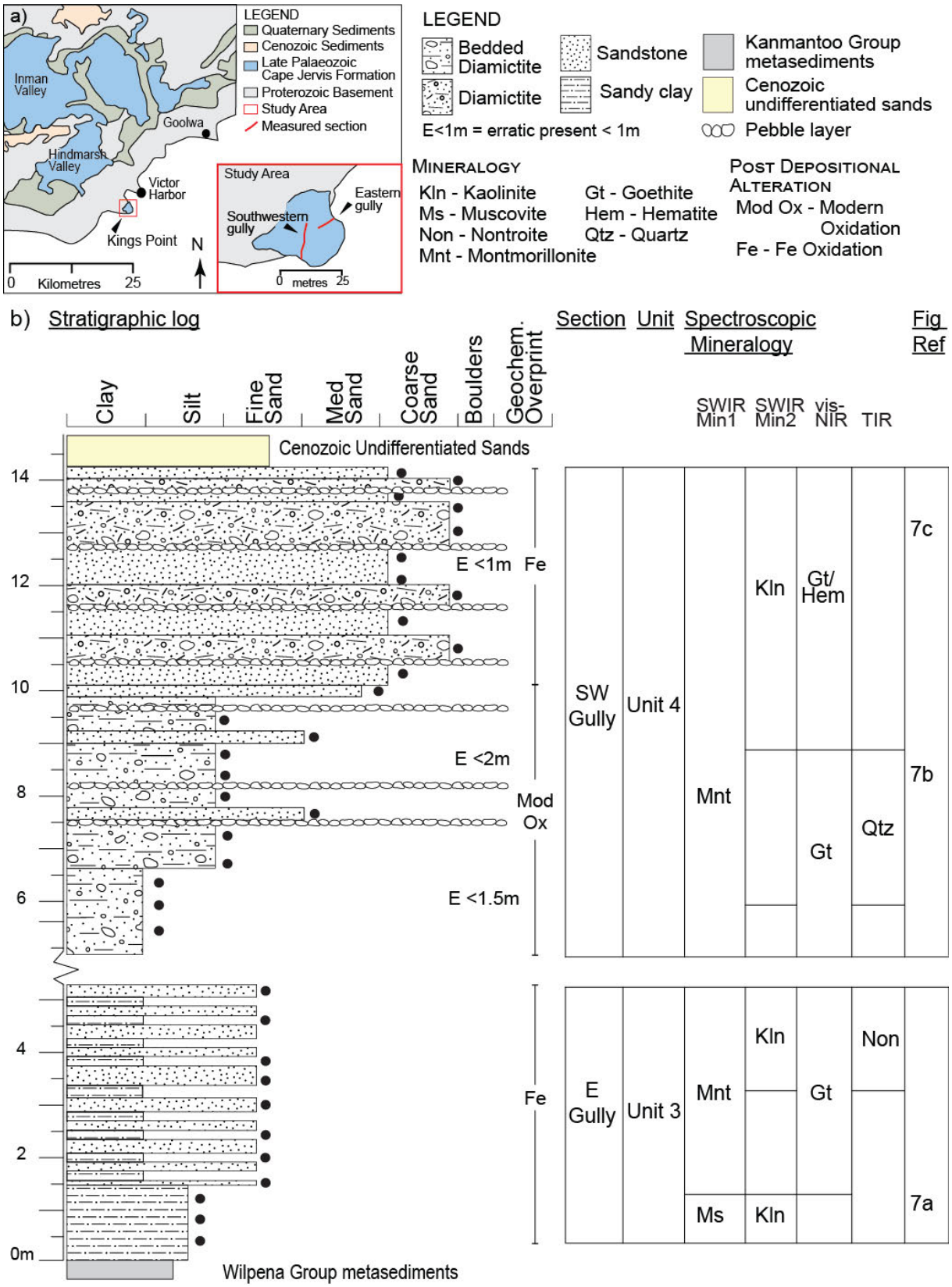

Figure 2:6 a) Simplified regional geology of the Kings Point area adapted from Bourman and Alley (1995) showing section locations; b) Stratigraphic log and spectroscopic mineralogy for the gullies investigated in the Kings Point area. The location of Kings Point is shown in Figure 2:1. Black dots: sample location for HyLogger™ analysis. Units as described by Bourman and Alley (1995).

Figure 2:7 Kings Point Section a) Clasts of Kanmantoo Group metasediment within the clay at 1.2 m in the eastern gully (unit three); b) Pebble lens within the matrix-supported diamictite beds at 8.2 m in the southwestern gully (unit four); c) Encounter Bay Granite erratics scatter the landscape in the southwestern gully, photo taken at 13 m looking down section. Geology hammer is approximately 30 cm long; approximate locations of photos are shown in Figure 2:6.

2.3.4 Waterloo Bay section

The Waterloo Bay section preserves approximately three metres of Cape Jervis Formation that are unconformably overlain by about four metres of Quaternary sedimentary rocks (Figures 2:8, 2.9a). The unconformity is well preserved and is an undulating surface. Units four and five are present in this section.

The Cape Jervis Formation in the Waterloo Bay section consists of bedded clay and diamictite of *unit four* (0 to 2 m) overlain by massive clay of unit five (2 to 3.2 m; Figure 2:8b). Unit four at Waterloo Bay is distinctive from that of the type section as matrix-supported diamictite (Figure 2:9b) has clay to silty clay and is interbedded with clay rather than the sandstone seen at the type section. Unit four at Waterloo Bay is also green to grey whereas at other sections, the sedimentary rocks are buff to yellow. The hard, red and orange mottles of hematite and goethite preserved on the surface of the silty clay beds (Figure 2:9b) are also not observed at the type section.

Unit five at Waterloo Bay is similar to the massive to bedded clay with lesser sandstone at the type section. At Waterloo Bay, red and orange mottles (Figure 2:9c) are preserved and a fine-grained, sandstone bed (<20 cm) at 2.6 m. The section is overlain by a palaeosol containing alunite and limestone and calcrete of the Quaternary Bridgewater Formation.

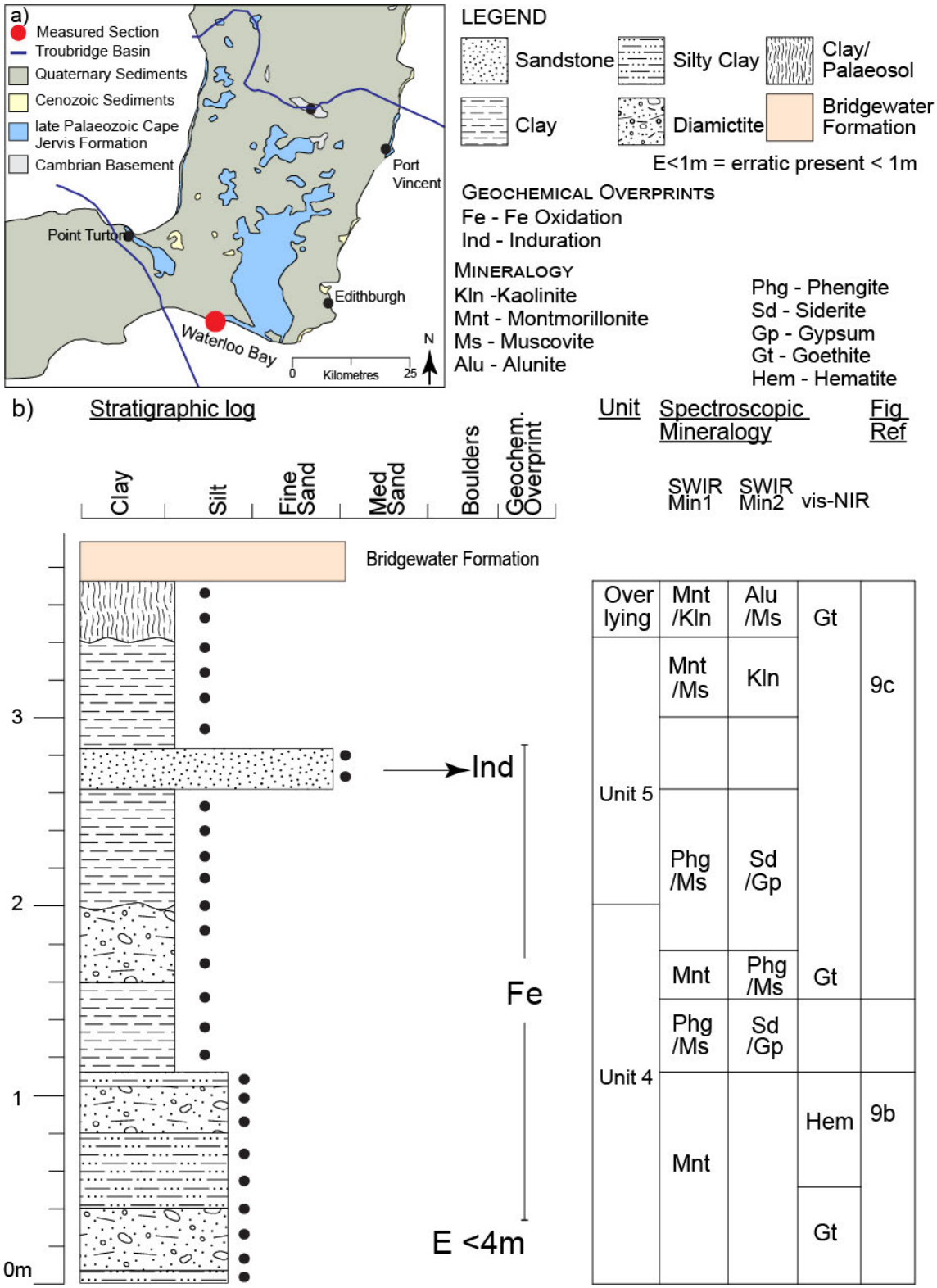

Figure 2:8 a) Simplified regional geology of the southern Yorke Peninsula showing the location of the Waterloo Bay profile adapted from Alley and Bourman (1995); b) Stratigraphic log and spectroscopic mineralogy for Waterloo Bay. The location of Yorke Peninsula is shown in Figure 2:1. Units were originally described by Foster (1974) as all glaciomarine sediments however using the unit descriptions of Alley and Bourman (1984) the units have been reclassified as shown. Black dots: sample location for HyLogger™ analysis.

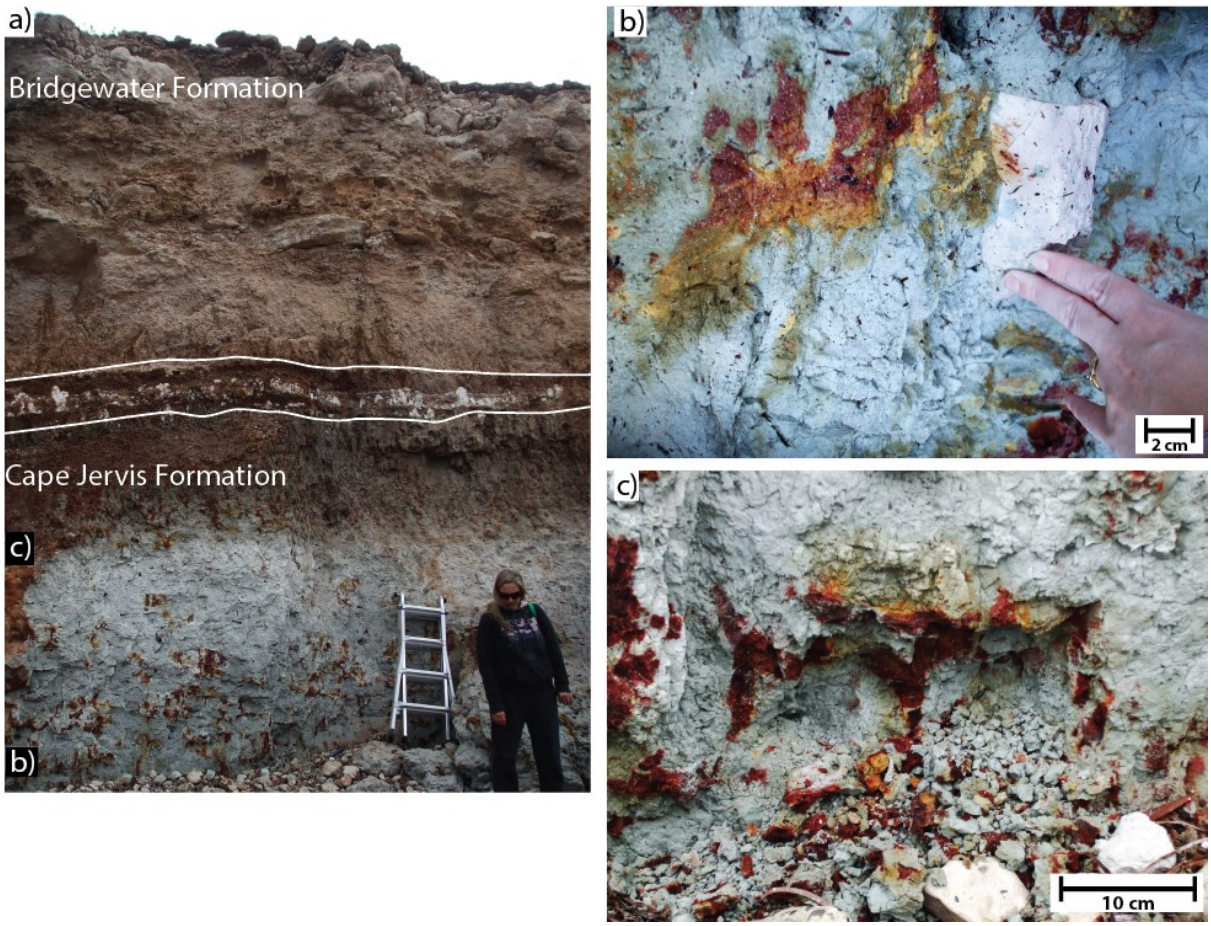

Figure 2:9 Waterloo Bay Section a) Cliff showing the Waterloo Bay section. Sedimentary rocks of the Cape Jervis Formation are overlain by Quaternary Bridgewater Formation, between the white lines is the palaeosol at 3.4 to 3.7 m; ladder is 1.5m high; b) Clasts of Encounter Bay Granite within the lowermost diamictite in the Waterloo Bay section at 1 m. Red and orange mottles can also be seen; c) Mottles of hematite and goethite within the massive clay at 3.2 m near the top of the exposed Cape Jervis Formation. Approximate locations of photos are shown in Figure 2:8. Location of photos in b) and c) is shown by black boxes in a).

2.3.5 Kingscote Composite section

The unit underlying the Cape Jervis Formation in the Bluff Quarry and Kingscote foreshore sections (Figure 2:10a) is unknown although it is interpreted that the sedimentary rocks are underlain by Cambrian Kanmantoo Group as seen at other locations on the Kangaroo Island (Bourman and Alley 1999). The sedimentary rocks of the Bluff Quarry section (0 to 4.5 m; Figure 2:10b) comprise interbedded silty clay, diamictite and sandstone (Figure 2:11a). The Cape Jervis Formation exposed in the coastal cliffs near the Kingscote Warf (5 to 10.7 m; Figure 2:10b) are a sequence of clay to sandstone beds (Figure 2:11e). The Cape Jervis Formation at both measured sections is unit three.

Unit three of the Kingscote Composite section (0 to 4.5 m) is similar to the upper portion of unit three at the type section. The sandstone beds (Figures 2:11b, c) are fine- to coarse-grained with minimal rock fragments and clasts. The cross-bedded sandstone at 2.2 m (Figure 2:11d) in the Kingscote composite section is not at the top of the section, rather, it is overlain by another eight metres of sandstone and clay beds. The clay beds from 5 to 7.5 m of the Kingscote composite section (Figures 2:10b, 2:11f) are similar in characteristics but thicker than the clay beds of the type section. The fine-grained sand that make up the top two metres of the section (9 to 10.7 m) has yellow with purple and orange mottles (Figure 2:11g) and is unconsolidated except in places where the beds are contorted. These contortions

were not observed at the type section. The section is overlain by Jurassic Wisanger Basalt (Figure 2:11a).

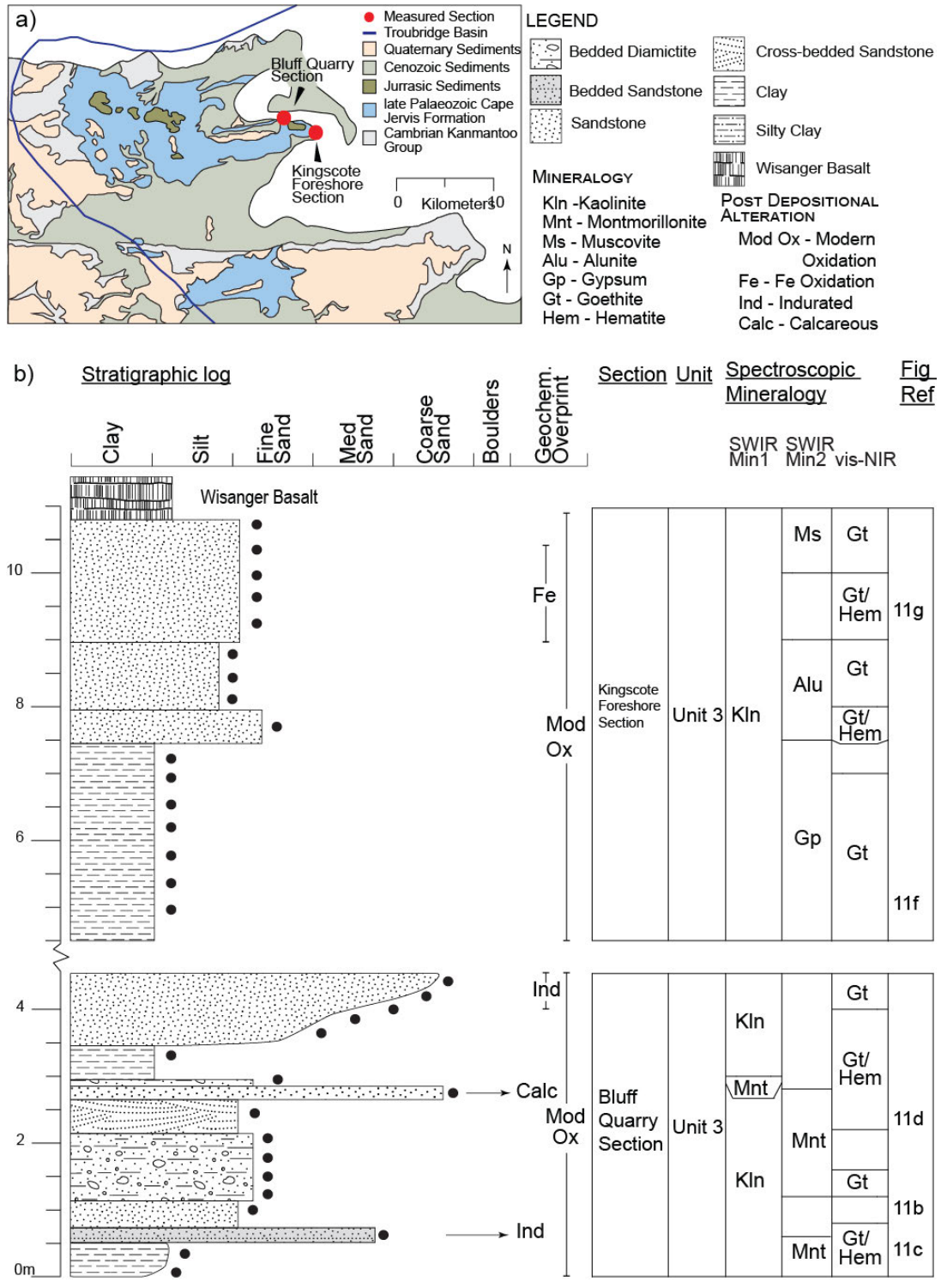

Figure 2:10 a) Simplified regional geology of northeastern Kangaroo Island adapted from Alley and Bourman (1995); b) Stratigraphic log and spectroscopic mineralogy of the Kingscote composite section. The location of Kingscote composite section is shown in Figure 2:1. Black dots: sample location for HyLogger™ analysis. Units as described by Alley et al. (2013).

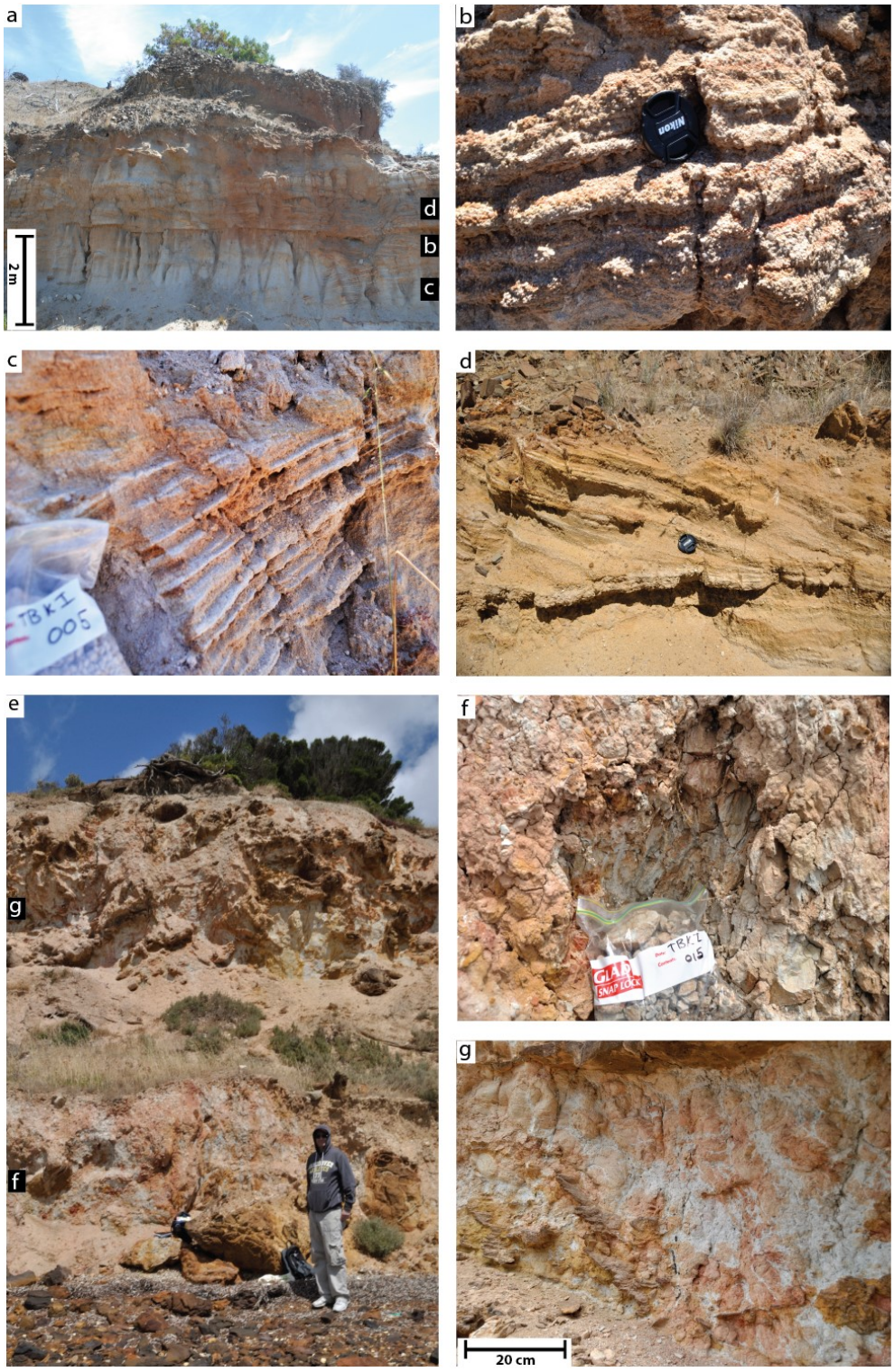

Figure 2:11 Kingscote composite section a) Bluff Quarry section (0 to 4.5 m), Cape Jervis Formations are overlain by Jurassic Wisanger Basalt; b) Pebbly sandstone beds at one metre, with angular, coarse-grained quartz grains bedding in preserved where the silty clay matrix remains; c) Hard, indurated, medium- to coarse-grained sandstone at 0.5 m, that preserves bedding at the base of the Bluff Quarry section; d) Poorly-preserved, planar cross-bedding within medium- to coarse-sandstone at 2.5 m of the Bluff Quarry section; e) Kingscote Foreshore section (5 to 10.7 m), the Cape Jervis Formation make up the entire cliff; f) Clay at the base (at 5.5 m of the composite section) of the Kingscote Foreshore section with prismatic fracturing and orange mottles; g) Sandstone of the upper part of the Kingscote section (9.5 m) with light orange mottles. Approximate locations of photos are shown in Figure 2:10. Location of photos in b), c) and d) are shown by black boxes in a) and location of photos in g) and h) are shown by black boxes in e).

2.4 Discussion

2.4.1 Stratigraphic correlations

Previous researchers (e.g. Alley and Bourman 1984, Bourman and Alley 1990, 1995, 1999) were able to recognise the units described by Alley and Bourman (1984) within sections away from the Cape Jervis type section. However, correlations between sections are yet to be made. With the exception of the Waterloo Bay section, all sections logged in this study were also investigated by Bourman and Alley (1984, 1990, 1995, 2013). Here, the sedimentary rocks observed in the Waterloo Bay section are suggested to represent units four and five of Alley and Bourman (1984; Figure 2:11b) based on similarity in the lithologies preserved and stratigraphic relationships of the lithologies. Where the units were described in relation to the sedimentary rocks at the other sections, specific unit boundaries have been established at each section (see stratigraphic logs above). The unit boundaries were positioned using the depositional setting described by Bourman and Alley (1984, 1990, 1995, 2013), however the units were not visually represented in the previous studies.

The correlation of units across the Troubridge Basin will allow spatial distribution to be assessed and for any lateral differences to be recognised, leading to better understanding of basin-wide variations in depositional setting. The stratigraphic correlations made here (Table 2:1; Figure 2:12) are based on the unit descriptions of Alley and Bourman (1984) together with interpretations based on the facies analysis approach of glacigene settings described by Eyles et al. (1983) and Miall (2000). The approach in facies analysis of glacigene rocks and the interpretation of the depositional processes is based on the identification of key sedimentary characteristics, in particular sedimentary structures and the relationship of these characteristics with depositional processes. Given the weathered nature and lack of well-preserved sedimentary structures in the sections it is not possible to use these facies definitions as intended by Eyles et al. (1983) and Miall (2000), however, where possible the relationships between the glacigene sedimentary rocks and depositional processes have been assessed.

Table 2:1 has a summary of the characteristics of each unit, the unique lithologies of the unit as well as the overall unit characteristics based on observations described in Section 2.3. The correlations between the measured sections are demonstrated in Figure 2:12, where the unique characteristics for each unit have been used to correlate the sections.

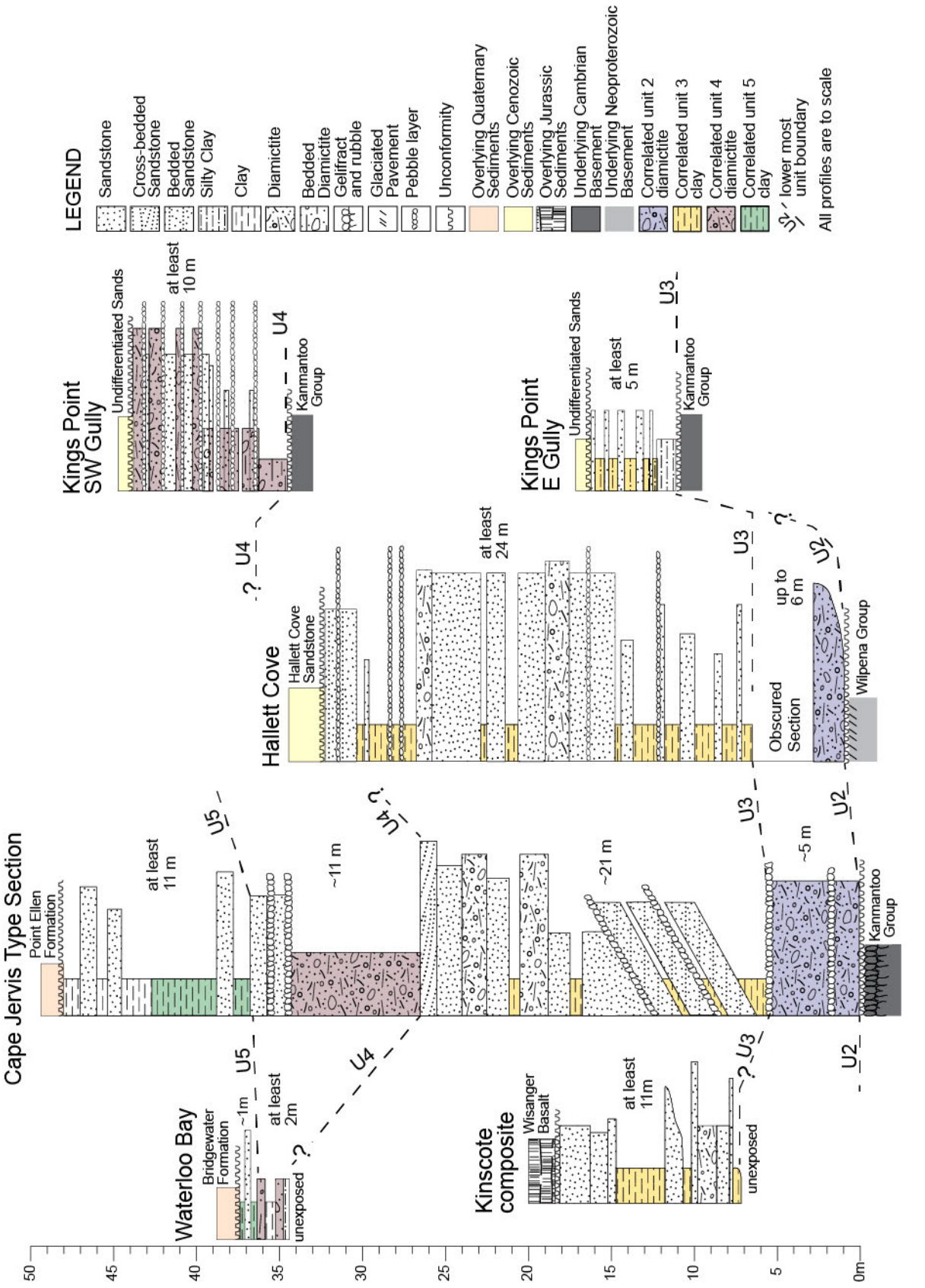

Figure 2:12 Correlation of measured sections from east to west across the basin. The approximate thickness of each unit is recorded within the unit boundaries. The unique lithology for each unit is highlighted. These lithologies were the basis for correlations detailed in the text and Table 2:1. Section locations are in Figure 2:1. Detailed stratigraphic logs of each section are in Appendix 1. Overlying and underlying stratigraphy from (left to right) Zang et al. (2006), Bourman and Alley (1990), Alley and Bourman (1984), and Bourman and Alley (1999, 1995).

2.4.2 Depositional setting of late Palaeozoic sedimentary rocks

Previous researchers (e.g. Crowell and Frakes 1971b, Alley and Bourman 1984, Crowell and Frakes 1971a, Alley et al. 1995, Bourman and Alley 1988, Bourman and Alley 1999) have proposed that during the Permo-Carboniferous glaciation Gondwana was at high latitudes and close to the South Pole. During this time a continental-scale, wet-based ice mass moved from Antarctica through southern Australia and advanced north and east to cover most of South Australia and extended into surrounding states. The ice mass then retreated in a south to southeasterly direction. This was followed by a marine transgression and subsequent regression. The Troubridge Basin was initially covered by the ice mass and was later covered by the transgressing sea.

The Cape Jervis Formation represents changing glacial environments as the ice mass advanced then retreated. The glacial conditions varied depending on the underlying substrate and surrounding landscape. These conditions are reflected not only in the differences between sections but also within the same unit.

Glaciated bedrock surfaces

Two types of glaciated basement surfaces are exposed; polished glacial pavements; and, frost-scattered bedrock (Figures 2:1b, 2:3a, 2:5a). Striated, polished pavements are present in close proximity to the Hallett Cove, Kings Point and Kingscote composite sections (Figure 2:1; Milnes and Bourman 1972, Bourman and Alley 1988, 1990, 1995, 1999). These surfaces have been eroded by the abrasive action of rock particles transported at the base of the ice mass to create a polished, striated and rock-scoured pavement (Figure 2:13a; Glasser and Bennett 2004, Bennett and Glasser 2009). Striations and other rock-scoured features such as chatter marks and concentric grooves provide an indication to the direction of ice movement (Bennett and Glasser 2009). These properties were all observed at Hallett Cove (Figures 2:6, 2:7a). A northwesterly ice movement direction was interpreted by Bourman et al. (1976), Bourman and Alley (1988) and Bourman and Alley (1990) from ice movement indicators across the Troubridge Basin.

Although the general ice movement direction is northwesterly there is some variation in the striae direction measured across the basin. Milnes and Bourman (1972), Bourman and Milnes (1976) and Bourman et al. (1976) observed an east to west ice movement near Mount Compass, at Port Elliot and in the Inman Valley (Figure 2:1b). While Milnes and Bourman (1972), Bourman and Alley (1990 and 1999) and Alley et al. (2013) observed northeast to north northeast ice movement directions at Hallett Cove and across Kangaroo Island. The difference in ice movement direction have been attributed to the presence of ice tongues that preceded the icesheet (Bourman and Miles 1976, Bourman and Alley 1999, Alley et al. 2013).

The basal melting of ice tongues typically causes the over-deepening of existing valleys (Alley et al. 1995, Nick et al. 2010) forming U-shaped valleys such as the Inman Valley and the valley at Hallett Cove. The polished pavements document the abrasion and quarrying of the underlying strata while the striations document the direction the ice flows (Benn et al. 2003).

Gelifract is not the product of direct contact with the ice mass, however, is an example of a glaciated bedrock surface (e.g. Alley and Bourman 1984). Gelifract was observed underlying the glacigene sedimentary rocks of the Cape Jervis section (Figures 2:2b, 2.3a). The fracturing of basement rocks has been attributed to frost shattering that occurred due to periglacial conditions prior to the beginning of the glaciation of the area (Alley and Bourman 1984, Matsuoka 1990). Though these glaciated bedrock

surfaces are not part of the Cape Jervis Formation, it is important to recognise their presence as it indicates that the overlying sedimentary rocks are glacial in nature.

Depositional setting of lodgement till (unit 2)

Diamictite of unit two are exposed at Cape Jervis and Hallett Cove. At both locations the lodgement till directly overlies bedrock. Although the Cape Jervis Formation overlies the bedrock at Kings Point, lodgement till is not exposed (Figure 2:7b). This may be an example of where the lodgement till was removed by the advancing ice mass or that no lodgement till was deposited in the area. This differs from Hallett Cove (Figure 2:4b) and Cape Jervis (Figure 2:2b) where the glaciated basement is directly overlain by lodgement till.

Lodgement till (unit two) represents deposition of debris that is transported subglacially (e.g. within or by a glacier) in crudely stratified basal layer with an intense abrasive action (Eyles and Miall 1984, Bennett and Glasser 2009; Figure 2:13a). Deposition occurs when the friction between the ice mass and the debris (sediment and rock fragments) is such that the debris stops moving or the debris is released by melting (Bennett and Glasser 2009; Figure 2:13a). The debris deposited is typically a dense, matrix-supported diamictite with a high concentration of locally-derived clasts (Eyles et al. 1983). A proportion of the clasts have glacially-faceted shapes which are characteristic and diagnostic (Eyles and Miall 1984). The debris is then deposited at the front and preserved underneath the advancing glacier. The typical geometry of lodgement till across sedimentary basins is 'sheet-like'; lying above local and regional unconformities (Eyles and Miall 1984, Hambrey and Glasser 2012). Hambrey and Glasser (2012) concluded that debris deposited in a subglacial, basal setting of a temperate glacier would have a rare abundance, when compared diamictites deposited in other glacial settings, be clast-rich (5 to 30%) with very angular to subrounded clasts where twice as many clasts were faceted then striated, poorly-sorted within a silt to sand matrix. The characteristics of unit two (Table 2:1) are consistent with the criteria for basal subglacial deposition within a temperate glacial setting of Eyles et al. (1983), Eyles and Miall (1984) and Hambrey and Glasser (2012).

Unit two of the Cape Jervis Formation was deposited at the front and base of the glacier (Figure 2:13a). Up to six metres of the diamictite of the lodgement till was been preserved across the basin; specifically as valley fill at the Cape Jervis and Hallett Cove sections (Figure 2:12). Bourman and Alley (1990) reported that they had not seen any greater thickness of lodgement till or pre-till glacigene sedimentary rocks in the Troubridge Basin and after extensive investigation no greater thickness was seen during this study. It is unlikely that a greater thickness would be found as the continual erosion of the till underneath the advancing ice mass would have minimised accumulation. Erosion of the unit may also have occurred during the retreat of the ice mass resulting in some reworking and resedimentation of the debris (Eyles and Miall 1984, Ashley et al. 1985, Hambrey and Glasser 2012).

As unit one was not observed, there is no evidence as to the change in depositional setting between units one and two. The contact between the underlying basement and the lodgement till is unconformable, which is caused by the erosion of sedimentary rocks by the glacier as it moved across the landscape. This fore fills the requirement of Eyles and Miall (1984) and Hambrey and Glasser (2012) for subglacial basal deposition. The overlying contact with sedimentary rocks of the fluviolacustrine beds is an abrupt contact between the diamictite of the lodgement till and fluviolacustrine clay beds (Figure 2:12). Where the contact was observed, there is no evidence of a pause in sedimentation by means of an erosional contact or palaeoweathering surface (Figures 2:2b, 2.4b).

The lack of other lithologies (e.g. sandstone and clay units) within unit two (Figure 2:2b and 2:4b) suggests that there was a limited supply of meltwater to deposit beds of smaller grain size at this time. Elyes and Miall (1984) suggested that a wide range of lithologies are commonly associated with subglacial basal deposition within cold based glacial settings where channel fill is a result of subglacial stream drainage. This expands on the depositional setting described by Alley and Bourman (1984) and (Bourman and Alley 1990, 1999, Alley et al. 2013) that the lodgement till was deposited by the advancing ice mass.

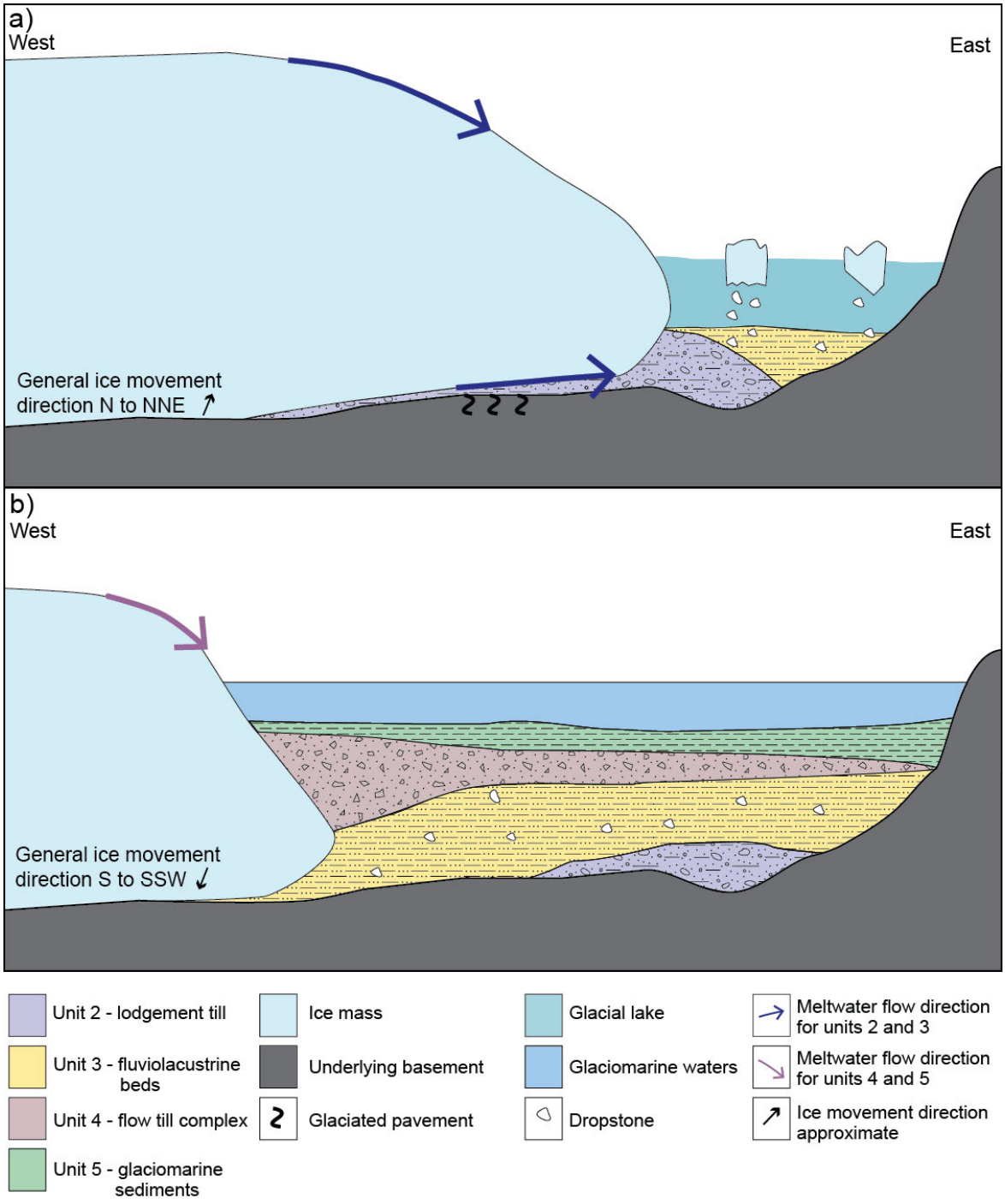

Figure 2:13 a) Stylised depositional setting during the migration and stagnation of the ice mass and the deposition of units two and three; b) Stylised depositional setting during the retreat of the ice mass and related marine transgression and the deposition of units four and five. These diagrams a representation of a perfect exposure and are based on what is seen typically along the coastal exposures of the basin such as the type section at Cape Jervis.

Depositional setting of the fluviolacustrine beds (unit 3)

The fluviolacustrine beds (unit three) were observed at all sections except for Waterloo Bay (Figure 2:12), the thickness of the unit varies from 5m at Kings Point up to at least 24 m at Hallett Cove (Figure 2:12) The varying lithologies (i.e. clay, sandstone and diamictite) within unit three suggest that the depositional processes for vary implying a dynamic, evolving depositional setting. Bourman and Alley (1990) and Bourman and Alley (1995) propose that the alternating clay, sand and diamictite beds of the fluviolacustrine beds (unit three; Table 2:1) are the result of variable ice decay rates. Investigating the depositional process of each lithology can provide a better understanding of the depositional setting of unit three.

The massive to finely laminated clay and silt beds were likely deposited in a low energy environment. Miall (2000) suggests that the fine laminations in the clay beds were deposited in an abandoned channel or waning flood plain setting; while, Hambrey and Glasser (2012) proposed that very fine-grained laminate with no clasts suggest deposition in an ice-proximal glaciolacustrine setting. Given that the ice mass was likely still proximal to the Troubridge Basin and the similarity of the clay beds in unit three to Hambrey and Glasser's (2012) description an ice-proximal glaciolacustrine is the most likely depositional setting.

Glacial lakes can develop in a number of environments, such as at the front of a stagnant glacier, or between moraines and the ice mass, or by the draining of glacial waters into pre-existing basins (Bennett and Glasser 2009). It is likely that the glacial lakes of the Troubridge Basin formed from glacial water draining into low-lying areas (Figure 2:13a) when the ice stagnated in the Gulf St Vincent. This depositional setting was also surmised by Bourman and Alley (1999) and Alley et al. (2013).

The fine- to medium-grained sandstone beds of unit three, are typically interbedded with the clay beds (Figure 2:13). The sandstone beds increase in frequency up section suggesting a gradual change in glacial conditions. Bennett and Glasser (2009) listed resedimentation by gravity flows, current reworking or shoreline sedimentation as mechanisms for sandstone deposition within a glaciofluvial environment. Eyles et al. (1983) and Miall (2000) both correlated horizontally bedded sandstone beds with sediment-heavy flows and laminated clays deposited into subglacial ponds. Hambrey and Glasser (2012) linked a high abundance of well sorted sand or silt beds with a very low (<5%) striated and faceted clast occurrence with fluvioglacial streams.

The sandstone beds of unit three are typically massive to thinly bedded with minor occurrences of poor-preserved planar and trough cross-beds in the Cape Jervis and Kingscote sections. Due to the poor-preservation of the cross-beds information such as palaeocurrent directions could not be established. Of the depositional processes listed by Bennett and Glasser (2009), gravity flows, current reworking and shoreline sedimentation can be ruled out due to the lack of sedimentary structures. The processes of Eyles et al. (1983), Miall (2000) and Hambrey and Glasser (2012) are similar in that they describe meltwater streams transporting sediment away from the ice mass. Meltwater streams (or channels) associated with the flow of water away from the ice mass can form subglacially (beneath the ice), laterally (along the ice margin; Figure 2:13a) and in proglacial locations (in front of the ice; Bennett and Glasser 2009). The cross-bedded sandstone beds are likely scour fill or minor channel fill deposits (Miall 2000). Given the discontinuous exposure of the sand and sandstone beds across the basin it is not possible to determine where the meltwater streams originated. It is likely that all three types of meltwater streams introduced sedimentary rocks into the glacial lake(s).

Dropstones occur sporadically throughout both the clay and sandstone beds of unit three, particularly at the Cape Jervis and Hallett Cove sections (Figures 2:3b, 2:5f, g). The presence of dropstones is indicative of glacial 'rain-out' or ice-rafted debris flows (Eyles et al. 1983, Miall 2000, Bennett and Glasser 2009, Hambrey and Glasser 2012). When icebergs and the resultant 'rain-out' is in low concentrations, isolated dropstones are deposited on the finer materials that have accumulated at the bottom of the lake (Bennett and Glasser 2009). The presence of dropstones in unit three suggests that there were ice bergs on the surface of the glacial lakes (Figure 2:13). The dropstones at Cape Jervis and Hallett Cove and contortion of the underlying beds and draping of overlying beds (Figures 2:5f, g, 2:13a) suggests they were deposited via gravity (underlying contortion) and remained undisturbed (overlying draped beds). Bourman and Alley (1990) also suggested that icebergs where the source of the dropstones and contorted beds associated with them in unit three at Hallett Cove.

Eyles et al. (1983) suggested that ice-rafted debris flows may also be the depositional process responsible for diamictite deposits. In unit three diamictite beds are interbedded with the sandstone and clay beds in the upper unit three (Figure 2:13). The irregular shape and lithological nature of the diamictite lenses and beds (e.g. sorting, clast shape) suggests deposition in an environment where there was the degree of disaggregation of grainsize and current activity was minimal, which occurs where the depth of the lake is at a minimum (Bennett and Glasser 2009). Eyles et al. (1983) attributed these characteristics with bank erosion and collapse into melt stream channels. Hambrey and Glasser (2012) extended the characteristics of the diamictite to boulder to gravel sized, very angular to rounded clasts within a sand to silt matrix that is well sorted. These clasts are deposited by supraglacial channels and deposited where water ponds.

The sandstone and diamictite of unit three (Figure 2:12) represent a transient influx of higher energy into the glacial lake system. This may have been triggered via several mechanisms, including deposition from meltwater flows, direct deposition from the front of the ice mass, 'rain-out' from icebergs, resedimentation by gravity flows, current reworking and shoreline sedimentation (Bennett and Glasser 2009).

Unit three of the Cape Jervis Formation was likely deposited in a subaqueous or subglacial fluviolacustrine setting. Where sediment heavy channel flows and ice rafted debris flows with minor channel flows supplying sediment and debris into glacial lakes. Bourman and Alley (1990) and Alley and Bourman (1984) postulated that the ice was likely stagnant in the Gulf St Vincent to enable the development of glacial lakes. The presence of the silt and clay beds in unit three are evidence of the glacial lakes that formed between the ice mass and palaeoshore. It is not known if the lakes were continuous along the coastline or if a series of discrete lakes formed. This is also reflected in the depositional setting postulated by Alley and Bourman (1984).

The lower section of the unit is dominated by clay and silt beds suggesting that the glacial lake was likely a very low energy environment and there was minor input from meltwater streams depositing the sandstone beds. The increased presence of sandstone beds and diamictite lenses and beds towards the top of the unit (Figure 2:12) suggest that at some point the conditions changed, perhaps initiated by a change in climate and retreat of the glacier. Additionally, the cross-bedded sandstone in the Cape Jervis and Kingscote sections (Figure 2:2b) suggest deposition within shallow water environment, such as channel flow following downwasting of the ice mass. It is therefore possible that the glacial lake became increasingly shallow due to the deposition of sediment and the decrease of water input via meltwater before the ice conditions changed to enable the deposition of the flow till complex (unit four). These changing depositional processes have caused the variations in thickness of unit three.

The tilting of the lower fluviolacustrine beds at Cape Jervis is likely due to sub-aqueous collapse of the saturated sedimentary rocks prior to consolidation. Similar tilting of unit three was not observed at any other section or above and below the tilted unit three sedimentary rocks at Cape Jervis.

The depositional setting change represented by the clay dominance of the lower part of the section and the sand dominance in the upper part of the section is important as it indicates a change from a dominantly lacustrine to fluvial settings. The damming of meltwater to create glacial lakes occurred during the stagnation of the ice mass causing thick beds of clay and silt to deposit between the deposition of thin sandstone and diamictite beds. The change to dominant sandstone and diamictite beds and thin clay and silt beds was triggered by the initiation of the melting of the ice mass. This change in depositional setting was also recognised by Alley and Bourman (1984) who suggested the formation of a series of a kame terraces that deposited fluvial sedimentary rocks intermittently causing the interfingering of alluvial and lacustrine sedimentary rocks.

Depositional setting of the flow till complex (unit 4)

Unit four is approximately 11 m thick at the type section; at Kings Point the unit is at least ten metres thick while at Waterloo Bay it is at least 2.5 m thick (Figure 2:12). At the type section the unit consists of unstratified and unconsolidated diamictite (Figure 2:2b) whereas at the other sections it consists of thin (<1 m) beds and lenses of diamictite interbedded with either clay or sand beds (Figures 2:6b, 2:8b). Sedimentary rocks similar to those at Kings Point were also observed at Hallett Cove and Kangaroo Island by Bourman and Alley (1999) and Alley et al. (2013). The different lithologies of the flow till complex across the Troubridge Basin reflects variable depositional conditions during the decay and retreat of the glacier.

Alley and Bourman (1984) and Bennett and Glasser (2009) suggest that the deposition of flow till complex is the result of highly unstable supraglacial debris flowing downslope. The debris is released due to constant ablation occurring on the surface of the melting ice mass. The unstable material accumulates on the constantly changing ice surface until enough debris has accumulated to be released down the melting ice slope where it is deposited (Figure 2:13b). The properties of the resulting diamictite is dependent on water content, debris character, (e.g. size of clasts, proportion of rock flour), the surface gradient and the composition of the depositional surface (Bennett and Glasser 2009). Broadly, the greater the water content the more debris is deposited. Sand and silt beds within the flow till complex are associated with the reworking of the debris by meltwater that originates from the base and top of the ice mass (Bennett and Glasser 2009). Miall (2000) suggested that unconsolidated to clast-supported diamictites are deposited as debris flows from valley glaciers. If the diamictites also have inverse grading. Miall (2000) proposed depositional processes such as low-strength and pseudoplastic debris flows.

The unconsolidated or clast-supported nature of the diamictite beds suggests reworked glaciofluvial materials according to Hambrey and Glasser (2012). Other properties associated with reworked glaciofluvial deposits include, deposits with 80 to 100% clasts that have a very low (<10%) occurrence of striated and faceted clasts within a sand to silt sized matrix that is moderately well sorted. Eyles et al. (1983) associate a diamictite that is mostly unconsolidated, with dominantly rounded clasts that have no orientation interbedded with fluvial lithologies and other resedimented diamictites with depositional processes within a valley glaciers. The resedimented diamictites extend into channel fills where they may become increasingly sandy with reduced clasts. Eyles et al. (1983) also suggest that coarsening-up of deposits, such as that seen in the diamictite matrix at the Kings Point section (Figure

2:6b), may be evidence of resedimentation in an environment with debris-rich and debris-poor glacial ice that is melting. While Bennett and Glasser (2009) attribute it to the preferential washing out of the clay and silt sized particles before coarser sedimentary rocks where deposited.

The interbedded clay and sand beds of unit four may have been deposited via meltwater, as suggested by Eyles et al. (1983), that either reworked the finer sedimentary rocks in the debris, or via the same mechanisms as the sand beds of the fluviolacustrine material in the underlying unit three (i.e. pooling glacial water such as glacial lakes and sediment laden meltwater streams). The variation in the degree of interaction with meltwater between the flow till complex sedimentary rocks deposited at the Cape Jervis versus Kings Point and Waterloo Bay sections may reflect the position of the ice mass in relation where the till was deposited. The mixing of meltwater flow and debris flow deposits at Kings Point and Hallett Cove is indicative that the ice mass was stagnant or slowly moving, which would permit the formation of meltwater streams (Bennett and Glasser 2009). The mass flow of the debris at Cape Jervis was likely at the front of the retreating ice mass.

The varied lithofacies within the flow till complex are due to the diversity of glacial environment and instability of the ice mass as it retreats and decays. Deposition occurred both subglacially and subaqueously with debris flows and intermittent fluviolacustrine depositional processes. The clay and silt beds were deposited via glacial lakes that remained or were formed by trapping water between the ice and the built up debris. The sand and sandstone beds were deposited via meltwater streams flowing out from the ice mass. The diamictite beds were deposited when the top of the ice mass released debris trapped in the upper ice mass. These varied depositional settings are the cause of the differing thicknesses of the individual beds and the total thickness of the flow till complex at each measured section.

These observations are consistent with Alley and Bourman (1984) and Bourman and Alley (1999) where it was surmised that the flow till complex was deposited during the downwasting and slow retreat of a large ice mass. Additionally the occurrence of temporal glacial lakes and the associated glaciolacustine sedimentary rocks was suggested by Bourman and Alley (1990) and Alley et al. (2013).

Compared to the diamictite of the lodgement till (unit two), the diamictite of the flow till complex (unit four) has larger clasts which are mostly angular and are both locally- and distally-derived. The clasts increase in size up-profile. The matrix of the diamictite also reflects the dynamic depositional conditions. The matrix consists of unconsolidated sand grains which increase in size up-profile. It is likely that the diamictite was deposited by an icesheet rather than an ice tongue. The ice tongues likely melted before the ice mass retreated to the Troubridge Basin, likely decaying first as the ice would have been not as thick as the icesheet. The angular clasts and mixed source are indicative of an icesheet deposition.

At Waterloo Bay the contact between the flow till complex and overlying glaciomarine clay is transitional (Figures 2:8a, 2:9b), which is suggested to be, indicative of a glacial environment where debris deposition continued during the influx of marine waters. The debris deposition occurred periodically allowing the silty clay beds to be deposited between deposition of debris beds. At Cape Jervis the contact between unit four and the clay of unit five is a sharp contact (Figure 2:2b).

Depositional setting of the glaciomarine sediments (unit 5)

The glaciomarine sediments preserved at Cape Jervis and Waterloo Bay vary in thickness up to at least 11 m (Figure 2:12). Unit five was deposited in a quiet, marine environment where it is likely that the marine waters were locally influenced by the downwasting and presence of glaciers or icesheets.

Previous studies (e.g. Ludbrook 1969b, Foster 1974, Alley and Bourman 1984) recognised the sedimentary rocks are glaciomarine and surmised that deposition occurred in marine waters influenced by the presence of glaciers or icesheets where meltwater continually introduced sedimentary rocks to the environment. Ludbrook (1969b) and Foster (1974) both recognised the effects of the glacial meltwater on the salinity and density of the marine waters which in turn affected the species of foraminifera. Foster (1974) added that the influence of the meltwater was likely to be isolated to the proximity of the meltwater inlet. Palynological studies conducted by Ludbrook (1969b) and Foster (1974) suggest that the marine waters were cold with low salinity during the deposition of the glaciomarine sediments. The cool temperatures of the water are likely a function of the climate and proximity of the ice and meltwater flow input.

The mechanisms of deposition of unit five are similar those that occur in glacial lakes however the presence of marine foraminifera suggests a low energy marine depositional setting. Bennett and Glasser (2009) listed these to be direct deposition from the ice mass front; 'rain-out' from icebergs; deposition from meltwater flows; settling of sedimentary rocks in suspension; current reworking; and shoreline sedimentation. Rhythmically laminated clay and silts in glacial successions are typically described as varves however similar deposits such as turbidites can form due to low-viscosity density flows. Turbidite deposits without ripples and slumping suggest proglacial or ice-distal deposition where tidal and seasonal-stimulated changes in meltwater discharge control the amount of finer grained materials transported from the ice and deposited via suspended sediment plumes. Ice-distal deposition of turbidites are typically associated continental ice margin settings (Eyles 1993, Miall 2000). Hambrey and Glasser (2012) observed that glaciomarine deposition of massive or laminated clay with minimal clasts (<5%) and some sandstone beds are typically deposited via a combination of settling from suspension (clay) and iceberg rafting (sandstone).

Given the fine-grained, clay and silty clay nature of the glaciomarine sediments, it is likely that the mechanism of deposition is largely due to settling of sedimentary rocks that are in suspension in a low energy environment as suggested by Eyles et al. (1983), Miall (2000), Bennett and Glasser (2009) and Hambrey and Glasser (2012). The increase of distinct bedding in the clay sedimentary rocks at Cape Jervis (Figure 2:2b) indicates that deposition occurred in a marine environment which was potentially deepening due to the increase melting of the ice mass, where sedimentary rocks were continually introduced to the environment via meltwater flows from the retreating glacier (Figure 2:13b; Alley and Bourman 1984).

Sandstone beds within the unit (Figure 2:12) are proposed to have been deposited via meltwater flows and iceberg 'rain-out' (Figure 2:13b). Deposition of the sandstone beds via current reworking or shoreline sedimentation would result in cross-bedded sandstone (Bennett and Glasser 2009), which was not observed. The lack of a significant population of dropstones indicates that deposition via 'rain-out' from icebergs is not a preferred mechanism for deposition of the sandstone beds.

2.5 Summary of glacial sedimentology of the Cape Jervis Formation

The deposition of the sedimentary rocks of the Cape Jervis Formation can be summarised as five depositional settings each signifying a change in the glacial environment (Figure 2:13).

1. Development of glaciated bedrock surfaces either due to pre-glacial freeze-thaw of the substrata to form gelifract as observed at Cape Jervis or due to the movement of the ice mass over the substrate forming glaciated pavements that were observed across the Troubridge Basin. This movement polished the underlying rock and caused the development of glacial movement indicators such as striations and chatter marks. Large erratics were deposited.
2. Deposition of lodgement till as the advancing of the ice mass moved generally from south to north. The diamictite is made up of dominantly locally-derived sedimentary rocks that were deposited in front of and under the ice mass.
3. The stagnation and subsequent melting and retreat of the ice mass in the Gulf St Vincent led to a series of glacial lakes forming between the ice and coastal cliffs. During this time clay and silt beds were deposited due to the settling of suspended fine material within the lakes. Sandstone beds of unit three were deposited due to the settling of suspended coarser-grained material and via the action of meltwater streams. Dropstones originated from the melting of icebergs within glacial lakes. Indications of a change in depositional settings are marked by an increase in the frequency and thickness sandstone and diamictite beds at the top of unit three, which was caused by an increase in melting of the ice mass.
4. Further down-wasting and the commencement of the southerly retreat of the glacier is signified by deposition of the flow till complex. The diamictite of unit four was deposited as saturated debris released by constant surface ablation and then deposited down slope. Sandstone beds and lenses between the diamictite beds were deposited via meltwater flows from the base of the ice mass.
5. A rise in sea-level, possibly initiated by the melting of the ice mass, led to a marine incursion where glaciomarine clay sedimentary rocks where deposited over the flow till complex. The presence of stagnant and retreating ice continued to supply meltwater and coarser (sand) sedimentary rocks to the marine water, ultimately lowering the salinity. The increasing bedding of the clay indicates a rapidly deepening environment.

Chapter 3: Sedimentology of late Palaeozoic sedimentary rocks of the Arckaringa Basin, South Australia

Foreword

This chapter describes the results of the sedimentology of the sedimentary rocks carried out on three measured sections of the Arckaringa Basin. Measured sections were systematically logged and sampled by the author and Dr. Steve Hill, Dr. Robert Dart and Steve Hore during a field trip during January 2011. Analytical methods include observations of the physical characteristics of the sedimentary rocks including detailed petrology and mineralogy. Petrological analysis was conducted by the author at Adelaide Microscopy at the University of Adelaide using thin sections prepared by Pontifex and Associated Pty. Ltd. in Adelaide. Mineralogical (spectroscopic) analysis and data processing was conducted by Georgina Gordon using the Hylogger^{TM} 3-3 at the Department of State Development, Geological Survey of South Australia Core Store Facility in Glenside, Adelaide.

This chapter builds on research initially conducted by Ludbrook (1961) and expanded upon by Townsend and Ludbrook (1975) which focused on the stratigraphic nomenclature of the Boorthanna, Stuart Range and Mount Toondina formations. Detailed studies at specific sites were also conducted by Heath (1963, 1965) and Freytag (1964, 1965). These are duly referenced throughout this chapter. The depositional settings of the sedimentary rocks of the Arckaringa Basin, based on their sedimentology are presented herein. This chapter has been written as an independent publication and is structured accordingly.

Abstract

Late Palaeozoic sedimentary rocks of the Arckaringa Basin in northern South Australia include diamictite and sandstone units of the Boorthanna Formation that were deposited as lodgement till under fluvioglacial conditions. The clast size and matrix sedimentology suggest that the diamictite units were sourced from both continental icesheet and valley or ice tongue glaciers, which is in contrast to accepted models that do not consider multiple glacial influences in sediment deposition. The sandstone units of the Boorthanna Formation were deposited in meltwater streams at the final stage of deglaciation. The uppermost unit of the late Palaeozoic Arckaringa Basin, the Mount Toondina Formation consists of carbonaceous sandstone and siltstone units. The interbedded nature of this unit as well as the sedimentology implies that the sedimentary rocks were deposited in an alternating lacustrine and fluvial setting.

Comparison with the depositional model for temporally equivalent late Palaeozoic sedimentary rocks of the Troubridge Basin shows that the lowermost sedimentary rocks in both basins comprise lodgement till that was deposited via the action of icesheets and valley glaciers. The depositional processes in the two basins then became different so that sedimentary rocks within the Arckaringa Basin were being deposited in a deepening marine setting whilst fluvioglacial and glaciomarine sedimentary rocks were being deposited in the Troubridge Basin. The depositional environment of the Arckaringa Basin then moved to being terrestrial, and alternating lacustrine and fluvial sedimentary rocks were deposited. At this time the Troubridge Basin moved to a deepening glaciomarine environment.

3.1 Introduction

Extensive glacigene sedimentary rocks are preserved across much of Australia as a result of a major glaciation event that covered most of the Gondwana supercontinent throughout the Carboniferous (Crowell and Frakes 1971a, 1971b, Alley et al. 1995, Veevers 2006). Within South Australia, the geological record for this time is preserved within discrete, remnant basins. One depocentre of late Palaeozoic sedimentary rocks is the Arckaringa Basin (Figure 3:1; Ludbrook 1961, McGowran 1973, Hibburt 1995). The glacigene sedimentary rocks within the Arckaringa Basin are deeply covered (up to 1000 m depth). Localised, disconnected exposures are preserved along the eastern and western margins of the basin. The poor exposure implies that comparisons between the depositional settings of temporally equivalent glacial sedimentary rocks within basins across South Australia have not been made.

Due to poor exposure combined with insufficient geophysical and drilling logs of the Arckaringa Basin, the stratigraphic definition of the late Palaeozoic sedimentary rocks is poor (Hibburt 1995). The stratigraphy has been broadly divided into three units (e.g. Ludbrook 1961, 1967, Harris and McGowran 1971, McGowran 1973, Townsend and Ludbrook 1975). The lowermost stratigraphic unit, the Boorthanna Formation, dominantly comprises basal glacial deposits that unconformably overlie the basement. The glacigene sedimentary rocks are unconformably overlain by the Stuart Range Formation, which was deposited in a marine setting (Figure 3:2). The Mount Toondina Formation forms the uppermost stratigraphy of the Arckaringa Basin and represents sedimentary rocks deposited in a marine to freshwater lacustrine and fluvial environment (Figure 3:2; Ludbrook 1961, Harris and McGowran 1971, McGowran 1973, Hibburt 1995).

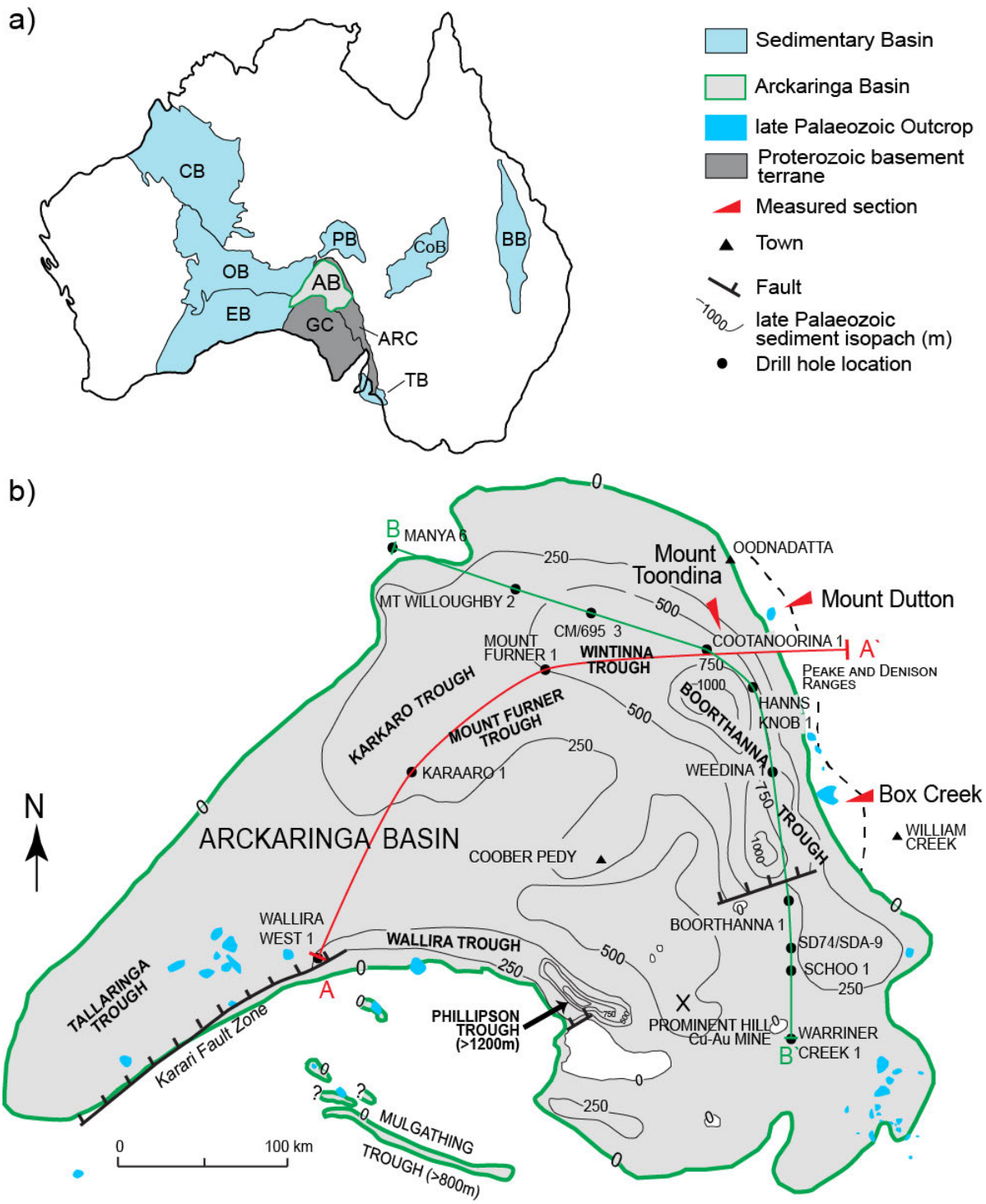

Figure 3:1 a) Approximate limits of the Arckaringa Basin. Locations of exposed late Palaeozoic sedimentary rocks at Box Creek, Mount Dutton and Mount Toondina are given. Significant geological elements such as major troughs and isopachs of late Palaeozoic sedimentary rocks, field locations and drill holes addressed in this chapter are shown adapted from Hibburt (1995) and Alley et al. (1995); b) Location of the Arckaringa Basin in South Australia. Other Late Palaeozoic sedimentary basins and Archean to Proterozoic basement rocks relevant to this study are also shown. ARC: Adelaide Rift Complex; AB: Arckaringa Basin; BB: Bowen Basin; PB: Pedirka Basin; CB: Canning Basin; CoB: Cooper Basin; EB: Eucla Basin; GC: Gawler Craton; OB: Officer Basin; TB: Troubridge Basin.

Depositional models for the late Palaeozoic sedimentary rocks in the Arckaringa Basin are mostly based on fitting rudimentary sedimentological observations into pre-existing, continental-scale reconstructions. These models suggest that the glacigene sedimentary rocks were deposited within various glacial environments including a continental-scale icesheet, glaciolacustrine and fluvioglacial (Crowell and Frakes 1971b, Alley et al. 1995). A detailed depositional model for the sedimentary rocks of the Arckaringa Basin itself is yet to be proposed.

This study details the sedimentology of late Palaeozoic sedimentary rocks exposed on the eastern Arckaringa Basin. These data are used to correlate the surface exposures with subsurface type sections (taken from drill holes) to develop a more holistic understanding of the depositional processes of glacigene sedimentary rocks within the Arckaringa Basin. A model of the depositional setting for the sedimentary rocks of the Arckaringa Basin is proposed. This model is then compared to the depositional model of similar aged sedimentary rocks in the Troubridge Basin.

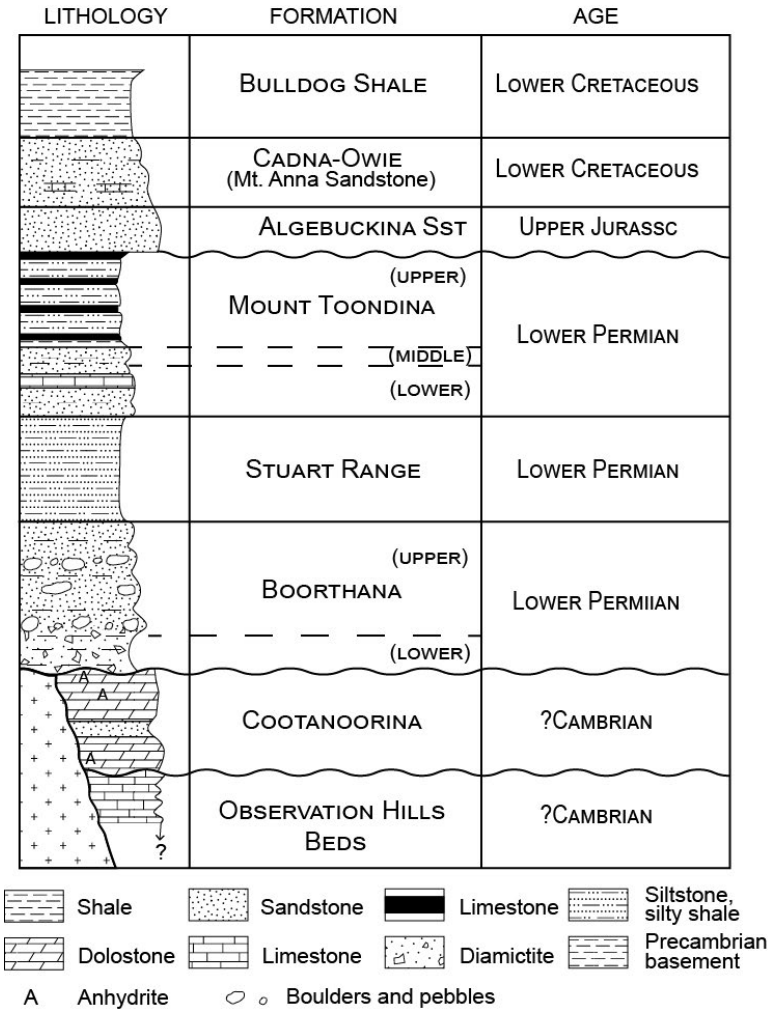

Figure 3:2 Idealised composite section of the Arckaringa Basin, succession from the Precambrian basement to the Cretaceous sediments that are typically exposed on the surface. Adapted from Townsend (1973).

3.1.1 Geological setting

The late Palaeozoic Arckaringa Basin is an intracratonic basin that covers approximately 80 000 km^2 of central South Australia (Figure 3:1). The basin is mostly covered by younger sedimentary rocks. Limited

exposures of late Palaeozoic sedimentary rocks are located along the north-eastern, eastern and southwestern margins of the basin (Figure 3:1; Hibburt 1995). The Boorthanna and Phillipson Troughs on the eastern and southern edge of the Arckaringa Basin respectively are the main depocentres (Figure 3:1; Hibburt 1995).

The Arckaringa Basin overlies Precambrian Gawler Craton basement (Figure 3:2). The basin is bound to the east by the Peake and Denison Ranges, to the south by the continuation of the Gawler Craton and to the west by the Officer Basin (Figure 3:1). Possible occurrences of late Palaeozoic sedimentary rocks in drill holes in the Everard Ranges suggest that the basin may extend at least 100 km further to the west (Alley et al. 1995).

Arckaringa Basin sedimentary rocks are thickest in the Boorthanna and Phillipson troughs (Figure 3:1). Both have at least 1000 m of late Palaeozoic sedimentary rocks as defined by drilling and geophysical surveys (Townsend 1973, Townsend and Ludbrook 1975, Hibburt 1995). Smaller, shallower troughs, including the Tallaringa, Wintinna, Karkaro, Mount Furner and Wallira troughs (Figure 3:1), have been identified in the west of the basin (Townsend 1973, Alley et al. 1995).

The eastern edge of the Boorthanna Trough (Figure 3:1) is bound by a NNW trending fault, movement along which resulted in horst-like uplift of the Peake and Denison Ranges (Figure 3:3; Townsend 1973). The southern margin of the Tallaringa Trough (Figure 3:1) is also fault bound (Figure 3:3; Townsend 1973). Townsend (1973) surmised that the network of troughs and basement highs within the Arckaringa Basin are all controlled by bounding faults. Wilmot (1987) suggested that development of the Boorthanna Trough was initiated during the late Proterozoic to Early Cambrian (ca 500-540 Ma) by extensional reactivation of the former Adelaide Rift Complex area, or by fault activity within a region of crustal weakness around the northeastern edge of the Gawler Craton. Syn-depositional faulting continued through the Neoproterozoic to the late Palaeozoic (Wilmot 1987, Rogers et al. 1996a, Alley et al. 1995). Menpes et al. (2010) proposed that the Phillipson and Wallira Troughs (Figure 3:1) were formed by glacial scouring. Seismic interpretations show the troughs are fault controlled and most likely deepened by glacial scouring during the Permo-Carboniferous glaciation (Wilmot 1987). These troughs were later filled with late Palaeozoic sedimentary rocks. Most of the Arckaringa Basin is covered with the lower Cretaceous Cadna-Owie Sandstone, Bulldog Shale or upper Jurassic Algebuckina Sandstone (Figure 3:2; Townsend 1973, Hibburt 1995).

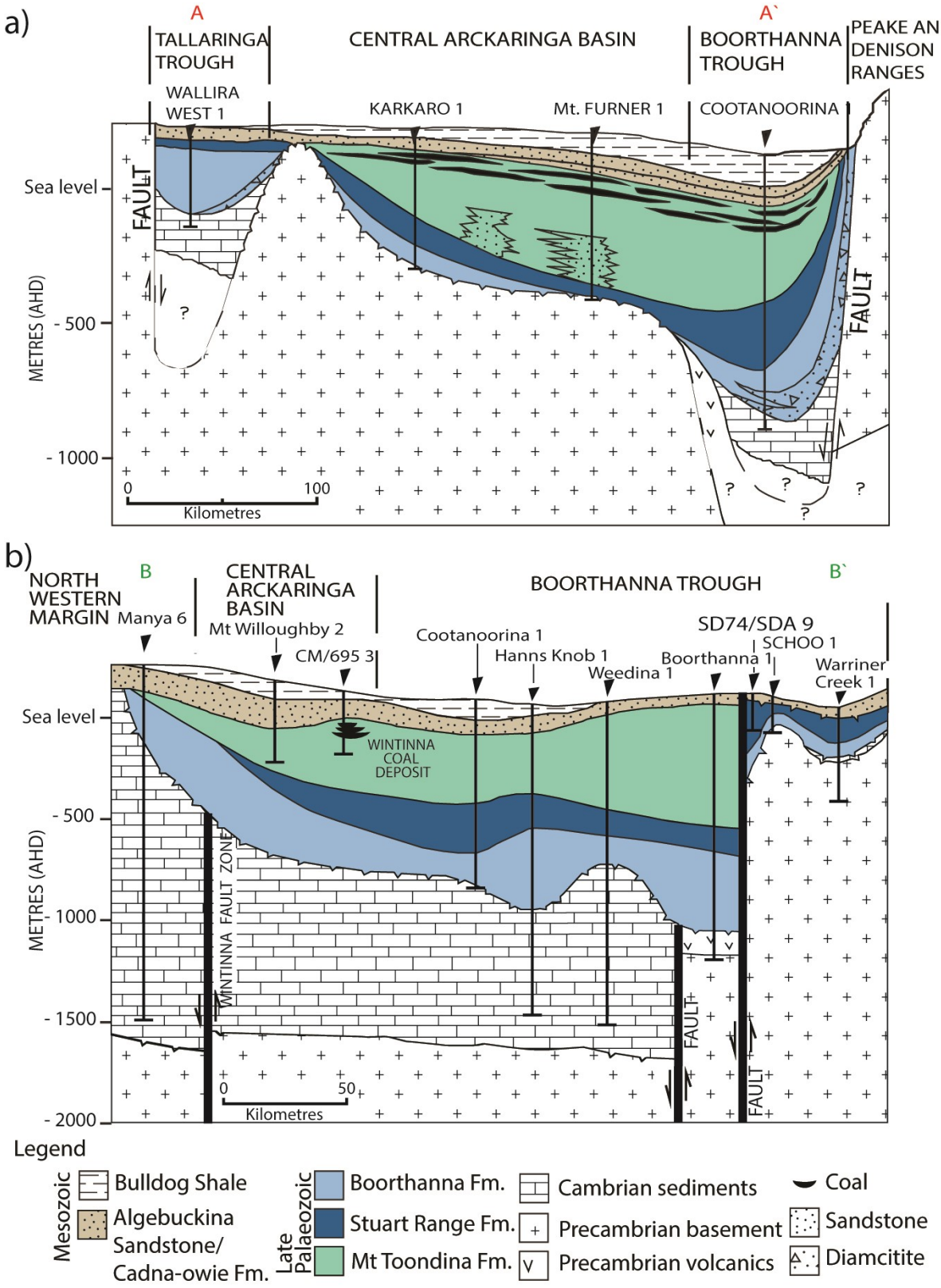

Figure 3:3 Schematic cross section of a) the Arckaringa Basin from the western Tallaringa Trough across the central basement high to the top of the Boorthanna Trough adapted from Townsend (1973); and b) Subsurface stratigraphy based on drilling from the north western margin on the Arckaringa Basin through the central basin to the southern Boorthanna Trough adapted from Hibburt (1995). Cross section locations shown in Figure 3:1.

Glacial sedimentology

Sediment deposited from continental, wet-based icesheets are typically thin (generally less than 100 m thick; Ashley et al. 1985). The glacial sedimentary rocks extend for hundreds, and in some instances thousands, of kilometres. Preserved sedimentary rocks are generally restricted to discrete basins where the continental glaciers caused depressions and forebulge, resulting in the formation of basins and topographic highs. The discrete basins were depocentres for the glacial sedimentary rocks (Ashley et al. 1985, Bennett and Glasser 2009).

Sedimentary rocks deposited by wet-based glaciers are typically dominated by a basal unit of lodgement till (Ashley et al. 1985, Bennett and Glasser 2009). The composition of the lodgement till varies depending on the underlying geology so that where the glacier has moved over hard basement rocks the majority of the lodgement till includes material it directly overlies. Where the glacier has moved over more easily eroded materials the lodgement till is deposited in a greater thickness in topographic lows such as basins. The till is a locally diverse sediment and may not possess a strong particle fabric (Bennett and Glasser 2009). The lodgement till can be interrupted locally by subglacial rivers, which rework the sedimentary rocks into sands and gravel beds (Bell 1998). Other sedimentary rocks typically in the glacial succession, such as glaciolacustrine and flow till sedimentary rocks, are not unique to wet-based glaciers (Ashley et al. 1985). Therefore the distribution and thickness of the lodgement till is the most diagnostic feature for a wet-based glacial environment (Ashley et al. 1985). Surface features such as glacially polished and striated pavements may also be indicative of wet-based glacial activity (Ashley et al. 1985).

Arckaringa Basin stratigraphy

The late Palaeozoic Boorthanna, Stuart Range and Mount Toondina Formations of the Arckaringa Basin are a succession of glacial, marine and freshwater deposited sedimentary rocks (Figures 3:1, 3:2, 3:3; Alley et al. 1995). These units have been defined based on lithological and geophysical logs of drill holes and in mapping of areas around Mount Toondina and the Peake and Denison Ranges (Freytag 1965, Allchurch and Wopfner 1967, Ludbrook 1967, Townsend and Ludbrook 1975, Holmes and Rayment 1970). Exposures of these sedimentary rocks are poor and not representative of complete formations; cored sections of drill holes are limited and existing stratigraphic and geophysical log quality is poor. The lack of reliable data implies that stratigraphic definitions are incomplete (Hibburt 1995). The age, sedimentology and depositional setting of the stratigraphic units are summarised in Table 3:1.

Table 3:1 Summary table of characteristics, age and depositional setting for each of the late Palaeozoic stratigraphic units within the Arckaringa Basin. Unit characteristics are based on observations by the author and Allchurch and Wopfner (1967), Townsend and Ludbrook (1975), Wilmot (1987), Hibburt (1995) and Rogers et al. (1996b). Age of the units is constrained by palynological studies by [1,2]Ludbrook (1961, 1967), [3]Jones (1987) and [4]Hibburt (1995). Palaeoenvironmental interpretation is based on observations made by [a]Freytag (1965), [b]Allchurch and Wopfner (1967), [c]Townsend and Ludbrook (1975), [d]Wilmot (1987), [e]Hibburt (1995), [f]Rogers et al. (1996b) and [g]Tucker (1997).

Unit, age	**Overall unit characteristic**	**Palaeoenvironmental interpretation**
Mount Toondina Formation, Artinskian to Sakmarian age (290 to 285 Ma)[5]	Upper: lacustrine shale and minor fluvial clastics, carbonaceous and includes intervals of coal Middle: sandstone and siltstone Lower: shale and minor beds of sandstone	Upper: freshwater origin with the characteristics of a lake-bottom with alternating with fluvial input; peat swamps [a,d,e] Middle: deltaic [d] Lower: anoxic marine lacustrine environment [e]
Stuart Range Formation	Homogeneous shale with minor clay and siltstone	restricted-marine lagoons and swamps with intermittent deposition of fluvial sands [c]
Boorthanna Formation, Sakmarian-Asselian age (295 – 290 Ma)[1,2,3,4,5]	Upper unit: rhythmically bedded sandstone and diamictite with boulder to pebble-sized clasts within a matrix of medium to coarse-grained sand Lower unit: Basal diamictites overlain by calcareous, sandy to bouldery claystone interbedded with shale, sandstone and carbonate beds	Upper: glacial debris deposited in a marine environment by turbidity currents [b,e,g] Lower: glacial debris transported by mudflows and meltwater flows [c,f,g]

3.2 Methods

3.2.1 Sample collection

Suitable sites for logging and sampling were selected based on the exposure being extensive enough to allow sampling through the stratigraphic profile. Profiles sampled for this study were from Mount Dutton, Box Creek and Mount Toondina (Figure 3:1). Some sections are in the same or similar locations to the locations as investigations by previous researchers. This occurred as these sites were the most complete, best exposed and accessible sections across the basin. The previous studies provided a guide to the basic lithology of the sedimentary rocks.

Samples were collected at each change in lithology or every metre if no change occurred. Five to ten centimetres of overlying material was removed prior to sample collection to reduce risk of surface contamination. Approximately 0.5 kg of sample was then removed using a geo pick and put into a clean, plastic, snap lock bag. Each bag was labelled with a predetermined sample number and location name. For each sample, a GPS location was recorded along with a description of the sediment lithology and any overprinting and weathering that was apparent. Surrounding field relationships were also recorded as well as information such as vegetation growth or proximity to possible contaminants such as dust from tracks. Samples were collected for investigations into the petrography and mineralogy of the sedimentary rocks as well as detailed sedimentological descriptions. Splits of selected samples

were also used for geochronological and geochemical analysis. The samples were of varied lithologies which included sand, clay, silt and diamictite with varying degrees of weathering.

3.2.2 Mineralogical analysis

The bulk mineralogy of samples was investigated using petrographic and spectroscopic analysis. Petrographic analysis of thin sections determined relationships between grains and matrix as well as alteration. Petrologic analysis was performed on representative samples from each section. Samples were selected so as to represent each of the preserved units, with minimal post-depositional alteration, and as being consolidated where possible.

Polished petrological thin sections (dimensions: 7.5 by 2.5 cm) of consolidated sediment were prepared by Pontifex and Associates Pty. Ltd., Adelaide. Petrographical analysis was done on selected samples from each measured section at Adelaide Microscopy, University of Adelaide using a Nikon Petrographic Microscope.

A representative split of rock chips from each sample collected was placed into black chip trays and analysed using the HyLogger™3-3 at the Department of State Development Core Storage Facility in Glenside, Adelaide. HyLogger™ Core Scanning and HyChips™ modes were used to detect the visible to shortwave infrared (Vis-SWIR: 380-2500nm) wavelengths, and the thermal infrared wavelengths (TIR: 6000-14500nm, core logging mode only). The minerals identified using infrared wavelengths include white micas, kaolinite, carbonate minerals in the SWIR, and tectosilicates such as pyroxene, silica, feldspars and garnets in the TIR. High resolution images were taken on every sample every 2mm. HyLogger™ core logging mode analysis was done by scanning across each sample four times, allowing for overlap to maximise the viable spectra. HyChips™ mode analysis was done by scanning three times using only Vis-SWIR wavelengths. Three readings were taken per sample.

Results were processed using The Spectral Geologist (TSG) HotCore software to allow viewing in the free TSG Viewer software provided by AusSpec International Inc. Data processing included removal of data from any non-sample material (e.g. black plastic of the chip trays). Processing did not account for geological context of the samples or removal of any specific mineral species prior to processing. Routine machine calibrations were performed prior and post-analyses.

3.3 Sedimentology and mineralogy

As exposures of late Palaeozoic sedimentary rocks are sparse and scattered along the eastern margin of the Arckaringa Basin, it was necessary to go to several sites. This enabled the observation of the changing facies of the formations as well as the sampling of these facies.

3.3.1 Mount Dutton sections

Mount Dutton is located to the NE of the Arckaringa Basin (Figure 3:1). Late Palaeozoic sedimentary rocks of the area have been previously described by Heath (1963, 1965). Sedimentary rocks were collected from five locations (Figure 3:4a).

The lowermost unit is best exposed at site one (0 to 1 m; Figure 3:4a) as approximately 2000 m long, 500 m wide field of scattered cobbles and boulders (Figure 3:4c, 3:5a). The cobbles and boulders are

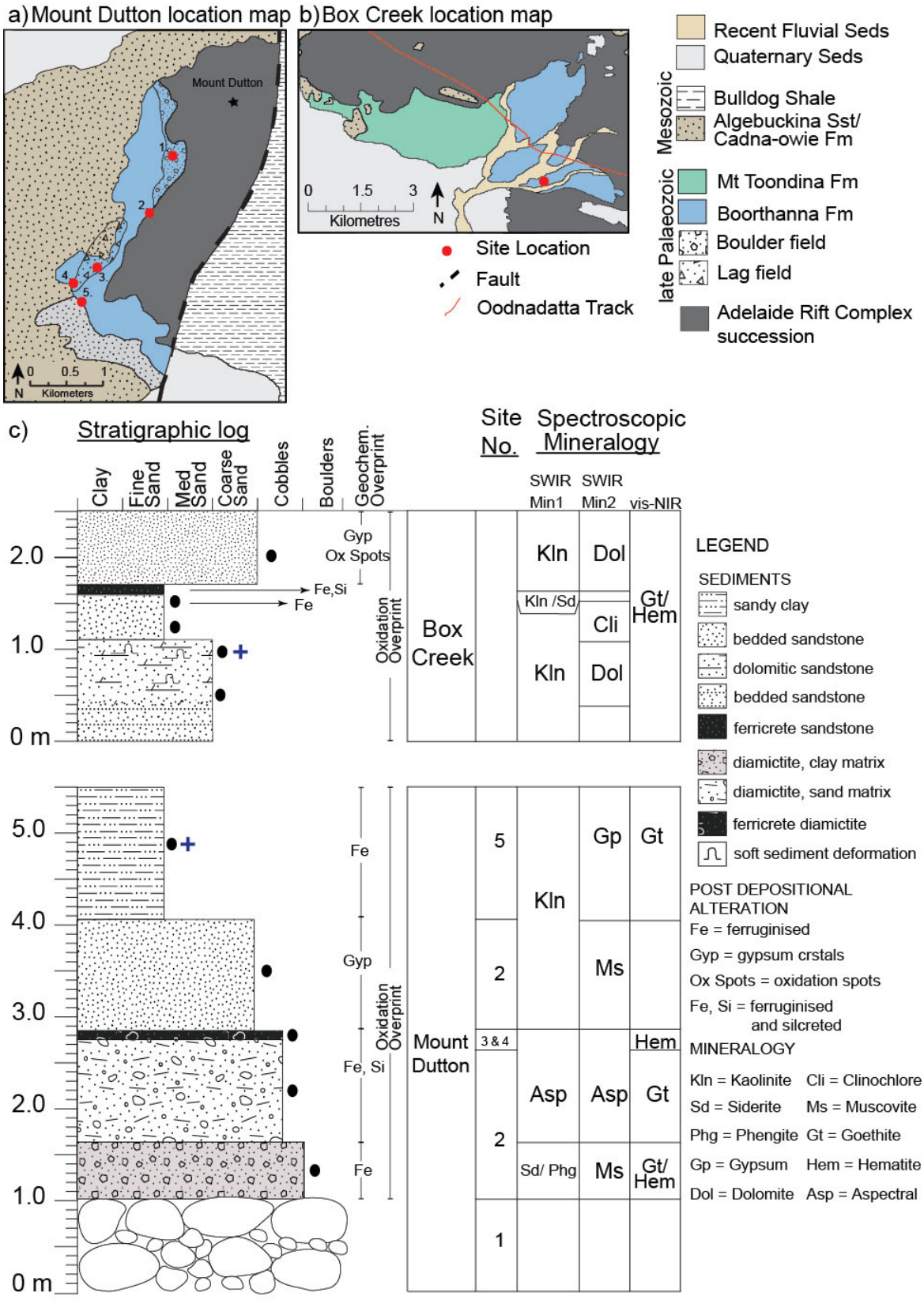

Figure 3:4 Broad regional geology of the a) Mount Dutton and b) Box Creek, adapted from Heath (1963) and Rogers et al. (1996a) showing sample site location; b) Composite stratigraphic log of the sedimentary rocks incorporating sample site locations and the spectroscopic mineralogy. The location of Box Creek and Mount Dutton is shown in Figure 3:1. Black dots: HyLogger™ sample; blue cross: sample used for petrographic analysis.

typically between 10 and 50 cm in diameter although some are several metres. Most of the cobbles and boulders (approximately 80%) are rounded, elliptical, fine-grained quartzite, with subordinate shale, dolomite and minor porphyry and granite gneiss. Approximately half of the cobbles and boulders are polished and have at least one striated and faceted surface.

The lowermost unit (1 to 1.6 m) passes conformably upward into a 0.6 m thick, pebbly, matrix-supported diamictite with a clay-sized purple matrix that is best exposed at site two (Figures 3:3a, 3:4b). The clasts are rounded to subangular, fine-grained quartzite up to 20 mm in diameter. Hyperspectral analysis identified siderite, phengite, muscovite, goethite and hematite within the matrix (Figure 3:4c).

The pebbly diamictite is overlain by a 1m thick, variably silicified and ferruginous pebbly, matrix-supported diamictite with a coarse-grained sandstone matrix (1.6 to 2.75 m). This diamictite contains subangular to rounded, dominantly quartzite clasts up to ten millimetres (Figures 3:5c, d). The upper surface of this unit (2.75 to 2.85 m), forming a 2000 by 200 m land surface exposed at sites three and four (Figure 3:4a), is dominated by 1 to 10 cm fragments of ferricrete and quartzite (Figure 3:5d).

The ferruginised diamictite passes upward into a 1.2 m thick of fine-grained sand with clay cement (2.85 to 4.1 m). The sand is unconsolidated and pale to grey-green with orange Fe-oxide mineral mottles. The sand-sized component is dominated by quartz, with trace muscovite and lithic fragments. The cement is dominantly Fe-oxide and kaolinite (Figure 3:4c).

The sand passes upward into an approximately one metre thick green, unconsolidated sandy clay that is best exposed at site five (Figure 3:4a, c). This unit from 4.1 to 5.5 m, is laminated at millimetre-scale with alternating clay and medium-grained sand beds (Figures 3:5e, f). The clay beds consist of closely packed and well sorted quartz and clay in roughly equal portions, with patches of Fe-oxide minerals (Figure 3:5c). Patches of high Fe-oxide mineral concentration within the clay beds are darker and quartz-poor (<5% quartz). The sand laminae contain subrounded to angular and poorly sorted quartz grains ranging between 10 and 100 µm size within a matrix of clay and Fe-oxide. Lithic fragments and muscovite account for approximately 2% of the rock (Figures 3:5e, f). The volume of pore space in the sand laminae is variable (0 to 15%); where pore space is minimal, Fe-oxide mineral cement is dominant.

Next page: Figure 3:5 Mount Dutton; a) Striated boulder approx. 100 cm long and 30 cm wide from the erratic field (site 1); b) lodgement till diamictite with rounded to angular clasts from 1.2 m; c) Ferricrete fragments that makes up the area between sites three and 4; d) Pieces of ferricrete that dominate the land surface of sites three and 4, small quartz pebbles can be seen within the samples from 2.8 m; e) Photomicrograph of the sandy clay showing clay and sand laminae from a sample collected from 4.9 m; f) Photomicrograph of very fine-grained sand laminae within sandy clay showing a dominant kaolinite and Fe-oxide mineral cement region amongst poorly sorted quartz grains. Sample is the same as the previous photomicrograph of 3:4e. Qtz: quartz; kln: kaolinite; Ms: muscovite; cly: clay minerals; Fe: Fe-oxide mineral cement; Fe/Kln: kaolinite and Fe-oxide mineral cement; PS: pore space.

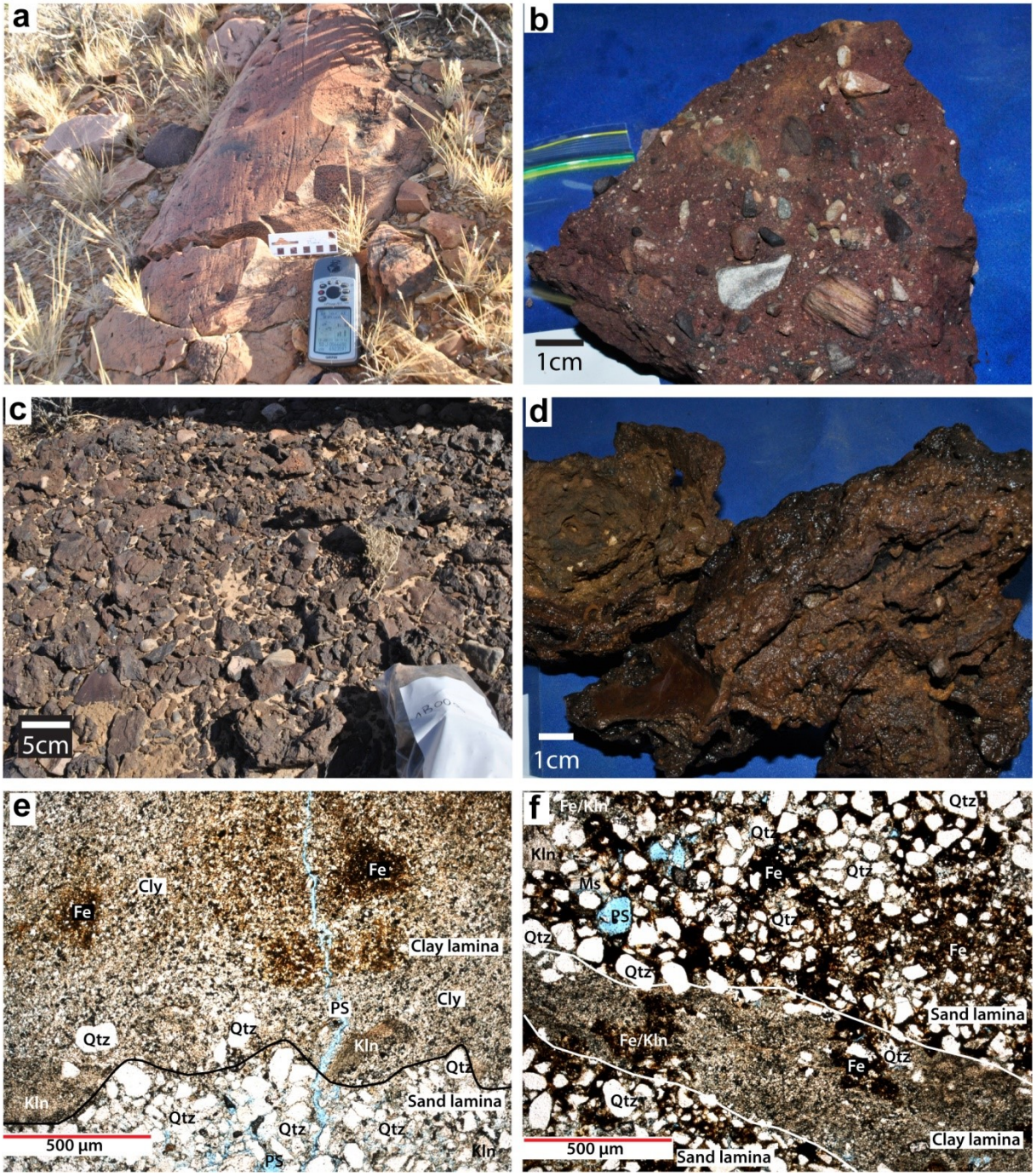

3.3.1 Box Creek area section

Box Creek crosses the Oodnadatta Track northwest of William Creek (Figure 3:1a) on the southeastern edge of the Arckaringa Basin. The site investigated (Figure 3:4b) is a ~2.5 m high creek terrace wall composed of sandstone (Figure 3:4c, 3:6a). The sedimentary rocks at Box Creek have not had any detailed sedimentological descriptions except for a brief reference in Parkin (1956).

The base of the section at Box Creek is a 1.2 m buff to yellow, fine-grained sandstone (Figure 3:4c). The sandstone is moderately-sorted with subrounded to angular quartz grains between 50 and 200 microns. The lower 0.5 m of this unit is thinly laminated, dominated by quartz in a cement of kaolinite, goethite and hematite (Figure 3:6c). From 0.5 to 1.2m, the sandstone cement becomes dolomitic, the

laminations become less frequent and there are decimetre-scale soft sediment deformation features (Figure 3:6b).

The basal sandstone (0 to 1.2 m) is overlain by 0.5 m of buff to pale pink, very fine-grained quartz sandstone (Figure 3:4c) with minor lithic fragments (1.2 to 1.7 m). The quartz grains have irregular, subrounded to angular shapes and range from 100 to 200 µm (Figures 3:7c, d). Millimetre-scale laminations are defined by subtle variation in grain size. Fine-grained laminations have closely packed quartz grains that average 50 µm (Figure 3:6d). Coarse-grained laminations are defined by grains from 100 to 200 µm and larger pore spaces than the fine-grained laminae (Figure 3:6d). The cement consists of Fe-oxide minerals (goethite and hematite), kaolinite and Mg-chlorite (Figures 3:6c, d). In the top ten centimetres of the unit (1.6 to 1.7 m), chlorite is absent and siderite is present (Figure 3:4c). This horizon has been ferruginised and silicified. The original cements have been replaced, and most pore space is filled by Fe-oxide minerals (Figure 3:5d). The fine-grained sandstone is overlain by a 0.8 metre thick (1.8 to 2.5 m) internally massive coarse-grained quartz sandstone with a cement of kaolinite, dolomite and Fe-oxide minerals (Figure 3:4c).

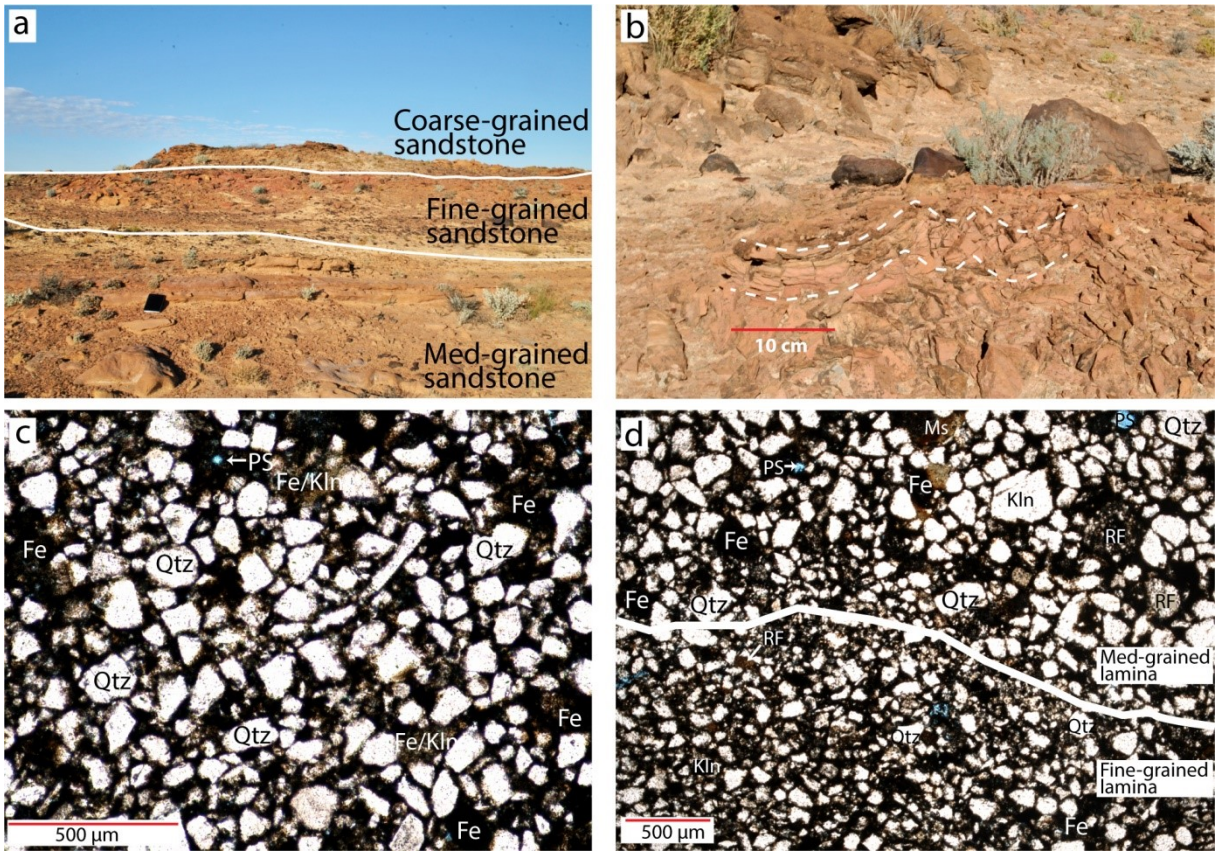

Figure 3:6 a) Box Creek sandstone profile showing different grain sizes throughout the profile. Profile is approximately 2.5 m height; b) Soft sediment deformation (highlighted by white dashed lines) at the 0.9 to 1.1 m; the top of the basal medium-grained sandstone; c) Photomicrograph of the medium-grained sandstone from Box Creek showing a coarse portion on the sandstone and the variation in grain shapes. Sample collected from 1.0 m; d) Photomicrograph of the medium-grained sandstone from Box Creek showing a lamina of very fine-grained to clay sized quartz grains within the fine-grained sandstone Sample is the same as the previous photomicrograph of 3:5c. Qtz: Quartz; Kln: Kaolinite; Ms: Muscovite; RF: rock fragment; Fe: Fe-oxide mineral cement; Fe/Kln: kaolinite and Fe-oxide mineral cement; PS: pore space.

3.3.2 Mount Toondina section

Mount Toondina is in the northeast of the Arckaringa Basin (Figure 3:1). Various levels of the late Palaeozoic stratigraphy are exposed due to the interplay of uplift and erosion (Figures 3:7a, 3:8a, b). These sedimentary rocks have been previously described by Freytag (1964, 1965), Youles (1976), Wopfner (1977), and (Hibburt 1995). An approximately 80m section of late Palaeozoic sedimentary rocks are exposed within a northeast to southwest oriented channel (Figures 3:7a, 3:8a).

The easternmost (and lowermost) 12m of the section is an upward fining sequence of laminated medium to fine grained quartz-rich sandstones and siltstones. This includes two 50 to 100 cm thick horizons of mixed silt and lignite that are laminated at millimetre to centimetre-scale (Figure 3:7b). The sandstone laminae consist of subangular quartz grains and occasional kaolinitic clasts up to 100 µm size. The sandstone has visible pore space between the quartz grains (Figure 3:7b, 3:8c). The pore space between these quartz grains has been in-filled with kaolinite and minor Fe-oxide minerals. Small, rounded lignite grains are preserved outside of the lignite bands (Figure 3:7b, 3:8c).

Carbonaceous units become more abundant from 30 to 65 m where they account for approximately 40% of the sequence (Figures 3:7b, 3:8a). These include shale, silt and sandstones interbedded at metre-scale, with variable organic content ranging from a few percent to near 100% within discrete 1 to 2m wide bands of lignite. The lignite is unconsolidated and poorly exposed (Figures 3:8b). The inorganic component of the carbonaceous sandstones is dominated by quartz with kaolinite cement (Figure 3:4c). The westernmost (uppermost) 15m of the section consists of fine to medium-grained sandstones and siltstones, within an upward coarsening sequence.

This sequence is steeply southwest dipping and dissected by numerous faults. No younging indicators were observed, and observations follow Freytag's (1965) interpretation that the sequence youngs to the southwest. The possibility that the apparent mirror symmetry of the section is the result of a structural repetition cannot be ruled out. The section consists of a sequence of dominantly fluvial and lacustrine, laminated, carbonaceous sandstones, siltstones and shales (Figure 3:7a).

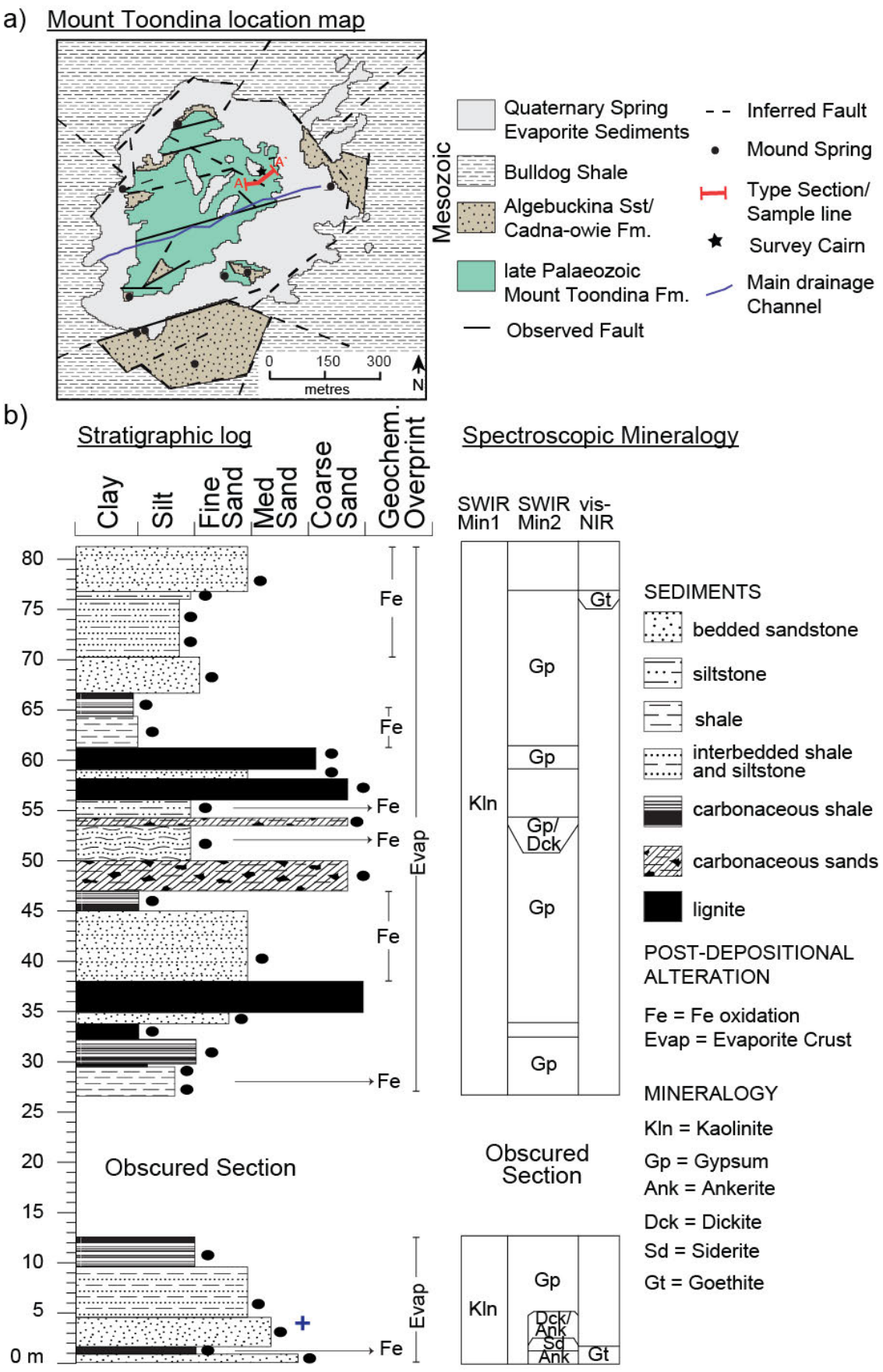

Figure 3:7 a) Regional geology of Mount Toondina adapted from Freytag (1965); b) Stratigraphic log of the sedimentary rocks incorporating the sample line (left) and spectroscopic mineralogy. The location of the Mount Toondina area is shown in Figure 3:1. Black dots: HyLogger™ sample; Blue cross: sample used for petrographic analysis.

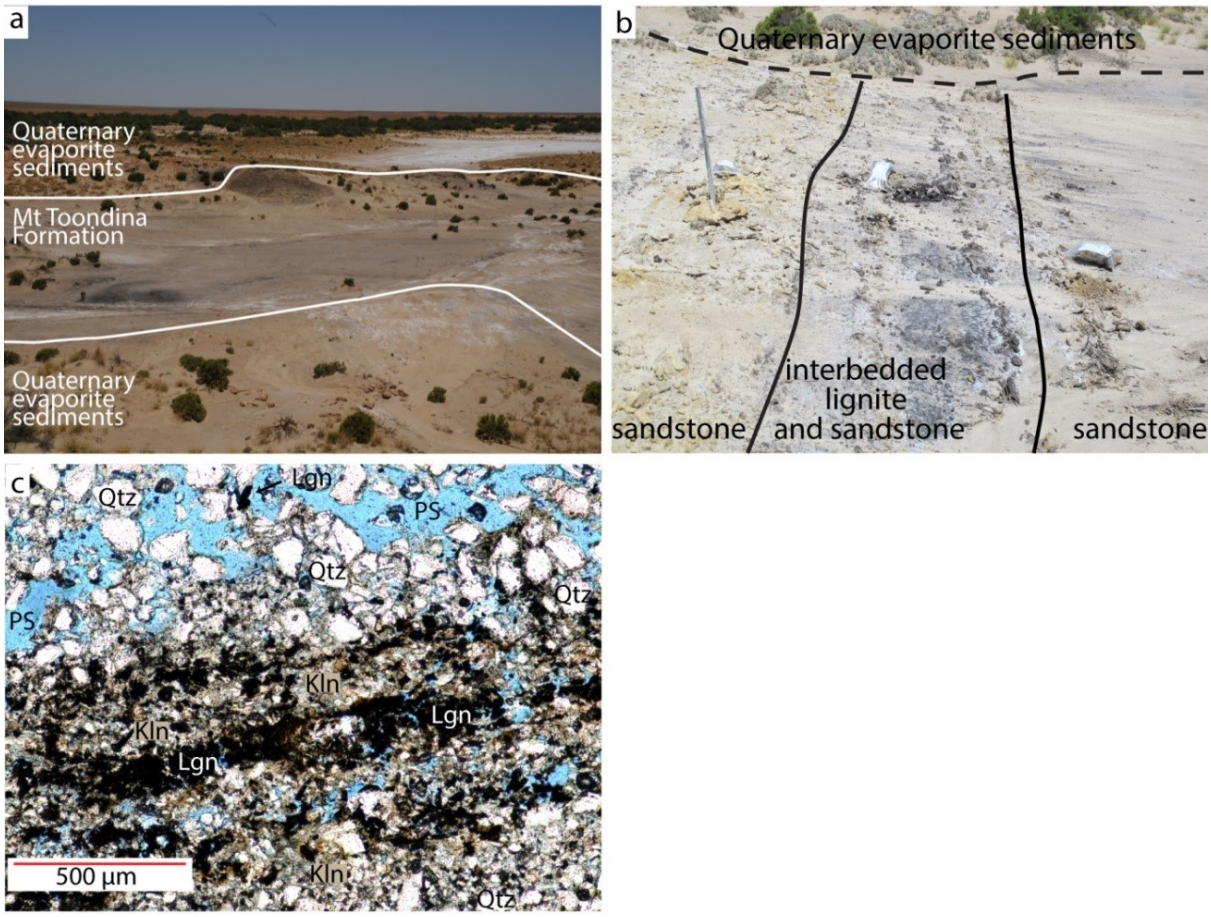

Figure 3:8 a) Part of the channel along which the Mount Toondina section was mapped showing the exposed stratigraphy as well as the younger evaporate crust that obscures the underlying late Palaeozoic sedimentary rocks. The late Palaeozoic carbonaceous sedimentary rocks are distinguishable by their dark grey colour. Photo taken looking northeast; b) Upper five metres of the section (76 to 81 m) showing interbedded sandstone and lignite. The stake signifies the top of the section; c) Photomicrograph of the interbedded sandstone and lignite from the base of the section (at four m). Small laminations of sandstone are observed within the lignite beds.

3.4 Discussion

3.4.1 Stratigraphic correlation

Given the discrete exposures of the Arckringa Basin succession in the Boorthanna Trough, there have been few detailed studies that correlate between the surface exposures of the Boorthanna and Mount Toondina formations or with the subsurface type sections. The exposed sedimentary rocks of the Arckaringa Basin investigated here have been compared with previously described subsurface type sections to place them in the correct stratigraphic context (Figure 3:8). The type section of the basal Boorthanna Formation is in the Boorthanna 1 drill hole (Figure 3:1). The type sections of the Stuart Range Formation and Mount Toondina Formation are in the Cootanoorina 1 drill hole (Figure 3:1; Townsend and Ludbrook 1975).

The correlation of units across the Boorthanna Trough will allow spatial distribution of the units to be assessed, leading to better understanding of basin-wide variations in depositional setting. The stratigraphic correlations made here (Table 3:1; Figure 3:8) are based on the unit descriptions of Townsend and Ludbrook (1975) together with interpretations based on the facies analysis approach

of glacigene settings described by Eyles et al. (1983), Miall (2000) and Hambrey and Glasser (2012). The approach in facies analysis of glacigene rocks and the interpretation of the depositional processes is based on the identification of key sedimentary characteristics, in particular sedimentary structures and the relationship of these characteristics with depositional processes. Given the weathered nature and lack of well-preserved sedimentary structures in the sections it is not possible to use these facies definitions as intended by Eyles et al. (1983) and Miall (2000), however, where possible the relationships between the glacigene sedimentary rocks and depositional processes have been assessed.

The diamictite at Mount Dutton (Figure 3:4c) has previously been described as being part of the Boorthanna Formation by Heath (1963) and Freytag et al. (1967), however no direct correlation to the type sections have been made. The diamictites in the lower Boorthanna Formation are the only diamictite unit recognised in the type sections of the late Palaeozoic sedimentary rocks in the Arckaringa Basin (Townsend and Ludbrook 1975). Here, the sedimentary rocks at Mount Dutton are correlated with the diamictite of the lower unit of the Boorthanna Formation type section (Figure 3:9).

The sandstone section and lag deposits at site one at Box Creek (Figure 3:4b) have also been correlated with the Boorthanna Formation. More specifically, the sedimentary rocks likely correlate with the upper part of the sandstone unit in the Boorthanna 1 that directly overlies the diamictite (Figure 3:9). Within this unit there are occasional clasts and erratics as well as rare pebbles that may be representative of the lag deposits scattered around site one. The sandstone section correlates with a sandstone bed between siltstone beds that dominate this part of the type section. This correlation was suggested by Rogers et al. (1996b) although no direct correlation with Boothanna 1 was made.

The section at Mount Toondina (Figure 3:7a) was the type section for the Mount Toondina Formation prior to the identification and interpretation of the more complete sedimentary rocks of the Mount Toondina Formation in Cootanoorina 1 (Freytag 1965, Townsend and Ludbrook 1975). The Mount Toondina section was then correlated with the upper part of the reinterpreted Mount Toondina Formation subsurface type section (Townsend and Ludbrook 1975; Figure 3:9). This correlation is based on the upper unit of the Mount Toondina Formation being more carbonaceous than the lower units and has been maintained in this study.

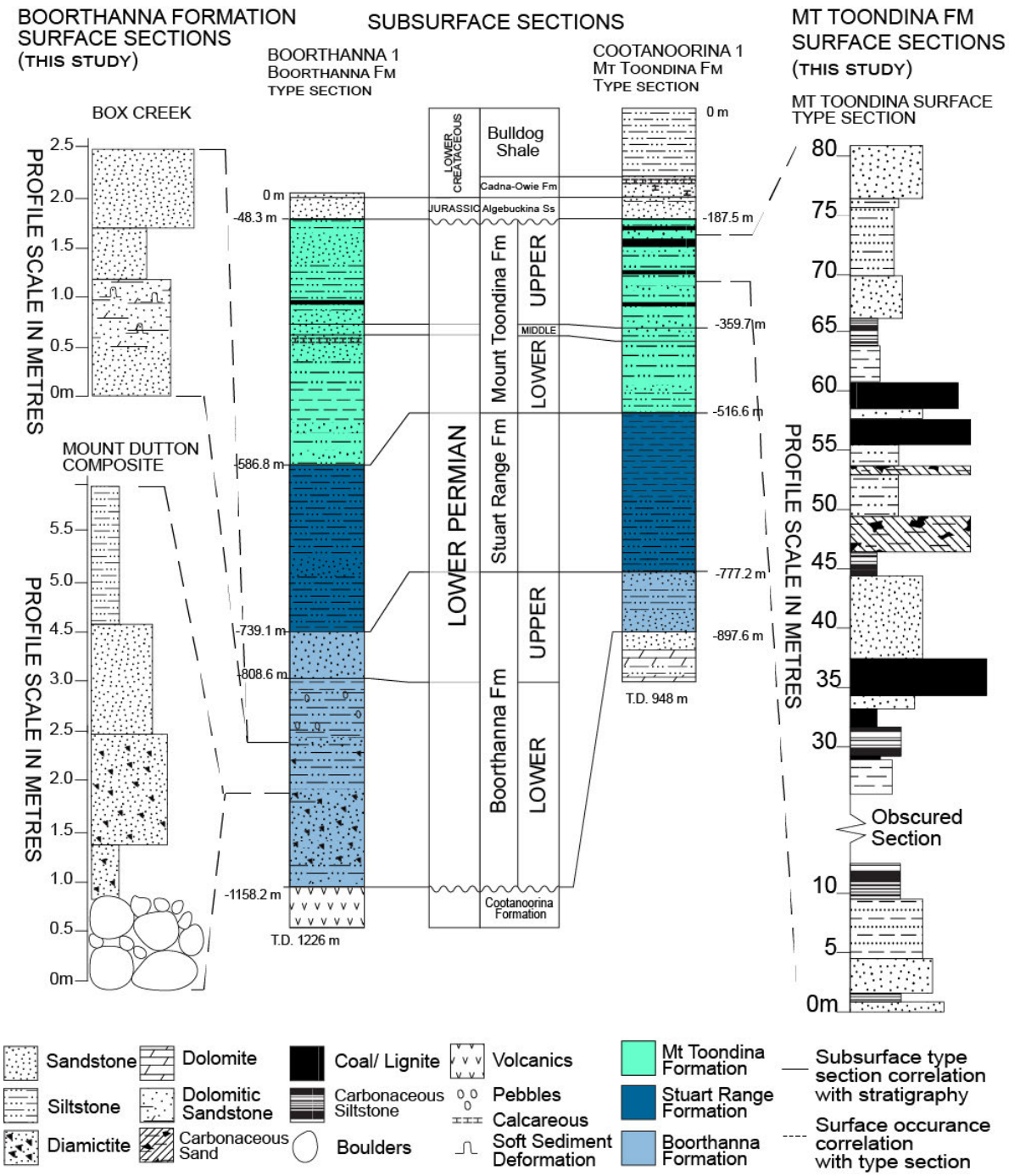

Figure 3:9 Stratigraphic columns showing the subsurface type sections for the Boorthanna, Stuart Range and Mount Toondina Formations within drill holes Boorthanna 1 and Cootanoorina 1 adapted from Townsend and Ludbrook (1975), and the correlative surface stratigraphic logs for each of the sites investigated in this study. The locations of drill holes are shown in Figure 3:1. See Figures 3:4c and 3:7b for detailed stratigraphic logs of surface sections.

3.4.2 Depositional setting of late Palaeozoic sedimentary rocks

Depositional reconstructions for the late Palaeozoic sedimentary rocks in southern Australia suggest that during the time when Gondwana was at high latitudes and close to the south pole a continental-scale, wet-based icesheet moved from Antarctica through southern Australia and rapidly advanced northward and eastward covering most of South Australia (e.g. Crowell and Frakes 1971a, 1971b, Alley

and Bourman 1984, Bourman and Alley 1988, 1995, 1999). The icesheet retreated in a south to south south-easterly direction followed by a marine transgression and subsequent regression. The basin was then dominated by freshwater conditions where fluvial and lacustrine conditions alternated. The late Palaeozoic stratigraphic units of the Arckaringa Basin reflect the major changes in the depositional processes as the climate transitioned from glacial (Boorthanna Formation) to marine (Stuart Range Formation) to terrestrial freshwater (Mount Toondina Formation; Townsend and Ludbrook 1975).

In this section, the depositional setting of each late Palaeozoic unit within the Arckaringa Basin is described. The previously suggested depositional processes are summarised, then the favoured depositional setting is described in detail with supporting evidence highlighted.

Depositional setting of the Boorthanna Formation

Diamictite and sandstone of Boorthanna Formation were observed at Mount Dutton and Box Creek (Figure 3:4). The sedimentary rocks at both sites have been correlated with the lower Boorthanna Formation in the subsurface type section (Figure 3:9; Townsend and Ludbrook 1975). It is largely accepted that the Boorthanna Formation was deposited during the glacial maximum and into the initial deglaciation (e.g. Freytag 1964, DeMaison 1969, Townsend 1973, Townsend and Ludbrook 1975, Wopfner 1977, Alley et al. 1995). The basal diamictites of the Boorthanna Formation are not as widespread as the rest of the formation, and are mainly restricted to the eastern edges of the troughs, especially the Boorthanna and Tallaringa troughs (Figures 3:3). Both Heath (1965) and Wopfner (1977) generally suggested that the diamictite of the Boorthanna Formation was deposited via an icesheet. However, the mechanisms for diamictite are varied and may include deposition via valley or ice tongue glaciers or icesheets (Bennett and Glasser 2009, Singh and Haritashya 2011) by way of direct glacial, glaciofluvial or glaciolacustrine deposition (Eyles et al. 1983, Ashley et al. 1985, Miall 2000, Hambrey and Glasser 2012).

As the exposures of the Boorthanna Formation investigated are far from complete and lack continuity it is difficult to assess the depositional mechanisms. However, using the characteristics of the sedimentary rocks, particularly the diamictites, the potential depositional mechanisms have been evaluated using principles of glaciology as well as facies analysis.

As the matrix of the cobbles and boulders of the erratic field was not observed it is difficult to assess the setting in which deposition occurred. The high proportion of faceted and striated clasts (~80%) at Mount Dutton (Figure 3:5a) suggest a temperate glacial setting (Eyles et al. 1983, Hambrey and Glasser 2012) as cold-based glaciers do not have the erosional capacity due to the lack of frictional force and associated meltwater streams (Miall 2000, Bennett and Glasser 2009, Hambrey and Glasser 2012). Eyles et al. (1983) observed that debris flows from wet-based, temperate glaciers typically result in faceted clasts observed as boulder pavements. Eyles et al. (1983) also associated boulder units with massive, matrix-supported diamictites filled the lee-side of glacially formed landforms (such as the side of a ridge as observed at site one of Mount Dutton; Figure 3:4) with supraglacial deposition within a valley glacier setting. Benn et al. (2003) suggests that basal diamictite units deposited at the terminus of valley glaciers are typically clast-supported and imbricated and that fluvially rounded clasts such as those observed in the erratic field at Mount Dutton are typically observed in deposits from debris-covered valley glaciers.

The characteristics of the diamictite of the Boorthanna Formation at Mount Dutton and Box Creek are that it is massive and matrix-supported with angular to rounded pebble-sized clasts within a clay to coarse-grained sandstone matrix. Eyles et al. (1983) have correlated massive, matrix-supported

diamictite deposits with angular to rounded clasts with no preferential orientation with supraglacial valley glacier deposition. When deposited in a sedimentary trough between a glacier and valley side, diamictites with these characteristics are frequently interbedded with fluvioglacial sediments (Eyles et al. 1983, Eyles and Miall 1984 and Miall 2000). Benn et al. (2003) also associated sandy diamictite with overlying laminated fine sediments with deposition at an ice/meltwater contact such as at the edge of a valley glacier. Bennett and Glasser (2009) suggest that icesheet deposited basal diamictite typically has a higher portion of angular, locally-derived clasts than the diamictite deposited by valley or ice tongue glaciers. The latter are typically deposited by a combination of meltwater and glacier debris flow with clasts that are rounded to angular and locally- and distally-derived within a matrix that is coarse-grained to clay (Bennett and Glasser 2009). Eyles et al. (1983), Miall (2000) and Hambrey and Glasser (2012) describe meltwater streams transporting sediment away from the ice mass. and Glasser 2009).

The sandstone and clay units at Mount Dutton and Box Creek are likely to be deposited in a glaciofluvial setting. Bennett and Glasser (2009) suggest gravity flows, current reworking and shoreline sedimentation as the main glaciofluvial depositional processes for siliciclastics, however, these can be ruled out due to the lack of sedimentary structures. Eyles et al. (1983), Miall (2000) and Hambrey and Glasser (2012) describe meltwater streams transporting sediment away from the ice mass. Additionally, Eyles et al. (1983) stated that massive to crudely-bedded sediments suggests rapid dewatering within a subaqueous environmentand Miall (2000) described similar siliciclastic sequences as deposited in a subaqueous valley glacier setting. Meltwater streams (or channels) associated with the flow of water away from the ice mass can form subglacially (beneath the ice), laterally (along the ice margin) and in proglacial locations (in front of the ice; Bennett and Glasser 2009). The ice mass that supplies the meltwater and debris is not easily distinguishable from the debris and sediment deposited especially when there are minimal diamictite interbeds.

Bennett and Glasser (2009) suggest that the distribution of the diamictite in continental glacier settings map out the maximum distribution of ice. In comparison to continental glaciers, valley glaciers carry relatively small amounts of supraglacial debris (Benn et al. 2003) and therefore the diamictite of the Boorthanna Formation is likely to have been deposited by the continental ice mass. Benn et al. (2003) postulated that glacial debris is transported to the ice margin and concentrated into landforms with high preservation potential such as troughs. The restricted distribution of diamictite to the Boorthanna and Tallaringa troughs (Figure 3.3) suggests that this occurred in the Arckaringa Basin. The absence of diamictite in the Boorthanna Formation in the west and north suggests that the continental glacier may not have completely covered the basin.

The clasts in the erratic field at Mount Dutton are typically rounded to subrounded, locally-derived clasts (Figure 3:5a), the diamictite that overlies the erratic field are rounded to subangular and locally-derived (Figure 3.5b). These characteristics are consistent with glacial deposition in an environment with high erosion and transport such as valley or tongue glacial environments. Given the proximity of the Boorthanna Trough to the Peake and Denison Ranges which during the Permian were topographically higher than the Arckaringa Basin (Veevers 2006, Hall et al. 2016) it is likely that valley glaciers occurred along the eastern margin of the basin. It is probable that that the valley glaciers flowed into the Boorthanna Trough. The diamictite observed in the Tallaringa Trough is reported to be reworked and water transported glacial sediments (Townsend 1973). There are no modern highlands and few drill holes that have reached basement at depth to the west of the Arckaringa Basin suggesting that the diamictites of the Tallinga Trough were deposited in the trough by the continental glacier.

Miall (2000) reported that fluvial and glaciolacustrine are often at the top of sequences deposited in a glaciated valley setting. These are typically overlying lodgement till and debris flows diamictites. Rogers et al. (1996b) interpreted the sandstones at Box Creek (Figure 3.4b) to be associated with subglacial deposits that formed at the end of a valley glacier. The absence of clasts in the sandstone units and the sparse occurrence of erratics are indicative of deposition by meltwater from a valley glacier (Benn et al. 2003). Bennett and Glasser (2009) suggest that the absence of clasts occurs when a glacier is in stages of stagnation and deglaciation and most clasts and erratics have already been extracted from the ice. The sandstone units include subrounded, elongate and rhombic-shaped grains that indicate less reworked, poorly-developed sediment (Figures 3:6c, d) when compared to the sedimentary rocks of Mount Dutton. The poorly-developed nature of this sediment indicates that it was likely derived from a local source as it has not been transported far.

Heath (1963) suggested the sedimentary rocks are fan deposits, however the mostly very flat-lying nature of the strata suggests that fan deposits are unlikely. As both the Boorthanna and Tallaringa troughs are largely fault-controlled depocentres (Hibburt 1995) rather than glacially scoured U-shaped valleys, it is possible that any localised tilting of the sedimentary rocks was due to fault activity. This would hold for the Boorthanna Trough as a large fault is located on the eastern margin (Figure 3:3), which is where the tilted Boorthanna Formation sedimentary rocks are located. Townsend and Ludbrook (1975) suggest that the basal diamictites of the Boorthanna Formation were deposited in a fluvial and occasional lacustrine environment.

It is not possible to determine which glacial setting was the more dominant depositional mechanism, however, it is likely that the diamictite was deposited by both the icesheet and smaller valley and ice tongue glaciers. Due to the mixed depositional mechanisms of the basal diamictite of the Boorthanna Formation it is likely that the diamictite is a lodgement till. In order to explain the westerly orientation of diamicitites in the Boorthanna Trough, previous researchers (e.g. McGowran 1973, Veevers 2006) have suggested deposition of the diamictites in the Boorthanna Formation to be associated with the presence of valley and upland glaciers within an alpine glacial system occurring within the Gawler Craton to the east of the Boorthanna Trough (Figure 3:1). This is consistent with the orientation of the sedimentary rocks would create depositional characteristics such as gentle slopes and partial deposition of the diamictites against basement highs, as is seen in the Boorthanna Trough and central Arckaringa Basin (Figure 3:3). Valley glaciers may have deposited the diamictites either directly or via meltwater streams in a westerly orientation as the glaciers would have been topographically higher and deposition would have occurred down slope. This may be indicative that valley and ice tongue glaciers were the dominant depositional setting, however, it is not conclusive.

Depositional Setting of the Stuart Range Formation

The Stuart Range Formation was not investigated as part of this study due to it being restricted to the subsurface in the Boorthanna Trough. The depositional setting described below has been constructed using facies analysis principles of the previously described lithology as well as any depositional environments inferred by previous researchers.

The Stuart Range Formation and associated coal beds are interpreted to have been deposited during a marine transgression (Townsend and Ludbrook 1975). However, there is limited understanding of the conditions of the marine transgression which follows the deglaciation of the icesheet and deposition of the Boorthanna Formation. The general consensus is that a rapid climate shift was accompanied by a global rise in eustacy in the late Sakmarian (Dickins 1996, Scheffler et al. 2003,

Wopfner and Jin 2009). The warming of the climate would have been a major factor in the initiation of the deglaciation and retreat of the late Palaeozoic glaciation (Isbell et al. 2012).

The direction of the marine transgression is widely debated. Crowell and Frakes (1971b) suggested that a discontinuous marine and lagoonal epeiric sea spread across the continent during the Early Permian from the Canning Basin in Western Australia to the Arckaringa Basin, and then extended northward and eastward to inundate the Pedirka, Cooper and Bowen basins (Figure 3:1a). Alternatively, Alley et al. (1995) suggested that the marine transgression accompanied the decay of ice and the transgression into tectonic basins and isostatically depressed lowlands along the margin of the icesheet, however no directional indicators were suggested. Heath (1974) and McGowran (1973) postulated a connection to the southwest through the area later occupied by the Eucla Basin (Figure 3:1a). Conversely, Wopfner (1964) and Veevers (2006) each argued that the sea came from the west, whereas Jones (1987) suggested the sea originated from the northwest. No matter the direction of the transgression it is widely agreed that the conditions were quiet, cold water restricted marine as indicated by fauna within the Stuart Range Formation (Allchurch and Wopfner 1967, Townsend and Ludbrook 1975, Alley et al. 1995, Rogers et al. 1996b).

As the Stuart Range Formation was not investigated as part of this study no further insight to the depositional setting can be provided. The favoured depositional setting of the author is that the marine transgression likely originated from the west as suggested by Crowell and Frakes (1971b). This is favoured as the decaying and southerly moving icesheet is likely to have occupied the space to the south of the basin blocking the northerly movement of the transgressing sea.

Depositional setting of the Mount Toondina Formation

The Mount Toondina Formation is interpreted to have been deposited in an alternating fluvial and marine conditions that became increasingly freshwater with fluvial and lacustrine conditions. Townsend and Ludbrook (1975) proposed that the unit was deposited in a series of non-marine lagoons and swamps with intermittent deposition of fluvial sands. Alley et al. (1995) added that a crustal isostatic recovery or eustatic fall resulted in the termination of the marine sedimentation and the resulting return to freshwater conditions led to the development of coal swamps. These conditions are reflected in the Mount Toondina Formation which are characterised by bedded and laminated clay and siltstone sedimentary rocks interbedded with carbonaceous sedimentary rocks and occasional sandstone and lignite units.

The controlling factors that effected the change from marine to freshwater conditions are poorly understood. It has been suggested by Veevers (2006) that the large amounts of sediment erosion that occurred during the Triassic removed evidence of these conditions. In some instances the change occurred gradually without a period of significantly reduced deposition, such as in the Arckaringa Basin. In other areas such as the Cooper Basin (Figure 3:1), distinct unconformities occur between the marine shale (Stuart Range Formation equivalent) and freshwater beds (Mount Toondina Formation equivalent; Wopfner 1972).

3.4.3 Comparisons to the sedimentology of the sedimentary rocks of the Troubridge Basin

The late Palaeozoic glacial setting of the Arckaringa Basin rapidly (from 295 to 285 Ma; Ludbrook 1961, 1967, Jones 1987, Hibburt 1995, Tucker 1997) changes from glacial to marine to fluvial and lacustrine. The glacial setting is recorded in the sedimentary rocks of Boorthanna Formation (295-290 Ma;

Ludbrook 1961, 1967, Jones 1987, Hibburt 1995,). The same period in time (298 to 290 Ma; Ludbrook 1967, 1969b, Harris and McGowran 1971, Foster 1974, Bourman and Alley 1990, Alley and Bourman 1995) is recorded in glacial sedimentary rocks of the Cape Jervis Formation in the Troubridge Basin in southern South Australia (Figure 3:1a). Sedimentary rocks of the Cape Jervis Formation are better exposed than sedimentary rocks of the Boorthanna Formation, therefore the evolution of the glacial setting and corresponding sedimentary rocks in the Troubridge Basin are better understood.

The Cape Jervis Formation is divided into five units and each unit is a sedimentological record of the glacial setting at the time of deposition (Chapter 2; Alley and Bourman 1984). The basal unit contains glaciated bedrock surfaces (e.g. gelifract) and glacially polished pavements, and is representative of the pre-glacial setting of the Troubridge Basin. Landscape features such as U-shaped valleys are also indicative of the initial stages of glaciation. As most of the Arckaringa Basin sedimentary rocks are covered, there have been no recorded occurrences of glaciated pavements, however, Menpes et al. (2010) suggested that the Wallira Trough is a series of U-shaped valleys.

The lowermost sedimentary rocks (unit two) of the Cape Jervis Formation are a lodgement till comprising non-stratified diamictite with rounded to angular clasts within a sandstone matrix. Similarly, the basal diamictite of the Boorthanna Formation is composed of angular, subrounded and rounded clasts within a clay to sandstone matrix and is interpreted as a lodgement till in this study. The lodgement till of the Boorthanna Formation is restricted to small depocentres on the basin margins and in troughs. The subrounded and rounded clasts are likely to be derived from the debris of the valley or ice tongue glaciers (Bennett and Glasser 2009). Conversely, icesheet-derived clasts tend to be angular and locally-derived as the slow moving icesheet tends to shear and break the clasts rather than the rounding that occurs in the faster movement of a valley or ice tongue glacier. The characteristics of the lodgement till diamictite in both the Cape Jervis Formation (Chapter 2) and the Boorthanna Formation therefore suggest that the diamictite in both units was derived from the debris of both an icesheet and a valley or ice tongue glacier.

The units that overlie the lodgement till in the Cape Jervis Formation include fluviolacustrine beds that comprise clay, silt and sandstone beds with occasional pebble and diamictite beds (unit three). The fluviolacustrine beds were deposited when the icesheet was stagnant and slowly decaying and glacial lakes formed from the increased meltwater flows. Fine-grained sedimentary rocks were deposited via settling of sediment within the glacial lakes, and fluviolacustrine (sandstone) beds were deposited via the action of meltwater streams (Chapter 2, Bourman and Alley 1990 , Bennett and Glasser 2009). These are in-turn overlain by the flow till complex (unit four). The flow till complex consists primarily of diamictite often interbedded with sandstone and pebble beds. The sedimentary rocks of the flow till complex are indicative of the retreat of the icesheet and associated rapid decay which released debris that was deposited in a mass flow (Chapter 2, Bennett and Glasser 2009). These glacial settings are not directly preserved in the glacial sedimentary rocks of the Boorthanna Formation or elsewhere in the Arckaringa Basin. The sandstone units at Box Creek that are part of the Boorthanna Formation (Figures 3:3b, 3:8) are suggested to be associated with subglacial fans deposited by meltwater action, and formed at the end of a valley glacier that was in the final stages of deglaciation (Bennett and Glasser 2009). The absence of any sedimentary rocks that indicate stagnation and retreat of the icesheet (e.g. akin to unit three of the Cape Jervis Formation) and deposition of the valley glacier sedimentary rocks (e.g. sandstones at Box Creek) suggests that the icesheet retreated at a time when the valley glaciers where stagnant or slowly retreating and meltwater was still flowing into the into the basin.

The uppermost unit (unit five) of the Cape Jervis Formation consists of clay beds interbedded with sandstones and deposited within a deepening glaciomarine setting with occasional input of fluviolacustrine material via meltwater (Bennett and Glasser 2009, Chapter 2). The upper Boorthanna Formation is interpreted to have been deposited via turbidity currents during the initial stages of a marine transgression (Allchurch and Wopfner 1967, Hibburt 1995, Tucker 1997), and may therefore represent the initiation of the marine transgression that ultimately deposited the glaciomarine sediments of the Cape Jervis Formation (unit five). Deposition of sedimentary rocks in a deepening marine environment is also supported by the presence of the shales, clays and siltstones of the Stuart Range Formation that mostly conformably overly the Boorthanna Formation, and are interpreted to have been deposited in a transgressional marine environment (Ludbrook 1961, Townsend and Ludbrook 1975).

Palaeontological investigations of the lodgement till (unit two) and glaciomarine sediments (unit five) of the Cape Jervis Formation estimate that the lodgement till is Asselian (295 to 298 Ma) age and the glaciomarine sediments are Sakmarian (290 – 295 Ma) age (Ludbrook 1967, 1969b, Harris and McGowran 1971, Foster 1974). The upper Boorthanna Formation has been constrained to an Asselian-Sakmarian (290 – 298 Ma) age, while it is suggested that the Mount Toondina Formation is Late Asselian to Sakmarian age (Ludbrook 1967, Jones 1987, Hibburt 1995, Tucker 1997). This suggests that most of the late Palaeozoic successions of the Arckaringa Basin were deposited at the same time as the late Palaeozoic Cape Jervis Formation of the Troubridge Basin.

Although the age of the successions is correlative, there are no direct sedimentological equivalents of the Stuart Range Formation and Mount Toondina Formation of the Arckaringa Basin in the Cape Jervis Formation in the Troubridge Basin. This suggests that there were variations in depositional settings across the two basins during this period. The presence of thick successions of marine sedimentary rocks of the Stuart Range Formation in the Arckaringa Basin that are temporally equivalent with glacial sedimentary rocks of the Troubridge Basin suggests that the Arckaringa Basin was inundated with seawater while the icesheet was still covering the Troubridge Basin. The alternating lacustrine and fluvial sedimentary rocks of the Mount Toondina Formation were then deposited after the marine waters had receded from the Arckaringa Basin region. The occurrence of the glaciomarine sedimentary rocks at the top of the Cape Jervis Formation indicates that the marine waters covered the Troubridge Basin at the same time as there were terrestrial conditions within the Arckaringa Basin during deposition of the Mount Toondina Formation. This indicates that the direction of marine regression was to the south southwest.

3.5 Conclusions

The physical characteristics of the late Palaeozoic sedimentary rocks of the Arckaringa Basin show that each exposed stratigraphic unit has unique and diagnostic features that can be related to individual depositional setting. The Boorthanna Formation can be largely recognised by the diamictite and sandstone sedimentary rocks that dominate the exposures at Mount Dutton and Box Creek. The Mount Toondina Formation sedimentary rocks are dominated by siltstone and shale units, some of which are calcareous. Lignite beds were recognised in the exposure of the upper Mount Toondina Formation. The Boorthanna Formation sedimentary rocks are also identifiable by the ferruginous materials they contain, although in the correct conditions ferruginous material could form in sedimentary rocks of

the Mount Toondina Formation therefore identification using ferruginous sedimentary rocks needs to be done carefully.

The clast shape and matrix sedimentology of the Boorthanna Formation diamictite units suggest both that the glacial influence during deposition was both a continental icesheet and valley glaciers. This is in contrast to the most popular model of deposition that does not take into account the possibility of several glacial influences on deposition.

Comparison of the sedimentology of late Palaeozoic sedimentary rocks within the Arckaringa Basin with temporally equivalent glacial sedimentary rocks of the Cape Jervis Formation in the Troubridge Basin demonstrates that the lowermost units in both basins comprise lodgement tills deposited via the action of an icesheet and valley or ice tongue glaciers. The depositional mechanisms occurring in the Arckaringa and Troubridge basins subsequently became variable. In the Arckaringa Basin, shales and clays of the Stuart Range Formation were deposited in a deepening marine setting and overlain by alternating lacustrine and fluvial sedimentary rocks of the Mount Toondina Formation that were deposited as the marine waters receded from the Arckaringa Basin region. Contemporarily equivalent sedimentation in the Troubridge Basin involved deposition of fluvioglacial and glaciomarine sedimentary rocks (units three and four of the Cape Jervis Formation) and overlain by interbedded silts and sandstone in a deepening glaciomarine environment with transient fluvioglacial input (unit five of the Cape Jervis Formation). This suggests that there were marine conditions in the Arckaringa Basin at the same time as the Troubridge Basin was covered in ice. The marine waters then regressed to the south so that terrestrial conditions were present in the Arckaringa Basin at the same time as the Troubridge Basin was in a deepening marine setting.

Chapter 4: Zircon provenance of Late Palaeozoic glacigene sedimentary rocks in the Troubridge and Arckaringa basins, South Australia

Foreword

This chapter presents the results of the LA-ICP-MS U-Pb zircon geochronology, carried out on selected samples of the Cape Jervis Formation of the Troubridge Basin and the Boorthanna Formation of the Arckaringa Basin. Samples used were collected during the sampling of the measured sections detailed in Chapters 2 and 3. Sample preparation, mineral separation and zircon mount preparation was conducted by the author at the University of Adelaide. Zircon imaging was conducted by the author using the Phillips XL-40 Scanning Electron Microscope at Adelaide Microscopy, University of Adelaide. Zircon U-Pb analysis were conducted by the author using the New Wave 213nm Nd-YAG laser coupled to an Aglient 7500cs/7500s ICP-MS at Adelaide Microscopy, University of Adelaide over in five sessions between June and December 2012. Dr. Ben Wade and Augus Netting of Adelaide Microscopy provided invaluable assistance in the operation of the apparatus at Adelaide Microscopy. U-Pb LA-ICP-MS data were processed using the GLITTER software (Griffin et al. 2008). Interpretation of the processed data was conducted by the author using the Microsoft Excel add in Isoplot 4.15 (Ludwig 2003). Dr Katie Howard (University of Adelaide) provided assistance in the use of the data processing and interpretation software. The provenance of the Cape Jervis and Boorthanna formations and associated implications on glacial sediment transport are presented here. This chapter has been written as an independent publication and is structured accordingly.

Abstract

U-Pb zircon geochronological data was collected from from eight samples taken from late Palaeozoic glacigene sedimentary rocks in the Troubridge and Arckaringa basins in South Australia. The zircon age distributions provide an opportunity to constrain and compare provenance of the glacigene sedimentary rocks at different geographic locations and stratigraphic levels as an aide to interpreting palaeogeography and evolution of the Palaeozoic Gondwanan icesheet. The zircon grains have heterogeneous morphology, including numerous fragmented grains, and varying patterns of internal zoning consistent with diverse source rocks. The zircon populations significantly predate the ca 285-300 Ma depositional age for the Troubridge and Arckaringa basins sedimentary rocks determined independently from palynology. Zircon populations from the Troubridge Basin are dominated by a significant mode at ca 550 to 650 Ma. Older zircons are more abundant in the glaciomarine sedimentary rocks in the upper part of the sequence. The Arckaringa Basin samples are characterised as having a large component of ca 900 to 1200 Ma and ca 1700 to 1900 Ma zircon age populations and containing a significant late Proterozoic to early Palaeozoic population. The resulting provenance assessment suggests that the sedimentary rocks from the Troubridge Basin were sourced almost exclusively from the Kanmantoo Group and the Transantarctic Mountains of Antarctica. Conversely, the Arckaringa Basin sedimentary rocks were primarily sourced from the Gawler Craton and Adelaide Rift Complex.

4.1 Introduction

Numerous studies investigating the provenance of sedimentary rocks and potential source regions within sedimentary basins have been conducted (e.g. Payne et al. 2006, Haines et al. 2011, Paulsen et al. 2013, Normington et al. 2015, 2016). These studies used known age constraints of surrounding basement terranes and U-Pb isotopic detrital zircon analyses to assess the potential of source regions of zircons within the basin sedimentary rocks. Identifying the potential source region of glacial sedimentary rocks can provided additional constraints on ice movement directions and processes of sediment deposition related to glacial activity (e.g. Haines et al. 2011). Additionally, provenance data can be linked into palaeogeographic reconstructions (e.g. Haines et al. 2011 and Normington et al. 2016).

A number of detailed continental (e.g. Crowell and Frakes 1971a, 1971b, Veevers 2006) to local-scale (e.g. Alley and Bourman 1984, Bourman and Alley 1990, 1999) palaeogeographic reconstructions that postulate ice movement directions have been proposed for the late Palaeozoic in southern Australia. However, there is no existing provenance data from the late Palaeozoic sedimentary rocks of South Australia and these reconstructions rely on the distribution of discrete remnants of glacigene sedimentary rocks and glacial pavements.

It is recognised that the maximum depositional ages interpreted from detrital zircons do not always accurately represent the true timing of deposition. The depositional age of glacigene sedimentary rocks in the Troubridge and Arckaringa Basins (Figure 4:1) have previously been constrained from palynological studies (Chapters 2 and 3, Ludbrook 1961, 1967, 1969b, Harris and McGowran 1971, Foster 1974, Jones 1987, Bourman and Alley 1990, Alley and Bourman 1995, Hibburt 1995, Tucker 1997). Bourman and Alley (1990) reported an Asselian age (298 – 295 Ma) for unit two of the Cape Jervis Formation and Ludbrook (1967) reported a Sakmarian age (290 – 295 Ma) for unit five, which

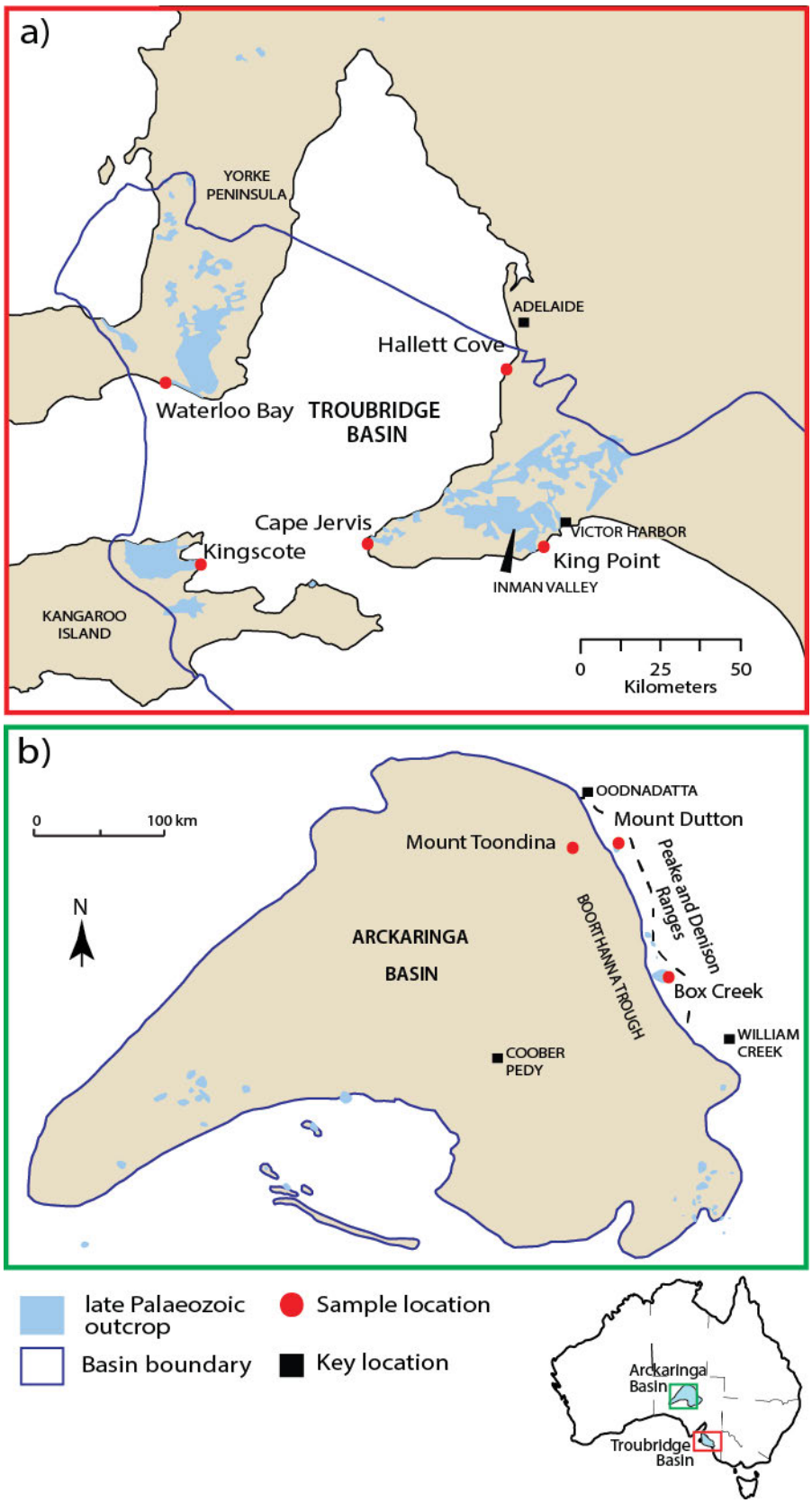

Figure 4:1 a) Approximate limits of the Troubridge Basin adapted from Alley and Bourman (1995), showing late Palaeozoic exposures adapted from Thompson and Horwitz (1962), Fairclough (2007), Belperio et al. (2009) and Zang and Crawford (2009). Measured sections and key locations are also shown; b) Limit of the Arckaringa Basin, showing the late Palaeozoic exposures adapted from Hibburt (1995), Rogers et al. (1996a) and Freytag et al. (1967). Measured sections and key locations are also shown. Inset: location of study areas in relation to Australia.

was later confirmed in other studies (Ludbrook 1969b, Harris and McGowran 1971, Foster 1974). Ludbrook (1969b) constrained the age of the Boorthanna Formation to Sakmarian (290 – 295 Ma) and Hibburt (1995) reported that the Mount Toondina Formation is Artinskian (283 – 290 Ma). The depositional age ranges determined from palynological studies are considered to be highly indicative of the actual timing of sedimentation as these ages are constrained using foraminifera that lived in the waters present at the time of deposition (Mory and Backhouse 1997, Eyles et al. 2002). Conversely, the geochronological maximum depositional age may only approximate the true timing of deposition if sedimentation occurred during or immediately after a zircon forming or alteration event such as volcanism or high-grade metamorphism. There are no known zircon forming events, or events that would have altered existing zircon grains during the timing of deposition of the glacigene sedimentary rocks of the Troubridge and Arckaringa basins. Therefore, zircon U-Pb ages from the Troubridge and Arckaringa basins are unlikely to add further constraint to the depositional age of the sedimentary rocks, but rather will be highly useful in determining the source region(s) of the sedimentary rocks, which in turn may be used to infer glacial flow directions.

Assessment of any given terrane as a potential source of sedimentary rocks in a region may be assessed as a potential source region as it will show similar age patterns in U-Pb probability plots to the sedimentary package being assessed. This has been successfully used to assess source regions of numerous sedimentary packages within sedimentary basins (e.g. Maidment et al. 2007, Haines et al. 2011, Normington et al. 2015, 2016). In the case of the late Palaeozoic glacigene sedimentary rocks of the Troubridge and Arckaringa basins, potential source regions were selected based on palaeogeography. During the time of glacigene sedimentation, Australia was part of the Gondwana Supercontinent (Crowell and Frakes 1971b, Caputo and Crowell 1982, Alley et al. 1995, Veevers 2006), and southern Australia was attached to the northern part of Antarctica (Figure 4:2). This implies that the Kanmantoo Group, the Cambrian portion of the Adelaide Rift Complex (ARC), Gawler Craton and Antarctica are considered potential proximal sources for the Troubridge Basin. The Gawler Craton, Mesoproterozoic to Paleoproterozoic portion of ARC and the Musgrave Province are considered proximal sources and the Kanmantoo Group, Arunta Region and Transantarctic Mountains (TAM) of Antarctica distal sources for the Arckaringa Basin. These potential source regions are the modern day above-surface expression of the highlands that were likely exposed during the Permo-Carboniferous glaciation.

This chapter will provide provenance analysis of late Palaeozoic glacigene sedimentary rocks from the Troubridge and Arckaringa basins (Figure 4:1) using zircon U-Pb geochronological analysis. The ages are discussed in relation to the provenance of the glacigene sedimentary rocks and known ice movement directions (e.g. Milnes and Bourman 1972, Bourman et al. 1976, Alley and Bourman 1984, Bourman and Alley 1988, 1990, 1999) provide a constraint on the sediment source direction. This subsequently allows a comprehensive assessment of the mechanisms of ice movement and processes of sediment deposition (e.g. fluvial input, ice melting).

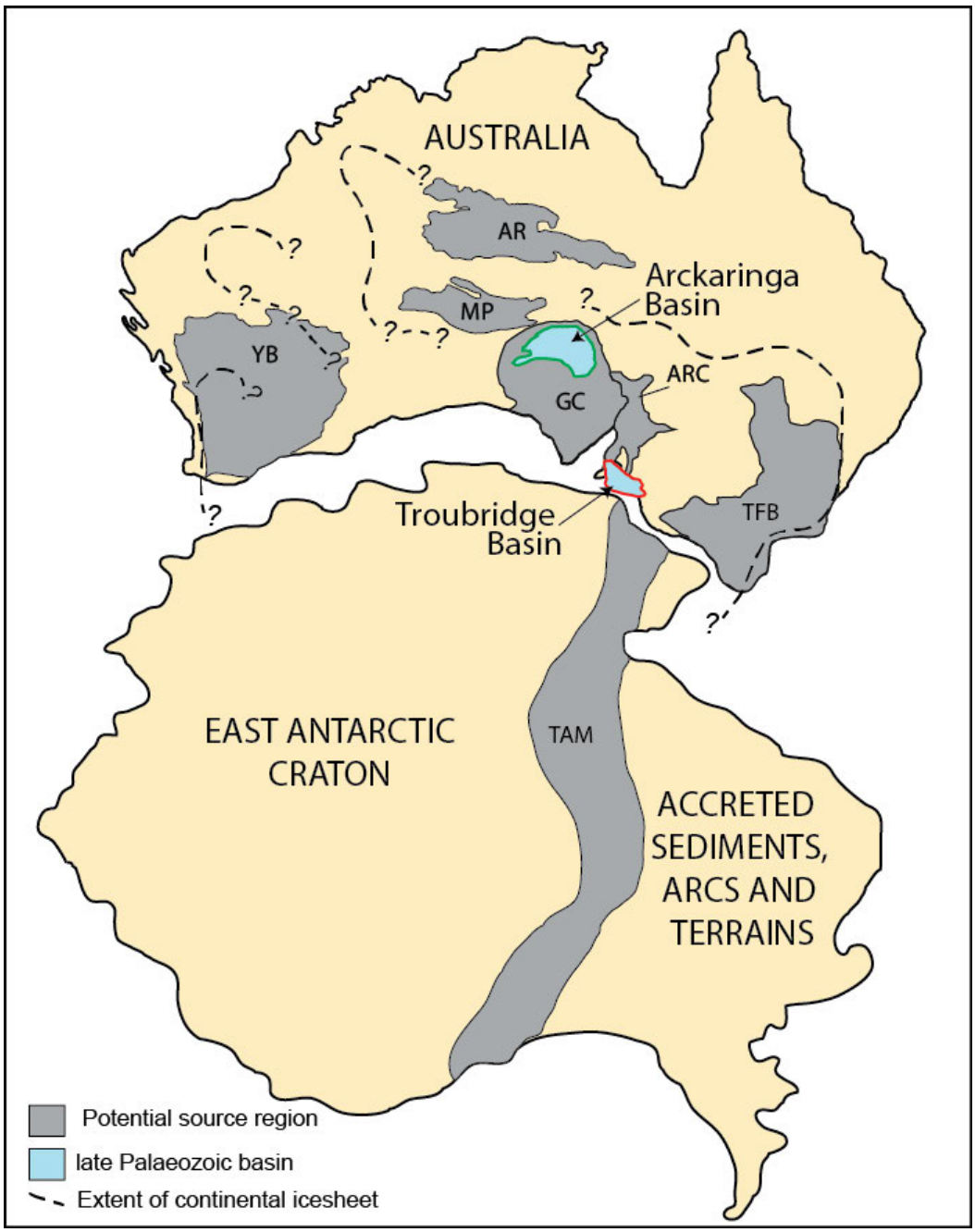

Figure 4:2 Potential source regions of Australia and Antarctica (grey) in relation to the Arckaringa Basin and Troubridge Basin in blue. The Australian extent of the continental ice mass during the early Permian is shown by the broken line adapted from Crowell and Frakes (1971b). Diagram is not to scale and adapted from Foden et al. (2006). AB: Arckaringa Basin; AR: Arunta Region; ARC: Adelaide Rift Complex; GC: Gawler Craton; MP: Musgrave Province; TAM: Transantarctic Mountains; TFB: Taman Fold Belt; YB: Yilgarn Block.

4.2 Methods

4.2.1 Sample selection

Nine samples from six key stratigraphic sections distributed within the Troubridge and Arckaringa basins were analysed. For detailed descriptions of the location, stratigraphy and sedimentology of the key sections refer to Chapters 2 and 3. In order to maximise the possibility of separating zircon

grains, individual samples were taken from intervals with Zr content >200 pm as determined by whole rock geochemical analysis (see Chapter 5 for whole rock geochemistry methods). Systematic mineralogical assessment using thin sections was not possible. Zircons were not observed during petrological investigations and no mineralogical differences were observed to allow provenance assessments. Six samples of the Cape Jervis Formation representative of units two, three, four and five are from key localities at Cape Jervis, Kings Point, Kingscote and Waterloo Bay in the Troubridge Basin (Figure 4:3). One sample was also taken from the Hallett Cove section but had low zircon yield was not suitable for analysis. Three samples are from the Box Creek, Mount Dutton and Mount Toondina key localities in the Arckaringa Basin and represent the Boorthanna Formation (Box Creek and Mount Dutton) and Mount Toondina Formation (Mount Toondina; Figure 4:4).

4.2.2 Zircon separation

Samples were prepared for zircon extraction by crushing in a jaw crusher, sieving and collecting the 79 – 400 micron fraction. Zircon concentrates were prepared through a process of panning, magnetic separation and heavy liquid separation. Highly magnetic minerals were removed via magnetic separation using a Franz isodynamic separator. The concentrate was further separated via heavy mineral separation using heavy liquid (methylene iodine) separation. Zircon grains were then handpicked from the concentrate and mounted onto epoxy resin blocks. The resin blocks were then polished with 0.25 µm diamond paste to reveal the grains and provide a smooth surface for analysis.

4.2.3 Imaging

The internal structure of the zircon grains was imaged using back scattered electron and Cathodeluminescence (CL) techniques on a Phillips XL-40 Scanning Electron Microscope (SEM) with an attached Gatan CL detector at Adelaide Microscopy, University of Adelaide. Images were used to target cores or rims within individual grains to maximise the analysis of a cohesive part of the grain.

4.2.4 Data acquisition and processing

Isotopic analysis was undertaken using Laser Ablation Inductively Coupled Plasma Mass Spectrometry (LA-ICP-MS) at Adelaide Microscopy, University of Adelaide and follow the methodology of Payne et al. (2006) and Howard et al. (2011). Due to the possibility that the ages obtained could range from 250 Ma to beyond 2000 Ma, the isotopic ratio used to determine the age of a zircon grain was dependant on the $^{207}Pb/^{206}Pb$ isotopic ratio (Cawood et al. 2003). Zircon grain ages older than 1500 Ma were calculated based on the $^{207}Pb/^{206}Pb$ ratio, and zircon grain ages younger than 1500 Ma were calculated using the $^{206}Pb/^{238}U$ isotopic ratio. Data were processed using the GLITTER software developed at Macquarie University, Sydney (Griffin et al. 2008).

Instrument drift and U-Pb fractionation were corrected using the GEMOC GJ-1 standard zircon (Jackson et al. 2004) and accuracy was checked using Plešovice zircon standard mean ID-TIMS (Slama et al. 2008). The normalised ages for the standards analysis during the study were within error as reported by Jackson et al. (2004) and Slama et al. (2008). The standard ages for each of these as well as the average normalised ages of GJ-1 and Plešovice are reported in Appendix 2.

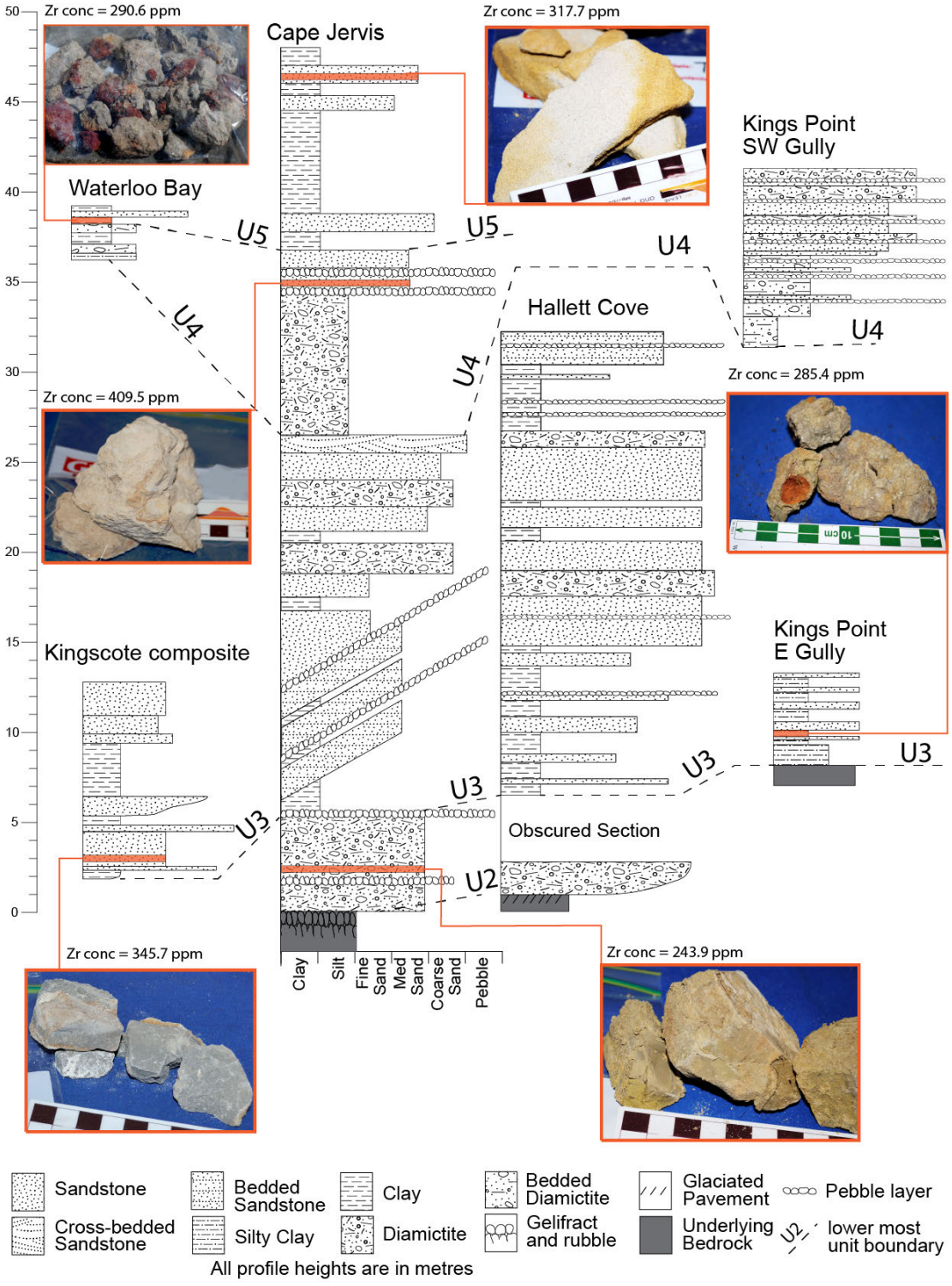

Figure 4:3 Stratigraphic sections of key locations within the Troubridge basin showing location of samples used for geochronological analysis. Photos of samples from which zircon grains were separated are shown. Dashed lines show correlation of stratigraphic units across the key locations. Location of the key sites are given in Figure 4:1. Detailed descriptions of the stratigraphic sections are given in Chapter 2.

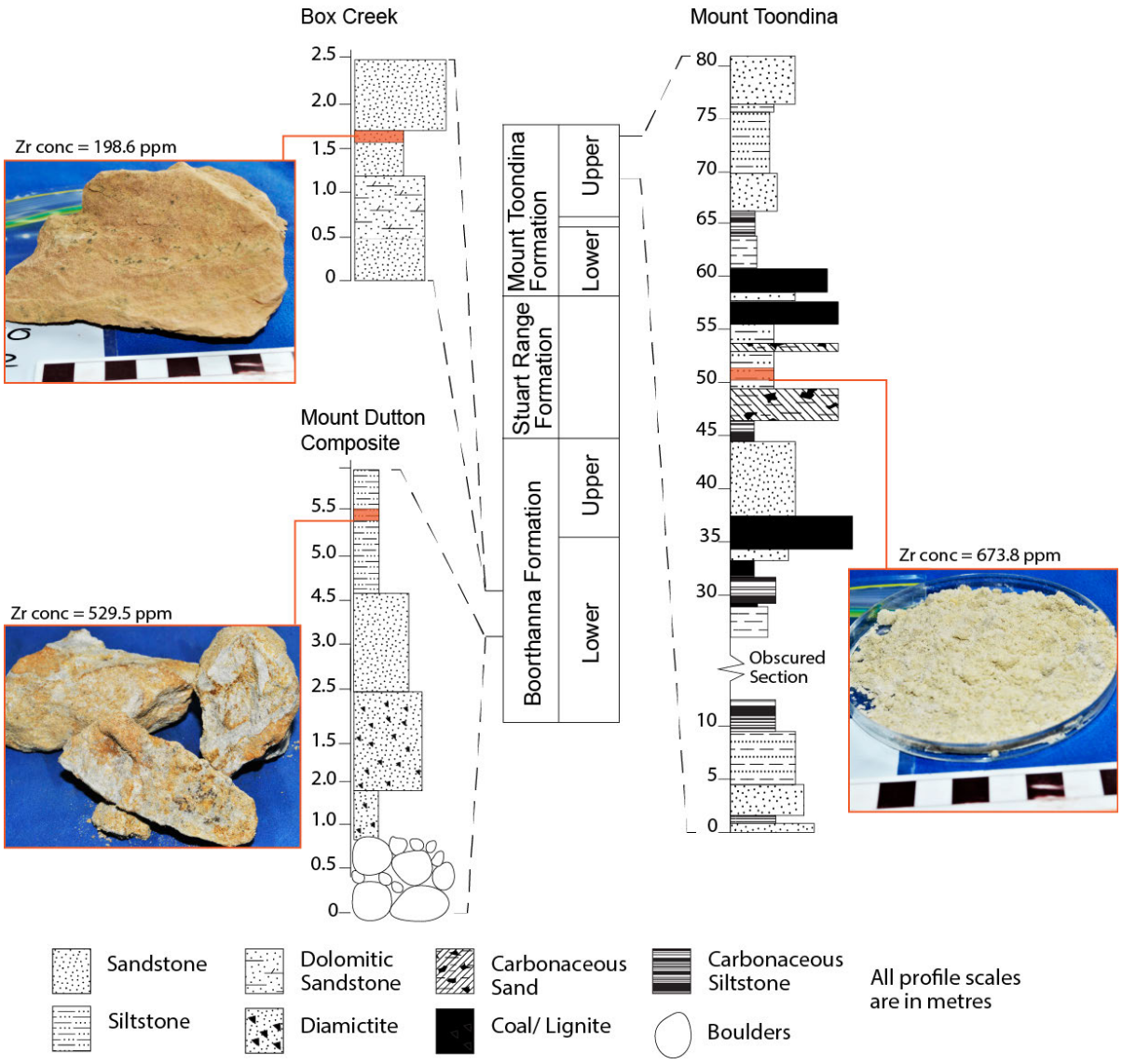

Figure 4:4 Sample locations, sample photos and section correlation of Arckaringa Basin measured section, section locations are shown in Figure 4:1. Sample locations are marked on sections in orange. Photos of samples from which zircon grains were separated are shown. Detailed descriptions of the stratigraphic sections are given in Chapter 3.

4.3 Results

4.3.1 Troubridge Basin

Zircon descriptions

Zircon grains have a comparable range of morphologies in the eight samples taken from the Troubridge Basin. Zircon grains range from approximately 50 to 250 µm in size, are euhedral to subhedral and typically elongate (Figure 4:5). Broken grain fragments are common (Figure 4:5). In cathodoluminescence (CL) images, zircon grains exhibit varying internal structure; most show zoning which includes complex growth zoning, sector zoning and broad zoning (Figure 4:5; Corfu et al. 2003). There is some indication of metamorphic recrystallisation and new growth as some zircon grains preserve cores and outer concentric zones. Some grains have rims with a brighter-CL response, while a small portion of grains have a darker-CL response where it is difficult to determine internal

structure. Examples of the internal structure of zircon grains from the Cape Jervis Formation are shown in Figure 4:5 and summaried in Table 4:1.

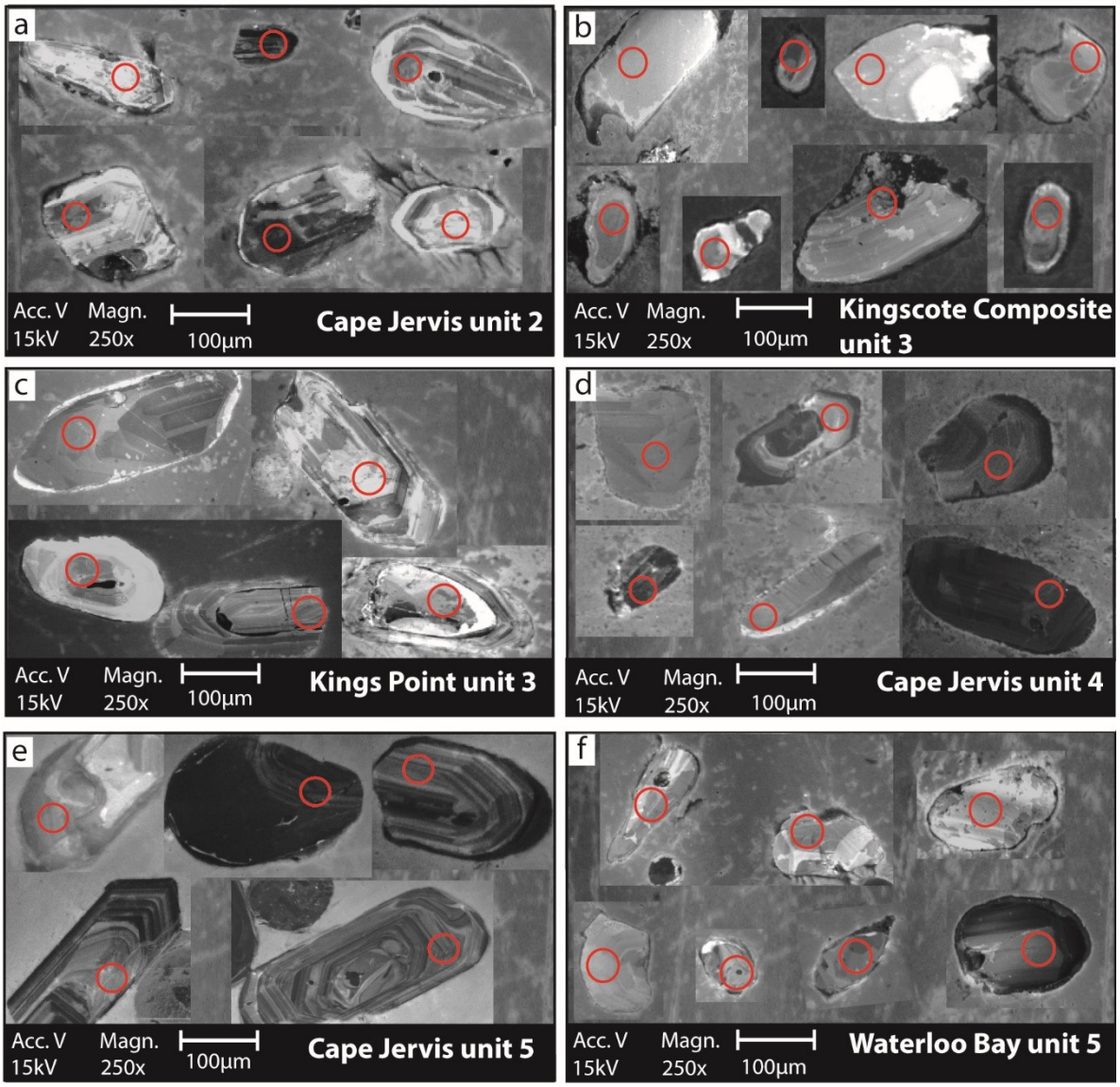

Figure 4:5 Representative CL images of zircon grains of the Cape Jervis Formation. Each sample is identified in the bottom right hand corner of each image. Laser spots (30 µm size) are shown in red. Zircon numbers relate to the figure reference guide in Table 4:1.

Table 4:1 Guide to internal structure of zircon grains in Figure 4:5 and 4:9.

Internal structure of zircon grains	Figure reference
Complex growth (oscillatory) zoning	Figure 4:5a) grains 1,5; c) grains 2, 4, 5; e) grains 3, 4, 5. Figure 4:9 grains 6, 9, 10.
Sector zoning	Figure 4:5b) grain 3; c) grain 1; d) grain 4; f) grain 7. Figure 4:9 grains 1, 5, 8.
Broad zoning	Figure 4:5a) grain 4; b) grain 5; e) grain 1; f) grain 7. Figure 4:9 grains 2. 7, 11.
Metamorphic recrystallization	Figure 4:5e) grains 4, 5. Figure 4:9 grains 3, 4, 5.
New growth	Figure 4:5d) grain 2; e) grain 5. Figure 4:9 grains 2, 13.
Brighter CL response	Figure 4:5a) grains 3, 4, 6; b) grains 1, 3; c) grains 2, 3, 5. Figure 4:9 grains 7, 11, 13.
Darker CL response	Figure 4:5) grains 3, 4, 6; e) grain 2; f) grain 7. Figure 4:9 grains 8, 12.

Zircon U-Pb geochronology

Unit 2 - lodgement till

Cape Jervis Section

One hundred and nineteen zircon grains were analysed from the unit two sample from the Cape Jervis section. Thirty-three analyses were within 10% concordance (Figures 4:6a, b). The concordant analyses range between ca 3460 and 580 Ma (Figure 4:7a). The strongest mode is from ca 565 to 690 Ma (n = 18). Lesser peaks occur at ca 890 to 1226 Ma (n = 7), ca 2263 to 3500 Ma (n = 7; Figure 4:7a).

Unit 3 - fluviolacustrine beds

Kings Point Section

One hundred zircon grains were analysed from the unit three sample at Kings Point with forty-four analyses within 10% concordance (Figures 4:6c, d). The U-Pb isotopic ages of the concordant analyses range from ca 3445 to 520 Ma (Figure 4:7b). The strongest mode is from ca 640 to 550 Ma (n = 29). Lesser modes occur at ca 700 to 1070 Ma (n = 5), ca 2000 to 3450 Ma (n = 10; Figure 4:7b).

Kingscote Composite Section

One hundred and nineteen grains were analysed from the unit three sample from the Kingscote Composite section, with 22 analyses within 10% concordance (Figures 4:6e, f). The U-Pb isotopic ages of the concordant analyses range from ca 3440 to 595 Ma (Figure 4:7c). The strongest mode is from ca 590 to 700 Ma (n = 15). Lesser modes occur at ca 860 to 1210 Ma (n = 5), ca 2190 to 3440 Ma (n = 2; Figure 4:7c).

Unit 4 - flow till complex

Cape Jervis Section

One hundred and eleven zircon grains were analysed from the flow till complex. Of these, 23 analyses were within 10% concordance (Figures 4:6g, h. The U-Pb isotopic ages of the concordant analyses range from ca 3235 and 530 Ma (Figure 4:7d). The strongest mode is between ca 530 and 630 Ma (n = 12). Lesser modes occur at ca 740 to 770 Ma (n = 2), ca 1025 to 1120 Ma (n = 3), ca 2010 to 3240 Ma (n = 6; Figure 4:7d).

Unit 5 - glaciomarine sediments

Cape Jervis Section

One hundred and fifty-seven zircon grains were analysed from the sandstone. Fifty-five analyses were within 10% concordance (Figures 4:6i, j). The U-Pb isotopic ages of the concordant analyses range from ca 3735 to 370 Ma (Figure 4:7e). The strongest mode is from ca 510 to 640 Ma (n = 18). Lesser modes occur at ca 370 to 475 Ma (n = 3), ca 730 to 870 Ma (n = 4), ca 950 to 1640 Ma (n = 17), ca 2205 to 3740 Ma (n = 13; Figure 4:7d).

Waterloo Bay section

One hundred and eleven zircon grains were analysed from the Waterloo Bay sample and 74 were within 10% concordance (Figures 4:6k, l). The U-Pb isotopic ages of the concordant analyses range from ca 3070 and ca 380 Ma (Figure 4:7e). The strongest mode is between ca 510 and 750 Ma (n = 28). Lesser modes occur at ca 380 Ma (n = 1), ca 900 to 1260 Ma (n = 19), ca 1500 to 1940 Ma (n = 9) and ca 2285 to 3070 Ma (n = 17; Figure 4:7f).

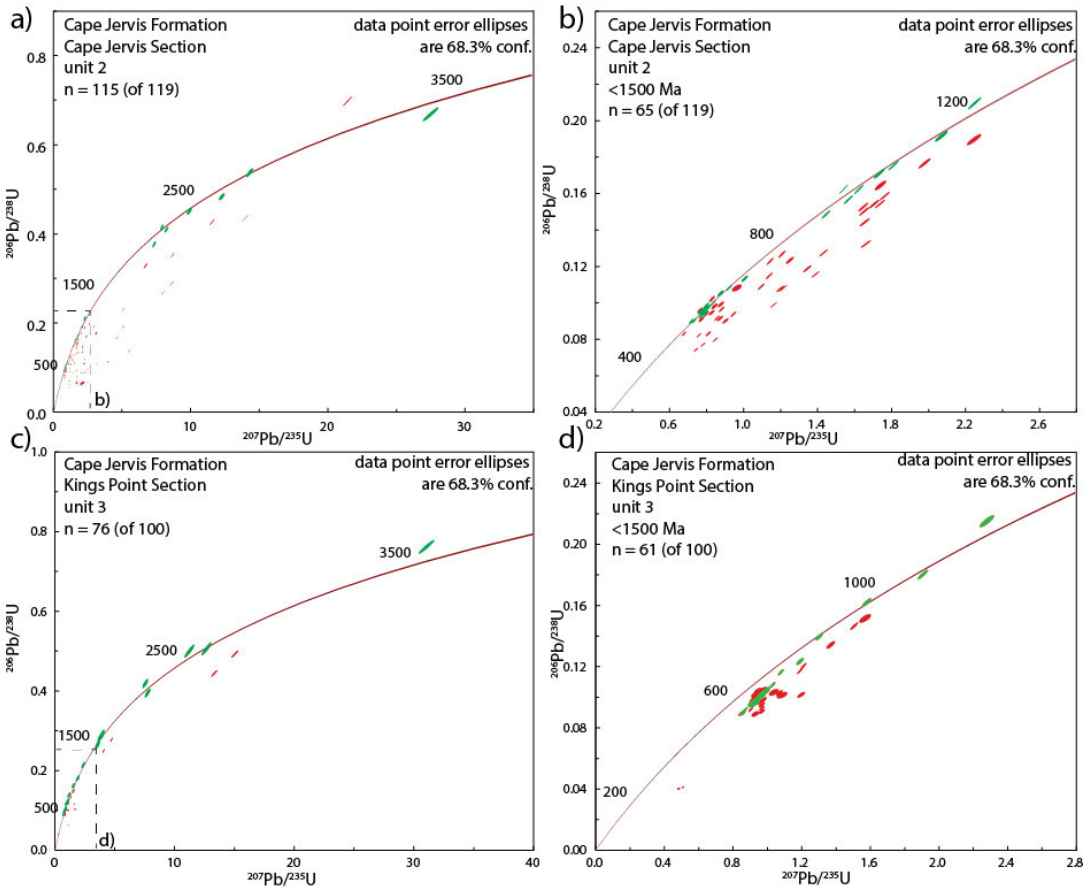

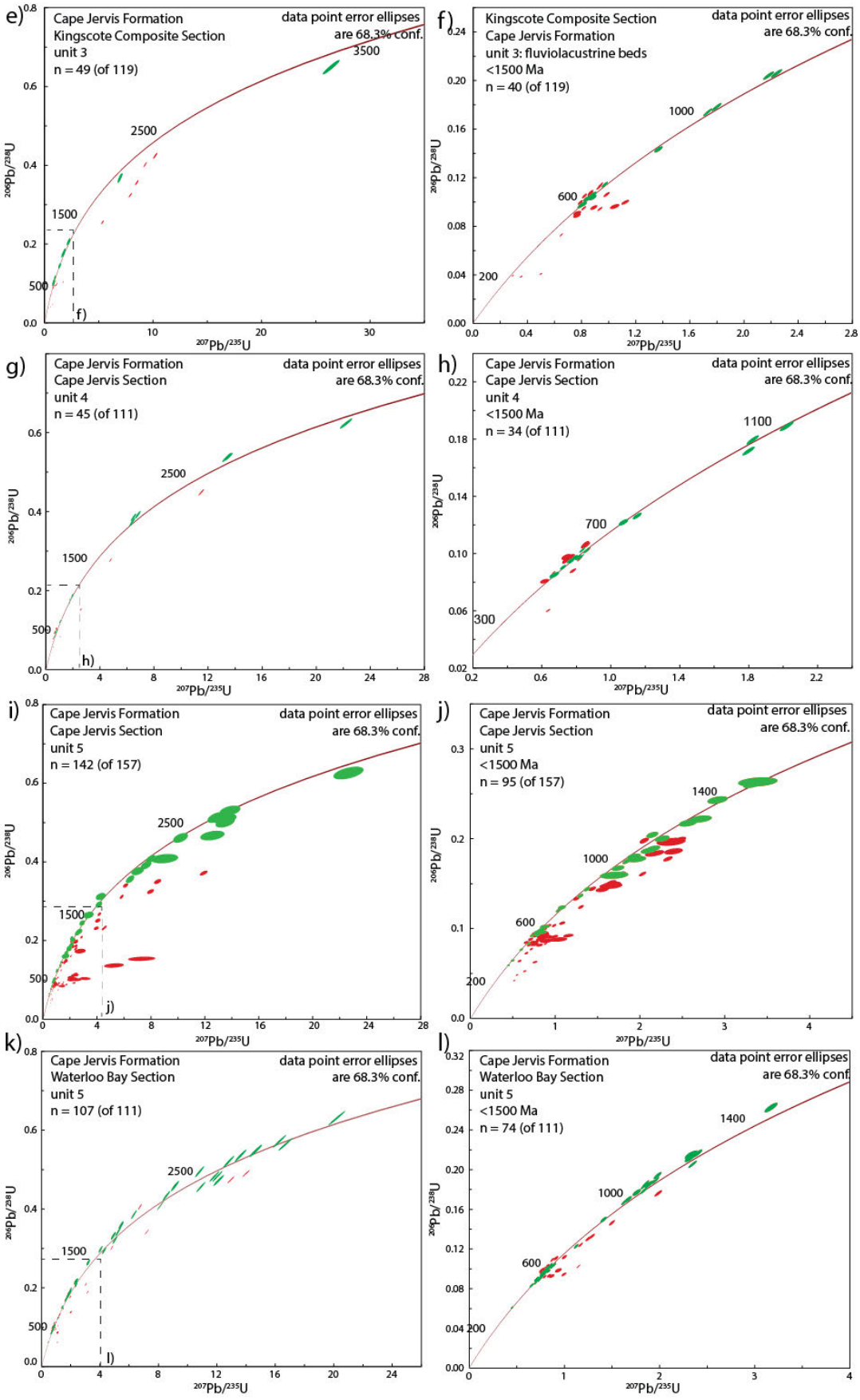
e)
Cape Jervis Formation
Kingscote Composite Section
unit 3
n = 49 (of 119)
data point error ellipses
are 68.3% conf.
3500
2500
1500
500
f)
f)
Kingscote Composite Section
Cape Jervis Formation
unit 3: fluviolacustrine beds
<1500 Ma
n = 40 (of 119)
data point error ellipses
are 68.3% conf.
1000
600
200
g)
Cape Jervis Formation
Cape Jervis Section
unit 4
n = 45 (of 111)
data point error ellipses
are 68.3% conf.
2500
1500
500
h)
h)
Cape Jervis Formation
Cape Jervis Section
unit 4
<1500 Ma
n = 34 (of 111)
data point error ellipses
are 68.3% conf.
1100
700
300
i)
Cape Jervis Formation
Cape Jervis Section
unit 5
n = 142 (of 157)
data point error ellipses
are 68.3% conf.
2500
1500
500
j)
j)
Cape Jervis Formation
Cape Jervis Section
unit 5
<1500 Ma
n = 95 (of 157)
data point error ellipses
are 68.3% conf.
1400
1000
600
200
k)
Cape Jervis Formation
Waterloo Bay Section
unit 5
n = 107 (of 111)
data point error ellipses
are 68.3% conf.
2500
1500
500
l)
l)
Cape Jervis Formation
Waterloo Bay Section
unit 5
<1500 Ma
n = 74 (of 111)
data point error ellipses
are 68.3% conf.
1400
1000
600
200
$^{206}Pb/^{238}U$
$^{207}Pb/^{235}U$

Previous Page: Figure 4:6 Concordia plots of all zircon grain analyses from the Cape Jervis Formation a) all analyses from unit two at Cape Jervis; b) analyses of zircon grains with ages <1500 Ma from unit two at Cape Jervis; c) all analyses from unit three at Kings Point; d); analyses of zircon grains with ages <1500 Ma from unit three at Kings Point; e) all analysis from unit three from the Kingscote composite; f) analyses of zircon grains with ages <1500 Ma from unit three from the Kingscote composite; g) all analyses from unit four at Cape Jervis; h) analyses of zircon grains with ages <1500 Ma from unit four at Cape Jervis; i) all analyses of unit five at Cape Jervis; j) analyses of zircon grains with ages <1500 Ma from unit five at Cape Jervis; k) all analyses of unit five at Waterloo Bay; l) analyses of zircons with ages <1500 Ma from unit five at Waterloo Bay. Red ellipses are non-concordant zircon grains; green ellipses are concordant zircon grains.

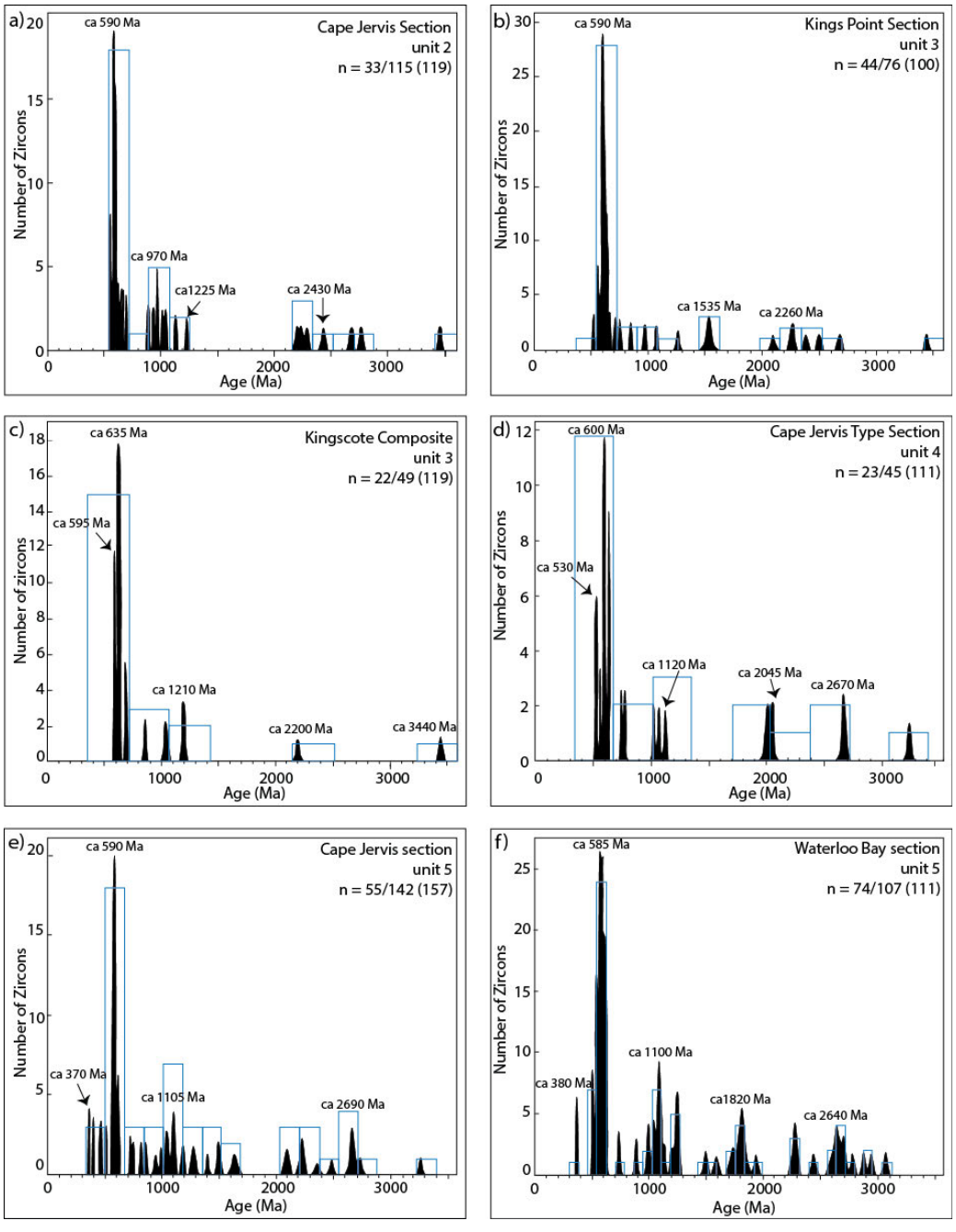

Figure 4:7 Age probability density plot for concordant and near concordant detrital zircons of the Cape Jervis Formation from a) unit two at the Cape Jervis section; b) unit three at the Kings Point section; c) unit three at the Kingscote composite section; d) unit four at the Cape Jervis section; e) unit five at the Cape Jervis section and f) unit five from the Waterloo Bay section. Blue bars show number of zircons included in analysis for each mode.

Combining of Cape Jervis Formation age data

Combing zircon age data from various samples allows the provenance of the unit and formation across the basin to be assessed instead of provenance at one isolated section. This is important as the glacial conditions can be variable across the basin simultaneously. The combining of the units with multiple samples was done here after considering the lithological and stratigraphic correlation as discussed in Chapter 2, and the shape of the individual provenance spectra.

The individual provenance sprectra of all units have a strong mode between ca 550-650 Ma, the proportion of concordant analyses within this age range was assessed. A similar proportion of grains and common stratigraphic features were used as justification for combining samples. This reasoning was also used to justify the combination of the analyses from units two, three and four. The provenance spectra for units two, three and four are remarkably similar with a main peak at ca 590 Ma and lesser Mesoproterozoic and Palaeoproterozoic modes (Figures 4:6a to d). The proportion of zircon grains within the 550-650 Ma age range is 45 to 50% in all of the units two to four samples. Combining the spectra allows assessment of the provenance of the sedimentary rocks during glacial activity, which in turn can be used to infer ice motion directions.

The combined of data for units two to four gives 112 analyses within 10% concordance. The U-Pb isotopic ages of the concordant analyses range from ca 3460 Ma to 526 Ma (Figure 4:8c). The strongest mode is ca 500 to 665 Ma (n = 68). Lesser modes occur within age ranges of ca 690 to 900 Ma (n = 10), ca 940 to 1255 Ma (n = 18), ca 1515 to 1540 Ma (n = 3), ca 2000 to 2290 Ma (n = 9), ca 2430 to 2765 Ma (n = 7) and ca 3230 to 3460 Ma (n = 4; Figure 4:8c).

Conversely, unit five of the Cape Jervis Formation was deposited in a glaciomarine setting where the influence from the retreating ice mass was not significant. The two samples from this unit were combined to assess the sediment provenance across the basins. The combined of data for unit five gives 129 analyses within 10% concordance. The U-Pb isotopic ages of the concordant analyses range from ca 3260 Ma to 370 Ma (Figure 4:8b). The strongest mode is ca 500 to 640 Ma (n = 49), like the underlying units, however a lesser, younger mode with an age range of ca 370 to 475 Ma (n = 4) is apparent (Figures 4:6e, f). Minor age populations at ca 730 to 1293 Ma (n = 43), ca 1400 to 1940 Ma (n = 15), ca 2080 to 2485 Ma (n = 11), ca 2590 to 2700 Ma (n = 10) and ca 2735 to 3260 Ma are also evidence (n = 7; Figure 4:8b).

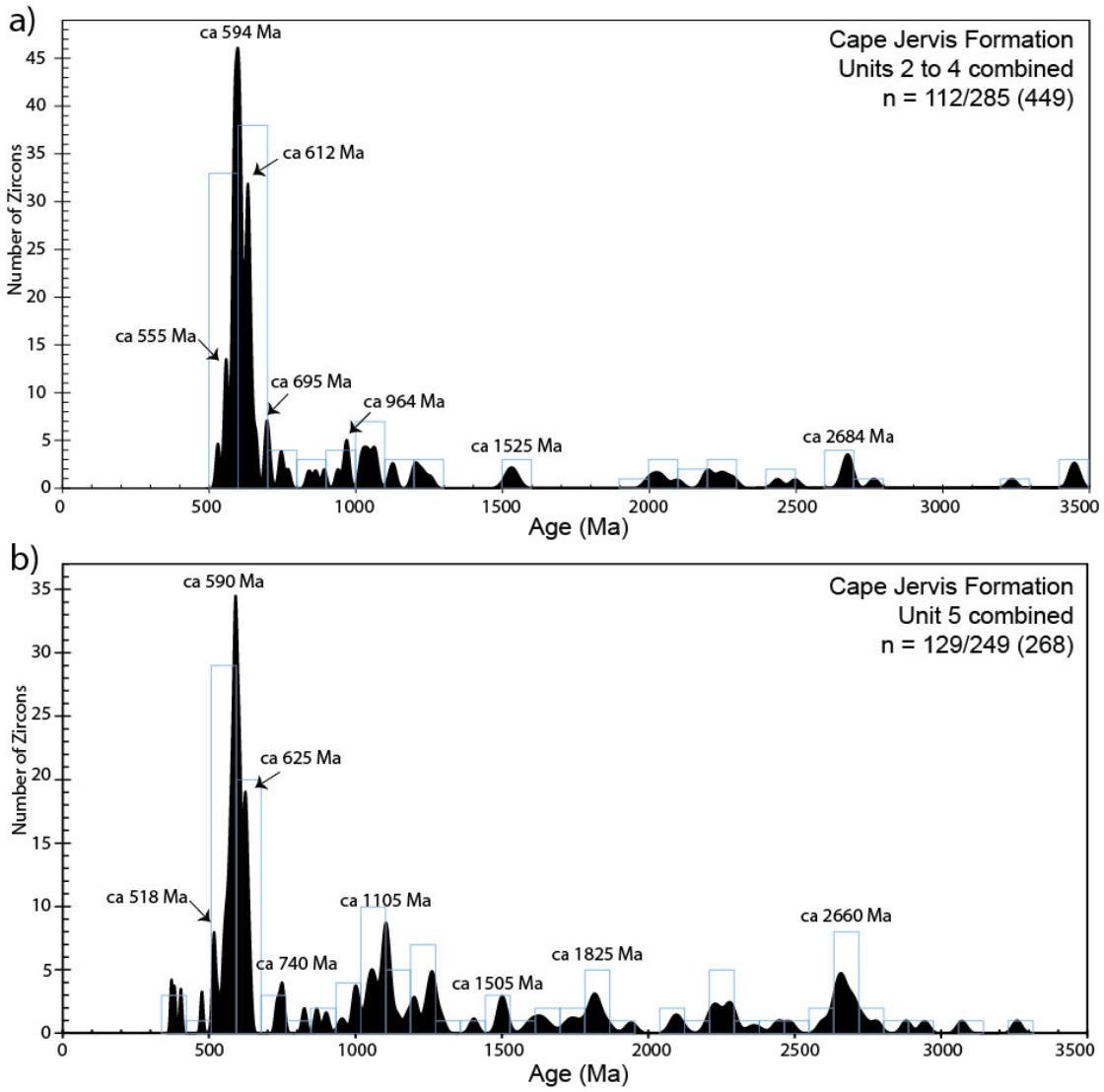

Figure 4:8 a) Combined provenance spectra of units two to four of the Cape Jervis Formation; b) Combined provenance spectra of unit five of the Cape Jervis Formation.

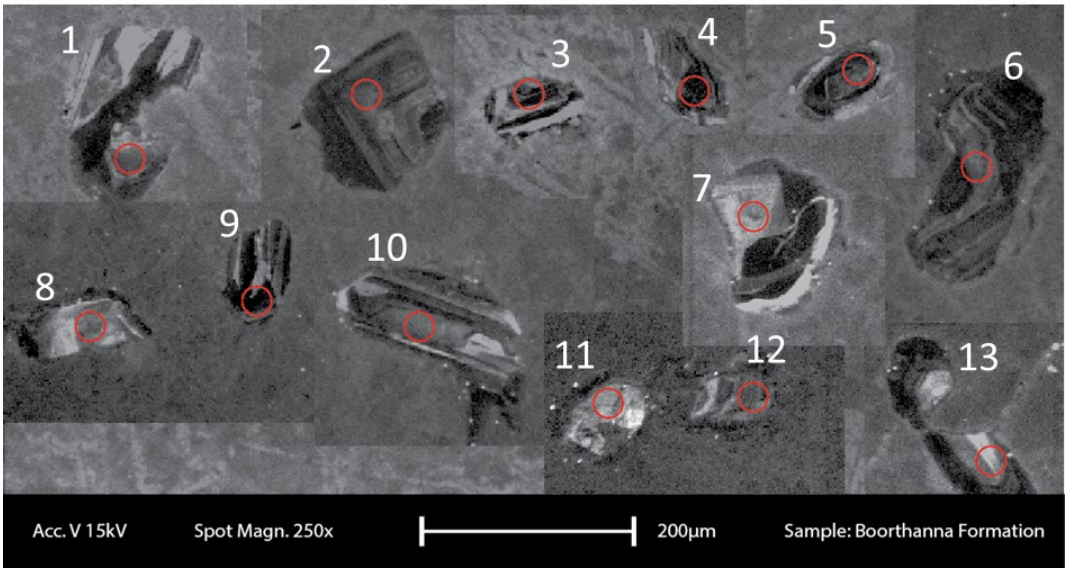

Figure 4:9 Representative cathodoluminescence images of zircon grains of the Boorthanna Formation. 30 µm laser spots are shown in red. Zircon numbers relate to the figure reference guide in Table 4:1.

4.3.2 Arckaringa Basin

Zircon descriptions

Zircon grains were extracted from all three samples from the Arckaringa Basin. Zircon grains from samples of Boorthanna Formation collected at Box Creek and Mount Dutton range from ~100 to ~250 µm size. The grains are typically elongate and show a rounded shape however, most grains are broken fragments (Figure 4:9). Most grains preserve zoning, including complex growth zoning, sector zoning and faint, broad zoning (Figure 4:9, Table 4:1). There is some evidence of metamorphic recrystalisation and new growth as some grains preserve cores with outer concentric zones (Figure 4:9, Table 4:1; Corfu et al. 2003). Most of the zircon grains extracted from the sample of Mount Toondina Formation collected at Mount Toodina were <40 µm in diameter, and therefore too small for use in LA-IC-PMS U-Pb isotopic analysis.

Zircon U-Pb geochronology

Mount Dutton section

One hundred and two zircon grains were analysed from the Mount Dutton section, of those 57 zircon grains were within ± 10% concordance (Figures 4:10a, b). The U-Pb isotopic ages of the concordant analyses range from ca 3180 and 490 Ma (Figure 4:11a). The strongest mode is from ca 1705 to 1950 Ma (n = 23). Lesser modes occur at ca 490 to 685 Ma (n = 11), ca 805 to 1020 Ma (n = 5), ca 1050 to 1280 Ma (n = 9), ca 1460 to 1610 Ma (n = 4) and ca 2220 to 3310 Ma (n = 5; Figure 4:11a).

Box Creek section

Of the 111 zircon grains analysed, 39 grains yielded analysis within 10% concordance (Figures 4:10c, d). These grains range in age from ca 3380 to 465 Ma (Figure 4:11b). The U-Pb isotopic ages of the concordant analyses range from ca 460 to 660 Ma (n = 14). Lesser modes occur at ca 930 to 1195 Ma (n = 12), ca 1435 to 1870 Ma (n = 8) and ca 2425 to 3380 Ma (n = 5; Figure 4:11b).

Combining of Boorthanna Formation age data

The sandstone samples of Boorthanna Formation from the Mount Dutton and Box Creek sections are recognised as being the similar lithology, as having been deposited within a similar glacial environment and as being stratigraphically equivalent (Chapter 3; Alley et al. 1995). Based on these correlations, the age spectra of the two samples were combined to assess the regional provenance of the Boorthanna Formation within the Boorthanna Trough.

The combined age spectra are shown in Figure 4:10c, and includes 96 concordant and near-concordant analyses. The U-Pb isotopic ages of the concordant analyses range from ca 3310 to 495 Ma (Figure 4:11c). The strongest modes occur at ca 1700 to 1945 Ma (n = 29) and lesser modes occur at ca 465 to 685 Ma (n = 22) and ca 1015 to 1280 Ma (n = 21; Figure 4:11c).

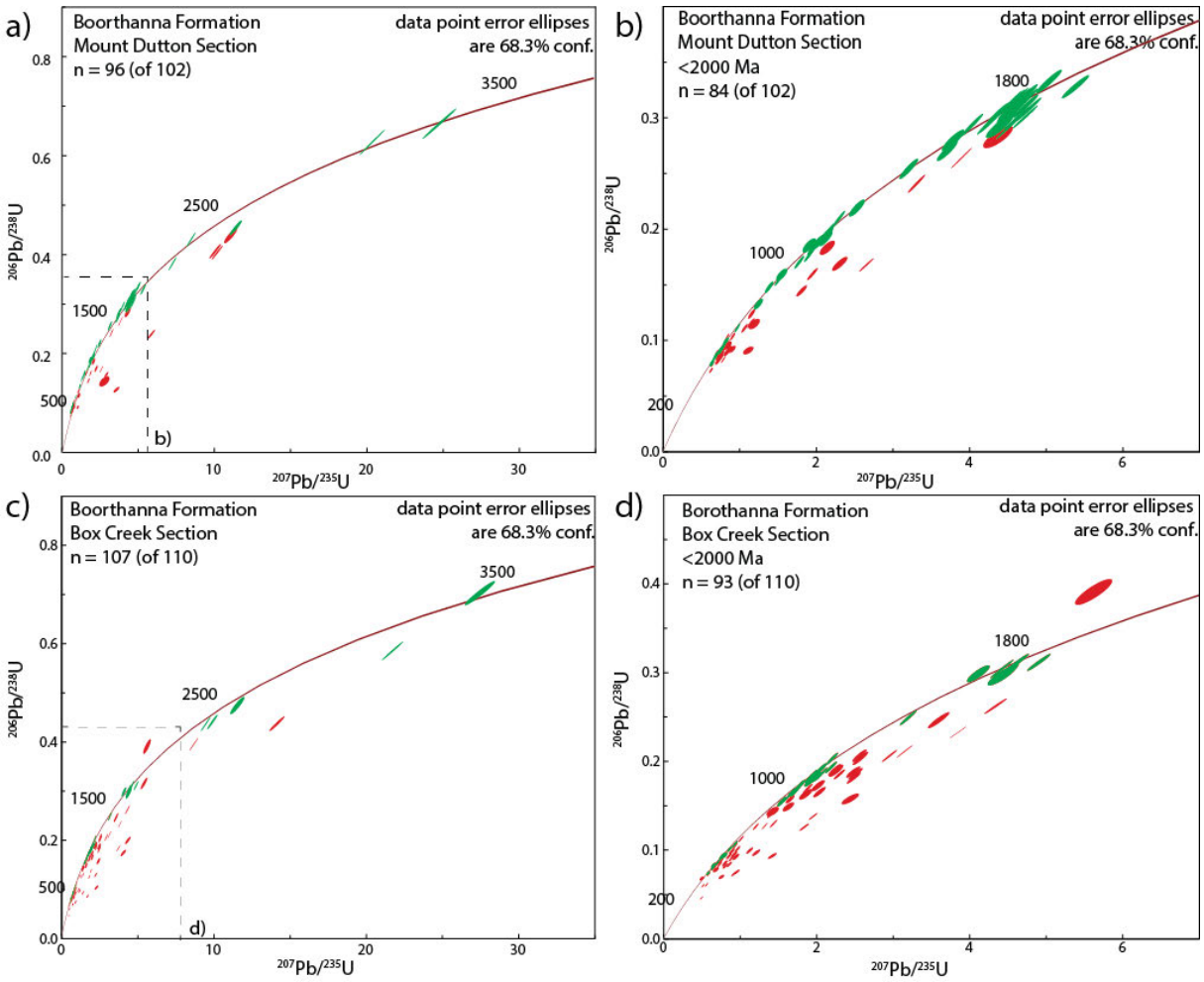

Figure 4:10 Concordia plot of all zircon grain analyses from the Boorthanna Formation a) all analyses from Mount Dutton; b) analyses of zircon grains with ages <2000 Ma from Mount Dutton; c) all analyses from Box Creek; d) analyses of zircon grains with ages <2000 Ma from Box Creek. Red ellipses are non-concordant zircon grains; green ellipses are concordant zircon grains.

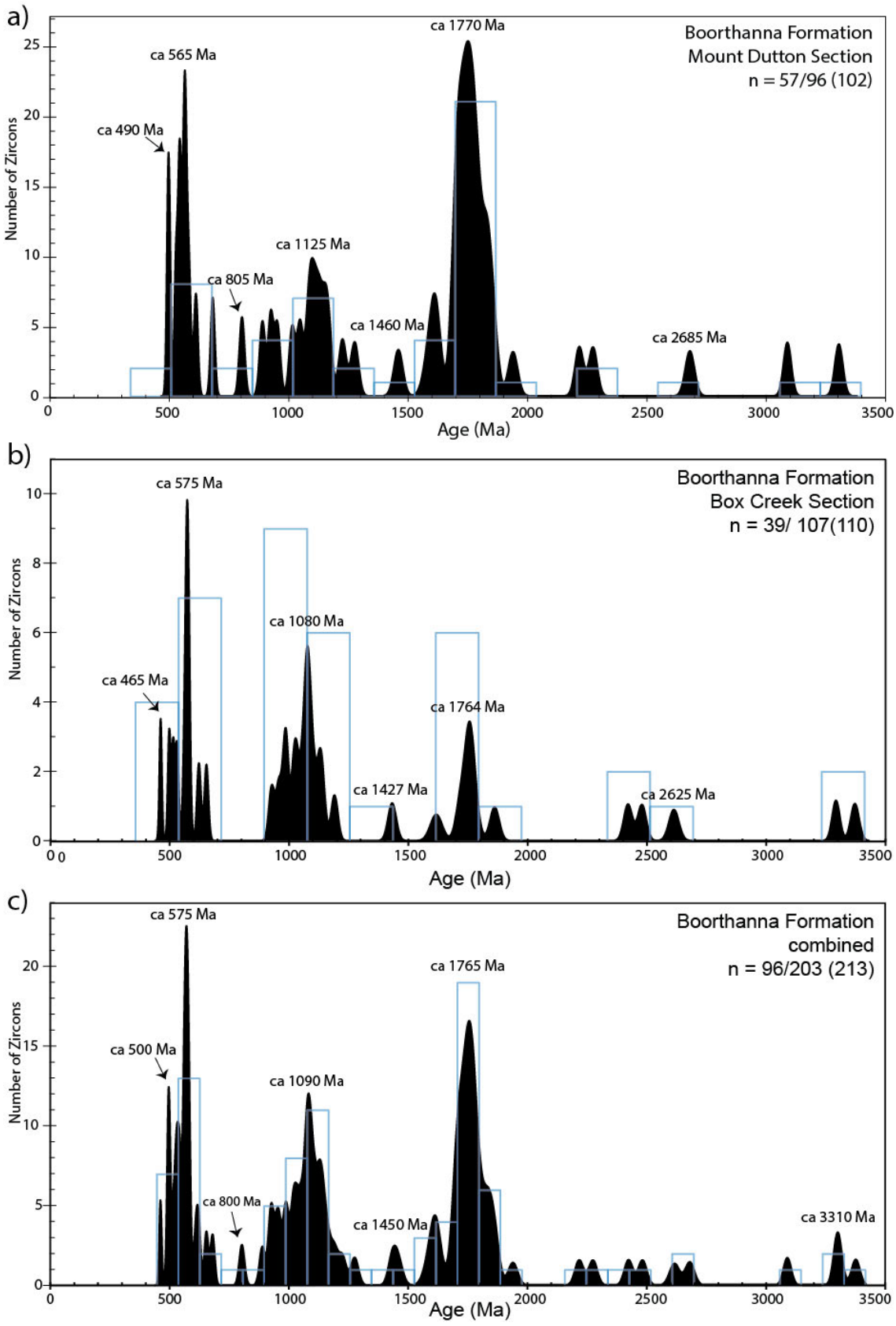

Figure 4:11 Age probability density plot for concordant and near concordant detrital zircons of the Boorthanna Formation from a) the Mount Dutton section; b) the Box section; c) Combined provenance spectra of the Boorthanna Formation. Blue bars show number of zircons included in analysis for each mode.

4.4 Discussion

The U-Pb isotopic dating of detrital zircon grains from the late Palaeozoic glacigene sedimentary rocks of the Troubridge and Arckaringa Basins can be used to assess sediment source region(s) and potentially infer glacial movement directions (Haines et al. 2011). Limitations of provenance analysis such as the representation of source regions in the sample population, the recognition of geological events capable of forming or altering significant numbers of zircon grains and the availability of age data within potential source regions need to be recognised. Without this recognition, the resulting provenance assessment may be an incorrect assessment of the sediment source region and consequently the interpreted glacial movement direction. Where possible, other observations also need to be used in conjunction with the detrital zircon age populations to assess the ice movement and fluvial flow directions and hence potential source regions. Indicators such as striae on glacial pavements and the distribution of erratics give direct indications of the ice movement direction (David and Howchin 1897, Milnes and Bourman 1972, Alley and Bourman 1984, Bourman and Alley 1988, Bourman and Alley 1990, Bourman and Alley 1999. Palaeocurrent indicators such as cross-beds or ripple marks can be used to assess the direction of deposition. Unfortunately, sedimentary structures are poorly preserved in the late Palaeozoic sedimentary rocks and cannot be used. The location of the sample in relation to the source region also requires consideration. An ice mass has the potential to transport sedimentary rocks large distances, at times a continental icesheet can move thousands of kilometres from its origin (Ashley et al. 1985, Bennett and Glasser 2009) and transport debris trapped in the ice. Conversely, the debris transport distances in fluvioglacial and meltwater streams are a relatively short as it is controlled by factors such as topography and sediment load (Bennett and Glasser 2009). Glacially influenced streams are often terminated by moraine deposits or uplifted strata causing damming and are therefore limited to transport distances of several kilometres (Bennett and Glasser 2009). Lastly, palaeogeography will dictate which potential source regions were proximal to the sedimentation depocentre.

Assessment of any given terrane as a potential source of sedimentary rocks in a region may be done using expected age histograms constructed from zircon age data and that show zircon forming or altering events that occurred within the potential source terrane (e.g. Pell et al. 1997, Maidment et al. 2007). Expected age histograms have been constructed based on the process outlined by Pell et al. (1997) from published age data for each of the terranes (e.g. Ireland et al. 1998, Camacho et al. 2002, Neumann and Fraser 2007, Maidment et al. 2007, Paulsen et al. 2007, Wade et al. 2008) and these are shown in Figure 4:12 along with the histograms of the Cape Jervis Formation and Boorthanna Formation.

Next page: Figure 4:12 Expected age histograms for potential source regions of glacigene sedimentary rocks in the Troubridge and Arckaringa basins. a) Gawler Craton adapted from Neumann and Fraser (2007) and Fanning et al. (2007); b) Arunta Region data from Maidment et al. (2007) and Camacho et al. (2002); diagram adapted after Pell et al. (1997); c) Musgrave Province data from Maidment et al. (2007), Camacho et al. (2002) and Wade et al. (2008); diagram adapted after Pell et al. (1997); d) Transantarctic Mountains of Antarctica adapted from Paulsen et al. (2013); e) Adelaide Rift Complex, light blue histogram is the expected age histogram of the Neoproterozoic sedimentary rocks of the ARC, dark blue histogram is the expected age histogram of the Cambrian sedimentary rocks of the Adelaide Rift Complex data from Ireland et al. (1998); diagram adapted after Pell et al. (1997); f) U-Pb age probability plot for units two to four of the Cape Jervis Formation; g) U-Pb age probability plot for unit five of the Cape Jervis Formation; h) U-Pb age probability plot for the Boorthanna Formation. Troubridge Basin sedimentary rocks are in red, Arckaringa Basin sedimentary rocks are in green, grey bars highlight age ranges of interest: 1: ca 470 to 700 Ma; 2: ca 900 to 1300 Ma; and 3: ca 1650 to 2000 Ma. Black, dark and light blue histograms of source regions for comparisons to the red and green histograms of the Troubridge and Arckaringa basins.

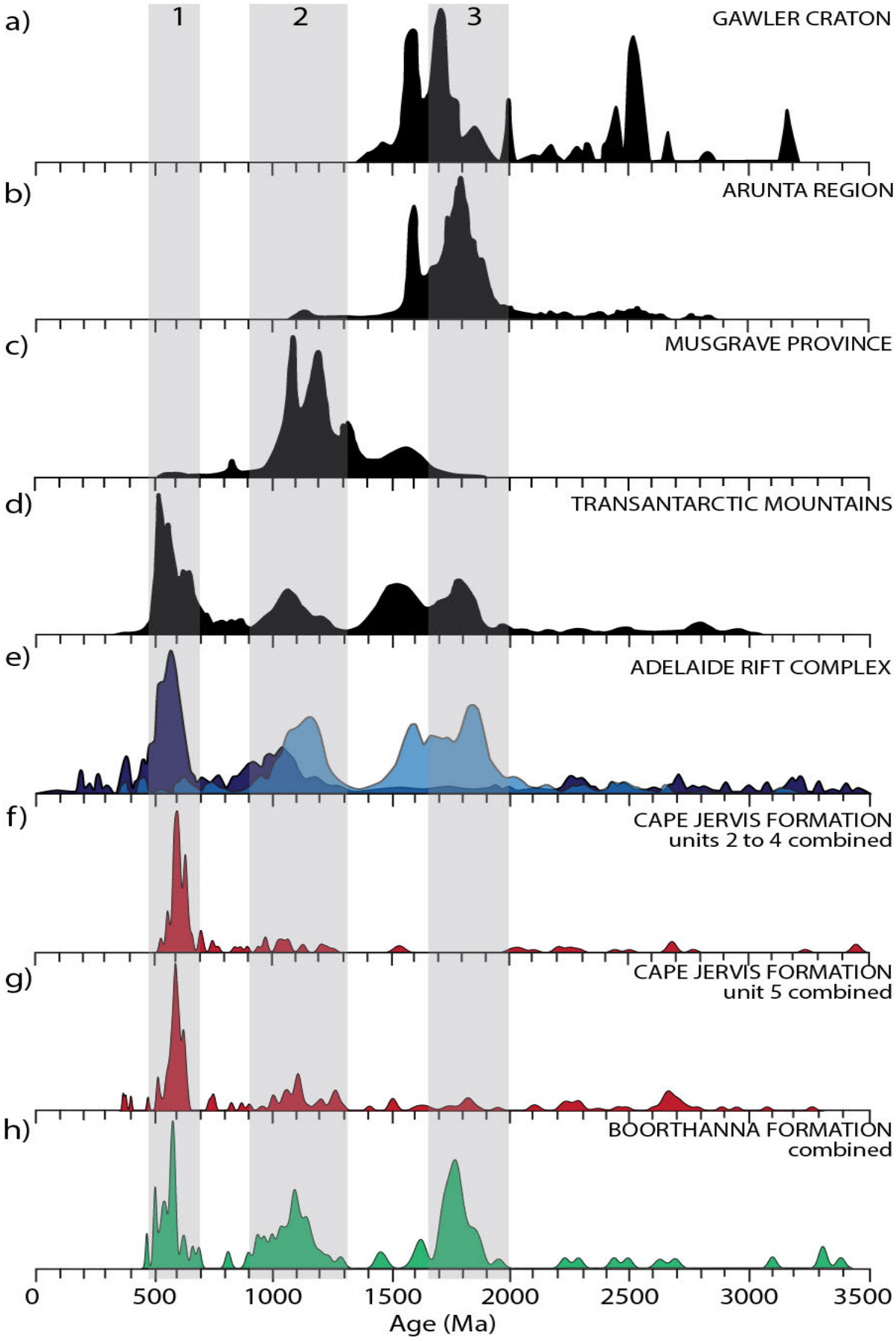
a)
1
2
3
GAWLER CRATON
b)
ARUNTA REGION
c)
MUSGRAVE PROVINCE
d)
TRANSANTARCTIC MOUNTAINS
e)
ADELAIDE RIFT COMPLEX
f)
CAPE JERVIS FORMATION
units 2 to 4 combined
g)
CAPE JERVIS FORMATION
unit 5 combined
h)
BOORTHANNA FORMATION
combined
0
500
1000
1500
2000
2500
3000
3500
Age (Ma)

4.4.1 Comparisons between of provenance spectra

There are some similarities between the provenance spectra of the Cape Jervis Formation and Boorthanna Formation (Figures 4:12f to h). Both units have a significant age population of ca 490 to 700 Ma. The most significant difference is the increased Mesoproterozoic (i.e. ca 900 to 1300 Ma) and Palaeoproterozoic (ca 1650 to 2000 Ma) occurrence in the Boorthanna Formation sedimentary rocks (Figure 4:12h) compared to the Cape Jervis Formation (Figures 4:12f, g). Units two to four of the Cape Jervis Formation have a minimal component of the Palaeoproterozoic ages grains, while unit five has a slight increase. Unit five also has a small proportion of sedimentary rocks Mesoproterozoic aged sedimentary rocks that are not present in units two to four (Figures 4:12f to h).

The detrital zircon age spectra for units two to four and unit five of the Cape Jervis Formation show some variation (Figures 4:12f, g), particularly away from the dominant age population. This difference can likely be attributed to the different depositional settings from the glacially influenced deposition of units two to four to the marine dominated depositional setting of unit five (e.g. Alley and Bourman 1984, 1995, Bourman and Alley 1999) and the associated differences in sediment transport mechanisms. The sedimentary rocks containing zircon grains of ca 500 to 620 Ma are dominant in both provenance spectra of the Cape Jervis Formation. The dominant mode for both spectra is ca 590 Ma and most grains are between ca 570 and 610 Ma (Figures 4:12f, g).

4.4.2 Source of ca 490 to 700 Ma zircon grains

Neoproterozoic to Cambrian (ca 490 to 700 Ma) zircon grains are dominant in the provenance spectrum of the Cape Jervis and Boorthanna Formation (Figure 4:12g to h). Zircon grains of this age range dominate both the combined unit two to four and the unit five of the Cape Jervis Formation spectra. This suggests that most of the zircon grains in Cape Jervis Formation was sourced from rocks with zircon grains between ca 490 and 700 Ma, specifically ca 570 and 640 Ma (Figures 4:12f, g). The Boorthanna Formation sedimentary rocks also have a significant proportion of grains aged ca 500 to 620 Ma (Figure 4:12h). The shape and age range of the ca 490 to 700 Ma portion of the histogram of the Boorthanna Formation is similar to the dominant peak seen of the glacigene sedimentary rocks of the Troubridge Basin (Figure 4:12f to h).

The dominance of the sedimentary rocks of this age range in the Cape Jervis Formation suggests a restricted source such as from a discrete metamorphic or magmatic event. The zircon grains from the Cape Jervis Formation are typically prismatic and preserve oscillatory zoning (Figure 4:5a, Table 4:1), which suggests the grains were sourced from an igneous rock within which the zircon grains grew. There are no known magmatic events of ca 590 Ma in the Adelaide Rift Complex. The expected age histogram for the Cambrian Kanmantoo Group sedimentary rocks has dominant ca 610-570 Ma sedimentary rocks (Figure 4:12d). As there are no known rocks of this age in the Kanmantoo Group; it is likely that these sedimentary rocks have been inherited from elsewhere.

The expected histogram of the TAM also has the dominant ca 610 to 570 Ma zircon population (Figure 4:12e). Provenance studies of sedimentary rocks of the TAM consistently show a dominant age population of ca 590 Ma (Veevers et al. 2006, Goodge et al. 2012, Paulsen et al. 2013). Potential source units in Antarctica with an age of ca 590 Ma age include the granitoids associated with the ca 555-590 Ma magmatism of the Ross Orogen as well as granites with igneous crystallisation ages of ca 555-590 Ma of the TAM (Goodge et al. 2012). Mikhalsky et al. (1997) reported evidence of

metamorphism and deformational events reflected in ca 540-590 Ma aged zircon grains from the Humboldt Mountains, which is also part of the TAM.

The sedimentary rocks of the Cape Jervis Formation were likely sourced from both the Kanmantoo Group and the TAM (Figure 4:2). It is likely that rocks from Antarctica are the source of the ca 570 to 610 Ma sedimentary rocks in both the Kanmantoo Group sedimentary rocks and the Cape Jervis Formation. The similarity of the shape of the ca 500-650 Ma sedimentary rocks in the expected histograms of the Kanmantoo Group and the TAM along with the absence of known ca 590 Ma rocks in the ARC implies that the 500-650 Ma sedimentary rocks were likely sourced from the TAM. This is further supported by the positon of Antarctica to relation to South Australia during the time of the deposition of the Kanmantoo Group; (Figure 4:2; Alley and Bourman 1995, Foden et al. 2006).

Distal sources of the ca 590 Ma zircon grains could be volcanic rocks within the Wonominta Block to the east of the ARC and Tasman Fold Belt (Figure 4:2). Crawford et al. (1997) reported the Mount Arrowsmith and Mount Wright Volcanics in western New South Wales have a SHRIMP U-Pb zircon age of ca 585 to 590 Ma. The Mount Wright Volcanics, are postulated to be geochemical correlatives of the ca 550 Ma Truro Volcanics in the ARC (Crawford et al. 1997). Lavas and dykes in western Tasmania with K-Ar dates of ca 590-600 Ma (Direen and Crawford 2003) are potential sediment source from the Wonominta Block and Tasman Fold Belt.

It is difficult to ascertain whether the source of the ca 590 Ma zircon grains within the Cape Jervis Formation were sourced from the TAM directly or recycled through the Kanmantoo Group. This is due to the possibility of the zircon grain being recycled through many cycles of deposition. Most of the zircon grains have at least one rounded edge suggesting that the majority of zircon grains have undergone some recycling. There is no apparent correlation between the internal structure and the U-Pb isotopic age of the zircon grains. Sedimentary rocks of the ca 590 Ma age range are absent from the Mesoproterozoic to Paleoproterozoic ARC sedimentary rocks (Figure 4:12e) or the Gawler Craton (Figure 4:12a) which are the most proximal potential source regions. Given the proximity of the Kanmantoo Group and the TAM (Figure 4:2) to the Troubridge Basin it is likely that these were the sediment source. The northwards advancement of the icesheet (Alley and Bourman 1984, Bourman and Alley 1988, Alley et al. 1995) from Antarctica into the Troubridge Basin may have transported the ca 610-570 Ma sedimentary rocks into the basin. Alternatively, the ca 610-570 Ma could have been sourced from the Kanmantoo Group sedimentary rocks that were eroded by the advancing ice, and that were likely originally sourced from the TAM (Ireland et al. 1998). It is also possible that the sedimentary rocks were sourced from both the Kanmantoo Group and TAM. A portion of the ca 590 Ma zircon grains may have also been sourced from the distal Wonominta Block and the Tasman Fold Belt.

The presence of erratics in units two to four of the Cape Jervis Formation can also be used to constrain potential sediment source regions. Locally-sourced erratics include metasedimentary rocks of the Kanmantoo Group (and Encounter Bay Granite at the Kings Point section). The local nature of these erratics implies they cannot be used to provide any indication of the ice movement directions. Distally-sourced erratics dominantly comprise the Neoproterozoic Encounter Bay Granite (Foster 1974, Alley and Bourman 1984, Bourman and Alley 1999), which is exposed on the southern Fleurieu Peninsula around Victor Harbor (Figure 4:1a; Thompson and Horwitz 1962, Gravestock et al. 1995). The Encounter Bay Granite is part of the Cambrian ARC succession and its presence as erratics in the

sedimentary rocks is further evidence that the sedimentary rocks were sourced from the Cambrian ARC (Gravestock et al. 1995).

The ca 500 to 620 Ma zircon grains of the Boorthanna Formation (Figure 4:12h) are not the most dominant population, however, the presence of zircon grains of this age cannot be discounted. Sedimentary rocks of this age are not in any of the local potential source regions, such as the Gawler Craton, Arunta Region and Musgrave Province (Figure 4:12a to c) it is probable that the ca 500 to 620 Ma aged sedimentary rocks were sourced from the ARC. The sedimentary rocks were probably carried north from the TAM and Kanmantoo Group by the advancing icesheet and associated ice tongues. Like the Cape Jervis Formation, it is not possible to determine the exact source of the ca 500 to 620 Ma sedimentary rocks, however, it can be determined that they were sourced from the south from either the Kanmantoo Group or TAM. This is supported by the generally northerly ice movement direction and the absence of younger sedimentary rocks in the Gawler Craton expected age histogram (Figure 4:12a).

4.4.3 Source of ca 900 to 1300 Ma zircon grains

The notable difference between the provenance spectra of the Cape Jervis Formation and the Boorthanna Formation is the increase in sedimentary rocks older than ca 900 Ma in the latter (Figures 4:12f to h). The younger Proterozoic population of the Boorthanna Formation (ca 900-1300 Ma) population is similar in shape and age range to populations seen in the ARC, TAM and Musgrave Province (Figures 4:12c to e). Given the proximity of the Mesoproterozoic to Paleoproterozoic ARC and the Musgrave Province to the Arckaringa Basin (Figure 4:2), it is probable that the sedimentary rocks of the Boorthanna Formation were primarily sourced from the Mesoproterozoic to Paleoproterozoic ARC and Musgrave Province rather than from the distal TAM. Veevers (2006) suggested a region of highlands was present during the Late Palaeozoic in the area that is now recognised as the Musgrave Province. This region of elevated topography during the late Palaeozoic would be susceptible to erosion and would be a potential local source of sedimentary rocks for the Boorthanna Formation. It is not known if debris from the Musgrave Province was transported via fluvial or glacial mechanisms. However, given the high latitude of Australia during the Permo-Carboniferous glaciation and the probability that the Musgrave Province was at an increased height compared to the modern landscape it is likely that alpine glaciers were present.

The older sedimentary rocks (<900 Ma) of the Boorthanna Formation were likely sourced from the Mesoproterozoic to Paleoproterozoic ARC and the Gawler Craton. The Peake and Denison Ranges which is adjacent to the Arckaringa Basin have sedimentary rocks from both the Mesoproterozoic to Paleoproterozoic ARC and the Gawler Craton. This interpretation is also supported by the observations of Heath (1963) and Ambrose et al. (1981) of erratics and clasts in the Boorthanna Formation that are of similar lithologies to rocks of the Peake and Denison Ranges. These sedimentary rocks were likely transported into the basin via montane and valley glaciers and the associated meltwater streams which were situated in the Gawler Craton highlands. Sedimentary rocks from distal source regions such as the Arunta Region and Musgrave Province were likely also transported via montane and valley glaciers.

There is a less significant proportion of the ca 900 to 1300 Ma-aged zircon grains in the provenance spectrum of the Cape Jervis Formation (Figure 4:12f, g) when compared to that of the Boorthanna Formation (Figure 4:12h). This can likely be attributed to the potential source of these zircon grains. The pattern of the ca 900 to 1300 Ma zircon grains in the Cape Jervis Formation spectra is similar in

shape of the expected histogram of the Cambrian rocks and Mesoproterozoic to Paleoproterozoic rocks of the ARC (Figure 4:12e), a minor peak of the TAM histogram (Figure 4:12d) as well as the main component of the Musgrave Province histogram (Figure 4:12c). Given that the majority of the zircon grains in the Cape Jervis Formation are sourced from rocks of the the Cambrian ARC and the TAM, it is likely that the ca 900 to 1300 Ma zircon grains are also primarily sourced from these rocks. The small portion of zircon grains of this age suggest that the primary source in the ARC and TAM rocks was likely the Musgrave Province. These were then reworked from the metasedimentary rocks of the ARC and TAM into the Cape Jervis Formation as part of the debris eroded from these terranes.

Studies of the exhumation history of the eastern Musgrave Province by Glorie et al. (2017) suggest that the Musgrave Province underwent at least three cooling events. Apatite fission track analysis infer that these cooling and exhumation events occurred during the late Neoproterozoic (ca 550 Ma), the Silurian to Devonian (ca 450 to 400 Ma) and the late Carboniferous (ca 310-290 Ma; Glorie et al. 2017). These events imply that at least a portion of the Musgrave Province was exposed during the Permo-Carboniferous glaciation, consequently, eroded debris from the associated rocks would have been available for transport via fluvial and/or glacial transport mechanisms and subsequent deposition.

4.4.4 Source of ca 1650 to 2000 Ma zircon grains

The most populated age range in the Boorthanna Formation is ca 1650 to 2000 Ma. The shape of the provenance spectra is similar to the shape of the Proterozoic sedimentary rocks in the ARC (Figure 4:12e). Ireland et al. (1998) and Pell et al. (1997) surmised that these were inherited from the Gawler Craton. Grains of this age are also a component of the TAM expected age histogram (Figure 4:12d).

The expected histogram for the Gawler Craton (Figure 4:12a) both have populations within this age range. The ca 1650-2000 Ma zircon grains are recognised within the basement rocks of the Peake and Denison Ranges (Figure 4:1) which include rocks of the Gawler Craton and ARC. Geochronology data for the Peake and Denison Ranges are limited, however, the rock packages with available age data mostly fall within the 1700 to 1900 Ma age range. The Tidnamurkana Volcanics have U-Pb SHRIMP zircon ages of 1774 ± 6 and 1789 ± 10 Ma (Fanning et al. 2007) and a less precise age of 1806 ± 27 Ma (Neumann and Fraser 2007). Felsic volcanics of the Peake and Denison Ranges have yielded an age of 1740 ± 6 Ma and the Wirriecurrie Granite has been dated as 1787 ± 8 Ma (Fanning et al. 2007).

A small ca 1590 Ma mode within the Boorthanna Formation spectra (Figure 4:12h) has been attributed to the ca 1592 Ma Gawler Range Volcanics (Drexel et al. 1993, Giles et al. 2004) and the ca 1575-1595 Ma Hiltaba Suite Granites (Cooper et al. 1985, Creaser and Cooper 1993). The Gawler Range Volcanics and Hiltaba Suite Granites are part of an extensive suite of felsic and mafic volcanics and intrusions that were extruded and emplaced across much of the Gawler Craton (Drexel et al. 1993). Furthermore, granites in the Peake and Denison Ranges (Figure 4:1b) that yield an age of ca 1590 (Fanning et al. 2007, Neumann and Fraser 2007), and may also account for the small ca 1590 Ma zircon age population recognised in the Boorthanna Formation.

Recent apatite fission track studies suggest that exhumation of the Peake and Denison Ranges occurred from ca 470 to 440 Ma and ca 320 to 280 Ma (Hall et al. 2016). The second exhumation event during Carboniferous to Early Permian (ca 320 to 280 Ma) brought the Peake and Denison Ranges to the surface (Hall et al. 2016). This suggests that the rocks of the Peake and Denison Ranges

were exposed during deposition of the Boorthanna Formation. Debris was likely eroded and transported into the Boorthanna Trough via valley glaciers and fluvial mechanisms.

Grains of this age are also present in the expected age histogram of the Arunta Region (Figure 4:12b), potential source rocks within the Arunta Region include the ca 1790-1810 Ma rocks of the Strangway Metamorphic Complex (Scrimgeour 2013). Although the Arunta Region is a potential sediment source for the Boorthanna Formation it is more probable that the sedimentary rocks were sourced from the proximal Gawler Craton and ARC. If a component of the ca 1650-2000 Ma sedimentary rocks were sourced from the TAM it is likely that the sedimentary rocks were transported into the basin via the advancing icesheet. The sedimentary rocks were likely eroded either directly from Antarctica (Mikhalsky et al. 1997, Goodge et al. 2012, Paulsen et al. 2013) or from the Kanmantoo Group sedimentary rocks (Ireland et al. 1998). Given the distal location of the TAM and the extensive distance the sediment would have to travel it is likely that only a small proportion of the sediment was sourced from the TAM.

Alley and Bourman (1995) suggested that the Boorthanna Formation sedimentary rocks were sourced from the Gawler Craton and deposited as a result of the northward advance of the icesheet as inferred by Alley and Bourman (1984). This northward advance would have transported a large proportion sedimentary rocks from the Gawler Craton as well as a smaller component from the Kanmantoo Group and TAM into the Arckaringa Basin. The presence of montane glaciers in the highlands of the Arunta Region and Musgrave Province may have provided some sedimentary rocks into the Arckaringa Basin. The most proximal source to the eastern margins of the Arckaringa Basin and the sample locations are the Gawler Craton and the Mesoproterozoic to Paleoproterozoic ARC (Figure 4:2).

This age range is less significant in the detrital zircon provenance spectra of the Cape Jervis Formation (Figure 4:12f, g). This is likely due to the majority of detritus in the Cape Jervis Formation being sourced from the Kanmantoo Group and TAM (Figure 4:12d, e). This is demonstrated by the greater proportion of ca 490 to 700 Ma zircon grains in the provenance spectrum of the Cape Jervis Formation (Figure 4:12f, g).

4.5 Conclusions

The most likely sediment source for the Cape Jervis Formation in the Troubridge Basin is the Cambrian Kanmantoo Group and TAM. The expected histograms of the Kanmantoo Group and TAM are similar in shape and age range to the Cape Jervis Formation. The Kanmantoo Group is the closest potential sediment source to the basin therefore it is reasonable to expect that the majority of sedimentary rocks are derived from the most local source. This is consistent throughout the units of the Cape Jervis Formation. As South Australia was connected to Antarctica during the late Palaeozoic it is possible that the TAM was a local potential sediment source. A small portion of sedimentary rocks may also have been sourced from the Proterozoic sedimentary rocks of the ARC.

The most likely sediment sources for the Boorthanna Formation in the Boorthanna Trough of the Arckaringa Basin are the Gawler Craton, Mesoproterozoic to Paleoproterozoic portion of the ARC and the Musgrave Province. The detrital provenance spectrum of the Boorthanna Formation is similar in shape to the expected histograms of the Mesoproterozoic to Paleoproterozoic portion of ARC and Musgrave Province. It is likely that the majority of the sedimentary rocks were sourced from the Gawler Craton and Mesoproterozoic to Paleoproterozoic ARC as they are the most local source

regions to the Boorthanna Trough. The Musgrave Province and Kanmantoo Group of the ARC are distal sources, however, is still a viable sediment source for the Arckaringa Basin. Other potential distal sources for the Boorthanna Formation include the Arunta Region and TAM.

These outcomes show that despite the capacity for a glacier to move debris long distances, the majority of glacigene sedimentary rocks are sourced from local terranes. The abrasive action from an advancing or regressing ice mass and from the meltwater streams erodes and reworks the local sedimentary rocks in to the glacigene sedimentary rocks. The local source regions provide the majority of sedimentary rocks to the late Palaeozoic glacigene sedimentary rocks this suggests that the glacier erodes and deposits debris within a short distance and only traps and transports a small proportion of the material. This results in small populations of probably distally-sourced sedimentary rocks within the provenance spectra of the Cape Jervis and Boorthanna formations.

Chapter 5: Geochemistry of late Palaeozoic glacigene sedimentary rocks of the Troubridge and Arckaringa basins

Foreword

This chapter documents the results of whole rock geochemical analysis, carried out on all samples collected from the Troubridge Basin and Arckaringa Basin. Samples analysed were collected during sampling of measured sections detailed in Chapters 2 and 3. Sample preparation and whole rock XRF and ICP-MS geochemical analysis was performed by ACME Laboratories, Canada. Statistical analysis and comparative geochemical plots were created by the author using the geochemical software package IoGAS. The lithological constraints of the whole rock geochemistry and associated process signals are presented here as a series of Harker plots. An examination into the geochemical background and implications using glacigene sediments as a geochemical exploration media is also presented in this chapter. This chapter has been written as an independent publication and is structured accordingly.

Abstract

Major element ratios in the geochemistry of the late Palaeozoic glacigene sedimentary rocks of the Troubridge and Arckaringa basins differentiate a number of geochemical signals suggesting depositional and weathering processes largely control the geochemistry. The depositional processes of the glacigene sedimentary rocks are distinguishable via Al_2O_3:SiO_2 ratios. Sedimentary rocks deposited in a high energy fluvial setting have high concentrations of SiO_2 and are dominated by quartz grains with few other minerals present. Subsequently, these sedimentary rocks have low trace and rare earth element concentrations. Sedimentary rocks deposited in low energy lacustrine environments are clay rich and therefore have high Al_2O_3 contents. The high clay content is also reflected in the high K_2O, trace and rare earth element concentrations. The intense weathering of the sedimentary rocks includes sulphate, carbonate, ferruginous and clay weathering. These can be identified using ratios of Al_2O_3, Fe_2O_3, K_2O, CaO and MgO. Sedimentary rocks that have geochemical signatures that are not controlled by depositional or weathering processes are typically moderately oxidised or minimally weathered. The geochemistry of these sedimentary rocks is reflective of their source rocks. The likely source rocks for the Palaeozoic glacigene sedimentary rocks include the Kanmantoo Group metasedimentary rocks. If the background geochemical signals related to provenance, depositional processes and weathering processes can be recognised and accounted for (for example by using simple normalisations) there is a better chance of isolating geochemical signals related to local enrichment of commodity elements that may be relevant to mineral exploration.

5.1 Introduction

Glacigene sedimentary rocks are common in the geologic record and cover large areas of potentially mineralised basement rocks, particularly at high latitudes in the northern hemisphere (e.g. Canada and Scandinavia) that were glaciated during the Neogene (Shilts 1993). The glacial sedimentary rocks present a challenge for mineral exploration, being both a potential hindrance (introducing a physical and chemical barrier of far-travelled material that may have little genetic relationship to the underlying basement) and a potential opportunity (as a regolith sample medium the provenance of which could be traced upstream of the glacial movement direction towards possible source rocks). Mineral exploration using glacigene sedimentary rocks has become more popular in the last 50 years and has paralleled a growing understanding of glacial transport mechanisms (McClenaghan and DiLabio 1993, Shilts 1993, McClenaghan et al. 2000, Forbes et al. 2015) and geochemistry as a tool for vectoring towards potential mineralisation (DiLabio and Coker 1987, McMartin and McClenaghan 2001, Sarala et al. 2009).

The utilisation of glacigene sedimentary rocks as a sample medium is not only applicable to sedimentary rocks of recent glaciations such as those in Canada but it is also relevant to ancient glacigene sedimentary rocks. Much of South Australia is covered with ancient glacigene sedimentary rocks, such as those preserved in the late Palaeozoic Arckaringa and Troubridge basins (Figure 5:1). Late Palaeozoic glacigene sedimentary rocks bury a large portion of the Gawler Craton, Adelaide Rift Complex and the overlying Kanmantoo Group, which host important mineral provinces such as the Olympic Province IOCG±U domain of the eastern Gawler Craton and the Kanmantoo Trough (Figure 5:1; Parker 1985, Creaser and Cooper 1993). In deeply weathered geological environments, such as

those in South Australia, the glacigene sedimentary rocks may have been subjected to a range of post-depositional near-surface processes (e.g. weathering, induration) with the potential to enhance or detract from their use as geochemical exploration sample media (Plumlee 1999, Taylor and Eggleton 2001, Anand 2005, McQueen 2006, Scott and Pain 2008).

Figure 5:1 Approximate limits of the late Palaeozoic basins in South Australia showing the Troubridge (red outline) and Arckaringa (green outline) basins. Other key Proterozoic provinces and mineralised domains are also shown as well as key mineral deposits. Adapted from Alley and Bourman (1995).

The use of glacigene sedimentary rocks as sampling media for mineral exploration requires a detailed understanding of their background geochemistry. The lithological and mineralogical controls on the geochemistry as well as the processes affecting the geochemistry, which may or may not be related to the presence of mineralisation, must be completely understood. The most important controls on the geochemistry of glacigene sedimentary rocks relate to 1) provenance of the detrital materials, 2)

depositional processes, in particular mineralogical sorting on the basis of grain size or density, and 3) post-depositional processes such as chemical weathering and induration. Ferruginous or calcareous induration during weathering is a common process in southern Australia and has the potential to dramatically alter the geochemistry of surface samples. Such indurated regolith materials have been favoured sample media for mineral exploration (Butt et al. 1997, Anand 2005) due to the potential for the weathering processes to enhance the exploration geochemical signal (for example by preferentially scavenging pathfinder elements from groundwater). From understanding the controls on the geochemistry, the concentration range that is background for the sedimentary rocks and therefore geochemically enriched samples can be determined.

This chapter presents geochemical analyses of sedimentary rocks from the late Palaeozoic Troubridge and Arckaringa basins. The lithogeochemistry of the sedimentary rocks is used to provide constraints on the weathering and depositional processes as well as remnant provenance signals. The geochemistry of the remnant provenance signals are then used to assess the possibility of the metasedimentary rocks of the Kanmantoo Group being the dominant source rocks of the glacigene sedimentary rocks. From the understanding of the processes controlling the geochemistry of the glacigene rocks the geochemical background of the glacigene rocks can be defined. The geochemical background of the glacigene sedimentary rocks is then used to provide a basis for the recognition of anomalies as an example of how glacigene rocks can be used as a sampling medium in future geochemical exploration programs.

5.2 Methods

5.2.1 Sampling

One hundred and eighty one surface samples of late Palaeozoic glacigene sedimentary rocks were collected; 144 from the Troubridge Basin and 37 from the Arckaringa Basin. The sample sites include eight key stratigraphic sections at which numerous samples were taken and 71 sites each represented by a single sample (Figure 5:2).

All samples from the Troubridge Basin were taken from the Cape Jervis Formation; 69 were taken from the measured sections (described in Chapter 2) and 75 were collected from surface exposures across the basin (Figure 5:2a). The regional surface samples were collected in order to assess lateral variations in geochemistry and to mimic an opportunistic exploration geochemical survey utilising glacigene sedimentary rocks from a restricted stratigraphic interval as sample media. Of the regional surface samples, 57 were collected from the Fleurieu Peninsula, eight from Kangaroo Island and ten from the Yorke Peninsula. Sample locations were selected based on 250k mapped exposures of the Cape Jervis Formation (Crawford 1960, Thompson and Horwitz 1962, Fairclough 2007, Belperio et al. 2009, Zang and Crawford 2009) and invariably were taken where the glacigene rocks are exposed along roadsides and in road cuttings. Where possible the samples were collected 0.5 to 1 km apart. These exposures were rarely more than one metre high and often oxidised and indurated.

Of the Arckaringa Basin samples, 12 were collected from measured sections of the Boorthanna Formation at Box Creek and Mount Dutton (Figure 5:2b) and 26 samples were taken from the Mount Toondina Formation at the Mount Toondina type section (Figure 5:2b). Due to limited surface exposures there were no opportunistic samples collected in the Arckaringa Basin. For detailed

descriptions of the location, stratigraphy and sedimentology of the key sections refer to Chapters 2 and 3.

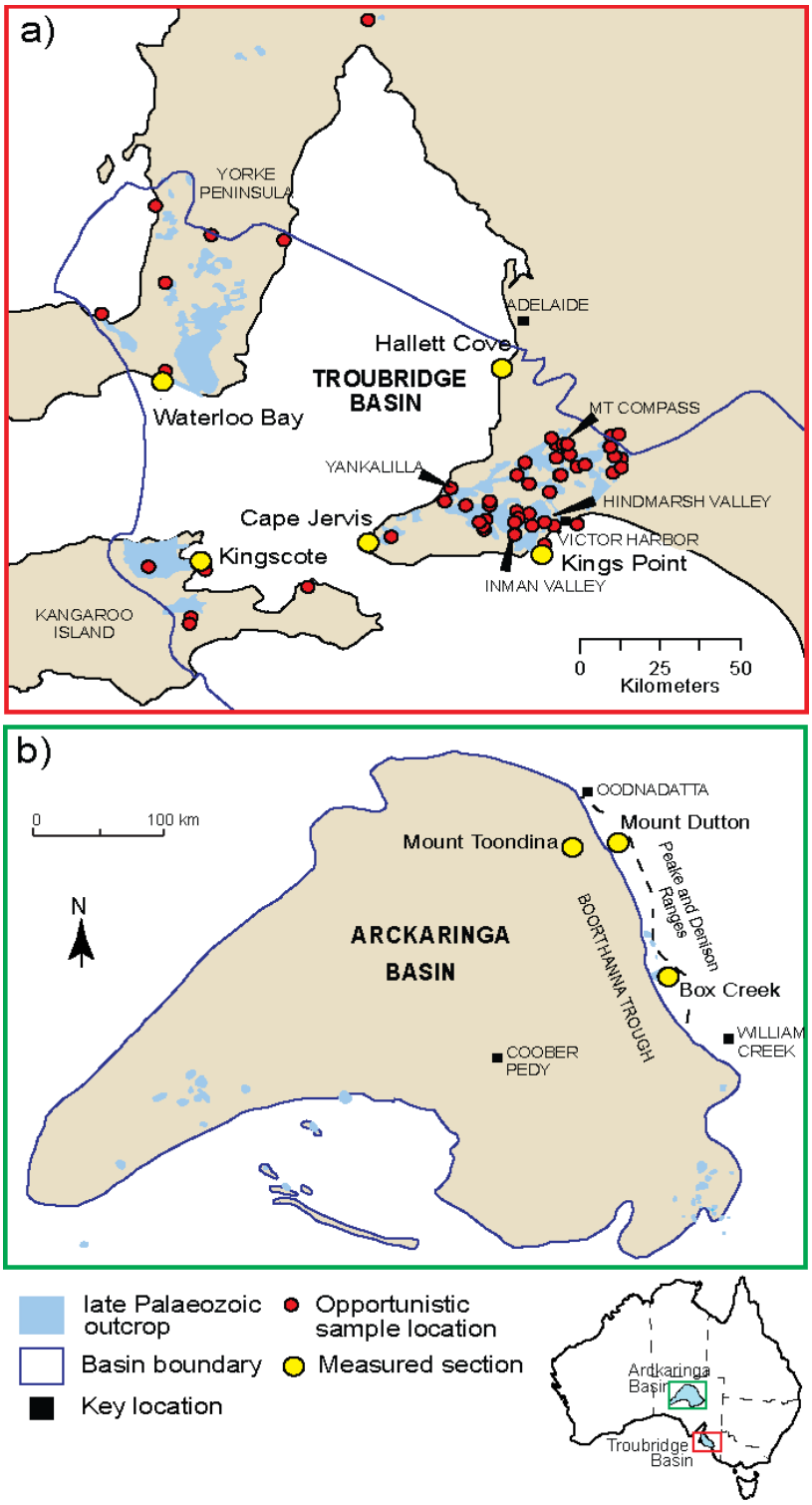

Figure 5:2 a) Sample locations within the Troubridge Basin. Distribution of late Palaeozoic exposures adapted from Belperio et al. (2009), Fairclough (2007), Thompson and Horwitz (1962) and Zang (2003). Key measured sections are also shown; b) Sample locations within the Arckaringa Basin, showing the late Palaeozoic exposures adapted from Hibburt (1995), Rogers et al. (1996) and Freytag et al. (1967). Key measured sections are also shown. Inset: location of study areas in relation to Australia.

Surface samples were used as the aim of this study was to emulate a mineral exploration project. In an exploration project often only the material on the surface is available for sampling especially in scoping studies. These samples are assessed to identify the less altered using geochemistry to compare for weathering, depositional and provenance signals. Drill hole samples are the optimal sampling medium, however, in both the Troubridge and Arckaringa basins, drill core would not have been adequate for this study as drill holes were sparsely distributed and stored only as 3-5 m chip composites and do not allow systematic sampling across the basins.

The sampling procedure involved removing approximately 0.5 kg of material from the exposed surface using a geological pick. The samples are of varied lithology including sand, clay, silt and diamictite all with varying degrees of weathering and induration (see section 5.3.1). Descriptions of key sections (Chapters 2 and 3) were used to target dominant lithologies. This diversity reflects the opportunistic nature of sampling. Samples taken from diamictites were carefully chosen to exclude clasts greater than five millimetres in diameter so as to reduce the potential for individual source rocks to influence the geochemistry. As such, the analysis of diamictite samples was of matrix with minimal clasts. Throughout this chapter the term matrix is used for any material smaller than 5 millimetres, which includes and cement which may have been introduced to the material during weathering processes such as Fe-oxide or clay minerals.

In all other respects care was taken to collect samples that were representative of exposed material at the sample site and free of overlying materials or other contaminants. Contamination risk from the sampling procedure was minimised by removing personal jewellery, hands were kept clear of sunscreen and sedimentary rocks from previous samples by washing and drying them before the collection of each sample. Samples were placed into a clean, plastic, snap-lock bag, labelled and transported to the University of Adelaide.

5.2.2 Geochemical analysis

A subsample weighing approximately 200 g was taken from each field sample and a duplicate sub-sample of equivalent mass was taken from every twenty fifth sample (giving a total of seven duplicate sub-samples). All sub-samples were sent to ACME Laboratories in Vancouver, Canada for crushing, preparation and geochemical analysis. Acme laboratories sample preparation includes crushing the sample until 80% of sample passes through a 2000 µm mesh, the crushed sample is then further pulverised until 85% of sample passes through a 75 µm mesh. This smaller fraction is then used in all analysis.

Geochemical data for 59 elements were collected using whole rock XRF (ACME code 4X) and Total Trace Element by ICP-MS analysis (ACME code 4B). Whole rock XRF analyses were conducted on fused disks in which 12 g of analytical pulp was fused utilising a lithium borate flux. Trace, refractory and rare earth elements were analysed by ICP-MS. Trace element analyses were conducted on 0.5 g of analytical pulp digested in an Aqua Regia, whereas refractory and rare earth element ICP-MS analyses were conducted on 0.2 g of analytical pulp, following lithium borate fusion and digestion in nitric acid.

Quality assurance and quality control (QA/QC)

In addition to the seven duplicate sub-samples, four samples of certified reference material from OREAS 22p and 42p (Ore Research and Exploration Pty Ltd) were intercalated with the field sub-samples (~1 reference sample for every 50 unknowns; 2 of each were sent) and submitted to ACME for

preparation and analysis. Analysis of these reference materials, sample duplicates as well as laboratory duplicates and standards provide a measure of QA/QC of the dataset.

5.2.3 Data treatment

The geochemical data were loaded into the IoGAS software package in order to conduct simple statistical analyses and generate comparative geochemical plots including bivariate, ternary and multi-element "spidergrams". Elements where the majority of samples were analysed to be at or below detection limit (including Cr_2O_3, Ba, Ag, Be, Bi, Cd, Hg, Se, Sn and Tl) were not included in any further data treatment. Where individual samples have concentrations at or below detection limit, the sample was assigned a concentration of half the detection limit of the given element.

Samples from the Troubridge and Arckaringa basins are lateral and temporal equivalents (Chapter 3), also have similar zircon populations (although, there are relatively more older grains within the Boorthanna Formation of the Arckaringa Basin; Chapter 4) and have near identical population statistics for many key elements (Figure 5:3). The differences in the provenance spectrums of the Cape Jervis Formation and Boorthanna Formation (Figure 4:12f to g) are based on the quantity of zircons within the samples rather than differences in age groupings. The provenance spectrums of both formations have zircon grains within the age ranges ca 470 to 700 Ma, ca 900 to 1300 Ma and ca 1650 to 2000 Ma, the shapes of these age ranges are also similar. The provenance studies also indicate that both formations have been sourced, at least in part from the Kanmantoo Group and the Transantarctic Mountains of Antarctica (Chapter 4).

Given these similarities of the Troubridge and Arckaringa basins data from both basins have been combined into a single dataset to assess the geochemical signatures of late Palaeozoic glacial sedimentary rocks across South Australia.

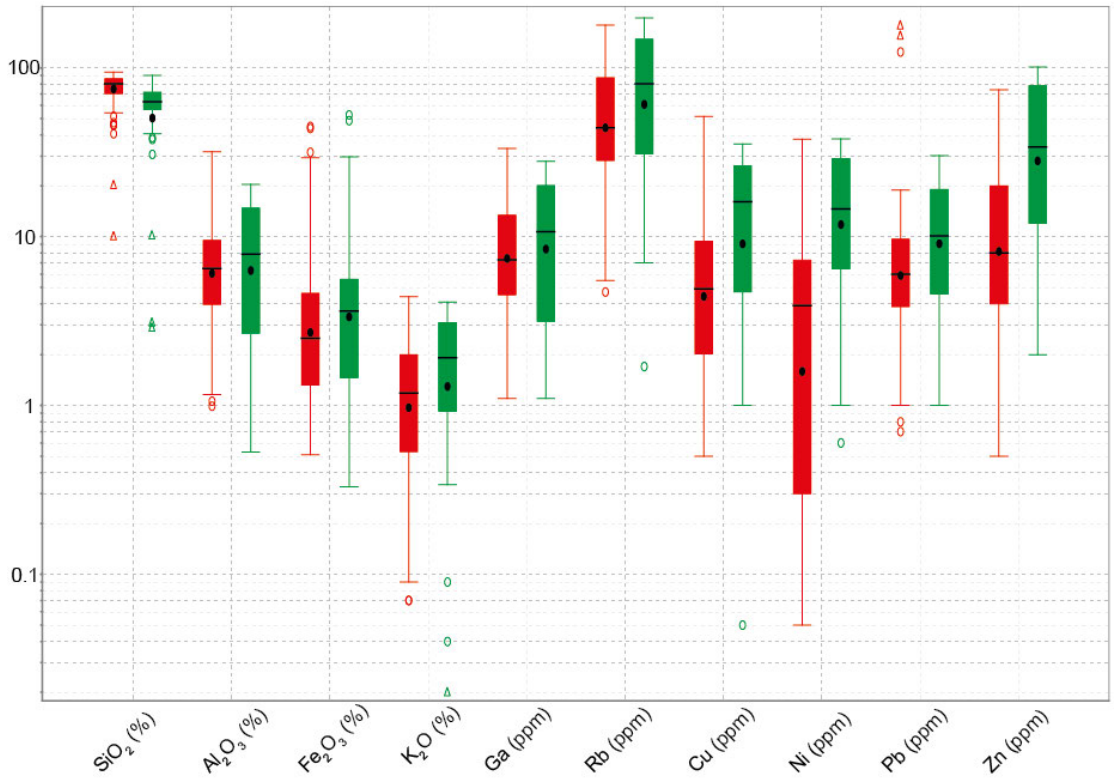

Figure 5:3 Turkey Plots showing the similarity in concentration in key elements between the samples of the Troubridge (red) and Arckaringa (green) basins. Black dots are the mean of logged values, black central bar is 50% of the values between Q1 and Q3, open circles are outliers further than 1.5 from Q3-Q1 and open triangles are far outliers further than 3x from Q3-Q1.

5.2.4 Comparative whole rock geochemistry

All of the geochemical plots presented in this study include the geochemical range of previously analysed samples from the Kanmantoo Group and Encounter Bay Granite (Foden et al. 2002, Haines et al. 2009, De Pretis 2011) which are likely source rocks of the Late Palaeozoic glacigene sedimentary rocks, as well as Post Archaean Average Shale (PAAS; McLennan 1989) which is a useful geochemical reference for generic sedimentary source material. A majority of the clasts in diamictite rocks of the Troubridge Basin resemble Kanmantoo Group metasedimentary rocks with a minor component of coarse-grained granite which has been correlated with the Encounter Bay Granite (Chapter 2; Alley and Bourman 1984). Zircon grains from the Troubridge Basin have a provenance spectrum which closely resembles the Cambrian Kanmantoo Group metasedimentary rocks (Chapter 4, Ireland et al. 1998). The clast population of Arckaringa Basin diamictites are dominated by low grade metasedimentary rocks (shales and sandstones) with minor metamorphic rocks consistent with derivation from proximal Neoproterozoic Adelaide Rift Complex and underlying Palaeoproterozoic Gawler Craton (Chapter 3, Ambrose et al. 1981). Zircon grains from the Boorthanna Formation of the Arckaringa Basin have a detrital zircon provenance spectrum consistent with proximal rocks of the Gawler Craton and Adelaide Rift Complex as well as a lesser Cambrian Kanmantoo Group component likely sourced distally (Chapter 4, Ireland et al. 1998).

The Kanmantoo Group geochemistry reported here is taken from Haines et al. (2009) and De Pretis (2011) in addition to three samples collected from the base of the Hallett Cove, Kings Point and Cape Jervis type sections presented in Chapter 2 (Figure 5:2, the individual sample results from this study are in Appendix 3). The range of Kanmantoo Group geochemistry presented in Figures 5:5 to 5:12

exclude 6 out of 44 analyses (13%) which were outliers of the main population. These included samples described as calcareous by Haines et al. (2009), which are likely to have been subject to regolith carbonate induration, as well as samples that are outliers with respect to alkali concentrations which are likely to have been subject to intense weathering (Nesbitt and Young (1989). The samples of Kanmantoo Group included are mudstone, siltstone and sandstone metasedimentary rocks. The range of Encounter Bay Granite is taken from Foden et al. (2002). The range excludes 1 of 8 samples (12%) that have elemental concentrations that are outliers in the Nesbitt and Young (1989) plots.

The Kanmantoo Group and Encounter Bay Granite analyses presented by were collected using different sampling and analytical methods from the methods used in this study. As the geochemical analyses are not directly comparative, the ranges are used as broad comparisons to the geochemical data of this study.

5.3 Results

5.3.1 Lithology and weathering

Samples were classified into seven lithological groups and five weathering groups based on field observations (Table 5:1; Appendix 3). Lithology of the sample material is described by dominant grainsize and include both consolidated and unconsolidated material. Table 5:1 summaries that descriptions of the lithology and weathering classifications while Table 5:2 shows the distribution of the classifications within the samples.

'Oxidised' sedimentary rocks were classified based on the presence Fe-oxide minerals distributed throughout the sample, either in the form of mottles (Figures 5:4e, i) or pervasive yellow, orange and/or red staining (Figures 5:4a, j). Despite the degree of induration in samples classified as 'Ferruginous', the primary sedimentary textures of the ferruginous samples are often preserved, for example on the weathered surfaces of ferruginous sand samples where individual quartz grains are contrasted against the Fe-oxide matrix or cement. All sulphate weathered samples were collected from an area adjacent to a mound spring at Mount Toondina (Figure 5:4n).

Table 5:1 Summary table of characteristics for each lithology and weathering classification used throughout the geochemical analysis. Unit characteristics are based on observations by the author.

Lithology	Characteristics	Figure reference
Sand	- Fine- to very coarse grained - Unconsolidated sand - Sandstone	Figure 5:4a to d
Clay	- Smooth texture - No visible quartz grains	Figure 5:4f to h
Silt	- Gritty texture - No visible quartz grains	Figure 5:4e
Sandy Clay	- Minor visible very fine- to fine-grained quartz grains - Dominant clay cement	Figure 5:4i
Diamictite	- > 5% clasts - Clasts > 5 mm	Figure 5:4j, k
Diamictite Clay	- Smooth or gritty texture - No visible quartz grains	Figure 5:4k
Diamictite Sand	- Fine- to very coarse grained - Unconsolidated sand - Sandstone	Figure 5:4j
Carbonaceous	- Black to grey - Interbedded with shale and sand	Figure 5:4l, m

	-	Previously described as lignite by Freytag et al. (1967)	
Weathering			
Ferruginous	-	Fe-oxide dominant cement or matrix	Figure 5:4e, h
	-	Typically red or purple	
	-	Hard and coherent	
Sulphate	-	Visible gypsum	Figure 5:4n
Carbonate	-	Chalky-texture	Figure 5:4c, d
	-	Visible Ca-carbonate on surfaces or distributed through the sample.	
Oxidised	-	Mottles	Figure 5:4e, i
	-	Pervasive yellow, orange and/or red staining	Figure 5:4a, j
	-	Quartz grains often coated with Fe-oxide minerals	
	-	Typically friable.	
Minimal	-	Green or grey	Figure 5:4f, g, k
	-	mm to cm-scale bedding	
	-	Friable along bedding planes	
	-	Fe-oxide mineral staining or calcium carbonate induration minimal +/or restricted to narrow fractures/sample surface.	

Table 5:2 Distribution of lithology and weathering of glacigene sedimentary rocks

Lithology / Weathering	Sand n = 62	Clay n = 42	Silt n = 9	Sandy Clay n = 21	Diamictite Clay n = 12	Diamictite Sand n = 25	Carbonaceous n = 10
Ferruginous n = 25	10-	10	-	1	12	3	-
Sulphate n = 26	8	2	6	-	-	-	10
Carbonate n = 13	9	-	-	1	1	2	-
Oxidised n = 92	32	15	2	17	6	20	-
Minimal n = 25	3	15	1	2	4	-	-

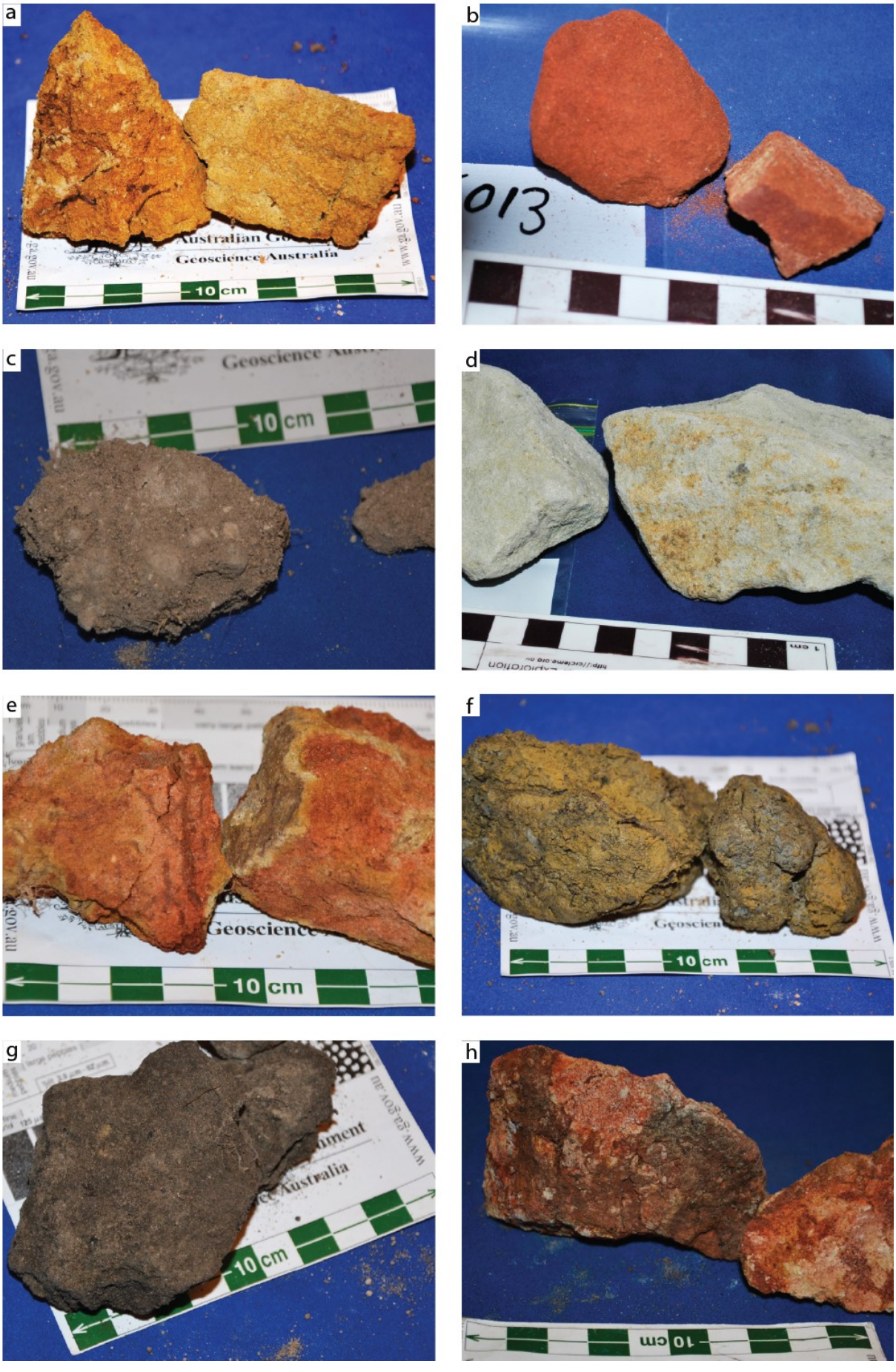
a
Geoscience Australia
10 cm
b
c
10 cm
d
e
10 cm
f
10 cm
g
10 cm
h
10 cm

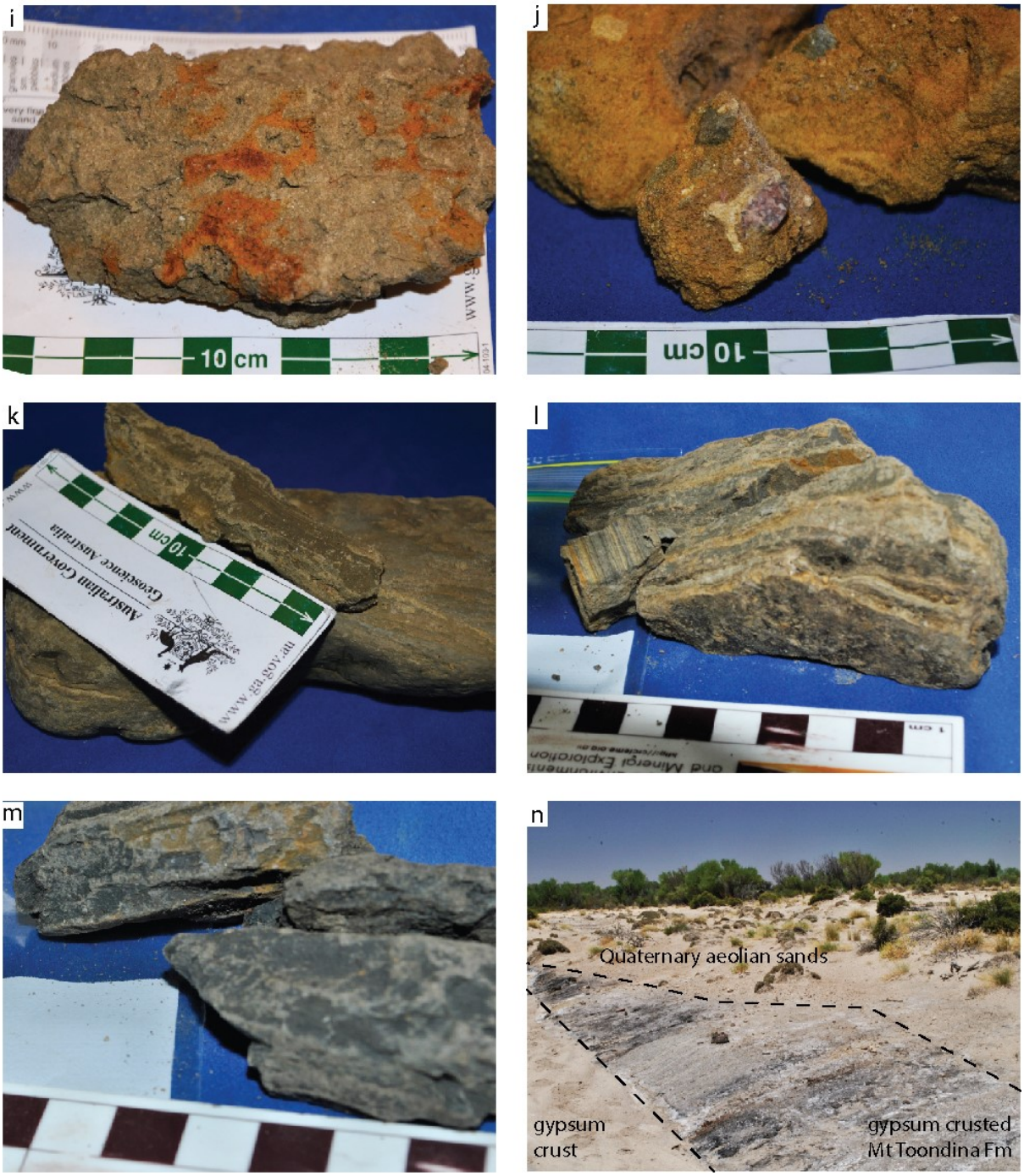

Figure 5:4 Examples of lithology and alteration classifications. a) Sand with oxidation alteration expressed as yellow Fe-oxide mineral staining: Inman Valley; b) Sand with ferruginous alteration: Kingscote composite measured section; c) sand with carbonate alteration, buff patches are calcium carbonate mineral dominated: central Yorke Peninsula; d) sand with carbonate alteration: Boorthanna Formation from the Box Creek section; e) silt with oxidation alteration (Fe-oxide surface/mottles): Hindmarsh Valley; f) clay with minimal alteration: Inman Valley; g) clay with minimal alteration: central Yorke Peninsula; h) clay with carbonate alteration: Mount Compass; i) sandy clay with oxidation alteration (Fe-oxide mottles): Waterloo Bay, Yorke Peninsula; i) sandy diamictite with oxidation alteration (Fe-oxide staining): Cape Jervis; k) clay diamictite with minimal alteration: Yankalilla; l) carbonaceous (grey beds interbedded with siltstone beds) with sulphate alteration: Mount Toondina Formation from the Mount Toondina type section; m) carbonaceous with sulphate alteration, : Mount Toondina Formation from the Mount Toondina type section; n) gypsum crust formed as part of the sulphate alteration process on the surface of the Mount Toondina type section. All samples were collected opportunistically and from the Cape Jervis Formation unless otherwise stated. Locations are shown on Figure 5:1.

5.3.2 Major element geochemistry

The glacigene samples fall into a number of groups on standard major elemental plots based on the concentrations of SiO_2, Al_2O_3, Fe_2O_3, MgO, CaO, Na_2O and K_2O.

On the SiO_2 vs Al_2O_3 plot, 65% of the samples occupy an array which lies within 4% SiO_2 of a line which projects to an SiO_2 intercept of 100%, has a slope of -2.11 and a maximum Al_2O_3 composition of 22% (Figure 5:5). Sand, sandy clay and diamictite sand samples of the minimal and oxidised weathering groups cluster toward the SiO_2-rich end of this array. Whereas silt, clay and diamictite clay of the minimal or oxidised weathering groups are drawn toward the Al_2O_3-rich end. The array overlaps with the broad field of Kanmantoo Group sedimentary rocks and the more restricted field of Encounter Bay granites toward the Al_2O_3-rich end and lies slightly below PAAS.

The 35% of remaining samples, occupy a triangular space between the SiO_2 vs Al_2O_3 array and the origin of the plot. This group includes a large proportion of the carbonaceous samples as well as samples with intense carbonate, ferruginous and sulphate weathering.

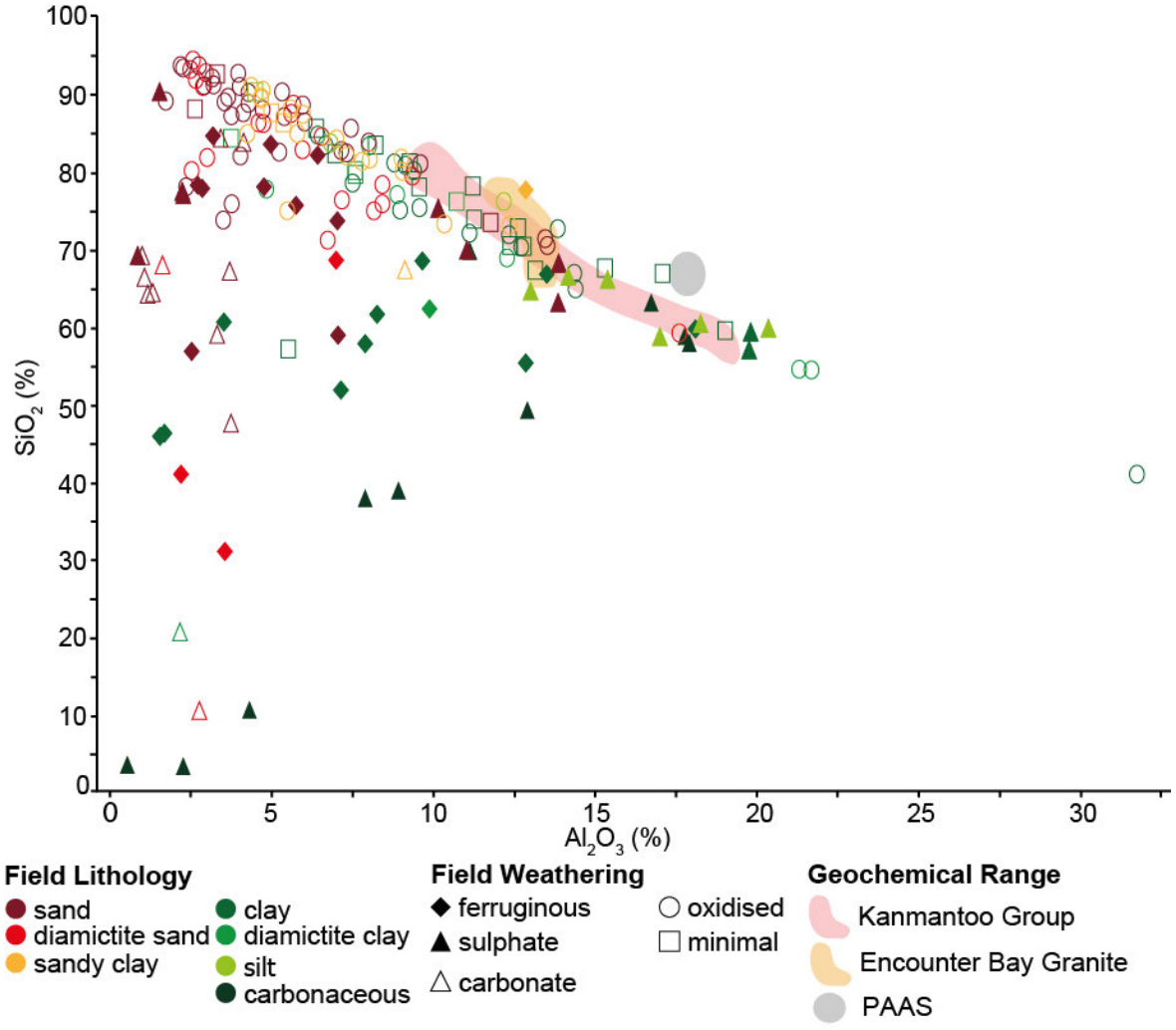

Figure 5:5 Al_2O_3 versus SiO_2 plot for all glacigene sedimentary rocks sampled.

Lithology and alteration is further mapped on the Al_2O_3 – $CaO+Na_2O+K_2O$ – $FeO+MgO$ (A-CNK-FM) diagram (Figure 5:6). This plot ignores the geochemical influence of detrital quartz (SiO_2) and accentuates variations as a result of minerals introduced due to regolith processes such as carbonate,

Fe-oxide and clay minerals. Forty percent of samples plot within a triangle bound by 45% FM, 20% CNK and 72% A (Figure 5:6), which includes PAAS and most Kanmantoo Group samples. The late Palaeozoic glacigene samples within this space are a mix of primary lithologies and are dominated by samples classified as having minimal or oxidised weathering.

A group of 28 oxidised samples, including all lithology types plot within a few percent of the A-FM axis. Ferruginous samples plot towards the FM apex (Figure 5:6). Samples with carbonate or sulphate weathering and a number of oxidised samples form a loose array between the central triangle and the CNK apex. A group of four sand samples consisting of two carbonate and two oxidised weathering samples plot close the dolomite end member (Figure 5:6). These samples contain dolomite as detected by spectroscopic analysis (Chapter 2 and 3).

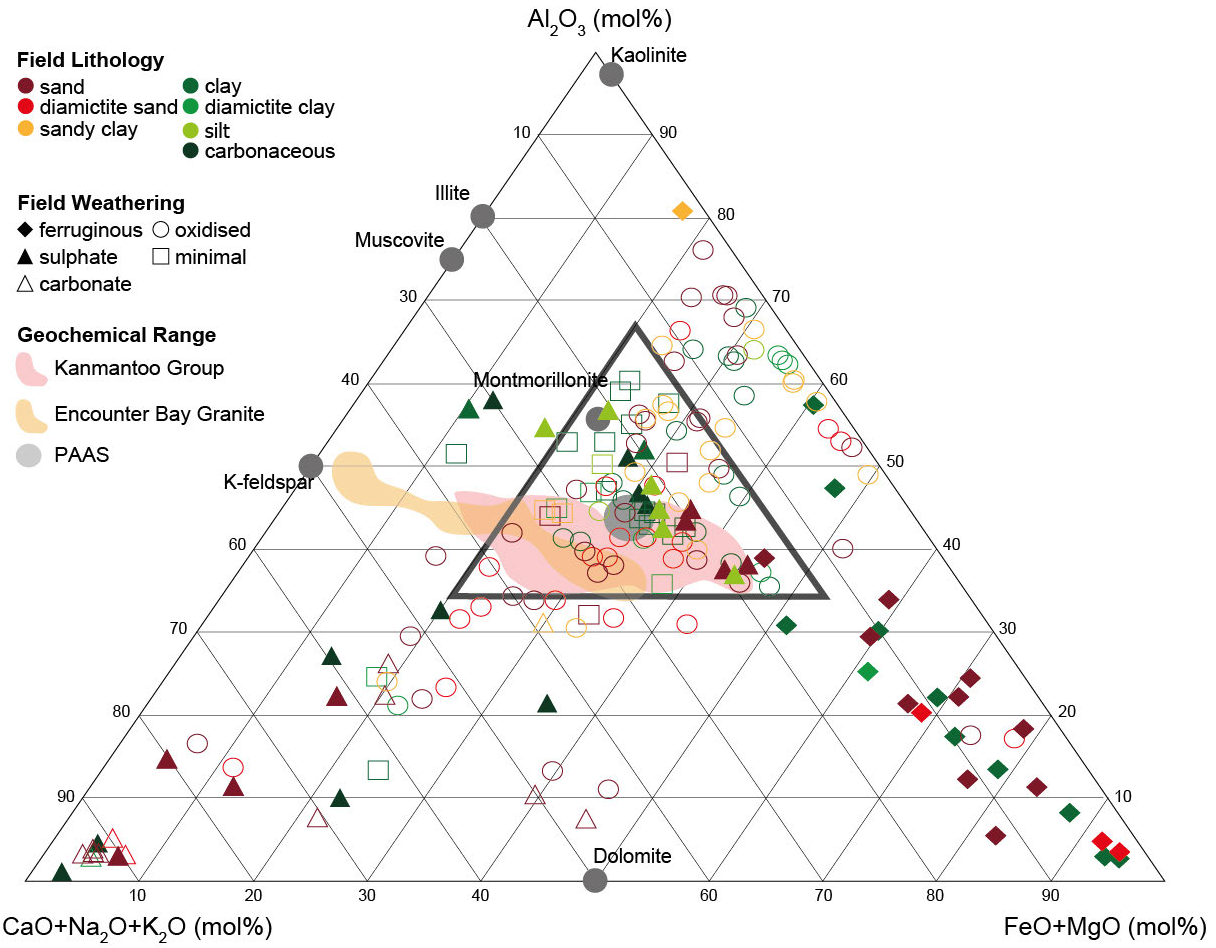

Figure 5:6 A-CNK-FM ternary showing all glacigene samples. The area bound in the thick black triangle shows where the majority of minimal weathered and oxidised samples plot. Small dark grey circles show the expected ratios for the mineral end members.

The Al_2O_3 – $CaO+Na_2O$ – K_2O (A-CN-K) plot is used to identify silicate and clay weathering processes in regolith (Nesbitt and Young 1989). The plot ignores the influence of ferruginisation but is strongly influenced by carbonate weathering and induration. The highest density of samples occurs within a triangle bound by 60% Al_2O_3, 12% K_2O and 8% $CaO+Na_2O$ (Figure 5:7) which accounts for 80 % of all the samples. This group includes all primary lithologies and weathering types. Approximately one third of the samples, dominated by oxidised and ferruginous weathering types, trend from this triangle towards A-K axis and ultimately towards the A apex (Figure 5:7). This group includes a tight cluster at the A apex, close to ideal kaolinite, which are the same samples that plot along the A-FM axis in Figure

5:6. Approximately 24% of samples plot in an array from the central triangle towards the CN apex (Figure 5:7). This group is dominated by samples of the oxidised, sulphate and carbonate weathering types. The cluster of samples closest to the CN apex correspond to samples with pervasive calcite or gypsum induration (Figure 5:7).

The field of Kanmantoo Group samples forms a loose array overlapping with PAAS and the highest density of glacigene sedimentary rocks (i.e. within the central triangle) and trending toward the mid-point of the A-CN axis. The field of Encounter Bay Granite samples plots just below the central triangle within the array of glacigene sedimentary rocks that trends toward the CN apex.

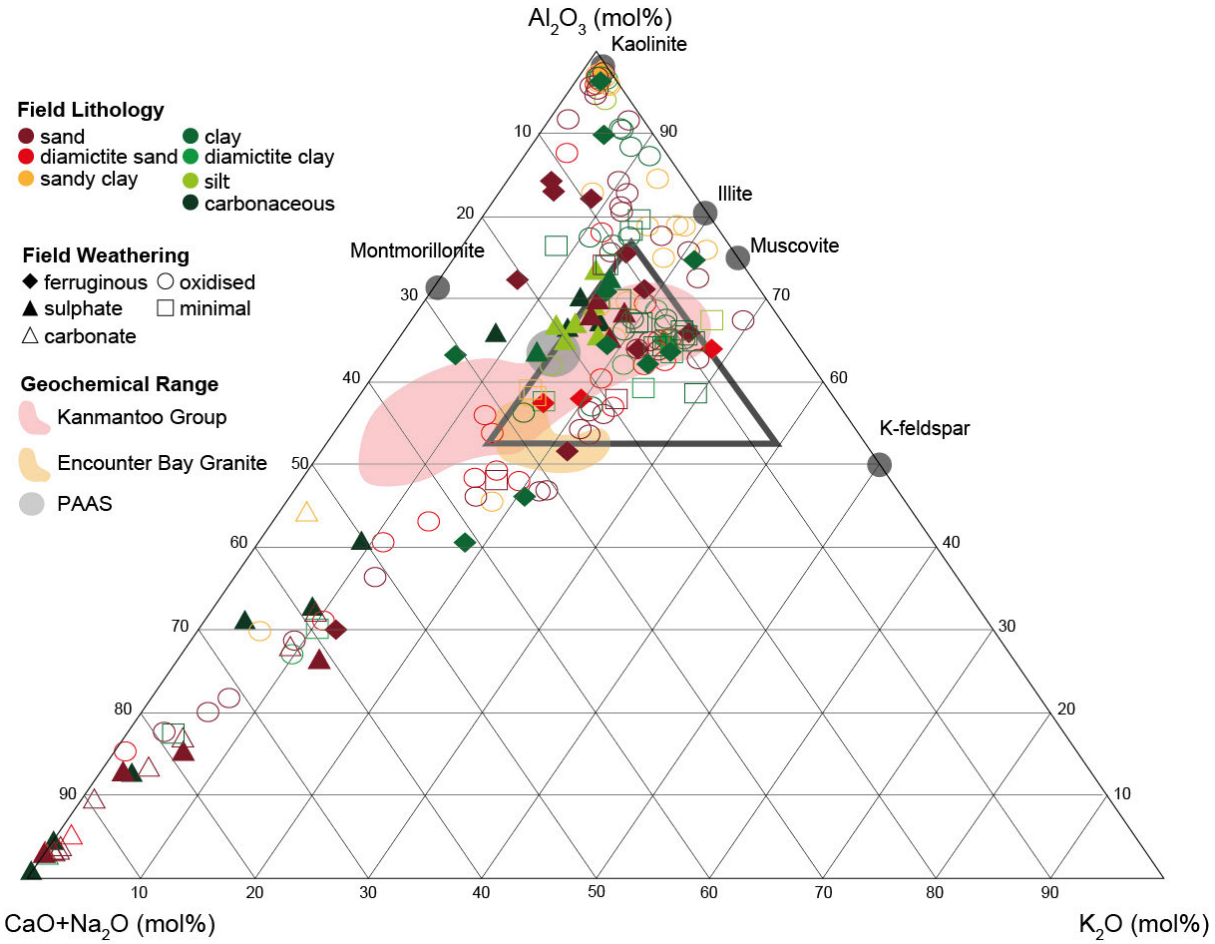

Figure 5:7 A-CN-K ternary showing all glacigene samples. The area bound in thick black triangle shows where the majority of minimal weathering and oxidised samples plot. Small dark grey circles show the expected ratios for the mineral end members.

5.3.3 Elementary relationships

Aluminium (Al_2O_3)

Given the ability for lithogeochemical discrimination based on Al_2O_3 content whereby clay-dominated and sand (quartz)-dominated samples have low and high Al_2O_3 content respectively (Figure 5:5), relationships between Al_2O_3 and the trace and rare earth elements were used to assess the influence of mineralogy on chemistry. Ga, Rb and K_2O have positive linear relationships with Al_2O_3 and are relatively enriched in clay and silt lithologies (Figures 5:8a to c) consistent with mineralogical controls for these elements related to the abundance of Al_2O_3 bearing minerals (ie clay minerals). The strong linear relationship between Ga and Al_2O_3 (Figure 5:8b) can be attributed to the common substitution of Ga for Al in clay minerals (Taylor and Eggleton 2001, Scott and Pain 2008). K and Rb have slightly

weaker correlations with Al_2O_3, in both cases with a near linear upper bounding array projecting toward the origin and a significant proportion of the samples being 'smeared' below this array toward the Al_2O_3 axis. The slope of the upper bounding array on the K_2O vs Al_2O_3 plot is approximately 1:3, consistent with the mass ratio of K_2O:Al_2O_3 in ideal muscovite. Samples with lower K_2O:Al_2O_3 are likely to represent mixtures of sheet silicates and clays with lower proportions of potassium (e.g. illite, montmorillonite, smectites and kaolinite). The similarity of the K_2O vs Al_2O_3 and Rb vs Al_2O_3 plots (Figure 5:8) and the strong correlation between K_2O and Rb (Figure 5:8) is consistent with the commonly observed lattice substitution of Rb for K in a range of K-bearing minerals (Taylor and Eggleton 2001, Scott and Pain 2008).

The rare earth elements (represented by Ce and Dy in Figures 5:8d and e) also have a broad positive relationship with Al_2O_3 and are relatively enriched in the clay and silt lithologies. This trend is commonly observed in sedimentary rocks and is consistent with the substitution of REEs into the lattice of clay minerals (Taylor and Eggleton 2001, Scott and Pain 2008).

The commodity elements, Pb, Cu, Ni and Zn have similar patterns when compared to Al_2O_3 (Figures 5:8f to i), although the pattern is somewhat obscured in the Pb vs Al_2O_3 plot due to a few very high Pb values (Figure 5:8). The patterns include three trends; 1) a low commodity element trend, hugging the Al_2O_3 axis and dominated by samples that also have low K_2O:Al_2O_3, 2) a moderate commodity element trend which most closely matches the field for Kanmantoo Group sedimentary rocks and PAAS, and tends to highest values in clay and silt rich and/or sulphate weathered lithologies and 3) a high commodity element trend, which for Pb, Ni and Zn is dominated by ferruginous samples but for Cu includes a range of protolith and weathering types. This is likely due to the varying clay mineral content in the samples. Samples within trend 1 are sand or ferruginous sediments with low clay mineral content; samples within trend 3 typically have clay and silt lithologies that are oxidised or have minimal alteration, these lithologies typically have high clay mineral content and therefore high Al_2O_3 concentrations.

When plotted against Al_2O_3 the siderophile elements (Figures 5:8j and k) have a lower bounding linear array which projects to the origin and a scattering of higher concentration samples which are almost exclusively of the ferruginous weathering type. The CaO vs Al_2O_3 plot has a similar pattern, however, samples enriched in CaO above the background trend are dominated by the carbonate and sulphate weathering types (Figure 5:8l).

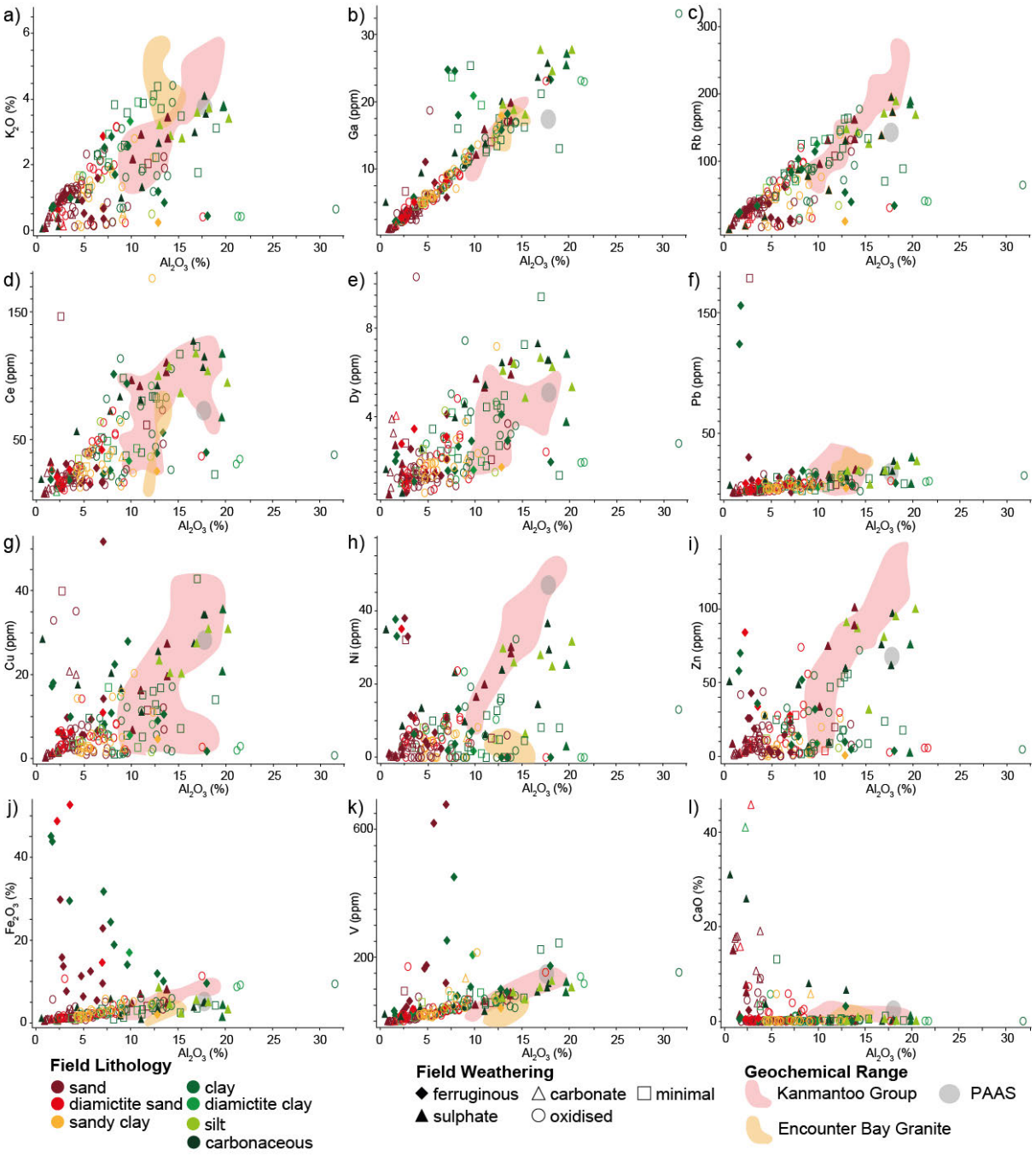

Figure 5:8 Harker diagrams of Al_2O_3 vs selected elements.

Iron (as Fe_2O_3)

Ratios Fe_2O_3 and K_2O, Ga, Rb, REEs and the commodity elements (Pb, Cu, Ni and Zn) display similar patterns (Figures 5:9a to i). In each case there is an approximately linear upper bounding array (for samples <10% Fe_2O_3) that overlaps with Kanmantoo Group sedimentary rocks and PAAS. Within this array, sand and sand-matrix diamictite samples plot near the origin and the clay, silt and clay matrix diamictite samples plot away from the origin. Samples with elevated Fe_2O_3 concentrations (up to ~50%) plot to the right of this array and are dominated by samples of the ferruginous weathering type. On the V vs Fe_2O_3 plot the majority of samples form a broad positive array, overlapping with the field of Kanmantoo Group sedimentary rocks, with a small group of samples projecting along this array but

significantly more enriched in V than Kanmantoo Group (up to ~600 ppm) and another group enriched in Fe_2O_3 without coincident V enrichment. The latter two groups are dominated by samples of the ferruginous weathering type. CaO-rich samples (i.e. sulphate and carbonate weathered sedimentary rocks) have very low concentrations of Fe_2O_3 (typically <3%) compared to the other alteration groups sampled (Figure 5:9k).

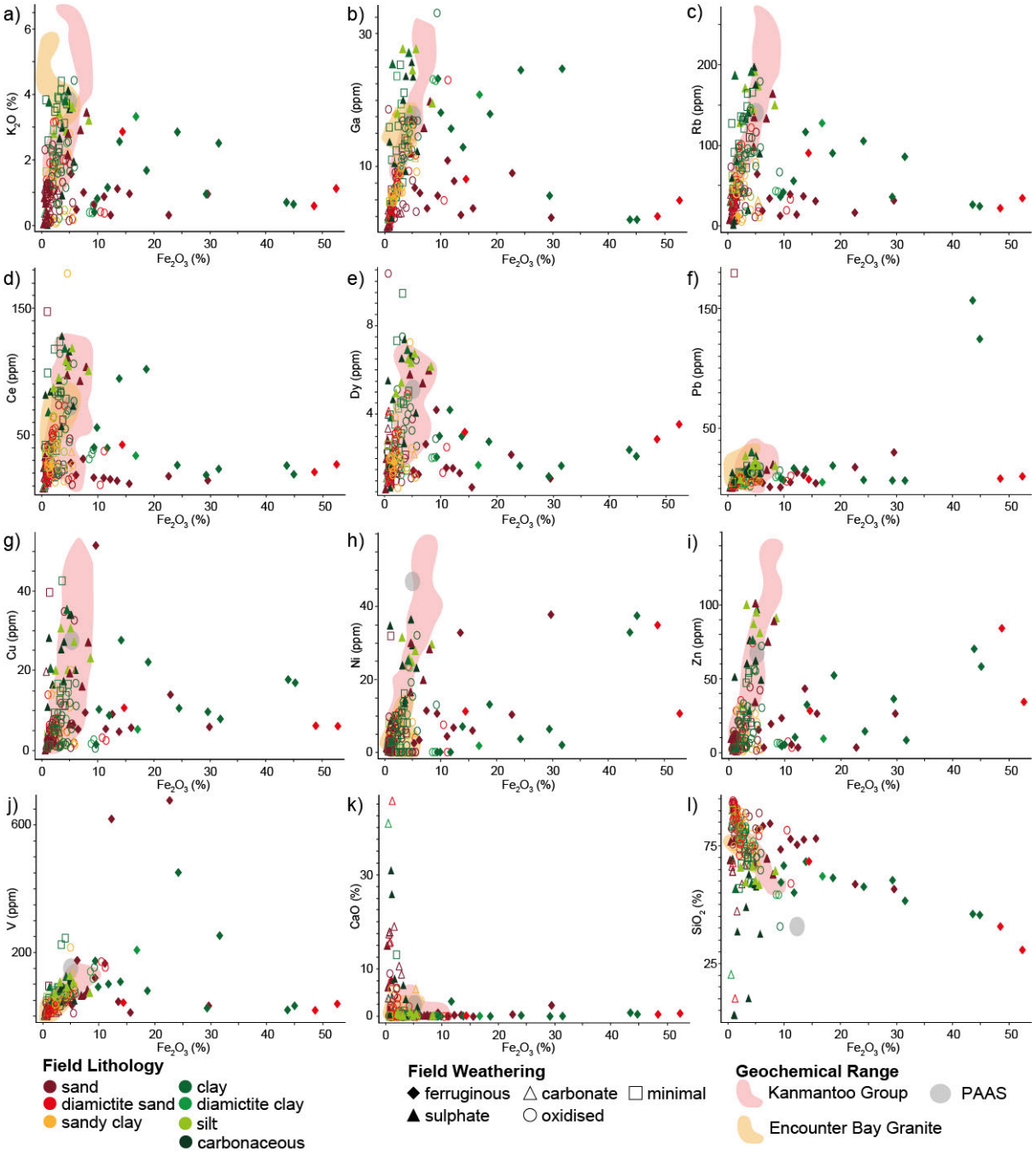

Figure 5:9 Harker diagrams of Fe_2O_3 vs selected elements.

Calcium (as CaO)

On the plot of C vs CaO the majority of samples, including most lithology and weathering types, form a broad linear array with highest concentrations occurring in carbonate weathered samples (Figure

5:10a). This array, passes close to the origin and is centred on a line with a slope of ~0.2 consistent with the mass ratio of C to CaO in calcium carbonate. Six samples depart from this array, all of which are sulphate weathered carbonaceous sedimentary rocks from the Mount Toondina section. The same small group of carbonaceous samples with sulphate weathering also form a linear array on the plot of S vs CaO (Figure 5:10b). This array passes close to the origin and is centred on a line with a slope of ~0.6 consistent with the mass ratio of S to CaO in gypsum.

On the plot of Sr vs CaO there are two dominant trends; a high CaO, moderate Sr trend which is dominated by sand-rich, carbonate weathered samples at higher concentrations of CaO, and a high Sr, low CaO trend which is dominated by clay-rich samples at the high Sr end (Figure 5:10d). A small number of samples lie between these trends, including a single carbonaceous, sulphate weathered sampled with a Sr concentration approaching 2000 ppm.

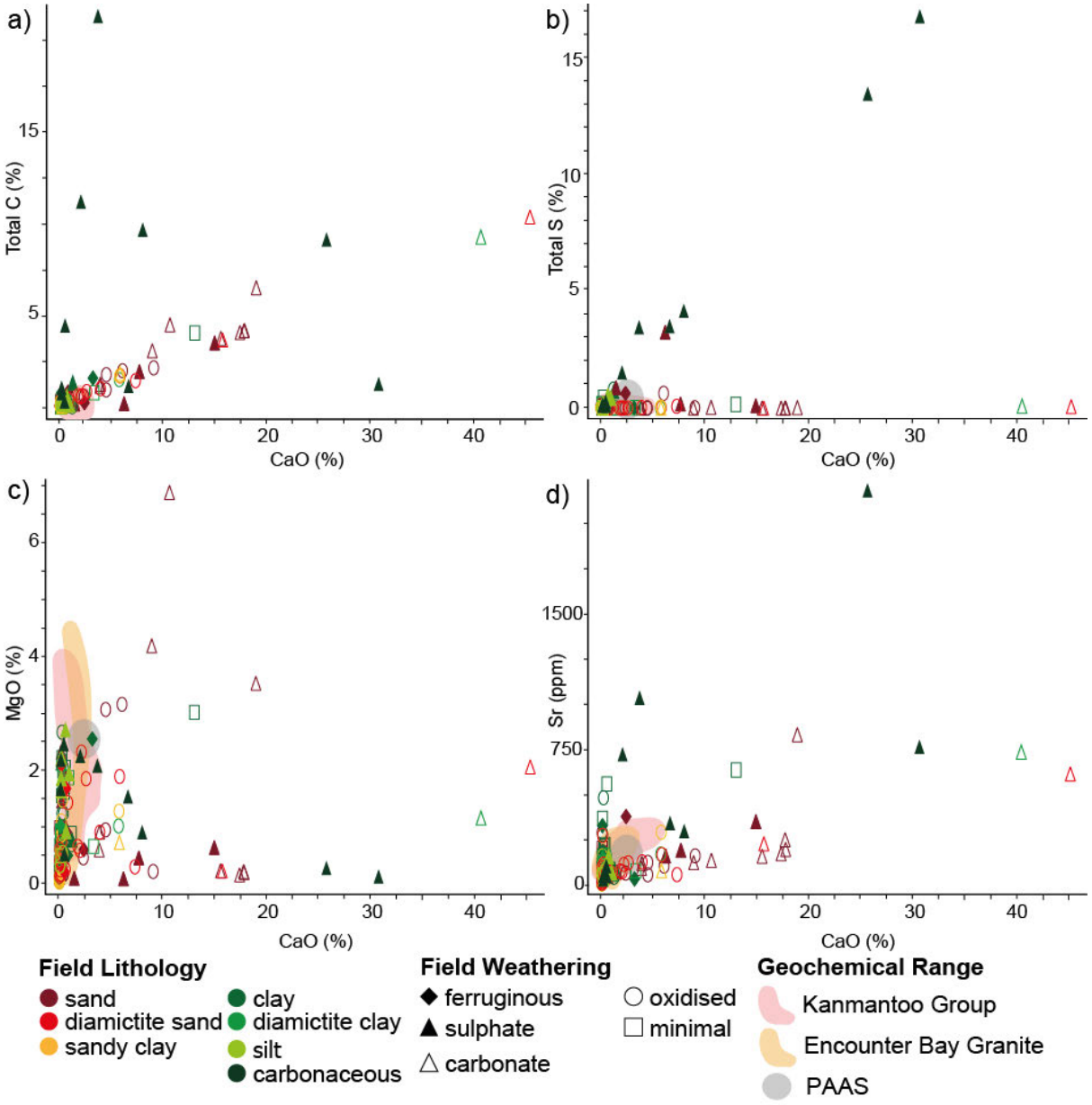

Figure 5:10 Harker diagrams of CaO vs selected elements.

Zirconium

A tight linear trend is observed between Zr and Hf (Figure 5:11a), consistent with the well-known mineralogical control of zircon on these two elements (Taylor and Eggleton 2001, Scott and Pain 2008). At zirconium concentrations <250 pm the trend overlaps with PAAS and Kanmantoo Group sedimentary rocks, with clay-rich samples more commonly at the high-Zr end and sand-rich samples at the low-Zr end. The group of samples with >250 ppm Zr a mixture of protolith and weathering types. The Al_2O_3 vs Zr plot shows a broad positive scatter whereby clay samples generally have higher Al_2O_3 and Zr content relative to sand samples (Figure 5:11b). At Zr concentrations >250 ppm, Al_2O_3 concentrations tend to decline forming an upper bounding broad linear array with a negative slope on the Al_2O_3 vs Zr plot. Plots of TiO_2% and Ce vs Zr have similar patterns with a broad positive scatter projecting toward the origin. On plots of Al_2O_3, TiO_2 and Ce vs Zr, Zr is relatively enriched (offset to the right) compared to Kanmantoo Group sedimentary rocks and PAAS.

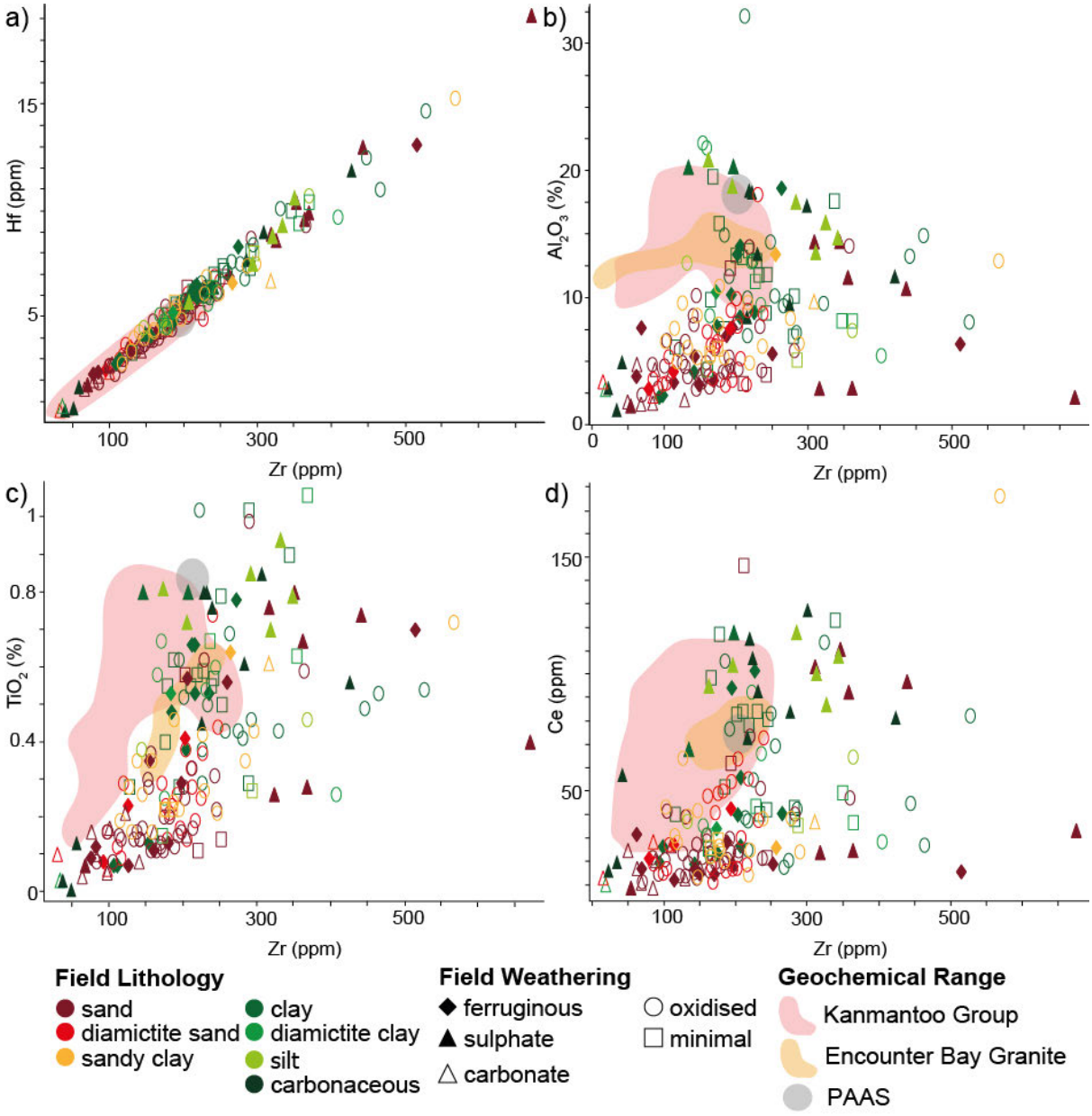

Figure 5:11 Harker diagrams of Zr vs selected elements to demonstrate the heavy and resistate mineral associations.

Rare Earth Elements

The minimal weathered and oxidised samples from all field lithology types have a similar REE patterns; with convex LREE enrichment, a negative Eu anomaly and relatively flat HREEs (Figure 5:12). Sand, sandy clay and diamictite sand samples have lower ΣREE compared to the clay sedimentary rocks. These patterns are similar to PAAS and Kanmantoo Group sedimentary rocks, although with lower ΣREE.

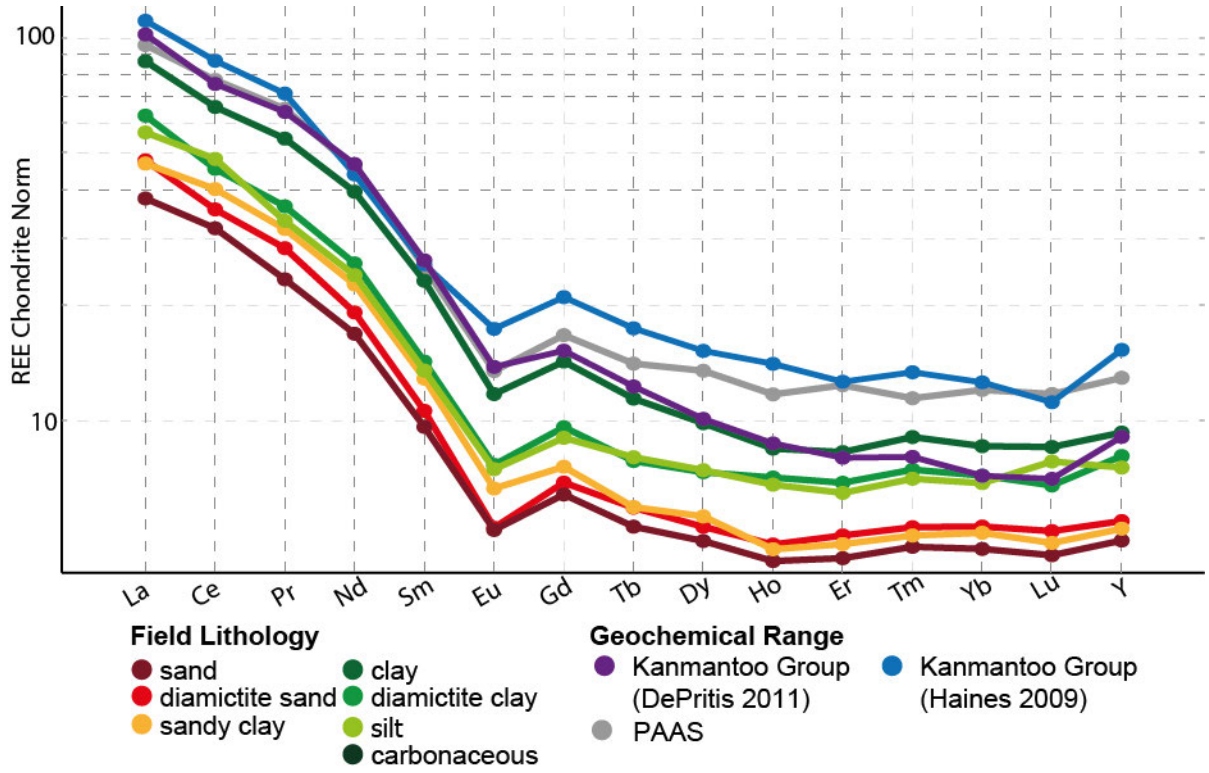

Figure 5:12 Chondrite REE normalisation of the oxidised and minimal weathering glacigene sedimentary rocks.

5.4 Discussion

5.4.1 Weathering signals in the geochemical data

The A-CNK-FM and A-CN-K plots (Figures 5:6, 5:7) were presented by Nesbitt and Young (1989) as a way of representing bulk chemical changes due to weathering. Different types of weathering recognised in this study are reflected in the major element geochemistry in terms of relative concentration of Al_2O_3 and the alkalis K_2O, Na_2O and CaO (formation of secondary clays), CaO and MgO (carbonate induration), CaO and S (sulphate deposition at mound springs) and Fe_2O_3 (oxidisation and iron induration). Isocons were not used as it was difficult to source true representation of weathered and fresh material to be able to make a fair comparison.

Origin of clays

The formation of secondary clays results in samples that are displaced away from the CNK apex and toward the A-FM axis on the A-CNK-FM diagram (Figure 5:6) and away from the CN apex and ultimately toward the A-apex on the A-CN-K diagram (Figure 5:7). The group of samples displaying this pattern includes all field lithologies and is dominated by samples of the oxidised weathering type. The pattern

can be interpreted to be the result of the weathering of Ca, Na and K bearing silicates (e.g. feldspars and micas) to a variety of secondary clays (e.g. illite, montmorillonite) and ultimately to kaolinite (Nesbitt and Young, 1989). The specific clay mineralogy is not obvious in hand sample as the clay minerals are fine-grained and occupy pore spaces. For samples collected from key sections, HyLogger™ analysis has enabled the identification of sample mineralogy (Chapter 2 and 3). The location of this group midway along the A-FM axis on the A-CNK-FM diagram and projecting through the central triangle from the CNK axis, demonstrates conservation of Fe:Al ratios during weathering and is consistent with in-situ conversion of Fe in detrital silicate minerals to Fe-oxides during weathering.

Carbonate

The majority of calcareous sedimentary rocks identified in this study are classified as regolith carbonates, rather than marine carbonates, on the basis of textural and morphological evidence (Chapter 2, 3). No marine carbonate sedimentary rocks were observed in the glaciomarine sedimentary rocks of the Cape Jervis and Boorthanna formations.

Regolith carbonates are broadly defined by Hill et al. (1998) as all carbonate materials of indeterminate composition and degree of induration found within the regolith. Most of the carbonate weathered samples analysed in this study are displaced towards the CNK apex on the A-CNK-FM diagram (Figure 5:6) and toward the CN apex on the A-CN-K diagram (Figure 5:7). This pattern is consistent with calcite, $CaCO_3$, being the dominant carbonate mineral. A smaller number of samples are displaced toward the midpoint of the CNK-FM axis on the A-CNK-FM diagram consistent with dolomite, $CaMg(CO_3)_2$, being the dominant carbonate. Hyperspectral analysis detected dolomite in these samples (Chapter 3). The dolomitic sedimentary rocks are not distinguishable using any of the other major element ratios such as Al_2O_3 and SiO_2 (Figure 5:5) or Al_2O_3 and K_2O (Figure 5:8). They are not distinguishable in any CaO elemental associations such as those shown in Figure 5:10.

The Ca in regolith carbonates is derived from two primary sources; the weathering of bedrock and the aeolian and precipitational deposition of Ca, ultimately derived from marine salt (Dart et al. 2007). Dart et al. (2007) proposed that approximately 90% of the Ca within regolith carbonates is sourced from an external marine source. This source is likely from sedimentary carbonates on the continental shelf and calcareous aeolianites that surround much of the southern and western Australian coastline. The winds that continually pass over these carbonates rework and transport the material over the Australian content where it is deposited and forms regolith carbonates (Lintern et al. 2006, Dart et al. 2007). A characteristic of regolith carbonates is that they have significantly higher Sr/Ca ratios than marine carbonates (van der Hoek and Forbes 2013). Wolff et al. (in review) has shown that regolith carbonates from the York Peninsula consistently have Sr/Ca >0.001 whereas marine carbonates have Sr/Ca <0.001. On this basis all of the samples in this study fall within the regolith carbonate field (Figure 5:10d).

A proportion of the oxidised weathering type (18 of 92 samples on the A-CN-K diagram; Figure 5:7) and a small number of the minimal weathering type (3 of 25 on the A-CN-K diagram) follow similar patterns to the carbonate weathered samples in all plots. Carbonate weathering has not been significant enough to be observed in hand specimen although calcite can be seen in thin section in the cement of fluviolacustrine sands as well as sands from the flow till complex and glaciomarine sands (Chapter 2). These samples were not identified from major element ratios.

Sulphate

The linear relationship between CaO and Total S for sulphate weathered samples is consistent with gypsum being the dominant sulphate mineral (Figure 5:10b). These samples were collected from the Mount Toondina section in an area prone to flooding from a mound spring where evaporate minerals such as gypsum saturate the landscape (Chapter 3). The glacigene sedimentary rocks at the Mount Toondina location include a significant proportion of carbonaceous samples and lignites, demonstrated by elevated C with no particular relationship to CaO in Figure 5:10a. Lignite commonly contains elevated S in the form of H_2S as it is a by-product of the decomposition of organic matter (Scott and Pain 2008). It is likely that the sulphate component of the gypsum at Mount Toondina is sourced from reduced S in these lignitic beds which has been oxidised to sulphate in the surficial environment (Saikia et al. 2014).

Ferruginous

Samples of the ferruginous weathering type are displaced toward the FM apex on the A-CNK-FM plot (Figure 5:6). This group are not differentiated from other samples in the A-CN-K plot (Figure 5:7, 5:13). This is because there is no Fe or Mg component on the diagram. Where the ferruginous sedimentary rocks plot on Figures 5:7 and 5:13 may reflect the lithogeochemistry of the original rock prior to ferruginous alteration provided the Fe-oxide minerals have not selectively replaced other minerals in the sediment.

Ferruginisation is a post-depositional process which overprints the sediment while often retaining the primary lithological characteristics of the sediment (Taylor and Eggleton 2001, Scott and Pain 2008). In sedimentary rocks that have been ferruginised, Fe-oxide minerals typically occupy pore space, and in-filling of the pore space preserves the primary mineralogy and texture of the sediment (Taylor and Eggleton 2001, Scott and Pain 2008). In sedimentary rocks that have been completely ferruginised, for example ferricrete, Fe-oxide minerals have overgrown the minerals of the sediment. In sandstones, the Fe-oxide minerals overgrows the minerals that make up the cement leaving only quartz grains and rock fragments. This is seen in the sandstone at Box Creek (Figure 3:6c, d) where the rock is made up of quartz grains and Fe-oxide mineral cement with very small amounts of kaolinite. Also observed in the ferruginous rocks in the Arckaringa Basin is the Fe-oxide mineral cement dissolving the quartz grains (Figure 3:5c). These textures can occur during diagenesis or due to weathering processes such as ferruginisation. Given the presence of lignite and unconsolidated material in the late Palaeozoic succession it is unlikely that diagenesis occurred therefore it is likely that this dissolution occurred during post-depostional weathering.

Iron is introduced in to sedimentary rocks through the weathering of rocks. When primary rock-forming minerals are exposed to oxygen and water the minerals begin to weather. An important product of this weathering is the oxidation of Fe to produce Fe^{3+} ions (Taylor and Eggleton 2001, Scott and Pain 2008). These Fe^{3+} ions are mobile in a reducing environment (i.e. below the water table), and are transported in groundwater until the conditions change to an oxidising environment. The Fe^{3+} ions become immobile in an oxidising environment and are precipitated as Fe-oxide minerals such as goethite and hematite (Bowell 1994, Taylor and Eggleton 2001, Scott and Pain 2008). When the weathering of primary rock-forming minerals occurs in an oxidising environment (i.e. above the water table), Fe^{3+} ions precipitate within the weathering solution as Fe-oxide minerals such as ferrihydrite which then upon further oxidation becomes goethite and/or hematite (Taylor and Eggleton 2001).

Environment of weathering

Deeply weathered sedimentary rocks with ferruginisation and mineral enrichment typically form in humid tropical to temperate environments of moderate relief that have been tectonically stable for long periods (Butt et al. 1997). In these conditions the water table typically rises and falls seasonally allowing oxidising, acidic conditions to initiate the chemical weathering of minerals in the sedimentary rocks. This chemical weathering includes the progressive destruction of minerals such as mica, feldspar and other sheet silicates which results in the depletion of Mg, Ca, Na, K and some depletion of Si and the retention of Al and Si in weathering products such as kaolinite and other clay minerals. Chemical weathering also initiates the mobilisation of trace elements hosted in the sedimentary rocks (Scott and Pain 2008, Taylor and Eggleton 2001). Weathering profiles of this kind characteristically form from granitods and volcanic rocks (Scott and Pain 2008, Butt et al. 1997). Although, weathering profiles that form mafic and ultramafic rocks have ferruginous zones that are better developed (Butt et al. 1997). Weathering profiles that form from detrital sedimentary rocks, such as the late Palaeozoic glacigene rocks often contain a higher proportion of accessory minerals. These accessory minerals are often the remnants of weathered quartz-rich source rock. These accessory minerals are less affected by chemical weathering (Scott and Pain 2008).

The weathering that occurred after the deposition of the glacigene sedimentary rocks was likely initiated during the Mesozoic. The climate during the Mesozoic varied from wet to dry, becoming warmer in the later Mesozoic (Drexel and Preiss 1995). While this climate was favourable for weathering and the associated ferruginisation and elemental enrichment, the sedimentary rocks that are being weathered are derived from rock types that are not favourable to forming Fe-oxide minerals and are unlikely to host an abundance of trace elements. While the Mesozoic may have potentially been wet and humid enough to facilitate the conditions favourable for trace element enrichment, these conditions were not continuous (Drexel and Preiss 1995) and the glacigene sedimentary rocks were not periodically saturated by oxidising acidic groundwaters.

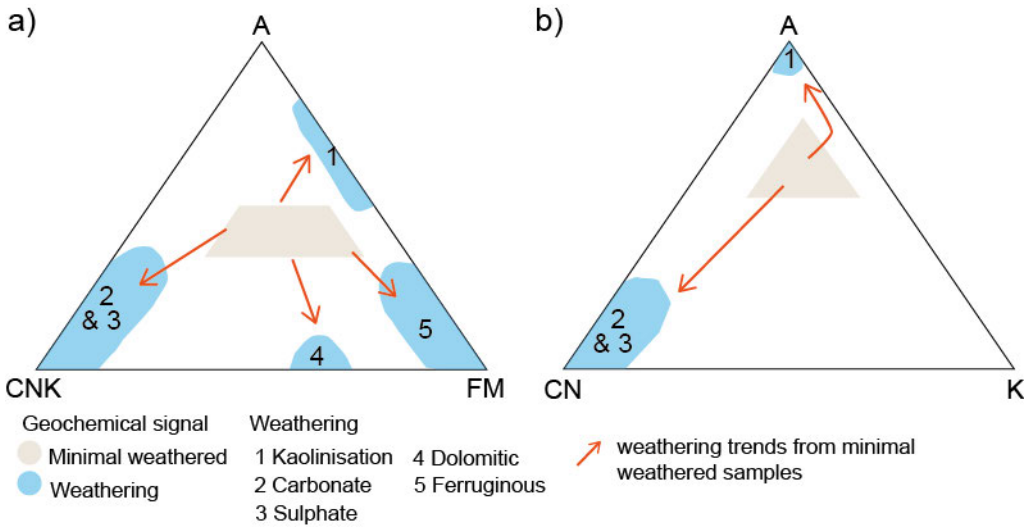

Figure 5:13 Geochemical signals and weathering types distinguished in the a) A-CNK-FM and b) A-CN-K ternary plots.

5.4.2 Depositional process signals

Grainsize and compositional variations with in the samples are related to depositional processes. Samples of the minimal weathering and oxidised weathering types dominate the least-altered regions

within Figures 5:6 and 5:7 (marked by the black triangles) and make up the dominant, linear trend in Figure 5:5. Most of these samples also closely overlap with PAAS and the field of Kanmantoo Group sedimentary rocks. The high silica end-members in Figure 5:5 are dominated by the coarser grained (sandy) sedimentary rocks while fine-grained clay and silt-rich samples dominate the high Al side of the plot.

The majority of the sand units, dominantly consisting of quartz, within the glacigene sedimentary package were deposited via medium to high energy meltwater streams during the melting of the ice mass (Chapters 2 and 3). Geochemically, the sand samples preserve low concentration of the major elements, Al_2O_3 and Fe_2O_3, as well as many of the trace and rare earth elements (Figures 5:8, 5:9). Elements other than Si are mostly concentrated within the sediment cement of clay, Fe-oxide or calcium carbonate minerals.

Conversely, the clay and silt sedimentary rocks within the glacigene sequence were deposited in a less energetic setting (e.g. glacial lake) during stagnation of the ice (Chapter 2). The clay and silt samples are geochemically more variable and contain higher concentrations of a range of trace elements (including Zr, Hf, REEs and the commodity elements Pb, Zn, Ni and Cu) compared to sand-rich sedimentary rocks. The relative concentration of such elements in the fine fraction of the sedimentary rocks could be the result of:

1) Elemental abundances controlled by sheet silicate and clay minerals (e.g. Al_2O_3, K_2O) including elements that substitute or are incorporated into the lattice of sheet silicate and clay minerals (e.g. Rb). REEs can also substitute into the lattice of clay minerals (Taylor and Eggleton 2001, Scott and Pain 2008) and the positive linear relationships between Ce, Dy and Al_2O_3 supports this as the dominant control on REE abundance in the glacigene sedimentary rocks. REEs deported in heavy mineral phases such as oxides or phosphates would be expected to form a separate high REE/low Al_2O_3 population (as seen for Zr and Hf deported in zirconium, see below).

2) Elemental abundances controlled by adsorption onto clay minerals. This is most likely the case for Ga and the commodity elements (Pb, Zn, Ni and Cu) which have been shown to have a strong affinity toward absorption onto clay minerals (Taylor and Eggleton 2001, Scott and Pain 2008).

3) Elemental abundances controlled by minerals that tend to be fine-grained (even though they may also be relatively dense). This appears to be the case for Zr and Hf which are most likely deported in zircon. At Zr concentrations <250 ppm, there is a tendency for Zr and Hf to be concentrated in fine-grained lithologies and a broad positive relationship between Zr and Al_2O_3. In contrast, the highest Zr and Hf samples (Zr >300 ppm) include a range of rock-types and have a broadly negative correlation with Al_2O_3. This implies that a high proportion of zircon typically resides in the fine fraction (which also includes the Al_2O_3-rich clays), however, heavy mineral sorting processes, that act to locally enrich zircon, tend to also remove the clay component.

The sand matrix diamictites presented in this study typically have a geochemical signature similar to sand samples, whereas the clay matrix diamictites are similar to the clay and silt-rich glacigene sedimentary rocks (Figures 5:5 to 5:11). This is not surprising given the sampling method employed for

the diamictites where any visible clasts (>0.5 cm) where removed before analyses. Thus, the geochemistry of the diamictites is representative of their matrix. A diamictite formed directly by the release of debris from a glacier, and without subsequent modification, might be expected to have a broad particle size distribution (potentially from rock powder to boulders) due to the ability of glaciers to transport a range of grainsizes with equal efficiency (Clark 1987). Such a rock should carry a geochemical signal which closely matches its source materials. However, in many cases the glacially deposited material might be overprinted by other depositional processes which act to modify the geochemical signal. For example, a diamictite deposited by a retreating glacier might be modified in a relatively high energy fluvial setting, whereby fine-grained materials are removed leaving a diamictite with a sandy matrix, or ultimately a fluvio-glacial conglomerate. The relative importance of such depositional processes acting on the diamictites appears to be the dominant control on SiO_2, Al_2O_3 and a range of elements that broadly correlate with Al_2O_3 including the REEs (Figure 5:11) and the commodity elements (Pb, Zn, Ni and Cu). It is also important to recognise that the weathering of the diamictite and hence the matrix has been influenced by the same mechanisms as the other lithologies within the glacigene succession. As such the mineralogical influence, particularly of secondary minerals, on the geochemistry of the diamictites is also responsible for the similar geochemistry between the sand matrix dominated diamictite samples and the sand samples and between the clay matrix diamictite samples and the clay and silt samples.

5.4.3 Provenance signals

As discussed above, the Arckaringa and Troubridge basin glacigene samples of the minimal and oxidised weathering types are concentrated in discrete regions of the major element plots (Figures 5:5 to 5:7). They have variable major element chemistry due to depositional processes and also form coherent populations defining 'background' trends on many of the trace element correlation diagrams. The Al_2O_3-rich component of this group of samples is most likely to be glacial rock flour which in turn is most likely to be representative of the mineralogy and geochemistry of the source region (provenance) of the glacigene rocks (Clark 1987, Glasser and Bennett 2004).

Major element concentrations are consistent with Kanmantoo Group, Encounter Bay Granite and PAAS as are most of the trace elements (Figures 5:5 to 5:11). The Chondrite REE normalisation plot (Figure 5:12) shows the same pattern for all minimally weathered and oxidised samples regardless of lithology, however each lithology has a differing bulk REE concentration. Clay is similar to the geochemistry of the average Kanmantoo Group, Encounter Bay Granite and PAAS (Figure 5:12). The remaining lithologies show that the minimal weathered and oxidised samples are displaced lower on the REE plot (Figure 5:12) resulting from dilution by quartz. This reflects the depositional processes previously described. These observations are consistent with the geochemistry of the average Kanmantoo Group, Encounter Bay Granite and PAAS, however, it cannot be used in isolation as proof of source rock as many upper crustal rocks have similar REE geochemical patterns.

5.4.4 Comparison with potential Kanmantoo Group source rocks

Here the geochemistry of the late Palaeozoic glacigene rocks of this study are compared with Post Archaean Australian Shale (PAAS), Kanmantoo Group metasedimentary rocks and the Encounter Bay Granite taken from previous publications.

Diamictites of the Cape Jervis Formation in the Troubridge basin contain two dominant clast types; i) metasedimentary rocks of comparable composition, texture and metamorphic grade to

metasedimentary rocks of the Kanmantoo Group which are exposed on the Fleurieu Peninsula and Kangaroo Island, ii) granitic rocks of similar composition and texture to the Encounter Bay Granite, exposed near Victor Harbour on the Fleurieu Peninsula (Chapter 4, Foden et al. 2002, Haines et al. 2009, De Pretis 2011). Detrital zircon spectra from the Cape Jervis Formation support the interpretation that Kanmantoo Group metasedimentary rocks and to a lesser extent the Encounter Bay Granites are likely source rocks (Chapter 4). In a glacial environment where the movement of ice is responsible for grinding and transportation of rocks, it can be expected that heavy minerals such as zircon would remain in the rock flour and be deposited in glacial sedimentary rocks with population distributions that are representative of the source rock.

The source of the glacigene sedimentary rocks of the Arckaringa Basin is likely to be more diverse than the Cape Jervis Formation and thus more difficult to characterise geochemically. Clasts within diamictite rocks of the Boorthanna Formation include sedimentary and metasedimentary rocks, granites and gneisses likely to be sourced from the Neoproterozoic Adelaide Rift Complex and underlying Meso- and Palaeoproterozoic basement exposed in the Peake and Denison Inlier (Chapter 4). This diversity of potential source rocks is supported by detrital zircon spectra that include a broader and older spread of ages than those from the Cape Jervis Formation (Chapter 4). Given the varied stratigraphy and basement geology of the Peake and Denison Ranges (Ambrose et al., 1981) it is difficult to independently ascertain their average geochemistry. The PAAS has instead been included as a useful geochemical representative of average Australian Proterozoic rocks.

The Kanmantoo Group range follows the same Al_2O_3:SiO_2 trend (Figure 5:5) as the late Palaeozoic glacigene sedimentary rocks. The Kanmantoo Group ranges from 85 to 60% SiO_2 and 10 to 20% Al_2O_3. The glacigene sedimentary rocks that plot within this range are dominated by clay and silt lithologies that are oxidised or have minimal weathering. Although plotting along the same trend, the sand-rich glacigene sedimentary rocks have higher SiO_2 and lower content Al_2O_3 when compared to the average of the Kanmantoo Group and Encounter Bay Granite (Figure 5:5). This relationship continues in the Harker plots of trace elements against Al_2O_3 (Figure 5:8) and Fe_2O_3 (Figure 5:9). The Kanmantoo Group has comparable trends to the 'background' trends defined by samples of the minimal and oxidised weathering types on most plots, overlapping with samples of the clay and silt-rich rock types. This suggests that the relationship between high trace elements and Al_2O_3 and Fe_2O_3 content in clay and silt lithologies in the glacigene sedimentary rocks are similar to the relationships within the Kanmantoo Group.

The Kanmantoo Group occupies the middle of the A-CNK-FM plot (Figure 5:6), at ~0.4 Al_2O_3 and ranging from 0.45 CNK, 0.15 FM to 0.15 CNK, 0.45 FM. This range overlaps with PAAS and occupies a similar space as a large group of late Palaeozoic samples of the minimal and oxidised weathering types. The Encounter Bay Granites include samples trending toward the mid-point of the A-CNK axis, consistent with the significant component of feldspar and mica observed in these rocks (Foden et al. 2002). On the A-CN-K plot (Figure 5:7) the Kanmantoo Group occupies an array between 0.50 A, 0.45 CN, 0.05 K and 0.70 A, 0.05 CN, 0.25 K. The CN-rich end of the Kanmantoo Group array sits mid-way along the A-CN axis, distinct from the carbonate weathering trend in the late Palaeozoic samples. This is consistent with plagioclase, or a Na/Ca bearing sheet silicate such as montmorillonite, being a significant component of the Kanmantoo Group as observed by Haines et al. (2009). A likely explanation for the trend toward more Al and K-rich compositions is the variable replacement of plagioclase by sheet silicates and clays during weathering or alteration. The Al and K-rich end of this trend overlaps with a

large group of late Palaeozoic glacigene samples of the minimal, oxidised and ferruginous weathering types.

That the Kanmantoo Group and late Palaeozoic glacigene sedimentary rocks have diverging trends on the A-CN-K plot does not rule out the Kanmantoo Group as a potential source. One possible interpretation of the data is that the Kanmantoo Group and the late Palaeozoic samples (all of which were taken from surface exposures) underwent similar surficial weathering processes in the relatively recent geological past, resulting in them being pulled toward similar locations on the A-CN-K plot. The Kanmantoo Group dataset, for reasons related to the particular sampling technique, location or local preservation has a larger component of less weathered samples than the late Palaeozoic group and thus preserves a trend toward the A-CN axis.

The favoured explanation, which more completely accounts for the observed trends, is that the Kanmantoo Group underwent weathering or alteration prior to being incorporated in the late Palaeozoic glacigene sedimentary rocks. Thus the end-point of pre-glacial alteration (the Al and K-rich end of the Kanmantoo Group trend) overlaps with the starting point of post-glacial alteration (the minimal and oxidised weathering types of the late Palaeozoic samples). Geochemical trends due to post depositional weathering and alteration diverge from this space, toward the A apex (clay weathering) and CN apex (carbonate and sulphate weathering) and toward the FM axis (Fe-induration) on the A-CNK-FM diagram (Figure 5:6).

The chondrite normalised Kanmantoo Group average REE geochemistry has a similar pattern to PAAS and to the late Palaeozoic glacigene sedimentary rocks (Figure 5:12), with elevated convex, upward LREE, a negative Eu anomaly and relatively flat HREE. There is a difference in the normalised REE patterns of the Kanmantoo Group averages from Haines et al. (2009) and De Pretis (2011). The higher average REE content in the Haines et al. (2009) samples is likely due to the larger number of finer-grained samples. These samples are likely to have an increased clay mineral content and therefore a higher capacity for REE substitutions into the clay mineral lattice. The normalised REE concentrations of the clay-rich late Palaeozoic glacigene rocks, most likely to be representative of their source rocks are almost identical to those of the Kanmantoo Group samples presented by De Pretis (2011).

5.4.5 Distinguishing background for exploration geochemistry

Although the sedimentary rocks of the Troubridge and Arckaringa basins do not host any mineralisation, the underlying basement rocks are host to a number of known mineral deposits. The Kanmantoo Group is host to a number of base metal deposits which include the Kanmantoo Cu-Au-Ag deposit and Angus Zn-Pb-Ag deposit (Figure 5:1; Geological Survey of South Australia 2016). The Talisker Pb-Au deposit is the only major deposit that is directly overlain by the Troubridge Basin sedimentary rocks in this study area. Known mineralisation of the northern Yorke Peninsula includes the Hillside IOCG-U deposit (Figure 5:1). This region is the southernmost extent of the Moonta-Wallaroo Cu-Au belt and the Olympic Dam IOCG±U Domain (Creaser and Cooper 1993). Sedimentary rocks of the Troubridge Basin are preserved in low-lying areas of the northern Yorke Peninsula and have been observed approximately 100 km north of the recognised boundary of the basin near Port Wakefield (Figure 5:2a). The Arckaringa Basin overlaps the northern extent of the Olympic Dam IOCG±U Domain (Creaser and Cooper 1993) and glacigene sedimentary rocks of the Boorthanna Formation directly overly the Prominent Hill IOCG deposit (Forbes et al. 2015). Forbes et al. (2015)

showed that diamictites of the Boorthanna Formation carry a geochemical signature resulting in a manifold increase in the exploration footprint of the Prominent Hill deposit.

Given the proximity to known mineral deposits it is important to understand how the late Palaeozoic sedimentary rocks can be utilised for the exploration of mineral deposits that are potentially covered by the sedimentary rocks. As discussed in the introduction of this chapter using geochemistry as a tool for vectoring towards potential mineralisation is commonly used in glaciated terrains such as Canada and Finland, where the geochemistry of glacigene sediments deposited during the Last Glacial Maximum can be used to vector towards potential mineralisation. Research such as that conducted by DiLabio and Coker (1987), McMartin and McClenaghan (2001) and Sarala et al. (2009) all suggest that understanding the background geochemistry is important in these types of studies. Forbes et al. (2015) used the geochemistry of mineralised sediments to show the reworking and redistribution of the mineralised sediments into the glacigene sediments in the Arckaringa Basin.

Most commonly explorers use raw geochemical data or normalise the data to reduce the effect of a known geochemical and lithological relationships (Lentz 1996, Harris et al. 1997, Liaghati et al. 2003, Corredeira et al. 2008). Normalising to Al_2O_3 or Fe_2O_3 are common approaches, as clay minerals and Fe-oxide minerals tend to have an ability to concentrate trace elements (Butt et al. 1997, Taylor and Eggleton 2001, Scott and Pain 2008). This may lead to false anomalies in geochemical datasets where enrichment is due to bulk mineralogy rather than elemental enrichment that may indicate proximity to mineralisation.

It is generally expected that ferruginous sedimentary rocks are enriched in metals such as Pb, Cu, Ni and Zn (e.g. Taylor and Eggleton 2001, McQueen 2006, Scott and Pain 2008). Trace elements can be incorporated in to Fe-oxide minerals by adsorption, followed by structural substitution, isomorphic substitution, growth of new trace-element specific minerals or overgrowth and inclusion of other resistate minerals (Scott and Pain 2008). It is likely that the enrichment of trace elements in the late Palaeozoic sedimentary rocks is from adsorption and substitution. Trace elements adhere and are substituted into Fe-oxides (and Mn-oxides) that are products of weathering such as goethite and hematite, thus enriching the ferruginous sedimentary rocks in trace elements (Scott and Pain 2008).

The generally low concentrations of commodity elements (Cu, Ni, Pb, Zn) in the late Palaeozoic sedimentary rocks and the observed relationships with other geochemical components presents an opportunity to define the geochemical background as a function of the provenance, depositional and weathering processes discussed above. This will help to determine the most suitable data treatment (for example normalisation) for highlighting enrichment that is not due to such processes and might instead be useful as an indicator of nearby mineralisation.

The commodity element geochemistry of the late Palaeozoic sedimentary rocks is largely controlled by the clay content (i.e. Al_2O_3) and Fe-oxide mineral content (i.e. Fe_2O_3). The three trends on the commodity element vs Al_2O_3 plots can be interpreted as the result of three separate controls:

1) The low commodity element trend is dominated by samples that also have low K_2O:Al_2O_3 and plot near the A apex on the A-CN-K plot and along the A-FM axis on the A-CNK-FM plot. These samples have undergone intense weathering and have kaolinite as the dominant clay mineral. Low levels of the commodity elements in these samples are consistent with cation leaching, which is commonly observed in highly weathered kaolinite-rich saprolites (Taylor and Eggleton 2001, Scott and Pain 2008).

2) The moderate commodity element trend most closely matches the field for Kanmantoo Group sedimentary rocks and PAAS, with the highest commodity element concentrations in clay and silt-rich rock types, and is best interpreted as a function of depositional processes. The broad positive background relationship can be attributed to the ability of trace elements to substitute into the mineral lattice of clay minerals (Taylor and Eggleton 2001, Scott and Pain 2008).
3) The high commodity element trend which includes a relatively small number of samples. In the case of Cu this trend includes a range of protolith and weathering types, whereas for Pb, Ni and Zn the high commodity element trend is dominated by ferruginous samples, suggesting a potential Fe-oxide control on trace element concentrations.

In the commodity elements vs Fe_2O_3 plots (Figures 5:9f to i) two groups are evident. At Fe_2O_3 concentrations <5%, Cu, Ni, Pb and Zn form linear arrays with relatively steep gradients. These arrays overlap with the range of Kanmantoo Group sedimentary rocks and PAAS and include the same samples as the low Fe_2O_3:Al_2O_3 trend on the Fe_2O_3 vs Al_2O_3 plot (Figure 5:8j).

The second grouping has Fe_2O_3 >5% and variable concentrations of commodity elements (Figures 5:8f to j). This group is dominated by samples with ferruginous alteration. Although the concentrations of commodity elements in the high-Fe_2O_3 samples are not systematically higher than the non-ferruginous sedimentary rocks there are a number of very high-Fe_2O_3 samples which also have high commodity element concentrations and partly constitute the high commodity element low Al_2O_3 groups in Figure 5:8f to i.

In an attempt to account for commodity element concentrations controlled by clay and Fe-oxide abundances, Pb, Zn, Ni and Cu concentrations have been normalised against Al_2O_3 and Fe_2O_3. This process can be visualised by plotting the commodity elements against Al_2O_3 + Fe_2O_3 (Figure 5:14). The majority of the samples on these diagrams form a scatter with an upper bounding line which effectively defines the background population. The term background is defined by Hawkes and Webb (1962) as elemental concentrations that are the normal abundance of an element in a non-mineralised earth material. It is also suggested that background concentrations are a range and not an absolute value. The samples with background concentrations are shaded in grey on Figure 5:14. Samples that are enriched over and above what might be expected due to the abundance of clay and Fe-oxides plot above the background population, toward the y-axis on these diagrams.

The enriched samples identified in this way include a range of sedimentary protoliths and weathering types (Figures 5:14; Table 5:2). The enriched samples from the Mount Toondina section and the diamictite clay from Waterloo Bay are likely enriched in Cu, Pb and Zn due to the presence of lignite/ carbonate materials in the sedimentary rocks. Riley et al. (2011) reported that copper is a residual component in carbonaceous sedimentary rocks. Pyrite, chalcopyrite and other sulphides are common in coal and lignite which also contributes to the Cu content in the carbonaceous and organic-rich sedimentary rocks. Gluskoter (1975) reported that Pb is inorganically incorporated into carbonaceous material. It is likely that the Pb is associated with the presence of sulphides (Riley et al. 2011). Zn in also present in coal and lignite. Typically, the Zn is associated with sulphides however Riley et al. (2011) reported an association between Zn and illite.

Table 5:2 Summary of samples outside of the background range of concentrations of commodity elements Cu, Ni, Pb and Zn. Sample ID refer to the samples labelled in Figure 5:14 and Appendix 3.

Sample ID	Lithology	Weathering	Sample location	Enriched in	Closest mineral occurrence/ potential source of commodity element
KI001	Clay	Minimal	Wisanger Hills	Cu	Overlain by Wisanger Basalt
KI003	Sand	Oxidised	Kingscote Composite Section	Cu, Zn	Overlain by Wisanger Basalt
KI004	Sand	Carbonate	Kingscote Composite Section	Cu	Overlain by Wisanger Basalt
KI007	Sand	Carbonate	Kingscote Composite Section	Cu	Overlain by Wisanger Basalt
Reg072	Sand	Ferruginous	Kingscote Composite Section	Cu	Overlain by Wisanger Basalt
CJ016	Diamictite sand	Oxidised	Cape Jervis Section	Zn	Talisker Pb-Ag-Zn deposit,5 km E
Reg075	Clay	Ferruginous	Cape Jervis Section	Pb	Talisker Pb-Ag deposit, 5 km E
Reg075	Clay	Ferruginous	Cape Jervis Section	Pb	Talisker Pb-Ag deposit, 5 km E
Reg007	Diamictite clay	Minimal	Waterloo Bay	Cu, Ni, Pb	Dark, reduced sediment potentially organic matter-rich
Reg045	Sand	Oxidised	Yankalilla	Cu, Zn	Yankalilla River Cu occurrence, 1.5 km SW Great Gorge Cu deposit, 1.5 km NW
MT004	Sand	Sulphate	Mt Toondina Section	Zn	Enrichment due to lignite/coal content
MT009	Carbonaceous	Sulphate	Mt Toondina Section	Cu, Ni, Zn	Enrichment due to lignite/coal content

The samples from the Kingscote Composite Section are all enriched in Cu (Table 5:2). This can likely be attributed to the Jurassic Wisanger Basalt (Milnes et al. 1981, Johnson 1982a, Johnson 1982b) that overlies the Cape Jervis Formation in the Kingscote region. Geochemical results in Hill et al. (2012) demonstrate elevated Cu and Zn content. The percolation of groundwater through the relatively Cu-rich basalt and glacigene sedimentary rocks provides a mechanism of enrichment of the sedimentary rocks in the Kingscote Composite section. Approximately 30 km to the SSW of Kingscote, there are a number of known Cu, Au, Zn and Pb occurrences associated with the Cygnet-Snelling Shear Zone (Hill et al. 2012). This mineralisation system may also be contributing to the Cu enrichment of the glacigene sedimentary rocks. The Cygnet-Snelling Shear Zone is topographically higher than Kingscote (Hill et al. 2012), it is reasonable to assume groundwaters would flow from the shear zone through the glacigene sediments before running out to sea.

The Cu enrichment of the oxidised sand sampled from Yankalilla might be attributed to known local mineral occurrences. The Yankalilla River Cu occurrence and Great Gorge Cu deposit are within 1.5 km upstream of the sample site (Becker and Horgath 2004). Enrichment of Pb and Zn from the Cape Jervis Section might also be attributed to known local mineral occurrences. The Talisker Pb-Ag-Zn deposit is exposed approximately five km to the east and topographically uphill of the Cape Jervis Section (Figure 5:1; Drexel 1978, Parker 1985) and the Talisker Formation of the Kanmantoo Group contains numerous minor occurrences of Pb and Zn mineralisation (Drexel 1978).

The enrichment of samples (disregarding enrichment due to carbonaceous and organic matter) can in all cases be attributed to known local enrichments including mineral occurrences in the underlying basement and trace element-rich overlying stratigraphy. This shows that using normalisation based on lithogeochemical relationships can differentiate between elemental abundances related to provenance, depositional and background weathering, or alteration processes and those that might be useful as indicators of proximal mineralisation. The type of normalisation needs to be assessed based on the sample lithology as well as the weathering alteration as demonstrated in this chapter. The reason this is required is that the anomalous data for one dataset may not be anomalous for another, just as the background ranges will differ between datasets.

Using copper as an example, Figure 5:15 demonstrates how using normalisations to Fe_2O_3, Al_2O_3, and Al_2O_3+Fe_2O_3 alter the population distribution to produce successively tighter log normal distributions with more clearly defined outliers at the high-Cu end (corresponding to the samples above the background population in Figure 5:14a).

To assess the validity of the normalisation of the glacigene sedimentary rocks the comparisons have been made between the raw data and normalised data. Using the samples from the Troubridge Basin, the raw Cu data and the Cu data normalised to Al_2O_3 and Fe_2O_3 have been plotted on a map of the basin (Figure 5:16) to allow spatial comparisons between the data sets. The statistical breaks in the data have been made based on the distribution of the data (Figures 5:15a, d). Samples with concentrations 2 standard deviations or more from normal have been assessed as the samples that are outside of the background range, these are plotted as red dots. These are the samples that are potentially enriched in Cu from processes other than lithology and weathering. Normalising the data for clay and Fe-oxide mineral content reduces the number of enriched samples from 16 samples using the raw Cu data (Figure 5:16a) to nine samples using the Al+Fe normalised Cu data (Figure 5:16b). Six of the enriched normalised samples are identified as enriched in the raw data as well as the normalised data the other three enriched Al+Fe samples were not identified. This validates what was shown in the normalisation histograms (Figure 5:15) that using normalisations based on the lithogeochemistry can improve the assessment of geochemical datasets obtained from exploration programs where glacigene sedimentary rocks cover potentially mineralised terranes

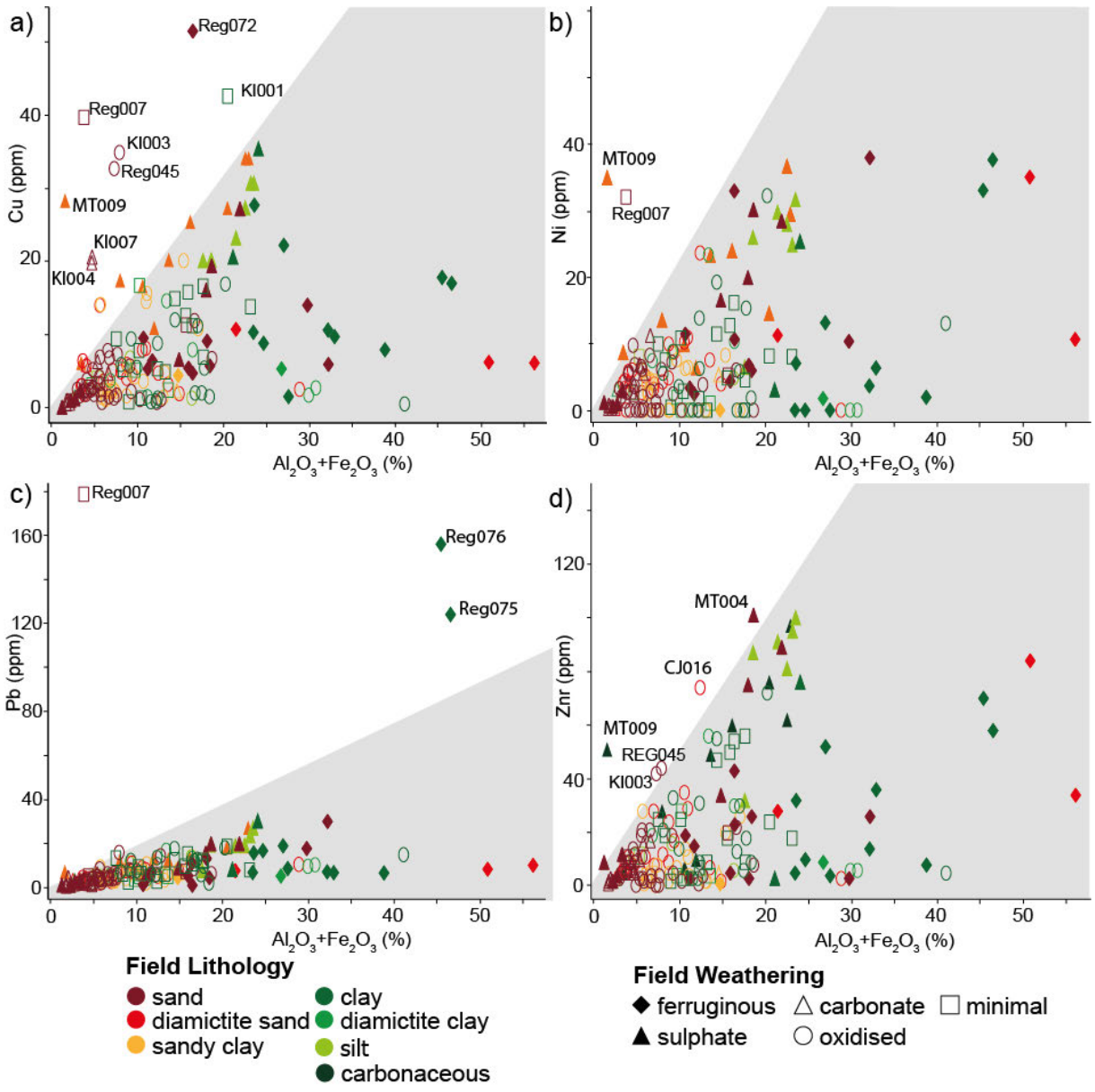

Figure 5:14 Commodity elements (Cu, Ni, Pb and Zn) vs (Al_2O_3+Fe_2O_3) Harker diagrams showing normalisation of samples to Fe-oxide and clay minerals. Samples that are considered as having background concentration or lower of commodity elements are shaded in grey. Further details on samples are in Appendix 3.

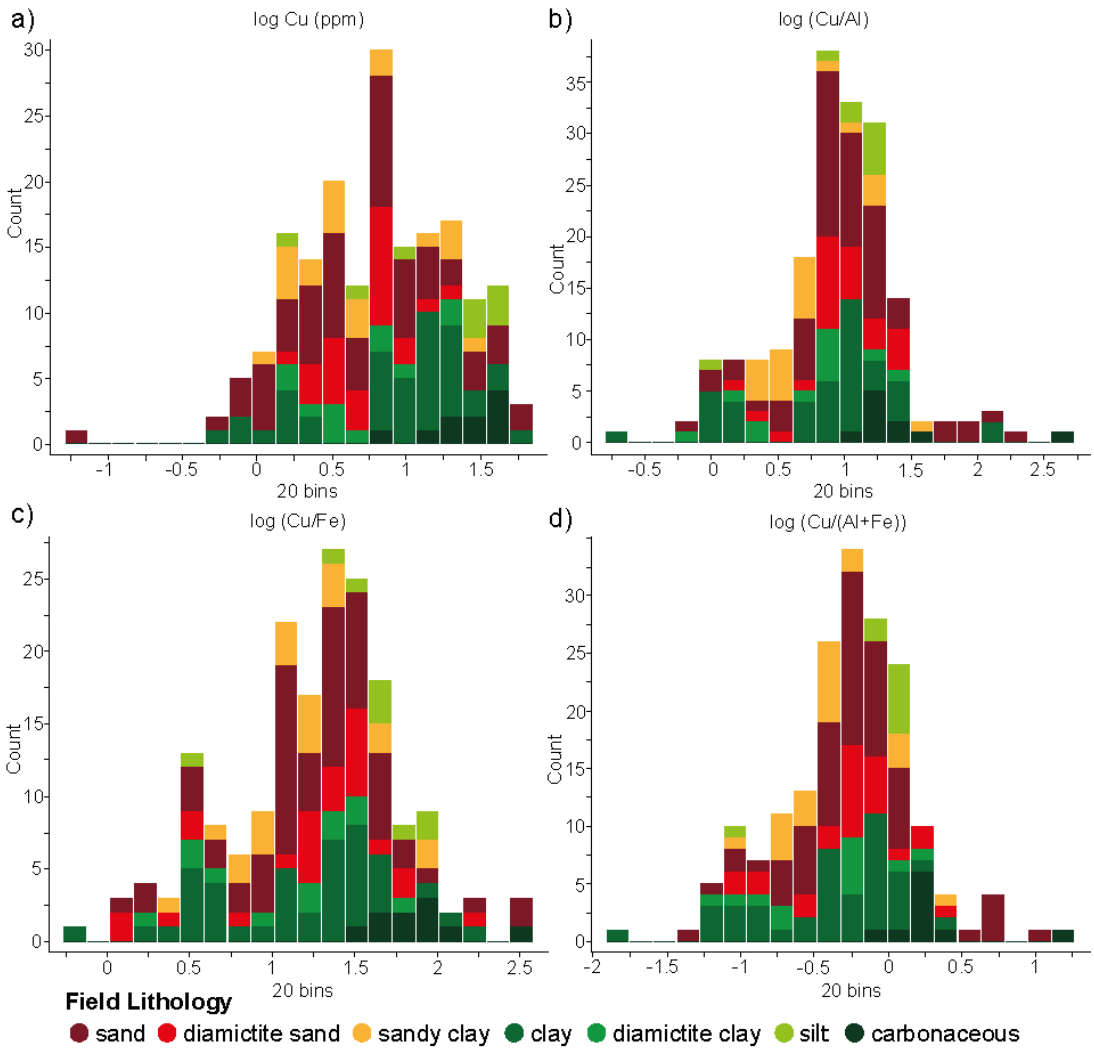

Figure 5:15 Histograms of glacigene sedimentary rocks showing distribution of samples showing a) log Cu; b) log Cu/Al_2O_3; c) log Cu/Fe_2O_3; d) log $Cu/(Al_2O_3+Fe_2O_3)$. Skewness is removed using automated power transformations within the IoGAS software package.

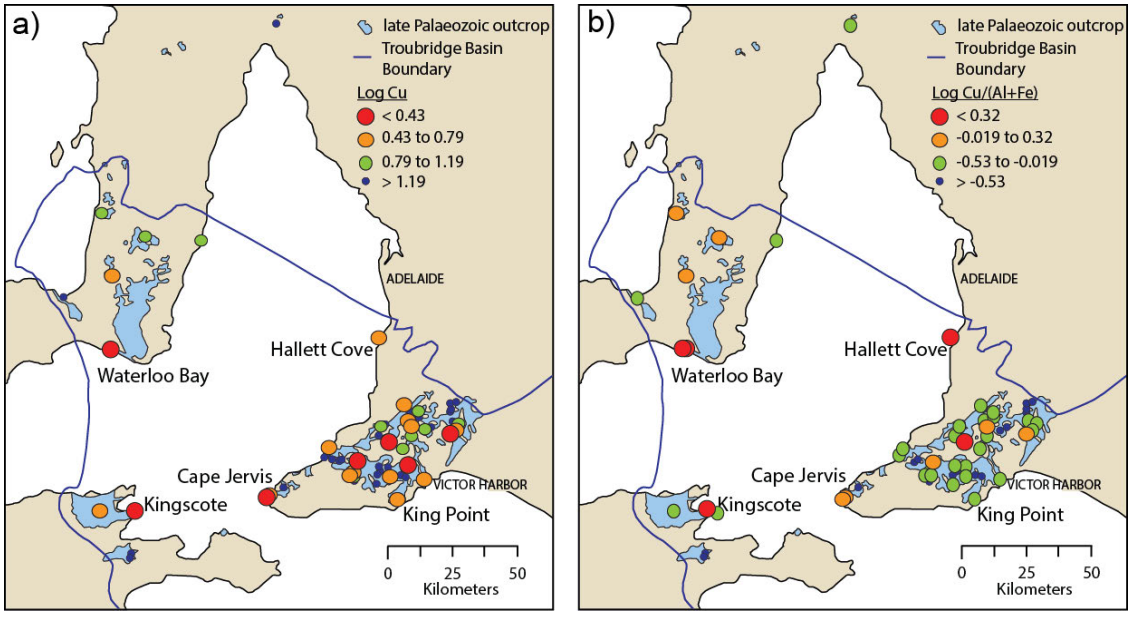

Figure 5:16 Spatial representation of the a) raw Cu and b) Cu normalised to Al_2O_3 + Fe_2O_3 data of the Troubridge Basin.

5.5 Conclusion

The geochemistry of the glacigene sedimentary rocks of the Troubridge and Arckaringa basins suggests that via major element ratios a number of signals can be interpreted. These include signals that indicate; the preservation of provenance geochemistry; the depositional processes of the glacigene rocks, and the types of post-deposition weathering the sedimentary rocks have undergone.

There are several different types of weathering that the glacigene sedimentary rocks have undergone. These are clearly differentiated in the geochemistry particularly in the A-CNK-FM and A-CN-K ternary diagrams. Additional weathering groups can also be distinguished in the A-CNK-FM ternary plots that are not observable in field observations.

Sedimentary rocks that have calcareous weathering (carbonate and sulphate) are distinguishable in both ternary plots. This is due to the Ca component in these sedimentary rocks likely in the form of calcium carbonate and calcium sulphate minerals. In the A-CN-K ternary plot, some oxidised sedimentary rocks are pulled towards the CN apex, shown by the arrow in Figure 5:14b. These are the sedimentary rocks that have a minor calcium carbonate or calcium sulphate component that are not observable in field observation. Additionally, sedimentary rocks with a significant amount of dolomite are differentiated from the other calcareous sedimentary rocks. These sedimentary rocks are pulled towards the FM apex due to the Mg component in the dolomite ($CaMg(CO_3)_2$). It is not possible to separate the sedimentary rocks with carbonate or sulphate weathering or dolomitic sedimentary rocks in the A-CN-K ternary plot. The ferruginous sedimentary rocks are only differentiated in the A-CNK-FM ternary diagram (Figure 5:6) and are pulled toward the FM apex due to the FeO and MgO content.

Broad depositional processes can be ascertained from the chemistry of the glacigene sedimentary rocks. Most of the samples with a sand lithology are geochemically barren, and have very high Si content (Figure 5:5) with low concentrations of Al and minor concentrations of Fe, Ca and K. This infers that the sedimentary rocks were deposited in an environment where the high energy meltwater removed most of the fine sedimentary rocks depositing sands that are primarily the quartz grains and rock fragments. The clay and silt sedimentary rocks have comparatively low Si and high Al concentrations. These were deposited in a quiet, low energy environment where the finer grained sedimentary rocks were deposited.

The geochemical signals that show a preservation of the geochemistry inherited from the source rock (or the provenance signal) in the sedimentary rocks that have minimal weathering or sedimentary rocks that have not been intensely weathered rather have undergone some oxidation that has resulted in the precipitated or formation of Fe-oxide minerals in the form of mottles or the staining of quartz grains. These sedimentary rocks are not restricted to a particular lithology and are expressed in the A-CNK-FM and A-CN-K ternary diagrams (Figures 5:6, 5:7) by plotting in a small region near the centre of the diagrams. The Kanmantoo Group geochemical average also plots in these areas (indicated in Figure 5:13) suggesting that the samples that plot near this have a similar geochemistry to the Kanmantoo Group. The minimal weathering and oxidation the sedimentary rocks have undergone have not influenced the major element geochemistry of these sedimentary rocks.

If the background geochemical signals related to provenance, depositional processes and weathering processes can be recognised and accounted for (for example by using simple normalisations) there is a

better chance of isolating geochemical signals related to local enrichment of commodity elements that may be relevant to mineral exploration.

Chapter 6: Palaeogeographic reconstruction of the late Palaeozoic glaciation in South Australia

Foreword

This chapter provides a series of palaeogeographic reconstructions of late Palaeozoic South Australia. The reconstructions are based on the observations and outcomes of Chapters 2 to 5 as well as previously published models and reconstructions. Previous reconstructions by Howchin (1912), Crowell and Frakes (1971a, 1971b), McGowran (1973), Alley and Bourman (1984) and Veevers (2006) have provided a foundation for the reconstructions depicted here and are duly referenced throughout the text. The palaeogeographic reconstructions in this chapter illustrate, through a number of state-wide, planar view reconstructions, the major depositional events that occurred during, and after the late Palaeozoic glaciation in South Australia. This chapter has been written as an independent publication and is structured accordingly.

Abstract

A series of new palaeogeographic reconstructions for South Australia during the glacial and post-glacial environments during the late Palaeozoic are presented. The reconstructions are a synthesis of existing models and new datasets including sedimentology, geochronology and geochemistry. The glacial environment has been separated into three depositional stages; glacial advance, glacial maximum and glacial retreat. These stages have been preserved in glacigene sedimentary rocks of the Troubridge and Arckaringa basins. The glacial environment, during which deposition occurred, has been reconstructed largely based on the extent and characteristics of the diamictite units. The shape, sorting, size and lithology of clasts in the diamictite facies deposited during each depositional stage are unique and can therefore be used to define the stage of glacial environment as well as the maximum extend of the glaciation. The glaciation was followed by a marine retreat. The sedimentary rocks preserving this post-glacial environment are restricted to the subsurface of the late Palaeozoic basins in the north of South Australia and sparse exposures in the Troubridge Basis in the south of the state. The marine transgression was followed by freshwater conditions in the north of South Australia. This depositional environment comprised of alternating fluvial and lacustrine conditions with occasional coal swamps. These alternating sandstone and clay units are largely preserved in the Arckaringa Basin, minor lignite, coal and carbonaceous sedimentary rocks are common within the main depocentres of the basin.

6.1 Introduction

Abundant evidence exists that large parts of Australia were covered by ice in Carboniferous and Early Permian times (Figure 6:1a; Crowell and Frakes 1971a, 1971b, Caputo and Crowell 1982, Veevers 2006, Playford 2011, Yang et al. 2014). Within South Australia, extensive research (e.g. David and Howchin 1897, Ludbrook 1961, 1967, Freytag 1964, DeMaison 1969, Townsend 1973, Heath 1974, Finlayson 1981, Alley and Bourman 1984, Bourman and Alley 1988, 1990, 1995, Hibburt 1995) into the sedimentary rocks of the late Palaeozoic basins established that these sedimentary rocks were deposited in glacial and post-glacial conditions during the Permo-Carboniferous glaciation. Studies such as Howchin (1912), Crowell and Frakes (1971a, 1971b; Figure 1:4), Crowell (1978), McGowran (1973), Townsend (1973), and Veevers (2006) have correlated the glacigene sedimentary rocks of South Australia with other known late Palaeozoic glacigene sedimentary rocks across Australia. The distribution of the sedimentary rocks and understanding of depositional processes during the late Palaeozoic offers the chance to study the interactions between global cycles of tectonics, eustacy and climate. Previously developed models by Crowell and Frakes (1971a, 1971b), Embleton and Schmidt (1977), Embleton and Valencio (1977), Crowell (1978), Veevers (2006), and Isbell et al. (2012) were largely based on observations and the distribution of late Palaeozoic glacigene sedimentary rocks in New South Wales, Victoria and Western Australia. The late Palaeozoic sedimentary rocks in South Australia are an important component to improve the understanding these interactions as they are situated between the previously investigated regions.

The sedimentary rocks of the Troubridge and Arckaringa basins of South Australia investigated in this study are an excellent example of how the sedimentology, inferred depositional settings and provenance from geochronology of isolated areas can provide an indication of the overall climate and depositional conditions occurring across the broader region, and in some cases, continental-scale climate and depositional mechanisms can be deduced (for example Veevers 2006, Isbell et al. 2012).

An improved understanding of the historical evidence from these sedimentary rocks can also provide a better understanding of the coal measures, shale gas, oil, and aquifers within the basin succession as well as the sedimentary rocks that cover mineral provinces.

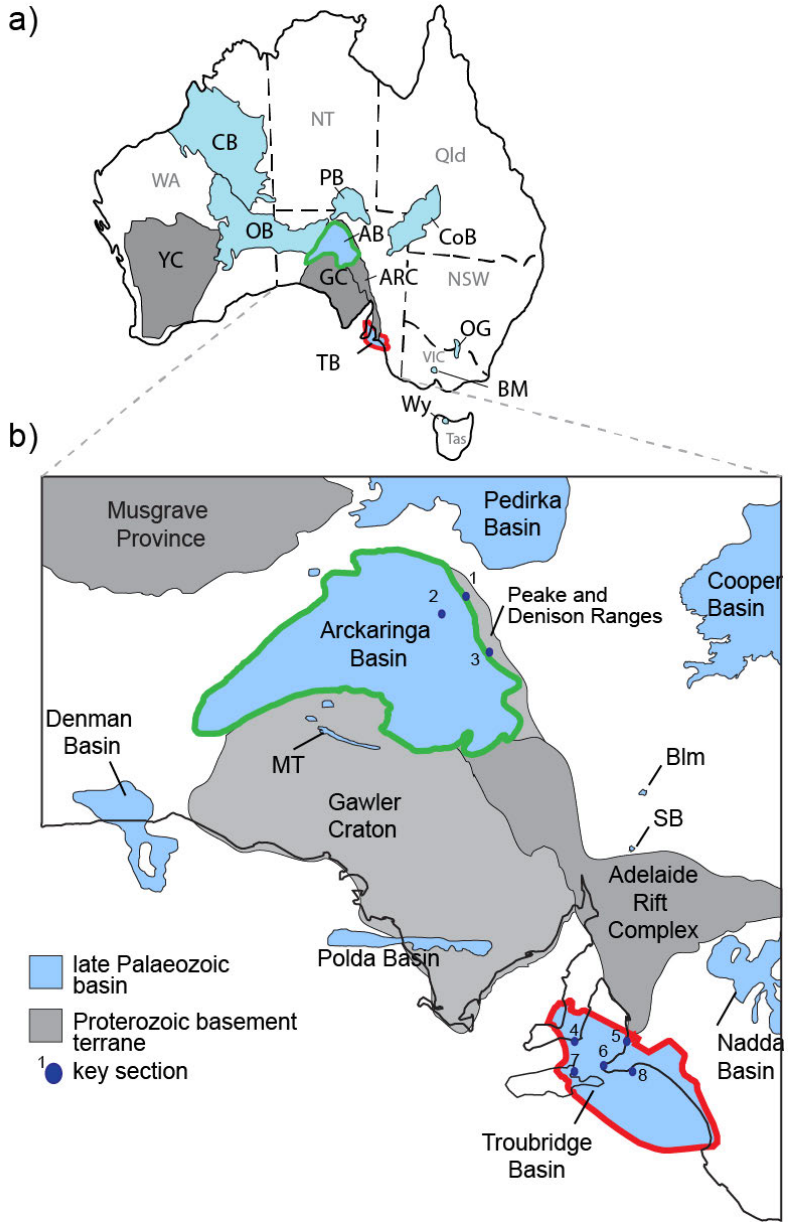

Figure 6:1 a) Location diagram of key late Palaeozoic basins and basement terranes of Australia, adapted from Pell et al. (1997); b) Late Palaeozoic basins and key basement terranes of South Australia, adapted from Alley et al. (1995). AB: Arckaringa Basin (green outline); ARC: Adelaide Rift Complex; BM: Bacchus Marsh; Blm: Blinman area; CB: Canning Basin; CoB: Cooper Basin; GC: Gawler Craton; MT: Mulgathing Trough; OB: Officer Basin; OG: Ovens Graben; PB: Pedirka Basin; SB: Springfield Basin; TB: Troubridge Basin (red outline); Wy: Wynyard; YC: Yilgarn Craton. Measured sections: 1: Mount Dutton; 2: Mount Toondina; 3: Box Creek; 4: Waterloo Bay; 5: Hallett Cove; 6: Cape Jervis; 7: Kingscote Composite; 8: Kings Point.

This chapter addresses the issue of delineating the nature and provenance of glacial deposits in the Troubridge and Arckaringa basins with inference on other late Palaeozoic basins in South Australia including the Cooper, Pedirka, Nadda and Denman basins (Figure 6:1b). These are regions of sparse exposure for which the basic understanding of the evolution of glacial and post-glacial sedimentary rocks is unknown. Here a holistic model, through palaeogeographic reconstructions, is presented that

accounts for changes in depositional mechanisms and gives an improved understanding of the sediment dispersal, their potential source regions, and the direction of ice flow. The palaeogeographic reconstructions encompass was constructed based on the sedimentological (Chapters 2 and 3), provenance (Chapter 4) and geochemical (Chapter 5) differences between the basins as well as between lithological units within the basin, together with the inferences made about the glacial setting from these differences.

6.1.1 Background geology

Remnants of the late Palaeozoic glaciation are preserved across Australia (Figure 6:1a). Glacigene sedimentary rocks deposited at this time are often floored by polished and striated pavements, and have been identified in the Bacchus Marsh area in central southern Victoria, the Ovens Graben in northeastern Victoria (Craig and Brown 1984, Roberts 1984, O'Brien 1986, Holdgate 1995, O'Brien et al. 2003), Wynyard in Tasmania (Banks 1962, Fielding et al. 2010) and the Canning Basin in Western Australia (Figure 6:1a; Crowell and Frakes 1971b, Towner 1981). Within South Australia, late Palaeozoic sedimentary rocks have been recognised in a number of basins Figure 6:1b), and are best preserved within the Troubridge and Arckaringa Basins (Figure 6:1b). The majority of the late Palaeozoic glacigene sedimentary rocks of South Australia are restricted to the subsurface with only small, discrete surface exposures typically on the margins of the basin (Alley et al. 1995).

Within South Australia, late Palaeozoic glacigene sedimentary rocks are best preserved within the Troubridge and Arckaringa Basins. Within the Troubridge Basin, the sedimentary rocks occur within five units of the well exposed Cape Jervis Formation. The Cape Jervis Formation has five informal units (Chapter 2). Units one to four were deposited during the glaciation and therefore their deposition was directly influenced by the glacier (Alley and Bourman 1984, Alley et al. 1995). These units comprise of diamictite, clay and sandstone. These lithologies are typically bedded within each unit although units two and four are dominated by diamictite beds where units one and three are dominated by beds of clay and sandstone (Ludbrook 1967, Alley and Bourman 1984, Alley and Bourman 1995). Unit five was deposited in a transgressing marine environment and as such is dominated by bedded clay with occasional sandstone beds. These sandstone beds are due to localised influence of glaciers (Alley and Bourman 1984, Alley et al. 1995).

Glacigene sedimentary rocks within the Arckaringa Basin are mostly restricted to the subsurface with limited exposures along the basin margins. The stratigraphic units of the Arckaringa Basin are representative of the major depositional events that occurred during the late Palaeozoic. The Boorthanna Formation was deposited during the Permo-Carboniferous glaciation (Townsend 1973, Hibburt 1995). The unit consists of beds of diamictite and sandstone with minor beds of carbonate and clay dominate the lower Boorthanna Formation. The upper Boorthanna Formation is dominated by sandstone and siltstone with minor diamictite lenses (Heath 1963, Townsend 1973, Hibburt 1995). The Stuart Range Formation was deposited during the marine incursion which followed the decay of the icesheet (Townsend and Ludbrook 1975, Hibburt 1995). The lower Stuart Range Formation is dominated by shale with minor siltstone and sandstone (Townsend and Ludbrook 1975, Hibburt 1995). The Mount Toondina Formation was deposited in an alternating lacustrine and fluvial environment (Freytag 1964, 1965, Townsend and Ludbrook 1975, Hibburt 1995). The unit consists of siltstone and sandstone interbedded with coal, shale and rare carbonate (Townsend 1973, Hibburt 1995).

6.2 Approach

Existing models and reconstructions provide an excellent basis to develop a comprehensive reconstruction of the depositional mechanisms of the late Palaeozoic sedimentary rocks in South Australia with emphasis on the Troubridge and Arckaringa basins. With the exception of Howchin (1912), the previous models (such as Crowell and Frakes 1971a, 1971b, Embleton and Valencio 1977, Caputo and Crowell 1982, Veevers 2006) were constructed using the distribution of till facies and glaciated pavements to relate the maximum extent of the glaciation. The types of glaciation proposed are based on observations from the last glacial maximum and current glacial conditions in the Northern Hemisphere. The presence of a continental-size glacier was deduced from the preservation of glaciated pavements in South Australia, Victoria, and Western Australia (e.g. Crowell and Frakes 1971a, 1971b, Caputo and Crowell 1982, Veevers 2006). The presence of alpine and valley glaciers was based on the palaeolatitude of the highlands during the late Palaeozoic (e.g. Embleton and Schmidt 1977, Embleton and Valencio 1977, Isbell et al. 2012) due to alpine glaciation typically only forming at high latitudes.

The new reconstructions for the South Australian late Palaeozoic glaciation presented here are based on observations within previous studies in combination with new data (Table 6:1). The period of glaciation has been divided into three stages; glacial transgression, maximum glaciation and glacial regression. Set criteria are used to define the overall glacial environment and the environment of deposition of sedimentary rocks. The criteria have been collated from glaciology and facies analysis, where as a single criteria has been linked to a glacial environment or environment of deposition, here multiple criteria have been linked together to create a series of multifaceted criteria that include modern landscape remnants of the glacial environment, sedimentology and provenance studies to reconstruct the paleogeography during and after the late Palaeozoic glaciation in South Australia. Criteria used in this study are given in Table 6:1, and includes collation of previously published criteria on glacial depositional environments and a summary of relevant observations from the glacial sediments of the Troubridge and Arckaringa basins made in this and previous studies.

Table 6:1 Summary of criteria for the deposition of diamictitie, observations made in this study and observations made by previous researchers. References for depositional criteria: [a]Eyles et al. (1983), [b]Eyles and Miall (1984), [c]Ashley et al. (1985), [d]Clark (1987), [e]Matsuoka (1990), [f]Bell (1998), [g]Miall (2000), [h]Benn et al. (2003), [i]Glasser and Bennet (2004), [j]Bennett and Glasser (2009), [k]Hambrey and Glasser (2012). Observations from other studies are from: [1]Crawford (1960), [2]Heath (1963, 1965), [3]Ludbrook (1967), [4]Allchurch and Wopfner (1967), [5]Townsend (1973), [6]Foster (1974), [7]Townsend and Ludbrook (1975), [8]Bourman et al. (1976), [9]Alley and Bourman (1984), [10, 11, 12, 13]Bourman and Alley (1984, 1998, 1990, 1995), [14]Hibburt (1995), [15]Alley and Bourman (1995), [16]Alley (1995), [17]Bourman and Alley (1999), [18]Veevers (2006), [19]Menpes et al. (2010), [20]Menpes (2013), [21]Alley et al. (2013), [22]Forbes et al. (2015).

Environment of deposition of diamictite	Criteria	Observations from this study		Observations from other studies	
		Troubridge Basin (Cape Jervis Formation)	Arckaringa Basin (Boorthanna Formation)	Troubridge Basin (Cape Jervis Formation)	Arckaringa Basin (Boorthanna Formation)
Icesheet-derived diamictite, deposited during icesheet advance	presence of glaciated pavement [a,c,e,h,i,j,k]			Hallett Cove[9,11,12,15], Inman Valley[9,11,13], Kingscote[9,11,18,22], Cape Jervis[4,9,10,15]	
	large, glacially polished erratics [a,b]	Cape Jervis, Hallett Cove	Box Creek	Cape Jervis[4,10,15]	presence of erratic at Box Creek[17]
	angular clasts, sand matrix diamictite [a,f,g,j,k]			diamicitie described at Cape Jervis[4,10] and Hallett Cove[12,15]	presence of diamictie in S Boorthanna Trough[8,14], drillholes[4,5,6,8,14], reported in Phillpson and and Mulgathing troughs[16,23] and Polda Basin[16]
Icesheet-derived diamictite, deposited during icesheet retreat	variable matrix from clay to coarse-grained sand [d,k]	Kings Point	Not observed	diamicitie described at Cape Jervis[4,10,15], Kings Point[13] and Waterloo Bay[1,7]	Not observed
	clasts up to 40 cm, dominated by subrounded to rounded, variably sourced [a,k]	Cape Jervis, Kings Point, Waterloo Bay			
	unconsolidated or clast-supported[k]	Cape Jervis, Kings Point			
	interbedded with sandstone and pebble beds [j]	Cape Jervis, Kings Point, Waterloo Bays			

Table 6:1 Continued from previous page.

Environment of deposition of diamictite	Criteria	Observations from this study		Observations from other studies	
		Troubridge Basin (Cape Jervis Formation)	**Arckaringa Basin (Boorthanna Formation)**	**Troubridge Basin (Cape Jervis Formation)**	**Arckaringa Basin (Boorthanna Formation)**
Valley glacier or ice tongue-derived diamictite	presence of U-shaped valleys[h]	Inman Valley (Kings Point), Hallett Cove		Hallett Cove[9,11], Inman Valley[9,11,13]	southern and southeastern troughs deepened U-shaped valleys[20,21]
	rounded to angular (higher portion of rounded), distally- and locally-derived clasts [a,c,g,j,k]	Kingscote, Kings Point, Cape Jervis, Hallett Cove	Mount Dutton	diamicitie described at Cape Jervis[4,10,15], Kings Point[13], Kingscote[18,22], Hallett Cove[12,15]	Diamictite described at Mount Dutton[2,3,6,8,14], described in Wallira and Tallaringa troughs from drillholes[5,6,8], Cooper Basin[16,19], Denman Basin[16], Nadda Basin[4,16] and at Blinman[16]
	mature, well sorted and subrounded to rounded matrix [h]				
	mud to sandstone matrix [h,j,k]				
	presence of the bedded silty clay unit above the diamictite [g,j]	Hallett Cove, Kings Point			

Criteria defining the glacial environment are the presence of landscape features such as:

- Polished pavements with striations, concentric grooves, chatter marks and winding channels,
- Roche Moutonńee, cirques and kettle holes, and
- U-shaped valleys, typically floored by polished pavement.

Differences in sedimentological properties between diamictite units deposited by an icesheet (referred to as icesheet-derived) versus by fluvial systems typical of ice tongues and valley glaciers (referred to as valley glacier-derived) is used to remodel the extent of the continental icesheet along with the probable extent of the ice tongue at the margin of the icesheet and the likely locations of valley glaciers. The presence of diamictite units is used to predict the extent of the depositing glacier as these sedimentary rocks are deposited at the front of the ice.

Criteria to describe icesheet-derived diamictites deposited during the advance of the icesheet are:

- Presence of glaciated basement,
- Large (up to several tens of metres), glacially polished erratics, and
- Diamictite with large angular clasts within a sand matrix.

Criteria to describe icesheet-derived diamictites deposited during the retreat of the icesheet are:

- Variable matrix from clay to coarse-grained sand,
- Clasts up to 40 cm, dominated by subrounded to rounded, variably sourced,
- Unconsolidated or clast-supported, and
- Interbedded with sandstone and pebble beds.

Diamictite deposited in an environment with both icesheet and ice tongue glaciers have the same criteria, however the clasts are rounded to angular. Valley glacier-derived diamictites are identified by:

- Presence of U-shaped valleys
- Rounded to angular (higher portion of rounded), distally- and locally-derived clasts,
- Mature, well sorted and subrounded to rounded matrix,
- Mud to sandstone matrix, and
- Presence of the bedded silty clay unit above the diamictite.

The glacial regression is defined by the presence of alternating fluviolacustrine clay and sand beds that vary in thickness. Minor diamictite beds may be present. Differences in the dominant sediment (i.e. clay dominated or sand dominated) within the unit are attributed to the dominant glacial setting (e.g. fluvioglacial or glaciolacustrine).

The extent of the marine transgression is defined by sedimentary rocks that are dominated by green, massive to bedded clay with prismatic fracturing and occasional sandstone beds. These sedimentary rocks are largely confined to the subsurface and therefore the extent of the maximum marine transgression is largely defined by the extent of marine sedimentary rocks in drill holes. Freshwater conditions are characterised by alternating fluvial and lacustrine, freshwater shale, siltstone and sandstone beds with intermittent occurrences of coal and carbonaceous sedimentary rocks. Both marine and freshwater depositional conditions are verified by the presence of foraminifera as described by Ludbrook (1961, 1967), Harris and McGowran (1971), Foster (1974), Alley (1995) and Hibburt (1995).

6.2.1 New data

New datasets used to constrain the palaeogeography of late Palaeozoic South Australia include a regional assessment of sedimentology of the glacigene sedimentary rocks across the Troubridge and Arckaringa Basins, geochronology and geochemistry. These new data are presented in detail in Chapters 2 to 5.

Sedimentology of the glacigene Cape Jervis Formation of the Troubridge Basin (Chapter 2) and the Boorthanna Formation of the Arckaringa Basin (Chapter 3) provide a record of the stages of glacial deposition from a wet-based glacier to fluvioglacial to glaciomarine. Detailed observations of locally-sourced, angular to rounded clasts within diamictite units lower in the stratigraphy suggest that smaller, more mobile ice tongue glaciers were likely dominant. Interbedded clay and sandstone beds in the middle of the glacial sequence are indicative of a stagnant icesheet. Large, poorly sorted clasts within diamictite units higher in the sequence suggests that the ice mass was rapidly melting. These diamictites are often interbedded with sandstone beds and lenses indicative of small glacial lakes and meltwater streams. The increase in occurrence of diamictite and sandstone beds towards the top of the unit is indicative of the increased melting of the ice mass. Massive to bedded clays at the top of the sequence are indicative of a marine incursion. Minor sandstone beds suggest periodic fluvioglacial input. The uppermost unit of the late Palaeozoic Arckaringa Basin, the Mount Toondina Formation

(Chapter 3) consists of carbonaceous sandstone and siltstone units. The interbedded nature of this unit as well as the sedimentology implies that the sedimentary rocks were deposited in an alternating lacustrine and fluvial setting.

Sedimentological observations suggest the Boorthanna and Cape Jervis formations are temporal equivalents. The sedimentary rocks of both formations comprise of diamictites that were deposited via the action of icesheets, ice tongues and valley glaciers. The depositional mechanisms of the two basins then became variable. Sedimentary rocks of the Arckaringa Basin were being deposited in a deepening marine setting whilst fluvioglacial and glaciomarine sedimentary rocks were being deposited in the Troubridge Basin. The environment of the Arckaringa Basin then became terrestrial and alternating lacustrine and fluvial sedimentary rocks were deposited. At this time the Troubridge Basin moved to a deepening glaciomarine environment. These sedimentological observations are substantiated by foraminiferal age evidence. Ludbrook (1691, 1967), Jones (1987) and Hibburt (1995) reported the Boorthanna Formation to be Asselian to Sakmarian (298 – 290 Ma) from palynogical studies. The Cape Jervis Formation is also reported to be Asselian to Sakmarian by Ludbrook (1967, 1969b), Harris and McGowran (1971), Foster (1974), Bourman and Alley (1990) and Alley and Bourman (1995).

Geochronology of the late Palaeozoic sedimentary rocks of the Troubridge and Arckaringa basins constrain the provenance of the glacigene sedimentary rocks at different geographic locations and stratigraphic levels (Chapter 4). Multiple zircon grain populations were identified to be significantly older than the ca 285-300 Ma depositional age previously determined from palynology (Ludbrook 1967, Alley et al. 1995). Zircon grain populations from the Troubridge Basin are dominated by ca 500 to 650 Ma, while sedimentary rocks of the Arckaringa Basin are dominated by significant zircon populations of ca 990 to 1200 Ma and ca 1700 to 1900 Ma. Provenance of the zircon grains suggests that the sedimentary rocks from the Troubridge Basin were sourced almost exclusively from the Kanmantoo Group and the Transantarctic Mountains of Antarctica. Conversely, the Arckaringa Basin sedimentary rocks were primarily sourced from the Gawler Craton and Adelaide Rift Complex.

The major element whole rock geochemistry of the glacigene sedimentary rocks is largely controlled by depositional and post-depositional weathering processes (Chapter 5). Ratios of Al_2O_3 and SiO_2 are indicative of depositional process including the degree of water activity that has the potential to wash away finer sediment fractions. The intense weathering of the sedimentary rocks includes sulphate, carbonate, ferruginous and clay weathering, and is identified from ratios of Al_2O_3, Fe_2O_3, K_2O, CaO and MgO. Sedimentary rocks that have geochemical signatures that are not controlled by depositional or weathering processes are typically moderately oxidised or minimally weathered. These sedimentary rocks preserve geochemical signatures similar to the sediment source rocks. The likely source rocks include the Kanmantoo Group metasedimentary rocks which have a similar geochemistry to the minimally weathered glacigene sedimentary rocks.

6.3 Palaeogeographic reconstructions

6.3.1 Maximum glaciation

The reconstruction models presented here (Figures 6:2 to 6:4) show the varying environments through the Permo-Carboniferous glaciation. The Cape Jervis Formation and Boorthanna Formation were deposited during this time. The geographical reconstructions are a combination of the northwards

moving, continental-scale icesheet of Alley et al. (1995) and the eastern alpine glacial system and a western continental icesheet suggested by Veevers (2006) and Isbell et al. (2012).

Glacial advance

Icesheet-derived diamictites (or lodgement till) are typically deposited at or underneath the front of an advancing ice mass (Bennett and Glasser 2009). Lodgement tills have been recorded extensively in late Palaeozoic basins across southern South Australia, including in the Troubridge and Polda Basin and the southern Arckaringa Basin (Figure 6:2; Alley et al. 1995). These lodgement tills have been recognised based on the criteria outlined in section 6.2.1.

Calculations from striae and till fabric orientation studies (Alley and Bourman 1984, Bourman and Alley 1988, 1990, 1995, 1999, Alley et al. 2013) indicate the continental icesheet moved in a north to northeasterly direction from Antarctica into South Australia. This ice movement direction is supported by provenance studies of the Cape Jervis and Boorthanna Formation. The Cape Jervis Formation is primarily sourced from the Kanmantoo Group as well as Transantarctic Mountains of Antarctica (Chapter 4). The presence of zircon grains sourced from Antarctica suggests that a portion of sedimentary rocks eroded by the advancing ice mass remained trapped in the ice and were consequently transported by the ice mass. The provenance spectra of the Boorthanna Formation also suggest that a portion of the sedimentary rocks may have been sourced from either the Kanmantoo Group or Antarctica (Chapter 4). It is probable that these sedimentary rocks were also transported by the icesheet and then into the Arckaringa Basin via ice tongue glaciers or meltwater streams.

The lodgement till of the Troubridge Basin (unit two of the Cape Jervis Formation) has both rounded and angular clasts that are predominantly locally-derived. The occurrence of both rounded and angular clasts suggests that the lodgement till was deposited in an environment that included both an icesheet (angular clasts) and tongue glaciers (rounded clasts). The ice tongues preceded the icesheet as it moved across the basin. The ice tongue movement deepened existing valleys, resulting in scouring and exposing of bedrock that was subsequently polished by the following icesheet to form glaciated pavements. Landscape features such as the cirque at Christmas Cove, Kangaroo Island (Bourman and Alley 1999) as well as the occurrences of glaciated pavements in proximity to the U-shaped valleys in the Fleurieu Peninsula (David and Howchin 1897, Bourman and Alley 1988, 1990, 1999) suggest smaller, more mobile ice masses preceded the main icesheet. The ice tongue glaciers tend to produce lodgement till with higher incidence of rounded clasts as these glaciers generally transport sedimentary rocks further (Ashley et al. 1985). The presence of locally-derived, angular clasts Kanmantoo Group are an example of icesheet-derived material. Conversely, large, continental-scale icesheets are not as mobile and tend to produce lodgement till that is typically locally-derived therefore clasts are subject to less transport and rounding.

The lodgement till of the Troubridge Basin (unit two of the Cape Jervis Formation) has both rounded and angular clasts that are predominantly locally-derived. The occurrence of both rounded and angular clasts suggests that the lodgement till was deposited in an environment that included both an icesheet (angular clasts) and tongue glaciers (rounded clasts). The ice tongues preceded the icesheet as it moved across the basin. The ice tongue movement deepened existing valleys, resulting in scouring and exposing of bedrock that was subsequently polished by the following icesheet to form glaciated pavements. Landscape features such as the cirque at Christmas Cove, Kangaroo Island (Bourman and Alley 1999) as well as the occurrences of glaciated pavements in proximity to the U-shaped valleys in the Fleurieu Peninsula (David and Howchin 1897, Bourman and Alley 1988, 1990, 1999) suggest

smaller, more mobile ice masses preceded the main icesheet. The ice tongue glaciers tend to produce lodgement till with higher incidence of rounded clasts as these glaciers generally transport sedimentary rocks further (Ashley et al. 1985). The presence of locally-derived, angular clasts Kanmantoo Group are an example of icesheet-derived material. Conversely, large, continental-scale icesheets are not as mobile and tend to produce lodgement till that is typically locally-derived therefore clasts are subject to less transport and rounding.

The lodgement till of the Troubridge Basin (unit two of the Cape Jervis Formation) has both rounded and angular clasts that are predominantly locally-derived. The occurrence of both rounded and angular clasts suggests that the lodgement till was deposited in an environment that included both an icesheet (angular clasts) and tongue glaciers (rounded clasts). The ice tongues preceded the icesheet as it moved across the basin. The ice tongue movement deepened existing valleys, resulting in scouring and exposing of bedrock that was subsequently polished by the following icesheet to form glaciated pavements. Landscape features such as the cirque at Christmas Cove, Kangaroo Island (Bourman and Alley 1999) as well as the occurrences of glaciated pavements in proximity to the U-shaped valleys in the Fleurieu Peninsula (David and Howchin 1897, Bourman and Alley 1988, 1990, 1999) suggest smaller, more mobile ice masses preceded the main icesheet. The ice tongue glaciers tend to produce lodgement till with higher incidence of rounded clasts as these glaciers generally transport sedimentary rocks further (Ashley et al. 1985). The presence of locally-derived, angular clasts Kanmantoo Group are an example of icesheet-derived material. Conversely, large, continental-scale icesheets are not as mobile and tend to produce lodgement till that is typically locally-derived therefore clasts are subject to less transport and rounding.

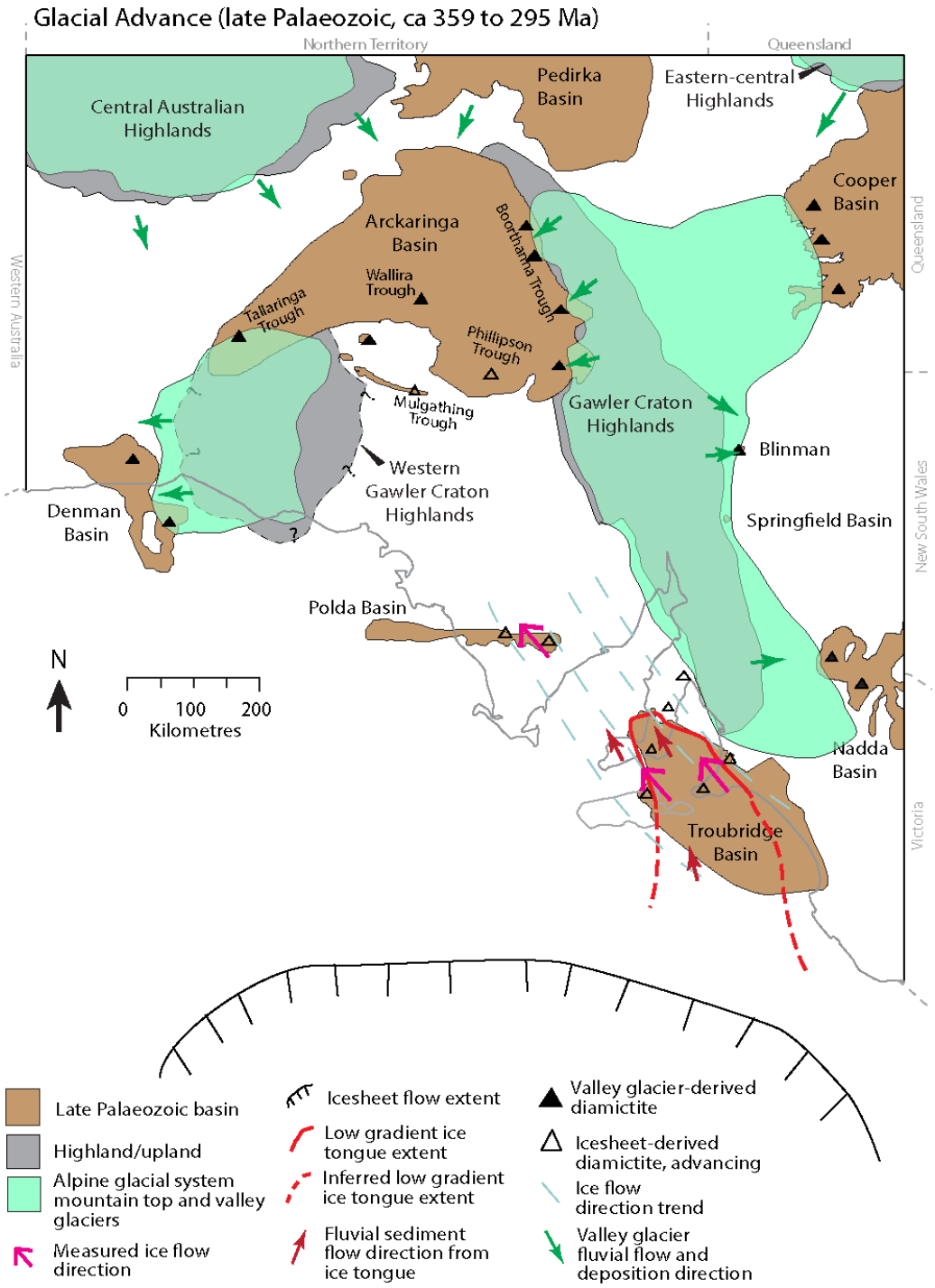

Figure 6:2 Palaeogeographic reconstruction of the glacial advance that occurred between the Late Carboniferous and earliest Permian (Asselian). Model is based on field observations (this study), Alley et al. (1995) and Veevers (2006).

Glacial maximum

A continental icesheet extended over most of the Troubridge Basin and continued north to the southern Arckaringa Basin (Figure 6:3). The northern extent of the ice tongue at the southern margin of the Arckaringa Basin coincides with the northern most occurrence of lodgement till (Figure 6:3). The limited occurrence lodgement till in the Arckaringa Basin is likely an indicator of the maximum northerly extent of the icesheet and associated ice tongue glaciers. The fluvial and reworked nature of the lower Boorthanna Formation diamictites in the Wallira, Phillipson and Tallaringa troughs (Townsend 1973, Townsend and Ludbrook 1975, Hibburt 1995) as well as the recognition of the

Phillipson Trough (Figure 6:3) as a glacially scoured depocentre (Menpes et al. 2010) suggests the presence of ice tongues at the northern extent of the continental icesheet (Figure 6:3).

Discrete occurrences of diamictite have been observed within the Arckaringa Basin (Chapter 3, Figure 3:3) in close proximity to the highlands such in the Boorthanna Trough adjacent to the Peake and Denison Ranges (Freytag et al. 1967, Townsend and Ludbrook 1975, Rogers et al. 1996a). These discrete occurrences have also been observed within the Cooper, Denman and Nadda basins (Figure 6:1; Alley et al. 1995). Previous models have assumed these were flow till successions deposited by the decaying continental icesheet (Crowell and Frakes 1971a, Alley et al. 1995). The discrete diamictite occurrences such as those at Mount Dutton (Figure 6:1) include rounded clasts and are typified by an alternating mud and sand matrix that is often interbedded with sand lenses and beds up to ten metres thick and overlying sandstone-matrix diamictite (Chapter 3). The clasts in the diamictite have previously been suggested to have been rounded by reworking and transport in meltwater streams that may be subglacial (e.g. ice tongues), or surficial (e.g. at the end of valley glaciers; Bennett and Glasser 2009). The rounded, well sorted clasts of the diamictite are indicative of a depositional setting that included the transport and rounding of the sedimentary rocks in a high energy environment such as a meltwater stream that was also transporting pebble and boulder-sized rocks such as the at the front of a valley glacier. The overlying bedded sandstone and siltstone is indicative of increasingly fluvially dominant environment (Figure 6:3b).

Provenance studies of the Boorthanna Formation within the Boorthanna Trough (Figure 6:1; Chapter 4) indicate sediment was primarily sourced from the Adelaide Rift Complex and Gawler Craton rocks of the Peake and Denison Ranges that are adjacent to the eastern margin of the basin. This is supported by the interpretation that the continental icesheet and associated ice tongues did not extend into the northern Arckaringa Basin, and therefore only reached the southernmost Boorthanna Trough. This suggests that the diamictite units were deposited by meltwater streams of variable sources, and are interpreted to be related to the presence of valley (or piedmont) glaciers that originated in the Gawler Craton Highlands (Figure 6:3), rather than the larger continental icesheet and ice tongue glaciers or associated meltwater flow deposits (Heath 1963, Bennett and Glasser 2009).

Following the initial advance of the icesheet into South Australia, the ice mass stagnated in the Troubridge Basin. Along the palaeo-coastline of the Troubridge Basin, this is similar to the modern coastline, glacial lakes formed due to the ice mass being stagnant trapping the meltwater. Lakes fed by meltwater formed between the ice mass and the shore as speculated by (Bourman and Alley 1990, Alley et al. 2013). The increased meltwater in the system would have carried an increased amount of sand-sized sediment into the glacial lakes, resulting in an increase in deposition of sand beds as reflected in unit three (fluviolacustrine beds) of the Cape Jervis Formation (Chapter 2). The lower fluviolacustrine beds are clay dominated, and were deposited as fine sedimentary rocks settling out of suspension from glacial lake water. The presence of sandstone beds within the unit suggests input of sand-sized sediment from meltwater streams directly from under the glacier and into the glacial lake. The increase in occurrence of diamictite and sandstone beds towards the top of the fluviolacustrine beds is indicative of the melting ice mass directly dumping debris into the lake. The presence of dropstones suggests icebergs were present on the lake surface. The variable thickness and widespread nature of the fluviolacustrine beds across the Troubridge Basin is attributed to the differing depths of the glacial lake as well as sediment availability. The period of stagnation and direction of the glacial retreat remain unresolved.

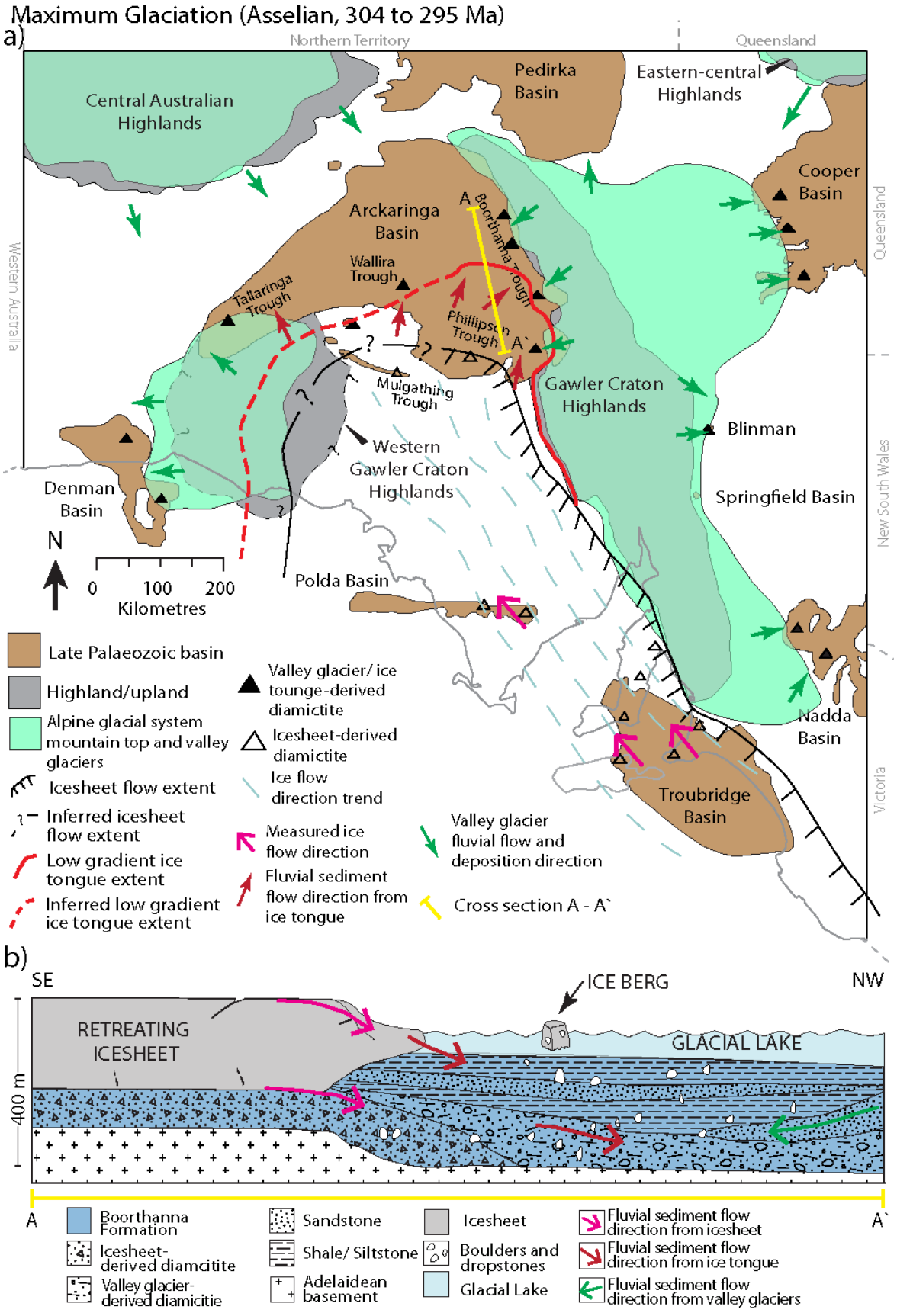

Figure 6:3 a) Palaeogeographic reconstruction of the maximum glaciation that occurred between the Late Carboniferous and earliest Permian (Asselian). Model is based on field observations (this study), Alley et al. (1995) and Veevers (2006); b) Stylised cross section of depositional mechanisms and sedimentary succession during the glacial maximum.

The distinctively different characteristics between icesheet and fluvially deposited diamictites of the Boorthanna Formation allows the tentative extent of the icesheet to be mapped out along the southern margin of the Arckaringa Basin (Figure 6:3), reaching the Mulgathing Trough, where icesheet-derived diamictites have been observed (Forbes et al. 2015), but not reaching the Arckaringa Basin. This is supported by the ice movement direction being in a northwesterly direction (Figure 6:3; Alley and Bourman 1984, Bourman and Alley 1990, 1999). Due to the absence of late Palaeozoic sedimentary rocks overlying, and glacial landforms within the Gawler Craton such as glaciated pavements it is unlikely that the icesheet covered most of South Australia as has been previously inferred by Crowell and Frakes (1971b) and Alley et al. (1995). The reconstruction presented here shows that the eastern edge of the icesheet continues towards Antarctica and follows the northeastern margin of the Troubridge Basin. The inferred western margin of the icesheet is to the east of the Denman Basin where it is likely to continue south towards Antarctica (Figure 6:3).

The Permo-Carboniferous reconstruction of Australia proposed by Veevers (2006) did not include a synthesis of the centre of the continent, therefore, it is difficult to compare it to the model proposed here. Veevers (2006) did however conclude that during the latest Carboniferous much of Western Australia was covered with icecaps and glaciers which had spread eastward towards the Arckaringa Basin. Further spreading north was prohibited by the Central Australian Highlands. It is feasible for the late Palaeozoic glacial system to have extended south of the Central Australian Highlands into South Australia. However, there is little evidence of this as any potential glacigene sedimentary rocks south of the Central Australian highlands are deeply covered by sedimentary rocks of the Great Victoria Desert (Drexel and Preiss 1995). Therefore, the extent of the icesheet has been placed east of the Denman Basin (Figure 6:3). The extent of the ice tongue glaciers associated with the icesheet is also difficult to ascertain due to poor exposure of the diamictite units and diagnostic landscape features such as polished and striated glacial pavements or glacially-carved U-shaped valleys.

Many authors (including Heath 1963, Crowell and Frakes 1971b, Alley et al. 1995, Veevers 2006, Isbell et al. 2012) have suggested the formation of alpine glaciers in the highlands of eastern Australia during the Permo-Carboniferous glaciation. In general it is accepted that these glacial systems were independent of the icesheet that covered South Australia (Isbell et al. 2012, Veevers 2006). Veevers (2006) also suggested the presence of similar icecap and valley glaciers in the Central Australian and Central Gawler Highlands which fed sediment into the Pedirka and Arckaringa basins via ice and fluvial deposition. Given the probable presence of an alpine glacial system in other highlands near the Arckaringa Basin, it is likely that the Gawler Craton highlands had a similar system. This system would have included icecap glaciers on top of the highest peaks and a series of valley glaciers travelling westwards downslope towards the Arckaringa Basin. These valley glaciers would have fed reworked, glacial sedimentary rocks into the Boorthanna Trough via meltwater streams. It is also likely that valley glaciers would have moved in an easterly direction onto the region now occupied by the Flinders Ranges (Figure 6:3). Small exposures of late Palaeozoic diamictite have been observed at Blinman in the northern Flinders Ranges. These sedimentary rocks have similar characteristics to the reworked diamictites in the Boorthanna Trough (Alley et al. 1995). The depositional mechanisms for these are poorly constrained, although from lithological descriptions it is likely that the sediment is valley glacier-derived diamictite.

The reconstructions shown in Figure 6:2 and 6:3 differs from the widely-accepted model that all of the diamictite occurrences across South Australia were deposited by the continental icesheet. It is unlikely

that the icesheet reached as far north as previous models indicated for several reasons: the absence of glacially polished pavements in places other than the Troubridge Basin; the differentiation of icesheet-derived diamictite deposits from ice tongue and valley glacier-derived diamictite deposits; and the acknowledgement of the already uplifted highlands (Figures 6:2 and 6:3). Remnants of the Central Australian Highlands and Gawler Craton Highlands (Figure 6:3) are now expressed as the Musgrave Province and Adelaide Rift Complex /Peake and Denison Ranges respectively, although the later has also undergone significant post-Mesozoic uplift. There is no surface expression of the Eastern-Central Highlands or the western Gawler Craton Highlands, which are now overlain by extensive, thick cover sequences of the Eromanga Basin and Eucla Basin respectively (Drexel and Preiss 1995). Veevers (2006) suggested the presence of the Eastern-Central Highlands due to the presence lithology of glacigene sedimentary rocks in the Cooper Basin. Based on evidence of similar valley glacier-derived glacigene sedimentary rocks recorded in the Nadda Basin, the reconstruction presented here (Figure 6:3) includes the presence of the western Gawler Craton Highlands that would have had ice cap and valley glaciers that may have deposited valley glacier-derived diamictite units into the Nadda Basin. The valley glacier-derived diamictite deposits in the Tallaringa Trough of the Arckaringa Basin may have been deposited by valley glaciers originating in these highlands, however, it remains difficult to distinguish the diamictite types due to lack of exposure and therefore detailed sedimentological descriptions.

Glacial retreat

The increase of diamictite towards the top of the fluviolacustrine beds of the Cape Jervis Formation signals the beginning of melting and retreat of the ice mass. Alley and Bourman (1984) linked the flow till complex (unit four) of the Cape Jervis Formation to the decay and retreat of the continental ice mass. The large, poorly sorted clasts of the diamictite within the flow till complex suggests that the ice mass was rapidly melting, leading to an accumulation of debris on the surface, which flowed downslope. Sandstone and pebble beds and lenses interbedded with the diamictite are likely due to small lakes and meltwater streams forming between the fall of debris.

The flow till complex varies in thickness and lithology across the Troubridge Basin (Figure 6:4). This is due to the position of the ice in relation to the section. At Cape Jervis, the ice was likely very close to the shoreline and no glacial lakes remained, therefore the meltwater likely flowed towards the west into Gulf St Vincent transporting the finer sand and clay-sized sedimentary rocks away from Cape Jervis leaving the larger debris to be deposited at Cape Jervis. At other sections, particularly Kings Point, the shoreline (assuming a similar configuration to the modern shoreline) is of a more favourable orientation to accommodate formation of glacial lakes. Evidence of the formation of such lakes is seen as the clay beds that are dominant within unit four of the Cape Jervis Formation at Kings Point.

In the Arckaringa Basin, Townsend and Ludbrook (1975) suggested sand and clay lenses and beds in the lower Boorthanna Formation were the result of alternating deposition of sand and mud by meltwater. These are deposited when larger clasts are either not available or meltwater is limited and the stream does not have sufficient energy to transport clasts and sand grains allowing only suspended mud particles to be transported and deposited (Bennett and Glasser 2009, Singh and Haritashya 2011). The alternating strata occur with clasts (as a diamictite) or without. The latter are interbedded with diamictite units or overlie the diamictite, and are an indication of the transition into non-glacial deposition. It is not clear if the fluviolacustrine sedimentary rocks in the lower Boorthanna Formation were deposited while the glacier was stagnant or after it had begun melting.

Large sandstone deposits such as at Box Creek (Figure 6:1) are mostly associated with subglacial fan deposits forming at the end of a valley glacier (Wilmot 1987, Rogers et al. 1996b, Bennett and Glasser 2009, Chapter 3). The absence of lithics in the form of pebble- and cobble-sized clasts in the sandstone units, the sparse occurrence of erratics and smaller, striated and faceted clasts is indicative of deposition by meltwater from a valley glacier that had very few larger clasts trapped in the ice. This occurs when the glacier is in final stages of deglaciation and most clasts and erratics have already been extracted from the ice (Bennett and Glasser 2009). The sandstone units include subrounded, elongate and rhombic-shaped grains that indicate less reworked, immature sediment when compared to the sedimentary rocks of Mount Dutton. Given the limited extent of the icesheet and associated ice tongue glaciers, it is more probable that the sand and clay lenses and beds were deposited via meltwater streams (Figure 6:4). Flow till complex sedimentary rocks have not been observed in the Arckaringa Basin. This is likely due to the icesheet not reaching the middle of the basin (Figure 6:3) as the deposition of the flow till complex is directly related to the presence of decaying ice. It is possible valley and alpine glaciers were also in retreat contemporaneously with decay of the continental icesheet, however evidence of related flow till complex diamictite is lacking.

The clay beds of the glaciomarine sediments (unit five) of the Cape Jervis Formation have been broadly correlated with the upper Boorthanna Formation (Chapter 3). These sedimentary rocks were deposited during the stages of the marine transgression. The sedimentary rocks are sparsely preserved across the Troubridge Basin although it is generally accepted that the marine transgression stretched across most of South Australia as temporally equivalent marine sedimentary rocks have been observed in many of the late Palaeozoic basin across the state (Alley et al. 1995).

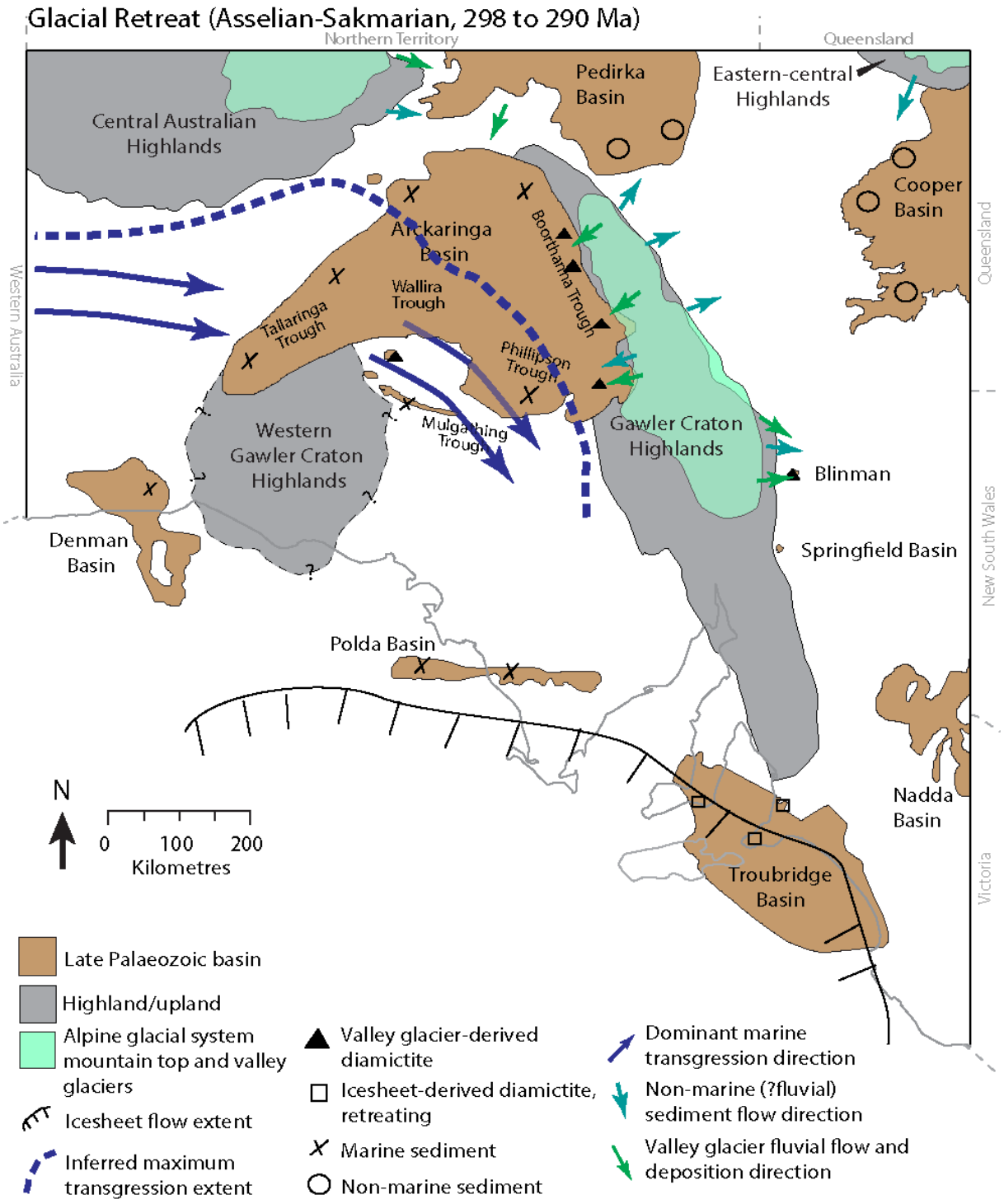

Figure 6:4 Palaeogeographic reconstruction of the glacial regression that occurred in the Asselian-Sakmarian. Model is based on field observations (this study), Alley et al. (1995) and Veevers (2006).

6.3.2 Maximum marine transgression

The palaeoenvironment during the maximum marine transgression is difficult to reconstruct due to limited exposure and drill logs preserving the Stuart Range Formation in the Arckaringa Basin and its equivalents. There are no sedimentary rocks associated with the maximum marine transgression preserved in the Troubridge Basin, however, the glaciomarine sedimentary rocks may be from the

beginning of the marine incursion (Alley and Bourman 1984). The debate surrounding the direction of the transgression adds difficulty to the reconstructions. The reconstruction given in Figure 6:5 indicates a westerly incursion as suggested by Veevers (2006) and Wopfner (1972). A westerly incursion is favoured as the western Gawler Craton Highlands (Figure 6:5) would have blocked a direct flow path into the centre of South Australia. A westerly transgression also supports the suggestion of Crowell and Frakes (1971a) for the existence of an epeiric sea that arched from the Canning Basin in Western Australia across the continent. A southwestern transgression direction was postulated by Heath (1974) and McGowran (1973). This may be possible, however, it is difficult to distinguish between a westerly or southwesterly marine transgression with currently available data.

Veevers (2006) suggested that the icesheet that covered most of southern Western Australia had melted by the Early Permian and that this meltwater is the likely source of the marine incursion into South Australia. It is possible that during the southward retreat of the icesheet further marine waters were able to advance from the southwest, which may account for the marine sedimentary rocks in the Polda and Denman basins. No flow direction indicators have been reported so it is not possible to prove or disprove this.

At maximum transgression, the shoreline reached the eastern edges of the Arckaringa Basin and Troubridge Basin, inundating these basins as well as the Polda Basin and Denman Basin (Figure 6:5). The shoreline extent between these basins is unknown, and has therefore been inferred based on the occurrence of late Palaeozoic marine sedimentary rocks (Figure 6:5; Alley et al. 1995). The presence of the Stuart Range Formation (approximately 300 m) in the Tallaringa Trough (Figure 6:5) suggests a period of marine sedimentation in the southwestern portion of the basin. Slightly thinner occurrences (150-200 m) in the Boorthanna Trough (Figure 6:3) may be indicative of a lesser time of marine sedimentation due to a shallower sea or differing rates of deposition. Scheffler et al. (2003) indicated that the climate during the early Sakmarian was subject to rapid change such as a rapid shift in temperature, which may be evidenced by the alternating sandstone and shale succession of the Stuart Range Formation that is reported in drill logs (Townsend and Ludbrook 1975). It is also possible that fault movement further deepened the existing depocentres such as the Boorthanna Trough. The absence of late Palaeozoic marine sedimentary rocks in the Nadda, Springfield, Cooper and Pedirka basins (Figure 6:5) suggests that the marine incursion did not cross the Gawler Craton Highlands or extend beyond the northern margins of the Arckaringa Basin (Figure 6:5).

It is difficult to hypothesise the direction of the regression due to lack of directional sedimentary structures in exposures. Based on seismic studies, Wilmot (1987) suggested that the regression was bi-directional to the southeast and southwest in the southern parts of the Boorthanna Trough. The Gawler Craton Highlands that extend from the east of the Arckaringa Basin and continue south to the southern coastline are likely to have prevented the regression in any other direction other than south to southwest (Figure 6:5), therefore it is likely that the regression was multidirectional and the shoreline stretched across much of the modern coastline (Figure 6:5). The absence of Mount Toondina Formation equivalent sedimentary rocks in the Polda Basin and Troubridge Basin (Alley et al. 1995) suggests the final stages of regression occurred with little deposition.

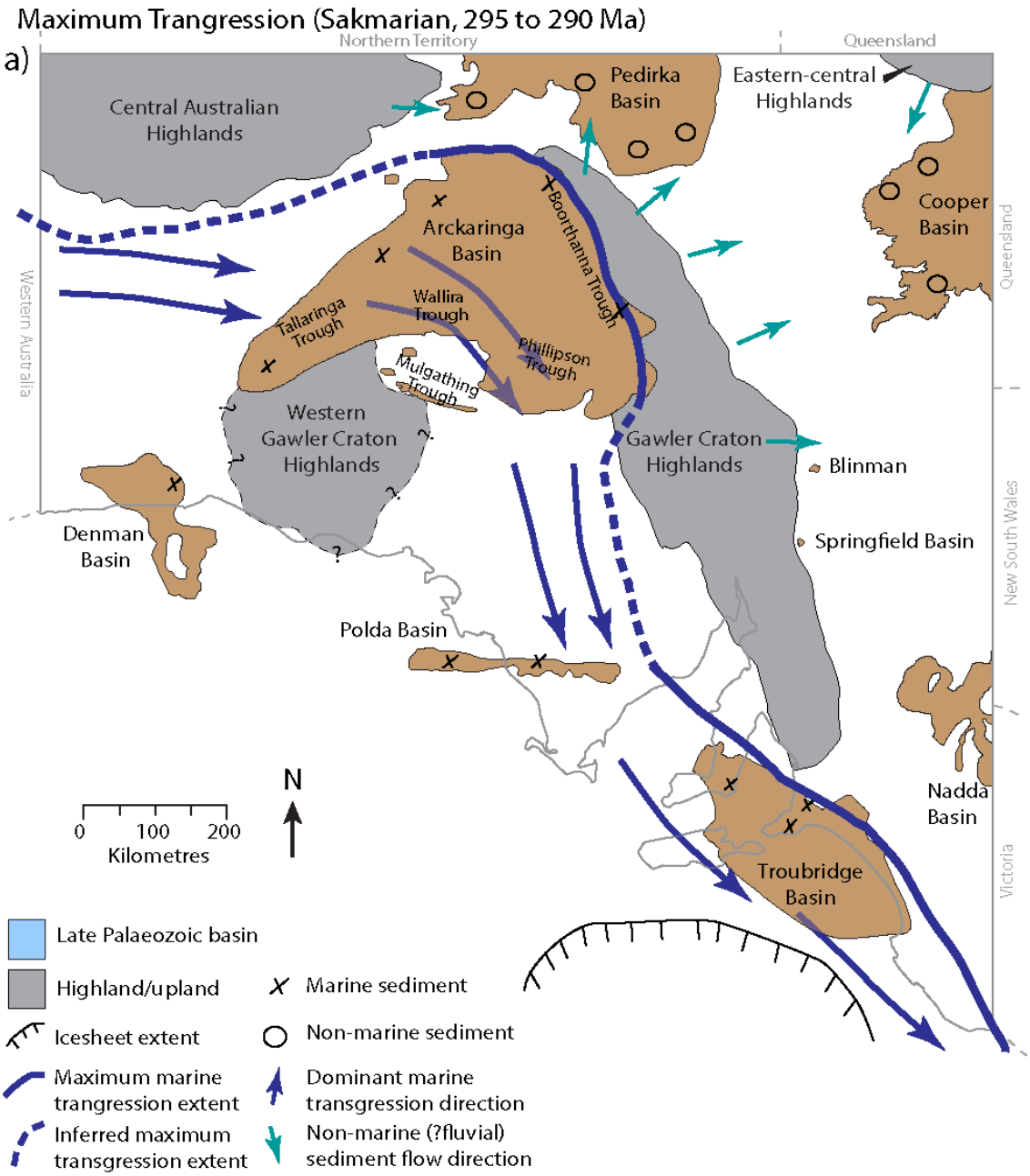

Figure 6:5 a) Palaeogeographic reconstruction of the maximum marine transgression that occurred during the Early Permian (early Sakmarian). Model is based on field observations (this study), Crowell and Frakes (1971a), Alley et al. (1995), Rogers et al. (1996b), Rogers (2000), Veevers (2006), Menpes (2013).

Previously proposed reconstructions mostly imply the sea covered most of the continent without explaining the role of the highlands such as the Central Australian, Eastern-central Australian, and western Gawler Craton highlands during this time (Crowell and Frakes 1971a, 1971b, Caputo and Crowell 1982, Alley and Bourman 1995). The sedimentary rocks of the Stuart Range Formation and other correlative late Palaeozoic marine sedimentary rocks are generally indicative of a quiet, cold-water, restricted marine environment with some periods of lagoonal conditions (Alley et al. 1995, Rogers et al. 1996b). Ludbrook (1967, 1967) observed foraminifera within the rocks of the Stuart Range Formation that supported a restricted marine environment. Sedimentary rocks in the Pedirka and Cooper basins to the north of the Central Gawler Highlands (Figure 6:5) have been assigned a similar

age and depositional conditions (Alley et al. 1995, Rogers et al. 1996b) as the upper Stuart Range Formation, however foraminiferal evidence suggests these are freshwater sedimentary rocks and have been interpreted to have been deposited in fluvial and alluvial fan conditions (Alley et al. 1995). These conditions are most likely a remnant of the waters released by alpine glacial systems in the highlands and indicate fluvial sediment transport off the highlands into the surrounding low-lying areas (Figure 6:5). Evidence of freshwater and/or fluvial sediment input is not recognised within the Arckaringa Basin. It is possible that the Gawler Craton Highlands were a series of islands during the maximum marine transgression, however, given that the marine conditions were shallow and restricted it is unlikely that this was the case. The shallow marine environment along with the absence of marine sedimentary rocks in the highlands suggests that the marine transgression did not cover the highlands. However, it is likely that the shoreline was very close if not in contact with the topographically lower parts of the Gawler Craton Highlands, which may also be the case for the Central Australian (Figure 6:5).

6.3.3 Freshwater conditions

Sedimentary rocks deposited during freshwater conditions are restricted to northern basins of South Australia and dominant only in the Arckaringa Basin (Figure 6:6). The mechanism for initiation of the marine regression and subsequent freshwater conditions during the Early Permian is largely unknown. Isostatic recovery of the continental crust after the compressional influence of the icesheet was removed may have initiated in the marine regression (Crowell and Frakes 1971a, Alley et al. 1995, Veevers 2006). Alternatively, Alley et al. (1995) suggested that the regression may have been caused by widespread eustatic fall. As the marine transgression was shallow and quiet with no significant change in depth or conditions, it is difficult to ascertain when the sedimentation regime changed from transgressive to regressive. Additionally, no sharp boundary from marine shale to freshwater fluvial sedimentary rocks is observed in the Arckaringa Basin, implying the change from marine to freshwater conditions was gradual. The gradual change in conditions favours post-glacial isostatic rebound as a mechanism for the change as this is a slow process that would allow for a gradual change in sedimentation. It is likely that the Troubridge Basin was inundated by the still regressing marine waters, as no sedimentary rocks indicating a freshwater environment have been observed in the basin.

The sedimentary rocks of the middle Mount Toondina Formation as seen at Box Creek are representative of a fluvial system active in the waning stages of the marine regression. These sedimentary rocks predominately consist of sand beds with occasional clay beds. The sand beds are suggested to have been deposited by subaqueous fans, and the clay beds were deposited during intermittent periods of quieter, lower energy fluvial flows (Wilmot 1987). Fluvial conditions became increasingly dominant and fluvial channels developed. In the southern Boorthanna Trough channels flowed in southerly and southwesterly directions.

The upper Mount Toondina Formation thickens in the northern Boorthanna Trough and is absent in the western margins of the basin (Chapter 3, Figure 3:3). This is likely due to the concentration of freshwater sedimentation in the main depocentres of the Arckaringa Basin, and are also indicated by the concentration of the major coal occurrences (Figure 6:6). The freshwater most likely flowed into the depocentres from the higher basin centre and from the surrounding highlands creating intricate fluvial systems with floodplains and lakes in the low-lying areas and swampy floodplains (Figure 6:6). Like the marine regression, the freshwater deposition is likely to have been multidirectional (Figure 6:6) both within the basin and in and out of the basin. Alley et al. (1995) suggested that minor coal

occurrences in the Cooper, Pedirka and Denman basins indicate similar depositional conditions. It is likely that these freshwater alternating fluvial and lacustrine environments were restricted to the larger, northern basins due to the freshwater flowing into the basins from the melting valley glacier systems.

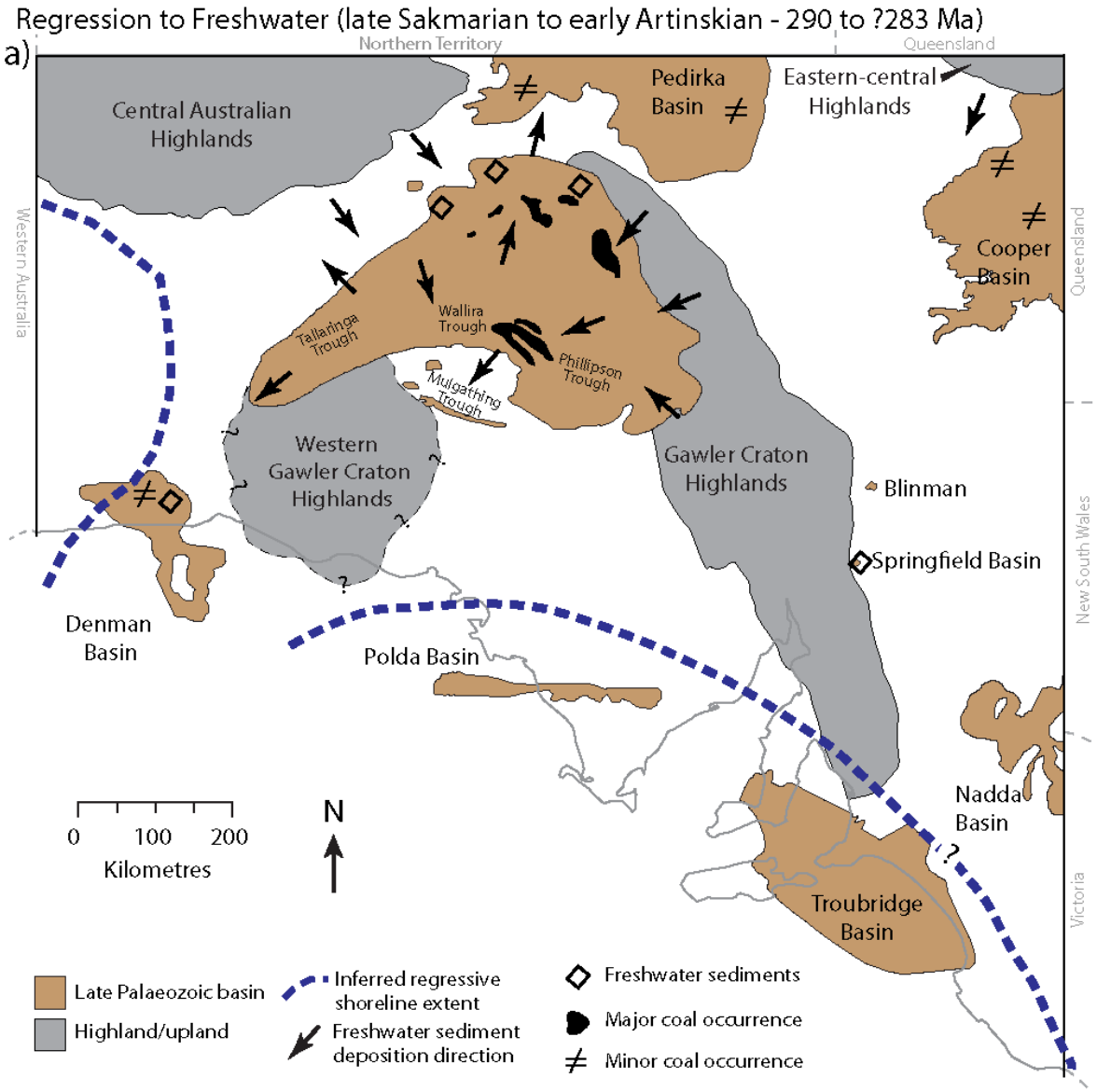

Figure 6:6 a) Palaeogeographic reconstruction of the transition from marine regression to freshwater environment that occurred during the Early Permian (Sakmarian to ?Artinskian). Data complied based on field observations and information provided in Crowell and Frakes (1971a), Alley et al. (1995), Rogers et al. (1996b), Rogers (2000), Veevers (2006), Menpes (2013).

6.4 Conclusions

The late Palaeozoic glaciation in South Australia consisted of two types of glaciation: alpine and continental. Alpine glaciers occupied areas including the Gawler Craton Highlands and Central Australia Highlands (now Musgrave Province). Valley glaciers were part of the alpine glaciation, and likely flowed from topographic highs to the basin margins. The continental icesheet spread rapidly north from Antarctica into central South Australia. Sedimentary rocks deposited by the valley glaciers are restricted to the northern late Palaeozoic basins. These sedimentary rocks suggest deposition occurred

via high energy meltwater streams that typically resulted in diamictite and coarse-grained sandstone deposits. The westerly orientation of the diamictite units in the Boorthanna Trough suggests that the valley glaciers that deposited these sedimentary rocks originated in the Gawler Craton Highlands that border the eastern margin of the Arckaringa Basin.

The advance of the continental icesheet is best recorded in the Troubridge Basin where units one to three of the Cape Jervis Formation preserve the glacial conditions of the icesheet. These units suggest that ice tongue glaciers preceded the continental icesheet prior to the ice stagnating. The ice tongue glaciers widened and deepened existing valleys and eroded sedimentary rocks, exposing the bedrock. The icesheet then scoured and polished the exposed bedrock and deposited diamictite with typically locally-derived clasts. The icesheet slowed as it moved northward so that the ice that occupied the Troubridge Basin stagnated, causing the formation of glacial lakes between the ice and the palaeoshoreline. The glacial lakes and meltwater streams from the icesheet facilitated deposition of the alternating clay and sand beds of unit three of the Cape Jervis Formation. The icesheet did not reach the Arckaringa Basin. Reworked, fluvially-deposited diamictites suggest that ice tongue glaciers may have moved into the Arckaringa Basin from the south.

The ice rapidly retreated from central South Australia; this is recorded in the Troubridge Basin in sedimentary rocks of unit four of the Cape Jervis Formation. Diamictite units with typically rounded clasts interbedded with sand beds signify an ice mass that was quickly decaying, periodically releasing debris into the surrounding environment. As the ice continued to retreat and decay, associated sea level rises covered the Troubridge Basin in a deepening marine environment which resulted in the deposition of unit five of the Cape Jervis Formation. There is no evidence of the rapid retreat of the icesheet recorded in other late Palaeozoic basins of South Australia. However, the rapid decay of valley glaciers is recorded in the sandstone units in the Boorthanna Trough, Arckaringa Basin. The timing of the retreat of the valley glaciers is not clearly understood although it is likely to have occurred simultaneously with the retreat of the icesheet.

Following the glacial retreat, much of South Australia was inundated by a transgressing sea. It is suggested that the incursion began in Western Australia and when at a maximum completely covered the Arckaringa and Troubridge basins. This incursion is recorded in the sedimentary rocks of the Stuart Range Formation of the Arckaringa Basin and its equivalents in the Polda and Denman basins. These sedimentary rocks are restricted to the subsurface, making accurate reconstructions difficult.

Once the sea waters retreated to the south, potentially covering the Troubridge Basin, freshwater conditions prevailed in the north of South Australia. This transition is recorded in the lower and middle Mount Toondina Formation. The marine regression was likely bi-directional to the southeast and southwest. Regressive marine sedimentary rocks interbedded with increasingly fluvial sedimentary rocks suggest that freshwater streams were active during the waning stags of the regression. As the fluvial conditions became dominant fluvial channels developed. Evidence of the south to southwesterly flowing fluvial channels is preserved in the upper Mount Toondina Formation in the southern Boorthanna Trough.

The Mount Toondina Formation in the northern Boorthanna Trough is a record of alternating fluvial and lacustrine environments in which coal swamps intermittently formed. Freshwater streams likely flowed into the middle of the basin from the topographically higher margins and the surrounding highlands creating fluvial systems with floodplains and lakes in the low-lying areas where coal swamps developed.

Chapter 7: Conclusions

This study involved characterising the late Palaeozoic glacigene sedimentary rocks of the Troubridge and Arckaringa Basin with the aim of reconstructing the palaeogeography of South Australia during the late Palaeozoic and establishing background geochemistry to enable effective use of the glacigene sedimentary rocks as mineral exploration sampling media. The methods used were sedimentology, U-Pb isotopic zircon geochronology and whole rock geochemistry. The palaeogeographic reconstructions are an amalgamation of the existing depositional models and reconstructions, and new data to provide a holistic palaeogeographic reconstruction of South Australia.

The sedimentology of the glacigene units, particularly the diamictite units of the late Palaeozoic glacigene sedimentary rocks of the Troubridge (lower Cape Jervis Formation) and Arckaringa (Boorthanna Formation) basins can be used to assess the depositional setting and feed into development of palaeogeographic reconstructions that depict the Permo-Carboniferous glacial environment throughout South Australia. Clast composition, size and shape are indicative of the glacial setting. Diamictite units deposited by an advancing icesheet will have angular, locally-derived clasts, and are observed throughout the Troubridge Basin and into the southern Arckaringa Basin. Diamictite units with rounded to angular, locally-derived clasts were deposited by an ice tongue, and are observed in the southern Arckaringa Basin. Diamictite units with subrounded to rounded clasts with both locally- and distally-derived clasts were deposited by valley glaciers, and are observed throughout the eastern and western Troubridge Basin and the eastern margin of the Arckaringa Basin.

Alternating clay and sandstone with lesser diamictite beds in the middle Cape Jervis Formation are indicative of an ice mass that has stagnated, forming glacial lakes that are fed by meltwater streams with alternating energy and sediment load due to the periodic melting of the ice mass. Similar depositional settings are indicated in the lower Boorthanna Formation. The increasing frequency of diamictite beds up-sequence is indicative of the rapid retreat and melting of the ice mass. These sedimentary rocks are overlain by shallow marine sedimentary rocks in the Troubridge Basin. These are indicative of the marine transgression initiated by the melting and retreat of the ice mass. The alternating clay and silt beds with minor carbonaceous occurrences in the Arckaringa Basin are indicative of the transition to fluviolacustrine environment that followed the marine transgression and subsequent regression. The fluvial to fluviolacustrine transition is due to the post-glacial isostatic rebound changing the dynamics of the landscape.

The Cape Jervis Formation and the Boorthanna Formation are equivalent units which comprise diamictite units deposited via the action of an icesheet and valley or ice tongue glaciers. Palynological (Ludbrook 1969b, Townsend and Ludbrook 1975) evidence suggests that both units were deposited in the Sakmarian (295 – 290 Ma). The extent and nature of these diamictite units was used to model the extent and location of icesheets, ice tongues and valley glaciers during the glacial maximum.

Following the glaciation, the depositional environment between the Arckaringa and Troubridge basins became variable. The marine transgression reached its maximum in the north of South Australia, including in the Arckaringa Basin, while the Troubridge Basin was covered in ice. Following the marine regression in the north a terrestrial, freshwater environment dominated, while the Troubridge Basin was in a deepening marine setting.

Despite the capacity for a glacier to move debris long distances, there is no requirement to seek source regions outside of the proximal Kanmantoo Group, the Transantarctic Mountains of Antarctica in the Troubridge Basin and the Gawler Craton and Adelaide Rift Complex in the Arckaringa Basin as a sourced of the glacigene sedimentary rocks. The provenance of the late Palaeozoic glacigene sedimentary rocks has previously been inferred from clast lithology and apparent ice movement directions (Crowell and Frakes 1971a, Alley et al. 1995, Veevers 2006). Here, this interpretation is further refined here using U-Pb isotopic zircon geochronology. The detrital zircon populations of the Troubridge Basin closely match the detrital populations of the Kanmantoo Group, in particular the prominent ca 570 Ma peak. Other possible sources in the Transantarctic Mountains have more prominent populations between ca 900 to 1200 Ma and ca 1700 to 1900 Ma. The Boorthanna Formation has prominent populations from ca 500 to 600 Ma, ca 900 to 1200 Ma and ca 1700 to 1900 Ma. There are multiple potential source regions for these sedimentary rocks including the Adelaide Rift Complex, Gawler Craton, Transantarctic Mountains, Arunta Region and the Musgrave Province. The ca 500 to 600 Ma population closely matches the pattern of the Cape Jervis Formation and the Kanmantoo Group, there are no populations of this age in the Gawler Craton, Adelaide Rift Complex, Musgrave Province and the Arunta Region. The ca 500 to 600 Ma peak in the Transantarctic Mountains have a younger mode at ca 510 Ma. Thus the preferred interpretation of the provenance of the Boorthanna Formation is a combination of Adelaide Rift Complex, Gawler Craton from the proximal Peake and Denison Ranges and the Kanmantoo Group, the nearest exposure of which is approximately 800 km to the south.

Detailed geochemical analysis of the late Palaeozoic sedimentary rocks was used to further interpret the depositional processes and effects of post-depositional weathering. The whole rock geochemistry of the glacigene sedimentary rocks of the Troubridge and Arckaringa basins can be interpreted as a combination of source rock geochemistry, depositional and weathering processes:

- The geochemistry of the source rocks. This is best seen in the minimally weathered clay and silt sedimentary rocks. The geochemistry of these rocks is similar to PAAS and likely source rocks of the Kanmantoo Group.

- The depositional setting of the glacigene sedimentary rocks. This is best seen in SiO_2:Al_2O_3 ratios with high silica end members representing sand-rich lithologies and high Al content representing clay-rich lithologies. The high Al end members include clay matrix diamictites which are most likely the result of glacial deposition (rock flour + clasts). At the silica-rich end represent lithologies where fluvial processes removed the fine-grained clay-rich component.

- The types of post-depositional weathering the sedimentary rocks have undergone. These include calcareous weathering (carbonate, sulphate and dolomite), ferruginous (and magniferous) weathering and kaolinitic weathering.

Trace element concentrations are low. The trace element geochemical signature is largely controlled by the clay mineral component and to a lesser extent the Fe-oxide mineral component of the sedimentary rocks. After normalisation against Al+Fe, elevated, normalised Cu concentrations occurred in glacigene sedimentary rocks adjacent to known sources of elevated Cu in the basement or overlying rocks.

The data presented here are consistent with a palaeogeographic reconstructions involving three stages; 1. Glacial advance; 2. Glacial retreat and marine transgression and 3. Post-glacial isostatic rebound and transition to fluviolacustrine conditions.

During the glacial maximum the South Australian landscape was dominated by 2 types of glaciation: continental and alpine. The continental icesheet spread rapidly north from Antarctica into central South Australia. Ice tongues at the front of the icesheet scoured, eroded and polished the exposed landscape, forming U-shaped valleys and polished, glaciated pavements. Alpine glaciers of which valley glaciers were part of occupied the highlands and the valley glaciers transported debris into the low-lying depocentres. The icesheet rapidly melted and retreated from northern South Australia and slowed as it moved south continuing to melt and shed debris into the Troubridge Basin. The retreat of the ice mass from northern South Australia opened a westerly seaway where the marine transgression originated. The maximum marine transgression covered most of South Australia west of the Gawler Craton Highlands. The marine waters retreated to the south, possibly continuing to cover the Troubridge Basin, in the north of South Australia freshwater conditions prevailed. Regressive marine sedimentary rocks interbedded with increasingly fluvial sedimentary rocks suggest that freshwater streams were active during the waning stages of the regression. The resulting terrestrial environment consisted of an alternating fluvial and lacustrine environment with intermittent formation of coal swamps.

The glaciated terrane of Myggbukta, eastern Greenland (Figures 1:1, 7:1a, b) is comparable to the maximum glaciation of late Palaeozoic South Australia. As the icesheet moved north into South Australia, ice tongues at the front of the ice-scoured large U-shaped valleys. This is occurring to the east and west of Myggbukta where the ice tongue is advancing into the ocean (Figures 7:1a, b). The valley glacier of late Palaeozoic South Australia would have been similar to the valley glaciers in the coastal highlands of Myggbukta. Glacial lakes forming between the shoreline and glaciers along the ice margins (Figures 7:1a, b) as the ice melt and retreat and the diverse fluvial sediment flow directions are analogous with the depositional setting of where the ice was stagnant and melting. The varying size and location of these lakes is reflective of the glacial lakes sedimentary rocks in the Troubridge Basin.

The post-glacial landscape of Hudson Bay, Canada in relation to glaciated terrane of Greenland (Figure 7:1c) demonstrates some of the proposed depositional settings of South Australia during the marine transgression and subsequent freshwater conditions. The deglaciation of the Greenland ice mass and its retreat towards the North Pole is a modern analogy of the maximum marine transgression. The increase in water supply into the ocean is causing a sea level rise which could potentially cause the inundation of the surrounding land mass. The meltwater input from the west of Greenland and east of Baffin Island (Figure 7:1c) is similar to the input of meltwater into the Arckaringa Basin as the marine transition occurred. The transition from marine to fluvial conditions is comparable to the margins of Hudson Bay (Figure 7:1c) where marine transgression followed the northward retreat of the icesheet. Subsequent post-glacial isostatic uplift has resulted transition to fluviolacustrine conditions and stranding of palaeoshorelines on the margins and islands of the bay (Figure 7:1c).

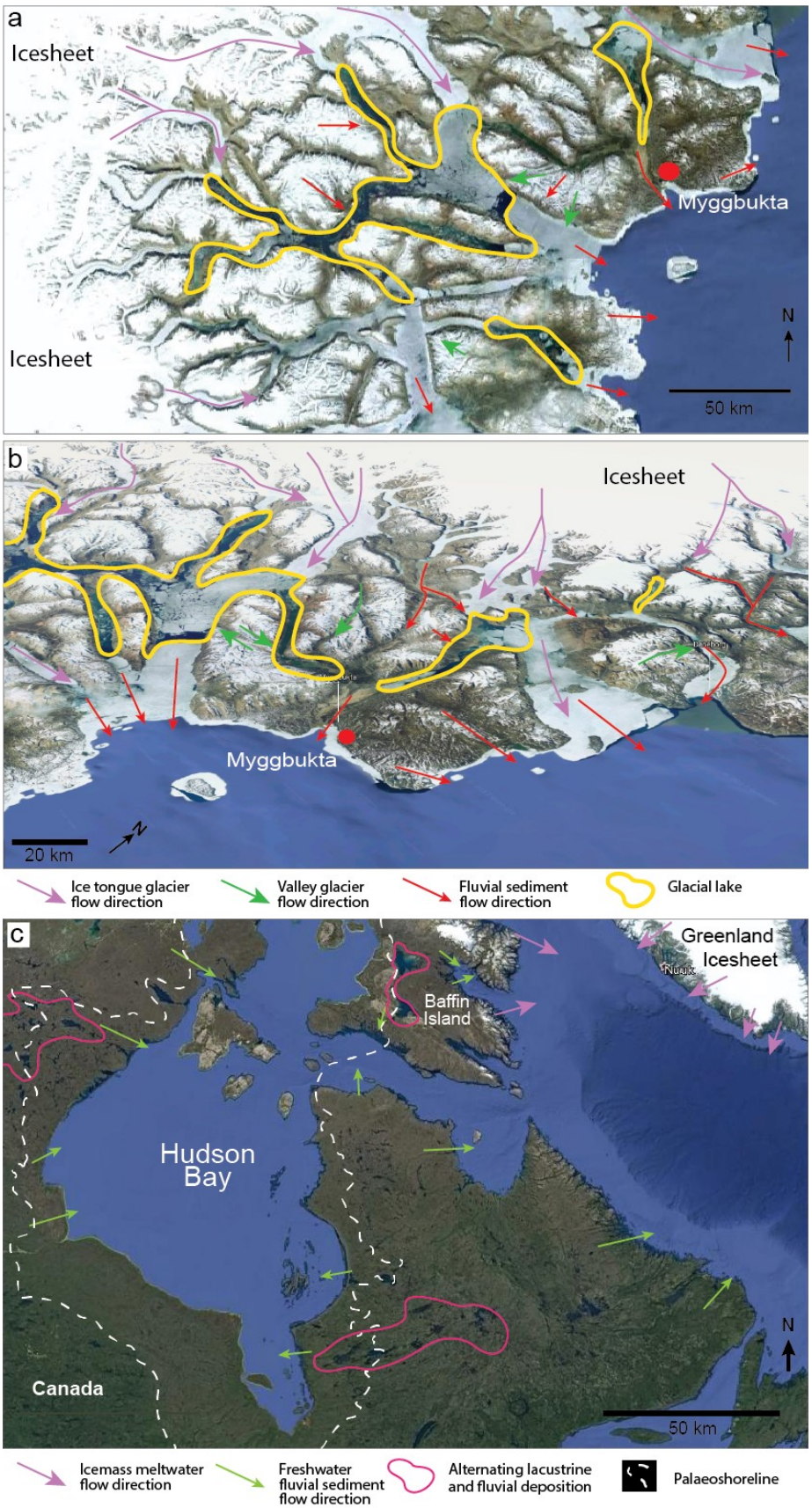

Figure 7:1 (a) Planar view and (b) tilted view of the modern glaciated terrane in eastern Greenland showing the interaction of ice masses and the surrounding landscape; (c) The post-glacial landscape of Hudson Bay, Canada. Palaeoshoreline adapted from Shilts (1986), stranding of the palaeoshoreline is evident by the lighter colour seen in islands in the northwest of the bay and on western Baffin Island. Locations of this figure are shown in Figure 1:1; images from Google Earth.

Future Work

Throughout the duration of this research project, many additional questions have arisen from the founding research aims and objectives. These include:

- What are the primary and secondary clay minerals within the matrix of the diamictite and sandstone units?
- What is the source of the primary clay minerals and do the primary clay minerals provide an indication of provenance?
- Are there any differences in the grain morphology between the rocks of differing depositional settings?
- Would performing U-Pb isotope provenance studies on the clasts within the glacigene sediments as well as the assumed source rocks provide more evidence for source rocks?
- Would the U-Pb isotopic provenance spectra of glacigene sediments from other southern Australian late Palaeozoic exposures show similar results? ie a strong local source with lesser distal source input.
- Would a more detailed palynological study better constrain the age of the sediments as well as provide another constraint on the depositional setting?
- Does assessing the geochemical background of late Palaeozoic glacigene sediments work in a known mineralised region such as the Bendigo region of Victoria?
- Are the unique characteristics identified in Chapters 2 and 3 applicable to other late Palaeozoic glacigene rocks elsewhere in Australia?
- Can the criteria use to generate the palaeogeographic reconstructions be applied to extend the reconstruction across southern Australia or further?

These points cannot be answered in the scope of the present study, it is the author's wish to continue to publish material concerning the sedimentology and mineralogy, the provenance and potential source rocks, the lithogeochemistry of late Palaeozoic glacigene rocks and the palaeogeographic reconstructions generated from the published studies.

References

ALLCHURCH P. D. & WOPFNER H. 1967 South Australian Government Cootanoorina No. 1 Well Completion Report, Report Book 65/104. Adelaide.

ALLEY N. F. & BOURMAN B. P. 1984 Sedimentology and origin of Late Palaeozoic glacigene deposits at Cape Jervis, South Australia, *Transactions of the Royal Society of South Australia,* vol. 108, no. 1, pp. 63-75.

ALLEY N. F. & BOURMAN B. P. 1995 Troubridge Basin. In DREXEL J. F. & PREISS W. V. (EDS). The geology of South Australia, Vol 2, The Phanerozoic*.* pp. Chaper 8: 65-70. Adelaide.

ALLEY N. F.*,* BOURMAN B.P, GRAVESTOCK D. I., HIBBURT J. E., HILL A. J. & RANKIN L. R. 1995 Late Palaeozoic. In DREXEL J. F. & PREISS W. V. (EDS). The geology of South Australia, Vol 2, The Phanerozoic*.* pp. Chapter 8: 63-91. Adelaide.

ALLEY N. F., BOURMAN B. P. & MILNES A. R. 2013 Late Palaeozoic Troubridge Basin sediments on Kangaroo Island, South Australia, *Mesa Journal,* vol. 70, no. 3, pp. 24-43.

AMBROSE G. J., FLINT R. B. & WEBB A. W. 1981 Precambrian and Palaeozoic Geology of the Peake and Denison Ranges. Bulletin 50*.* Geological Survey of South Australia, Adelaide.

ANAND R. R. 2005 Weathering history, landscape evolution and implications for mineral exploration. In ANAND R. R. & DE BROEKERT P. (EDS). Regolith Landscape Evolution Across Australia. A compliation of regolith case studies with regolith landscape evolution models*.* pp. 2-40. CRC LEME.

ARCHBOLD N. W. 1982 Correlation of the Early Permian faunas of Gandwana: Implication for the Gondwanan Carboniferous-Permian boundary, *Australian Journal of Earth Sciences,* vol. 29, no. 3, pp. 267-276.

ASHLEY G. M., SHAW J. & SMITH N. D. 1985 Glacial sedimentary environments. SEPM Short Course No. 16. Oklahoma, USA: Society of Palaeotologists and Mineralogists.

BANKS M. R. 1962 Permian, *Australian Journal of Earth Sciences,* vol. 9, no. 2, pp. 189-215.

BECKER E. & HORGATH P. 2004 Paladin Resources Ltd. EL 2892 Yankalilla Annual and final reports to licence expiry for the period 22/10/2001 to 21/10/2003. Geological Survey of South Australia Open File Envelope No. 9919.

BELL F. G. 1998 Environmental Geology: Principles and Practice*.* (First Edition edition). Blackwell Science Ltd, Oxford.

BELPERIO A. P., FAIRCLOUGH M. C. & RANDALBEL J. P. J. 2009 Kingscote 1:250 000 geological map. 2nd Edition ed. Adelaide.

BENN D. I., KIRKBRIDE M. P., OWEN L. A. & BRAZIER V. 2003 Glaciated Valley Landsystems In EVANS D. J. A. (EDS). Glacial Landsystems, pp. 372-406. Arnold, London

BENNETT M. R. & GLASSER N. F. 2009 Glacial geology: ice sheets and landforms*.* (2nd edition). John Wiley and Sons, West Sussex, UK.

BOURMAN B. P. 1973 Geomorphic Evolution of southeastern Fleurieu Peninsula. Department of Geography*.* University of Adelaide.

BOURMAN B. P. 1986 A review of controversial issues related to the Late Palaeozoic glaciation of southern South Australia, *International Geomorphology,* vol. Part II, pp. 725-742.

BOURMAN B. P. & ALLEY N. F. 1988 Permian glacial features, northwestern Fleurieu Peninsula, South Australia., *Quarterly Geological Notes,* vol. October 1988, no. 108, pp. 2-6.

BOURMAN B. P. & ALLEY N. F. 1990 Stratigraphy and Environments of Deposition at Hallett Cove during the Late Palaeozoic, *Mines and Energy Review, South Australia,* vol. 157, pp. 68-82.

BOURMAN B. P. & ALLEY N. F. 1995 Late Palaeozoic sediments at King Point, southeastern Troubridge Basin, South Australia, *Quarterly Geological Notes,* vol. 128, pp. 2-7.

BOURMAN B. P. & ALLEY N. F. 1999 Permian glaciated bedrock surfaces and associated sediments on Kangaroo Island, South Australia: implications for local Gondwanan ice-mass dynamics, *Australian Journal of Earth Sciences*, no. 46, pp. 523-531.

BOURMAN B. P., MAUD R. R. & MILNES A. R. 1976 Late Palaeozoic Glacial Features near Mount Compass, South Australia, *Search,* vol. 7, no. 11-12, pp. 488-490.

BOURMAN B. P. & MILNES A. R. 1976 Exhumed Roche Moutonnee, *Australian Geographer,* vol. 13, pp. 214-216.

BOWELL R. J. 1994 Sorption of arsenic by iron oxides and oxyhydroxides in soils, *Applied Geochemistry,* vol. 9, pp. 279-286.

BUTT C. R. M., LINTERN M. J. & ANAND R. R. 1997 Evolution of regoliths and landscapes in deeply weathered terrain - implications for geochemical exploration. In GUBINS A. G. (EDS). Proceedings of Forth Decennial International Conference on Mineral Exploration.

CADMAN S. J., PAIN L. & VUCKOVIC V. 1994 Australian Petroleum Accumulations Report 10: Perth Basin, Western Australia. In BRANCH P. R. (ED). Perth: GSWA.

CAMACHO A., HENSEN B. J. & ARMSTRONG R. 2002 Isotopic test of a thermally driven intraplate orogenic model, Australia, *Geology,* vol. 30, no. 10, pp. 887-890.

CAMPBELL K. S. W., DERRINGTON S. S., ISBELL R. F., LARING A. C. M., MORGAN K. H., MOTT W. D., PHILLIPS K., ROWE S. M., TWEEDALE G.W. & WEBB E. A. 1960 The Bowen Basin. In CAMPBELL K. S. W. & DERRINGTON S. S. (EDS). Geology of Queensland. pp. 184-185.

CAPUTO M. V. & CROWELL J. C. 1982 Migration of glacial centres across Gondwana during Palaeozoic Era, *Geological Society of America Bulletin,* vol. 96, pp. 1020-1036.

CAWOOD P. A., NEMCHIN A. A., SMITH M. & LOWEY S. 2003 Source of Dalradian Supergroup contrained by U-Pb dating of detrital zircon and implication for the East Laurentian margin, *Journal of Geological Society, London,* vol. 160, no. 2003, pp. 231-246.

CLARK P. U. 1987 Subglacial sediment dispersal and till composition, *Journal of Geology,* vol. 95, pp. 527-541.

COOPER J. A., MORTIMER G. E., ROSIER C. M. & UPPILL R. K. 1985 Gawler Range magmatism - further isotopic age data, *Australian Journal of Earth Sciences,* vol. 32, pp. 115-123.

CORFU F., HANCHAR L. M., HOSKIN P. W. O. & KINNY P. 2003 Atlas of Zircon Textures, *Journal of Mineralogy and Geochemistry,* vol. 53, pp. 469-500.

CORREDEIRA C., ARAÚJO M. F. & JOUANNEAU J.-M. 2008 Copper, zinc and lead impact in SW Iberian shelf sediments: An assessment of recent historical changes in Guadiana Rver Bsin, *Geochemical Journal,* vol. 42, pp. 319-329.

CRAIG M. A. & BROWN M. C. 1984 Permian glacial pavements and ice movement near Moyhu, north-east Victoria, *Australian Journal of Earth Sciences,* vol. 31, pp. 439-444.

CRAWFORD A. R. 1960 MAITLAND map sheet. South Australia Geological Altas, 1: 250 000 series, Sheet SI 53-12.

CRAWFORD A. R. 1965 The geology of Yorke Peninsula. GSSA Bulletin 39. Adelaide.

CRAWFORD A. R., STEVENS B. P. J. & FANNING M. 1997 Geochemistry and tectonic setting of some Neoproterozoic and Early Cambrian volcanics in western New South Wales, *Australian Journal of Earth Sciences,* vol. 44, pp. 831-852.

CREASER R. A. & COOPER J. A. 1993 U-Pb geochronology of Middle Proterozoic felsic magmatism surrounding the Olympic Dam Cu-U-Au-Ag and Moonta Cu-Au-Ag deposits, South Australia, *Economic Geology,* vol. 88, pp. 186-197.

CREER K. M. 1968 Palaeozoic Palaeomagnetism, *Nature,* vol. 219, no. July 20, pp. 246-250.

CROWELL J. C. 1978 Gondwanan glaciation, cyclotherms, continental positioning, and climate change, *American Journal of Science,* vol. 278, no. December, pp. 1345-1372.

CROWELL J. C. & FRAKES L. A. 1971a Late Palaeozoic glaciation of Australia, *Australian Journal of Earth Sciences,* vol. 17, no. 2, pp. 115-155.

CROWELL J. C. & FRAKES L. A. 1971b Late Palaeozoic glaciation: Part IV, Australia, *Geological Society of America Bulletin,* vol. 82, no. September, 1971, pp. 2515-2540.

DART R. C., BAROVICH K. M., CHITTLEBOROUGH D. J. & HILL S.M. 2007 Calcium in regolith carbonates of central and southern Australia: Its source and implications for the global carbon cycle, *Palaeogeography, Palaeoclimatology, Palaeoecology,* vol. 249, pp. 32-334.

DAVID T. E. W. & HOWCHIN W. 1897 Notes on the glacial features of the Inman Valley, Yankalilla and Cape Jervis District, *Transactions of the Royal Society of South Australia*, pp. 61-67.

DE PRETIS D. 2011 Application of lithogeochemistry to identify stratographic units and provenance of the Kanmantoo Group, Kangaroo Island. University of Adelaide unpublished Honours Thesis.

DEMAISON G. 1969 Strarigraphic drilling in the Arckaringa Sub-basin, *Quarterly Geological Notes,* vol. 34, no. July 1969, pp. 4-9.

DERRINGTON S. S. & MORGAN K. H. 1960 South-eastern and South Central Bowen Basin. In CAMPBELL K. S. W. & DERRINGTON S. S. eds. Geology of Queensland. pp. 204-212.

DICKINS J. M. 1989 Youngest Permian marine macrofossil fauna from the Bowen and Sydney Basins, eastern Australia, *BMR Journal of Australian Geology and Geophysics,* vol. 11, no. 1, pp. 63-79.

DICKINS J. M. 1996 Problems of a Late Palaeozoic glaciation in Australia and subsequent climate in the Permian *Palaeogeography, Palaeoclimatology, Palaeoecology,* vol. 125, no. 1996, pp. 185-197.

DILABIO R. N. W. & COKER W. B. 1987 Mineral Exploration in Glaciated Terrian Using Till Geochemistry, *Episodes,* vol. 10, no. 1, pp. 32-34.

DIREEN N. G. & CRAWFORD A. R. 2003 Fossil seaward-dipping reflector sequences preserved in southeastern Australia: a 600 Ma volcanic passive margin in eastern Gondwanaland, *Journal of the Geological Society, London,* vol. 160, pp. 985-990.

DREXEL J. F. 1978 An historical summary of the mines of Fleurieu Peninsula. Geological Survey of South Australia Report Book 78/27.

DREXEL J. F. & PREISS W. V. (EDS) 1995 The geology of South Australia. Vol. 2, The Phanerozoic. South Australia. Bulletin 54. Government of South Australia, Adelaide.

DREXEL J. F., PREISS W. V. & PARKER A. J. (EDS) 1993 The geology of South Australia. Vol 1, The Precambrian. South Australia. Bulletin 54 Geological Survey of South Australia, Adelaide.

EHLERS J. & GIBBARD P. 2007 The extent and chronology of Cenozoic Global Glaciation, *Quaternary International,* vol. 164-165, no. April 2007, pp. 6-20.

EMBLETON B. J. J. & SCHMIDT P. W. 1977 Revised palaeomagnetic data for the Australian Mesozoic and a synthesis of Late Palaeozoic-Mesozoic results for Gondwanaland, *Tectonophysics,* vol. 38, no. 1977, pp. 355-364.

EMBLETON B. J. J. & VALENCIO D. A. 1977 Palaeomagnetism and the reconstruction of Gondwanaland, *Tectonophysics,* vol. 40, no. 1977, pp. 1-12.

Eyles N. 1993 Earth's glacial record and it's tectonic setting, Earth-Science Reviews, vol. 35, pp. 1-248

EYLES N., EYLES C. H. & MIALL A. D. 1983 Lithofacies types and vertical profile models: an alternative approach to the description and environmental interpretation of glacial diamict and diamictite sequences, *Sedimentology*, vol 30, pp. 393-410

EYLES N. & MIALL A. D. 1984 Glacial Facies. In WALKER R. G. (ED) Facies models (2nd Edition), Geoscience Canada Reprint Series 1, Geological Society of Canada, Ainsworth Press Limited.

EYLES N., MORY A. J. & BACKHOUSE J. 2002 Carboniferous-Permian palynostratigraphy of west Australian marine rift basins: resolving tectonic and eustatic controls during Gondwanan glaciations, *Palaeogeography, Palaeoclimatology, Palaeoecology,* vol. 184, pp. 305-319.

FAIRCLOUGH M. C. 2007 Kingscote Special 1:250 000 geological map, *Mesa Journal,* vol. 47, no. December, pp. 28-31.

FANNING C. M., REID A. & TEALE G. S. 2007 A geochronological framework for the Gawler Craton, South Australia, *South Australia Geological Survey Bulletin,* vol. 55, p. 80.

FIELDING C. R., FRANK T. D., ISBELL J. L., HENRY L. C. & DOMACK E. W. 2010 Stratigraphic signature of the Late Palaeozoic Ice Age in the Parmeener Supergroup of Tasmania, SE Australia, and inter-regional comparisons, *Palaeogeography, Palaeoclimatology, Palaeoecology,* vol. 298, pp. 70-90.

FIELDING C. R., FRANK T. D. & ISBELL R. F. 2008 The late Palaeozoic - A review of current understanding and synthsis of global climate patterns, *The geological Society of America,* vol. Special Paper 441.

FINLAYSON B. 1981 Exploration of the Arckaringa Basin: An outline of a work programme to upgrade knowledge of this Permian intercratonic basin, Report Book No 81/51. Adelaide.

FLÖTTMANN T. & COCKSHELL C. D. 1996 Palaeozoic basins of southern South Australia: New insights into their structural history from regional seismic data, *Australian Journal of Earth Sciences,* vol. 43, no. 1, pp. 45-55.

FLÖTTMANN T., HAND M., CLOSE D. J., EDGOOSE C. J. & SCRIMGEOUR I. R. 2004 Thrust tectonic styles of the intracratonic Alice Springs and Petermann orogenies, central Australia. In MCCLAY M. R. (ED) Thrust tectonics and hydrocarbon systems. pp. 538-557. American Association of Petroleum Geologists, Memoir 82.

FODEN J., ELBURG M. A., DOUGHERTY-PAGE J. & BURTT A. 2006 The timing and duration of the Delamerian Orogeny: Correlation with the Ross Orogen and implications for Gondwana Assembly, *The Journal of Geology,* vol. 114, no. 2 (March 2006), pp. 189-210.

FODEN J. D., ELBURG M. A., TURNER S. P., SANDIFORD M., O'CALLAGHAN J. & MITCHELL S. 2002 Granite production in the Delamerian Orogen, South Australia, *Journal of the Geological Society, London,* vol. 159, pp. 557-575.

FORBES C. J., GILES D., FREEMAN H., SAWYER M., & NORMINGTON V. J. 2015 Glacial dispersion of hydrothermal monazite in the Prominent HIll deposit: An exploration tool., *Journal of Geochemical Exploration,* vol. 156, pp. 10-33.

FOSTER C. B. 1974 Stratigraphy and palynology of the Permian at Waterloo Bay, Yorke Peninsula, South Australia, *Transactions of the Royal Society of South Australia,* vol. 98, no. 1, pp. 29-42.

FREYTAG I. B. 1964 Summary of recent investigations in the Mount Toondina area of the Arckaringa sub-basin, Report Book 58/120. Adelaide.

FREYTAG I. B. 1965 Mount Toondina Beds - Permian sediments in a probable piercement structure, *Transactions of the Royal Society of South Australia,* vol. 89, pp. 61-76.

FREYTAG I. B., HEATH G. R. & WOPFNER H. 1967 OODNADATTA map sheet. South Australia Geological Atlas, 250 000 Series, Sheet SG53-15. Geological Atlas 1: 250 000 Series. Adelaide.

GEOLOGICAL SURVEY OF SOUTH AUSTRALIA. 2016 South Australia's Major Operating/Approved Mines. Department of State Development. Government of South Australia.

GILES D., BETTS P. G. & LISTER G. S. 2004 1.8–1.5-Ga links between the North and South Australian Cratons and the Early–Middle Proterozoic configuration of Australia, *Tectonophysics,* vol. 380, no. 1, pp. 27-41.

GLASSER N. F. & BENNETT M. R. 2004 Glacial erosional landforms: origins and significance for palaeoglaciology, *Progress in Physical Geography,* vol. 28, no. 1, pp. 43-75.

GLORIE S., AGOSTINO K., & Pawley M. 2017 Low-temperature exhumation history of the eastern Musgrave Province, *Mesa Journal,* vol. 84, no. 3 pp. 19-22.

GLUSKOTER H. J. 1975 Mineral matter and trace elements in coal, *Trace Elements in Fuel*, no. 141, pp. 1-22.

GOODGE J. W., FANNING C. M., NORMAN M. D. & BENNETT V. C. 2012 Temporal, Isotopic and Spatial Relations of Early Palaeozoic Gondwana-Margin Arc Magmatism, Central Transantarctic Mountains, Antarctica, *Journal of Petrology*.

GRAVESTOCK D. I., ALLEY N. F., BENBOW M. C., COWLEY W. M., FARRAND M. G., FLINT R. B., GATEHOUSE C. G., KREIG R. B. & Preiss W. V. 1995 Early and Middle Palaeozoic. In DREXEL J. F. & PREISS (EDS) W. V. eds. The geology of South Australia, Vol 2, The Phanerozoic. pp. Chapter 7: 3-62. Adelaide: South Australian Geological Survey.

GRIFFIN W. L., POWELL W. L., POWELL W. L., PEARSON N. J. & O'REILLY S. Y. 2008 GLITTER: Laser ablation ICP-MS In SYLVESTER P. ed. Laser ablation ICP-MS in the earth sciences. Mineral Association of Canada Short Course Series. pp. 204-207.

HALL J. W., GLORIE S., COLLINS A. S., REID A., EVANS N., MC INNES B & FODEN J. 2016 Exhumation history of the Peake and Denison Inliers: insights from low-temperature thermochronology, *Australian Journal of Earth Sciences,* vol. 63, no. 7, pp. 805-820.

HAINES P. W., ALLEN H.-J., WINGATE M. T. D., KIRKLAND C. L. & HOCKING R. M. 2011 Ice movement direction and detrital zircon provenance data for early Permian glacial deposits, Amadeus Basin, eastern Western Australia. In HAKANSSAN E. & TROTTER J. (EDS). Programme & Abstracts, The XVII Internation Congress on the Carboniferous and Permian, Perth 3-8 July 2001. pp. 63. Geological Survey of Western Australia, Record 2011/20.

HAINES P. W., TURNER S. P., FODEN J. D. & JAGO J. B. 2009 Isotopic and geochemical characterisation of the Cambrian Kanmantoo Group, South Australia: implications for stratigraphy and provenance, *Australian Journal of Earth Sciences,* vol. 56, no. 8, pp. 1095-1110.

HAMBREY M. J. & GLASSER N. F. 2012 Discriminating glacier thermal and dynamic regimes in the sedimentray record, Sedimentary Geology vol. 251-252, pp. 1-33.

HARRIS W. K. & MCGOWRAN B. 1971 Permian and reworked Devonian microfossils from the Troubridge Basin, *Quarterly Geological Notes,* vol. 40, no. October 1971, pp. 5-11.

HARRIS J. R., WILKINSON L., GRUNSKY E., HEATHER K. & AYER J. 1997 Techniques for analysis and visualisation of lithogeochemical data with applications to the Swayze greenstone belt, Ontario, *Journal of Geochemical Exploration,* vol. 67, pp. 301-334.

HAWKES H. E. & WEBB J. S. 1962 Geochemistry in Mineral Exploration. Harper & Row, New York.

HEATH G. R. 1963 The Geology of the Mount Dutton Area: Oodnadatta 4-Mile Sheet, Report Book No. 57/72. PIRSA Adelaide.

HEATH G. R. 1965 Permian sediments of the Mount Dutton Inlier, *Quarterly Geological Notes,* vol. 14, no. April 1965, pp. 4-6.

HEATH R. S. 1974 Permian foraminifera in the Arckaringa Basin and their environmental significance. University of Adelaide.

HIBBURT J. E. 1995 Arckaringa Basin. In DREXEL J. F. & PREISS W. V. (EDS) The geology of South Australia, Vol 2, The Phanerozoic. pp. Chaper 8: 73-76. Adelaide: South Australian Geological Survey.

HILL S. M., STOATE, K., NORMINGTON V.J. & SWAIN G. 2012 Kanagroo Island Field Guide: DET CRC Project 3.3: Geochemical Sampling the Deep Cover. Deep Exploration Technologies Cooperative Research Centre (DET CRC) Annual Conference 2012. Adelaide.

HILL S. M., TAYLOR G. & MCQUEEN K. G. 1998 Genesis of some calcretes in the southern Yilgarn craton, Western Australia: implications for mineral exploration - Discussion, *Australian Journal of Earth Sciences,* vol. 45, pp. 177-178.

HOFFMAN P. F. & SCHRAG D. P. 2002 The Snowball Earth hypothesis: testing the limits if global change, *Palaeogeography, Palaeoclimatology, Palaeoecology,* vol. 258, pp. 129-155.

HOLDGATE G. R. 1995 The exploration potential of the Permian Numurkah Trough and Ovens Graben, Victoria, VIMP Report 3. In GEOLOGICAL SURVEY of VICTORIA (ED).

HOLMES D. A. & RAYMENT P. 1970 Oxymin Boorthanna No. 1 Well Completion Report. Open File Envelope 1313, unpublished. pp. 9-100. Adelaide.

HOWARD K. E., HAND M., BAROVICH K. M. & BELOUSOVA E. 2011 U-Pb zircon, zircon Hf and whole-rock Sm-Nd isotopic constraints on the evolution of Palaeoproterozoic rocks in the northern Gawler Craton, *Australian Journal of Earth Sciences,* vol. 58, no. 6, pp. 615-638.

HOWCHIN W. 1912 Australian Glaciation, *The Journal of Geology,* vol. 20, no. 3, pp. 193-227.

IRELAND T. R., FLÖTTMAN T., FANNING D., & PRIESS W. V. 1998 Development of the early Palaeozoic Pacific margin of Gondwana from detrital ages across the Delamerian orogen, *Geology,* vol. 26, no. 3, pp. 243-246.

ISBELL J. L., HENRY, L. C., GULBRANSON E. L., FRAISER M. L., KOCH Z. J., COCCIOLO P. L. & DINEEN A. A. 2012 Glacial paradoxes during the late Palaeozoic ice age: Evaluating the equilibrium line altitude as a control on glaciation, *Gondwana Research,* vol. 22, pp. 1-19.

JACKSON S. E., PEARSON N., J., GRIFFIN W. L. & BELOUSOVA E. A. 2004 The application of laser ablation-inductively coupled plasma-mass spectrometry to in situ U-Pb zircon geochronology, *Chemical Geology,* vol. 211, pp. 47-69.

JOHNSON P. D. 1982a The Bluff Basalt Quarry, Kangaroo Island, E.M.L. 2983. GSSA Report Book No. 82/29.

JOHNSON P. D. 1982b The Geology of Chapman Basalt Quarry near Kingscote, Kangaroo Island. GSSA Report Book No. 82/18.

JONES M. J. 1987 Review of palynology, Arckaringa Basin, (NB/SR 12, Birribiana 1 and Hanns Knob 1). Palynological laboratory report No 542/1. Open file Envelope 4878, unpublished. pp. 739-756. Adelaide.

LE BLANC SMITH G. & ERIKSSON K. A. 1979 A fluvioglacial and glaciolacustrine deltaic depositional model for Permo-Carboniferous coals of the northeastern Karoo Basin, South Africa, *Palaeogeography, Palaeoclimatology, Palaeoecology,* vol. 27, pp. 67-84.

LENTZ D. R. 1996 Recent advances in lithogeochemical exploration for massive sulphide deposits in volcano-sedimentary environments: Petrogenetic, chemostratigraphic and alteration aspects with examples from the Bathurst Camp, New Brunswick. In CARROLL B. M. W. (ED). Current Research 1995, New Brunswick Department of Natural Resources and Energy, Minerals and Energy Division, Mineral Resource Report 96-1. pp. 73-119.

LIAGHATI T., PREDA M. & COX M. 2003 Heavy metal distribution and controlling factors within coastal plain sediments, Bells Creek catchment, southeast Queensland, Australia, *Environment International,* vol. 29, pp. 935-948.

LINTERN M. J., SHEARD M. J. & CHIVAS A. R. 2006 The source of pedogenic carbonate associated with gold-calcrete anomalies in the western Gawler Craton, South Australia. , *Chemical Geology,* vol. 235, pp. 299-324.

LÓPEZ-GAMUNDI O. R. & BUATOIS L. A. 2010 Introduction: Late Palaeozoic glacial events and post glacial transgressions in Gondwana, Geological Society of America Special Papers 2010, pp v-viii.

LUDBROOK N. H. 1961 Permian to Cretaceous subsurface stratigraphy between Lake Phillipson and the Peake and Denison Ranges, South Australia, *Transactions of the Royal Society of South Australia,* vol. 85, pp. 67-80.

LUDBROOK N. H. 1967 Permian deposits of South Australia and their fauna, *Transactions of the Royal Society of South Australia,* vol. 91, pp. 65-92.

LUDBROOK N. H. 1969a Palaeozoic: The Permian Period. In PARKIN L. W. ed. Handbook of South Australian Geology. pp. Chapter 3: 117-132. Adelaide: Geological Survey of South Australia.

LUDBROOK N. H. 1969b Permian of South Australia - A review, *Geological Society of Australia - Special Publication,* vol. 2, pp. 39-45.

LUDWIG K. R. 2003 User's manual for Isoplot 3.6: a geochronological toolkit for Microsoft Excel, *Berkeley Geochronology Center,* vol. Special Publication 4.

MAIDMENT D. W., WILLIAMS I. S. & HAND M. 2007 Testing long-term patterns of basin sedimentation by detrital zircon geochronology, Centralian Superbasin, Australia, *Basin Research,* vol. 19, no. 3, pp. 335-360.

MIALL A. D. 2000 Principles of Sedimentary Basin Analysis (3rd edition). Springer, Berlin, Germany.

MARGOLD M., STOKES C. R., & CLARK C. D. 2015 Ice Streams in the Laurentide Ice Sheet: Identification, characteristics and comparison to modern ice sheets, Earth-Science Reviews, vol 143, pp. 117-146.

MARTIN H. 1981 The Late Palaeozoic Gondwana glaciation, *Geologische Rundschau,* vol. 70, pp. 480-496.

MATSUOKA N. 1990 The rate of bedrock weathering by frost action: Field measurements and a predictive model, *Earth Surface Processes and Landforms,* vol. 15, no. 1, pp. 73-90.

MAWSON D. 1962 Varve shales associated with the Permo-Carboniferous glacial strata of South Australia, *Transactions of the Royal Society of South Australia*, pp. 160-161.

MCCLENAGHAN M. B. & DILABIO R. N. W. 1993 Till geochemistry and its implications for mineral exploration: Southeastern Cape Breton Island, Nova Scotia, Canada, *Quaternary International,* vol. 20, pp. 107-122.

MCCLENAGHAN M. B., THORLEIFSON L. H. & DILABIO R. N. W. 2000 Till geochemical and indicator mineral methods in mineral exploration, *Ore Geology Review,* vol. 16, pp. 145-166.

MCGOWRAN B. 1973 Rifting and drift of australia and the migration of mammals, *Science (New York, NY),* vol. 180, no. 4087, p. 759.

MCLENNAN S. M. 1989 Rare earth elements in sedimentary rocks: Influence of provenance and sedimentary processes. In LIPIN B. R. & MCKAY G. (EDS). Geochemistry and mineralogy of rare earth elements Vol. Reviews in Mineralogy 21. pp. 169-200.

MCMARTIN L. & MCCLENAGHAN M. B. 2001 Till geochemistry and sampling techniques in glaciated shield terrain: A review. In MCCLENAGHAN M. B.*, et al.* eds. Drift Exploration in Glaciated Terrain. pp. 19-43. Geological Society, London, Special Publications 185.

MCQUEEN K. G. 2006 Unravelling the Regolith with geochemistry. Regolith 2006 - Consolidation and Dispersion of Ideas.

MENPES S. 2013 Organic rich shale in Permian fjords - A potential resource play in the Arckaringa Basin, South Australia. American Association of Petroleum Geologists.

MENPES S., KORSCH R. J. & CARR L. K. 2010 2008 Gawler Craton-Office Basin-Musgrave Province-Amadeus Basin (GOMA) seismic survey, 08GA-OM1: Geological interpretation of the Arckaringa Basin.

MII H.-D., SHI G. R., CHENG C-J. & CHEN Y-Y. 2011 Permian Gondwanaland palaeoenvironment inferred from carbon and oxygen isotope records of brachiopod fossils from the Sydney Basin, southeast Australia, *Chemical Geology*.

MIKHALSKY E. V., BELIATSKY B. V., SAVVA E. V., WETZEL H-U., FEDOROV L. V., WEOSER TH. & HAHNE K. 1997 Reconnasissance Geochronologic Data on Polymetamorphic and Igneous Rocks of the Humboldt Mountains, Central Queen Maud Land, East Antarctica, *The Antarctic Region: Geological Evolution and Processes*, pp. 45-53.

MILNES A. R. & BOURMAN B. P. 1972 A Late Palaeozoic glaciated granite surface at Port Elliot, South Australia, *Transactions of the Royal Society of South Australia,* vol. 96, no. 3, pp. 149-155.

MILNES A. R., COOPER B. J. & COOPER J. A. 1981 The Jurassic Wisanger Basalt of Kangaroo Island, South Australia. GSSA Report Book No. 81/83. Adelaide.

MORY A. J. & BACKHOUSE J. 1997 Permian Stratigraphy and palynology of the Carnarvon Basin, Western Australia, Report 51. Geological Survey of Western Australia.

MORY A. J., HAIG D. W., MCLOUGHLIN S. & HOCKING R. M. 2005 Geology of the Northern Perth Basin, Western Australia - A field guide, Record 2005/9. Geological Survey of Western Australia.

NESBITT R. W. & YOUNG G. M. 1989 Formation and diagenesis of Weathering Profiles, *The Journal of Geology,* vol. 97, no. 2, pp. 129-147.

NEUMANN N. L. & FRASER G. L. 2007 Geochronological sythesis and Time-Space plots for Proterozoic Australia. Geoscience Australia Record 2007/06.

NORMINGTON V., DONNELLAN N. & EDGOOSE C. 2016 Central Australia, an island paradise: Were the Musgrave Province and Arunta Region exposed during Neoproterozoic sedimentation in the Amadeus Basin? 2016 Australian Earth Sciences Convention Abstracts. Adelaide, South Australia: Geological Society of Australia.

NORMINGTON V. J., DONNELLAN N. & EDGOOSE C. 2015 Neoproterozoic evolution of the Amadeus Basin: evidence from sediment provenance and mafic magmatism. NTGS record 2015-002. Annual Geoscience Exploration Seminar (AGES) 2015. Record of abstracts. Northern Territory Geological Survey.

O'BRIEN P. E. 1986 The Permian glacial sediments of central Victoria and the Murray Basin - their sedimentology and geochemisty. Department of Geology. Melbourne: University of Melbourne.

O'BRIEN P. E., BROWEN R. L., THOMAS G. A., CRAIG M. A. & HOLDGATE G. R. 2003 Permian: sedimentation around a continental ice sheet. In BIRCH W. D. (ED). Geology of Victoria.

PARKER A. J. 1985 Tectonic development and metallogeny of the Kanmantoo Trough in South Australia. Geological Survey of South Australia Report Book 85/10.

PARKIN L. W. 1956 Notes on the younger glacial remnants for northern South Australia, *Transactions of the Royal Society of South Australia,* vol. 79, pp. 148-151.

PAULSEN T. S., ENCARNACION J., GRUNOW A. M., LAYER P. W. & WATKEYS M. 2007 New age constraints for a short pulse in Ross orogen deformation triggered by East-West Gonwana suturing, *Gondwana Research,* vol. 12, pp. 417-427.

PAULSEN T. S., ENCARNACION J., GRUNOW A. M., VALENCIA V. A., PEACHA M., LAYER P. W., STUMP E., ROESKA S., THAO S. & RASAZANAMPARANY C. 2013 Detrital mineral ages from the Ross Supergroup, Antarctica: Implicaitons for the Queen Maud terrane and outboard sediment provenance on the Gondwana margin, *Gondwana Research*.

PAYNE J. L., BAROVICH K. M. & HAND M. 2006 Provenance of metasedimentary rocks in the northen Gawler Craton, Australia: Implications for Palaeoproterozoic reconstructions, *Precambrian Research,* vol. 148, pp. 275-291.

PELL S. D., WILLIAMS I. S. & CHIVAS A. R. 1997 The use of protolith zircon-age fingerprints in determining the protosource areas for some Australian dune sands, *Sedimentary Geology,* vol. 109, pp. 233-260.

PILLANS B. 2007 Pre-Quaternary landscape inheritance in Australia, *Journal of Quternary Science,* vol. 22, pp. 439-447.

PLAYFORD P. 2011 The Permo-Carboniferous glaciation of Gondwana: its legacy in Western Australia. XVII International Congress on the Carboniferous and Permian. pp. 103. Perth, Australia.

PLAYFORD P. E., COCKBAIN A. E. & LOW G. H. 1976 Geology of the Perth Basin, Western Australia, Bulletin 124, unpublished. Perth.

PLUMLEE G. S. 1999 The environmental geology of mineral deposits. . The Environmental Geology of Mineral Deposits. Part A. pp. 71-116. Society of Economic Geologists

RILEY K. W., FRENCH D. H., FARRELL O. P., WOOD R. A. & HUGGINS F. E. 2011 Modes of occurrence of Trace and Minor Elements in Some Australian Coals, *International Journal of Coal Geology*.

ROBERTS P. S. 1984 Explanatory Notes on Bacchus Marsh and Ballan 1:50,000 Geological Maps.

ROGERS P. A. 2000 Giles, South Australia - Explanatory Notes. Government of South Australia, Adelaide.

ROGERS P. A., AMBROSE G. J., FLINT R. B. & BELPERIO A. P. 1996a WARRINA map sheet. South Australia Geological Atlas, 250 000 Series, Sheet SH 53-3. Adelaide.

ROGERS P. A., FREEMAN P. J., ALDAM R. G. & KWITKO G. 1996b Warrina, South Australia - Explanatory Notes. Goverment of South Australia, Adelaide.

SAIKIA B. K., WARD C. R., OLIVEIRA M. L. S., HOWER J. C., BARUAH B. P., BRAGA M. & SILVA L. F. 2014 Geochemistry and nano-mineralogy of two medium sulfur northeast Indian coals, *International Journal of Coal Geology,* vol. 121, pp. 26-34.

SARALA P., PULKKINEN E., OJALA V. J. & PELTONIEMI-TAIVALKOSKI A, 2009 Gold exploration using till at Petajalehto, northern Finland, *Geochemistry: Exploration, Environmental Analysis,* vol. 9, pp. 247-255.

SCHEFFLER K., HOERNES S. & SCHWARK L. 2003 Global changes during Carboniferous-Permian glaciation of Gondwana: Linking polar and equatorial climate evolution by geochemical proxies, *Geology,* vol. 31, no. 7, pp. 605-608.

SCOTT K. M. & PAIN C. F. 2008 Regolith science. CSIRO Publishing.

SCRIMGEOUR I. R. 2013 Aileron Province. In AHMAD M. & MUNSON T. J. eds. Geology and mineral resources of the Northern Territory; Special Publication 5. Northern Territory Government.

SHEARER A. 1994 Distribution of Permian sediments in the eastern Officer Basin, S.A, Open File Envelope 008591 R16, unpublished. In PIRSA ed. Adelaide.

SHILTS W. W. 1986 Glaciation of the Hudson Bay Region. In MARTINI I. P. (ED). Canadian Inland Seas, Elsevier Oceanography Series 44. Canada: Elsevier.

SHILTS W. W. 1993 Geological Survey of Canada's contribution to understanding the composition of glacial sediments, *Canadian Journal of Earth Science,* vol. 30, pp. 333-353.

SINGH V. P. & HARITASHYA U. K. 2011 Encyclopedia of snow, ice and glaciers. Springer.

SLAMA J.*, et al.* 2008 Plesovice zircon - A new natural reference material for U-Pb and Hf isotopic microanalysis, *Chemical Geology,* vol. 249, pp. 1-35.

TAYLOR G. & EGGLETON R. A. 2001 Regolith Geology and Geomorphology. Wiley and Sons, Brisbane.

THOMPSON B. P. & HORWITZ D. 1962 BARKER map sheet. South Australia Geological Altas, 1: 250 000 series, Sheet SI 54-13. Adelaide.

TOWNER R. R. 1981 Late Palaeozoic tillites of the Canning Basin, Western Australia. In HAMBERY M. J. & HARLAND W. B. (EDS). Earth's pre-Pleistocene glacial record. pp. 449-452. New York: Cambridge University Press.

TOWNSEND I. J. 1973 A synthesis of stratigraphic drilling in the Arckaringa Basin 1969 - 1971, Report Book No. 73/98. Adelaide.

TOWNSEND I. J. & LUDBROOK N. H. 1975 Revision of Permian and Devonian nomenclature of four formations in and below the Arckaringa Basin, *Quarterly Geological Notes,* vol. 54, no. April 1975, pp. 2-5.

TUCKER L. R. 1997 Correlation of Permian sandstones in the Officer, Arckaringa and Pedirka Basins, Open File Report Book 96/0019. Adelaide.

VAN DER HOEK B. & FORBES C. J. (EDS) 2013 Geological and Hydrological Atlas of the Gawler Craton, South Australia. First Edition. Deep Exploration Technologies Cooperative Research Centre. Internal Report 2013/326.

VEEVERS J. J. 2006 Updated Gondwana (Permian - Cretaceous) earth history of Australia, *Gondwana Research,* vol. 9, pp. 231-260.

VEEVERS J. J.*,* BELOUSOVA E., SAEED A., SIRCOMBE K., COOPER A. F. & READ S. E. 2006 Pan-Gondwanaland detrital zircons from Australia analysed for Hf-isotopes and trace elements reflect an ice-covered Antarctic provenance of 700 - 500 Ma age, T_{DM} of 2.0-1.0 Ga, and alkaline affinity, *Earth-Science Reviews,* vol. 76, pp. 135-174.

WADE B. P.*,* KELSEY D. E., HAND M. & BAROVICH K. M. 2008 The Musgrave Province: stitching north, west and south Australia, *Precambrian Research,* vol. 166, no. 1, pp. 370-386.

WILMOT J. G. 1987 Geophysical interpretation report 1985 Morphett-Arc seismic survey. Arckaringa block. Arckaringa North, Central and South areas, Open File Envelope 559, unpublished. Adelaide.

WOLFF K., GILES, D., TIDDY C., & GORDON G. in review. Using Ca/Sr ratios to identify pedogenic carbonates derived from weathered marine limestones: Implications for mineral exploration using calcrete sampling, *Journal of Geochemical Exploration*.

WOPFNER H. 1964 Permian-Jurassic history of the western Great Artesian Basin, *Transactions of the Royal Society of South Australia,* vol. 88, no. 117-132.

WOPFNER H. 1972 Depositional history and tectonics of South Australian sedimentary basins, *Mineral Resources Review,* vol. 133, pp. 32-50.

WOPFNER H. 1977 Mount Toondina - ?Diapir or Astrobleme, *Quarterly Geological Notes,* vol. 62, no. April 1977, pp. 21-24.

WOPFNER H. & JIN X. C. 2009 Pangea megasequences of the Tethyan Gondwana-margin reflect global changes of climate and tectonism in Late Palaeozoic and Early Triassic times - A review, *Palaeoworld,* vol. 18, pp. 169-192.

YANG J., CAWOOD P. A., DU Y., FENG B. & YAN J. 2014 Global continental weathering trends across the Early Permian glacial to postglacial transition: Correlating high-and low-paleolatitude sedimentary records, *Geology,* vol. 42, no. 10, pp. 835-838.

YOULES I. P. 1976 Mount Toondina impact structure, *Quarterly Geological Notes, Geological Survey of South Australia,* vol. 60, pp. 10-12.

ZANG W.-L. & CRAWFORD A. R. 2009 Maitland 1:250 000 geological map. 2nd Edition ed. Adelaide.

ZANG W.-L. & HORE S. 2001 TER 1, Yorke Peninsula. Well completion report. GSSA Report Book 2001/017. South Australia.

ZANG W.-L. & HORE S. 2003 Yorke Peninsula basement drilling and contribution to regional geology, *Mesa Journal,* vol. 28, no. January pp. 53-55.

Appendix 1: Detailed descriptions of measured sections in the Troubridge Basin

Hallett Cove section

The northernmost known occurrence of the Cape Jervis Formation on the Fleurieu Peninsula is in the coastal cliffs of Hallett Cove (Figures 2:1, 2.4a). The area is host to a well-preserved exposure of Cape Jervis Formation and the underlying glaciated pavements. The section investigated is begins at the edge of the shore platform and is exposed in a 30m interval in the incised gullies of Sugarloaf Creek (Figure 2:4a).

The basement rocks within the Hallett Cove area dominantly comprise Neoproterozoic Wilpena Group sedimentary rocks. These sedimentary rocks are well preserved as a glaciated pavement, which is best exposed at the top of Black Cliff, north of Sugarloaf Creek (Figure 2:5a). The glaciated pavement has been polished and striated and preserves chatter marks and grooves (Figure 2:5a). Bourman and Alley (1990) calculated a northwesterly ice movement direction using measurements of the striae and till fabric studies. There is no exposed glacial bedrock pavement at the base of the measured section, at Sugarloaf Creek, however, diamictites overlie polished pavement at Black Cliff (Figure 2:5b).

The lowermost 2 metres of the Sugarloaf Creek section consists of diamictite that is exposed on the shore platform and in the mouth of the creek. The diamictite has been assigned to unit two of the Cape Jervis Formation (Bourman and Alley 1990). Clasts comprise up to 70% of the whole rock, range from 1 to 45 cm in size and are rounded to angular, though angular clasts are more common. Many of the rounded to subrounded clasts are polished, striated and faceted. The majority of clasts are locally-derived Wilpena Group sedimentary rocks with lesser (~5%) Encounter Bay Granite clasts. The diamictite matrix coarsens upward from grey-green sandy clay to buff coloured coarse-grained sand (Figure 2:4b). The shore platform is also littered boulders and pebbles that have been eroded from the sedimentary rocks above and with erratics (Figure 2:5c). Larger erratics (up to five m), comprise locally-derived shale of the Neoproterozoic basement. Smaller erratics (up to one m) also comprise largest Encounter Bay Granite.

At the mouth of the Sugarloaf Creek there is an accumulation of polished, rounded and striated rocks that are on average greater than 50 cm in diameter (Figure 2:5d). These boulders are derived from diamictite units higher in the section. The top of unit two and bottom of unit three in this area is obscured by approximately four metres of grasses and aeolian sands (Figure 2:4b).

Unit three in the Hallett Cove area comprises ~28 m of clay, silt and medium to coarse-grained sand beds with minor diamictite and pebble beds (Figures 2:4b, 2:5e to g). The lowermost ten metres of unit three comprises silty clay (clay with 50 to 70% silt) beds interbedded with lesser medium to coarse-grained sand beds. The silty clay beds are pale grey with orange and red mottles and up to two metres thick. The sand beds are buff coloured, up to 8m thick and dominantly comprise coarse-grained quartz dominated, unconsolidated sand with clay mineral cement. A pebble layer (~10 cm thick) is preserved within this part of the section (Figure 2:4b). Pebbles make up 50% of the layer, are up to 35 cm size and comprise dominantly of Wilpena Group sedimentary rocks. Dropstones are also occasionally preserved. The dropstones are up to 50 cm size and also comprise Wilpena Group sedimentary rocks.

The dropstones deform the sediment underneath them and are draped by sediment on top (Figure 2:5f, g).

The silty clay beds are overlain by about seven metres of red and purple medium- to coarse-grained sandstone beds interbedded with occasional diamictite and clay beds (Figure 2:5e). The sandstone beds vary from consolidated to friable. The sandstone comprises coarse-grained, angular quartz sand with clay mineral cement. The diamictite beds are 0.5 to 2 m thick. The clasts comprise 40% of the whole rock, are angular, up to 5cm and consists mostly of Wilpena Group sedimentary rocks. The matrix of the diamictite is coarse- to very coarse-grained sand. A pebble lens is preserved within one of the lower sandstone beds (Figure 2:4b). The pebble lens is up to 50 cm thick and is dominated by subangular Neoproterozoic Wilpena Group sedimentary rocks.

The red and purple sandstone dominated beds are overlain by about five metres of coarse-grained, buff to yellow sandstone and a thick (~50 cm) diamictite lens. The sandstone contains occasional layers of fine- to medium-grained, red, unconsolidated sand up to 20cm thick. These red sand beds also preserve red and orange Fe-oxide mottles (goethite; Figure 2:4b) and thin red laminations (Figure 2:5e). The diamictite at the top of the sandstone comprises clasts up to 50 cm in diameter and comprise of Wilpena Group sediment and lesser Encounter Bay Granites. The matrix of the diamictite is a very coarse-grained sand. Several <1m size dropstones occur within the sandstone. The majority of the dropstones are between the diamictite lenses and are rounded, polished and some are striated. Some of the dropstones have disturbed the sedimentary rocks directly below them (Figure 2:5f).

At the top of the exposed unit three and directly behind and including much of the Sugarloaf is 2 to 3 m of partially consolidated, medium- to coarse-grained, yellow, bedded sandstone. The sandstone comprises of subrounded to rounded, coarse-grained quartz grains with clay mineral (kaolinite and montmorillonite) cement (Figure 2:4b). A thin (20 cm) pebble lens is preserved in the middle of the sandstone (Figure 2:4b). The pebbles are rounded and are all locally-derived, Wilpena Group sedimentary rocks and between 5 and 10 cm in diameter. Several metres of loosely consolidated Pliocene Hallett Cove Sandstone overlie the top of the exposed Cape Jervis Formation in this area.

Kings Point section

The coastal cliffs of Kings Point preserve 14 m of Cape Jervis Formation exposed in two erosional gullies (Figure 2:6a). Both sections unconformably overlie the Cambrian Petrel Cove Formation of the Kanmantoo Group (Bourman and Alley 1995). It is not clear whether the late Palaeozoic sedimentary rocks of the southwestern gully directly overlie the late Palaeozoic sedimentary rocks of the eastern gully or if some late Palaeozoic sedimentary rocks have been eroded creating a disconformity between the sections.

The base of the section is exposed in the eastern erosional gully and are part of unit three (Figure 2:6b). Approximately 1m of dark red, massive, silty clay beds contain occasional rounded and polished, 5cm clasts typical of the underlying strata. Overlying the silty clay beds is 4.5 m of alternating fine-grained sand and silty clay beds. The fine-grained sand beds are grey-green with orange mottles of goethite (Figure 2:6b). The sand comprises of coarse-grained quartz with clay mineral (montmorillonite and kaolinite) cement. The 0.2 to 1 m thick clay beds comprise montmorillonite, kaolinite and nontonite (Figure 2:6b) and include rounded and polished 40 cm clasts derived from the local metasedimentary rocks (Figure 2:7a). Smaller (up to 20 cm) granitic clasts also occur throughout the clay beds. These are typical of the Encounter Bay Granite exposed a kilometre to the east. Rounded, polished and

occasionally faceted erratics (up to five m) typical of the Encounter Bay Granite and Kanmantoo Group metasedimentary rocks within the gully have Cape Jervis Formation deposited against them.

The unit four of the Cape Jervis Formation is exposed in the southwestern gully (Figure 2:6a). The unit comprises ~8.5 m of diamictite interbedded with sandstone. The lowermost diamictite beds are up to two metres thick (Figure 2:6b). Clasts comprise of 25 to 75% of the whole rock, are mostly 20 cm, can be up 40 cm, and are rounded to angular in shape. Rounded clasts are often polished and striated. The clasts are typical of Kanmantoo Group metasedimentary rocks and Encounter Bay Granite. The diamictite matrix coarsens upward from clay to coarse-grained sand (Figure 2:6b). The lowermost 1.5 m of diamictite is faintly laminated with a grey clay matrix consisting of montmorillonite and kaolinite (Figure 2:6b). Higher in the sequence the diamictite comprises of fine-grained, friable sand. The buff coloured, medium-grained sandstone interbeds are up to two metres thick. Lenses of pebbles throughout the diamictite consist of the same lithology as the diamictite clasts. The pebbles are up to 50 cm and are typically rounded and polished (Figure 2:7b).

The upper four metres of sediment exposed in the southwestern gully exposes diamictite and coarse-grained sandstone beds. The diamictite beds are up to one metre thick, and are massive with either coarse-grained sandstone matrix or clast-supported with minimal coarse-grained sandstone matrix. Clasts typical of Kanmantoo Group metasedimentary rocks and Encounter Bay Granite are rounded to subangular and up to 50 cm. The base of each diamictite bed is defined by a pebble bed consisting of clasts with the same features as the diamictite clasts. The diamictite matrix comprises montmorillonite, kaolinite, quartz as well as goethite and hematite (Figure 2:6b). Medium-grained sandstone beds and lenses are throughout the unit. The sandstone is yellow with angular to rounded, poorly sorted quartz with lesser rock fragments that are of the same composition as the clasts within the diamictite. The gully is littered with Encounter Bay Granite erratics that are up to 2.5 m, rounded and polished (Figure 2:7c). The Cape Jervis Formation is overlain by up to ten metres of Tertiary sands.

Waterloo Bay section

The Waterloo Bay section preserves approximately three metres of Cape Jervis Formation that are unconformably overlain by about four metres of Quaternary sedimentary rocks (Figures 2:8a, 2.9a). The Quaternary sedimentary rocks unconformity is well preserved and is an undulating surface.

The Cape Jervis Formation in the Waterloo Bay section consists of bedded clay and diamictite of unit four overlain by massive clay of unit five. The lowermost metre of the exposed sedimentary rocks comprises alternating 30 to 50 cm thick silty clay and diamictite beds (Figure 2:8b). The beds are green in colour and dominantly comprise montmorillonite, phengite and muscovite (Figure 2:8b). Hard, red and orange mottles of hematite and goethite are also preserved on the surface of the silty clay beds (Figure 2:9b). Clasts within the diamictite are subrounded and range from <1 to 15 cm. The clast lithology is variable. Larger clasts (<10 cm) are typical of Encounter Bay Granite (Figure 2:9b) and smaller clasts are typical of locally-derived granite, sandstone and metamorphic basement and Kanmantoo Group metasedimentary rocks. The matrix of the diamictite beds is the same material as the silty clay beds and preserves the same colour and mottling and mineralogy.

Approximately two metres of unit five overlies the interbedded clay and diamictite beds consisting of clay with lesser sandstone (Figure 2:8b). Clay beds are up to 50 cm thick, massive, prismatic fractured, and green in colour with red and orange mottles of hematite and goethite (Figure 2:9c). The fine-grained, sandstone bed (<20 cm) is red with some patches of white, the sandstone is extremely hard.

Mottles in the clay decrease towards the top of the section. Larger erratics of the same lithologies as the clasts in the diamictites are scattered along the shore line near the section and along Waterloo Bay. The section is overlain by a palaeosol containing alunite and Quaternary limestone and calcrete.

Kingscote Composite section

The unit underlying the Cape Jervis Formation sedimentary rocks in the Bluff Quarry and Kingscote foreshore sections is unknown although it is interpreted that the sedimentary rocks are underlain by Cambrian Kanmantoo Group metasedimentary rocks as seen at other locations on the Kangaroo Island (Bourman and Alley 1999). The sedimentary rocks of the Bluff Quarry section comprise interbedded silty clay, diamictite and sandstone (Figure 2:10b). The silty clay beds are 0.5 to 3 m thick (Figure 2:10b), and comprise grey-green, bedded, clay (kaolinite) with some thin (<0.1 cm) beds of goethite (Figure 2:11a). Diamictite beds are up to one metre thick (Figure 2:10b). Clasts within the diamictite are less than 0.5 cm size, rounded to angular, and comprise metasedimentary rocks typical of the Kanmantoo Group. The matrix of the diamictite is fine-grained silty sand and preserves bedding Sandstone beds have variable bed thickness and grain size. The lowermost sandstone has bedding preserved by hard, pink, medium- to coarse-grained sandstone beds (Figure 2:11c). More commonly, the sandstone is fine- to coarse-grained, with subrounded to rounded quartz (Figure 2:11b) with clay mineral (kaolinite and montmorillonite) cement. Planar and trough cross-bedding occurs sporadically throughout the section (Figure 2:11d) although it is typically poorly-preserved (Figure 2:10b). The uppermost sandstone in the Bluff Quarry section is a fine- to coarse-grained, upward coarsening buff coloured sandstone that is ~40 cm thickness. The section is overlain by Jurassic Wisanger Basalt (Figure 2:11a).

The Cape Jervis Formation sedimentary rocks exposed in the coastal cliffs near the Kingscote Warf (Figure 2:10a) are a sequence of clay to sandstone beds (Figure 2:11e). The lowermost 3m are dominated by silty to fine-grained sandstone beds (Figure 2:10b) with kaolinite and gypsum cement (Figure 2:10b). Approximately three metres of buff coloured, massive clay overlie the indurated sandstone (Figure 2:11f). The base of this clay has prismatic fractures and orange mottles (Figure 2:11g) are throughout the clay unit. The uppermost three metres of the section consists of fine-grained sandstone. The sandstone is yellow with purple and orange (hematite and goethite) mottles. This unit is unconsolidated except in places where the beds are contorted.

Appendix 2: Geochronology

Reported U-Pb zircon standard values and values generated during analysis

Standard	n	$^{207}Pb/^{206}Pb$ age (Ma)	$^{206}Pb/^{238}U$ age (Ma)	$^{207}Pb/^{235}U$ age (Ma)	Reference
GJ-1 (TIMS)		608.3	600.7	602.2	Jackson *et al.* (2004)
GJ-1*	145	603.3 ± 6.8	591.5 ± 4.9	593.6 ± 4.8	This study
Plešovice (TIMS)			337.13 ± 0.37		Slama *et al.* (2008)
Plešovice*	44	372 ± 30	333.5 ± 5.5	336.9 ± 7	This study

*Normalised standard is reported. Errors provided are 2σ

Troubridge Basin – Cape Jervis Formation

Cape Jervis Section - unit 2

Spot No.	$^{207}Pb/^{235}U$	Error ±2 σ	$^{206}Pb/^{238}U$	Error ±2 σ	$^{207}Pb/^{235}U$	Error ±2 σ	$^{207}Pb/^{206}Pb$ age (Ma)	Error ± (Ma)	$^{206}Pb/^{238}U$ age (Ma)	Error ± (Ma)
z01-1	11.5225	0.1155	0.4268	0.0042	11.5225	0.1155	2792.20	16.83	2291.20	19.10
z02-1	0.9240	0.0097	0.1083	0.0011	0.9240	0.0097	671.80	23.06	662.60	6.21
z03-1	0.7812	0.0082	0.0965	0.0010	0.7812	0.0082	556.50	23.56	594.00	5.60
z04-1	2.0659	0.1060	0.0653	0.0023	2.0659	0.1060	3049.70	93.75	407.60	14.08
z05-1	0.8296	0.0102	0.0947	0.0010	0.8296	0.0102	728.10	26.82	583.00	5.66
z06-1	1.1648	0.0117	0.0989	0.0010	1.1648	0.0117	1326.10	19.90	607.80	5.69
z07-1	0.7662	0.0090	0.0960	0.0010	0.7662	0.0090	526.70	26.73	590.70	5.66
z08-1	0.7194	0.0080	0.0898	0.0009	0.7194	0.0080	533.10	25.47	554.60	5.28
z09-1	1.6681	0.0166	0.0800	0.0008	1.6681	0.0166	2359.80	17.47	496.30	4.70
z10-1	2.3655	0.0277	0.1702	0.0017	2.3655	0.0277	1639.40	22.54	1013.30	9.61
z11-1	0.9478	0.0104	0.0938	0.0010	0.9478	0.0104	1022.20	22.28	577.90	5.60
z12-1	4.5989	0.0460	0.1672	0.0017	4.5989	0.0460	2822.30	16.37	996.50	9.23
z13-1	0.8797	0.0111	0.0993	0.0010	0.8797	0.0111	750.90	26.96	610.00	6.04
z14-1	1.0585	0.0121	0.0703	0.0007	1.0585	0.0121	1786.60	21.29	437.90	4.37
z15-1	0.7966	0.0089	0.0971	0.0010	0.7966	0.0089	586.20	24.56	597.20	5.79
z16-1	0.9666	0.0170	0.1083	0.0012	0.9666	0.0170	766.70	38.09	662.60	7.17
z17-1	2.0738	0.0228	0.1916	0.0020	2.0738	0.0228	1159.90	22.03	1129.90	10.55
z18-1	1.6554	0.0173	0.1503	0.0015	1.6554	0.0173	1193.90	20.70	902.70	8.48
z19-1	1.1749	0.0123	0.0698	0.0007	1.1749	0.0123	1986.60	18.84	435.00	4.25
z20-1	13.957	0.1392	0.4359	0.0044	13.957	0.1392	3067.60	15.95	2332.10	19.55
z21-1	7.9578	0.0800	0.2683	0.0027	7.9578	0.0800	2944.60	16.16	1532.20	13.73
z22-1	0.8455	0.0109	0.0982	0.0010	0.8455	0.0109	690.80	27.94	603.60	6.05
z23-1	5.0652	0.0510	0.1912	0.0019	5.0652	0.0510	2761.00	16.44	1127.70	10.42
z24-1	0.8325	0.0099	0.1022	0.0011	0.8325	0.0099	569.60	25.56	627.50	6.17
z25-1	0.7792	0.0092	0.0952	0.0010	0.7792	0.0092	580.70	25.71	586.20	5.77
z26-1	1.1472	0.0122	0.1230	0.0013	1.1472	0.0122	858.00	22.06	747.80	7.16
z27-1	1.6583	0.0177	0.1443	0.0015	1.6583	0.0177	1277.40	20.88	869.00	8.27
z28-1	14.256	0.1447	0.5368	0.0054	14.256	0.1447	2764.90	16.58	2769.90	22.78
z29-1	1.6265	0.0168	0.1623	0.0016	1.6265	0.0168	1005.90	20.93	969.30	9.09
z30-1	0.8013	0.0087	0.0938	0.0010	0.8013	0.0087	673.30	23.25	577.90	5.62
z31-1	0.8754	0.0106	0.0915	0.0010	0.8754	0.0106	910.90	25.41	564.30	5.59
z32-1	7.3187	0.0755	0.3767	0.0038	7.3187	0.0755	2238.60	17.91	2061.00	17.84
z33-1	1.0981	0.0117	0.1090	0.0011	1.0981	0.0117	1015.90	21.66	667.00	6.40
z34-1	5.4898	0.0555	0.1373	0.0014	5.4898	0.0555	3417.40	15.80	829.60	7.84
z35-1	0.7983	0.0094	0.0946	0.0010	0.7983	0.0094	647.10	25.44	582.60	5.70
z36-1	1.4504	0.0149	0.0887	0.0009	1.4504	0.0149	1936.00	18.50	547.70	5.29
z37-1	0.7741	0.0110	0.0950	0.0010	0.7741	0.0110	570.80	31.58	585.10	5.95
z38-1	2.0357	0.0205	0.0599	0.0006	2.0357	0.0205	3163.70	15.99	374.80	3.65

Spot No.	$^{207}Pb/^{235}U$	Error ±2 σ	$^{206}Pb/^{238}U$	Error ±2 σ	$^{207}Pb/^{235}U$	Error ±2 σ	$^{207}Pb/^{206}Pb$ age (Ma)	Error ± (Ma)	$^{206}Pb/^{238}U$ age (Ma)	Error ± (Ma)
z39-1	2.2237	0.0224	0.1184	0.0012	2.2237	0.0224	2180.40	17.58	721.20	6.84
z40-1	2.2148	0.0359	0.1090	0.0013	2.2148	0.0359	2315.40	29.68	667.10	7.80
z41-1	1.7927	0.0183	0.1334	0.0013	1.7927	0.0183	1576.70	19.33	807.10	7.57
z42-1	0.7446	0.0079	0.0743	0.0007	0.7446	0.0079	1006.40	21.82	461.80	4.47
z43-1	1.1908	0.0124	0.0905	0.0009	1.1908	0.0124	1537.40	19.86	558.30	5.36
z44-1	0.8495	0.0088	0.0799	0.0008	0.8495	0.0088	1125.00	20.97	495.30	4.76
z45-1	2.4350	0.0244	0.0627	0.0006	2.4350	0.0244	3373.60	15.86	391.70	3.79
z46-1	2.5879	0.0272	0.1984	0.0020	2.5879	0.0272	1520.80	20.09	1166.50	10.72
z47-1	1.3923	0.0142	0.1157	0.0012	1.3923	0.0142	1366.40	19.81	705.90	6.66
z48-1	1.0434	0.0108	0.0539	0.0005	1.0434	0.0108	2231.10	18.25	338.60	3.31
z49-1	2.4506	0.0245	0.0954	0.0010	2.4506	0.0245	2710.80	16.68	587.10	5.58
z50-1	0.8127	0.0092	0.0975	0.0010	0.8127	0.0092	619.60	24.80	599.90	5.79
z51-1	2.9353	0.0296	0.1921	0.0019	2.9353	0.0296	1813.10	18.49	1132.70	10.36
z52-1	0.8781	0.0108	0.1051	0.0011	0.8781	0.0108	624.80	27.08	644.30	6.30
z53-1	144.72	3.2608	1.5017	0.0357	144.72	3.2608	4728.60	28.97	5911.20	92.05
z54-1	1.7420	0.0178	0.1545	0.0015	1.7420	0.0178	1240.80	20.25	925.90	8.61
z56-1	2.2193	0.0220	0.0903	0.0009	2.2193	0.0220	2637.30	16.60	557.10	5.31
z57-1	1.4485	0.0151	0.1485	0.0015	1.4485	0.0151	950.10	21.55	892.50	8.34
z58-1	3.0749	0.0437	0.1771	0.0020	3.0749	0.0437	2042.10	26.33	1051.00	11.01
z59-1	1.7667	0.0181	0.1587	0.0016	1.7667	0.0181	1215.20	20.41	949.60	8.82
z60-1	1.5695	0.0162	0.1566	0.0016	1.5695	0.0162	1005.20	21.13	938.00	8.72
z61-1	1.4364	0.0148	0.1276	0.0013	1.4364	0.0148	1238.10	20.42	773.90	7.31
z62-1	1.8137	0.0186	0.1754	0.0018	1.8137	0.0186	1069.20	20.68	1041.70	9.62
z63-1	27.406	0.2769	0.6668	0.0067	27.406	0.2769	3460.60	15.77	3293.70	26.02
z64-1	3.1201	0.0312	0.1081	0.0011	3.1201	0.0312	2900.60	16.35	661.80	6.28
z65-1	2.2814	0.0228	0.0878	0.0009	2.2814	0.0228	2730.10	16.57	542.20	5.19
z66-1	0.8003	0.0086	0.0983	0.0010	0.8003	0.0086	570.50	23.59	604.10	5.80
z67-1	12.221	0.1239	0.4836	0.0049	12.221	0.1239	2683.20	16.89	2542.90	21.13
z68-1	0.8586	0.0092	0.0917	0.0009	0.8586	0.0092	865.50	22.41	565.80	5.45
z69-1	1.6651	0.0497	0.0658	0.0013	1.6651	0.0497	2685.50	55.22	410.80	7.99
z70-1	1.7443	0.0204	0.1646	0.0017	1.7443	0.0204	1118.20	23.75	982.20	9.37
z71-1	7.2576	0.0775	0.1830	0.0019	7.2576	0.0775	3404.80	16.94	1083.50	10.46
z72-1	1.0084	0.0119	0.1133	0.0012	1.0084	0.0119	760.50	25.07	691.70	6.78
z73-1	1.2178	0.0125	0.1082	0.0011	1.2178	0.0125	1237.50	20.08	662.10	6.36
z74-1	2.2540	0.0236	0.2096	0.0021	2.2540	0.0236	1146.70	20.72	1226.80	11.33
z75-1	1.2536	0.0143	0.1235	0.0013	1.2536	0.0143	1031.70	22.93	750.50	7.30
z76-1	2.1160	0.0215	0.1490	0.0015	2.1160	0.0215	1678.80	18.63	895.40	8.43
z77-1	0.7607	0.0080	0.0823	0.0008	0.7607	0.0080	840.00	21.87	509.60	4.96
z78-1	3.1298	0.0315	0.0811	0.0008	3.1298	0.0315	3363.50	15.64	502.40	4.88
z79-1	2.0247	0.0254	0.0885	0.0010	2.0247	0.0254	2517.40	22.04	546.60	5.78
z80-1	3.9408	0.0417	0.1132	0.0012	3.9408	0.0417	3200.50	16.97	691.40	6.80
z81-1	1.6718	0.0170	0.0939	0.0010	1.6718	0.0170	2086.40	17.77	578.70	5.66
z82-1	1.3480	0.0148	0.1188	0.0012	1.3480	0.0148	1253.20	21.19	723.70	7.08
z83-1	7.8661	0.0803	0.4145	0.0043	7.8661	0.0803	2198.30	17.56	2235.60	19.39
z84-1	6.6808	0.0768	0.3285	0.0035	6.6808	0.0768	2317.70	19.93	1831.30	17.15
z85-1	9.8403	0.1014	0.4515	0.0047	9.8403	0.1014	2435.90	17.32	2402.00	20.70
z86-1	0.8840	0.0100	0.0965	0.0010	0.8840	0.0100	820.60	23.60	594.10	5.88
z87-1	1.6550	0.0165	0.0609	0.0006	1.6550	0.0165	2802.40	16.16	381.20	3.77
z88-1	1.5442	0.0156	0.1624	0.0017	1.5442	0.0156	899.10	20.57	969.90	9.16
z89-1	0.8394	0.0088	0.0999	0.0010	0.8394	0.0088	638.20	22.29	613.80	5.98
z90-1	0.8008	0.0090	0.0986	0.0010	0.8008	0.0090	564.60	24.51	606.20	5.98
z91-1	0.9047	0.0110	0.0902	0.0010	0.9047	0.0110	1006.90	24.68	556.70	5.63
z92-1	1.1447	0.0119	0.0636	0.0007	1.1447	0.0119	2106.60	17.94	397.20	3.96
z93-1	1.7089	0.0185	0.1543	0.0016	1.7089	0.0185	1205.00	21.04	925.00	8.91
z94-1	2.0677	0.0216	0.1348	0.0014	2.0677	0.0216	1819.40	18.57	815.40	7.87
z95-1	2.4638	0.0254	0.0681	0.0007	2.4638	0.0254	3261.00	15.87	424.70	4.22
z96-1	1.6507	0.0178	0.1527	0.0016	1.6507	0.0178	1156.70	20.99	916.20	8.81
z97-1	0.7744	0.0099	0.0910	0.0010	0.7744	0.0099	663.40	27.51	561.70	5.71
z98-1	1.6647	0.0177	0.1324	0.0014	1.6647	0.0177	1450.40	19.85	801.50	7.76
z99-1	2.0849	0.0224	0.1445	0.0015	2.0849	0.0224	1708.40	19.54	869.90	8.42
z100-1	1.6948	0.0176	0.0714	0.0007	1.6948	0.0176	2579.50	17.02	444.40	4.41
z101-1	0.7727	0.0088	0.0927	0.0010	0.7727	0.0088	620.30	24.74	571.60	5.61
z102-1	0.6802	0.0076	0.0831	0.0009	0.6802	0.0076	582.40	24.13	514.40	5.04
z103-1	0.8119	0.0092	0.0831	0.0009	0.8119	0.0092	954.60	23.37	514.60	5.08
z104-1	1.2105	0.0129	0.1268	0.0013	1.2105	0.0129	907.50	21.96	769.30	7.37
z105-1	8.5645	0.0867	0.2886	0.0029	8.5645	0.0867	2946.20	16.27	1634.50	14.59

Spot No.	$^{207}Pb/^{235}U$	Error ±2 σ	$^{206}Pb/^{238}U$	Error ±2 σ	$^{207}Pb/^{235}U$	Error ±2 σ	$^{207}Pb/^{206}Pb$ age (Ma)	Error ± (Ma)	$^{206}Pb/^{238}U$ age (Ma)	Error ± (Ma)
z106-1	1.2014	0.0132	0.1077	0.0011	1.2014	0.0132	1219.40	21.67	659.60	6.42
z107-1	0.7848	0.0107	0.0950	0.0010	0.7848	0.0107	601.80	29.87	585.00	5.93
z108-1	5.0593	0.0511	0.2308	0.0023	5.0593	0.0511	2446.10	16.99	1338.40	12.19
z109-1	8.1936	0.0849	0.4101	0.0042	8.1936	0.0849	2287.60	17.78	2215.20	19.09
z110-1	2.0653	0.0214	0.1354	0.0014	2.0653	0.0214	1810.50	18.77	818.70	7.79
z111-1	8.6500	0.0889	0.3529	0.0036	8.6500	0.0889	2632.60	16.80	1948.50	17.19
z112-1	1.5117	0.0175	0.1103	0.0012	1.5117	0.0175	1613.20	21.66	674.60	6.72
z113-1	0.7358	0.0082	0.0902	0.0009	0.7358	0.0082	573.60	23.84	556.80	5.49
z114-1	0.7850	0.0089	0.0940	0.0010	0.7850	0.0089	624.50	24.13	579.20	5.72
z115-1	1.7365	0.0191	0.1709	0.0018	1.7365	0.0191	1033.60	21.75	1017.10	9.71
z116-1	0.7835	0.0083	0.0772	0.0008	0.7835	0.0083	1032.20	21.18	479.20	4.73
z117-1	2.2505	0.0257	0.1897	0.0020	2.2505	0.0257	1339.40	22.06	1119.90	10.73
z118-1	1.1412	0.0123	0.1149	0.0012	1.1412	0.0123	988.00	21.89	700.90	6.82
z119-1	21.3979	0.2207	0.6982	0.0072	21.3979	0.2207	2997.70	16.30	3413.90	27.18
z120-1	1.9823	0.0215	0.1767	0.0018	1.9823	0.0215	1230.70	21.02	1049.00	9.97

Spot No.	Preferred age (Ma)	Error ± (Ma)	rho	Conc.
z01-1	2792.20	16.83	0.99	82
z02-1	662.60	6.21	0.94	99
z03-1	594.00	5.60	0.93	107
z04-1	3049.70	93.75	0.70	13
z05-1	583.00	5.66	0.83	80
z06-1	607.80	5.69	0.98	46
z07-1	590.70	5.66	0.85	112
z08-1	554.60	5.28	0.89	104
z09-1	2359.80	17.47	0.99	21
z10-1	1639.40	22.54	0.87	62
z11-1	577.90	5.60	0.93	57
z12-1	2822.30	16.37	1.00	35
z13-1	610.00	6.04	0.83	81
z14-1	1786.60	21.29	0.91	25
z15-1	597.20	5.79	0.91	102
z16-1	662.60	7.17	0.65	86
z17-1	1129.90	10.55	0.92	97
z18-1	902.70	8.48	0.96	76
z19-1	1986.60	18.84	0.97	22
z20-1	3067.60	15.95	1.00	76
z21-1	2944.60	16.16	1.00	52
z22-1	603.60	6.05	0.81	87
z23-1	2761.00	16.44	1.00	41
z24-1	627.50	6.17	0.86	110
z25-1	586.20	5.77	0.87	101
z26-1	747.80	7.16	0.95	87
z27-1	869.00	8.27	0.96	68
z28-1	2764.90	16.58	1.00	100
z29-1	969.30	9.09	0.98	96
z30-1	577.90	5.62	0.93	86
z31-1	564.30	5.59	0.85	62
z32-1	2238.60	17.91	0.98	92
z33-1	667.00	6.40	0.95	66
z34-1	3417.40	15.80	0.99	24
z35-1	582.60	5.70	0.87	90
z36-1	1936.00	18.50	0.98	28
z37-1	585.10	5.95	0.75	103
z38-1	3163.70	15.99	1.00	12
z39-1	2180.40	17.58	1.00	33
z40-1	2315.40	29.68	0.76	29
z41-1	1576.70	19.33	0.98	51
z42-1	461.80	4.47	0.94	46
z43-1	1537.40	19.86	0.97	36
z44-1	495.30	4.76	0.96	44
z45-1	3373.60	15.86	1.00	12
z46-1	1520.80	20.09	0.95	77
z47-1	705.90	6.66	0.98	52

Spot No.	Preferred age (Ma)	Error ± (Ma)	rho	Conc.
z48-1	2231.10	18.25	0.97	15
z49-1	2710.80	16.68	1.00	22
z50-1	599.90	5.79	0.90	97
z51-1	1813.10	18.49	0.99	62
z52-1	644.30	6.30	0.83	103
z53-1	4728.60	28.97	0.95	125
z54-1	925.90	8.61	0.98	75
z56-1	2637.30	16.60	0.99	21
z57-1	892.50	8.34	0.96	94
z58-1	2042.10	26.33	0.80	51
z59-1	949.60	8.82	0.98	78
z60-1	938.00	8.72	0.97	93
z61-1	773.90	7.31	0.97	63
z62-1	1041.70	9.62	0.98	97
z63-1	3460.60	15.77	1.00	95
z64-1	2900.60	16.35	1.00	23
z65-1	2730.10	16.57	1.00	20
z66-1	604.10	5.80	0.94	106
z67-1	2683.20	16.89	0.99	95
z68-1	565.80	5.45	0.94	65
z69-1	2685.50	55.22	0.67	15
z70-1	982.20	9.37	0.88	88
z71-1	3404.80	16.94	0.98	32
z72-1	691.70	6.78	0.87	91
z73-1	662.10	6.36	0.98	54
z74-1	1226.80	11.33	0.97	107
z75-1	750.50	7.30	0.90	73
z76-1	1678.80	18.63	0.99	53
z77-1	509.60	4.96	0.96	61
z78-1	3363.50	15.64	0.99	15
z79-1	2517.40	22.04	0.88	22
z80-1	3200.50	16.97	0.98	22
z81-1	2086.40	17.77	1.00	28
z82-1	723.70	7.08	0.95	58
z83-1	2198.30	17.56	0.99	102
z84-1	2317.70	19.93	0.93	79
z85-1	2435.90	17.32	1.00	99
z86-1	594.10	5.88	0.92	72
z87-1	2802.40	16.16	0.98	14
z88-1	969.90	9.16	0.99	108
z89-1	613.80	5.98	0.98	96
z90-1	606.20	5.98	0.92	107
z91-1	556.70	5.63	0.86	55
z92-1	2106.60	17.94	0.98	19
z93-1	925.00	8.91	0.96	77
z94-1	1819.40	18.57	0.99	45
z95-1	3261.00	15.87	1.00	13
z96-1	916.20	8.81	0.96	79
z97-1	561.70	5.71	0.83	85
z98-1	801.50	7.76	0.97	55
z99-1	1708.40	19.54	0.96	51
z100-1	2579.50	17.02	0.99	17
z101-1	571.60	5.61	0.90	92
z102-1	514.40	5.04	0.92	88
z103-1	514.60	5.08	0.90	54
z104-1	769.30	7.37	0.95	85
z105-1	2946.20	16.27	1.00	55
z106-1	659.60	6.42	0.93	54
z107-1	585.00	5.93	0.78	97
z108-1	2446.10	16.99	1.00	55
z109-1	2287.60	17.78	0.98	97
z110-1	1810.50	18.77	0.98	45
z111-1	2632.60	16.80	0.99	74
z112-1	1613.20	21.66	0.91	42
z113-1	556.80	5.49	0.93	97
z114-1	579.20	5.72	0.92	93
z115-1	1017.10	9.71	0.94	98

Spot No.	Preferred age (Ma)	Error ± (Ma)	rho	Conc.
z116-1	479.20	4.73	0.96	46
z117-1	1119.90	10.73	0.91	84
z118-1	700.90	6.82	0.95	71
z119-1	2997.70	16.30	0.99	114
z120-1	1049.00	9.97	0.95	85

Kings Point Section - unit 3

Spot No.	$^{207}Pb/^{235}U$	Error ±2 σ	$^{206}Pb/^{238}U$	Error ±2 σ	$^{207}Pb/^{235}U$	Error ±2 σ	$^{207}Pb/^{206}Pb$ age (Ma)	Error ± (Ma)	$^{206}Pb/^{238}U$ age (Ma)	Error ± (Ma)
Z01-1	0.7080	0.0129	0.0890	0.0011	0.0578	0.0011	521.00	40.10	549.30	6.30
Z02-1	3.8260	0.0456	0.2914	0.0032	0.0953	0.0011	1533.80	21.28	1648.70	16.05
Z03-1	0.7859	0.0093	0.0943	0.0010	0.0605	0.0007	620.20	24.01	581.10	6.07
Z04-1	0.8284	0.0113	0.0969	0.0011	0.0621	0.0008	676.70	28.29	596.00	6.38
Z05-1	1.0832	0.0123	0.0642	0.0007	0.1224	0.0013	1991.40	18.91	401.40	4.24
Z06-1	1.9513	0.0236	0.1797	0.0020	0.0788	0.0009	1167.50	22.78	1065.30	10.82
Z07-1	1.4775	0.0178	0.1459	0.0016	0.0735	0.0009	1028.20	23.07	877.90	9.02
Z08-1	0.6928	0.0092	0.0886	0.0010	0.0567	0.0007	480.60	28.58	547.40	5.84
Z09-1	1.1282	0.0137	0.1198	0.0013	0.0684	0.0008	879.40	23.97	729.40	7.58
Z10-1	3.4985	0.0391	0.2688	0.0029	0.0945	0.0010	1517.70	19.70	1534.60	14.82
Z12-1	0.8140	0.0176	0.1012	0.0013	0.0583	0.0013	541.30	47.90	621.70	7.67
Z13-1	0.8283	0.0168	0.0991	0.0013	0.0606	0.0012	625.80	43.47	609.30	7.40
Z14-1	1.6553	0.0272	0.1035	0.0013	0.1160	0.0019	1896.10	29.49	634.80	7.64
Z15-1	0.7790	0.0141	0.0945	0.0012	0.0598	0.0011	595.10	39.04	582.40	6.83
Z16-1	0.8421	0.0132	0.0900	0.0011	0.0679	0.0010	864.40	31.43	555.60	6.34
Z17-1	0.9803	0.0238	0.1007	0.0014	0.0707	0.0018	947.30	50.16	618.30	8.22
Z18-1	1.1049	0.0167	0.1228	0.0015	0.0653	0.0010	783.90	30.46	746.40	8.32
Z19-1	0.8490	0.0132	0.1004	0.0012	0.0614	0.0009	652.10	32.23	616.50	6.96
Z20-1	0.9618	0.0149	0.1021	0.0012	0.0683	0.0010	878.50	30.89	626.80	7.10
Z21-1	0.8118	0.0119	0.0989	0.0012	0.0596	0.0009	590.40	30.60	607.90	6.74
Z22-1	0.8209	0.0110	0.0986	0.0011	0.0605	0.0008	619.80	27.28	606.50	6.61
Z26-1	7.7673	0.0923	0.3963	0.0045	0.1424	0.0016	2256.40	18.86	2151.80	20.71
Z27-1	1.5529	0.0263	0.1510	0.0019	0.0747	0.0013	1061.20	33.60	906.30	10.37
Z28-1	0.7975	0.0116	0.0964	0.0011	0.0601	0.0008	606.80	30.12	593.30	6.58
Z29-1	0.8409	0.0137	0.0945	0.0011	0.0647	0.0010	763.70	33.60	581.80	6.65
Z30-1	0.7962	0.0118	0.0975	0.0011	0.0593	0.0009	579.40	30.94	599.60	6.67
Z31-1	2.3924	0.0325	0.2146	0.0025	0.0809	0.0010	1218.80	24.83	1253.40	13.47
Z32-1	0.9725	0.0132	0.1157	0.0014	0.0610	0.0008	638.90	26.95	705.80	7.82
Z33-1	0.8214	0.0111	0.0993	0.0012	0.0600	0.0008	604.30	26.95	610.40	6.81
Z34-1	0.8122	0.0119	0.0972	0.0012	0.0606	0.0009	626.60	29.91	598.00	6.78
Z35-1	3.7130	0.0451	0.2819	0.0033	0.0956	0.0011	1539.50	20.55	1601.00	16.38
Z36-1	0.8748	0.0145	0.1034	0.0013	0.0614	0.0010	654.20	34.24	634.00	7.37
Z37-1	4.0323	0.0495	0.2500	0.0029	0.1170	0.0013	1911.40	19.92	1438.70	14.97
Z38-1	1.2374	0.0171	0.1391	0.0016	0.0646	0.0008	760.30	27.05	839.40	9.26
Z39-1	0.8522	0.0145	0.0976	0.0012	0.0634	0.0011	720.50	35.15	600.30	7.06
Z40-1	0.8235	0.0119	0.1004	0.0012	0.0595	0.0008	586.40	29.48	616.70	6.96
Z41-1	0.9149	0.0129	0.1074	0.0013	0.0618	0.0008	668.00	28.26	657.40	7.37
Z42-1	0.8013	0.0120	0.0964	0.0012	0.0603	0.0009	615.30	30.54	593.10	6.75
Z43-1	13.284	0.1576	0.4446	0.0051	0.2168	0.0023	2957.00	17.02	2371.30	22.86
Z46-1	0.8414	0.0121	0.0922	0.0011	0.0662	0.0009	813.60	28.26	568.40	6.45
Z47-1	14.992	0.1767	0.4931	0.0057	0.2206	0.0023	2985.00	16.81	2584.10	24.45
Z48-1	0.7292	0.0094	0.0912	0.0011	0.0580	0.0007	529.00	26.10	562.90	6.25
Z50-1	0.8308	0.0120	0.0963	0.0011	0.0626	0.0009	695.20	28.92	592.50	6.71
Z51-1	0.7826	0.0117	0.0956	0.0012	0.0594	0.0008	582.60	30.47	588.40	6.74
Z52-1	0.7634	0.0128	0.0950	0.0012	0.0583	0.0010	539.80	36.03	585.20	6.88
Z53-1	0.8064	0.0123	0.0957	0.0012	0.0611	0.0009	643.40	31.03	589.30	6.79
Z54-1	1.3163	0.0196	0.1336	0.0016	0.0715	0.0010	971.00	28.69	808.50	9.19
Z55-1	0.9234	0.0220	0.1026	0.0014	0.0653	0.0016	785.20	50.14	629.30	8.35
Z56-1	0.8500	0.0137	0.1026	0.0013	0.0601	0.0009	608.60	33.35	629.30	7.32
Z57-1	1.1034	0.0137	0.1165	0.0014	0.0687	0.0008	890.80	23.06	710.20	7.83
Z58-1	1.1127	0.0177	0.1009	0.0013	0.0800	0.0012	1196.60	30.22	619.90	7.31
Z60-1	0.8455	0.0152	0.1040	0.0013	0.0590	0.0010	566.40	38.00	637.90	7.60
Z63-1	0.7189	0.0091	0.0907	0.0010	0.0575	0.0007	510.70	25.43	559.70	6.14
Z65-1	0.7647	0.0105	0.0913	0.0011	0.0608	0.0008	631.30	27.65	563.20	6.26
Z67-1	0.2677	0.0065	0.0394	0.0005	0.0493	0.0012	160.50	57.05	249.30	3.23
Z68-1	0.8746	0.0132	0.1043	0.0012	0.0608	0.0009	633.60	31.20	639.60	7.21
Z70-1	11.329	0.1340	0.5015	0.0057	0.1639	0.0018	2496.50	17.98	2620.20	24.60
Z71-1	31.004	0.3671	0.7624	0.0090	0.2950	0.0031	3444.20	16.30	3653.00	32.74
Z72-1	0.7995	0.0131	0.0999	0.0012	0.0581	0.0009	532.10	34.91	613.60	7.17
Z73-1	0.2968	0.0050	0.0404	0.0005	0.0533	0.0009	342.60	36.90	255.10	3.06
Z74-1	0.8613	0.0131	0.1032	0.0013	0.0605	0.0009	622.20	31.19	633.40	7.29
Z75-1	0.8544	0.0113	0.1045	0.0012	0.0593	0.0007	578.90	26.51	640.60	7.17
Z76-1	0.7935	0.0171	0.1011	0.0013	0.0570	0.0012	489.20	47.29	620.60	7.81
Z77-1	12.778	0.1504	0.5074	0.0059	0.1827	0.0019	2677.50	17.24	2645.40	25.23

Spot No.	$^{207}Pb/^{235}U$	Error ±2 σ	$^{206}Pb/^{238}U$	Error ±2 σ	$^{207}Pb/^{235}U$	Error ±2 σ	$^{207}Pb/^{206}Pb$ age (Ma)	Error ± (Ma)	$^{206}Pb/^{238}U$ age (Ma)	Error ± (Ma)
Z78-1	0.8146	0.0178	0.1035	0.0014	0.0571	0.0013	495.50	48.36	634.60	8.01
Z79-1	4.6984	0.0595	0.2781	0.0033	0.1226	0.0014	1994.00	20.52	1581.60	16.63
Z80-1	0.8350	0.0117	0.1027	0.0012	0.0590	0.0008	566.80	27.97	630.10	7.12
Z81-1	1.5795	0.0203	0.1165	0.0014	0.0983	0.0012	1592.70	22.26	710.60	7.89
Z82-1	0.7966	0.0175	0.0884	0.0012	0.0654	0.0015	787.00	46.05	546.00	7.01
Z84-1	0.7698	0.0102	0.0975	0.0011	0.0573	0.0007	502.90	26.93	599.50	6.67
Z85-1	0.8326	0.0135	0.1012	0.0012	0.0597	0.0009	591.60	33.78	621.60	7.19
Z86-1	7.4912	0.0895	0.4186	0.0048	0.1298	0.0014	2095.70	18.88	2254.20	22.01
Z87-1	0.7723	0.0109	0.0961	0.0011	0.0583	0.0008	540.90	29.66	591.40	6.66
Z88-1	1.5630	0.0209	0.1614	0.0019	0.0703	0.0009	936.50	25.51	964.30	10.52
Z89-1	0.8011	0.0171	0.0972	0.0013	0.0598	0.0013	596.50	45.82	597.90	7.49
Z90-1	0.6636	0.0165	0.0839	0.0012	0.0574	0.0015	505.80	55.25	519.40	6.87
Z91-1	3.6589	0.0428	0.2447	0.0028	0.1086	0.0012	1775.90	19.29	1411.00	14.35
Z92-1	4.1731	0.1213	0.2383	0.0043	0.1272	0.0039	2059.60	53.45	1377.60	22.50
Z93-1	7.9089	0.0966	0.4005	0.0046	0.1434	0.0016	2268.70	19.32	2171.30	21.27
Z96-1	0.8113	0.0193	0.0952	0.0013	0.0619	0.0015	671.20	51.20	585.90	7.62
Z97-1	8.6037	0.1032	0.4086	0.0047	0.1529	0.0017	2378.70	18.65	2208.60	21.45
Z98-1	1.2841	0.0192	0.0946	0.0012	0.0986	0.0015	1596.90	27.21	582.80	6.74
Z99-1	0.7711	0.0127	0.0985	0.0012	0.0569	0.0009	486.20	35.55	605.30	6.93
Z100-1	0.7842	0.0146	0.0949	0.0012	0.0600	0.0011	603.10	39.58	584.70	6.94
Not Used										
Z11-1	-	-	6.0867	0.9655	0.9503	0.0645	5165.60	92.34	-	-
Z23-1	-	-	4.9958	2.7620	-	4.4482	0.10	0.00	-	-
Z24-1	-	-	8.8812	5.4394	-	2.6621	0.10	0.00	-	-
Z25-1	-	-	2.5805	2.9042	1.9132	2.1010	6134.00	995.19	-	-
Z44-1	-	-	-	32.350	0.9307	0.1472	5136.30	206.33	-	-
Z45-1	-	-	3.7979	1.7683	-	2.1053	0.10	5857.97	-	-
Z49-1	474.54	48.153	3.4054	0.3657	1.0111	0.0670	5252.90	89.91	9559.00	-
Z58-2	-	-	4.0191	2.2791	0.9918	0.3248	5225.70	395.19	-	-
Z61-1	97.468	15.071	0.7169	0.1401	0.9865	0.1961	5218.30	253.64	3484.50	-
Z64-1	81.819	3.0955	0.6074	0.0272	0.9775	0.0433	5205.40	60.86	3059.40	-
Z66-1	0.9766	4.5215	-	0.0173	-	0.5385	0.10	3989.30	-	-
Z69-1	163.70	11.446	1.1874	0.0945	1.0004	0.0686	5238.00	93.03	5045.70	-
Z83-1	-	-	3.4124	1.4898	0.7964	0.2212	4915.20	346.55	-	-
Z94-1	-	-	2.6087	0.0304	0.8153	0.0086	4948.70	14.90	8273.00	54.31
Z95-1	-	-	0.9355	0.5665	3.0865	1.4878	6779.20	522.94	4256.80	-

Kingscote Composite Section - unit 3

Spot No.	$^{207}Pb/^{235}U$	Error ±2 σ	$^{206}Pb/^{238}U$	Error ±2 σ	$^{207}Pb/^{235}U$	Error ±2 σ	$^{207}Pb/^{206}Pb$ age (Ma)	Error ± (Ma)	$^{206}Pb/^{238}U$ age (Ma)	Error ± (Ma)
z10-1	0.2943	0.0031	0.6486	0.0070	26.3563	0.2937	3440.40	16.13	3222.80	27.55
z13-1	0.0618	0.0008	0.1141	0.0013	0.9730	0.0135	667.20	27.83	696.70	7.66
z23-1	0.1377	0.0015	0.3691	0.0041	7.0040	0.0811	2198.00	18.19	2025.00	19.47
z28-1	0.0672	0.0010	0.0386	0.0005	0.3575	0.0052	845.30	29.30	243.90	2.79
z29-1	0.0544	0.0008	0.0393	0.0005	0.2949	0.0043	387.60	31.51	248.60	2.83
z36-1	0.1126	0.0014	0.0473	0.0006	0.7340	0.0097	1841.20	22.82	298.10	3.36
z37-1	0.0896	0.0012	0.0408	0.0005	0.5030	0.0070	1416.10	25.43	257.50	2.93
z38-1	0.1761	0.0019	0.3245	0.0037	7.8730	0.0937	2616.50	18.16	1811.50	17.80
z44-1	0.0578	0.0008	0.0997	0.0012	0.7948	0.0118	522.50	31.00	612.90	6.98
z45-1	0.0590	0.0008	0.1026	0.0012	0.8344	0.0124	567.00	30.47	629.70	7.16
z46-1	0.0603	0.0007	0.1122	0.0013	0.9318	0.0119	613.20	25.05	685.30	7.56
z47-1	0.0619	0.0007	0.1146	0.0013	0.9776	0.0125	670.40	24.89	699.30	7.71
z57-1	0.1167	0.0015	0.1038	0.0013	1.6697	0.0228	1906.50	22.72	636.70	7.39
z58-1	0.0734	0.0009	0.1783	0.0021	1.8019	0.0232	1023.70	23.34	1057.40	11.58
z59-1	0.0724	0.0008	0.1739	0.0021	1.7364	0.0219	998.30	22.71	1033.70	11.29
z61-1	0.0602	0.0010	0.1045	0.0013	0.8667	0.0145	609.10	34.56	640.90	7.58
z62-1	0.0600	0.0010	0.1034	0.0013	0.8554	0.0144	604.20	34.69	634.30	7.51
z63-1	0.0607	0.0010	0.1063	0.0013	0.8898	0.0155	628.60	36.00	651.50	7.78
z64-1	0.0623	0.0010	0.1037	0.0013	0.8904	0.0147	683.20	33.55	636.30	7.52
z67-1	0.0592	0.0008	0.0980	0.0012	0.7993	0.0119	572.80	30.21	602.80	6.97
z68-1	0.0616	0.0010	0.1035	0.0013	0.8781	0.0150	658.30	34.93	635.00	7.55
z72-1	0.0675	0.0009	0.1062	0.0013	0.9881	0.0145	854.50	28.52	650.70	7.50
z74-1	0.0603	0.0007	0.1130	0.0013	0.9392	0.0116	615.80	23.45	690.20	7.67
z83-1	0.0589	0.0008	0.1068	0.0013	0.8675	0.0126	564.00	29.87	654.30	7.42
z84-1	0.0594	0.0008	0.1023	0.0012	0.8375	0.0121	581.30	29.39	628.00	7.12
z85-1	0.0592	0.0008	0.1023	0.0012	0.8353	0.0122	575.20	29.74	628.00	7.14
z86-1	0.0603	0.0008	0.1035	0.0012	0.8595	0.0120	613.00	27.95	634.80	7.15
z89-1	0.0818	0.0013	0.0999	0.0013	1.1263	0.0184	1241.70	31.18	613.50	7.31
z90-1	0.0679	0.0013	0.0955	0.0012	0.8941	0.0168	866.10	38.23	588.00	7.20
z91-1	0.0651	0.0007	0.0729	0.0008	0.6537	0.0080	776.20	23.24	453.60	5.05
z92-1	0.0616	0.0015	0.0908	0.0013	0.7717	0.0188	661.50	52.42	560.50	7.44
z93-1	0.0628	0.0015	0.0889	0.0012	0.7695	0.0183	701.70	50.94	548.90	7.26
z94-1	0.0789	0.0018	0.0964	0.0013	1.0483	0.0227	1170.50	43.19	593.00	7.78
z95-1	0.0600	0.0007	0.1142	0.0013	0.9442	0.0116	602.80	24.03	697.10	7.62
z99-1	0.0586	0.0008	0.1079	0.0013	0.8708	0.0126	551.10	29.98	660.40	7.45
z100-1	0.0570	0.0008	0.1051	0.0012	0.8251	0.0117	490.20	29.92	644.00	7.24
z101-1	0.0601	0.0009	0.0990	0.0011	0.8198	0.0119	607.50	30.50	608.70	6.59
z102-1	0.0608	0.0009	0.0982	0.0011	0.8227	0.0123	632.10	31.58	604.10	6.59
z104-1	0.0627	0.0008	0.0949	0.0011	0.8194	0.0107	698.10	26.74	584.40	6.22
z106-1	0.0695	0.0010	0.1434	0.0016	1.3717	0.0197	912.80	28.85	863.60	9.23
z107-1	0.0600	0.0008	0.0967	0.0011	0.7989	0.0114	603.40	29.90	594.90	6.42
z113-1	0.1667	0.0018	0.4023	0.0043	9.2446	0.1031	2524.90	17.81	2179.40	19.97
z114-1	0.0777	0.0009	0.2041	0.0022	2.1854	0.0260	1138.90	22.78	1197.10	11.86
z115-1	0.0791	0.0009	0.2059	0.0022	2.2452	0.0267	1174.70	22.55	1206.90	11.94
z116-1	0.0592	0.0008	0.0967	0.0011	0.7891	0.0102	574.70	27.32	594.90	6.22
z117-1	0.0723	0.0009	0.0943	0.0010	0.9394	0.0118	993.30	24.82	580.90	6.08
z118-1	0.1724	0.0020	0.3565	0.0040	8.4702	0.1018	2580.80	19.51	1965.30	18.94
z119-1	0.1737	0.0020	0.4245	0.0047	10.163	0.1197	2593.30	18.94	2281.00	21.29
z120-1	0.1507	0.0019	0.2557	0.0029	5.3107	0.0671	2353.60	21.23	1467.70	14.87
Not Used										
z01-1	0.8082	0.0084	-	305.38	-	-	4936.20	14.69	-	265.90
z02-1	1.0762	0.4467	2.3225	1.3103	345.12	174.73	5340.30	481.52	7740.40	2542.18
z03-1	0.8215	0.0089	-	441.60	-	-	4959.40	15.38	-	927.22
z04-1	0.8182	0.0091	-	-	-	-	4953.80	15.72	-	5785.82
z05-1	0.8097	0.0089	-	-	-	-	4938.90	15.52	-	1671.08
z06-1	0.8171	0.0085	-	493.23	-	-	4951.90	14.71	-	404.67
z07-1	0.8088	0.0085	-	562.99	-	-	4937.30	14.92	-	727.61
z08-1	0.3593	0.1854	-6.4608	5.0439	-	273.93	3747.10	620.05	-	-
z09-1	0.8187	0.0085	-	-	-	-	4954.70	14.72	-	622.22
z11-1	0.8051	0.0085	-	184.41	-	-	4930.70	14.95	-	343.32
z103-1	0.8549	0.0089	-	-	-	-	5016.10	14.64	-	441.97
z105-1	0.8372	0.0087	-	531.33	-	-	4986.40	14.66	-	326.59
z108-1	-0.1813	0.1441	-30.629	27.606	764.75	358.48	0.10	0.00	-	-
z109-1	0.8436	0.0088	-	-	-	-	4997.20	14.79	-	754.16

Spot No.	$^{207}Pb/^{235}U$	Error ±2 σ	$^{206}Pb/^{238}U$	Error ±2 σ	$^{207}Pb/^{235}U$	Error ±2 σ	$^{207}Pb/^{206}Pb$ age (Ma)	Error ± (Ma)	$^{206}Pb/^{238}U$ age (Ma)	Error ± (Ma)
z110-1	0.8423	0.0088	-	166.85	-	-	4995.00	14.66	-	248.42
z12-1	0.8245	0.0087	-	-	-	-	4964.70	14.93	-	717.08
z14-1	0.8204	0.0088	411.73	15.73	-	-	4957.60	15.22	-	245.75
z15-1	0.8494	0.0103	-	-	-	-	5006.90	17.08	-	3660.29
z16-1	2.0265	2.4569	6.7393	8.4096	-	580.08	6212.20	1063.37	-	7004.73
z17-1	1.0333	0.2753	-	0.3876	-	54.738	5283.40	329.19	-	3768.51
z18-1	0.8207	0.0086	-	138.40	-	-	4958.10	14.86	-	208.94
z19-1	0.8122	0.0086	-	208.05	-	-	4943.30	15.05	-	465.31
z20-1	0.8287	0.0087	-	169.20	-	-	4971.80	14.88	-	289.22
z21-1	0.8215	0.0086	-	150.04	-	-	4959.50	14.80	-	305.97
z22-1	0.8166	0.0085	-	220.71	-	-	4950.90	14.77	-	268.09
z24-1	0.8248	0.0087	231.56	4.3877	-	503.44	4965.20	14.84	-	121.63
z25-1	0.8293	0.0087	-	559.58	-	-	4972.90	14.76	-	405.07
z26-1	0.8128	0.0085	-	136.67	-	-	4944.30	14.78	-	253.66
z27-1	-0.1222	0.0966	2.0882	2.6802	-	36.520	0.10	0.00	7269.00	5594.72
z30-1	0.8323	0.0087	-	121.71	-	-	4978.00	14.74	-	210.57
z31-1	0.6316	0.5645	13.861	5.8826	-	-	4582.40	905.33	-	2551.79
z32-1	0.8359	0.0089	-	330.85	-	-	4984.10	15.06	-	530.73
z33-1	0.8351	0.0089	-	-	-	-	4982.90	15.03	-	831.52
z34-1	0.8352	0.0088	-	220.05	-	-	4983.00	14.94	-	338.33
z35-1	0.8486	0.0090	-	352.05	-	-	5005.60	14.89	-	308.72
z39-1	0.8485	0.0090	-	26.034	-	-	5005.40	14.88	-	130.49
z40-1	0.8243	0.0087	-	233.05	-	-	4964.30	14.92	-	279.04
z41-1	0.8444	0.0090	-	546.72	-	-	4998.50	14.98	-	541.17
z42-1	0.8245	0.0086	-	125.69	-	-	4964.70	14.66	-	248.04
z43-1	0.8327	0.0086	-	271.41	-	-	4978.80	14.65	-	325.32
z48-1	0.8385	0.0091	26.468	0.4472	-	51.872	4988.60	15.26	-	104.96
z49-1	0.8459	0.0099	350.82	29.20	-	-	5001.10	16.54	-	535.00
z50-1	0.8265	0.0086	-	-	-	-	4968.10	14.64	-	425.21
z51-1	1.3754	0.4288	1.630	0.6753	309.02	109.59	5681.40	372.59	6234.30	1654.97
z52-1	0.8250	0.0085	-	147.67	-	-	4965.50	14.57	-	249.09
z53-1	0.8151	0.0084	-	239.63	-	-	4948.40	14.62	-	355.60
z54-1	0.8259	0.0085	-	100.89	-	-	4967.10	14.57	-	216.24
z55-1	-2.8844	2.7809	2.445	0.9400	-	963.24	0.10	0.00	7974.50	1758.71
z56-1	0.8435	0.0087	-	-	-	-	4997.10	14.55	-	500.68
z60-1	0.8243	0.0085	888.79	24.059	-	-	4964.30	14.61	-	174.30
z65-1	0.8440	0.0088	-	45.163	-	-	4997.80	14.74	-	176.56
z66-1	0.8437	0.0088	-	196.11	-	-	4997.30	14.75	-	298.60
z69-1	0.8281	0.0087	-	-	-	-	4970.90	14.77	-	873.60
z70-1	0.8330	0.0087	-	-	-	-	4979.30	14.74	-	464.04
z71-1	0.8252	0.0085	-	498.85	-	-	4965.80	14.63	-	396.90
z73-1	0.8322	0.0087	-	999.35	-	-	4977.80	14.69	-	664.85
z75-1	0.8306	0.0086	-	403.48	-	-	4975.10	14.60	-	300.17
z76-1	0.8432	0.0088	542.50	18.538	-	-	4996.50	14.78	-	219.88
z77-1	0.8250	0.0086	-	549.69	-	-	4965.40	14.66	-	472.54
z78-1	0.9908	0.1095	-	70.539	-	-	5224.40	146.93	-	-
z79-1	-0.1015	0.0815	-	56.958	818.78	495.15	0.10	0.00	-	-
z80-1	0.8399	0.0154	13.072	0.5732	-	65.349	4991.00	25.78	-	262.58
z81-1	0.8282	0.0086	-	336.45	-	-	4970.90	14.67	-	495.95
z82-1	0.8284	0.0087	-	-	-	-	4971.30	14.89	-	2075.32
z87-1	0.8321	0.0086	240.91	3.8341	-	441.90	4977.70	14.57	-	102.17
z96-1	0.8078	0.0083	-	233.19	-	-	4935.60	14.50	-	461.56
z97-1	0.7925	0.0081	-	32.090	-	-	4908.20	14.41	-	188.98
z98-1	0.8203	0.0084	-	356.89	-	-	4957.40	14.50	-	559.23
z111-1	0.8381	0.0086	-	299.92	-	-	4987.90	14.47	-	322.71
z112-1	0.7074	0.0876	118.89	119.42	-	-	4745.70	166.92	-	6421.32

Spot No.	Preferred age (Ma)	Error ± (Ma)	rho	Conc.
z10-1	3440.40	16.13	0.97	94
z13-1	696.70	7.66	0.83	104
z23-1	2198.00	18.19	0.97	92
z28-1	243.90	2.79	0.80	29
z29-1	248.60	2.83	0.79	64
z36-1	1841.20	22.82	0.88	16

Spot No.	Preferred age (Ma)	Error ± (Ma)	rho	Conc.
z37-1	1416.10	25.43	0.83	18
z38-1	2616.50	18.16	0.95	69
z44-1	612.90	6.98	0.80	117
z45-1	629.70	7.16	0.80	111
z46-1	685.30	7.56	0.91	112
z47-1	699.30	7.71	0.91	104
z57-1	1906.50	22.72	0.89	33
z58-1	1057.40	11.58	0.92	103
z59-1	1033.70	11.29	0.94	104
z61-1	640.90	7.58	0.74	105
z62-1	634.30	7.51	0.74	105
z63-1	651.50	7.78	0.72	104
z64-1	636.30	7.52	0.75	93
z67-1	602.80	6.97	0.81	105
z68-1	635.00	7.55	0.73	96
z72-1	650.70	7.50	0.83	76
z74-1	690.20	7.67	0.95	112
z83-1	654.30	7.42	0.82	116
z84-1	628.00	7.12	0.83	108
z85-1	628.00	7.14	0.82	109
z86-1	634.80	7.15	0.85	104
z89-1	1241.70	31.18	0.76	49
z90-1	588.00	7.20	0.68	68
z91-1	453.60	5.05	0.95	58
z92-1	560.50	7.44	0.57	85
z93-1	548.90	7.26	0.58	78
z94-1	593.00	7.78	0.63	51
z95-1	697.10	7.62	0.94	116
z99-1	660.40	7.45	0.82	120
z100-1	644.00	7.24	0.83	131
z101-1	608.70	6.59	0.78	100
z102-1	604.10	6.59	0.76	96
z104-1	584.40	6.22	0.85	84
z106-1	863.60	9.23	0.80	95
z107-1	594.90	6.42	0.79	99
z113-1	2524.90	17.81	0.97	86
z114-1	1197.10	11.86	0.91	105
z115-1	1206.90	11.94	0.91	103
z116-1	594.90	6.22	0.85	104
z117-1	580.90	6.08	0.87	58
z118-1	2580.80	19.51	0.93	76
z119-1	2593.30	18.94	0.94	88
z120-1	2353.60	21.23	0.90	62
Not Used				
z01-1			-	-
z02-1	5340.30	481.52	0.90	145
z03-1			-	-
z04-1			-	-
z05-1			-	-
z06-1			-	-
z07-1			-	-
z08-1			-	-
z09-1			-	-
z11-1			-	-
z103-1			-	-
z105-1			-	-
z108-1			-1.92	-
z109-1			-	-
z110-1			-	-
z12-1			-	-
z14-1			-	-
z15-1			-	-
z16-1			-	-
z17-1			1.01	-
z18-1			-	-
z19-1			-	-
z20-1			-	-

Spot No.	Preferred age (Ma)	Error ± (Ma)	rho	Conc.
z21-1			-	-
z22-1			-	-
z24-1			-	-
z25-1			-	-
z26-1			-	-
z27-1			-	7269000
z30-1			-	-
z31-1			-	-
z32-1			-	-
z33-1			-	-
z34-1			-	-
z35-1			-	-
z39-1			-	-
z40-1			-	-
z41-1			-	-
z42-1			-	-
z43-1			-	-
z48-1			-	-
z49-1			-	-
z50-1			-	-
z51-1	5681.40	372.59	0.86	110
z52-1			-	-
z53-1			-	-
z54-1			-	-
z55-1			-	-
z56-1			-	-
z60-1			-	-
z65-1			-	-
z66-1			-	-
z69-1			-	-
z70-1			-	-
z71-1			-	-
z73-1			-	-
z75-1			-	-
z76-1			-	-
z77-1			-	-
z78-1			-	-
z79-1			-1.61	-
z80-1			-	-
z81-1			-	-
z82-1			-	-
z87-1			-	-
z96-1			-	-
z97-1			-	-
z98-1			-	-
z111-1			-	-
z112-1			-	-

Cape Jervis Section - unit 4

Spot No.	$^{207}Pb/^{235}U$	Error ±2 σ	$^{206}Pb/^{238}U$	Error ±2 σ	$^{207}Pb/^{235}U$	Error ±2 σ	$^{207}Pb/^{206}Pb$ age (Ma)	Error ± (Ma)	$^{206}Pb/^{238}U$ age (Ma)	Error ± (Ma)
Z01-1	0.0578	0.0011	0.0890	0.0011	0.7080	0.0129	521.00	40.10	549.30	6.30
Z02-1	0.0953	0.0011	0.2914	0.0032	3.8260	0.0456	1533.80	21.28	1648.70	16.05
Z03-1	0.0605	0.0007	0.0943	0.0010	0.7859	0.0093	620.20	24.01	581.10	6.07
Z04-1	0.0621	0.0008	0.0969	0.0011	0.8284	0.0113	676.70	28.29	596.00	6.38
Z05-1	0.1224	0.0013	0.0642	0.0007	1.0832	0.0123	1991.40	18.91	401.40	4.24
Z06-1	0.0788	0.0009	0.1797	0.0020	1.9513	0.0236	1167.50	22.78	1065.30	10.82
Z07-1	0.0735	0.0009	0.1459	0.0016	1.4775	0.0178	1028.20	23.07	877.90	9.02
Z08-1	0.0567	0.0007	0.0886	0.0010	0.6928	0.0092	480.60	28.58	547.40	5.84
Z09-1	0.0684	0.0008	0.1198	0.0013	1.1282	0.0137	879.40	23.97	729.40	7.58
Z10-1	0.0945	0.0010	0.2688	0.0029	3.4985	0.0391	1517.70	19.70	1534.60	14.82
Z12-1	0.0583	0.0013	0.1012	0.0013	0.8140	0.0176	541.30	47.90	621.70	7.67
Z13-1	0.0606	0.0012	0.0991	0.0013	0.8283	0.0168	625.80	43.47	609.30	7.40
Z14-1	0.1160	0.0019	0.1035	0.0013	1.6553	0.0272	1896.10	29.49	634.80	7.64
Z15-1	0.0598	0.0011	0.0945	0.0012	0.7790	0.0141	595.10	39.04	582.40	6.83
Z16-1	0.0679	0.0010	0.0900	0.0011	0.8421	0.0132	864.40	31.43	555.60	6.34
Z17-1	0.0707	0.0018	0.1007	0.0014	0.9803	0.0238	947.30	50.16	618.30	8.22
Z18-1	0.0653	0.0010	0.1228	0.0015	1.1049	0.0167	783.90	30.46	746.40	8.32
Z19-1	0.0614	0.0009	0.1004	0.0012	0.8490	0.0132	652.10	32.23	616.50	6.96
Z20-1	0.0683	0.0010	0.1021	0.0012	0.9618	0.0149	878.50	30.89	626.80	7.10
Z21-1	0.0596	0.0009	0.0989	0.0012	0.8118	0.0119	590.40	30.60	607.90	6.74
Z22-1	0.0605	0.0008	0.0986	0.0011	0.8209	0.0110	619.80	27.28	606.50	6.61
Z26-1	0.1424	0.0016	0.3963	0.0045	7.7673	0.0923	2256.40	18.86	2151.80	20.71
Z27-1	0.0747	0.0013	0.1510	0.0019	1.5529	0.0263	1061.20	33.60	906.30	10.37
Z28-1	0.0601	0.0008	0.0964	0.0011	0.7975	0.0116	606.80	30.12	593.30	6.58
Z29-1	0.0647	0.0010	0.0945	0.0011	0.8409	0.0137	763.70	33.60	581.80	6.65
Z30-1	0.0593	0.0009	0.0975	0.0011	0.7962	0.0118	579.40	30.94	599.60	6.67
Z31-1	0.0809	0.0010	0.2146	0.0025	2.3924	0.0325	1218.80	24.83	1253.40	13.47
Z32-1	0.0610	0.0008	0.1157	0.0014	0.9725	0.0132	638.90	26.95	705.80	7.82
Z33-1	0.0600	0.0008	0.0993	0.0012	0.8214	0.0111	604.30	26.95	610.40	6.81
Z34-1	0.0606	0.0009	0.0972	0.0012	0.8122	0.0119	626.60	29.91	598.00	6.78
Z35-1	0.0956	0.0011	0.2819	0.0033	3.7130	0.0451	1539.50	20.55	1601.00	16.38
Z36-1	0.0614	0.0010	0.1034	0.0013	0.8748	0.0145	654.20	34.24	634.00	7.37
Z37-1	0.1170	0.0013	0.2500	0.0029	4.0323	0.0495	1911.40	19.92	1438.70	14.97
Z38-1	0.0646	0.0008	0.1391	0.0016	1.2374	0.0171	760.30	27.05	839.40	9.26
Z39-1	0.0634	0.0011	0.0976	0.0012	0.8522	0.0145	720.50	35.15	600.30	7.06
Z40-1	0.0595	0.0008	0.1004	0.0012	0.8235	0.0119	586.40	29.48	616.70	6.96
Z41-1	0.0618	0.0008	0.1074	0.0013	0.9149	0.0129	668.00	28.26	657.40	7.37
Z42-1	0.0603	0.0009	0.0964	0.0012	0.8013	0.0120	615.30	30.54	593.10	6.75
Z43-1	0.2168	0.0023	0.4446	0.0051	13.2849	0.1576	2957.00	17.02	2371.30	22.86
Z46-1	0.0662	0.0009	0.0922	0.0011	0.8414	0.0121	813.60	28.26	568.40	6.45
Z47-1	0.2206	0.0023	0.4931	0.0057	14.9922	0.1767	2985.00	16.81	2584.10	24.45
Z48-1	0.0580	0.0007	0.0912	0.0011	0.7292	0.0094	529.00	26.10	562.90	6.25
Z50-1	0.0626	0.0009	0.0963	0.0011	0.8308	0.0120	695.20	28.92	592.50	6.71
Z51-1	0.0594	0.0008	0.0956	0.0012	0.7826	0.0117	582.60	30.47	588.40	6.74
Z52-1	0.0583	0.0010	0.0950	0.0012	0.7634	0.0128	539.80	36.03	585.20	6.88
Z53-1	0.0611	0.0009	0.0957	0.0012	0.8064	0.0123	643.40	31.03	589.30	6.79
Z54-1	0.0715	0.0010	0.1336	0.0016	1.3163	0.0196	971.00	28.69	808.50	9.19
Z55-1	0.0653	0.0016	0.1026	0.0014	0.9234	0.0220	785.20	50.14	629.30	8.35
Z56-1	0.0601	0.0009	0.1026	0.0013	0.8500	0.0137	608.60	33.35	629.30	7.32
Z57-1	0.0687	0.0008	0.1165	0.0014	1.1034	0.0137	890.80	23.06	710.20	7.83
Z58-1	0.0800	0.0012	0.1009	0.0013	1.1127	0.0177	1196.60	30.22	619.90	7.31
Z60-1	0.0590	0.0010	0.1040	0.0013	0.8455	0.0152	566.40	38.00	637.90	7.60
Z62-1	0.4346	0.0161	0.1564	0.0044	9.3685	0.2807	4033.30	54.34	936.90	24.67
Z63-1	0.0575	0.0007	0.0907	0.0010	0.7189	0.0091	510.70	25.43	559.70	6.14
Z65-1	0.0608	0.0008	0.0913	0.0011	0.7647	0.0105	631.30	27.65	563.20	6.26
Z67-1	0.0493	0.0012	0.0394	0.0005	0.2677	0.0065	160.50	57.05	249.30	3.23
Z68-1	0.0608	0.0009	0.1043	0.0012	0.8746	0.0132	633.60	31.20	639.60	7.21
Z70-1	0.1639	0.0018	0.5015	0.0057	11.329	0.1340	2496.50	17.98	2620.20	24.60
Z71-1	0.2950	0.0031	0.7624	0.0090	31.005	0.3671	3444.20	16.30	3653.00	32.74
Z72-1	0.0581	0.0009	0.0999	0.0012	0.7995	0.0131	532.10	34.91	613.60	7.17
Z73-1	0.0533	0.0009	0.0404	0.0005	0.2968	0.0050	342.60	36.90	255.10	3.06
Z74-1	0.0605	0.0009	0.1032	0.0013	0.8613	0.0131	622.20	31.19	633.40	7.29
Z75-1	0.0593	0.0007	0.1045	0.0012	0.8544	0.0113	578.90	26.51	640.60	7.17
Z76-1	0.0570	0.0012	0.1011	0.0013	0.7935	0.0171	489.20	47.29	620.60	7.81

Spot No.	$^{207}Pb/^{235}U$	Error ±2 σ	$^{206}Pb/^{238}U$	Error ±2 σ	$^{207}Pb/^{235}U$	Error ±2 σ	$^{207}Pb/^{206}Pb$ age (Ma)	Error ± (Ma)	$^{206}Pb/^{238}U$ age (Ma)	Error ± (Ma)
Z77-1	0.1827	0.0019	0.5074	0.0059	12.778	0.1504	2677.50	17.24	2645.40	25.23
Z78-1	0.0571	0.0013	0.1035	0.0014	0.8146	0.0178	495.50	48.36	634.60	8.01
Z79-1	0.1226	0.0014	0.2781	0.0033	4.6984	0.0595	1994.00	20.52	1581.60	16.63
Z80-1	0.0590	0.0008	0.1027	0.0012	0.8350	0.0117	566.80	27.97	630.10	7.12
Z81-1	0.0983	0.0012	0.1165	0.0014	1.5795	0.0203	1592.70	22.26	710.60	7.89
Z82-1	0.0654	0.0015	0.0884	0.0012	0.7966	0.0175	787.00	46.05	546.00	7.01
Z84-1	0.0573	0.0007	0.0975	0.0011	0.7698	0.0102	502.90	26.93	599.50	6.67
Z85-1	0.0597	0.0009	0.1012	0.0012	0.8326	0.0135	591.60	33.78	621.60	7.19
Z86-1	0.1298	0.0014	0.4186	0.0048	7.4912	0.0895	2095.70	18.88	2254.20	22.01
Z87-1	0.0583	0.0008	0.0961	0.0011	0.7723	0.0109	540.90	29.66	591.40	6.66
Z88-1	0.0703	0.0009	0.1614	0.0019	1.5630	0.0209	936.50	25.51	964.30	10.52
Z89-1	0.0598	0.0013	0.0972	0.0013	0.8011	0.0171	596.50	45.82	597.90	7.49
Z90-1	0.0574	0.0015	0.0839	0.0012	0.6636	0.0165	505.80	55.25	519.40	6.87
Z91-1	0.1086	0.0012	0.2447	0.0028	3.6589	0.0428	1775.90	19.29	1411.00	14.35
Z92-1	0.1272	0.0039	0.2383	0.0043	4.1731	0.1213	2059.60	53.45	1377.60	22.50
Z93-1	0.1434	0.0016	0.4005	0.0046	7.9089	0.0966	2268.70	19.32	2171.30	21.27
Z96-1	0.0619	0.0015	0.0952	0.0013	0.8113	0.0193	671.20	51.20	585.90	7.62
Z97-1	0.1529	0.0017	0.4086	0.0047	8.6037	0.1032	2378.70	18.65	2208.60	21.45
Z98-1	0.0986	0.0015	0.0946	0.0012	1.2841	0.0192	1596.90	27.21	582.80	6.74
Z99-1	0.0569	0.0009	0.0985	0.0012	0.7711	0.0127	486.20	35.55	605.30	6.93
Z100-1	0.0600	0.0011	0.0949	0.0012	0.7842	0.0146	603.10	39.58	584.70	6.94
Not Used										
Z11-1	0.9503	0.0645	6.0867	0.9655	797.29	123.03	5165.60	92.34	-	878.3
Z23-1	-	4.4482	4.9958	2.7620	-	-	0.10	0.00	-	-
Z24-1	-	2.6621	8.8812	5.4394	-	-	0.10	0.00	-	-
Z25-1	1.9132	2.1010	2.5805	2.9042	679.64	273.25	6134.00	995.19	8222.40	-
Z44-1	0.9307	0.1472	-	-	-	-	5136.30	206.33	-	-
Z45-1	-	2.1053	3.7979	1.7683	-	-	0.10	-	-	-
Z49-1	1.0111	0.0670	3.4054	0.3657	474.55	48.15	5252.90	89.91	9559.00	-
Z58-2	0.9918	0.3248	4.0191	2.2791	549.34	293.71	5225.70	395.19	-	-
Z61-1	0.9865	0.1961	0.7169	0.1401	97.47	15.07	5218.30	253.64	3484.50	525.9
Z64-1	0.9775	0.0433	0.6074	0.0272	81.82	3.10	5205.40	60.86	3059.40	109.0
Z66-1	-	0.5385	-	0.0173	0.98	4.52	0.10	-	-	118.8
Z69-1	1.0004	0.0686	1.1874	0.0945	163.71	11.45	5238.00	93.03	5045.70	278.5
Z83-1	0.7964	0.2212	3.4124	1.4898	374.55	155.51	4915.20	346.55	9569.20	-
Z94-1	0.8153	0.0086	2.6087	0.0304	292.89	3.46	4948.70	14.90	8273.00	54.3
Z95-1	3.0865	1.4878	0.9355	0.5665	397.58	177.38	6779.20	522.94	4256.80	-

Spot No.	Preferred age (Ma)	Error ± (Ma)	rho	Conc.
Z01-1	549.30	6.30	0.65	105
Z02-1	1533.80	21.28	0.93	107
Z03-1	581.10	6.07	0.93	94
Z04-1	596.00	6.38	0.82	88
Z05-1	1991.40	18.91	0.96	20
Z06-1	1065.30	10.82	0.91	91
Z07-1	877.90	9.02	0.91	85
Z08-1	547.40	5.84	0.84	114
Z09-1	729.40	7.58	0.91	83
Z10-1	1517.70	19.70	0.97	101
Z12-1	621.70	7.67	0.60	115
Z13-1	609.30	7.40	0.63	97
Z14-1	1896.10	29.49	0.77	33
Z15-1	582.40	6.83	0.68	98
Z16-1	555.60	6.34	0.76	64
Z17-1	618.30	8.22	0.57	65
Z18-1	746.40	8.32	0.78	95
Z19-1	616.50	6.96	0.76	95
Z20-1	626.80	7.10	0.77	71
Z21-1	607.90	6.74	0.79	103
Z22-1	606.50	6.61	0.86	98
Z26-1	2256.40	18.86	0.95	95
Z27-1	906.30	10.37	0.72	85
Z28-1	593.30	6.58	0.80	98
Z29-1	581.80	6.65	0.73	76

Spot No.	Preferred age (Ma)	Error ± (Ma)	rho	Conc.
Z30-1	599.60	6.67	0.78	103
Z31-1	1253.40	13.47	0.87	103
Z32-1	705.80	7.82	0.86	110
Z33-1	610.40	6.81	0.87	101
Z34-1	598.00	6.78	0.81	95
Z35-1	1539.50	20.55	0.95	104
Z36-1	634.00	7.37	0.74	97
Z37-1	1911.40	19.92	0.95	75
Z38-1	839.40	9.26	0.86	110
Z39-1	600.30	7.06	0.72	83
Z40-1	616.70	6.96	0.82	105
Z41-1	657.40	7.37	0.84	98
Z42-1	593.10	6.75	0.80	96
Z43-1	2957.00	17.02	0.97	80
Z46-1	568.40	6.45	0.82	70
Z47-1	2985.00	16.81	0.97	87
Z48-1	562.90	6.25	0.90	106
Z50-1	592.50	6.71	0.82	85
Z51-1	588.40	6.74	0.81	101
Z52-1	585.20	6.88	0.73	108
Z53-1	589.30	6.79	0.79	92
Z54-1	808.50	9.19	0.82	83
Z55-1	629.30	8.35	0.59	80
Z56-1	629.30	7.32	0.76	103
Z57-1	710.20	7.83	0.94	80
Z58-1	619.90	7.31	0.78	52
Z60-1	637.90	7.60	0.70	113
Z62-1	4033.30	54.34	0.94	23
Z63-1	559.70	6.14	0.90	110
Z65-1	563.20	6.26	0.85	89
Z67-1	249.30	3.23	0.54	155
Z68-1	639.60	7.21	0.79	101
Z70-1	2496.50	17.98	0.97	105
Z71-1	3444.20	16.30	0.99	106
Z72-1	613.60	7.17	0.75	115
Z73-1	255.10	3.06	0.72	74
Z74-1	633.40	7.29	0.79	102
Z75-1	640.60	7.17	0.89	111
Z76-1	620.60	7.81	0.61	127
Z77-1	2677.50	17.24	0.99	99
Z78-1	634.60	8.01	0.61	128
Z79-1	1994.00	20.52	0.94	79
Z80-1	630.10	7.12	0.85	111
Z81-1	1592.70	22.26	0.91	45
Z82-1	546.00	7.01	0.61	69
Z84-1	599.50	6.67	0.88	119
Z85-1	621.60	7.19	0.75	105
Z86-1	2095.70	18.88	0.97	108
Z87-1	591.40	6.66	0.83	109
Z88-1	964.30	10.52	0.88	103
Z89-1	597.90	7.49	0.61	100
Z90-1	519.40	6.87	0.56	103
Z91-1	1775.90	19.29	0.97	79
Z92-1	2059.60	53.45	0.62	67
Z93-1	2268.70	19.32	0.94	96
Z96-1	585.90	7.62	0.57	87
Z97-1	2378.70	18.65	0.96	93
Z98-1	1596.90	27.21	0.81	36
Z99-1	605.30	6.93	0.73	124
Z100-1	584.70	6.94	0.67	97
Not Used				
Z11-1			0.97	-
Z23-1			-	-
Z24-1			-	-
Z25-1			0.36	134
Z44-1			-	-
Z45-1			-	-

Spot No.	Preferred age (Ma)	Error ± (Ma)	rho	Conc.
Z49-1			0.94	182
Z58-2			0.94	-
Z61-1			0.79	67
Z64-1			0.85	59
Z66-1			-	-
Z69-1			0.88	96
Z83-1			0.95	195
Z94-1			0.99	167
Z95-1			0.74	63

Cape Jervis Section - unit 5

Spot No.	$^{207}Pb/^{235}U$	Error ±2 σ	$^{206}Pb/^{238}U$	Error ±2 σ	$^{207}Pb/^{235}U$	Error ±2 σ	$^{207}Pb/^{206}Pb$ age (Ma)	Error ± (Ma)	$^{206}Pb/^{238}U$ age (Ma)	Error ± (Ma)
z01-1	0.0758	0.0031	0.0880	0.0016	1.0396	0.0674	1088.50	79.65	543.70	9.51
z02-1	0.0560	0.0009	0.0766	0.0008	0.5995	0.0121	449.90	34.42	475.60	4.99
z04-1	0.2871	0.0106	0.1368	0.0035	5.1942	0.4730	3401.80	56.50	826.50	19.97
z06-1	0.1768	0.0019	0.3240	0.0038	7.8811	0.1609	2623.30	18.17	1809.40	18.24
z07-1	0.1293	0.0014	0.3540	0.0039	6.4441	0.1238	2088.40	19.16	1953.60	18.59
z08-1	0.0968	0.0011	0.0500	0.0005	0.6695	0.0088	1562.90	21.20	314.70	3.26
z09-1	0.0619	0.0008	0.0848	0.0009	0.7130	0.0118	669.10	27.92	524.90	5.43
z10-1	0.2782	0.0032	0.4548	0.0048	17.218	0.4686	3352.60	17.63	2416.50	21.17
z11-1	0.0650	0.0011	0.0935	0.0010	0.8374	0.0185	774.10	33.60	576.10	6.13
z13-1	0.0605	0.0009	0.1009	0.0011	0.8441	0.0167	622.80	31.35	619.80	6.51
z14-1	0.0652	0.0011	0.0728	0.0008	0.6619	0.0139	779.30	33.59	453.00	4.98
z15-1	0.0655	0.0010	0.0928	0.0011	0.8276	0.0172	789.30	31.84	572.30	6.32
z16-1	0.1409	0.0016	0.2295	0.0024	4.4129	0.0719	2238.10	18.84	1331.90	12.49
z17-1	0.0613	0.0011	0.1024	0.0012	0.8555	0.0218	650.90	38.24	628.20	6.93
z18-1	0.2008	0.0056	0.1029	0.0019	3.1909	0.1916	2832.50	44.77	631.20	10.83
z19-1	0.0779	0.0011	0.1873	0.0021	2.1187	0.0513	1143.60	28.16	1106.90	11.27
z21-1	0.0754	0.0012	0.1805	0.0021	1.9299	0.0528	1079.70	31.32	1069.60	11.28
z22-1	0.1051	0.0012	0.0748	0.0008	1.0841	0.0148	1715.70	20.57	465.20	4.77
z23-1	0.0686	0.0025	0.0865	0.0014	0.8939	0.0502	886.00	74.38	534.90	8.51
z24-1	0.1004	0.0013	0.2900	0.0032	4.1470	0.0978	1630.80	23.04	1641.70	15.78
z25-1	0.0575	0.0010	0.0921	0.0010	0.7663	0.0175	512.10	36.70	567.70	6.12
z26-1	0.0853	0.0014	0.2222	0.0026	2.7137	0.0871	1322.60	31.41	1293.50	13.50
z27-1	0.1843	0.0020	0.5274	0.0053	13.787	0.3164	2692.10	18.03	2730.70	22.26
z28-1	0.1313	0.0049	0.1125	0.0023	2.3306	0.1761	2116.00	63.28	687.10	13.06
z29-1	0.2851	0.0077	0.4963	0.0105	36.001	6.1389	3390.80	41.51	2597.70	45.35
z30-1	0.0982	0.0012	0.2085	0.0021	2.8136	0.0552	1589.40	22.75	1220.90	11.33
z31-1	0.0743	0.0009	0.1982	0.0021	2.0509	0.0354	1048.90	23.69	1165.80	11.34
z32-1	0.1514	0.0023	0.4062	0.0047	8.9769	0.4083	2361.70	25.70	2197.40	21.75
z33-1	0.0731	0.0016	0.0818	0.0010	0.8161	0.0254	1016.40	43.61	506.50	6.14
z34-1	0.1627	0.0018	0.4585	0.0050	10.153	0.2191	2483.80	18.34	2433.00	22.03
z35-1	0.0752	0.0009	0.1750	0.0019	1.8409	0.0296	1072.80	23.08	1039.40	10.17
z36-1	0.0605	0.0014	0.0962	0.0012	0.8565	0.0281	620.50	47.49	592.20	7.04
z37-1	0.1405	0.0015	0.4052	0.0043	7.9492	0.1407	2232.80	18.30	2192.90	19.56
z38-1	0.0637	0.0012	0.1238	0.0014	1.0791	0.0301	730.60	38.54	752.10	8.14
z39-1	0.0625	0.0013	0.0852	0.0010	0.7720	0.0228	690.70	43.95	527.20	6.17
z40-1	0.0873	0.0014	0.0527	0.0006	0.6421	0.0128	1367.00	29.99	331.40	3.59
z41-1	0.1799	0.0021	0.4645	0.0050	12.495	0.3640	2651.90	19.41	2459.40	21.79
z42-1	0.0683	0.0020	0.0827	0.0013	0.7553	0.0320	878.00	60.31	512.10	7.46
z43-1	0.0724	0.0012	0.1675	0.0019	1.7405	0.0492	996.60	33.36	998.10	10.42
z44-1	0.0785	0.0010	0.2046	0.0022	2.1459	0.0453	1158.50	25.89	1199.90	11.73
z45-1	0.1632	0.0095	0.1018	0.0033	2.1296	0.2420	2488.90	95.30	624.80	19.03
z46-1	0.0679	0.0018	0.0881	0.0012	0.8227	0.0324	865.70	54.78	544.50	7.13
z47-1	0.0643	0.0008	0.0935	0.0010	0.8332	0.0137	751.60	26.98	576.30	5.91
z48-1	0.0942	0.0032	0.0850	0.0015	1.2265	0.0693	1511.90	63.36	526.10	8.65
z49-1	0.1129	0.0013	0.0947	0.0010	1.4833	0.0203	1846.00	19.85	583.00	5.98
z50-1	0.0641	0.0010	0.1034	0.0012	0.9244	0.0188	745.80	30.96	634.40	7.09
z51-1	0.1403	0.0016	0.3896	0.0041	7.6173	0.1593	2230.40	19.30	2120.90	19.17
z52-1	0.0744	0.0013	0.0868	0.0010	0.8875	0.0217	1051.50	34.66	536.60	6.00
z53-1	0.0821	0.0013	0.1835	0.0020	2.1481	0.0573	1246.70	29.28	1086.00	10.89
z54-1	0.0619	0.0011	0.0927	0.0011	0.7891	0.0197	669.30	38.08	571.40	6.28
z55-1	0.0763	0.0012	0.0915	0.0011	0.9994	0.0232	1103.00	32.28	564.40	6.34
z56-1	0.0765	0.0009	0.0834	0.0009	0.8873	0.0122	1108.20	22.64	516.20	5.24
z57-1	0.1809	0.0019	0.5101	0.0054	12.718	0.2404	2661.20	17.21	2657.20	23.05
z59-1	0.0947	0.0011	0.0497	0.0005	0.6395	0.0085	1522.90	21.57	312.50	3.24
z60-1	0.0565	0.0011	0.0847	0.0010	0.6584	0.0181	471.70	44.65	524.20	5.91
z61-1	0.0777	0.0015	0.1435	0.0017	1.5554	0.0503	1139.40	37.51	864.50	9.83
z62-1	0.0912	0.0018	0.2636	0.0034	3.3910	0.1529	1451.00	37.42	1508.10	17.16
z63-1	0.0729	0.0010	0.1445	0.0015	1.4388	0.0276	1009.90	26.70	870.10	8.70
z64-1	0.1425	0.0015	0.2341	0.0023	4.5536	0.0705	2257.80	18.57	1355.80	12.21
z65-1	0.2971	0.0031	0.5890	0.0059	24.4595	0.4508	3454.90	16.00	2985.50	23.84
z66-1	0.0799	0.0011	0.1894	0.0021	2.1587	0.0526	1193.60	28.01	1117.90	11.26
z67-1	0.0871	0.0021	0.1968	0.0029	2.3675	0.1132	1362.10	45.60	1158.30	15.39
z68-1	0.0699	0.0008	0.0934	0.0010	0.9106	0.0130	925.90	23.80	575.80	5.80
z69-1	0.0906	0.0013	0.2434	0.0027	2.9151	0.0785	1438.80	27.12	1404.30	14.15

Spot No.	$^{207}Pb/^{235}U$	Error ±2 σ	$^{206}Pb/^{238}U$	Error ±2 σ	$^{207}Pb/^{235}U$	Error ±2 σ	$^{207}Pb/^{206}Pb$ age (Ma)	Error ± (Ma)	$^{206}Pb/^{238}U$ age (Ma)	Error ± (Ma)
z70-1	0.1681	0.0064	0.1007	0.0022	2.5026	0.1982	2539.20	62.66	618.70	12.91
z71-1	0.0571	0.0009	0.0946	0.0011	0.7485	0.0167	494.30	36.18	582.60	6.27
z72-1	0.1095	0.0013	0.2667	0.0029	4.1225	0.0785	1790.90	20.88	1524.20	14.50
z73-1	0.0829	0.0011	0.0485	0.0005	0.5515	0.0085	1266.10	24.77	305.30	3.32
z74-1	0.1880	0.0061	0.1042	0.0021	2.9617	0.2033	2724.60	52.07	639.20	12.07
z75-1	0.0676	0.0009	0.0774	0.0008	0.7199	0.0119	854.90	27.25	480.40	5.01
z76-1	0.0660	0.0013	0.0640	0.0008	0.5806	0.0143	807.30	39.20	400.00	4.75
z77-1	0.0676	0.0008	0.1366	0.0015	1.2978	0.0222	855.00	25.69	825.20	8.30
z78-1	0.1522	0.0032	0.1156	0.0016	2.3771	0.0938	2370.60	35.01	704.90	9.29
z80-1	0.0658	0.0010	0.0930	0.0010	0.8511	0.0170	799.70	30.87	573.00	5.95
z81-1	0.0645	0.0011	0.0997	0.0011	0.8703	0.0216	758.70	36.68	612.70	6.63
z82-1	0.0599	0.0010	0.0931	0.0011	0.7948	0.0176	598.90	34.74	573.60	6.18
z83-1	0.0580	0.0008	0.0924	0.0010	0.7230	0.0131	529.60	31.03	570.00	5.90
z84-1	0.1230	0.0106	0.0862	0.0034	3.0289	0.5853	2000.60	145.40	533.10	20.15
z85-1	0.0679	0.0009	0.1035	0.0011	0.9871	0.0162	866.00	26.14	635.00	6.25
z86-1	0.0588	0.0009	0.0939	0.0010	0.7810	0.0153	558.00	31.97	578.70	5.96
z87-1	0.0597	0.0009	0.0959	0.0010	0.8147	0.0168	590.80	32.91	590.50	6.08
z88-1	0.0614	0.0010	0.0851	0.0011	0.7330	0.0152	654.50	32.76	526.80	6.21
z89-1	0.0592	0.0010	0.0836	0.0009	0.6859	0.0146	573.30	34.86	517.30	5.54
z90-1	0.0570	0.0011	0.0883	0.0011	0.7104	0.0183	491.30	41.17	545.30	6.30
z91-1	0.0848	0.0015	0.0629	0.0008	0.7626	0.0183	1309.60	34.11	393.10	4.62
z92-1	0.1172	0.0017	0.2312	0.0026	3.9025	0.1149	1913.20	25.60	1340.90	13.77
z93-1	0.0772	0.0010	0.1610	0.0018	1.7811	0.0354	1126.30	25.76	962.60	9.72
z94.1	0.0633	0.0026	0.0910	0.0016	0.8715	0.0554	718.80	85.47	561.60	9.36
z95-1	0.0613	0.0013	0.1024	0.0012	0.8914	0.0274	651.20	44.32	628.30	7.24
z96-1	0.0719	0.0024	0.1596	0.0026	1.6959	0.1095	982.10	67.72	954.40	14.15
z97-1	0.0779	0.0011	0.1868	0.0021	2.0862	0.0495	1144.90	27.92	1104.10	11.20
z98-1	0.0746	0.0011	0.1063	0.0012	1.0836	0.0227	1056.00	29.79	651.20	6.97
z100-1	0.0596	0.0008	0.0985	0.0010	0.8120	0.0128	587.20	27.07	605.30	6.09
z101-1	0.0541	0.0012	0.0646	0.0008	0.4992	0.0137	376.40	47.56	403.80	4.64
z103-1	0.0544	0.0010	0.0593	0.0007	0.4493	0.0096	385.90	38.64	371.20	4.07
z104-1	0.0875	0.0011	0.0422	0.0005	0.5181	0.0075	1371.30	23.73	266.60	2.88
z105-1	0.1374	0.0025	0.0885	0.0011	1.6954	0.0496	2195.20	30.62	546.40	6.49
z106-1	0.1088	0.0024	0.0898	0.0012	1.4081	0.0500	1780.00	39.03	554.60	7.07
z107-1	0.0596	0.0008	0.0956	0.0010	0.8003	0.0123	590.50	26.89	588.80	5.72
z108-1	0.0618	0.0009	0.0926	0.0010	0.7759	0.0144	665.40	30.26	571.00	6.03
z109-1	0.0962	0.0012	0.1800	0.0019	2.4188	0.0456	1551.30	22.84	1067.10	10.46
z110-1	0.0592	0.0012	0.0962	0.0012	0.8048	0.0235	575.10	43.93	591.80	6.76
z111-1	0.1677	0.0032	0.0926	0.0013	2.2549	0.0758	2535.30	31.18	570.60	7.39
z112-1	0.0701	0.0010	0.1335	0.0014	1.2502	0.0247	930.10	28.22	808.00	7.97
z113-1	0.0585	0.0011	0.0963	0.0011	0.7819	0.0193	548.70	38.56	592.90	6.42
z114-1	0.2621	0.0027	0.6229	0.0065	22.498	0.4515	3259.60	16.37	3121.40	25.65
z115-1	0.1313	0.0014	0.3106	0.0034	5.7615	0.0895	2115.20	18.14	1743.70	16.70
z116-1	0.0605	0.0009	0.0961	0.0010	0.7913	0.0146	621.90	30.37	591.50	5.99
z117-1	0.1323	0.0052	0.1069	0.0023	2.0255	0.1542	2129.20	67.72	654.50	13.29
z118-1	0.1015	0.0015	0.3103	0.0036	4.2902	0.1467	1651.50	27.95	1742.10	17.84
z120-1	0.0691	0.0009	0.1441	0.0015	1.3750	0.0239	902.10	25.78	867.80	8.46
z121-1	0.0656	0.0014	0.0948	0.0012	0.8808	0.0282	793.30	45.10	583.90	6.97
z122-1	0.0881	0.0011	0.1992	0.0021	2.4730	0.0470	1384.90	23.23	1171.00	11.37
z123-1	0.0897	0.0012	0.1844	0.0020	2.2091	0.0511	1417.90	26.26	1091.00	10.99
z124-1	0.1750	0.0019	0.3493	0.0039	8.4019	0.1689	2606.10	18.16	1931.00	18.81
z125-1	0.1150	0.0017	0.2504	0.0032	4.0063	0.1247	1879.80	26.65	1440.50	16.38
z126-1	0.0627	0.0008	0.1203	0.0013	1.0324	0.0162	697.50	25.77	732.20	7.36
z127-1	0.0607	0.0011	0.0989	0.0011	0.8413	0.0222	627.60	39.53	607.90	6.72
z128-1	0.0885	0.0014	0.1862	0.0023	2.3964	0.0724	1393.10	30.88	1100.60	12.45
z129-1	0.0778	0.0011	0.2004	0.0022	2.2614	0.0574	1141.10	28.52	1177.30	12.05
z130-1	0.0595	0.0010	0.0817	0.0009	0.6924	0.0158	586.30	36.67	506.30	5.58
z131-1	0.0925	0.0010	0.1610	0.0017	2.0313	0.0283	1477.20	20.60	962.40	9.34
z132-1	0.0764	0.0011	0.1516	0.0017	1.6671	0.0364	1105.70	28.03	909.70	9.32
z134-1	0.0592	0.0007	0.0962	0.0010	0.7798	0.0115	575.70	25.96	592.30	6.01
z135-1	0.0591	0.0009	0.0941	0.0010	0.7631	0.0159	570.00	33.65	579.90	6.15
z136-1	0.0989	0.0046	0.0846	0.0019	1.4214	0.1164	1604.30	84.40	523.30	11.01
z137-1	0.1306	0.0016	0.3745	0.0041	6.9975	0.1878	2106.60	21.34	2050.50	19.28
z138-1	0.0698	0.0014	0.0905	0.0011	0.9542	0.0285	922.40	40.79	558.60	6.54
z140-1	0.0827	0.0012	0.2177	0.0025	2.5666	0.0698	1260.90	28.50	1269.50	13.01
z141-1	0.2283	0.0023	0.3710	0.0039	11.791	0.1822	3040.30	16.24	2033.90	18.51

Spot No.	$^{207}Pb/^{235}U$	Error ±2 σ	$^{206}Pb/^{238}U$	Error ±2 σ	$^{207}Pb/^{235}U$	Error ±2 σ	$^{207}Pb/^{206}Pb$ age (Ma)	Error ± (Ma)	$^{206}Pb/^{238}U$ age (Ma)	Error ± (Ma)
z142-1	0.1358	0.0015	0.3394	0.0034	6.0434	0.1156	2174.80	19.40	1883.50	16.33
z143-1	0.2857	0.0089	0.1537	0.0034	7.2317	0.6579	3394.10	47.86	921.60	19.05
z144-1	0.0602	0.0010	0.0980	0.0011	0.8208	0.0194	611.80	36.47	602.70	6.36
z145-1	0.1814	0.0021	0.5071	0.0052	13.409	0.3516	2665.40	18.65	2644.30	22.05
z147-1	0.1038	0.0045	0.1731	0.0038	2.7073	0.2642	1693.90	78.16	1029.20	20.73
z148-1	0.0757	0.0022	0.1477	0.0022	1.6574	0.0884	1087.30	56.97	888.20	12.29
z149-1	0.1895	0.0021	0.4975	0.0050	13.432	0.2869	2737.60	17.69	2603.10	21.69
z150-1	0.1384	0.0015	0.3750	0.0038	7.0323	0.1079	2207.60	18.10	2052.70	17.86
z151-1	0.0918	0.0011	0.2610	0.0028	3.3228	0.0693	1463.50	23.01	1494.90	14.31
z152-1	0.0913	0.0020	0.0924	0.0012	1.1565	0.0390	1452.60	40.89	569.60	7.17
z153-1	0.3568	0.0036	0.7994	0.0083	40.353	0.7102	3736.30	15.32	3786.90	29.68
z154-1	0.0813	0.0013	0.1608	0.0018	1.7649	0.0453	1228.30	30.23	961.40	10.21
z155-1	0.1036	0.0013	0.0332	0.0003	0.4728	0.0066	1688.80	23.00	210.70	2.15
z156-1	0.0931	0.0011	0.1778	0.0018	2.3306	0.0365	1490.10	21.29	1055.00	10.09
z157-1	0.0799	0.0019	0.1495	0.0020	1.6728	0.0693	1193.20	45.30	898.30	11.40
z158-1	0.0781	0.0016	0.1775	0.0022	1.9605	0.0740	1150.40	39.80	1053.20	12.22
z159-1	0.0759	0.0009	0.1243	0.0014	1.3051	0.0217	1091.00	24.32	755.00	7.88
Not Used										
z03-1	0.7266	0.0102	0.9150	0.0136	154.054	16.722	4784.30	19.90	4188.30	45.74
z05-1	-	0.0330	-	24.401	-	-	0.10	0.00	-	-
z06-1	1.7193	1.1327	-	-	-	-	5988.20	685.2	-	-
z12-1	0.8849	0.0134	14.837	0.5642	-	-	5065.00	21.22	-	229.7
z20-1	0.5919	0.0903	0.7861	0.1196	23.254	27.659	4488.30	205.5	3739.10	431.7
z58-1	0.5170	0.0240	0.9565	0.0441	-	-	4290.50	66.44	4326.50	145.4
z79-1	1.2049	0.1948	0.8841	0.1653	-	-	5497.90	207.6	4083.50	565.4
z99-1	0.0706	0.0045	0.0951	0.0024	1.1317	0.1190	945.10	124.5	585.70	14.10
z102-1	0.5666	0.0115	0.3281	0.0059	38.4478	4.1205	4424.50	29.28	1828.90	28.62
z119-1	0.6896	0.0163	0.5308	0.0121	71.1527	11.463	4709.30	33.62	2744.80	51.00
z133-1	0.6707	0.0247	0.2926	0.0094	20.7865	3.2128	4669.20	52.14	1654.70	47.09
z139-1	0.6467	0.1049	0.0827	0.0103	-	-	4616.70	216.0	512.00	61.44
z146-1	0.1314	0.0078	0.1244	0.0037	2.8223	0.3878	2116.20	100.6	755.60	21.40

Spot No.	Preferred age (Ma)	Error ± (Ma)	rho	Conc.
z01-1	543.70	9.51	0.28	50
z02-1	475.60	4.99	0.54	106
z04-1	3401.80	56.50	0.28	24
z06-1	2623.30	18.17	0.57	69
z07-1	2088.40	19.16	0.57	94
z08-1	1562.90	21.20	0.81	20
z09-1	524.90	5.43	0.65	78
z10-1	3352.60	17.63	0.39	72
z11-1	576.10	6.13	0.50	74
z13-1	619.80	6.51	0.56	100
z14-1	453.00	4.98	0.54	58
z15-1	572.30	6.32	0.56	73
z16-1	2238.10	18.84	0.64	60
z17-1	628.20	6.93	0.45	97
z18-1	2832.50	44.77	0.30	22
z19-1	1106.90	11.27	0.46	97
z21-1	1069.60	11.28	0.42	99
z22-1	1715.70	20.57	0.78	27
z23-1	534.90	8.51	0.30	60
z24-1	1630.80	23.04	0.46	101
z25-1	567.70	6.12	0.50	111
z26-1	1293.50	13.50	0.36	98
z27-1	2692.10	18.03	0.44	101
z28-1	2116.00	63.28	0.26	32
z29-1	3390.80	41.51	0.12	77
z30-1	1589.40	22.75	0.52	77
z31-1	1165.80	11.34	0.62	111
z32-1	2361.70	25.70	0.26	93
z33-1	506.50	6.14	0.41	50
z34-1	2483.80	18.34	0.50	98
z35-1	1039.40	10.17	0.66	97

Spot No.	Preferred age (Ma)	Error ± (Ma)	rho	Conc.
z36-1	592.20	7.04	0.38	95
z37-1	2232.80	18.30	0.59	98
z38-1	752.10	8.14	0.41	103
z39-1	527.20	6.17	0.41	76
z40-1	331.40	3.59	0.56	24
z41-1	2651.90	19.41	0.37	93
z42-1	512.10	7.46	0.36	58
z43-1	998.10	10.42	0.40	100
z44-1	1199.90	11.73	0.51	104
z45-1	2488.90	95.30	0.28	25
z46-1	544.50	7.13	0.35	63
z47-1	576.30	5.91	0.65	77
z48-1	1511.90	63.36	0.30	35
z49-1	1846.00	19.85	0.79	32
z50-1	634.40	7.09	0.57	85
z51-1	2230.40	19.30	0.51	95
z52-1	536.60	6.00	0.48	51
z53-1	1086.00	10.89	0.41	87
z54-1	571.40	6.28	0.46	85
z55-1	564.40	6.34	0.50	51
z56-1	516.20	5.24	0.77	47
z57-1	2661.20	17.21	0.56	100
z59-1	1522.90	21.57	0.81	21
z60-1	524.20	5.91	0.43	111
z61-1	864.50	9.83	0.37	76
z62-1	1508.10	17.16	0.28	104
z63-1	870.10	8.70	0.56	86
z64-1	2257.80	18.57	0.65	60
z65-1	3454.90	16.00	0.54	86
z66-1	1117.90	11.26	0.45	94
z67-1	1158.30	15.39	0.30	85
z68-1	575.80	5.80	0.74	62
z69-1	1404.30	14.15	0.42	98
z70-1	2539.20	62.66	0.28	24
z71-1	582.60	6.27	0.50	118
z72-1	1790.90	20.88	0.56	85
z73-1	305.30	3.32	0.73	24
z74-1	2724.60	52.07	0.29	23
z75-1	480.40	5.01	0.66	56
z76-1	400.00	4.75	0.49	50
z77-1	825.20	8.30	0.62	97
z78-1	2370.60	35.01	0.35	30
z80-1	573.00	5.95	0.54	72
z81-1	612.70	6.63	0.46	81
z82-1	573.60	6.18	0.51	96
z83-1	570.00	5.90	0.60	108
z84-1	2000.60	145.40	0.20	27
z85-1	635.00	6.25	0.63	73
z86-1	578.70	5.96	0.55	104
z87-1	590.50	6.08	0.52	100
z88-1	526.80	6.21	0.60	80
z89-1	517.30	5.54	0.52	90
z90-1	545.30	6.30	0.47	111
z91-1	393.10	4.62	0.51	30
z92-1	1913.20	25.60	0.39	70
z93-1	962.60	9.72	0.55	85
z94.1	561.60	9.36	0.27	78
z95-1	628.30	7.24	0.39	96
z96-1	954.40	14.15	0.25	97
z97-1	1104.10	11.20	0.46	96
z98-1	651.20	6.97	0.54	62
z100-1	605.30	6.09	0.67	103
z101-1	403.80	4.64	0.43	107
z103-1	371.20	4.07	0.53	96
z104-1	266.60	2.88	0.76	19
z105-1	2195.20	30.62	0.43	25
z106-1	1780.00	39.03	0.37	31

Spot No.	Preferred age (Ma)	Error ± (Ma)	rho	Conc.
z107-1	588.80	5.72	0.66	100
z108-1	571.00	6.03	0.59	86
z109-1	1551.30	22.84	0.56	69
z110-1	591.80	6.76	0.41	103
z111-1	2535.30	31.18	0.40	23
z112-1	808.00	7.97	0.53	87
z113-1	592.90	6.42	0.46	108
z114-1	3259.60	16.37	0.52	96
z115-1	2115.20	18.14	0.70	82
z116-1	591.50	5.99	0.57	95
z117-1	2129.20	67.72	0.28	31
z118-1	1651.50	27.95	0.34	105
z120-1	867.80	8.46	0.60	96
z121-1	583.90	6.97	0.39	74
z122-1	1171.00	11.37	0.56	85
z123-1	1091.00	10.99	0.47	77
z124-1	2606.10	18.16	0.56	74
z125-1	1879.80	26.65	0.41	77
z126-1	732.20	7.36	0.68	105
z127-1	607.90	6.72	0.44	97
z128-1	1100.60	12.45	0.41	79
z129-1	1177.30	12.05	0.44	103
z130-1	506.30	5.58	0.50	86
z131-1	962.40	9.34	0.75	65
z132-1	909.70	9.32	0.50	82
z134-1	592.30	6.01	0.72	103
z135-1	579.90	6.15	0.53	102
z136-1	1604.30	84.40	0.27	33
z137-1	2106.60	21.34	0.41	97
z138-1	558.60	6.54	0.41	61
z140-1	1269.50	13.01	0.42	101
z141-1	3040.30	16.24	0.69	67
z142-1	2174.80	19.40	0.52	87
z143-1	3394.10	47.86	0.24	27
z144-1	602.70	6.36	0.47	99
z145-1	2665.40	18.65	0.39	99
z147-1	1693.90	78.16	0.22	61
z148-1	888.20	12.29	0.28	82
z149-1	2737.60	17.69	0.47	95
z150-1	2207.60	18.10	0.66	93
z151-1	1494.90	14.31	0.51	102
z152-1	569.60	7.17	0.39	39
z153-1	3736.30	15.32	0.59	101
z154-1	961.40	10.21	0.45	78
z155-1	1688.80	23.00	0.73	12
z156-1	1055.00	10.09	0.66	71
z157-1	898.30	11.40	0.33	75
z158-1	1053.20	12.22	0.33	92
z159-1	755.00	7.88	0.66	69
Not Used				
z03-1			0.14	88
z05-1			-	-
z06-1			-	-
z12-1			-	-
z20-1			0.13	83
z58-1			-	101
z79-1			-	74
z99-1			0.24	62
z102-1			0.17	41
z119-1			0.14	58
z133-1			0.21	35
z139-1			-	11
z146-1			0.22	36

Waterloo Bay Section - unit 5

Spot No.	$^{207}Pb/^{235}U$	Error ±2 σ	$^{206}Pb/^{238}U$	Error ±2 σ	$^{207}Pb/^{235}U$	Error ±2 σ	$^{207}Pb/^{206}Pb$ age (Ma)	Error ± (Ma)	$^{206}Pb/^{238}U$ age (Ma)	Error ± (Ma)
Z02-1	0.1739	0.0018	0.4542	0.0052	10.881	0.1253	2595.80	17.48	2413.80	22.82
Z04-1	0.0592	0.0007	0.0951	0.0011	0.7758	0.0094	574.70	24.33	585.80	6.34
Z05-1	0.1538	0.0016	0.3414	0.0038	7.2330	0.0818	2388.90	17.41	1893.30	18.44
Z06-1	0.0588	0.0007	0.0978	0.0011	0.7915	0.0097	559.30	24.69	601.20	6.51
Z07-1	0.0589	0.0008	0.1010	0.0012	0.8195	0.0114	564.30	29.17	620.10	6.85
Z08-1	0.0571	0.0008	0.0829	0.0010	0.6525	0.0094	496.30	30.53	513.40	5.74
Z09-1	0.0728	0.0008	0.1837	0.0021	1.8428	0.0227	1009.10	23.21	1087.20	11.40
Z10-1	0.0878	0.0012	0.2628	0.0031	3.1796	0.0445	1378.70	25.73	1504.30	15.89
Z11-1	0.0725	0.0008	0.1862	0.0021	1.8609	0.0225	999.70	22.64	1100.90	11.52
Z12-1	0.1064	0.0011	0.2084	0.0024	3.0568	0.0357	1738.80	19.58	1220.30	12.63
Z13-1	0.0741	0.0010	0.1942	0.0023	1.9847	0.0266	1045.00	25.62	1144.30	12.21
Z14-1	0.0574	0.0008	0.0965	0.0011	0.7639	0.0113	508.10	30.90	593.70	6.66
Z15-1	0.0741	0.0011	0.1854	0.0022	1.8930	0.0279	1043.70	28.72	1096.30	12.02
Z16-1	0.1811	0.0019	0.4812	0.0055	12.015	0.1388	2663.20	17.46	2532.70	23.90
Z17-1	0.0814	0.0009	0.1026	0.0012	1.1516	0.0135	1231.50	21.07	629.70	6.80
Z18-1	0.0568	0.0006	0.1004	0.0011	0.7851	0.0096	481.10	25.08	616.50	6.68
Z19-1	0.0746	0.0008	0.1866	0.0021	1.9172	0.0227	1056.00	22.13	1102.80	11.50
Z20-1	0.0622	0.0008	0.1023	0.0012	0.8771	0.0113	681.80	25.89	627.60	6.87
Z21-1	0.1113	0.0012	0.3377	0.0039	5.1805	0.0596	1820.80	18.84	1875.40	18.59
Z22-1	0.1789	0.0020	0.5186	0.0061	12.788	0.1517	2642.60	17.99	2693.30	25.67
Z23-1	0.1136	0.0013	0.3194	0.0037	5.0023	0.0606	1857.90	20.12	1787.00	18.11
Z24-1	0.1190	0.0013	0.3845	0.0044	6.3092	0.0745	1941.70	19.22	2097.40	20.64
Z25-1	0.2068	0.0021	0.5703	0.0065	16.259	0.1833	2881.00	16.38	2908.80	26.67
Z26-1	0.0666	0.0009	0.1230	0.0015	1.1293	0.0158	825.40	27.62	747.90	8.32
Z27-1	0.0575	0.0011	0.0978	0.0012	0.7748	0.0141	510.30	39.86	601.30	7.14
Z28-1	0.1431	0.0016	0.4318	0.0050	8.5198	0.1010	2265.50	18.65	2313.90	22.52
Z29-1	0.1315	0.0024	0.0615	0.0008	1.1148	0.0195	2118.50	31.34	384.70	5.00
Z30-1	0.1210	0.0013	0.4051	0.0047	6.7553	0.0790	1970.70	18.91	2192.40	21.37
Z31-1	0.0744	0.0010	0.1466	0.0017	1.5040	0.0204	1053.10	25.81	881.70	9.65
Z32-1	0.0595	0.0008	0.1013	0.0012	0.8315	0.0121	586.00	30.18	622.20	6.98
Z33-1	0.0602	0.0009	0.0888	0.0011	0.7364	0.0111	609.80	31.20	548.30	6.23
Z34-1	0.0685	0.0008	0.1243	0.0014	1.1740	0.0153	884.10	25.13	755.30	8.25
Z35-1	0.0597	0.0008	0.0987	0.0012	0.8123	0.0119	593.80	30.24	606.50	6.82
Z36-1	0.2327	0.0025	0.6293	0.0073	20.188	0.2346	3070.80	16.82	3146.70	28.68
Z37-1	0.1111	0.0012	0.3557	0.0041	5.4477	0.0631	1817.40	19.00	1961.80	19.26
Z38-1	0.0714	0.0010	0.1704	0.0020	1.6759	0.0240	967.60	27.96	1014.10	11.12
Z39-1	0.0589	0.0007	0.0960	0.0011	0.7795	0.0094	562.60	24.01	591.10	6.44
Z40-1	0.1448	0.0015	0.4068	0.0046	8.1206	0.0923	2285.20	17.56	2200.50	21.14
Z41-1	0.0598	0.0010	0.1110	0.0013	0.9153	0.0155	597.40	36.08	678.40	7.79
Z42-1	0.0650	0.0011	0.1121	0.0014	1.0034	0.0165	772.60	33.92	684.80	7.84
Z43-1	0.0584	0.0009	0.1010	0.0012	0.8130	0.0126	544.10	32.90	620.40	6.99
Z44-1	0.1848	0.0020	0.5338	0.0061	13.598	0.1587	2696.30	17.68	2757.60	25.60
Z45-1	0.0708	0.0009	0.1675	0.0019	1.6351	0.0208	951.80	24.41	998.40	10.58
Z46-1	0.0565	0.0012	0.0982	0.0013	0.7644	0.0163	471.10	47.62	603.50	7.41
Z47-1	0.0599	0.0008	0.0973	0.0011	0.8036	0.0112	600.60	28.72	598.50	6.61
Z48-1	0.0582	0.0007	0.0963	0.0011	0.7724	0.0102	535.80	27.73	592.70	6.48
Z49-1	0.0575	0.0012	0.0981	0.0012	0.7784	0.0158	511.80	44.65	603.50	7.30
Z50-1	0.0581	0.0009	0.0902	0.0011	0.7221	0.0113	531.60	33.54	556.90	6.31
Z51-1	0.1863	0.0020	0.4712	0.0055	12.102	0.1450	2710.10	17.96	2488.70	24.05
Z52-1	0.0946	0.0039	0.0860	0.0017	1.1203	0.0434	1519.20	75.95	531.60	10.22
Z53-1	0.1113	0.0012	0.3414	0.0039	5.2375	0.0620	1820.80	19.39	1893.20	18.85
Z54-1	0.0602	0.0009	0.0993	0.0012	0.8229	0.0126	608.80	31.65	610.10	6.95
Z55-1	0.0609	0.0007	0.0950	0.0011	0.7968	0.0101	634.50	25.03	584.90	6.45
Z56-1	0.0766	0.0013	0.0946	0.0012	0.9988	0.0166	1110.80	32.57	582.70	6.91
Z57-1	0.0591	0.0008	0.0859	0.0010	0.6998	0.0102	570.10	29.99	531.40	6.02
Z58-1	0.1166	0.0012	0.3013	0.0035	4.8408	0.0563	1903.90	18.72	1697.80	17.07
Z59-1	0.0581	0.0009	0.1031	0.0012	0.8259	0.0130	532.90	33.51	632.70	7.23
Z60-1	0.0606	0.0011	0.1028	0.0013	0.8587	0.0160	625.80	39.57	630.60	7.55
Z61-1	0.0587	0.0007	0.0951	0.0011	0.7691	0.0097	555.60	25.36	585.30	6.40
Z62-1	0.1097	0.0012	0.3577	0.0041	5.4112	0.0645	1795.00	19.79	1971.10	19.41
Z63-1	0.0607	0.0007	0.0913	0.0011	0.7631	0.0098	626.90	25.74	563.00	6.19
Z64-1	0.0565	0.0010	0.0979	0.0012	0.7625	0.0134	471.00	38.42	602.10	7.00
Z65-1	0.0582	0.0008	0.1093	0.0013	0.8762	0.0123	535.30	29.66	668.50	7.40
Z66-1	0.0806	0.0010	0.2166	0.0025	2.4056	0.0322	1211.00	24.79	1263.70	13.41

Spot No.	$^{207}Pb/^{235}U$	Error ±2 σ	$^{206}Pb/^{238}U$	Error ±2 σ	$^{207}Pb/^{235}U$	Error ±2 σ	$^{207}Pb/^{206}Pb$ age (Ma)	Error ± (Ma)	$^{206}Pb/^{238}U$ age (Ma)	Error ± (Ma)
Z67-1	0.0603	0.0009	0.0980	0.0012	0.8147	0.0128	614.40	32.78	602.70	6.87
Z68-1	0.0986	0.0011	0.2963	0.0034	4.0259	0.0501	1597.00	21.45	1672.90	17.01
Z69-1	0.0787	0.0013	0.2149	0.0027	2.3317	0.0391	1164.50	32.53	1254.90	14.20
Z70-1	0.0753	0.0009	0.1892	0.0022	1.9634	0.0241	1075.40	22.59	1117.20	11.73
Z71-1	0.2150	0.0023	0.5622	0.0065	16.660	0.1945	2943.40	17.12	2875.70	26.81
Z72-1	0.0686	0.0010	0.1499	0.0018	1.4172	0.0210	886.60	29.37	900.20	10.03
Z73-1	0.0591	0.0010	0.0942	0.0011	0.7674	0.0127	570.50	34.95	580.40	6.72
Z74-1	0.0598	0.0007	0.1020	0.0012	0.8398	0.0109	594.50	26.28	625.80	6.88
Z75-1	0.1075	0.0013	0.3307	0.0039	4.8978	0.0639	1756.60	22.35	1841.60	18.94
Z76-1	0.1057	0.0012	0.2930	0.0034	4.2708	0.0531	1727.20	21.10	1656.50	16.98
Z77-1	0.0575	0.0008	0.0907	0.0011	0.7183	0.0105	508.90	30.55	559.60	6.32
Z79-1	0.0796	0.0012	0.2118	0.0026	2.3249	0.0353	1187.50	28.96	1238.60	13.68
Z80-1	0.1224	0.0013	0.1889	0.0022	3.1887	0.0374	1992.10	18.94	1115.50	11.72
Z81-1	0.2076	0.0021	0.4900	0.0055	14.022	0.1577	2886.80	16.62	2570.60	23.67
Z82-1	0.0680	0.0015	0.0929	0.0012	0.8707	0.0182	867.70	43.58	572.80	7.14
Z83-1	0.0706	0.0010	0.1331	0.0016	1.2950	0.0183	945.10	27.79	805.60	8.81
Z84-1	0.0594	0.0013	0.0944	0.0012	0.7726	0.0161	580.70	45.39	581.50	7.12
Z85-1	0.1588	0.0017	0.4930	0.0056	10.792	0.1244	2442.90	17.90	2583.60	23.99
Z86-1	0.1988	0.0021	0.4738	0.0053	12.986	0.1472	2816.30	16.91	2500.40	23.23
Z87-1	0.0597	0.0010	0.0930	0.0011	0.7652	0.0126	593.00	34.37	573.20	6.54
Z88-1	0.0618	0.0010	0.0981	0.0012	0.8357	0.0138	667.80	34.62	603.10	6.89
Z90-1	0.1780	0.0019	0.4810	0.0054	11.805	0.1344	2634.60	17.30	2531.60	23.50
Z91-1	0.0600	0.0008	0.1043	0.0012	0.8622	0.0115	602.60	27.12	639.40	7.01
Z92-1	0.0597	0.0011	0.0924	0.0012	0.7613	0.0141	593.90	39.40	569.90	6.76
Z93-1	0.0819	0.0010	0.1763	0.0021	1.9913	0.0265	1243.30	24.49	1046.90	11.24
Z94-1	0.0563	0.0010	0.0992	0.0012	0.7693	0.0132	461.30	37.31	609.70	7.04
Z95-1	0.0623	0.0010	0.1043	0.0013	0.8953	0.0142	684.00	32.70	639.30	7.27
Z96-1	0.1071	0.0018	0.1378	0.0018	2.0342	0.0337	1750.00	30.12	832.30	9.90
Z97-1	0.0583	0.0009	0.0967	0.0012	0.7767	0.0123	539.50	34.01	594.90	6.76
Z98-1	0.1944	0.0021	0.5461	0.0063	14.638	0.1725	2779.90	17.57	2808.80	26.08
Z99-1	0.0697	0.0010	0.1305	0.0015	1.2536	0.0181	919.30	28.29	790.50	8.75
Z100-1	0.0655	0.0011	0.0932	0.0011	0.8419	0.0140	789.90	34.16	574.70	6.67
Z101-1	0.0595	0.0009	0.1008	0.0012	0.8265	0.0127	586.20	32.23	618.90	7.01
Z102-1	0.0627	0.0009	0.0923	0.0011	0.7968	0.0122	696.50	31.49	569.20	6.48
Z103-1	0.0580	0.0013	0.0890	0.0012	0.7115	0.0159	529.30	49.31	549.80	6.94
Z104-1	0.0539	0.0009	0.0611	0.0007	0.4531	0.0079	364.50	38.65	382.10	4.50
Z105-1	0.1448	0.0016	0.4568	0.0053	9.1113	0.1098	2285.10	19.00	2425.20	23.32
Z106-1	0.0691	0.0017	0.0987	0.0014	0.9398	0.0225	902.50	49.81	606.60	8.05
Z107-1	0.0746	0.0009	0.1792	0.0021	1.8410	0.0232	1057.00	23.72	1062.30	11.25
Z108-1	0.0575	0.0008	0.0840	0.0010	0.6652	0.0101	509.90	31.57	519.80	5.89
Z109-1	0.0831	0.0009	0.2056	0.0024	2.3537	0.0289	1271.50	21.90	1205.20	12.58
Z110-1	0.0792	0.0010	0.2158	0.0025	2.3535	0.0311	1176.10	24.50	1259.50	13.31
Z111-1	0.0723	0.0011	0.1771	0.0021	1.7654	0.0277	995.40	30.86	1051.30	11.73
Not Used										
Z01-1	0.8020	0.0111	318.09	50.211	-	-	4925.40	19.52	-	1014.4
Z03-1	-	0.9560	-	11.289	552.14	196.29	0.10	3784	-	-
Z78-1	0.7929	0.0085	6.3582	0.0862	694.98	9.2876	4909.00	15.18	-	75.54
Z89-1	0.8312	0.0109	-	5.8615	-	670.18	4976.10	18.57	-	-

Spot No.	Preferred age (Ma)	Error ± (Ma)	rho	Conc.
Z02-1	2595.80	17.48	0.98	93
Z04-1	585.80	6.34	0.93	102
Z05-1	2388.90	17.41	0.99	79
Z06-1	601.20	6.51	0.93	107
Z07-1	620.10	6.85	0.83	110
Z08-1	513.40	5.74	0.81	103
Z09-1	1087.20	11.40	0.92	108
Z10-1	1504.30	15.89	0.84	109
Z11-1	1100.90	11.52	0.94	110
Z12-1	1738.80	19.58	0.97	70
Z13-1	1144.30	12.21	0.87	110
Z14-1	593.70	6.66	0.80	117
Z15-1	1096.30	12.02	0.81	105
Z16-1	2663.20	17.46	0.99	95
Z17-1	629.70	6.80	0.96	51
Z18-1	616.50	6.68	0.93	128
Z19-1	1102.80	11.50	0.96	104
Z20-1	627.60	6.87	0.88	92
Z21-1	1820.80	18.84	0.99	103
Z22-1	2642.60	17.99	0.98	102
Z23-1	1857.90	20.12	0.96	96
Z24-1	1941.70	19.22	0.98	108
Z25-1	2881.00	16.38	0.99	101
Z26-1	747.90	8.32	0.85	91
Z27-1	601.30	7.14	0.68	118
Z28-1	2265.50	18.65	0.98	102
Z29-1	2118.50	31.34	0.76	18
Z30-1	1970.70	18.91	0.98	111
Z31-1	881.70	9.65	0.87	84
Z32-1	622.20	6.98	0.81	106
Z33-1	548.30	6.23	0.79	90
Z34-1	755.30	8.25	0.89	85
Z35-1	606.50	6.82	0.80	102
Z36-1	3070.80	16.82	0.99	102
Z37-1	1817.40	19.00	0.98	108
Z38-1	1014.10	11.12	0.83	105
Z39-1	591.10	6.44	0.94	105
Z40-1	2285.20	17.56	1.00	96
Z41-1	678.40	7.79	0.71	114
Z42-1	684.80	7.84	0.73	89
Z43-1	620.40	6.99	0.76	114
Z44-1	2696.30	17.68	0.98	102
Z45-1	998.40	10.58	0.90	105
Z46-1	603.50	7.41	0.60	128
Z47-1	598.50	6.61	0.83	100
Z48-1	592.70	6.48	0.87	111
Z49-1	603.50	7.30	0.62	118
Z50-1	556.90	6.31	0.76	105
Z51-1	2710.10	17.96	0.97	92
Z52-1	1519.20	75.95	0.52	35
Z53-1	1820.80	19.39	0.97	104
Z54-1	610.10	6.95	0.78	100
Z55-1	584.90	6.45	0.92	92
Z56-1	582.70	6.91	0.74	52
Z57-1	531.40	6.02	0.81	93
Z58-1	1903.90	18.72	0.98	89
Z59-1	632.70	7.23	0.77	119
Z60-1	630.60	7.55	0.67	101
Z61-1	585.30	6.40	0.91	105
Z62-1	1795.00	19.79	0.96	110
Z63-1	563.00	6.19	0.90	90
Z64-1	602.10	7.00	0.69	128
Z65-1	668.50	7.40	0.83	125
Z66-1	1263.70	13.41	0.87	104
Z67-1	602.70	6.87	0.76	98
Z68-1	1597.00	21.45	0.93	105
Z69-1	1254.90	14.20	0.74	108

Spot No.	Preferred age (Ma)	Error ± (Ma)	Rho	Conc.
Z70-1	1117.20	11.73	0.93	104
Z71-1	2943.40	17.12	0.99	98
Z72-1	900.20	10.03	0.81	102
Z73-1	580.40	6.72	0.73	102
Z74-1	625.80	6.88	0.90	105
Z75-1	1756.60	22.35	0.91	105
Z76-1	1727.20	21.10	0.94	96
Z77-1	559.60	6.32	0.80	110
Z79-1	1238.60	13.68	0.80	104
Z80-1	1992.10	18.94	0.98	56
Z81-1	2886.80	16.62	0.99	89
Z82-1	572.80	7.14	0.62	66
Z83-1	805.60	8.81	0.83	85
Z84-1	581.50	7.12	0.61	100
Z85-1	2442.90	17.90	0.98	106
Z86-1	2816.30	16.91	0.99	89
Z87-1	573.20	6.54	0.73	97
Z88-1	603.10	6.89	0.72	90
Z90-1	2634.60	17.30	0.99	96
Z91-1	639.40	7.01	0.86	106
Z92-1	569.90	6.76	0.67	96
Z93-1	1046.90	11.24	0.87	84
Z94-1	609.70	7.04	0.71	132
Z95-1	639.30	7.27	0.76	93
Z96-1	1750.00	30.12	0.77	48
Z97-1	594.90	6.76	0.75	110
Z98-1	2779.90	17.57	0.97	101
Z99-1	790.50	8.75	0.81	86
Z100-1	574.70	6.67	0.73	73
Z101-1	618.90	7.01	0.77	106
Z102-1	569.20	6.48	0.78	82
Z103-1	549.80	6.94	0.59	104
Z104-1	382.10	4.50	0.69	105
Z105-1	2285.10	19.00	0.96	106
Z106-1	606.60	8.05	0.58	67
Z107-1	1062.30	11.25	0.91	101
Z108-1	519.80	5.89	0.78	102
Z109-1	1205.20	12.58	0.93	95
Z110-1	1259.50	13.31	0.88	107
Z111-1	1051.30	11.73	0.77	106
Z01-1			-	-
Z03-1			-	-
Z78-1			0.99	-
Z89-1			-	-

Arckaringa Basin – Boorthanna Formation

Mount Dutton Section

Spot No.	$^{207}Pb/^{235}U$	Error ±2 σ	$^{206}Pb/^{238}U$	Error ±2 σ	$^{207}Pb/^{235}U$	Error ±2 σ	$^{207}Pb/^{206}Pb$ age (Ma)	Error ± (Ma)	$^{206}Pb/^{238}U$ age (Ma)	Error ± (Ma)
Z1	0.0996	0.0012	0.2706	0.0037	3.7168	0.0556	1617.10	23.03	1544.00	18.81
Z2	0.0757	0.0010	0.1614	0.0022	1.6842	0.0256	1086.50	25.23	964.80	12.30
Z3	0.0615	0.0011	0.0904	0.0013	0.7663	0.0148	657.10	37.61	557.80	7.68
Z4	0.0679	0.0009	0.1241	0.0017	1.1607	0.0185	864.70	27.86	753.90	9.90
Z5	0.0909	0.0012	0.1447	0.0020	1.8133	0.0280	1444.20	24.15	871.40	11.33
Z6	0.1088	0.0014	0.2975	0.0042	4.4622	0.0686	1779.30	22.85	1679.10	20.60
Z7	0.0839	0.0012	0.2194	0.0031	2.5374	0.0417	1290.20	26.88	1278.70	16.42
Z8	0.0982	0.0013	0.2802	0.0039	3.7930	0.0596	1590.40	23.84	1592.20	19.82
Z9	0.0679	0.0012	0.0896	0.0013	0.8378	0.0166	863.80	36.87	553.10	7.83
Z10	0.1091	0.0014	0.2924	0.0042	4.3963	0.0710	1783.80	23.98	1653.60	20.71
Z11	0.0604	0.0008	0.0949	0.0013	0.7900	0.0129	617.50	29.57	584.30	7.83
Z12	0.1079	0.0014	0.3055	0.0043	4.5446	0.0700	1764.00	22.81	1718.60	21.12
Z13	0.1446	0.0074	0.1435	0.0041	2.8595	0.1352	2282.90	85.61	864.10	23.13
Z14	0.1842	0.0024	0.4378	0.0062	11.117	0.1749	2690.80	21.23	2340.80	27.93
Z15	0.0681	0.0012	0.1332	0.0020	1.2503	0.0241	871.40	35.62	806.00	11.19
Z16	0.0794	0.0011	0.1958	0.0028	2.1440	0.0355	1183.00	27.33	1152.50	15.12
Z17	0.0626	0.0013	0.0880	0.0014	0.7596	0.0170	694.70	44.44	543.80	8.01
Z18	0.0755	0.0018	0.1150	0.0019	1.1962	0.0292	1080.70	46.61	701.70	10.73
Z19	0.0600	0.0010	0.0997	0.0015	0.8250	0.0154	604.60	35.26	612.60	8.63
Z20	0.0782	0.0012	0.1887	0.0028	2.0346	0.0362	1152.30	29.96	1114.40	15.08
Z22	0.1070	0.0012	0.3074	0.0046	4.5362	0.0699	1749.40	20.98	1728.00	22.65
Z23	0.1124	0.0012	0.2921	0.0043	4.5249	0.0674	1837.90	19.37	1652.00	21.58
Z24	0.0598	0.0009	0.0923	0.0014	0.7615	0.0133	597.20	31.08	569.30	8.25
Z26	0.1802	0.0022	0.2383	0.0036	5.9203	0.0928	2654.70	19.99	1377.90	18.82
Z27	0.0679	0.0010	0.0920	0.0014	0.8611	0.0154	864.60	30.97	567.50	8.29
Z28	0.0591	0.0007	0.0916	0.0014	0.7464	0.0118	572.10	26.08	564.70	8.05
Z31	0.0637	0.0008	0.1041	0.0014	0.9155	0.0131	730.20	25.85	638.10	7.95
Z32	0.0622	0.0008	0.0735	0.0010	0.6315	0.0094	681.20	27.78	456.90	5.81
Z33	0.0848	0.0015	0.1835	0.0026	2.1488	0.0400	1309.60	34.00	1085.80	14.04
Z34	0.1045	0.0011	0.2971	0.0039	4.2894	0.0569	1704.80	19.96	1676.90	19.19
Z35	0.0583	0.0009	0.0799	0.0011	0.6436	0.0112	540.30	35.55	495.40	6.44
Z37	0.0886	0.0022	0.0912	0.0014	1.1169	0.0275	1395.20	46.52	562.70	8.31
Z38	0.1119	0.0019	0.2831	0.0041	4.3773	0.0788	1830.10	30.66	1606.90	20.45
Z39	0.1041	0.0011	0.2948	0.0038	4.2438	0.0558	1699.20	19.71	1665.60	19.04
Z40	0.0708	0.0014	0.0924	0.0013	0.9041	0.0189	952.70	40.85	569.40	7.79
Z41	0.1048	0.0011	0.3139	0.0044	4.5345	0.0629	1710.70	19.31	1759.70	21.44
Z42	0.0789	0.0009	0.1988	0.0028	2.1618	0.0306	1168.80	21.59	1169.00	14.92
Z43	0.0680	0.0009	0.1483	0.0021	1.3911	0.0223	869.60	27.74	891.50	11.85
Z44	0.0698	0.0009	0.1112	0.0016	1.0698	0.0167	922.80	26.49	679.50	9.14
Z45	0.4013	0.0058	0.1622	0.0026	8.9730	0.1418	3913.80	21.66	969.00	14.13
Z46	0.1053	0.0011	0.3152	0.0044	4.5739	0.0643	1719.10	19.83	1766.00	21.59
Z47	0.1395	0.0015	0.3798	0.0053	7.3036	0.1008	2220.80	18.03	2075.40	24.71
Z48	0.1125	0.0013	0.3081	0.0043	4.7811	0.0681	1840.90	20.00	1731.60	21.30
Z49	0.0645	0.0011	0.0852	0.0013	0.7569	0.0146	756.80	36.99	526.90	7.46
Z50	0.0591	0.0007	0.1029	0.0014	0.8381	0.0124	570.40	24.84	631.30	8.42
Z51	0.1119	0.0013	0.2995	0.0042	4.6211	0.0660	1830.20	20.09	1689.10	20.83
Z52	0.1840	0.0019	0.4035	0.0056	10.233	0.1409	2688.80	17.06	2185.00	25.78
Z53	0.1063	0.0012	0.3097	0.0043	4.5401	0.0650	1737.20	20.41	1739.30	21.38
Z54	0.1071	0.0011	0.2642	0.0037	3.9025	0.0543	1750.90	19.17	1511.40	18.75
Z55	0.0614	0.0009	0.0854	0.0012	0.7222	0.0119	651.60	29.97	528.10	7.22
Z56	0.1140	0.0012	0.3012	0.0042	4.7351	0.0667	1864.50	19.50	1697.20	20.85
Z57	0.1074	0.0012	0.3086	0.0043	4.5693	0.0639	1755.30	19.40	1734.00	21.19
Z58	0.0796	0.0009	0.2097	0.0029	2.3016	0.0332	1186.80	22.21	1227.40	15.64
Z59	0.0577	0.0007	0.0880	0.0012	0.6993	0.0108	516.40	27.83	543.50	7.34
Z60	0.0646	0.0014	0.0958	0.0015	0.8523	0.0189	759.80	43.86	589.50	8.60
Z61	0.1804	0.0021	0.4061	0.0059	10.102	0.1507	2656.70	19.14	2197.20	27.25
Z62	0.1148	0.0012	0.1681	0.0024	2.6597	0.0376	1876.00	18.56	1001.70	13.25
Z63	0.0992	0.0015	0.1691	0.0026	2.3119	0.0408	1608.20	28.49	1007.30	14.10
Z64	0.2082	0.0043	0.1268	0.0022	3.6401	0.0759	2891.90	33.20	769.60	12.73
Z65	0.0691	0.0008	0.0832	0.0012	0.7930	0.0118	902.10	23.23	515.40	7.12
Z66	0.0916	0.0012	0.2545	0.0037	3.2141	0.0503	1458.80	23.76	1461.90	19.11

Spot No.	$^{207}Pb/^{235}U$	Error ±2 σ	$^{206}Pb/^{238}U$	Error ±2 σ	$^{207}Pb/^{235}U$	Error ±2 σ	$^{207}Pb/^{206}Pb$ age (Ma)	Error ± (Ma)	$^{206}Pb/^{238}U$ age (Ma)	Error ± (Ma)
Z67	0.0723	0.0010	0.1158	0.0017	1.1543	0.0190	994.30	27.63	706.40	9.81
Z68	0.0619	0.0008	0.0958	0.0014	0.8172	0.0134	670.60	28.63	589.50	8.21
Z69	0.2706	0.0030	0.6631	0.0097	24.739	0.3587	3309.60	17.06	3279.10	37.40
Z70	0.0598	0.0010	0.0915	0.0014	0.7544	0.0146	595.10	37.64	564.60	8.12
Z71	0.1088	0.0012	0.3087	0.0044	4.6296	0.0669	1778.80	19.68	1734.50	21.84
Z72	0.0641	0.0011	0.0816	0.0012	0.7203	0.0136	743.60	35.24	505.40	7.29
Z73	0.0747	0.0013	0.1858	0.0026	1.9128	0.0351	1059.20	34.89	1098.60	13.99
Z74	0.0707	0.0013	0.1596	0.0022	1.5549	0.0292	947.90	36.16	954.40	12.31
Z75	0.0711	0.0008	0.1545	0.0020	1.5137	0.0206	958.80	23.24	926.30	11.11
Z76	0.0614	0.0015	0.0940	0.0014	0.7962	0.0201	653.60	53.01	579.30	8.29
Z77	0.1099	0.0013	0.3330	0.0043	5.0459	0.0688	1797.80	20.83	1852.90	20.89
Z78	0.0784	0.0009	0.1767	0.0023	1.9108	0.0258	1157.40	22.23	1049.10	12.46
Z79	0.1074	0.0012	0.3204	0.0041	4.7428	0.0632	1755.20	20.08	1791.60	20.15
Z80	0.0580	0.0009	0.0855	0.0011	0.6837	0.0118	529.50	35.00	528.80	6.79
Z81	0.1191	0.0013	0.3283	0.0043	5.3917	0.0725	1942.80	20.03	1830.30	20.61
Z82	0.1835	0.0022	0.4526	0.0060	11.452	0.1593	2684.80	19.65	2406.90	26.62
Z83	0.0634	0.0008	0.1118	0.0016	0.9767	0.0145	720.60	25.15	683.20	8.97
Z84	0.1088	0.0012	0.3160	0.0044	4.7383	0.0663	1779.00	19.59	1770.00	21.32
Z85	0.0998	0.0011	0.2941	0.0041	4.0453	0.0571	1619.60	20.30	1662.20	20.21
Z86	0.2361	0.0025	0.6261	0.0086	20.377	0.2798	3093.80	16.51	3134.00	34.14
Z87	0.1044	0.0012	0.3038	0.0042	4.3710	0.0626	1703.40	20.66	1709.90	20.81
Z88	0.0575	0.0008	0.0809	0.0011	0.6405	0.0102	508.90	29.11	501.20	6.74
Z89	0.0630	0.0007	0.0976	0.0013	0.8477	0.0121	707.40	23.42	600.50	7.89
Z90	0.1058	0.0011	0.3166	0.0043	4.6181	0.0637	1728.20	19.15	1773.30	21.27
Z91	0.1442	0.0015	0.4286	0.0059	8.5208	0.1181	2278.50	18.16	2299.30	26.63
Z92	0.1380	0.0020	0.1568	0.0023	2.9842	0.0494	2202.50	25.23	939.20	12.79
Z93	0.0598	0.0007	0.0791	0.0011	0.6525	0.0097	596.60	26.03	490.90	6.49
Z94	0.0758	0.0009	0.1708	0.0024	1.7847	0.0259	1089.70	23.15	1016.40	12.91
Z95	0.0778	0.0010	0.1831	0.0025	1.9633	0.0300	1141.40	25.07	1083.60	13.85
Z96	0.0608	0.0009	0.0877	0.0012	0.7349	0.0126	630.80	32.03	542.00	7.32
Z97	0.0887	0.0010	0.1599	0.0022	1.9554	0.0281	1397.20	21.67	956.40	12.20
Z98	0.0807	0.0011	0.1918	0.0027	2.1335	0.0342	1213.50	26.72	1131.10	14.57
Z99	0.1106	0.0012	0.3110	0.0043	4.7424	0.0669	1809.00	19.94	1745.80	20.96
Z100	0.1066	0.0011	0.3163	0.0043	4.6494	0.0646	1742.00	19.54	1771.80	21.14
Z101	0.0581	0.0008	0.0884	0.0012	0.7078	0.0118	532.70	31.70	545.90	7.32
Z102	0.0997	0.0011	0.2410	0.0033	3.3143	0.0458	1618.90	19.63	1392.10	17.05
Not Used										
Z21	0.8672	0.1012	9.3891	2.0676	-	239.34	5036.30	155.94	-	1282.97
Z25	0.6297	0.3181	4.1210	0.3979	357.76	182.30	4578.00	583.89	-	500.83
Z29	0.1102	0.0326	0.1400	0.0185	2.1279	0.5761	1802.90	458.56	844.90	104.65
Z30	0.0013	0.0037	0.0910	0.0022	0.0160	0.0468	0.10	0.00	561.30	12.67
Z36	0.1229	0.0108	0.6358	0.0317	10.801	0.9034	1998.80	148.35	3172.60	125.09

Spot No.	Preferred age (Ma)	Error ± (Ma)	rho	Conc.
Z1	1617.10	23.03	0.92	95
Z2	964.80	12.30	0.90	89
Z3	557.80	7.68	0.75	85
Z4	753.90	9.90	0.87	87
Z5	871.40	11.33	0.90	60
Z6	1779.30	22.85	0.91	94
Z7	1278.70	16.42	0.86	99
Z8	1590.40	23.84	0.89	100
Z9	553.10	7.83	0.75	64
Z10	1783.80	23.98	0.88	93
Z11	584.30	7.83	0.86	95
Z12	1764.00	22.81	0.91	97
Z13	2282.90	85.61	0.60	38
Z14	2690.80	21.23	0.90	87
Z15	806.00	11.19	0.77	92
Z16	1152.50	15.12	0.86	97
Z17	543.80	8.01	0.68	78
Z18	701.70	10.73	0.66	65
Z19	612.60	8.63	0.79	101
Z20	1114.40	15.08	0.83	97

Spot No.	Preferred age (Ma)	Error ± (Ma)	rho	Conc.
Z22	1749.40	20.98	0.97	99
Z23	1837.90	19.37	1.00	90
Z24	569.30	8.25	0.87	95
Z26	2654.70	19.99	0.97	52
Z27	567.50	8.29	0.85	66
Z28	564.70	8.05	0.94	99
Z31	638.10	7.95	0.91	87
Z32	456.90	5.81	0.88	67
Z33	1085.80	14.04	0.75	83
Z34	1704.80	19.96	0.98	98
Z35	495.40	6.44	0.78	92
Z37	562.70	8.31	0.63	40
Z38	1830.10	30.66	0.80	88
Z39	1699.20	19.71	0.99	98
Z40	569.40	7.79	0.69	60
Z41	1710.70	19.31	1.00	103
Z42	1169.00	14.92	0.98	100
Z43	891.50	11.85	0.89	103
Z44	679.50	9.14	0.91	74
Z45	3913.80	21.66	0.99	25
Z46	1719.10	19.83	0.99	103
Z47	2220.80	18.03	0.99	93
Z48	1840.90	20.00	0.98	94
Z49	526.90	7.46	0.76	70
Z50	631.30	8.42	0.95	111
Z51	1830.20	20.09	0.98	92
Z52	2688.80	17.06	0.99	81
Z53	1737.20	20.41	0.98	100
Z54	1750.90	19.17	1.00	86
Z55	528.10	7.22	0.87	81
Z56	1864.50	19.50	0.99	91
Z57	1755.30	19.40	1.00	99
Z58	1227.40	15.64	0.97	103
Z59	543.50	7.34	0.92	105
Z60	589.50	8.60	0.69	78
Z61	2656.70	19.14	0.98	83
Z62	1876.00	18.56	0.99	53
Z63	1608.20	28.49	0.86	63
Z64	2891.90	33.20	0.84	27
Z65	515.40	7.12	0.97	57
Z66	1461.90	19.11	0.93	100
Z67	706.40	9.81	0.89	71
Z68	589.50	8.21	0.89	88
Z69	3309.60	17.06	1.00	99
Z70	564.60	8.12	0.77	95
Z71	1778.80	19.68	0.99	98
Z72	505.40	7.29	0.79	68
Z73	1098.60	13.99	0.75	104
Z74	954.40	12.31	0.74	101
Z75	926.30	11.11	0.95	97
Z76	579.30	8.29	0.60	89
Z77	1797.80	20.83	0.95	103
Z78	1049.10	12.46	0.95	91
Z79	1755.20	20.08	0.97	102
Z80	528.80	6.79	0.77	100
Z81	1942.80	20.03	0.96	94
Z82	2684.80	19.65	0.95	90
Z83	683.20	8.97	0.94	95
Z84	1779.00	19.59	0.98	99
Z85	1619.60	20.30	0.98	103
Z86	3093.80	16.51	1.00	101
Z87	1703.40	20.66	0.97	100
Z88	501.20	6.74	0.88	98
Z89	600.50	7.89	0.97	85
Z90	1728.20	19.15	0.99	103
Z91	2278.50	18.16	0.99	101
Z92	2202.50	25.23	0.88	43

Spot No.	Preferred age (Ma)	Error ± (Ma)	rho	Conc.
Z93	490.90	6.49	0.93	82
Z94	1016.40	12.91	0.95	93
Z95	1083.60	13.85	0.91	95
Z96	542.00	7.32	0.82	86
Z97	956.40	12.20	0.95	68
Z98	1131.10	14.57	0.88	93
Z99	1809.00	19.94	0.97	97
Z100	1742.00	19.54	0.98	102
Z101	545.90	7.32	0.84	102
Z102	1618.90	19.63	0.99	86
Not Used				
Z21			-	-
Z25			0.19	-
Z29			0.49	47
Z30			0.01	-
Z36			0.60	159

Box Creek Section

Spot No.	$^{207}Pb/^{235}U$	Error ±2 σ	$^{206}Pb/^{238}U$	Error ±2 σ	$^{207}Pb/^{235}U$	Error ±2 σ	$^{207}Pb/^{206}Pb$ age (Ma)	Error ± (Ma)	$^{206}Pb/^{238}U$ age (Ma)	Error ± (Ma)
Z1	0.0767	0.0010	0.1821	0.0024	1.9228	0.0274	1112.80	24.43	1078.60	12.88
Z2	0.0797	0.0014	0.1491	0.0021	1.6355	0.0298	1188.50	33.76	896.00	11.57
Z3	0.0637	0.0014	0.0784	0.0011	0.6870	0.0153	730.80	45.75	486.30	6.73
Z4	0.0722	0.0016	0.1440	0.0021	1.4309	0.0328	991.30	45.45	867.00	12.01
Z5	0.0783	0.0011	0.1781	0.0024	1.9192	0.0298	1153.30	27.57	1056.70	12.90
Z6	0.0601	0.0009	0.0941	0.0012	0.7785	0.0122	607.20	30.35	579.60	7.28
Z7	0.1060	0.0012	0.1262	0.0016	1.8414	0.0246	1732.00	20.45	765.90	9.27
Z8	0.0573	0.0011	0.0835	0.0011	0.6594	0.0127	504.00	40.25	517.10	6.79
Z9	0.0610	0.0013	0.0947	0.0013	0.7946	0.0171	638.10	44.53	583.00	7.89
Z10	0.1447	0.0021	0.0867	0.0012	1.7272	0.0269	2283.60	24.63	536.10	7.01
Z12	0.0787	0.0014	0.1825	0.0025	1.9809	0.0364	1165.70	35.09	1080.80	13.40
Z13	0.1142	0.0012	0.3121	0.0038	4.9128	0.0616	1867.50	19.37	1751.10	18.77
Z14	0.1261	0.0016	0.1299	0.0016	2.2569	0.0313	2044.50	22.20	787.00	9.36
Z15	0.0999	0.0014	0.2993	0.0038	4.1208	0.0603	1622.40	24.85	1687.80	18.97
Z17	0.0741	0.0010	0.1658	0.0021	1.6940	0.0256	1045.10	27.98	989.00	11.62
Z18	0.0592	0.0010	0.0813	0.0011	0.6625	0.0114	572.70	35.46	503.70	6.24
Z19	0.0583	0.0008	0.0807	0.0010	0.6490	0.0100	542.70	30.89	500.40	6.06
Z20	0.0900	0.0010	0.1858	0.0023	2.3030	0.0297	1424.40	21.30	1098.40	12.41
Z21	0.0598	0.0008	0.0936	0.0012	0.7710	0.0113	594.80	27.50	576.90	7.28
Z22	0.0788	0.0009	0.2036	0.0027	2.2106	0.0303	1166.80	22.30	1194.90	14.29
Z23	0.1595	0.0017	0.3956	0.0052	8.6915	0.1130	2450.10	17.44	2148.60	23.78
Z24	0.0626	0.0007	0.0603	0.0008	0.5195	0.0072	693.40	24.63	377.30	4.80
Z25	0.1574	0.0017	0.4371	0.0057	9.4770	0.1248	2427.70	17.90	2337.50	25.65
Z26	0.0958	0.0013	0.1883	0.0025	2.4850	0.0374	1543.30	24.60	1112.30	13.75
Z27	0.2692	0.0028	0.5866	0.0077	21.7557	0.2828	3301.40	16.19	2975.40	31.13
Z28	0.0866	0.0010	0.1897	0.0025	2.2643	0.0318	1352.30	22.62	1119.80	13.56
Z29	0.0780	0.0010	0.1921	0.0025	2.0639	0.0298	1146.60	24.29	1132.60	13.75
Z30	0.0625	0.0007	0.0885	0.0012	0.7618	0.0104	689.60	23.94	546.90	6.85
Z31	0.0932	0.0010	0.2497	0.0034	3.2047	0.0442	1490.90	20.65	1437.00	17.33
Z32	0.1082	0.0011	0.2118	0.0028	3.1583	0.0424	1769.90	19.08	1238.30	15.08
Z33	0.0737	0.0008	0.1608	0.0022	1.6334	0.0221	1034.40	21.06	961.10	11.95
Z34	0.0597	0.0007	0.0863	0.0012	0.7098	0.0105	592.90	25.91	533.70	6.93
Z35	0.0757	0.0008	0.1661	0.0022	1.7336	0.0233	1088.10	20.89	990.80	12.28
Z36	0.0654	0.0007	0.1130	0.0015	1.0182	0.0142	786.90	23.42	690.20	8.80
Z37	0.0803	0.0009	0.1302	0.0018	1.4412	0.0199	1205.30	21.57	789.00	9.98
Z38	0.0658	0.0009	0.0990	0.0014	0.8973	0.0146	799.90	29.61	608.40	8.01
Z39	0.1478	0.0015	0.1844	0.0025	3.7555	0.0497	2320.70	17.40	1091.00	13.40
Z40	0.0585	0.0008	0.0737	0.0010	0.5942	0.0093	548.40	28.96	458.60	6.04
Z41	0.1197	0.0013	0.2331	0.0026	3.8549	0.0437	1952.10	18.62	1350.90	13.79
Z42	0.0785	0.0015	0.0702	0.0009	0.7607	0.0144	1159.50	37.82	437.20	5.45
Z43	0.0682	0.0009	0.0860	0.0010	0.8100	0.0112	873.50	27.65	532.10	5.96
Z44	0.0570	0.0009	0.0747	0.0009	0.5878	0.0094	489.60	34.71	464.50	5.34
Z46	0.0754	0.0008	0.1274	0.0014	1.3266	0.0152	1079.10	21.15	773.00	8.22
Z47	0.0691	0.0008	0.1268	0.0014	1.2102	0.0145	901.30	23.11	769.80	8.24
Z48	0.0534	0.0012	0.0683	0.0009	0.5041	0.0113	346.00	50.71	426.20	5.37
Z49	0.1025	0.0011	0.1384	0.0016	1.9602	0.0228	1670.60	19.92	835.70	8.90
Z50	0.0762	0.0010	0.1577	0.0019	1.6588	0.0230	1099.30	26.75	944.00	10.33
Z51	0.3392	0.0056	0.1541	0.0025	7.2061	0.1218	3659.30	25.00	923.90	13.76
Z52	0.1039	0.0011	0.2064	0.0028	2.9559	0.0405	1694.90	19.61	1209.40	14.92
Z53	0.0711	0.0009	0.0906	0.0012	0.8874	0.0131	959.40	24.51	558.90	7.34
Z54	0.0604	0.0008	0.0841	0.0012	0.6994	0.0105	616.60	26.75	520.30	6.88
Z55	0.4437	0.0102	0.1891	0.0038	11.5699	0.2419	4064.30	33.91	1116.70	20.76
Z56	0.2346	0.0026	0.4378	0.0060	14.1573	0.1981	3083.40	17.36	2340.80	26.87
Z57	0.0724	0.0010	0.1553	0.0022	1.5512	0.0247	998.10	27.22	930.80	12.16
Z59	0.0592	0.0009	0.0801	0.0012	0.6529	0.0116	572.80	33.95	496.50	6.84
Z60	0.0748	0.0009	0.1738	0.0024	1.7922	0.0269	1063.30	24.27	1032.90	13.32
Z61	0.0620	0.0008	0.1019	0.0014	0.8701	0.0135	672.80	27.15	625.40	8.36
Z62	0.0805	0.0009	0.1872	0.0026	2.0771	0.0295	1209.50	21.45	1106.10	14.09
Z63	0.0773	0.0009	0.1819	0.0025	1.9375	0.0283	1128.00	22.92	1077.60	13.83
Z64	0.0850	0.0013	0.1730	0.0025	2.0256	0.0348	1314.60	29.12	1028.50	13.78
Z65	0.0764	0.0009	0.1847	0.0026	1.9452	0.0280	1105.50	22.34	1092.70	13.96
Z66	0.1055	0.0011	0.3046	0.0042	4.4281	0.0617	1722.40	19.33	1714.20	20.82
Z67	0.0669	0.0008	0.0613	0.0009	0.5650	0.0083	835.70	24.11	383.20	5.17
Z68	0.0851	0.0011	0.1908	0.0027	2.2389	0.0339	1318.40	23.79	1125.80	14.52

Spot No.	$^{207}Pb/^{235}U$	Error ±2 σ	$^{206}Pb/^{238}U$	Error ±2 σ	$^{207}Pb/^{235}U$	Error ±2 σ	$^{207}Pb/^{206}Pb$ age (Ma)	Error ± (Ma)	$^{206}Pb/^{238}U$ age (Ma)	Error ± (Ma)
Z69	0.0822	0.0011	0.0998	0.0014	1.1304	0.0179	1250.00	25.66	613.20	8.29
Z70	0.0694	0.0009	0.1016	0.0014	0.9712	0.0148	909.20	25.31	623.80	8.32
Z71	0.0918	0.0011	0.2037	0.0030	2.5783	0.0410	1463.60	22.84	1195.00	16.21
Z72	0.1058	0.0013	0.2467	0.0037	3.6001	0.0572	1729.00	22.10	1421.60	18.97
Z73	0.1245	0.0016	0.3164	0.0047	5.4308	0.0878	2021.90	22.12	1771.90	23.17
Z74	0.1765	0.0022	0.4752	0.0072	11.5645	0.1881	2620.60	20.96	2506.20	31.23
Z75	0.1083	0.0013	0.2997	0.0045	4.4730	0.0716	1770.10	22.26	1690.00	22.07
Z76	0.1122	0.0018	0.1580	0.0025	2.4439	0.0460	1835.60	29.27	945.50	13.72
Z77	0.1607	0.0030	0.1044	0.0017	2.3143	0.0464	2463.50	30.66	640.40	9.97
Z78	0.0743	0.0011	0.0927	0.0014	0.9499	0.0173	1050.70	30.53	571.40	8.31
Z79	0.1081	0.0015	0.2971	0.0045	4.4295	0.0759	1768.30	25.14	1677.10	22.24
Z80	0.1043	0.0015	0.3913	0.0059	5.6275	0.0990	1702.70	26.37	2128.70	27.48
Z81	0.0864	0.0012	0.1898	0.0028	2.2605	0.0379	1346.50	27.27	1120.50	14.89
Z82	0.0894	0.0012	0.1656	0.0024	2.0420	0.0329	1413.20	25.29	988.00	13.13
Z83	0.1585	0.0022	0.2003	0.0029	4.3758	0.0711	2439.80	23.03	1176.60	15.74
Z84	0.0912	0.0011	0.0736	0.0010	0.9245	0.0143	1450.00	23.56	457.50	6.27
Z85	0.1102	0.0015	0.0938	0.0014	1.4255	0.0234	1803.10	24.83	578.00	7.99
Z86	0.0714	0.0010	0.0824	0.0012	0.8112	0.0133	969.40	27.42	510.40	7.01
Z87	0.0828	0.0014	0.1631	0.0024	1.8612	0.0343	1263.60	31.52	974.10	13.37
Z88	0.0705	0.0010	0.0954	0.0014	0.9267	0.0160	941.60	29.84	587.40	8.11
Z89	0.0666	0.0009	0.0934	0.0013	0.8581	0.0138	826.60	27.18	575.60	7.84
Z90	0.0745	0.0010	0.0842	0.0012	0.8639	0.0139	1053.70	26.49	520.90	7.13
Z91	0.0684	0.0009	0.0852	0.0012	0.8030	0.0130	879.30	27.60	527.10	7.25
Z92	0.0904	0.0013	0.0974	0.0014	1.2143	0.0209	1433.90	28.10	599.20	8.39
Z93	0.0635	0.0008	0.0844	0.0012	0.7383	0.0113	724.20	25.51	522.00	7.12
Z94	0.1076	0.0013	0.2976	0.0043	4.4157	0.0674	1759.10	21.93	1679.60	21.15
Z95	0.2832	0.0032	0.7037	0.0100	27.4815	0.4051	3380.80	17.58	3434.60	37.94
Z96	0.0780	0.0009	0.0465	0.0007	0.4997	0.0075	1146.00	23.15	292.90	4.07
Z97	0.0995	0.0012	0.1817	0.0026	2.4918	0.0375	1614.20	21.70	1076.10	14.13
Z98	0.0615	0.0009	0.0872	0.0013	0.7399	0.0124	657.30	29.92	539.10	7.50
Z99	0.0598	0.0007	0.0917	0.0013	0.7559	0.0118	596.40	26.72	565.40	7.76
Z100	0.0979	0.0012	0.1863	0.0027	2.5146	0.0384	1584.60	22.34	1101.20	14.51
Z101	0.1200	0.0013	0.2624	0.0036	4.3428	0.0594	1956.60	18.48	1502.20	18.14
Z102	0.1077	0.0012	0.3113	0.0042	4.6233	0.0643	1761.00	19.48	1747.10	20.80
Z103	0.0900	0.0011	0.2067	0.0029	2.5649	0.0383	1425.00	23.14	1211.40	15.23
Z104	0.0808	0.0009	0.1695	0.0023	1.8870	0.0267	1215.60	21.71	1009.10	12.72
Z105	0.0634	0.0008	0.1073	0.0015	0.9382	0.0138	722.50	25.14	656.90	8.54
Z106	0.1629	0.0018	0.4421	0.0060	9.9324	0.1383	2486.30	18.10	2360.10	26.98
Z107	0.0919	0.0013	0.0758	0.0011	0.9602	0.0156	1465.60	26.76	470.80	6.39
Z108	0.0649	0.0008	0.1046	0.0014	0.9360	0.0136	770.20	24.19	641.60	8.33
Z109	0.1691	0.0026	0.1750	0.0026	4.0784	0.0694	2548.50	25.77	1039.30	14.28
Z110	0.0821	0.0009	0.1939	0.0026	2.1951	0.0311	1248.40	21.71	1142.30	14.26
Z111	0.0724	0.0009	0.1414	0.0019	1.4107	0.0211	995.80	24.75	852.60	10.97
Z112	0.0745	0.0008	0.1725	0.0024	1.7710	0.0252	1053.70	22.71	1025.90	12.91
Z113	0.0595	0.0008	0.0929	0.0012	0.7624	0.0116	586.90	30.30	572.70	6.89
Not Used										
Z58	0.5943	0.0074	0.2449	0.0036	20.0640	0.2967	4494.20	17.98	1412.00	18.36

Appendix 3: Geochemistry

Sample No	Formation	Profile name	East	North	Zone	Depositional setting	Field lithology	Field Alteration
Troubringe Basin								
CJ002	Cape Jervis	Cape Jervis	237417	6056750	54	lodgement till	diamictite sandy	Oxidised
CJ003	Cape Jervis	Cape Jervis	237417	6056750	54	lodgement till	diamictite sandy	Oxidised
CJ004	Cape Jervis	Cape Jervis	237417	6056750	54	lodgement till	diamictite sandy	Oxidised
CJ005	Cape Jervis	Cape Jervis	237371	6056675	54	fluviolacustrine	clay	Oxidised
CJ006	Cape Jervis	Cape Jervis	237371	6056675	54	fluviolacustrine	sand	Oxidised
CJ007	Cape Jervis	Cape Jervis	237371	6056675	54	fluviolacustrine	diamictite sandy	Oxidised
CJ008	Cape Jervis	Cape Jervis	237371	6056675	54	fluviolacustrine	sand	Oxidised
CJ009	Cape Jervis	Cape Jervis	237371	6056675	54	fluviolacustrine	diamictite sandy	Oxidised
CJ010	Cape Jervis	Cape Jervis	237371	6056675	54	fluviolacustrine	clay	minimal
CJ011	Cape Jervis	Cape Jervis	237369	6056663	54	fluviolacustrine	sand	Oxidised
CJ012	Cape Jervis	Cape Jervis	237369	6056663	54	fluviolacustrine	sand	carbonate
CJ013	Cape Jervis	Cape Jervis	237428	6056732	54	fluviolacustrine	sand	Oxidised
CJ014	Cape Jervis	Cape Jervis	237428	6056732	54	fluviolacustrine	sand	minimal
CJ015	Cape Jervis	Cape Jervis	237369	6056663	54	fluviolacustrine	sand	carbonate
CJ016	Cape Jervis	Cape Jervis	237369	6056663	54	flowtill complex	diamictite sandy	Oxidised
CJ017	Cape Jervis	Cape Jervis	237465	6056741	54	flowtill complex	diamictite clay	minimal
CJ018	Cape Jervis	Cape Jervis	237369	6056663	54	flowtill complex	diamictite sandy	carbonate
CJ019	Cape Jervis	Cape Jervis	237465	6056741	54	flowtill complex	diamictite clay	Oxidised
CJ020	Cape Jervis	Cape Jervis	237378	6056631	54	flowtill complex	sand	carbonate
CJ021	Cape Jervis	Cape Jervis	237378	6056631	54	glaciomarine	clay	minimal
CJ022	Cape Jervis	Cape Jervis	237378	6056631	54	glaciomarine	sand	carbonate
CJ023	Cape Jervis	Cape Jervis	237378	6056631	54	glaciomarine	clay	minimal
CJ024	Cape Jervis	Cape Jervis	237378	6056631	54	glaciomarine	clay	minimal
CJ025	Cape Jervis	Cape Jervis	237407	6056628	54	glaciomarine	clay	Oxidised
CJ026	Cape Jervis	Cape Jervis	237350	6056612	54	glaciomarine	clay	minimal
CJ027	Cape Jervis	Cape Jervis	237350	6056612	54	glaciomarine	sandy clay	Oxidised
CJ028	Cape Jervis	Cape Jervis	237350	6056612	54	glaciomarine	clay	minimal
HC002	Cape Jervis	Hallett Cove	271727	6115709	54	lodgement till	diamictite sandy	Oxidised
HC003	Cape Jervis	Hallett Cove	271860	6115619	54	fluviolacustrine	clay	Oxidised
HC004	Cape Jervis	Hallett Cove	271860	6115619	54	fluviolacustrine	sand	Oxidised
HC005	Cape Jervis	Hallett Cove	271898	6115620	54	fluviolacustrine	sandy clay	Oxidised
HC006	Cape Jervis	Hallett Cove	271898	6115620	54	fluviolacustrine	diamictite sandy	Oxidised
HC007	Cape Jervis	Hallett Cove	271898	6115620	54	fluviolacustrine	sand	Oxidised
HC008	Cape Jervis	Hallett Cove	271897	6115590	54	fluviolacustrine	sand	Oxidised
HC009	Cape Jervis	Hallett Cove	271897	6115577	54	flowtill complex	sand	Oxidised
HC010	Cape Jervis	Hallett Cove	271897	6115577	54	flowtill complex	diamictite sandy	Oxidised
HC011	Cape Jervis	Hallett Cove	271897	6115577	54	flowtill complex	diamictite clay	Oxidised
HC013	Cape Jervis	Hallett Cove	271959	6115567	54	flowtill complex	sand	Oxidised
HC014	Cape Jervis	Hallett Cove	271959	6115567	54	flowtill complex	clay	Oxidised
KI001	Cape Jervis	Kangaroo Is	737088	6053141	53	fluviolacustrine	clay	minimal
KI003	Cape Jervis	Kangaroo Is	737088	6053141	53	fluviolacustrine	sand	Oxidised
KI004	Cape Jervis	Kangaroo Is	737088	6053141	53	fluviolacustrine	sand	carbonate
KI005	Cape Jervis	Kangaroo Is	737088	6053141	53	fluviolacustrine	diamictite sandy	Oxidised
KI006	Cape Jervis	Kangaroo Is	737088	6053141	53	fluviolacustrine	sandy clay	Oxidised
KI007	Cape Jervis	Kangaroo Is	737088	6053141	53	fluviolacustrine	sand	carbonate
KI008	Cape Jervis	Kangaroo Is	737088	6053141	53	fluviolacustrine	sand	Ferruginous
KI009	Cape Jervis	Kangaroo Is	739262	6051536	53	fluviolacustrine	clay	Oxidised
KI010	Cape Jervis	Kangaroo Is	739262	6051536	53	fluviolacustrine	sand	Ferruginous
KI011	Cape Jervis	Kangaroo Is	739262	6051536	53	fluviolacustrine	sand	Ferruginous
KI012	Cape Jervis	Kangaroo Is	739262	6051536	53	fluviolacustrine	clay	minimal
KI013	Cape Jervis	Kangaroo Is	739262	6051536	53	fluviolacustrine	sand	minimal
KI014	Cape Jervis	Kangaroo Is	739262	6051536	53	fluviolacustrine	clay	minimal
KI015	Cape Jervis	Kangaroo Is	739262	6051536	53	fluviolacustrine	sand	Oxidised
KI016	Cape Jervis	Kangaroo Is	739262	6051536	53	fluviolacustrine	sand	Oxidised
KI017	Cape Jervis	Kangaroo Is	739262	6051536	53	fluviolacustrine	clay	Ferruginous
KI018	Cape Jervis	Kangaroo Is	739262	6051536	53	fluviolacustrine	clay	Ferruginous
KP002	Cape Jervis	Kings Point	280926	6057329	54	fluviolacustrine	clay	Oxidised
KP003	Cape Jervis	Kings Point	280913	6057322	54	fluviolacustrine	sandy clay	Oxidised
KP005	Cape Jervis	Kings Point	280878	6057315	54	fluviolacustrine	diamictite sandy	Oxidised
KP006	Cape Jervis	Kings Point	280868	6057194	54	flowtill complex	diamictite clay	Oxidised
KP007	Cape Jervis	Kings Point	280800	6057264	54	flowtill complex	diamictite sandy	Oxidised

Sample No	Formation	Profile name	East	North	Zone	Depositional setting	Field lithology	Field Alteration
KP008	Cape Jervis	Kings Point	280806	6057277	54	flowtill complex	diamictite sandy	Oxidised
Reg001	Cape Jervis	opportunistic	235287	6229048	53	lodgement till	diamictite sandy	Oxidised
Reg002	Cape Jervis	opportunistic	762058	6149871	53	flowtill complex	diamictite sandy	Oxidised
Reg003	Cape Jervis	opportunistic	743219	6151939	53	fluviolacustrine	sand	carbonate
Reg004	Cape Jervis	opportunistic	728518	6161045	53	flowtill complex	diamictite sandy	carbonate
Reg005	Cape Jervis	opportunistic	731432	6137935	53	fluviolacustrine	clay	minimal
Reg006	Cape Jervis	opportunistic	714896	6130886	53	flowtill complex	diamictite clay	carbonate
Reg007	Cape Jervis	opportunistic	730635	6111375	53	glaciomarine	sand	minimal
Reg008	Cape Jervis	opportunistic	730635	6111375	53	glaciomarine	sandy clay	Oxidised
Reg009	Cape Jervis	opportunistic	730406	6111491	53	glaciomarine	clay	Ferruginous
Reg011	Cape Jervis	opportunistic	730406	6111491	53	glaciomarine	diamictite clay	minimal
Reg012	Cape Jervis	opportunistic	271897	6115590	54	flowtill complex	sand	Ferruginous
Reg013	Cape Jervis	opportunistic	289638	6064942	54	fluviolacustrine	clay	Oxidised
Reg014	Cape Jervis	opportunistic	283581	6065318	54	fluviolacustrine	sand	Oxidised
Reg015	Cape Jervis	opportunistic	281293	6066155	54	lodgement till	sandy clay	Oxidised
Reg016	Cape Jervis	opportunistic	277470	6068785	54	flowtill complex	sandy clay	minimal
Reg017	Cape Jervis	opportunistic	274855	6067229	54	fluviolacustrine	clay	Oxidised
Reg018	Cape Jervis	opportunistic	273901	6065940	54	flowtill complex	sand	Oxidised
Reg019	Cape Jervis	opportunistic	278463	6065414	54	fluviolacustrine	clay	minimal
Reg020	Cape Jervis	opportunistic	274341	6069060	54	lodgement till	diamictite sandy	Oxidised
Reg021	Cape Jervis	opportunistic	274341	6069060	54	lodgement till	sand	Oxidised
Reg022	Cape Jervis	opportunistic	298010	6081468	54	fluviolacustrine	clay	Ferruginous
Reg023	Cape Jervis	opportunistic	298557	6086065	54	flowtill complex	sand	Oxidised
Reg024	Cape Jervis	opportunistic	300461	6085342	54	fluviolacustrine	sandy clay	Oxidised
Reg025	Cape Jervis	opportunistic	300036	6082810	54	fluviolacustrine	silt	Oxidised
Reg026	Cape Jervis	opportunistic	299688	6093099	54	fluviolacustrine	silt	Oxidised
Reg027	Cape Jervis	opportunistic	297426	6092532	54	flowtill complex	diamictite sandy	Oxidised
Reg028	Cape Jervis	opportunistic	297930	6090357	54	flowtill complex	sand	Oxidised
Reg029	Cape Jervis	opportunistic	297757	6089434	54	flowtill complex	sand	Oxidised
Reg030	Cape Jervis	opportunistic	271673	6115323	54	flowtill complex	sandy clay	minimal
Reg031	Cape Jervis	opportunistic	261238	6070931	54	lodgement till	sandy clay	Oxidised
Reg032	Cape Jervis	opportunistic	261957	6071207	54	lodgement till	sand	Oxidised
Reg033	Cape Jervis	opportunistic	267241	6070850	54	flowtill complex	diamictite clay	minimal
Reg034	Cape Jervis	opportunistic	265941	6066701	54	flowtill complex	sand	Oxidised
Reg035	Cape Jervis	opportunistic	266457	6066605	54	flowtill complex	clay	Oxidised
Reg036	Cape Jervis	opportunistic	265127	6065576	54	flowtill complex	sand	Oxidised
Reg037	Cape Jervis	opportunistic	265971	6064879	54	flowtill complex	sand	Oxidised
Reg038	Cape Jervis	opportunistic	266279	6063682	54	flowtill complex	clay	Oxidised
Reg039	Cape Jervis	opportunistic	238356	6057295	54	lodgement till	sand	Oxidised
Reg040	Cape Jervis	opportunistic	242841	6060693	54	flowtill complex	clay	Oxidised
Reg041	Cape Jervis	opportunistic	256496	6072341	54	lodgement till	sand	Oxidised
Reg042	Cape Jervis	opportunistic	256299	6072011	54	lodgement till	diamictite sandy	Oxidised
Reg043	Cape Jervis	opportunistic	257373	6075467	54	lodgement till	sandy clay	Oxidised
Reg044	Cape Jervis	opportunistic	274047	6080081	54	lodgement till	sand	Oxidised
Reg045	Cape Jervis	opportunistic	277444	6078079	54	flowtill complex	sand	Oxidised
Reg046	Cape Jervis	opportunistic	282304	6075294	54	flowtill complex	sand	Oxidised
Reg047	Cape Jervis	opportunistic	283424	6089960	54	lodgement till	diamictite sandy	Oxidised
Reg048	Cape Jervis	opportunistic	282503	6091554	54	lodgement till	clay	Ferruginous
Reg049	Cape Jervis	opportunistic	273837	6062573	54	flowtill complex	sandy clay	Oxidised
Reg050	Cape Jervis	opportunistic	274999	6083601	54	flowtill complex	sandy clay	Ferruginous
Reg051	Cape Jervis	opportunistic	276002	6084210	54	flowtill complex	diamictite clay	Oxidised
Reg052	Cape Jervis	opportunistic	283734	6085808	54	flowtill complex	clay	Ferruginous
Reg053	Cape Jervis	opportunistic	284760	6080366	54	flowtill complex	sandy clay	Oxidised
Reg054	Cape Jervis	opportunistic	285102	6083666	54	flowtill complex	sandy clay	Oxidised
Reg055	Cape Jervis	opportunistic	289120	6083120	54	lodgement till	diamictite clay	Oxidised
Reg056	Cape Jervis	opportunistic	291267	6083564	54	flowtill complex	sandy clay	Oxidised
Reg057	Cape Jervis	opportunistic	285829	6089410	54	flowtill complex	sandy clay	Oxidised
Reg058	Cape Jervis	opportunistic	286701	6089510	54	flowtill complex	sand	Oxidised
Reg059	Cape Jervis	opportunistic	287080	6087310	54	flowtill complex	sand	Oxidised
Reg060	Cape Jervis	opportunistic	765539	6043299	54	lodgement till	sandy clay	Oxidised
Reg061	Cape Jervis	opportunistic	286701	6089510	54	flowtill complex	sandy clay	Oxidised
Reg062	Cape Jervis	opportunistic	287080	6087310	54	flowtill complex	sandy clay	Oxidised
Reg063	Cape Jervis	opportunistic	765539	6043299	54	lodgement till	clay	Minimal
Reg064	Cape Jervis	opportunistic	242841	6060693	54	flowtill complex	clay	Oxidised
Reg065	Cape Jervis	opportunistic	282503	6091554	54	lodgement till	clay	Ferruginous
Reg066	Cape Jervis	opportunistic	289120	6083120	54	lodgement till	diamictite clay	Oxidised

Sample No	Formation	Profile name	East	North	Zone	Depositional setting	Field lithology	Field Alteration
Reg068	Cape Jervis	opportunistic	724983	6052730	53	fluviolacustrine	Sand	Ferruginous
Reg069	Cape Jervis	opportunistic	724983	6052730	53	fluviolacustrine	sandy clay	carbonate
Reg070	Cape Jervis	opportunistic	724983	6052730	53	fluviolacustrine	Sand	Ferruginous
Reg071	Cape Jervis	opportunistic	724983	6052730	53	fluviolacustrine	Sand	Ferruginous
Reg072	Cape Jervis	opportunistic	737163	6053123	53	fluviolacustrine	Sand	Ferruginous
Reg073	Cape Jervis	opportunistic	735216	6037312	53	fluviolacustrine	Clay	Oxidised
Reg074	Cape Jervis	opportunistic	734896	6035434	53	fluviolacustrine	Clay	Oxidised
Reg075	Cape Jervis	opportunistic	237378	6056631	54	glaciomarine	clay	Ferruginous
Reg076	Cape Jervis	opportunistic	237378	6056631	54	glaciomarine	clay	Ferruginous
Reg078	Cape Jervis	opportunistic	271897	6115577	54	flowtill complex	diamictite sandy	Oxidised
WB001	Cape Jervis	Waterloo Bay	730059	6111525	53	flowtill complex	diamictite clay	minimal
WB002	Cape Jervis	Waterloo Bay	730059	6111525	53	flowtill complex	diamictite clay	Ferruginous
WB003	Cape Jervis	Waterloo Bay	730059	6111525	53	glaciomarine	clay	minimal
WB004	Cape Jervis	Waterloo Bay	730059	6111525	53	glaciomarine	clay	Ferruginous
WB005	Cape Jervis	Waterloo Bay	730059	6111525	53	glaciomarine	clay	minimal
WB006	Cape Jervis	Waterloo Bay	730127	6111530	53	glaciomarine	sand	Oxidised
WB007	Cape Jervis	Waterloo Bay	730059	6111525	53	glaciomarine	clay	minimal
CJ029	Cape Jervis	Cape Jervis	237354	6056697	53	basement	N/A	N/A
KP009	Cape Jervis	Kings Point	280926	6057329	53	basement	N/A	N/A
HC015	Wilpena Group	Hallett Cove	271727	6115709	53	basement	N/A	N/A
Arckaringa Basin								
BC001	Boorthanna	Box Creek	595562	6823784	53	lodgement till	sand	Oxidised
BC002	Boorthanna	Box Creek	595562	6823784	53	lodgement till	sand	Oxidised
BC003	Boorthanna	Box Creek	595562	6823784	53	lodgement till	sand	Ferruginous
BC004	Boorthanna	Box Creek	595562	6823784	53	lodgement till	sand	carbonate
BC005	Boorthanna	Box Creek	595562	6823784	53	lodgement till	sand	Ferruginous
BC006	Boorthanna	Box Creek	595562	6823784	53	lodgement till	sand	carbonate
MD001	Boorthanna	Mt Dutton	566258	6923054	53	flowtill complex	diamictite sandy	Ferruginous
MD002	Boorthanna	Mt Dutton	566258	6923054	53	flowtill complex	diamictite sandy	Ferruginous
MD003	Boorthanna	Mt Dutton	566258	6923054	53	flowtill complex	diamictite sandy	Ferruginous
MD004	Boorthanna	Mt Dutton	565279	6922389	53	flowtill complex	silt	minimal
MD005	Boorthanna	Mt Dutton	565262	6922076	53	fluviolacustrine	clay	Oxidised
MT001	Mt Toondina	Mt Toondina	535385	6908893	53	fluviolacustrine	sand	sulphate
MT002	Mt Toondina	Mt Toondina	535385	6908893	53	fluviolacustrine	silt	sulphate
MT003	Mt Toondina	Mt Toondina	535371	6908898	53	fluviolacustrine	silt	sulphate
MT004	Mt Toondina	Mt Toondina	535371	6908898	53	fluviolacustrine	sand	sulphate
MT005	Mt Toondina	Mt Toondina	535388	6908899	53	fluvioswamp	carbonaceous	sulphate
MT006	Mt Toondina	Mt Toondina	535399	6908901	53	fluviolacustrine	clay	sulphate
MT007	Mt Toondina	Mt Toondina	535402	6908910	53	fluvioswamp	carbonaceous	sulphate
MT008	Mt Toondina	Mt Toondina	535402	6908910	53	fluvioswamp	sand	sulphate
MT009	Mt Toondina	Mt Toondina	535406	6908916	53	fluvioswamp	carbonaceous	sulphate
MT010	Mt Toondina	Mt Toondina	535418	6908919	53	fluvioswamp	silt	sulphate
MT011	Mt Toondina	Mt Toondina	535418	6908919	53	fluvioswamp	carbonaceous	sulphate
MT012	Mt Toondina	Mt Toondina	535416	6908915	53	fluvioswamp	silt	sulphate
MT013	Mt Toondina	Mt Toondina	535416	6908915	53	fluvioswamp	sand	sulphate
MT014	Mt Toondina	Mt Toondina	535415	6908914	53	fluvioswamp	carbonaceous	sulphate
MT015	Mt Toondina	Mt Toondina	535430	6908920	53	fluvioswamp	sand	sulphate
MT016	Mt Toondina	Mt Toondina	535480	6908925	53	fluvioswamp	carbonaceous	sulphate
MT017	Mt Toondina	Mt Toondina	535480	6908925	53	fluvioswamp	sand	sulphate
MT018	Mt Toondina	Mt Toondina	535488	6908927	53	fluvioswamp	carbonaceous	sulphate
MT019	Mt Toondina	Mt Toondina	535466	6908956	53	fluvioswamp	clay	sulphate
MT020	Mt Toondina	Mt Toondina	535466	6908956	53	fluvioswamp	carbonaceous	sulphate
MT021	Mt Toondina	Mt Toondina	535466	6908956	53	fluvioswamp	silt	sulphate
MT023	Mt Toondina	Mt Toondina	535488	6908961	53	fluvioswamp	carbonaceous	sulphate
MT024	Mt Toondina	Mt Toondina	535488	6908961	53	fluvioswamp	silt	sulphate
MT025	Mt Toondina	Mt Toondina	353481	6908978	53	fluvioswamp	sand	sulphate
MT026	Mt Toondina	Mt Toondina	353481	6908978	53	fluvioswamp	carbonaceous	sulphate
MT027	Mt Toondina	Mt Toondina	353481	6908978	53	fluvioswamp	sand	sulphate

	SiO2	Al2O3	Fe2O3	CaO	MgO	Na2O	K2O	MnO	TiO2	P2O5	Cr2O3	Ba	Tot/C
	%	%	%	%	%	%	%	%	%	%	%	%	%
Analysis	**XRF**	**XRF**	**XRF**	**XRF**	**XRF**	**XRF**	**XRF**	**XRF**	**XRF**	**XRF**	**XRF**	**XRF**	**XRF**
Det. limit	**0.01**	**0.01**	**0.04**	**0.01**	**0.01**	**0.01**	**0.01**	**0.01**	**0.01**	**0.01**	**0.001**	**5**	**0.002**
Sample No													
Troubridge Basin													
CJ002	78.20	8.42	2.50	0.84	1.43	0.87	3.15	0.03	0.37	0.09	0.00	0.06	0.42
CJ003	71.00	6.73	1.99	5.84	1.89	1.22	2.12	0.07	0.29	0.07	0.00	0.06	1.72
CJ004	75.70	8.42	2.11	2.60	1.85	0.62	3.13	0.03	0.38	0.10	0.00	0.06	0.86
CJ005	84.60	6.42	1.64	0.19	0.80	0.37	2.30	0.01	0.29	0.03	0.00	0.04	0.12
CJ006	82.60	7.15	1.93	0.37	0.96	0.45	2.45	0.02	0.31	0.03	0.00	0.04	0.27
CJ007	86.20	4.59	1.39	2.00	0.59	0.58	1.36	0.02	0.19	0.03	0.00	0.04	0.57
CJ008	93.60	2.18	1.04	0.30	0.21	0.26	0.80	0.02	0.11	0.02	0.00	0.02	0.09
CJ009	76.20	7.17	2.18	3.93	0.91	0.85	1.81	0.02	0.28	0.07	0.00	0.05	1.02
CJ010	85.50	6.37	1.92	0.16	0.84	0.37	2.26	0.03	0.29	0.05	0.00	0.08	0.14
CJ011	75.70	3.76	0.80	9.07	0.22	0.21	0.66	0.36	0.13	0.03	0.00	0.02	2.15
CJ012	64.20	1.32	0.76	17.84	0.20	0.12	0.37	0.15	0.08	0.01	0.00	0.01	4.19
CJ013	87.10	3.75	0.99	2.34	0.46	0.62	1.19	0.02	0.17	0.02	0.00	0.03	0.59
CJ014	92.50	3.31	0.98	0.08	0.22	0.58	1.21	0.08	0.14	0.01	0.00	0.03	0.03
CJ015	66.20	1.06	0.63	17.40	0.16	0.09	0.28	0.26	0.05	0.01	0.00	0.01	4.08
CJ016	74.80	8.16	4.21	2.16	2.32	0.58	1.97	0.09	0.44	0.09	0.00	0.04	0.63
CJ017	84.20	3.74	0.91	3.33	0.66	0.80	1.21	0.02	0.15	0.04	0.00	0.03	0.79
CJ018	67.80	1.62	0.87	15.73	0.23	0.11	0.40	0.37	0.06	0.01	0.00	0.02	3.67
CJ019	77.60	4.83	1.96	5.74	1.02	0.51	1.63	0.06	0.26	0.07	0.00	0.08	1.51
CJ020	69.00	0.99	0.73	15.56	0.23	0.06	0.20	0.27	0.10	0.01	0.00	0.01	3.76
CJ021	70.20	12.80	3.53	0.36	1.99	0.70	4.38	0.04	0.55	0.14	0.00	0.07	0.35
CJ022	64.00	1.16	0.78	17.79	0.22	0.05	0.38	0.10	0.04	0.02	0.00	0.01	4.17
CJ023	70.30	12.38	3.46	0.60	2.05	0.82	4.11	0.04	0.55	0.13	0.00	0.07	0.24
CJ024	73.70	11.26	3.06	0.52	1.72	0.69	3.86	0.05	0.50	0.14	0.00	0.06	0.13
CJ025	64.70	14.40	5.79	0.27	2.19	1.00	4.41	0.09	0.62	0.14	0.00	0.07	0.28
CJ026	67.40	15.31	2.32	0.51	1.61	1.15	3.47	0.02	0.62	0.13	0.00	0.06	0.36
CJ027	74.80	5.48	1.01	5.78	1.28	0.82	0.96	0.01	0.26	0.03	0.00	0.02	1.71
CJ028	81.00	9.27	1.14	0.35	0.88	0.69	2.57	0.01	0.40	0.06	0.00	0.05	0.26
HC002	80.00	2.52	1.08	7.31	0.30	0.30	0.17	0.01	0.25	0.04	0.00	0.01	1.45
HC003	83.30	6.66	2.57	0.30	1.64	0.30	2.09	0.02	0.46	0.10	0.01	0.04	0.03
HC004	81.90	4.03	1.57	4.48	0.95	0.35	1.20	0.07	0.25	0.05	0.00	0.03	0.95
HC005	84.80	4.25	1.42	0.23	1.11	1.81	1.57	0.02	0.27	0.06	0.01	0.03	0.07
HC006	92.70	2.96	1.06	0.20	0.53	0.11	0.97	0.03	0.16	0.03	0.00	0.02	0.04
HC007	92.00	3.16	0.91	0.08	0.46	0.64	1.18	0.03	0.17	0.03	0.01	0.02	0.01
HC008	89.50	3.65	1.10	0.09	0.68	0.78	1.27	0.02	0.22	0.04	0.00	0.03	0.01
HC009	87.90	4.72	1.78	0.14	1.01	0.49	1.48	0.02	0.28	0.06	0.00	0.04	0.04
HC010	93.10	2.48	1.04	0.08	0.42	0.27	0.86	0.02	0.17	0.03	0.00	0.02	0.01
HC011	76.90	8.88	4.47	0.20	2.08	0.59	2.51	0.04	0.60	0.15	0.01	0.04	0.02
HC013	93.30	2.26	0.70	0.08	0.38	0.84	0.97	0.01	0.08	0.02	0.00	0.02	0.01
HC014	75.20	9.57	4.75	0.27	2.67	0.82	2.55	0.03	0.69	0.16	0.01	0.05	0.01
KI001	66.70	17.09	3.36	1.18	0.89	0.77	1.73	0.02	0.90	0.04	0.00	0.04	0.60
KI003	87.50	4.12	3.74	0.24	0.14	0.23	1.31	0.01	0.16	0.01	0.00	0.03	0.14
KI004	83.70	4.13	0.52	3.91	0.91	0.24	1.11	0.01	0.16	0.01	0.00	0.03	1.26
KI005	86.10	4.74	0.83	1.81	0.66	0.17	1.38	0.01	0.29	0.01	0.00	0.03	0.64
KI006	81.50	8.03	2.94	0.16	0.37	0.88	1.69	0.01	0.35	0.02	0.00	0.04	0.27
KI007	84.20	3.42	1.26	3.87	0.60	0.38	1.04	0.01	0.21	0.01	0.00	0.03	1.15
KI008	84.50	3.18	7.48	0.32	0.17	0.08	1.00	0.49	0.09	0.01	0.00	0.06	0.28
KI009	71.90	11.12	5.85	0.11	0.79	0.78	1.78	0.04	0.52	0.09	0.00	0.05	0.23
KI010	82.00	6.42	5.27	0.06	0.30	0.49	1.56	0.01	0.29	0.05	0.00	0.05	0.13
KI011	78.10	2.71	15.68	0.02	0.07	0.20	0.96	0.21	0.07	0.09	0.00	0.03	0.07
KI012	78.00	11.22	1.97	0.06	0.68	0.61	1.86	0.01	0.57	0.03	0.00	0.03	0.18
KI013	73.30	11.77	3.87	0.07	0.99	1.10	2.01	0.03	0.58	0.07	0.00	0.05	0.28
KI014	72.60	12.62	2.93	0.10	0.84	1.13	2.20	0.02	0.58	0.10	0.00	0.05	0.10
KI015	71.20	13.46	3.13	0.06	0.97	1.11	2.22	0.02	0.62	0.09	0.00	0.05	0.06
KI016	93.60	2.75	0.93	0.07	0.10	0.18	1.12	0.01	0.11	0.02	0.00	0.03	0.02
KI017	60.40	3.52	29.37	0.07	0.31	0.48	0.95	0.32	0.13	0.11	0.00	0.02	0.06
KI018	61.40	8.26	18.72	0.09	0.78	0.87	1.67	0.15	0.53	0.14	0.00	0.05	0.09
KP002	70.10	12.72	5.02	0.26	1.24	0.89	1.64	0.02	0.49	0.03	0.01	0.02	0.35
KP003	81.20	7.79	2.86	0.32	0.88	0.49	1.85	0.01	0.35	0.02	0.01	0.03	0.04
KP005	82.70	5.95	2.07	0.27	0.74	0.86	1.85	0.02	0.23	0.03	0.01	0.04	0.08

Sample No	SiO2	Al2O3	Fe2O3	CaO	MgO	Na2O	K2O	MnO	TiO2	P2O5	Cr2O3	Ba	Tot/C
KP006	68.70	12.28	4.08	0.48	1.90	1.46	3.92	0.02	0.54	0.05	0.01	0.06	0.38
KP007	84.40	6.54	2.16	0.06	0.61	0.56	1.71	0.01	0.26	0.04	0.01	0.04	0.36
KP008	81.70	3.00	10.51	0.04	0.14	0.20	0.41	0.01	0.14	0.03	0.02	0.01	0.16
Reg001	88.60	5.67	1.28	0.21	0.17	0.11	0.22	0.01	0.23	0.01	0.02	0.25	0.07
Reg002	87.40	5.60	1.43	0.10	0.54	0.45	1.90	0.02	0.21	0.06	0.00	0.03	0.03
Reg003	47.30	3.74	1.57	18.97	3.53	0.18	0.45	0.02	0.17	0.05	0.00	0.02	6.52
Reg004	10.10	2.76	1.22	45.42	2.06	0.16	0.09	0.02	0.10	0.02	0.00	0.01	10.38
Reg005	56.90	5.51	1.98	13.04	3.02	0.62	1.24	0.04	0.28	0.06	0.01	0.03	4.05
Reg006	20.30	2.16	0.51	40.67	1.16	0.22	0.37	0.01	0.03	0.03	0.00	0.02	9.29
Reg007	88.00	2.62	1.11	0.17	0.52	0.96	0.87	2.43	0.11	0.01	0.01	0.08	0.03
Reg008	73.10	10.34	4.99	0.35	1.47	1.12	2.78	0.05	0.46	0.03	0.01	0.03	0.06
Reg009	51.60	7.14	31.61	0.13	0.73	0.86	2.50	0.02	0.48	0.10	0.03	0.04	0.17
Reg011	80.00	7.58	2.10	0.10	0.55	1.15	2.91	0.01	1.06	0.03	0.01	0.07	0.16
Reg012	77.90	4.76	11.14	0.07	0.41	0.29	0.87	0.01	0.35	0.07	0.01	0.02	0.21
Reg013	74.90	8.97	3.32	0.19	0.77	1.88	3.08	0.04	0.43	0.11	0.01	0.06	0.12
Reg014	85.50	7.45	1.78	0.15	0.30	0.15	0.81	0.01	0.33	0.01	0.00	0.13	0.19
Reg015	89.50	4.67	1.61	0.02	0.10	0.08	1.01	0.01	0.22	0.01	0.00	0.02	0.09
Reg016	87.50	4.98	1.21	0.22	0.41	1.12	1.23	0.02	0.22	0.01	0.00	0.03	0.08
Reg017	80.00	9.40	2.91	0.21	0.58	0.38	1.59	0.01	0.38	0.01	0.01	0.05	0.28
Reg018	80.90	9.60	3.10	0.04	0.27	0.04	0.69	0.01	0.37	0.02	0.01	0.02	0.51
Reg019	82.20	6.96	3.15	0.22	0.78	0.49	2.34	0.03	0.28	0.07	0.00	0.05	0.24
Reg020	90.90	2.87	1.59	0.35	0.48	0.82	0.90	0.02	0.14	0.06	0.01	0.02	0.04
Reg021	91.00	2.91	0.93	0.26	0.39	1.15	0.96	0.02	0.12	0.03	0.00	0.03	0.02
Reg022	68.30	9.66	13.90	0.13	0.57	0.17	2.55	0.02	0.38	0.10	0.01	0.06	0.08
Reg023	88.70	4.28	1.41	0.06	0.06	0.07	1.06	0.01	0.12	0.01	0.00	0.03	0.06
Reg024	84.10	7.00	2.64	0.23	0.39	0.20	0.65	0.01	0.28	0.02	0.00	0.02	0.18
Reg025	83.60	6.82	2.27	0.35	0.55	1.15	1.54	0.03	0.46	0.02	0.01	0.04	0.14
Reg026	76.00	12.18	4.10	0.08	0.32	0.08	0.46	0.01	0.38	0.02	0.01	0.01	0.14
Reg027	79.30	9.35	5.47	0.09	0.16	0.02	0.19	0.01	0.33	0.01	0.01	0.01	0.14
Reg028	90.20	5.32	1.32	0.04	0.10	0.03	0.13	0.01	0.14	0.01	0.00	0.01	0.11
Reg029	88.50	5.96	1.59	0.06	0.07	0.03	0.10	0.01	0.14	0.02	0.00	0.02	0.04
Reg030	86.20	5.36	1.39	0.24	0.49	1.18	1.24	0.02	0.22	0.01	0.00	0.03	0.05
Reg031	90.40	4.72	1.55	0.03	0.10	0.09	0.98	0.01	0.22	0.01	0.00	0.02	0.06
Reg032	86.30	6.02	1.20	0.04	0.06	0.01	0.10	0.01	0.14	0.02	0.00	0.02	0.03
Reg033	79.50	7.59	2.61	0.95	1.87	1.01	2.03	0.03	0.63	0.15	0.01	0.04	0.21
Reg034	70.30	13.53	5.09	0.49	0.44	0.22	1.87	0.01	0.59	0.03	0.01	0.03	0.19
Reg035	72.50	13.85	3.58	0.08	0.45	0.07	1.63	0.01	0.43	0.06	0.02	0.04	0.29
Reg036	87.00	5.39	2.24	0.08	0.41	0.14	1.09	0.01	0.20	0.01	0.00	0.02	0.15
Reg037	90.90	4.01	1.32	0.16	0.22	0.04	0.53	0.01	0.15	0.02	0.00	0.01	0.20
Reg038	71.70	12.34	4.32	0.10	0.63	0.12	1.15	0.01	0.50	0.02	0.01	0.03	0.60
Reg039	88.90	3.54	3.16	0.02	0.21	0.13	0.45	0.01	0.15	0.01	0.00	0.01	0.07
Reg040	80.70	9.13	2.97	0.05	0.27	0.10	0.64	0.01	0.41	0.01	0.01	0.02	0.39
Reg041	83.70	8.00	2.23	0.12	0.18	0.01	0.21	0.01	0.30	0.01	0.01	0.01	0.08
Reg042	91.80	2.65	1.09	0.61	0.26	0.24	0.54	0.01	0.09	0.01	0.00	0.03	0.12
Reg043	72.90	12.35	4.67	0.16	0.85	0.40	2.20	0.02	0.72	0.02	0.01	0.06	0.13
Reg044	91.10	3.20	0.98	0.41	0.16	0.41	1.25	0.01	0.11	0.03	0.01	0.03	0.10
Reg045	89.00	1.72	5.53	0.02	0.10	0.03	0.69	0.03	0.08	0.03	0.00	0.01	0.04
Reg046	90.10	4.28	1.33	0.11	0.20	0.05	1.24	0.01	0.16	0.03	0.00	0.03	0.06
Reg047	59.00	17.61	11.20	0.11	0.25	0.04	0.37	0.01	0.74	0.02	0.02	0.01	0.32
Reg048	66.60	13.51	9.93	0.08	0.32	0.31	0.81	0.01	0.53	0.02	0.01	0.02	0.21
Reg049	88.00	5.58	1.78	0.03	0.15	0.07	1.48	0.01	0.21	0.03	0.00	0.04	0.05
Reg050	77.50	12.86	1.84	0.04	0.15	0.01	0.20	0.01	0.64	0.02	0.01	0.01	0.06
Reg051	83.20	8.01	3.11	0.03	0.14	0.01	0.21	0.01	0.25	0.02	0.01	0.01	0.23
Reg052	55.10	12.86	11.77	3.20	2.55	0.26	1.15	0.05	0.66	0.04	0.01	0.02	1.59
Reg053	84.80	5.79	3.04	0.17	0.18	0.12	1.32	0.01	0.43	0.02	0.01	0.03	0.32
Reg054	81.60	9.01	2.05	0.09	0.26	0.05	1.30	0.01	0.35	0.05	0.01	0.03	0.29
Reg055	54.20	21.70	9.01	0.12	0.36	0.04	0.38	0.01	0.58	0.03	0.02	0.01	0.48
Reg056	90.90	4.36	1.47	0.02	0.05	0.01	0.13	0.01	0.16	0.02	0.00	0.01	0.05
Reg057	81.90	7.33	5.63	0.03	0.08	0.01	0.17	0.01	0.24	0.02	0.01	0.01	0.09
Reg058	82.30	7.31	4.89	0.02	0.09	0.01	0.14	0.01	0.28	0.01	0.01	0.01	0.11
Reg059	92.60	3.96	0.94	0.02	0.04	0.15	0.07	0.01	0.14	0.01	0.01	0.01	0.07
Reg060	87.30	5.96	2.73	0.04	0.07	0.02	0.12	0.01	0.19	0.03	0.01	0.01	0.24
Reg061	79.90	9.04	4.09	0.03	0.15	0.02	0.29	0.01	0.42	0.01	0.02	0.01	0.13
Reg062	89.30	4.67	2.50	0.03	0.03	0.01	0.07	0.01	0.16	0.01	0.01	0.01	0.07
Reg063	67.10	13.16	4.43	0.28	2.22	1.17	3.70	0.06	0.59	0.13	0.01	0.07	0.07
Reg064	81.00	8.79	2.72	0.04	0.27	0.10	0.64	0.01	0.43	0.01	0.01	0.01	0.33
Reg065	59.50	18.11	9.42	0.11	0.28	0.04	0.40	0.01	0.78	0.02	0.01	0.01	0.33

Sample No	SiO2	Al2O3	Fe2O3	CaO	MgO	Na2O	K2O	MnO	TiO2	P2O5	Cr2O3	Ba	Tot/C
Reg066	54.30	21.32	8.55	0.14	0.37	0.05	0.39	0.01	0.67	0.03	0.02	0.01	0.54
Reg068	75.50	5.75	12.31	0.32	0.38	0.16	0.31	0.01	0.70	0.01	0.00	0.06	0.18
Reg069	67.20	9.12	5.42	5.81	0.73	0.23	0.48	0.01	0.61	0.01	0.00	0.02	1.84
Reg070	83.40	4.97	6.20	0.22	0.28	0.10	0.48	0.01	0.56	0.01	0.00	0.03	0.26
Reg071	58.70	7.05	22.69	0.46	0.55	0.09	0.31	0.01	0.57	0.02	0.02	0.06	0.09
Reg072	73.50	7.03	9.37	0.80	0.89	0.34	0.63	0.02	0.12	0.03	0.00	0.03	0.83
Reg073	66.70	14.36	3.97	0.42	1.24	1.44	3.89	0.02	0.53	0.01	0.01	0.06	0.04
Reg074	40.70	31.77	9.26	0.10	0.51	0.11	0.61	0.05	1.02	0.02	0.01	0.01	0.09
Reg075	45.60	1.54	44.97	0.51	0.47	0.11	0.64	0.11	0.07	0.05	0.00	0.10	0.23
Reg076	46.00	1.68	43.71	0.83	0.50	0.12	0.70	0.23	0.07	0.04	0.00	0.04	0.28
Reg078	94.30	2.56	0.84	0.06	0.40	0.25	0.94	0.02	0.12	0.03	0.01	0.02	0.01
WB001	76.00	10.72	2.85	0.11	0.93	1.07	3.90	0.02	0.67	0.03	0.00	0.06	0.05
WB002	62.10	9.88	16.84	0.14	1.02	0.91	3.31	0.01	0.53	0.11	0.00	0.05	0.07
WB003	83.30	8.21	0.73	0.07	0.39	0.94	3.82	0.01	0.79	0.01	0.00	0.07	0.02
WB004	57.60	7.89	24.23	0.27	0.92	0.58	2.84	0.02	0.66	0.07	0.00	0.07	0.16
WB005	77.90	9.56	2.70	0.13	0.84	0.66	3.57	0.01	1.02	0.02	0.00	0.11	0.03
WB006	82.40	5.23	0.59	0.14	0.57	1.94	2.30	0.01	0.99	0.02	0.00	0.11	0.02
WB007	59.30	19.03	4.06	0.23	1.55	0.67	3.10	0.03	0.55	0.03	0.00	0.03	0.06
CJ029	72.20	12.45	4.77	1.41	2.02	1.91	2.64	0.07	0.59	0.18	0.0005	0.06	0.18
KP009	67.70	14.06	5.97	1.84	2.89	2.52	2.77	0.06	0.70	0.12	0.0240	0.06	0.06
HC015	59.10	15.93	9.80	1.02	3.05	1.76	3.67	0.07	1.41	0.30	0.01	0.04	0.24
Arckaringa Basin													
BC001	77.90	2.35	1.64	4.49	3.07	0.31	0.65	0.07	0.20	0.04	0.00	0.02	1.78
BC002	73.60	3.50	2.03	6.06	3.16	0.28	1.04	0.08	0.16	0.05	0.00	0.03	1.99
BC003	56.60	2.52	29.65	2.38	0.60	0.32	0.95	0.08	0.11	0.08	0.00	0.07	0.25
BC004	58.80	3.31	2.44	10.64	6.89	0.58	0.93	0.08	0.16	0.07	0.00	0.03	4.50
BC005	77.70	2.85	13.52	0.35	0.30	0.51	1.11	0.02	0.13	0.04	0.00	0.02	0.13
BC006	67.00	3.70	2.87	8.93	4.19	0.42	1.07	0.10	0.15	0.10	0.00	0.04	3.08
MD001	68.40	6.99	14.43	0.21	2.10	0.29	2.85	0.40	0.41	0.10	0.00	0.03	0.04
MD002	30.70	3.55	52.58	0.68	1.68	0.08	1.12	0.67	0.23	0.16	0.00	0.03	0.13
MD003	40.70	2.19	48.64	0.48	0.22	0.07	0.59	0.67	0.08	0.20	0.00	0.08	0.07
MD004	90.20	4.49	0.79	0.16	0.50	0.07	1.63	0.02	0.27	0.05	0.00	0.03	0.01
MD005	78.40	7.50	2.40	1.20	0.69	0.96	1.92	0.06	0.54	0.10	0.00	0.04	0.03
MT001	75.10	10.15	4.65	0.64	1.00	0.78	2.15	0.13	0.74	0.14	0.00	0.05	0.12
MT002	60.20	18.27	4.87	0.22	2.23	2.25	3.72	0.04	0.72	0.08	0.00	0.07	0.22
MT003	66.30	14.17	4.37	0.97	1.94	1.27	2.87	0.05	0.79	0.12	0.00	0.05	0.11
MT004	68.00	13.88	4.71	0.41	2.02	1.34	2.79	0.05	0.80	0.12	0.00	0.06	0.10
MT005	57.70	17.92	4.98	0.46	2.46	2.63	3.55	0.04	0.80	0.10	0.00	0.06	0.31
MT006	59.10	19.82	4.21	0.17	2.13	1.89	3.79	0.04	0.80	0.10	0.00	0.07	0.37
MT007	2.90	2.26	1.15	25.77	0.28	0.25	0.09	0.01	0.03	0.05	0.00	0.02	9.15
MT008	76.90	2.26	0.45	6.21	0.09	0.16	0.84	0.01	0.28	0.01	0.00	0.02	0.20
MT009	3.10	0.53	1.01	30.80	0.13	0.02	0.02	0.28	0.01	0.01	0.00	0.01	1.27
MT010	58.50	17.01	5.49	0.61	2.71	2.53	3.59	0.05	0.85	0.14	0.00	0.08	0.39
MT011	49.00	12.91	3.19	6.64	1.54	2.30	2.65	0.04	0.76	0.30	0.00	0.04	1.16
MT012	64.40	13.01	8.41	0.20	1.85	1.83	3.20	0.17	0.70	0.13	0.00	0.08	0.23
MT013	69.70	11.04	6.92	0.24	1.46	1.39	2.91	0.11	0.67	0.11	0.00	0.06	0.22
MT014	58.60	17.78	4.73	0.17	2.18	2.38	4.10	0.05	0.80	0.09	0.00	0.06	1.06
MT015	62.90	13.86	8.02	0.19	2.32	1.43	3.44	0.15	0.76	0.12	0.00	0.07	0.36
MT016	37.60	7.89	5.71	2.04	2.25	6.27	1.94	0.16	0.45	0.28	0.00	0.08	11.22
MT017	90.20	1.53	0.68	1.46	0.10	0.53	0.67	0.03	0.40	0.01	0.00	0.02	0.19
MT018	10.20	4.31	3.63	3.69	2.08	13.22	0.92	0.05	0.13	0.38	0.00	0.10	21.34
MT019	56.80	19.77	1.30	1.25	0.77	3.03	3.75	0.01	0.80	0.04	0.00	0.06	1.33
MT020	38.60	8.92	1.64	8.01	0.91	2.46	0.96	0.01	0.61	0.03	0.00	0.03	9.68
MT021	65.90	15.39	2.19	0.68	0.92	2.05	2.79	0.02	0.94	0.05	0.00	0.04	0.57
MT023	62.90	16.74	3.69	0.15	1.67	2.18	2.98	0.04	0.85	0.07	0.00	0.05	0.77
MT024	59.60	20.37	3.13	0.18	1.64	2.03	3.40	0.03	0.81	0.03	0.00	0.06	0.46
MT025	77.30	2.23	1.05	7.69	0.46	0.44	0.34	0.01	0.26	0.01	0.00	0.01	1.95
MT026	69.60	11.13	0.77	0.51	0.52	2.08	1.29	0.01	0.56	0.02	0.00	0.02	4.46
MT027	69.00	0.85	0.33	14.96	0.64	0.01	0.04	0.01	0.07	0.01	0.00	0.01	3.51

	Tot/S	Ba	Be	Co	Cs	Ga	Hf	Nb	Rb	Sn
	%	ppm	ppm	ppm	ppm	ppm	ppm	ppm	ppm	ppm
Analysis	**XRF**	**ICP-MS**	**ICP-MS**	**ICP-MS**	**ICP-MS**	**ICP-MS**	**ICP-MS**	**ICP-MS**	**ICP-MS**	**ICP-MS**
Det. limit	**0.002**	**1**	**1**	**0.2**	**0.1**	**0.5**	**0.1**	**0.1**	**0.1**	**1**
Sample No										
Troubridge Basin										
CJ002	0.01	535.00	1.00	4.40	5.40	9.20	6.10	7.10	100.80	2.00
CJ003	0.03	517.00	1.00	4.60	3.40	7.30	5.10	5.80	75.80	2.00
CJ004	0.01	599.00	0.50	5.50	4.00	9.00	6.10	6.80	99.10	2.00
CJ005	0.01	439.00	0.50	3.50	3.30	6.90	6.00	6.00	81.10	2.00
CJ006	0.01	472.00	0.50	3.90	3.80	8.50	6.10	6.80	96.70	2.00
CJ007	0.01	374.00	0.50	2.80	1.90	5.00	5.90	4.40	56.80	1.00
CJ008	0.01	214.00	0.50	1.20	0.80	2.10	3.90	2.20	30.00	2.00
CJ009	0.03	491.00	0.50	3.90	3.10	7.80	5.80	6.50	90.90	2.00
CJ010	0.01	876.00	0.50	4.90	3.80	6.90	7.30	6.20	83.70	2.00
CJ011	0.02	247.00	2.00	10.30	1.00	2.40	4.30	1.80	30.90	2.00
CJ012	0.01	145.00	0.50	0.50	0.40	1.40	3.40	1.20	18.80	0.50
CJ013	0.01	294.00	0.50	1.70	1.50	3.40	5.80	3.10	41.90	0.50
CJ014	0.01	246.00	0.50	1.70	1.20	2.60	6.90	2.90	40.60	0.50
CJ015	0.01	108.00	0.50	0.30	0.30	1.10	2.70	1.00	13.90	0.50
CJ016	0.01	359.00	0.50	12.70	7.30	9.50	6.70	9.40	121.90	3.00
CJ017	0.03	338.00	0.50	0.90	1.30	4.50	4.60	3.40	45.80	0.50
CJ018	0.01	170.00	0.50	0.80	0.80	1.70	2.40	1.30	22.40	0.50
CJ019	0.01	728.00	1.00	4.10	3.10	5.50	9.70	5.50	72.20	1.00
CJ020	0.01	98.00	0.50	0.40	0.30	1.20	2.20	0.80	11.70	0.50
CJ021	0.02	686.00	2.00	7.40	8.00	14.40	6.20	12.60	164.30	3.00
CJ022	0.01	147.00	0.50	0.60	0.50	1.20	1.60	0.80	19.00	0.50
CJ023	0.09	558.00	2.00	6.20	7.70	13.50	7.00	11.20	148.00	3.00
CJ024	0.03	556.00	2.00	6.60	6.30	13.00	7.20	10.70	134.90	3.00
CJ025	0.05	551.00	2.00	12.60	12.90	17.10	5.70	13.40	179.10	4.00
CJ026	0.05	477.00	2.00	4.40	8.60	16.30	5.60	12.60	135.50	4.00
CJ027	0.05	270.00	0.50	3.30	2.00	5.80	4.00	3.70	49.70	1.00
CJ028	0.03	394.00	1.00	1.70	5.00	11.20	5.10	7.90	91.30	2.00
HC002	0.08	64.00	1.00	2.10	0.50	4.20	4.90	5.20	9.00	0.50
HC003	0.01	431.00	1.00	7.70	4.60	7.30	8.40	7.10	69.20	2.00
HC004	0.01	311.00	1.00	4.00	1.50	5.20	5.00	3.90	44.00	0.50
HC005	0.07	354.00	1.00	3.80	1.90	5.20	6.90	4.30	48.00	2.00
HC006	0.01	210.00	2.00	2.20	1.50	3.70	2.70	2.50	32.80	0.50
HC007	0.01	261.00	0.50	2.40	1.70	3.50	3.70	2.80	38.90	0.50
HC008	0.03	280.00	0.50	2.40	2.00	3.60	6.20	4.00	40.70	0.50
HC009	0.05	368.00	2.00	3.60	3.20	6.20	5.50	4.60	53.10	0.50
HC010	0.01	191.00	1.00	1.40	1.20	2.30	5.40	2.70	28.10	0.50
HC011	0.01	436.00	3.00	10.50	5.00	11.70	6.20	9.60	93.00	2.00
HC013	0.12	203.00	1.00	1.70	0.90	2.10	2.30	1.60	28.70	0.50
HC014	0.01	463.00	4.00	9.40	5.20	12.70	7.60	9.50	92.00	2.00
KI001	0.01	316.00	2.00	15.40	4.30	21.30	10.00	14.50	72.20	3.00
KI003	0.01	260.00	0.50	7.50	1.20	4.00	2.70	2.30	42.30	0.50
KI004	0.01	248.00	0.50	1.70	1.20	3.60	2.00	2.00	39.00	0.50
KI005	0.01	287.00	0.50	3.00	0.70	4.60	3.70	4.30	44.20	0.50
KI006	0.01	350.00	1.00	3.20	0.50	7.10	4.40	5.60	51.20	1.00
KI007	0.01	235.00	0.50	3.60	0.60	3.20	3.50	3.00	35.90	0.50
KI008	0.01	568.00	1.00	60.40	0.50	3.90	2.30	1.70	34.10	0.50
KI009	0.05	406.00	1.00	5.60	5.10	14.70	5.80	11.80	97.30	3.00
KI010	0.03	498.00	0.50	1.50	2.40	7.00	5.40	5.70	64.30	1.00
KI011	0.01	222.00	0.50	3.30	0.60	3.90	3.30	2.00	30.80	0.50
KI012	0.03	290.00	2.00	2.00	4.90	12.60	6.80	12.60	101.50	3.00
KI013	0.08	388.00	2.00	5.70	6.40	14.10	6.40	12.80	109.80	4.00
KI014	0.20	504.00	2.00	4.00	6.80	17.60	6.10	14.70	120.90	4.00
KI015	0.06	429.00	2.00	4.30	7.70	17.10	6.40	16.20	133.60	4.00
KI016	0.01	271.00	0.50	1.00	1.20	3.10	4.00	2.80	41.90	0.50
KI017	0.01	243.00	0.50	5.10	1.10	5.80	4.10	3.60	36.00	1.00
KI018	0.04	458.00	2.00	10.20	4.80	18.10	6.40	13.20	90.20	3.00
KP002	0.04	151.00	0.50	7.40	3.90	16.50	12.50	7.80	74.10	3.00
KP003	0.01	324.00	2.00	3.60	3.50	10.00	7.40	7.50	74.90	2.00
KP005	0.02	421.00	2.00	2.80	2.70	7.50	5.20	4.60	72.70	1.00

Sample No	Tot/S	Ba	Be	Co	Cs	Ga	Hf	Nb	Rb	Sn
KP006	0.07	639.00	5.00	6.50	6.80	15.90	5.60	10.60	145.90	3.00
KP007	0.01	363.00	3.00	2.30	2.60	8.60	5.00	7.30	64.80	1.00
KP008	0.04	82.00	0.50	4.80	0.70	5.10	4.60	3.90	19.40	0.50
Reg001	0.07	2649.00	2.00	3.70	0.80	5.60	4.40	3.60	5.70	0.50
Reg002	0.01	348.00	1.00	1.80	2.50	5.30	4.70	3.80	61.10	1.00
Reg003	0.03	171.00	2.00	4.80	1.10	4.30	2.80	2.10	26.60	0.50
Reg004	0.07	89.00	0.50	3.70	0.70	3.50	0.60	1.00	16.80	0.50
Reg005	0.16	253.00	0.50	6.10	1.40	5.60	3.30	3.20	49.60	1.00
Reg006	0.09	220.00	0.50	2.90	0.70	2.30	0.80	0.70	30.00	0.50
Reg007	0.05	812.00	0.50	571.10	0.70	6.70	5.20	1.80	23.40	0.50
Reg008	0.03	383.00	0.50	10.00	3.30	13.70	5.50	6.80	78.80	2.00
Reg009	0.10	417.00	1.00	3.40	4.20	24.90	4.80	10.10	85.80	3.00
Reg011	0.16	790.00	0.50	2.10	3.90	23.80	10.40	17.10	95.70	5.00
Reg012	0.02	213.00	0.50	2.50	2.30	11.10	4.00	4.90	39.20	2.00
Reg013	0.15	545.00	0.50	5.50	3.20	11.40	10.10	8.80	89.60	2.00
Reg014	0.03	1402.00	0.50	3.10	2.80	9.30	5.70	5.40	41.80	2.00
Reg015	0.01	257.00	0.50	1.40	1.70	5.30	4.90	4.70	40.10	2.00
Reg016	0.01	297.00	2.00	2.30	1.30	6.30	4.50	4.80	46.10	1.00
Reg017	0.01	542.00	0.50	3.90	4.30	11.30	6.30	6.90	87.80	2.00
Reg018	0.01	156.00	0.50	2.40	3.20	11.80	4.80	6.20	45.40	1.00
Reg019	0.01	456.00	2.00	6.30	3.00	7.80	5.50	6.50	86.10	2.00
Reg020	0.01	214.00	0.50	2.10	1.80	3.40	5.10	3.20	38.80	0.50
Reg021	0.01	233.00	0.50	1.70	1.00	3.40	5.30	2.30	33.70	0.50
Reg022	0.01	534.00	3.00	4.80	8.60	13.10	5.60	9.40	116.40	3.00
Reg023	0.01	266.00	0.50	1.40	0.90	4.70	4.40	2.70	35.00	2.00
Reg024	0.01	192.00	0.50	5.00	2.30	9.10	3.40	4.60	36.80	2.00
Reg025	0.01	386.00	0.50	12.50	1.70	7.30	10.70	9.10	57.80	2.00
Reg026	0.01	90.00	0.50	3.40	3.40	14.60	4.50	5.80	36.50	2.00
Reg027	0.01	53.00	0.50	2.90	1.80	11.90	6.10	5.00	17.80	3.00
Reg028	0.01	68.00	0.50	1.60	0.90	5.70	3.40	2.30	10.50	1.00
Reg029	0.01	190.00	0.50	1.00	0.60	5.70	3.60	2.70	6.80	1.00
Reg030	0.01	272.00	0.50	2.40	1.30	6.10	5.70	4.80	46.20	2.00
Reg031	0.01	227.00	2.00	1.00	1.20	5.00	4.60	4.00	39.70	1.00
Reg032	0.01	203.00	3.00	0.80	0.70	6.40	3.00	2.50	6.80	1.00
Reg033	0.01	414.00	0.50	2.80	2.60	9.10	9.40	9.40	72.50	5.00
Reg034	0.01	351.00	0.50	4.60	4.10	17.10	9.30	7.90	116.40	3.00
Reg035	0.01	391.00	1.00	3.00	4.20	16.00	7.10	7.50	96.00	3.00
Reg036	0.01	234.00	0.50	1.70	2.10	6.30	4.40	3.70	51.00	3.00
Reg037	0.01	124.00	2.00	0.80	1.20	4.50	2.70	2.40	23.80	2.00
Reg038	0.01	203.00	3.00	4.90	5.40	15.30	5.90	7.80	109.20	2.00
Reg039	0.01	117.00	2.00	1.40	1.30	4.50	5.10	2.60	24.40	0.50
Reg040	0.01	161.00	1.00	2.70	2.80	10.90	6.80	5.60	41.50	1.00
Reg041	0.01	42.00	0.50	1.60	1.50	9.60	3.90	3.90	14.80	1.00
Reg042	0.01	315.00	0.50	1.10	1.30	2.60	3.20	1.20	24.00	0.50
Reg043	0.01	516.00	0.50	8.80	6.30	16.40	15.30	12.50	141.50	3.00
Reg044	0.03	327.00	2.00	1.60	1.10	2.50	5.50	2.60	43.10	0.50
Reg045	0.13	142.00	0.50	1.80	0.70	3.40	1.90	0.80	23.10	0.50
Reg046	0.01	261.00	0.50	1.70	2.10	5.20	3.60	2.40	45.80	0.50
Reg047	0.05	71.00	2.00	6.30	3.90	23.20	6.90	10.70	33.10	2.00
Reg048	0.05	123.00	3.00	3.90	1.90	18.30	5.90	7.50	41.80	2.00
Reg049	0.01	371.00	0.50	1.00	1.80	5.80	6.10	4.30	55.20	0.50
Reg050	0.01	54.00	0.50	2.00	1.10	18.00	6.60	9.40	13.00	2.00
Reg051	0.01	45.00	0.50	2.20	1.50	9.70	4.50	3.80	17.60	0.50
Reg052	0.01	192.00	0.50	7.50	3.60	15.90	6.40	10.50	55.80	2.00
Reg053	0.01	291.00	2.00	2.20	2.50	6.30	7.50	7.30	63.10	0.50
Reg054	0.01	278.00	0.50	1.90	3.60	11.30	4.30	6.60	67.30	2.00
Reg055	0.03	71.00	0.50	7.50	4.10	23.10	5.10	7.90	42.40	3.00
Reg056	0.01	47.00	0.50	0.60	0.70	4.80	4.00	2.00	8.80	0.50
Reg057	0.02	56.00	0.50	1.30	1.00	9.40	5.30	3.90	11.00	0.50
Reg058	0.01	43.00	0.50	1.70	1.10	8.10	4.20	3.90	11.20	0.50
Reg059	0.01	30.00	0.50	0.50	0.40	3.80	3.90	2.20	4.70	0.50
Reg060	0.01	39.00	0.50	0.90	0.80	6.30	2.80	2.60	8.80	0.50
Reg061	0.01	66.00	0.50	1.90	1.20	12.50	6.10	7.10	19.80	1.00
Reg062	0.01	24.00	1.00	0.50	0.40	6.30	4.30	3.70	5.50	0.50
Reg063	0.01	600.00	2.00	15.90	9.40	17.10	6.00	13.50	165.80	4.00
Reg064	0.01	167.00	1.00	3.00	2.70	10.30	7.50	7.00	43.00	1.00

Sample No	Tot/S	Ba	Be	Co	Cs	Ga	Hf	Nb	Rb	Sn
Reg065	0.04	76.00	2.00	6.80	4.20	23.40	8.30	11.30	36.30	3.00
Reg066	0.02	73.00	2.00	7.70	4.30	23.30	4.80	7.60	43.30	4.00
Reg068	0.04	683.00	0.50	8.60	1.00	8.00	13.10	8.80	14.10	1.00
Reg069	0.01	212.00	1.00	6.00	2.20	11.50	6.70	8.80	31.30	1.00
Reg070	0.01	269.00	0.50	4.80	1.00	6.20	6.90	6.50	18.70	1.00
Reg071	0.03	649.00	0.50	11.90	0.90	9.20	6.00	7.40	16.50	1.00
Reg072	0.01	229.00	0.50	4.90	0.05	5.80	2.40	2.10	12.60	0.50
Reg073	0.02	654.00	3.00	4.00	6.40	16.90	11.00	115.50	142.80	4.00
Reg074	0.02	90.00	11.00	20.00	7.00	33.30	6.60	12.70	66.80	6.00
Reg075	0.05	940.00	1.00	74.80	1.30	2.20	2.80	2.20	24.40	0.50
Reg076	0.34	430.00	1.00	85.40	1.30	2.20	3.00	2.10	26.40	0.50
Reg078	0.01	208.00	2.00	1.80	1.20	2.80	3.00	1.90	30.90	0.50
WB001	0.01	629.00	2.00	1.60	6.00	19.60	6.40	16.30	134.10	5.00
WB002	0.01	609.00	2.00	2.60	7.90	21.00	5.20	12.80	127.50	4.00
WB003	0.01	832.00	1.00	0.80	4.60	16.10	7.40	18.50	127.20	6.00
WB004	0.10	776.00	1.00	2.60	6.00	24.70	6.50	13.00	105.30	4.00
WB005	0.03	1237.00	2.00	2.20	6.20	25.50	8.10	18.90	131.20	5.00
WB006	0.14	1163.00	0.50	0.70	2.20	18.80	8.70	17.70	73.30	6.00
WB007	0.47	289.00	2.00	5.00	5.50	13.10	4.70	8.40	91.00	2.00
CJ029	0.01	561.00	2.00	13.10	7.70	15.30	4.50	12.60	153.90	4.00
KP009	0.01	544.00	2.00	15.70	7.20	18.40	4.50	13.40	149.60	5.00
HC015	0.01	278.00	4.00	25.30	7.40	21.60	6.50	21.20	169.60	4.00
Arckaringa Basin										
BC001	0.01	268.00	0.50	2.40	0.60	2.40	4.90	2.40	29.00	0.50
BC002	0.64	301.00	0.50	2.70	0.90	3.40	5.20	3.10	40.40	0.50
BC003	0.64	752.00	0.50	12.70	0.60	2.50	4.20	2.50	31.60	0.50
BC004	0.04	387.00	0.50	1.70	0.70	3.10	4.30	2.90	37.10	0.50
BC005	0.03	292.00	1.00	6.60	0.60	2.90	4.60	2.50	36.80	0.50
BC006	0.01	411.00	0.50	5.10	0.90	3.20	5.50	3.30	41.60	0.50
MD001	0.08	345.00	1.00	8.40	2.10	8.30	5.70	7.10	90.40	2.00
MD002	0.28	239.00	2.00	8.00	1.20	5.10	3.60	4.00	34.50	1.00
MD003	0.26	774.00	2.00	26.40	1.10	2.70	2.50	1.90	22.00	0.50
MD004	0.01	315.00	0.50	5.10	2.20	4.90	8.00	5.00	62.10	1.00
MD005	0.82	387.00	1.00	3.00	2.10	9.30	14.70	10.80	76.10	2.00
MT001	0.16	450.00	1.00	9.00	3.10	12.20	13.00	17.20	98.30	6.00
MT002	0.16	675.00	4.00	11.00	10.00	24.70	5.70	21.20	191.20	6.00
MT003	0.43	571.00	3.00	10.80	6.80	18.90	10.60	21.70	145.50	5.00
MT004	0.19	572.00	2.00	13.90	6.30	17.30	10.40	21.30	135.00	5.00
MT005	0.28	632.00	4.00	14.30	9.30	23.70	6.40	23.20	175.00	6.00
MT006	0.13	725.00	4.00	17.20	9.40	27.30	6.10	23.60	191.30	7.00
MT007	13.49	176.00	0.50	2.90	0.30	2.50	0.60	2.20	7.00	0.50
MT008	3.26	156.00	0.50	3.20	1.00	2.60	9.90	6.20	30.20	0.50
MT009	16.82	96.00	0.50	21.10	0.10	5.10	0.70	1.60	1.70	0.50
MT010	0.41	745.00	2.00	11.30	8.00	27.90	7.50	24.10	173.10	6.00
MT011	3.52	453.00	4.00	11.50	8.30	20.20	6.40	17.60	132.80	4.00
MT012	0.16	740.00	2.00	12.90	6.70	19.70	8.80	19.70	149.80	4.00
MT013	0.13	568.00	2.00	11.20	5.50	16.00	9.60	18.50	133.40	4.00
MT014	0.10	598.00	4.00	14.20	11.70	25.90	6.20	22.40	197.10	6.00
MT015	0.14	611.00	2.00	14.90	8.10	20.00	8.90	20.10	164.00	5.00
MT016	1.53	873.00	3.00	8.10	4.60	12.50	6.30	12.60	90.00	4.00
MT017	0.88	140.00	0.50	0.60	0.90	1.50	19.20	9.10	24.00	0.50
MT018	3.47	1025.00	0.50	9.40	2.40	9.50	1.70	4.50	20.00	1.00
MT019	0.72	686.00	2.00	3.50	10.10	25.60	4.20	21.70	186.70	7.00
MT020	4.18	239.00	2.00	8.80	8.50	10.70	7.70	11.80	80.40	3.00
MT021	0.53	521.00	2.00	4.00	5.70	18.20	9.30	23.10	128.10	6.00
MT023	0.15	518.00	2.00	6.50	7.50	23.80	9.00	29.80	140.50	7.00
MT024	0.17	594.00	3.00	16.20	9.70	27.90	4.90	25.90	170.90	7.00
MT025	0.18	80.00	0.50	1.80	2.40	3.50	8.60	7.20	23.50	0.50
MT026	0.10	164.00	1.00	2.70	4.50	13.90	11.90	27.70	59.50	5.00
MT027	0.11	28.00	0.50	0.90	0.50	1.10	1.80	1.40	7.70	0.50
MT001	0.16	450.00	1.00	9.00	3.10	12.20	13.00	17.20	98.30	6.00
MT002	0.16	675.00	4.00	11.00	10.00	24.70	5.70	21.20	191.20	6.00
MT003	0.43	571.00	3.00	10.80	6.80	18.90	10.60	21.70	145.50	5.00
MT004	0.19	572.00	2.00	13.90	6.30	17.30	10.40	21.30	135.00	5.00
MT005	0.28	632.00	4.00	14.30	9.30	23.70	6.40	23.20	175.00	6.00
MT006	0.13	725.00	4.00	17.20	9.40	27.30	6.10	23.60	191.30	7.00

Sample No	Tot/S	Ba	Be	Co	Cs	Ga	Hf	Nb	Rb	Sn
MT007	13.49	176.00	0.50	2.90	0.30	2.50	0.60	2.20	7.00	0.50
MT008	3.26	156.00	0.50	3.20	1.00	2.60	9.90	6.20	30.20	0.50
MT009	16.82	96.00	0.50	21.10	0.10	5.10	0.70	1.60	1.70	0.50
MT010	0.41	745.00	2.00	11.30	8.00	27.90	7.50	24.10	173.10	6.00
MT011	3.52	453.00	4.00	11.50	8.30	20.20	6.40	17.60	132.80	4.00
MT012	0.16	740.00	2.00	12.90	6.70	19.70	8.80	19.70	149.80	4.00
MT013	0.13	568.00	2.00	11.20	5.50	16.00	9.60	18.50	133.40	4.00
MT014	0.10	598.00	4.00	14.20	11.70	25.90	6.20	22.40	197.10	6.00
MT015	0.14	611.00	2.00	14.90	8.10	20.00	8.90	20.10	164.00	5.00
MT016	1.53	873.00	3.00	8.10	4.60	12.50	6.30	12.60	90.00	4.00
MT017	0.88	140.00	0.50	0.60	0.90	1.50	19.20	9.10	24.00	0.50
MT018	3.47	1025.00	0.50	9.40	2.40	9.50	1.70	4.50	20.00	1.00
MT019	0.72	686.00	2.00	3.50	10.10	25.60	4.20	21.70	186.70	7.00
MT020	4.18	239.00	2.00	8.80	8.50	10.70	7.70	11.80	80.40	3.00
MT021	0.53	521.00	2.00	4.00	5.70	18.20	9.30	23.10	128.10	6.00
MT023	0.15	518.00	2.00	6.50	7.50	23.80	9.00	29.80	140.50	7.00
MT024	0.17	594.00	3.00	16.20	9.70	27.90	4.90	25.90	170.90	7.00
MT025	0.18	80.00	0.50	1.80	2.40	3.50	8.60	7.20	23.50	0.50
MT026	0.10	164.00	1.00	2.70	4.50	13.90	11.90	27.70	59.50	5.00
MT027	0.11	28.00	0.50	0.90	0.50	1.10	1.80	1.40	7.70	0.50

	Sr	Ta	Th	U	V	W	Zr	Y	La	Ce
	ppm	ppm	ppm	ppm	ppm	ppm	ppm	ppm	ppm	ppm
Analysis	**ICP-MS**	**ICP-MS**	**ICP-MS**	**ICP-MS**	**ICP-MS**	**ICP-MS**	**ICP-MS**	**ICP-MS**	**ICP-MS**	**ICP-MS**
Det. limit	**0.5**	**0.1**	**0.2**	**0.1**	**8**	**0.5**	**0.1**	**0.1**	**0.1**	**0.1**
Sample No		**Ta**	**Th**	**U**	**V**	**W**	**Zr**	**Y**	**La**	**Ce**
Troubridge Basin										
CJ002	79.00	0.60	10.30	1.40	38.00	1.60	227.40	18.70	27.20	55.40
CJ003	176.50	0.50	9.30	1.40	31.00	1.10	171.90	16.50	24.10	48.00
CJ004	131.50	0.60	10.60	2.10	41.00	1.40	204.30	17.10	26.70	54.20
CJ005	64.10	0.50	7.10	1.50	28.00	1.10	226.80	12.30	19.00	37.30
CJ006	76.60	0.50	9.80	1.40	37.00	1.30	243.90	14.10	25.80	51.30
CJ007	81.80	0.40	7.00	0.90	22.00	0.50	217.40	9.70	17.30	30.00
CJ008	34.20	0.20	2.30	0.60	8.00	0.25	157.10	7.00	6.00	12.50
CJ009	136.50	0.50	14.00	1.30	35.00	0.90	213.20	15.90	33.00	64.00
CJ010	73.40	0.50	8.30	1.30	30.00	1.00	289.80	13.80	21.30	43.00
CJ011	169.80	0.40	2.50	1.00	10.00	0.25	170.10	61.80	15.60	31.00
CJ012	205.50	0.10	1.80	0.60	4.00	0.25	141.00	25.30	6.00	12.30
CJ013	75.20	0.30	4.70	1.00	17.00	0.60	214.10	8.20	11.90	24.40
CJ014	43.60	0.40	3.90	0.90	12.00	0.25	252.60	7.00	8.10	21.40
CJ015	181.70	0.05	1.60	0.90	4.00	0.25	97.40	6.50	4.40	8.30
CJ016	122.90	0.70	13.70	2.20	49.00	0.70	248.20	27.10	35.70	73.10
CJ017	88.00	0.30	4.50	0.70	16.00	0.25	172.70	9.70	12.80	25.20
CJ018	236.10	0.10	2.20	1.90	4.00	0.25	97.80	23.40	16.50	28.30
CJ019	179.50	0.40	5.10	1.30	25.00	0.90	409.50	22.00	15.20	28.30
CJ020	167.40	0.05	1.50	0.70	4.00	0.25	81.60	11.70	5.60	10.50
CJ021	84.80	0.90	17.80	3.00	62.00	2.40	211.40	23.70	43.10	83.30
CJ022	258.40	0.05	1.80	2.60	4.00	0.25	63.40	23.00	13.20	24.50
CJ023	82.00	1.00	17.20	4.90	63.00	2.40	239.60	26.00	41.30	84.50
CJ024	83.20	0.90	15.70	5.40	61.00	1.90	253.80	25.40	39.60	81.00
CJ025	90.90	1.00	20.90	3.80	83.00	2.10	195.50	39.70	50.90	106.20
CJ026	564.30	1.00	20.70	2.60	76.00	2.60	188.10	28.30	52.60	117.80
CJ027	299.00	0.30	5.40	1.40	29.00	0.60	145.10	8.30	15.90	39.30
CJ028	230.90	0.70	13.80	2.70	58.00	1.40	176.60	15.10	40.00	99.00
HC002	66.40	0.60	3.50	0.80	24.00	1.00	225.40	8.60	9.50	18.40
HC003	70.50	0.50	7.90	1.40	46.00	1.20	293.70	16.50	20.30	42.40
HC004	65.60	0.30	4.40	1.10	27.00	0.25	203.20	14.90	11.80	23.80
HC005	56.20	0.30	3.90	0.80	24.00	0.70	229.80	11.60	12.40	24.60
HC006	35.30	0.10	3.00	0.70	18.00	1.70	98.00	7.40	9.00	18.70
HC007	42.30	0.20	2.80	0.40	13.00	0.25	145.30	7.60	9.20	19.10
HC008	43.10	0.20	3.40	0.80	18.00	0.70	246.40	9.60	11.00	21.10
HC009	54.10	0.50	5.10	0.70	31.00	0.80	201.80	12.40	15.20	29.70
HC010	29.20	0.20	2.80	0.50	11.00	0.25	196.80	9.10	8.10	15.70

Sample No	Sr	Ta	Th	U	V	W	Zr	Y	La	Ce
HC011	91.00	0.70	10.90	1.40	61.00	1.40	245.00	30.70	31.80	66.30
HC013	33.80	0.05	2.20	0.40	10.00	0.60	105.00	6.70	7.50	14.30
HC014	89.60	0.90	11.30	1.30	69.00	1.70	264.10	27.40	35.40	69.60
KI001	71.90	1.10	23.60	3.20	226.00	2.10	345.70	47.00	64.70	123.80
KI003	39.30	0.20	4.30	0.90	79.00	0.25	97.10	10.40	10.60	21.40
KI004	127.90	0.10	3.00	0.60	25.00	0.25	75.90	7.90	8.70	16.70
KI005	85.70	0.30	5.80	0.80	31.00	0.25	119.50	10.60	13.30	27.00
KI006	61.30	0.40	7.60	1.10	77.00	0.70	158.30	15.30	20.00	41.70
KI007	101.80	0.20	6.30	0.90	39.00	0.25	122.20	9.80	12.80	26.50
KI008	50.60	0.10	2.80	1.30	66.00	0.25	75.30	15.80	11.70	31.40
KI009	288.00	0.80	18.00	2.40	73.00	1.40	201.80	11.60	39.20	76.90
KI010	108.40	0.40	14.50	1.70	37.00	0.70	198.40	7.10	14.60	28.20
KI011	47.80	0.10	10.80	1.80	14.00	0.25	126.40	3.60	6.20	11.80
KI012	98.00	1.10	9.70	2.50	56.00	1.60	242.70	10.60	22.70	40.30
KI013	211.50	1.10	14.00	2.50	61.00	1.70	203.50	11.30	35.50	62.10
KI014	375.60	1.10	14.10	3.20	82.00	1.80	219.90	12.60	42.10	84.50
KI015	298.70	1.20	15.40	3.30	90.00	2.00	229.50	13.80	37.90	73.80
KI016	79.50	0.20	4.20	0.80	15.00	0.25	164.60	4.80	10.90	21.50
KI017	93.10	0.30	13.50	2.40	28.00	0.25	154.00	6.70	10.70	18.60
KI018	335.10	1.00	28.40	2.70	82.00	1.60	236.10	14.40	48.90	102.00
KP002	56.20	0.50	9.70	1.10	70.00	1.00	448.30	18.10	21.80	44.80
KP003	92.30	0.70	8.90	1.10	52.00	1.00	285.50	11.20	19.80	38.40
KP005	104.50	0.40	8.80	0.80	25.00	0.90	186.00	11.50	25.00	49.10
KP006	174.10	1.20	16.40	1.80	65.00	2.30	231.90	24.70	46.20	92.80
KP007	108.40	0.60	7.10	1.10	22.00	1.70	192.70	12.60	33.60	50.10
KP008	18.30	0.30	14.40	1.00	173.00	0.90	179.10	7.00	6.90	10.90
Reg001	124.80	0.50	5.20	1.10	46.00	0.25	177.20	5.20	5.80	17.60
Reg002	281.60	0.30	5.40	1.20	22.00	0.80	182.30	9.00	18.00	40.80
Reg003	835.30	0.30	3.80	0.70	39.00	0.25	100.80	9.30	11.20	20.20
Reg004	619.80	0.05	2.80	0.70	24.00	0.50	29.60	6.00	7.30	12.70
Reg005	641.90	0.40	5.70	5.10	21.00	0.70	128.00	21.00	21.90	40.10
Reg006	739.60	0.05	1.40	0.80	4.00	0.25	33.10	7.00	5.80	9.70
Reg007	90.60	0.20	2.90	1.30	97.00	0.80	221.20	10.10	8.20	147.40
Reg008	90.60	0.60	11.10	1.30	217.00	1.60	188.60	13.60	14.10	24.50
Reg009	89.50	0.80	24.60	2.90	254.00	1.60	185.20	9.00	13.30	23.40
Reg011	162.20	1.40	11.30	2.40	82.00	2.20	370.30	15.20	23.90	36.50
Reg012	28.40	0.40	12.50	1.90	167.00	1.00	154.80	7.50	9.00	16.30
Reg013	488.90	0.70	9.10	2.20	70.00	6.00	330.80	22.40	48.50	114.30
Reg014	56.90	0.40	5.60	0.80	40.00	1.20	213.00	11.10	17.70	22.40
Reg015	51.00	0.40	5.20	1.10	26.00	1.40	195.40	7.20	10.90	19.90
Reg016	62.10	0.50	5.10	1.00	26.00	1.10	175.90	10.90	14.10	25.70
Reg017	60.80	0.70	7.80	1.40	52.00	1.30	226.80	11.70	14.70	24.70
Reg018	50.10	0.40	9.50	1.30	57.00	0.80	157.00	7.50	13.80	27.20
Reg019	103.50	0.60	8.80	1.80	36.00	1.10	195.30	16.00	25.60	52.00
Reg020	49.20	0.20	2.90	1.10	13.00	1.00	206.00	8.70	8.70	16.50
Reg021	58.10	0.20	2.90	1.00	11.00	0.70	189.30	8.90	9.00	17.70
Reg022	193.50	0.60	19.40	1.80	110.00	1.60	204.80	13.60	44.70	94.60
Reg023	70.70	0.10	4.60	0.70	19.00	0.25	170.60	6.40	14.30	28.60
Reg024	48.50	0.30	5.90	0.80	49.00	1.30	127.20	12.00	13.60	30.90
Reg025	85.50	0.80	7.50	1.50	40.00	2.40	370.00	23.00	26.50	64.80
Reg026	69.60	0.60	10.90	1.30	76.00	1.20	144.20	9.50	19.00	37.00
Reg027	41.40	0.30	12.10	1.20	71.00	1.40	211.90	7.00	9.50	16.80
Reg028	23.60	0.10	4.60	0.60	24.00	0.25	133.70	4.50	8.30	13.60
Reg029	52.50	0.10	5.60	0.80	28.00	0.25	142.00	4.70	19.00	39.00
Reg030	63.10	0.30	5.50	0.80	19.00	0.90	186.20	10.10	14.50	29.10
Reg031	48.60	0.20	5.30	1.00	20.00	1.60	176.30	6.50	10.10	22.00
Reg032	55.50	0.05	4.90	0.70	28.00	0.50	116.50	5.80	22.00	41.50
Reg033	66.60	0.80	9.70	2.30	42.00	1.30	355.90	21.90	25.00	49.40
Reg034	47.80	0.80	14.10	2.80	67.00	0.80	365.70	18.90	22.90	47.20
Reg035	188.20	0.80	13.80	1.50	50.00	1.60	258.30	13.50	42.20	83.60
Reg036	49.70	0.40	5.60	0.80	24.00	0.60	182.30	7.40	11.70	19.30
Reg037	37.40	0.20	6.70	0.70	16.00	0.25	113.70	5.30	11.50	20.50
Reg038	64.40	0.70	11.30	2.00	62.00	1.10	234.20	21.20	26.90	55.00
Reg039	25.90	0.30	11.20	0.80	33.00	0.25	193.90	5.60	12.00	19.10
Reg040	34.60	0.50	6.90	1.40	47.00	0.70	282.20	8.90	11.70	20.20
Reg041	38.00	0.40	10.20	1.20	38.00	0.60	152.80	5.60	13.50	21.90

Sample No	Sr	Ta	Th	U	V	W	Zr	Y	La	Ce
Reg042	58.20	0.20	4.20	0.70	11.00	0.25	116.20	5.80	9.40	16.60
Reg043	57.50	1.20	20.30	3.80	71.00	1.50	569.70	33.40	49.70	177.40
Reg044	143.60	0.20	2.70	0.90	8.00	0.25	174.00	7.10	9.20	23.30
Reg045	24.90	0.10	3.60	0.90	12.00	0.25	82.90	6.40	5.60	11.00
Reg046	55.40	0.20	6.20	1.10	22.00	0.50	138.00	7.10	12.10	23.20
Reg047	22.70	0.90	20.50	3.30	155.00	1.00	241.00	14.60	19.00	37.50
Reg048	17.40	0.70	25.30	2.60	94.00	0.25	217.00	14.90	28.10	56.00
Reg049	93.20	0.60	5.70	0.80	16.00	0.25	247.30	7.30	18.80	38.20
Reg050	46.20	0.70	15.50	1.50	44.00	1.60	265.30	10.80	14.50	25.70
Reg051	30.70	0.30	7.10	1.30	42.00	0.25	175.50	6.80	11.70	21.90
Reg052	42.80	0.90	12.20	4.60	103.00	1.20	213.00	18.80	18.50	39.90
Reg053	47.60	0.60	7.20	1.50	39.00	0.50	297.40	12.50	12.70	23.90
Reg054	169.60	0.60	12.20	2.20	45.00	1.30	138.10	18.70	32.00	64.30
Reg055	56.30	0.80	18.50	3.10	120.00	0.70	165.80	12.70	17.80	35.20
Reg056	47.40	0.30	5.50	0.80	20.00	0.25	130.80	5.90	13.40	28.00
Reg057	46.80	0.40	10.70	1.10	97.00	1.70	187.60	6.50	13.00	26.40
Reg058	20.80	0.30	7.00	1.30	54.00	0.50	153.80	6.50	8.10	15.00
Reg059	26.50	0.30	4.00	0.60	12.00	0.90	141.90	5.20	7.00	13.50
Reg060	45.00	0.30	8.30	1.20	23.00	0.70	114.80	5.40	21.80	43.20
Reg061	15.20	0.60	12.90	1.30	63.00	0.80	227.40	7.40	8.70	14.00
Reg062	29.40	0.20	6.80	1.00	29.00	0.70	158.50	3.90	8.20	13.00
Reg063	71.90	1.00	16.60	2.30	88.00	2.40	228.30	27.00	40.40	78.50
Reg064	35.20	0.60	6.00	1.20	52.00	1.10	275.90	8.80	10.20	17.30
Reg065	24.80	0.80	22.60	3.20	175.00	0.90	273.40	12.90	20.90	40.40
Reg066	58.60	0.70	18.40	3.30	142.00	1.20	171.20	12.00	17.50	31.30
Reg068	43.00	1.00	9.90	1.10	618.00	0.80	517.30	9.90	9.00	15.30
Reg069	87.90	0.60	10.30	1.20	137.00	0.60	317.70	13.30	19.50	36.90
Reg070	29.10	0.40	8.00	0.90	177.00	0.60	260.90	8.90	12.10	18.60
Reg071	51.20	0.60	13.90	1.10	676.00	<0.5	206.70	11.80	14.50	17.70
Reg072	63.70	0.20	3.50	0.80	122.00	0.25	82.10	27.00	6.80	16.60
Reg073	91.50	6.90	14.40	1.60	45.00	2.50	467.20	22.90	17.20	26.80
Reg074	55.70	1.40	29.60	3.60	155.00	2.60	223.10	13.50	15.80	38.60
Reg075	103.20	0.10	2.90	5.10	35.00	0.80	106.50	13.20	9.00	19.20
Reg076	69.80	0.20	3.00	5.50	22.00	1.10	111.20	14.50	10.50	26.10
Reg078	30.80	0.05	2.70	0.40	4.00	0.80	111.30	6.80	7.50	14.70
WB001	132.20	1.30	15.40	2.60	92.00	2.20	237.40	13.30	25.20	43.60
WB002	154.40	1.00	27.00	2.70	209.00	2.10	184.10	10.90	20.10	33.90
WB003	122.30	1.50	12.00	2.40	51.00	2.70	252.40	13.90	23.90	42.10
WB004	148.30	1.00	24.70	2.90	451.00	1.60	216.70	10.20	15.80	26.40
WB005	145.10	1.40	13.40	2.50	92.00	2.60	290.60	15.20	23.10	37.90
WB006	191.10	1.40	11.30	2.70	44.00	2.60	290.90	13.90	23.60	40.20
WB007	223.90	0.60	10.10	3.00	246.00	1.30	179.50	9.30	27.40	23.20
CJ029	185.60	0.90	14.50	2.80	86.00	1.70	159.30	26.10	38.40	74.70
KP009	202.30	1.10	14.10	2.40	86.00	1.80	183.90	29.80	39.20	79.70
HC015	53.30	1.60	15.40	2.70	136.00	3.00	241.50	36.80	45.90	95.40
Arckaringa Basin										
BC001	133.50	0.20	2.60	0.90	13.00	0.25	175.00	7.80	7.40	15.60
BC002	113.50	0.30	4.10	1.90	19.00	0.60	198.60	11.10	10.00	20.60
BC003	385.40	0.20	2.70	5.00	35.00	0.25	160.90	6.50	7.00	14.40
BC004	144.90	0.20	2.80	0.90	14.00	0.50	161.50	8.40	8.30	17.00
BC005	84.60	0.20	2.60	6.80	48.00	0.25	180.90	8.40	7.20	14.10
BC006	132.60	0.30	3.60	1.50	19.00	0.60	205.70	9.90	9.20	18.90
MD001	61.20	0.70	9.00	2.60	45.00	1.10	203.60	21.90	21.00	42.50
MD002	85.80	0.30	5.50	3.20	41.00	0.60	125.90	22.10	11.80	27.00
MD003	111.80	0.20	2.80	1.10	21.00	0.25	92.20	19.30	9.40	21.00
MD004	65.00	0.40	5.40	2.20	62.00	0.90	294.80	14.80	16.10	35.30
MD005	51.90	1.00	14.30	3.20	39.00	1.60	529.50	30.00	40.00	82.60
MT001	57.20	1.50	17.70	3.60	55.00	3.70	443.50	30.80	46.70	97.40
MT002	50.60	1.70	25.80	4.60	129.00	3.20	206.10	33.30	50.10	104.40
MT003	78.10	1.80	22.30	4.60	94.00	2.90	350.10	36.00	52.70	108.30
MT004	74.50	1.70	20.70	4.60	93.00	2.80	352.60	34.70	52.00	111.30
MT005	112.70	1.70	26.50	5.60	121.00	3.20	229.10	34.10	54.30	115.90
MT006	94.80	1.90	27.70	5.80	126.00	3.30	207.60	35.10	56.10	118.40
MT007	2177.70	0.10	1.70	4.30	19.00	0.25	36.80	4.50	9.50	15.80
MT008	169.30	0.60	4.60	1.40	17.00	0.70	369.80	11.80	12.20	24.50
MT009	768.60	0.05	2.10	0.40	26.00	0.60	48.40	8.00	9.10	19.50

Sample No	Sr	Ta	Th	U	V	W	Zr	Y	La	Ce
MT010	78.70	1.80	25.80	5.40	109.00	3.00	293.00	39.10	58.80	118.50
MT011	349.50	1.40	18.00	4.50	88.00	1.90	240.40	41.80	44.80	93.20
MT012	50.90	1.70	18.60	3.70	76.00	2.40	320.10	36.50	48.60	100.80
MT013	54.80	1.60	16.40	3.30	67.00	2.00	364.00	31.20	44.10	92.80
MT014	62.20	1.70	24.50	4.50	108.00	2.80	233.10	37.30	52.50	107.50
MT015	52.40	1.70	19.50	3.70	85.00	2.60	318.20	34.60	50.20	103.80
MT016	727.80	1.10	13.00	2.80	51.00	2.10	226.20	25.10	34.90	73.10
MT017	80.00	0.90	6.70	2.10	4.00	1.10	673.80	17.90	15.70	33.10
MT018	1038.10	0.30	5.40	7.20	49.00	0.70	55.70	13.70	32.70	57.10
MT019	96.30	2.00	26.10	2.70	94.00	3.20	146.30	22.20	36.80	68.10
MT020	306.20	1.10	16.50	4.40	49.00	1.70	284.30	28.90	38.90	84.40
MT021	163.50	1.80	19.60	4.50	72.00	2.70	333.60	28.40	42.30	87.30
MT023	39.50	2.30	26.30	4.50	95.00	3.40	308.00	37.00	60.00	128.20
MT024	44.40	2.10	27.00	3.60	109.00	3.30	173.60	28.60	45.60	95.40
MT025	200.40	0.40	3.80	1.00	14.00	0.50	325.10	10.50	12.00	23.60
MT026	58.20	3.20	20.90	3.00	35.00	1.90	428.00	29.00	36.00	81.80
MT027	357.70	0.10	1.50	0.50	4.00	0.25	67.50	3.40	4.40	8.30
MT001	57.20	1.50	17.70	3.60	55.00	3.70	443.50	30.80	46.70	97.40
MT002	50.60	1.70	25.80	4.60	129.00	3.20	206.10	33.30	50.10	104.40
MT003	78.10	1.80	22.30	4.60	94.00	2.90	350.10	36.00	52.70	108.30
MT004	74.50	1.70	20.70	4.60	93.00	2.80	352.60	34.70	52.00	111.30
MT005	112.70	1.70	26.50	5.60	121.00	3.20	229.10	34.10	54.30	115.90
MT006	94.80	1.90	27.70	5.80	126.00	3.30	207.60	35.10	56.10	118.40
MT007	2177.70	0.10	1.70	4.30	19.00	0.25	36.80	4.50	9.50	15.80
MT008	169.30	0.60	4.60	1.40	17.00	0.70	369.80	11.80	12.20	24.50
MT009	768.60	0.05	2.10	0.40	26.00	0.60	48.40	8.00	9.10	19.50
MT010	78.70	1.80	25.80	5.40	109.00	3.00	293.00	39.10	58.80	118.50
MT011	349.50	1.40	18.00	4.50	88.00	1.90	240.40	41.80	44.80	93.20
MT012	50.90	1.70	18.60	3.70	76.00	2.40	320.10	36.50	48.60	100.80
MT013	54.80	1.60	16.40	3.30	67.00	2.00	364.00	31.20	44.10	92.80
MT014	62.20	1.70	24.50	4.50	108.00	2.80	233.10	37.30	52.50	107.50
MT015	52.40	1.70	19.50	3.70	85.00	2.60	318.20	34.60	50.20	103.80
MT016	727.80	1.10	13.00	2.80	51.00	2.10	226.20	25.10	34.90	73.10
MT017	80.00	0.90	6.70	2.10	4.00	1.10	673.80	17.90	15.70	33.10
MT018	1038.10	0.30	5.40	7.20	49.00	0.70	55.70	13.70	32.70	57.10
MT019	96.30	2.00	26.10	2.70	94.00	3.20	146.30	22.20	36.80	68.10
MT020	306.20	1.10	16.50	4.40	49.00	1.70	284.30	28.90	38.90	84.40
MT021	163.50	1.80	19.60	4.50	72.00	2.70	333.60	28.40	42.30	87.30
MT023	39.50	2.30	26.30	4.50	95.00	3.40	308.00	37.00	60.00	128.20
MT024	44.40	2.10	27.00	3.60	109.00	3.30	173.60	28.60	45.60	95.40
MT025	200.40	0.40	3.80	1.00	14.00	0.50	325.10	10.50	12.00	23.60
MT026	58.20	3.20	20.90	3.00	35.00	1.90	428.00	29.00	36.00	81.80
MT027	357.70	0.10	1.50	0.50	4.00	0.25	67.50	3.40	4.40	8.30

	Pr	Nd	Sm	Eu	Gd	Tb	Dy	Ho	Er	Tm
	Ppm	ppm	ppm	ppm	ppm	ppm	ppm	ppm	ppm	ppm
Analysis	**ICP-MS**	**ICP-MS**	**ICP-MS**	**ICP-MS**	**ICP-MS**	**ICP-MS**	**ICP-MS**	**ICP-MS**	**ICP-MS**	**ICP-MS**
Det. limit	**0.02**	**0.3**	**0.05**	**0.02**	**0.05**	**0.01**	**0.05**	**0.02**	**0.03**	**0.01**
Sample No										
Troubridge Basin										
CJ002	6.41	22.40	4.21	0.83	3.68	0.58	3.23	0.64	1.91	0.28
CJ003	5.54	19.50	3.66	0.73	3.21	0.53	3.06	0.59	1.74	0.25
CJ004	6.18	22.10	3.95	0.78	3.39	0.55	3.10	0.60	1.84	0.28
CJ005	4.46	17.00	2.91	0.55	2.44	0.37	2.21	0.43	1.25	0.19
CJ006	5.88	22.60	3.76	0.68	2.99	0.45	2.59	0.51	1.52	0.24
CJ007	3.66	14.10	2.32	0.43	1.86	0.30	1.69	0.34	1.03	0.16
CJ008	1.25	4.70	0.89	0.19	0.97	0.18	1.13	0.25	0.75	0.12
CJ009	6.85	24.90	4.09	0.61	3.37	0.51	2.82	0.56	1.66	0.24
CJ010	5.06	19.00	3.25	0.61	2.67	0.43	2.50	0.50	1.45	0.24
CJ011	5.61	26.70	6.55	1.58	9.08	1.67	10.30	2.17	5.73	0.76
CJ012	1.63	7.10	1.70	0.47	2.38	0.49	3.32	0.75	2.02	0.27
CJ013	2.72	9.40	1.68	0.33	1.38	0.23	1.49	0.28	0.87	0.14
CJ014	1.94	7.90	1.24	0.28	1.15	0.21	1.25	0.30	0.81	0.13

Sample No	Pr	Nd	Sm	Eu	Gd	Tb	Dy	Ho	Er	Tm
CJ015	0.99	3.90	0.68	0.15	0.70	0.13	0.88	0.19	0.56	0.09
CJ016	8.68	33.10	5.75	0.87	5.10	0.84	4.86	0.99	2.83	0.41
CJ017	2.97	10.80	2.00	0.36	1.66	0.28	1.60	0.32	0.84	0.15
CJ018	4.07	17.80	3.47	0.84	3.89	0.69	4.10	0.81	2.10	0.25
CJ019	3.67	14.50	2.62	0.56	2.87	0.48	2.83	0.67	1.86	0.28
CJ020	1.31	5.50	1.03	0.24	1.20	0.24	1.57	0.36	0.99	0.14
CJ021	9.80	38.70	6.20	1.17	5.22	0.81	4.43	0.87	2.61	0.38
CJ022	3.07	12.50	2.82	0.65	3.36	0.66	3.95	0.81	2.14	0.28
CJ023	9.28	32.40	6.02	1.11	5.14	0.82	4.56	0.90	2.82	0.40
CJ024	8.97	32.10	5.93	1.09	5.04	0.80	4.48	0.88	2.59	0.38
CJ025	11.72	41.60	7.60	1.44	7.26	1.17	6.40	1.30	3.76	0.53
CJ026	14.85	58.00	12.48	2.49	10.54	1.54	7.27	1.20	3.05	0.43
CJ027	4.70	17.80	3.72	0.70	2.45	0.37	1.95	0.33	0.98	0.14
CJ028	11.37	45.40	9.69	1.75	6.16	0.85	3.93	0.66	1.79	0.26
HC002	2.03	6.20	1.56	0.28	1.36	0.24	1.66	0.29	1.09	0.16
HC003	4.49	13.90	3.21	0.73	3.01	0.50	3.15	0.71	1.46	0.29
HC004	3.01	11.30	2.46	0.59	2.45	0.44	2.45	0.48	1.41	0.21
HC005	2.85	8.80	1.80	0.47	1.62	0.31	2.05	0.42	1.18	0.16
HC006	1.90	6.30	1.46	0.30	1.34	0.22	1.02	0.33	0.90	0.12
HC007	2.10	7.40	1.44	0.29	1.22	0.21	1.25	0.27	0.69	0.11
HC008	2.49	8.60	1.68	0.33	1.49	0.26	1.74	0.38	1.03	0.17
HC009	3.39	11.90	2.52	0.55	2.23	0.37	2.27	0.43	1.11	0.23
HC010	1.85	6.00	1.21	0.26	1.40	0.21	1.31	0.32	0.90	0.14
HC011	7.34	26.80	4.91	1.18	5.01	0.83	4.70	1.21	3.12	0.45
HC013	1.76	5.60	1.43	0.28	1.12	0.17	1.23	0.22	0.71	0.10
HC014	8.04	27.00	5.87	1.18	5.06	0.84	4.26	1.00	2.56	0.40
KI001	17.13	65.70	13.15	2.64	10.54	1.66	9.41	1.80	5.60	0.88
KI003	2.82	10.90	2.41	0.50	2.12	0.35	1.97	0.45	1.37	0.21
KI004	2.35	8.70	1.87	0.45	1.57	0.25	1.44	0.29	0.89	0.14
KI005	3.20	11.00	2.30	0.48	1.89	0.31	1.84	0.38	1.15	0.17
KI006	5.24	19.70	3.71	0.84	3.13	0.51	3.03	0.60	1.93	0.29
KI007	3.00	10.50	2.10	0.31	1.74	0.27	1.64	0.34	1.15	0.17
KI008	3.23	12.80	2.66	0.52	2.52	0.44	2.60	0.59	1.86	0.29
KI009	8.47	29.40	5.15	0.91	3.48	0.48	2.52	0.46	1.50	0.24
KI010	2.98	9.80	1.94	0.38	1.44	0.24	1.41	0.27	0.94	0.15
KI011	1.35	4.80	0.93	0.19	0.75	0.12	0.66	0.13	0.41	0.07
KI012	4.05	12.90	2.29	0.39	1.74	0.28	1.85	0.40	1.27	0.22
KI013	6.14	18.00	2.99	0.50	2.35	0.37	2.12	0.43	1.53	0.25
KI014	9.41	38.20	6.92	1.22	4.71	0.59	2.76	0.50	1.53	0.25
KI015	8.12	31.50	5.77	0.98	3.98	0.53	2.76	0.50	1.54	0.26
KI016	2.34	8.80	1.42	0.27	1.05	0.15	0.88	0.16	0.50	0.09
KI017	2.01	7.30	1.27	0.26	1.17	0.19	1.15	0.23	0.70	0.11
KI018	10.35	37.50	5.70	0.96	3.85	0.52	2.72	0.50	1.47	0.25
KP002	5.13	19.70	3.71	0.80	3.27	0.54	3.22	0.72	1.62	0.30
KP003	4.39	18.70	3.12	0.59	2.39	0.36	1.79	0.45	1.26	0.23
KP005	5.27	18.40	2.81	0.58	2.17	0.37	2.36	0.37	1.26	0.21
KP006	10.00	37.60	6.69	1.30	5.57	0.83	4.70	0.93	2.55	0.37
KP007	5.75	18.10	3.10	0.56	2.44	0.39	2.22	0.39	1.35	0.19
KP008	1.43	5.60	1.11	0.21	1.07	0.21	1.32	0.31	0.92	0.16
Reg001	1.29	4.10	0.88	0.19	0.70	0.15	0.80	0.25	0.63	0.11
Reg002	4.60	17.40	2.65	0.57	1.81	0.32	1.63	0.35	1.04	0.16
Reg003	2.43	9.10	1.57	0.39	1.64	0.27	1.33	0.33	0.92	0.15
Reg004	1.59	5.20	1.25	0.26	1.28	0.16	0.89	0.21	0.58	0.09
Reg005	5.35	20.80	3.95	0.87	3.77	0.55	3.49	0.66	1.56	0.26
Reg006	1.39	6.20	1.11	0.28	1.31	0.16	1.08	0.26	0.53	0.08
Reg007	3.16	13.50	4.03	0.95	3.51	0.58	2.87	0.59	1.55	0.26
Reg008	2.70	10.60	2.07	0.53	2.02	0.35	2.41	0.53	1.63	0.25
Reg009	2.44	9.10	1.46	0.30	1.20	0.22	1.63	0.31	0.93	0.16
Reg011	4.16	13.70	2.65	0.48	2.23	0.36	2.49	0.61	1.89	0.29
Reg012	1.86	6.00	1.41	0.30	1.31	0.23	1.54	0.31	0.91	0.15
Reg013	16.16	77.70	16.89	3.12	11.35	1.44	7.45	0.97	2.26	0.35
Reg014	3.23	11.40	2.06	0.33	1.71	0.26	1.30	0.32	0.90	0.14
Reg015	2.32	8.80	1.54	0.29	1.20	0.22	1.22	0.27	0.97	0.13
Reg016	3.19	11.00	2.28	0.48	1.95	0.34	1.92	0.41	1.14	0.19
Reg017	3.04	12.00	2.07	0.43	1.83	0.32	2.02	0.48	1.31	0.23
Reg018	2.85	12.30	1.90	0.34	1.56	0.24	1.45	0.32	0.86	0.14

Sample No	Pr	Nd	Sm	Eu	Gd	Tb	Dy	Ho	Er	Tm
Reg019	5.81	20.90	3.68	0.72	3.33	0.53	3.08	0.54	1.77	0.24
Reg020	1.92	6.10	1.45	0.27	1.34	0.23	1.54	0.28	1.00	0.16
Reg021	1.95	8.50	1.26	0.28	1.32	0.22	1.36	0.27	0.90	0.15
Reg022	9.47	30.90	4.91	0.83	3.49	0.52	2.96	0.56	1.77	0.30
Reg023	3.47	11.80	1.96	0.45	1.44	0.22	1.15	0.23	0.73	0.10
Reg024	3.32	12.40	2.43	0.51	1.95	0.35	2.15	0.39	1.29	0.19
Reg025	5.81	21.50	4.27	0.93	4.00	0.68	4.31	0.85	2.21	0.36
Reg026	3.92	14.60	2.35	0.47	1.74	0.29	1.56	0.37	1.07	0.15
Reg027	1.97	6.60	1.22	0.28	1.17	0.20	1.26	0.26	0.92	0.14
Reg028	1.56	6.80	0.86	0.20	0.73	0.12	0.73	0.15	0.64	0.07
Reg029	4.08	15.40	1.80	0.40	1.31	0.20	1.27	0.20	0.54	0.09
Reg030	3.37	9.80	2.59	0.42	1.93	0.36	1.98	0.40	1.10	0.17
Reg031	2.37	7.80	1.58	0.32	1.10	0.21	1.33	0.27	0.79	0.12
Reg032	4.48	13.40	2.16	0.54	1.44	0.22	1.11	0.21	0.73	0.09
Reg033	6.63	26.40	5.06	1.00	4.53	0.60	4.22	0.76	2.02	0.34
Reg034	6.32	22.80	4.60	0.92	4.13	0.56	3.74	0.65	2.23	0.31
Reg035	11.54	41.70	6.90	1.33	4.61	0.58	3.27	0.51	1.42	0.21
Reg036	2.37	9.10	1.43	0.28	1.29	0.18	1.31	0.27	0.81	0.12
Reg037	2.61	9.60	1.42	0.21	1.15	0.14	0.93	0.16	0.53	0.09
Reg038	6.63	24.50	4.28	0.84	3.97	0.57	3.95	0.66	2.05	0.30
Reg039	2.25	7.40	1.38	0.25	1.06	0.14	0.90	0.15	0.59	0.08
Reg040	2.41	7.70	1.47	0.26	1.34	0.20	1.78	0.28	0.91	0.14
Reg041	2.80	8.30	1.29	0.20	1.03	0.13	0.95	0.18	0.63	0.10
Reg042	2.07	6.70	1.27	0.25	1.29	0.16	0.97	0.17	0.55	0.08
Reg043	13.76	53.80	9.70	1.67	8.15	1.10	7.19	1.20	3.47	0.52
Reg044	3.97	19.40	4.00	0.78	2.77	0.31	1.78	0.27	0.81	0.10
Reg045	1.52	6.50	1.28	0.27	1.35	0.19	1.29	0.23	0.66	0.10
Reg046	2.89	9.80	1.75	0.35	1.46	0.19	1.32	0.23	0.74	0.10
Reg047	4.30	15.00	2.54	0.40	2.49	0.34	2.47	0.43	1.51	0.22
Reg048	6.87	24.60	4.28	0.51	3.20	0.39	2.97	0.46	1.53	0.24
Reg049	5.00	18.70	3.13	0.58	2.07	0.24	1.38	0.25	0.74	0.11
Reg050	3.20	11.70	1.87	0.31	1.65	0.25	1.79	0.34	1.07	0.18
Reg051	2.72	10.10	1.66	0.30	1.26	0.17	1.23	0.21	0.76	0.11
Reg052	5.35	21.70	4.37	1.01	4.07	0.56	4.15	0.69	2.02	0.32
Reg053	2.97	10.60	2.08	0.35	1.83	0.28	1.98	0.38	1.21	0.20
Reg054	8.29	30.00	5.23	1.12	4.55	0.59	3.81	0.55	1.74	0.25
Reg055	3.68	13.50	2.38	0.51	2.08	0.31	2.01	0.40	1.29	0.19
Reg056	4.35	17.10	2.61	0.50	1.92	0.21	1.55	0.21	0.53	0.07
Reg057	3.52	14.20	2.52	0.45	1.53	0.19	1.11	0.19	0.60	0.09
Reg058	1.89	7.50	1.21	0.25	1.21	0.17	1.08	0.21	0.67	0.10
Reg059	1.79	6.70	1.29	0.24	1.14	0.13	1.19	0.18	0.52	0.07
Reg060	5.93	23.00	4.18	0.82	2.50	0.28	1.64	0.20	0.61	0.08
Reg061	1.77	6.30	1.09	0.18	1.00	0.16	1.45	0.25	0.83	0.13
Reg062	1.60	4.70	0.79	0.13	0.58	0.10	0.64	0.14	0.46	0.06
Reg063	9.91	35.80	6.62	1.15	5.55	0.77	4.99	0.97	2.57	0.39
Reg064	2.28	8.70	1.58	0.31	1.26	0.24	1.54	0.34	1.02	0.17
Reg065	4.45	16.50	2.78	0.40	2.58	0.35	2.02	0.50	1.35	0.23
Reg066	3.67	12.50	2.38	0.50	2.09	0.33	1.99	0.47	1.27	0.22
Reg068	2.06	7.70	1.38	0.30	1.37	0.24	1.52	0.31	1.04	0.18
Reg069	4.43	16.00	3.02	0.52	2.43	0.36	2.16	0.45	1.27	0.22
Reg070	2.27	8.60	1.39	0.23	1.23	0.19	1.24	0.27	0.89	0.13
Reg071	3.19	13.70	2.17	0.47	2.09	0.32	2.13	0.43	1.01	0.16
Reg072	1.94	7.10	2.07	0.53	2.72	0.58	4.15	0.98	3.15	0.50
Reg073	2.86	11.30	2.81	0.59	3.45	0.60	3.64	0.86	2.63	0.44
Reg074	2.85	9.30	2.26	0.46	2.43	0.38	2.85	0.50	1.70	0.30
Reg075	2.13	8.70	1.64	0.31	1.83	0.33	2.06	0.45	1.34	0.18
Reg076	2.33	9.60	1.82	0.36	2.13	0.37	2.35	0.50	1.44	0.20
Reg078	1.73	6.90	1.20	0.23	0.92	0.19	0.96	0.21	0.67	0.10
WB001	4.39	15.60	2.39	0.45	1.97	0.34	2.05	0.44	1.47	0.24
WB002	3.38	12.60	1.95	0.35	1.69	0.26	1.66	0.37	1.16	0.20
WB003	4.29	15.00	2.53	0.45	2.01	0.35	2.18	0.46	1.51	0.26
WB004	2.89	10.00	1.67	0.31	1.46	0.26	1.63	0.36	1.18	0.19
WB005	4.03	13.90	2.28	0.45	2.06	0.37	2.30	0.51	1.65	0.28
WB006	4.33	15.50	2.51	0.47	2.13	0.37	2.27	0.48	1.57	0.28
WB007	2.87	9.30	1.42	0.31	1.30	0.24	1.42	0.32	1.07	0.17
CJ029	9.00	35.20	6.22	1.21	5.45	0.85	4.64	0.91	2.58	0.39

Sample No	Pr	Nd	Sm	Eu	Gd	Tb	Dy	Ho	Er	Tm
KP009	9.26	31.60	6.39	1.39	5.70	0.96	5.33	1.12	2.88	0.46
HC015	10.76	41.50	8.70	1.90	7.99	1.20	7.30	1.54	3.92	0.57
Arckaringa Basin										
BC001	1.80	7.10	1.27	0.27	1.31	0.22	1.24	0.26	0.78	0.14
BC002	2.35	8.60	1.78	0.40	1.83	0.32	1.81	0.38	1.06	0.17
BC003	1.56	5.70	1.07	0.23	1.01	0.18	1.06	0.22	0.70	0.10
BC004	1.93	7.90	1.40	0.30	1.30	0.23	1.31	0.27	0.80	0.14
BC005	1.60	5.80	1.12	0.26	1.18	0.22	1.30	0.28	0.86	0.13
BC006	2.13	8.60	1.55	0.33	1.53	0.27	1.50	0.32	0.96	0.15
MD001	4.74	18.70	3.28	0.63	3.19	0.56	3.15	0.67	2.13	0.32
MD002	3.03	12.60	2.55	0.54	2.92	0.56	3.50	0.76	2.37	0.36
MD003	2.31	10.60	2.21	0.52	2.91	0.48	2.83	0.58	1.58	0.23
MD004	3.80	14.60	2.68	0.54	2.50	0.42	2.58	0.51	1.54	0.24
MD005	9.32	36.80	6.25	1.07	5.59	0.93	5.07	1.09	3.27	0.50
MT001	10.89	41.30	7.19	1.16	6.33	1.00	5.75	1.09	3.22	0.50
MT002	11.71	44.00	7.82	1.40	6.86	1.12	6.27	1.27	3.68	0.54
MT003	12.03	46.80	8.14	1.36	7.24	1.17	6.43	1.28	3.90	0.58
MT004	11.86	46.50	8.09	1.33	7.21	1.16	6.54	1.28	3.81	0.57
MT005	12.64	46.90	8.33	1.52	7.43	1.19	6.59	1.29	3.71	0.56
MT006	12.85	49.20	8.56	1.54	7.60	1.26	6.86	1.34	3.84	0.56
MT007	1.67	5.80	0.90	0.19	0.83	0.13	0.65	0.15	0.37	0.06
MT008	2.73	10.20	1.76	0.31	1.71	0.30	1.95	0.43	1.22	0.21
MT009	2.28	9.50	1.80	0.40	1.81	0.30	1.70	0.32	0.82	0.11
MT010	13.49	52.90	9.00	1.57	7.54	1.23	6.69	1.33	3.83	0.59
MT011	10.19	41.30	7.35	1.41	7.19	1.15	6.48	1.29	3.78	0.56
MT012	11.16	44.00	7.50	1.25	6.62	1.08	6.11	1.22	3.51	0.54
MT013	10.33	40.20	6.90	1.13	5.98	0.98	5.36	1.05	3.04	0.47
MT014	12.21	48.60	8.29	1.51	7.28	1.18	6.59	1.25	3.60	0.57
MT015	11.46	45.20	7.59	1.31	6.62	1.08	5.94	1.17	3.30	0.50
MT016	7.62	31.00	5.36	0.84	4.69	0.73	4.02	0.80	2.25	0.35
MT017	3.48	13.90	2.48	0.40	2.44	0.45	2.78	0.57	1.82	0.30
MT018	5.55	23.80	3.86	0.64	3.31	0.48	2.65	0.48	1.30	0.19
MT019	7.81	29.10	5.05	0.81	4.04	0.67	3.82	0.77	2.30	0.34
MT020	9.10	37.00	6.33	1.12	5.43	0.83	4.63	0.93	2.91	0.44
MT021	9.61	36.80	6.36	1.01	5.15	0.84	4.90	0.98	2.79	0.44
MT023	14.00	55.10	9.64	1.50	7.79	1.30	7.33	1.31	3.62	0.53
MT024	10.17	39.30	6.79	1.19	5.83	0.92	5.38	1.01	2.80	0.43
MT025	2.58	9.90	1.70	0.27	1.48	0.26	1.59	0.35	1.10	0.19
MT026	8.59	33.80	6.29	0.95	5.43	0.93	5.48	1.06	3.07	0.49
MT027	0.96	3.50	0.60	0.10	0.52	0.10	0.58	0.12	0.36	0.07
MT001	10.89	41.30	7.19	1.16	6.33	1.00	5.75	1.09	3.22	0.50
MT002	11.71	44.00	7.82	1.40	6.86	1.12	6.27	1.27	3.68	0.54
MT003	12.03	46.80	8.14	1.36	7.24	1.17	6.43	1.28	3.90	0.58
MT004	11.86	46.50	8.09	1.33	7.21	1.16	6.54	1.28	3.81	0.57
MT005	12.64	46.90	8.33	1.52	7.43	1.19	6.59	1.29	3.71	0.56
MT006	12.85	49.20	8.56	1.54	7.60	1.26	6.86	1.34	3.84	0.56
MT007	1.67	5.80	0.90	0.19	0.83	0.13	0.65	0.15	0.37	0.06
MT008	2.73	10.20	1.76	0.31	1.71	0.30	1.95	0.43	1.22	0.21
MT009	2.28	9.50	1.80	0.40	1.81	0.30	1.70	0.32	0.82	0.11
MT010	13.49	52.90	9.00	1.57	7.54	1.23	6.69	1.33	3.83	0.59
MT011	10.19	41.30	7.35	1.41	7.19	1.15	6.48	1.29	3.78	0.56
MT012	11.16	44.00	7.50	1.25	6.62	1.08	6.11	1.22	3.51	0.54
MT013	10.33	40.20	6.90	1.13	5.98	0.98	5.36	1.05	3.04	0.47
MT014	12.21	48.60	8.29	1.51	7.28	1.18	6.59	1.25	3.60	0.57
MT015	11.46	45.20	7.59	1.31	6.62	1.08	5.94	1.17	3.30	0.50
MT016	7.62	31.00	5.36	0.84	4.69	0.73	4.02	0.80	2.25	0.35
MT017	3.48	13.90	2.48	0.40	2.44	0.45	2.78	0.57	1.82	0.30
MT018	5.55	23.80	3.86	0.64	3.31	0.48	2.65	0.48	1.30	0.19
MT019	7.81	29.10	5.05	0.81	4.04	0.67	3.82	0.77	2.30	0.34
MT020	9.10	37.00	6.33	1.12	5.43	0.83	4.63	0.93	2.91	0.44
MT021	9.61	36.80	6.36	1.01	5.15	0.84	4.90	0.98	2.79	0.44
MT023	14.00	55.10	9.64	1.50	7.79	1.30	7.33	1.31	3.62	0.53
MT024	10.17	39.30	6.79	1.19	5.83	0.92	5.38	1.01	2.80	0.43
MT025	2.58	9.90	1.70	0.27	1.48	0.26	1.59	0.35	1.10	0.19
MT026	8.59	33.80	6.29	0.95	5.43	0.93	5.48	1.06	3.07	0.49
MT027	0.96	3.50	0.60	0.10	0.52	0.10	0.58	0.12	0.36	0.07

	Yb	Lu	Mo	Cu	Pb	Zn	Ni	As	Cd	Sb
	ppm	ppm	ppm	ppm	ppm	ppm	ppm	ppm	ppm	ppm
Analysis	ICP-MS	ICP-MS	ICP-MS	ICP-MS	ICP-MS	ICP-MS	ICP-MS	ICP-MS	ICP-MS	ICP-MS
Det. limit	0.05	0.01	0.1	0.1	0.1	1	0.1	1	0.1	0.1
Sample No										
Troubridge Basin										
CJ002	1.85	0.29	0.20	8.10	8.20	29.00	11.00	2.30	0.05	0.05
CJ003	1.62	0.24	0.10	5.90	7.60	24.00	10.00	2.90	0.05	0.05
CJ004	1.78	0.27	0.10	7.90	8.90	35.00	10.30	4.60	0.05	0.05
CJ005	1.35	0.20	0.05	5.90	7.20	21.00	5.60	1.00	0.05	0.05
CJ006	1.63	0.25	0.05	5.70	8.10	19.00	7.30	1.10	0.05	0.05
CJ007	1.10	0.17	0.10	3.60	4.00	11.00	5.20	2.20	0.05	0.05
CJ008	0.80	0.13	0.20	1.60	1.80	5.00	2.10	1.40	0.05	0.05
CJ009	1.66	0.24	0.10	4.50	11.10	17.00	8.80	3.40	0.05	0.05
CJ010	1.65	0.25	0.05	5.20	6.10	19.00	7.60	1.80	0.05	0.05
CJ011	4.75	0.67	0.20	2.40	1.80	14.00	9.80	2.40	0.30	0.05
CJ012	1.58	0.22	0.05	0.60	1.00	2.00	0.30	2.80	0.05	0.05
CJ013	0.96	0.15	0.05	2.70	4.20	9.00	3.60	1.30	0.05	0.05
CJ014	1.04	0.15	0.05	2.80	5.20	7.00	2.80	0.90	0.05	0.05
CJ015	0.59	0.09	0.05	0.50	0.70	1.00	0.30	2.10	0.05	0.05
CJ016	2.81	0.43	0.05	4.70	5.10	74.00	23.70	1.80	0.05	0.05
CJ017	0.93	0.16	0.05	3.10	2.60	11.00	2.70	0.60	0.05	0.05
CJ018	1.60	0.23	0.10	1.30	3.30	3.00	0.30	2.20	0.10	0.05
CJ019	1.97	0.28	0.10	3.70	5.50	19.00	7.50	1.90	0.05	0.05
CJ020	0.85	0.13	0.05	1.00	0.80	2.00	0.80	2.20	0.05	0.05
CJ021	2.53	0.39	0.05	11.20	10.80	54.00	16.20	2.90	0.05	0.05
CJ022	1.75	0.26	0.05	1.00	4.60	3.00	0.60	3.90	0.05	0.10
CJ023	2.65	0.39	0.10	15.80	15.30	50.00	12.80	1.80	0.10	0.05
CJ024	2.61	0.37	0.05	14.90	12.60	47.00	11.50	2.80	0.05	0.05
CJ025	3.41	0.49	0.20	16.90	18.00	72.00	32.30	3.20	0.10	0.05
CJ026	2.86	0.39	0.05	6.90	12.30	9.00	4.60	1.50	0.05	0.05
CJ027	0.99	0.14	0.10	2.20	3.70	4.00	4.70	2.40	0.05	0.05
CJ028	1.69	0.25	0.05	1.30	6.40	3.00	2.90	1.20	0.05	0.05
HC002	0.89	0.17	0.50	6.40	4.60	9.00	4.50	7.10	0.05	0.05
HC003	1.71	0.30	0.10	9.40	12.30	33.00	8.90	2.50	0.05	0.05
HC004	1.53	0.22	0.20	6.90	8.40	21.00	6.20	1.20	0.10	0.05
HC005	0.93	0.19	0.40	14.10	9.30	28.00	6.00	2.90	0.10	0.10
HC006	0.88	0.11	0.20	5.70	4.00	11.00	5.90	0.80	0.05	0.05
HC007	0.88	0.12	0.30	3.80	3.60	9.00	5.70	0.70	0.05	0.05
HC008	1.01	0.17	0.60	5.20	3.80	12.00	6.90	1.50	0.05	0.05
HC009	1.04	0.21	0.20	7.80	6.20	21.00	8.30	8.10	0.05	0.05
HC010	1.07	0.17	0.10	3.00	2.40	6.00	3.30	0.90	0.05	0.05
HC011	2.52	0.37	0.20	14.60	16.90	56.00	23.40	3.60	0.05	0.05
HC013	0.64	0.11	0.30	2.50	1.60	3.00	3.30	2.50	0.05	0.05
HC014	2.52	0.38	0.05	12.00	17.70	55.00	19.30	3.60	0.05	0.10
KI001	5.74	0.97	1.30	42.60	18.70	24.00	8.20	25.90	0.05	0.05
KI003	1.39	0.24	1.90	34.90	15.90	44.00	6.20	10.30	0.05	0.30
KI004	0.96	0.15	0.10	19.80	1.70	5.00	2.40	0.80	0.05	0.05
KI005	1.27	0.21	0.20	14.00	2.00	5.00	2.70	0.25	0.05	0.05
KI006	2.06	0.34	0.30	14.50	2.00	11.00	6.50	1.40	0.05	0.05
KI007	1.10	0.19	0.40	20.60	1.30	6.00	3.90	1.00	0.05	0.05
KI008	1.87	0.30	0.70	9.50	1.30	19.00	11.50	1.70	0.05	0.05
KI009	1.58	0.25	0.40	11.20	12.80	30.00	5.90	4.00	0.05	0.05
KI010	0.98	0.16	0.40	6.40	7.10	15.00	2.50	3.50	0.05	0.05
KI011	0.48	0.08	0.70	5.70	4.40	26.00	6.00	5.00	0.05	0.05
KI012	1.58	0.25	0.05	4.90	6.10	9.00	0.05	0.70	0.05	0.05
KI013	1.72	0.27	0.20	11.30	7.30	20.00	5.30	2.10	0.05	0.05
KI014	1.76	0.26	0.20	12.60	9.70	18.00	4.90	4.20	0.05	0.05
KI015	1.88	0.28	0.20	11.90	8.60	22.00	6.10	4.10	0.05	0.05
KI016	0.62	0.10	0.10	2.10	2.60	6.00	1.40	2.00	0.05	0.05
KI017	0.73	0.11	0.80	9.70	6.70	36.00	6.40	3.80	0.05	0.05
KI018	1.78	0.27	1.10	22.20	18.90	52.00	13.20	7.40	0.05	0.10
KP002	1.86	0.29	0.20	5.40	9.70	18.00	15.40	9.40	0.05	0.05

Sample No	Yb	Lu	Mo	Cu	Pb	Zn	Ni	As	Cd	Sb
KP003	1.17	0.23	0.20	3.60	7.50	14.00	6.30	11.40	0.05	0.05
KP005	1.12	0.16	0.10	4.90	7.10	12.00	4.30	2.30	0.05	0.05
KP006	2.66	0.39	0.05	7.90	13.20	30.00	10.40	3.20	0.05	0.05
KP007	1.54	0.22	0.20	4.00	7.70	9.00	4.90	2.00	0.05	0.05
KP008	1.19	0.22	1.70	3.20	6.00	7.00	7.60	58.80	0.05	0.30
Reg001	0.81	0.12	0.10	2.20	2.70	28.00	3.20	3.40	0.05	0.05
Reg002	1.13	0.20	0.20	5.10	5.40	8.00	4.00	7.00	0.05	0.05
Reg003	0.95	0.15	0.20	6.30	6.30	10.00	6.90	3.50	0.05	0.05
Reg004	0.39	0.09	0.05	5.90	4.10	6.00	4.40	9.00	0.05	0.10
Reg005	1.82	0.27	0.20	9.40	13.40	25.00	10.00	11.30	0.10	0.05
Reg006	0.49	0.09	0.20	1.40	2.90	3.00	3.20	3.80	0.05	0.10
Reg007	1.72	0.24	51.90	39.70	178.80	11.00	32.10	4.40	0.05	0.20
Reg008	1.53	0.23	0.60	20.10	6.70	20.00	8.30	33.50	0.05	0.05
Reg009	1.25	0.20	6.20	7.90	6.60	8.00	2.00	20.80	0.05	0.10
Reg011	2.13	0.31	0.20	5.10	3.70	4.00	2.00	1.20	0.05	0.05
Reg012	1.05	0.15	0.90	5.40	5.30	5.00	4.40	57.50	0.05	0.10
Reg013	2.31	0.36	1.70	8.80	13.60	31.00	13.90	26.90	0.05	0.30
Reg014	0.84	0.16	0.05	2.20	7.40	5.00	2.50	1.90	0.05	0.05
Reg015	1.00	0.15	0.30	1.30	4.00	2.00	2.80	2.60	0.05	0.05
Reg016	1.18	0.16	0.10	2.30	4.10	4.00	4.20	0.50	0.05	0.05
Reg017	1.38	0.17	0.10	1.30	10.40	9.00	6.30	2.50	0.05	0.05
Reg018	0.76	0.16	0.30	1.10	14.40	4.00	3.90	3.80	0.05	0.05
Reg019	1.62	0.26	0.20	7.80	9.40	25.00	10.90	2.70	0.05	0.05
Reg020	1.07	0.13	0.30	2.40	4.00	8.00	6.10	0.80	0.05	0.10
Reg021	0.94	0.14	0.05	2.40	1.80	5.00	2.70	0.25	0.05	0.05
Reg022	1.92	0.27	0.70	27.70	15.70	32.00	7.10	23.70	0.05	0.20
Reg023	0.74	0.13	0.40	1.80	4.20	3.00	2.10	3.40	0.05	0.05
Reg024	0.97	0.19	0.30	4.20	6.50	7.00	7.60	5.50	0.05	0.05
Reg025	2.45	0.44	0.05	6.80	11.00	16.00	8.70	1.60	0.05	0.05
Reg026	1.06	0.21	0.40	1.30	14.00	6.00	4.90	6.70	0.05	0.05
Reg027	1.02	0.13	0.30	1.90	7.70	2.00	4.00	6.60	0.05	0.05
Reg028	0.65	0.07	0.20	1.50	4.30	2.00	2.90	1.80	0.05	0.05
Reg029	0.60	0.10	0.20	1.70	4.40	0.50	3.00	2.70	0.05	0.05
Reg030	1.21	0.21	0.10	2.70	4.50	5.00	4.40	0.70	0.05	0.05
Reg031	0.96	0.13	0.30	1.10	4.00	2.00	2.50	2.40	0.05	0.05
Reg032	0.74	0.09	0.10	1.30	4.20	0.50	1.30	2.20	0.05	0.05
Reg033	2.15	0.30	0.20	16.70	5.00	28.00	0.05	10.50	4.30	0.25
Reg034	2.31	0.30	0.40	6.70	6.30	8.00	0.05	13.10	2.80	0.25
Reg035	1.43	0.21	0.20	2.00	5.80	6.00	0.05	5.90	2.90	0.25
Reg036	0.86	0.12	0.05	7.30	5.70	4.00	0.05	2.70	3.70	0.60
Reg037	0.59	0.06	0.20	3.30	5.00	3.00	0.05	1.80	1.60	0.25
Reg038	2.07	0.28	0.30	2.00	12.20	13.00	0.05	12.30	4.80	0.25
Reg039	0.71	0.08	0.30	6.80	4.70	4.00	0.05	3.40	12.70	0.25
Reg040	0.95	0.14	0.20	0.90	5.60	3.00	0.05	3.20	2.60	1.10
Reg041	0.74	0.09	0.40	1.10	6.70	2.00	0.05	2.10	9.30	0.70
Reg042	0.72	0.08	0.10	1.80	1.90	5.00	0.05	2.70	0.50	0.60
Reg043	3.98	0.50	0.40	10.80	12.60	26.00	0.05	18.40	4.60	0.25
Reg044	0.84	0.11	0.30	2.30	2.00	6.00	0.05	2.90	1.60	0.25
Reg045	0.74	0.11	1.20	32.70	6.40	42.00	0.05	2.80	4.50	0.25
Reg046	0.94	0.10	0.30	3.30	3.30	11.00	0.05	4.40	4.10	0.70
Reg047	1.68	0.22	1.20	2.50	10.50	3.00	0.05	5.80	9.30	0.25
Reg048	1.76	0.25	0.90	10.30	6.80	5.00	0.05	5.20	8.30	0.25
Reg049	0.88	0.10	0.05	2.20	2.80	8.00	0.05	1.00	1.20	0.25
Reg050	1.37	0.19	0.05	4.40	4.50	1.00	0.05	2.80	0.90	0.25
Reg051	0.83	0.11	0.30	1.50	4.00	3.00	0.05	3.70	3.50	0.25
Reg052	1.89	0.27	0.90	8.80	16.70	10.00	0.05	11.80	34.50	0.25
Reg053	1.53	0.20	0.40	5.60	8.10	5.00	0.05	4.10	5.00	0.25
Reg054	1.72	0.21	0.20	15.60	10.80	4.00	0.05	4.80	3.50	0.70
Reg055	1.51	0.19	1.10	2.70	10.30	6.00	0.05	10.50	9.00	0.80
Reg056	0.67	0.08	0.05	1.40	3.10	1.00	0.05	1.20	3.60	0.25
Reg057	0.78	0.11	0.60	1.40	5.80	2.00	0.05	2.50	43.10	0.25
Reg058	0.91	0.11	0.30	0.70	6.00	1.00	0.05	2.60	5.60	0.25
Reg059	0.62	0.08	0.20	1.80	2.00	0.50	0.05	1.20	3.10	0.25
Reg060	0.77	0.08	0.50	1.60	4.10	2.00	0.05	2.20	3.80	0.25

Sample No	Yb	Lu	Mo	Cu	Pb	Zn	Ni	As	Cd	Sb
Reg061	1.10	0.15	0.40	4.80	3.30	2.00	0.05	2.70	4.80	0.25
Reg062	0.50	0.06	0.60	2.50	3.00	0.50	0.05	1.40	7.50	0.25
Reg063	2.57	0.38	0.20	16.60	11.70	56.00	0.05	25.50	5.80	0.25
Reg064	1.12	0.19	0.20	0.80	6.00	3.00	0.05	4.20	2.50	0.25
Reg065	1.55	0.22	1.10	1.50	8.60	4.00	0.05	5.60	8.30	0.25
Reg066	1.40	0.20	1.10	1.70	9.60	6.00	0.05	9.90	8.30	0.25
Reg068	1.05	0.19	1.10	9.10	13.20	3.00	6.80	13.50	0.05	0.05
Reg069	1.29	0.21	0.20	2.30	7.80	5.00	5.40	3.70	0.05	0.05
Reg070	0.90	0.15	0.30	5.30	4.70	3.00	3.40	3.70	0.05	0.05
Reg071	1.14	0.16	0.70	14.00	17.70	3.00	10.40	10.20	0.05	0.05
Reg072	3.32	0.56	0.20	51.50	1.00	23.00	10.70	3.70	0.05	0.05
Reg073	2.90	0.44	0.05	1.50	2.00	9.00	1.90	1.20	0.05	0.05
Reg074	1.61	0.30	1.00	0.50	14.90	5.00	13.10	5.60	0.05	0.05
Reg075	1.17	0.17	9.20	17.00	124.10	58.00	37.70	666.90	0.05	29.00
Reg076	1.27	0.18	11.80	17.80	156.10	70.00	33.10	564.00	0.10	23.00
Reg078	0.95	0.13	0.30	3.00	2.10	6.00	4.20	0.60	0.05	0.05
WB001	1.65	0.26	0.20	2.40	5.00	4.00	1.10	2.80	0.05	0.05
WB002	1.37	0.21	4.20	5.30	5.20	9.00	1.80	24.60	0.05	0.05
WB003	1.82	0.28	0.05	0.80	2.40	2.00	0.50	0.25	0.05	0.05
WB004	1.37	0.21	7.90	10.60	7.10	14.00	3.70	44.50	0.05	0.20
WB005	2.00	0.31	0.10	5.30	2.80	7.00	1.80	1.10	0.05	0.05
WB006	1.83	0.29	0.05	0.70	2.20	2.00	0.40	0.50	0.05	0.05
WB007	1.18	0.18	0.30	13.80	8.00	18.00	8.10	14.80	0.05	0.05
CJ029	2.73	0.38	0.80	12.90	9.50	74.00	25.60	7.20	0.05	0.10
KP009	3.08	0.44	0.20	8.50	7.10	75.00	41.80	1.70	0.05	0.05
HC015	3.50	0.45	0.60	2.90	20.40	78.00	39.70	3.90	0.05	0.40
Arckaringa Basin										
BC001	0.93	0.14	0.30	1.80	2.80	9.00	5.50	2.90	0.05	0.10
BC002	1.13	0.17	0.30	4.20	4.10	19.00	6.60	2.70	0.10	0.05
BC003	0.71	0.11	12.80	5.90	30.00	26.00	38.00	28.40	0.30	0.80
BC004	0.88	0.14	0.10	2.50	3.80	16.00	5.60	2.40	0.05	0.05
BC005	0.91	0.13	6.70	4.70	11.10	43.00	33.00	21.90	0.05	1.00
BC006	1.04	0.16	0.50	4.70	3.90	17.00	11.30	4.40	0.05	0.10
MD001	2.06	0.32	0.50	10.70	7.60	28.00	11.30	5.70	0.05	0.05
MD002	2.33	0.38	0.80	6.10	10.10	34.00	10.70	13.80	0.60	0.10
MD003	1.38	0.21	0.60	6.20	8.30	84.00	35.10	4.70	0.50	0.05
MD004	1.58	0.24	0.05	4.00	5.10	12.00	8.10	4.20	0.05	0.05
MD005	3.23	0.51	0.05	5.50	7.70	14.00	3.60	1.30	0.05	0.05
MT001	3.22	0.48	0.40	6.60	8.90	34.00	16.60	4.30	0.05	0.05
MT002	3.53	0.51	0.30	30.70	23.50	95.00	24.90	4.40	0.05	0.30
MT003	3.73	0.56	0.30	20.20	19.30	87.00	26.00	6.40	0.05	0.10
MT004	3.71	0.54	0.30	19.40	19.90	101.00	30.20	7.00	0.05	0.10
MT005	3.61	0.52	0.60	34.10	27.10	97.00	29.50	3.80	0.05	0.10
MT006	3.50	0.54	0.80	35.40	30.20	76.00	25.40	2.60	0.05	0.05
MT007	0.34	0.06	4.60	6.10	3.60	5.00	8.70	4.50	0.05	0.05
MT008	1.29	0.21	0.05	1.20	2.60	4.00	1.00	0.90	0.05	0.05
MT009	0.69	0.10	2.00	28.30	7.10	51.00	35.00	6.50	0.05	0.20
MT010	3.63	0.55	0.10	27.30	19.20	81.00	28.00	1.40	0.05	0.05
MT011	3.42	0.50	0.40	25.40	13.90	60.00	24.00	7.20	0.05	0.20
MT012	3.38	0.50	0.50	23.20	18.90	91.00	29.80	3.50	0.10	0.10
MT013	3.05	0.45	0.40	16.10	15.60	75.00	20.00	4.40	0.05	0.20
MT014	3.56	0.53	0.30	34.10	18.70	62.00	36.70	1.70	0.05	0.10
MT015	3.20	0.46	0.40	27.20	19.90	89.00	28.50	3.70	0.10	0.20
MT016	2.19	0.32	1.60	20.20	12.70	49.00	23.30	3.50	0.05	0.20
MT017	2.03	0.32	0.20	1.00	1.00	2.00	0.60	0.25	0.05	0.05
MT018	1.13	0.17	9.00	17.40	12.20	28.00	13.60	8.60	0.30	0.30
MT019	2.21	0.36	0.20	20.60	8.20	3.00	3.10	0.70	0.05	0.05
MT020	2.79	0.43	0.70	16.60	6.90	7.00	9.90	2.20	0.05	0.05
MT021	2.92	0.41	0.20	20.10	7.60	32.00	6.50	2.30	0.05	0.10
MT023	3.32	0.47	0.05	27.30	18.20	76.00	14.60	1.90	0.05	0.10
MT024	2.83	0.41	0.20	30.70	27.00	100.00	31.70	2.60	0.05	0.05
MT025	1.17	0.20	0.40	2.30	3.20	12.00	3.00	3.30	0.05	0.10
MT026	3.22	0.47	0.10	10.90	13.30	10.00	6.40	1.30	0.05	0.05
MT027	0.35	0.07	0.10	0.05	1.10	9.00	1.20	1.90	0.05	0.30

	Bi	Ag	Au	Hg	Tl	Se
	ppm	ppm	ppb	ppm	ppm	ppm
Analysis	**ICP-MS**	**ICP-MS**	**ICP-MS**	**ICP-MS**	**ICP-MS**	**ICP-MS**
Det. limit	**0.1**	**0.1**	**0.5**	**0.1**	**0.1**	**0.5**
Sample No						
Troubridge Basin						
CJ002	0.20	0.05	0.25	0.01	0.20	0.25
CJ003	0.10	0.05	0.25	0.01	0.10	0.25
CJ004	0.10	0.05	0.25	0.01	0.10	0.25
CJ005	0.05	0.05	1.30	0.01	0.05	0.25
CJ006	0.05	0.05	0.25	0.01	0.10	0.25
CJ007	0.05	0.05	0.25	0.01	0.10	0.25
CJ008	0.05	0.05	0.25	0.01	0.05	0.25
CJ009	0.20	0.05	0.25	0.01	0.20	0.25
CJ010	0.10	0.05	0.25	0.01	0.10	0.25
CJ011	0.05	0.05	0.25	0.01	0.05	0.25
CJ012	0.05	0.05	0.25	0.01	0.05	0.25
CJ013	0.05	0.05	0.25	0.01	0.05	0.25
CJ014	0.05	0.05	0.25	0.01	0.05	0.25
CJ015	0.05	0.05	0.25	0.01	0.05	0.25
CJ016	0.20	0.05	0.25	0.01	0.50	0.25
CJ017	0.05	0.05	0.25	0.01	0.05	0.25
CJ018	0.05	0.05	0.25	0.01	0.05	0.25
CJ019	0.05	0.05	0.25	0.01	0.10	0.25
CJ020	0.05	0.05	0.25	0.01	0.05	0.25
CJ021	0.20	0.05	0.25	0.01	0.20	0.25
CJ022	0.05	0.05	0.25	0.01	0.05	0.25
CJ023	0.30	0.05	1.00	0.02	0.20	0.25
CJ024	0.20	0.05	1.10	0.01	0.10	0.25
CJ025	0.30	0.05	1.50	0.01	0.30	0.25
CJ026	0.30	0.05	1.00	0.01	0.10	0.25
CJ027	0.05	0.05	0.70	0.02	0.05	0.25
CJ028	0.10	0.05	0.25	0.01	0.05	0.25
HC002	0.05	0.05	0.25	0.01	0.05	0.25
HC003	0.05	0.05	0.80	0.01	0.05	0.25
HC004	0.05	0.05	0.25	0.01	0.05	0.25
HC005	0.40	0.05	4.30	0.01	0.05	0.25
HC006	0.05	0.05	1.00	0.01	0.05	0.25
HC007	0.05	0.05	2.70	0.01	0.05	0.25
HC008	0.05	0.05	1.10	0.01	0.05	0.25
HC009	0.05	0.05	0.60	0.01	0.05	0.25
HC010	0.05	0.05	0.25	0.01	0.05	0.25
HC011	0.20	0.05	1.90	0.01	0.10	0.25
HC013	0.05	0.05	0.25	0.01	0.05	0.25
HC014	0.20	0.05	0.25	0.01	0.10	0.25
KI001	0.20	0.05	7.70	0.02	0.10	0.25
KI003	0.05	0.05	1.40	0.01	0.20	0.25
KI004	0.05	0.05	2.80	0.02	0.05	0.25
KI005	0.05	0.05	1.60	0.01	0.05	0.25
KI006	0.05	0.05	3.10	0.01	0.05	0.25
KI007	0.05	0.05	5.20	0.01	0.05	0.25
KI008	0.05	0.40	0.25	0.01	1.50	0.25
KI009	0.20	0.05	0.25	0.01	0.20	0.25
KI010	0.20	0.05	0.25	0.01	0.05	1.40
KI011	0.05	0.05	0.25	0.01	0.05	1.10
KI012	0.10	0.05	0.25	0.01	0.20	0.25
KI013	0.20	0.05	0.25	0.01	0.30	0.25
KI014	0.20	0.05	6.00	0.01	0.20	0.25
KI015	0.20	0.05	0.25	0.01	0.30	0.25
KI016	0.05	0.05	1.80	0.01	0.05	0.25
KI017	0.05	0.05	1.50	0.01	0.05	0.25
KI018	0.30	0.05	0.25	0.01	0.10	1.60
KP002	0.10	0.05	0.25	0.08	0.20	0.25
KP003	0.10	0.05	0.25	0.01	0.10	0.25
KP005	0.05	0.05	0.50	0.01	0.10	0.25
KP006	0.20	0.05	0.25	0.01	0.20	0.25

Sample No	Bi	Ag	Au	Hg	Tl	Se
KP007	0.05	0.05	0.80	0.01	0.10	0.25
KP008	0.10	0.05	0.25	0.01	0.05	3.60
Reg001	0.05	0.05	0.25	0.01	0.05	0.25
Reg002	0.05	0.05	0.25	0.01	0.05	0.25
Reg003	0.05	0.05	2.40	0.02	0.10	0.25
Reg004	0.05	0.05	0.60	0.01	0.05	0.25
Reg005	0.30	0.20	3.80	0.01	0.10	1.00
Reg006	0.05	0.05	0.25	0.01	0.05	0.25
Reg007	0.05	0.05	0.25	0.01	3.10	0.25
Reg008	0.20	0.05	0.25	0.01	0.20	0.25
Reg009	1.00	0.05	0.25	0.01	0.05	4.60
Reg011	0.05	0.05	2.60	0.01	0.05	0.25
Reg012	0.20	0.05	0.60	0.01	0.05	1.40
Reg013	0.10	0.05	0.60	0.01	0.20	0.25
Reg014	0.10	0.05	0.90	0.01	0.20	0.25
Reg015	0.05	0.05	2.30	0.01	0.10	0.25
Reg016	0.05	0.05	1.40	0.01	0.05	0.25
Reg017	0.10	0.05	0.70	0.01	0.20	0.25
Reg018	0.05	0.05	2.00	0.02	0.05	0.25
Reg019	0.10	0.05	0.80	0.01	0.10	0.25
Reg020	0.05	0.05	0.25	0.01	0.05	0.25
Reg021	0.05	0.05	0.25	0.01	0.05	0.25
Reg022	0.30	0.05	0.60	0.01	0.20	1.60
Reg023	0.05	0.05	0.25	0.01	0.05	0.25
Reg024	0.05	0.05	0.70	0.01	0.05	0.25
Reg025	0.05	0.05	0.60	0.01	0.20	0.25
Reg026	0.10	0.05	1.00	0.01	0.05	0.25
Reg027	0.05	0.05	0.25	0.01	0.05	0.25
Reg028	0.05	0.05	0.25	0.01	0.05	0.25
Reg029	0.05	0.05	0.60	0.01	0.05	0.25
Reg030	0.05	0.05	0.25	0.01	0.05	0.25
Reg031	0.05	0.05	0.25	0.01	0.05	0.25
Reg032	0.05	0.05	0.25	0.01	0.05	0.25
Reg033	0.05	0.05	0.05	0.01	0.10	0.25
Reg034	0.05	0.05	0.05	0.02	0.20	0.25
Reg035	0.05	0.05	0.05	0.02	0.20	0.60
Reg036	0.05	0.05	0.05	0.01	0.10	0.25
Reg037	0.05	0.05	0.05	0.01	0.05	0.25
Reg038	0.05	0.05	0.10	0.06	0.30	0.25
Reg039	0.05	0.05	0.05	0.01	0.05	0.25
Reg040	0.05	0.05	0.05	0.06	0.10	0.25
Reg041	0.05	0.05	0.05	0.01	0.05	0.25
Reg042	0.05	0.05	0.05	0.01	0.05	0.25
Reg043	0.05	0.05	0.20	0.01	0.50	0.80
Reg044	0.05	0.05	0.05	0.01	0.05	0.25
Reg045	0.05	0.30	0.05	0.01	0.05	0.25
Reg046	0.05	0.05	0.05	0.01	0.05	0.25
Reg047	0.05	0.05	0.20	0.07	0.10	1.70
Reg048	0.05	0.05	0.05	0.02	0.05	0.60
Reg049	0.05	0.05	0.05	0.01	0.05	0.25
Reg050	0.05	0.05	0.10	0.01	0.05	0.25
Reg051	0.05	0.05	0.05	0.01	0.05	0.25
Reg052	0.05	0.10	0.20	0.03	0.10	0.80
Reg053	0.05	0.05	0.05	0.01	0.05	0.25
Reg054	0.05	0.05	0.10	0.01	0.20	0.60
Reg055	0.05	0.05	0.20	0.08	0.10	1.60
Reg056	0.05	0.05	0.05	0.01	0.05	0.25
Reg057	0.05	0.30	0.05	0.01	0.05	0.90
Reg058	0.05	0.05	0.05	0.03	0.05	0.25
Reg059	0.05	0.05	0.05	0.01	0.05	0.25
Reg060	0.05	0.05	0.05	0.01	0.05	0.25
Reg061	0.05	0.05	0.10	0.01	0.05	0.25
Reg062	0.05	0.05	0.05	0.01	0.05	0.50
Reg063	0.05	0.05	0.20	0.01	0.30	0.25
Reg064	0.05	0.05	0.05	0.05	0.10	0.25
Reg065	0.05	0.05	0.10	0.06	0.10	1.40
Reg066	0.05	0.05	0.10	0.08	0.10	1.30

Sample No	Bi	Ag	Au	Hg	Tl	Se
Reg068	0.05	0.05	0.25	0.01	0.05	0.60
Reg069	0.05	0.05	2.20	0.04	0.05	0.25
Reg070	0.05	0.05	0.25	0.01	0.05	0.25
Reg071	0.05	0.05	487.80	0.01	0.05	1.20
Reg072	0.05	0.05	31.50	0.06	0.05	0.25
Reg073	0.05	0.05	0.50	0.02	0.10	0.25
Reg074	0.30	0.05	0.25	0.06	0.05	2.10
Reg075	0.05	0.30	0.50	0.19	0.20	2.00
Reg076	0.05	2.00	2.90	0.57	0.70	2.80
Reg078	0.05	0.05	0.25	0.01	0.05	0.25
WB001	0.20	0.05	1.10	0.01	0.05	0.25
WB002	0.90	0.05	0.25	0.01	0.05	2.90
WB003	0.05	0.05	0.25	0.01	0.05	0.25
WB004	1.10	0.05	0.25	0.01	0.05	7.40
WB005	0.10	0.05	0.90	0.01	0.05	0.25
WB006	0.05	0.05	0.25	0.01	0.05	0.25
WB007	0.20	0.05	0.25	0.01	0.05	0.25
CJ029	0.20	0.05	2.00	0.01	0.70	0.60
KP009	0.20	0.05	0.25	0.01	0.70	0.25
HC015	0.30	0.05	0.25	0.01	0.10	0.25
Arckaringa Basin						
BC001	0.05	0.05	0.25	0.01	0.05	0.25
BC002	0.05	0.05	0.80	0.01	0.10	0.25
BC003	0.05	0.05	0.80	0.01	0.05	3.80
BC004	0.05	0.05	0.50	0.01	0.05	0.25
BC005	0.05	0.05	6.20	0.01	0.05	0.25
BC006	0.05	0.05	0.80	0.01	0.05	0.25
MD001	0.20	0.05	0.25	0.01	0.30	0.25
MD002	0.10	0.30	0.60	0.02	0.70	0.25
MD003	0.05	0.05	0.25	0.01	0.50	0.25
MD004	0.05	0.05	0.25	0.01	0.05	0.25
MD005	0.10	0.05	0.25	0.01	0.10	0.25
MT001	0.20	0.05	0.25	0.01	0.20	0.25
MT002	0.70	0.05	0.70	0.01	0.20	0.25
MT003	0.40	0.05	0.25	0.01	0.30	0.25
MT004	0.30	0.05	0.25	0.01	0.30	0.25
MT005	0.70	0.05	0.25	0.01	0.20	0.25
MT006	0.80	0.05	5.90	0.03	0.10	0.25
MT007	0.10	0.05	1.10	0.01	0.05	2.10
MT008	0.05	0.05	0.25	0.02	0.05	0.25
MT009	0.05	0.05	1.60	0.01	0.30	0.25
MT010	0.50	0.05	2.30	0.02	0.30	0.80
MT011	0.30	0.05	1.40	0.01	0.20	0.25
MT012	0.30	0.05	0.25	0.01	0.30	0.25
MT013	0.20	0.05	0.25	0.01	0.20	0.60
MT014	0.60	0.05	0.70	0.02	0.10	0.60
MT015	0.30	0.05	0.25	0.01	0.30	0.25
MT016	0.20	0.05	0.70	0.04	0.20	1.00
MT017	0.05	0.05	0.25	0.01	0.05	0.25
MT018	0.20	0.05	1.00	0.08	0.10	5.80
MT019	0.70	0.05	0.25	0.02	0.10	0.25
MT020	0.30	0.05	0.25	0.03	0.10	1.10
MT021	0.20	0.05	0.90	0.03	0.20	0.25
MT023	0.40	0.05	0.25	0.02	0.10	0.25
MT024	0.60	0.05	0.25	0.01	0.30	0.25
MT025	0.05	0.05	0.25	0.01	0.30	0.25
MT026	0.10	0.05	0.25	0.04	0.10	0.25
MT027	0.05	0.05	0.25	0.01	0.10	0.25